

**Cold Metal Transfer-Gas Metal Arc Welding (CMT-GMAW) Wire + Arc Additive  
Manufacturing (WAAM) Process Control Implementation**

by

Wesley Scott Hunko

A dissertation submitted to the Graduate Faculty of  
Auburn University  
in partial fulfillment of the  
requirements for the Degree of  
Doctor of Philosophy

Auburn, Alabama  
May 5, 2018

Keywords: Additive Manufacturing, Wire + Arc Additive Manufacturing, Cold Metal  
Transfer

Copyright 2018 by Wesley Scott Hunko

Approved by

Lewis N. Payton, Chair, Associate Research Professor of Mechanical Engineering  
Ruel A. (Tony) Overfelt, Professor of Materials Engineering  
Dan B. Marghitu, Professor of Mechanical Engineering  
John L. Evans, Department Chair of Industrial and Systems Engineering

## **Abstract**

While additive manufacturing is comprised of metal and polymer fabrication, current additively manufactured polymer-based products are much further from being put into industrial applications. Metal-based additive manufacturing is comprised into wire- and powder-based processes. While the powder processes have the advantage of fine detailed resolution, they are limited by the production rate it takes to produce these fine details. Wire processes have much higher deposition rates, while at the same time having lower start-up, production, and consumable costs. Due to these reasons, a wire-based system was chosen for this research. A Fronius Cold Metal Transfer (CMT) welder has been modified to a CNC 3-Axis gantry system for the purposes of a Wire + Arc Additive Manufacturing (WAAM) system.

One of the biggest issues currently with additive manufacturing is the lack of control over the process. Issues such as scale error, thermal management, and variable control plague the technology. Many work-arounds have been developed to increase productivity, repeatability, and reliability (such as scaling, pausing, or trail-and-error); however, no real-time process control has been implemented successively on a broad basis. This research attempts to close the gap on control over the WAAM process via multiple control schemes. The three biggest issues noted in literature are issues with scale error, thermal management, and process variable control. Closed-loop feedback control systems have been developed, analyzed, and quantified to address these specific issues.

The control schemes have been successfully evaluated and have indeed improved the WAAM process. Mechanical properties such as ultimate tensile strength, yield strength, and hardness have been characterized at multiple temperatures and via different welding control lines. Support material such as wiring diagrams, operating manuals, and operational machine codes have also been developed for replication of this research and to further the research started here. Using the results found in this research, future users can easily produce quality additive metal parts quickly, efficiently, and easily thanks to the controls developed to aid in the ease of using WAAM.

The use of all the control schemes in conjunction with each other is highly recommended for all future users for all occasions. This not only benefits the user and the 'printed' part, but also the machine. In additive manufacturing the need for optimal mechanical properties is not always necessary. Often a simple working prototype for proof of concept is all that is necessary. In this case the fastest method, without compromising the machine, is best. If material strength is to be optimized, maintaining a low temperature set point, without sacrificing time, is recommended for both materials (steel, stainless). Isotropic tendencies were found in steel, and near-isotropic properties were found in stainless with the combined control schemes.

## **Acknowledgements**

Many people contributed to this project and deserve recognition for its success. I would like to thank my committee for their guidance and support. I want to thank Dr. Payton for giving me the opportunity to work in the DML and providing support throughout my time at Auburn. I also want to thank the National Institute of Standards and Technology (NIST) for providing funding for this project.

I am grateful for the many colleagues I have had the pleasure to work with over the years. Our experiences together have helped mold me into the person I am today. Particularly I want to thank Jeffrey Gaddes for his initial work with me on this project. Also, I want to especially thank Conyers Coupland for his efforts alongside me throughout this research. I want to thank Dr. Jordan Roberts and Justin Evans for their guidance, support, and friendships throughout my time at Auburn University.

I would also like to thank my family for their love and support throughout my college career. I am especially thankful for the love, commitment, and encouragement from Alx Kelley. Finally, I would like to thank God for all the blessings and opportunities he has presented me throughout my life.

## Table of Contents

Abstract .....	ii
Acknowledgements .....	iv
List of Tables .....	x
List of Figures .....	xii
I. Introduction .....	1
II. Literature Review .....	3
Metal Additive Manufacturing .....	3
Wire and Arc Additive Manufacturing .....	6
GMAW Deposition Processes .....	7
Wire and Arc Additive Manufacturing using Short Circuit Transfer GMAW .....	10
Wire and Arc Additive Manufacturing using Cold Metal Transfer GMAW .....	43
Process Control .....	60
Fronius CMT Welding .....	64
Weld Temperature .....	66
Wire Offset Distance .....	71
Evaluation Techniques for CMT-GMAW Additive Manufacturing .....	72
Summary of Research Opportunities .....	72
III. Scope and Objectives .....	74
IV. Design and Construction of Equipment .....	77

IV. Design and Construction of Equipment.....	77
Previous Machine Design .....	77
CMT Weld System .....	80
Robot – Welder Integration .....	86
Instruments.....	93
Materials .....	102
V. Methodology and Statistical Design of Experiments.....	104
Tensile Strength Evaluation .....	104
Hardness Evaluation .....	111
Macrostructure & Microstructure Evaluation.....	114
Wire Offset Distance Control .....	116
Wire Feed Speed/Voltage/Current Control.....	119
Temperature Control.....	121
Operators’ Manual .....	126
Summary .....	126
VI. Results.....	128
Standard Specimen Data Sheet .....	128
Closed-Loop Process Control .....	130
Contact Tip to Work Distance Control Evaluation.....	135
Cold Metal Transfer Control Evaluation .....	165
Temperature Monitoring Control Evaluation .....	196
VII. Discussion .....	231
Closed-Loop Process Control Discussion.....	231

Contact Tip to Work Distance Control Discussion.....	231
Cold Metal Transfer Control Discussion .....	232
Temperature Monitoring Control Discussion .....	232
General Discussion .....	233
Summary .....	234
VII. Conclusion and Future Work .....	236
Recommendations for Future Work.....	237
Outstanding Objectives.....	239
References.....	241
Appendix I – Data Results .....	249
Synergic ‘Standard Mode’ Data.....	250
CTWD Control Data.....	251
Temperature Control ER70S-6 .....	252
Temperature Control ER308L .....	253
Baseline Comparison Data.....	254
Repeatability Study in ER70S-6 - Tensile .....	255
Repeatability Study in ER70S-6 - Hardness .....	256
Appendix II – Experiment Sheets/Notes.....	257
Appendix III – Machine Codes.....	274
Appendix IV – Statistics .....	277
Repeatability Stats for Hardness for ER70S-6.....	278
Repeatability Stats for Tensile for ER70S-6.....	296
CTWD Control Stats for ER70S-6 .....	313

CTWD Control Stats for ER308L.....	323
CMT Control Stats for ER70S-6 .....	335
CMT Control Stats for ER308L.....	344
Temperature Control Stats for ER70S-6.....	356
Temperature Control Stats for ER308L.....	383
ER70S-6 ANOVA – CTWD.....	428
ER70S-6 ANOVA – CMT .....	439
ER70S-6 ANOVA – Temperature .....	450
ER308L ANOVA – CTWD.....	461
ER308L ANOVA – CMT.....	472
ER308L ANOVA – Temperature .....	483
Appendix V – Material Data Sheets .....	494
Appendix VI – Wiring Diagram .....	497
Appendix VII – Operating Manual.....	500
Turning Everything On/Off .....	501
Controls Overview .....	501
G-code.....	502
Loading the Wire .....	505
Loading the Build Plate .....	506
Setting the Gas Flow Rate.....	506
Preparing Mach3 for Printing .....	506
Measuring the Voltage and Current and Wire Feed Speed.....	507
Varying parameters in operation.....	508



Appendix VIII – Continuation of Manual; Provided via Fronius..... 509

## List of Tables

Table 1: Interactions observed by Dickens et al. [18] .....	16
Table 2: Tensile Properties of Deposited 2319 Alloy and Wrought 2219 Alloy [41] .....	54
Table 3: Directly Proportional (X) and Inversely Proportional (1/X) Responses to Current and Travel Speed [45] .....	58
Table 4: Fronius CMT Advance 4000 MV R Power Source Specs [57] .....	82
Table 5: Machine Codes used to Operate the Welder .....	89
Table 6: ER308L filler material properties .....	102
Table 7: ER70S-6 filler material properties [National Standard] .....	103
Table 8: ER70S-6 Repeatability Perpendicular Tensile Results .....	107
Table 9: ER70S-6 Perpendicular Repeatability T-Test Results .....	108
Table 10: ER70S-6 Repeatability Parallel Tensile Results .....	108
Table 11: ER70S-6 Parallel Repeatability T-Test Results .....	109
Table 12: Parallel Vs Perpendicular T-Test Results .....	110
Table 13: Tensile Standard Deviations ( $\sigma$ ) .....	111
Table 14: ER70S-6 Repeatability Perpendicular Hardness Results Rockwell B .....	112
Table 15: ER70S-6 Perpendicular Repeatability T-Test Results .....	112
Table 16: ER70S-6 Repeatability Parallel Hardness Results Rockwell B .....	113
Table 17: ER70S-6 Parallel Repeatability T-Test Results .....	113
Table 18: Average Hardness T-Test Results .....	114

Table 19: Hardness Tests Standard Deviations ( $\sigma$ ).....	114
Table 20: Mixing Solution for %3 Nital Etchant, ASTM No. 74a.....	115
Table 21: Mixing Solution for Kroll’s Reagent Etchant, ASTM No. 88.....	115
Table 22: Wire Offset Distance Control Scheme Combinations .....	118
Table 23: WFS/Voltage/Current Control Scheme Combinations.....	121
Table 24: Temperature Control Scheme Combinations.....	123
Table 25: ER70S-6 With v. Without CTWD Control P-Values.....	136
Table 26: ER308L With v. Without CTWD Control P-Values .....	137
Table 27: CTWD Control Print Time and Machining Evaluation.....	160
Table 28: ER70S-6 CMT v. Standard Control P-Values.....	165
Table 29: ER308L CMT v. Standard Control P-Values.....	166
Table 30: CMT Control Deposition Rate, Machining, and Layer Height Evaluation....	190
Table 31: Average WFS, V, C for Representative Wall for Different Modes.....	192
Table 32: ER70S-6 With v. Without Temperature Control P-Values .....	197
Table 33: With V. Without Temperature Control for ER308L P-Values.....	211
Table 34: Temp Control Deposition Rate, Machining, and Layer Height Evaluation ...	223

## List of Figures

Figure 1: Typical Powder Bed System Setup [1].....	4
Figure 2: Typical Powder Fed System Setup [1].....	5
Figure 3: Typical Wire Feed System Setup (E-Beam Energy Source Process) [1].....	6
Figure 4: GMAW Short Circuit Transfer [4].....	8
Figure 5: GMAW Globular Transfer [4] .....	9
Figure 6: GMAW Spray Arc Transfer [4] .....	9
Figure 7: GMAW Cold Metal Transfer [5].....	10
Figure 8: Baker’s Patent [8].....	11
Figure 9: Box Produced using GMAW Process [18].....	15
Figure 10: Truncated Hollow Pyramid using GMAW Process [18].....	15
Figure 11: Geometries studied by Spencer et al [19].....	18
Figure 12: Procedure for depositing adjacent layers by Spencer et al. [19] .....	19
Figure 13: Voids in adjacent beads as shown in dye penetrant test by Spencer et al. [19] .....	19
Figure 14: First successful integration of CAD and welder controls [22].....	21
Figure 15: Complex geometry produced by Ribeiro et al. [26].....	22
Figure 16: Relationship between layer width and travel speed by Ribeiro et al. [21] .....	23
Figure 17: Tube shaped part with the same layer start point by Zhang et al. [30] .....	26
Figure 18: Tube shaped part with varied layer start point by Zhang et al. [30].....	26

Figure 19: Speed control for the start and stop of the path by Zhang et al. [30] .....	27
Figure 20: Wall section without start and end-point control by Zhang et al. [30].....	27
Figure 21: Wall section with start and end-point control by Zhang et al. [30].....	28
Figure 22: Thin-walled part before and after machining by Song et al. [32] .....	29
Figure 23: Integrated welding and milling machine created by Song et al. [32].....	29
Figure 24: (A) Upper Region of the Wall; (B) Lower Region of the Wall [32].....	30
Figure 25: Solid part before and after machining by Song et al. [32] .....	31
Figure 26: Build Strategies for Solid Layers [33].....	33
Figure 27: Low-Cost Open-Source GMAW Printer by Anzalone et al. [35] .....	35
Figure 28: Sprocket manufactured by Anzalone et al. [35] .....	36
Figure 29: WAAM Machined Produced at Auburn University [2] .....	37
Figure 30: Solid Infill vs. Infill with Shells [2] .....	38
Figure 31: Outward and Inward Facing Geometry Test [2] .....	38
Figure 32: Bridge Geometry Test [2].....	38
Figure 33: Stainless Steel Nozzle as Printed and Post Processed [2] .....	39
Figure 34: Wire Diameter Study Voltage Results [2].....	40
Figure 35: Wire Diameter Study Current Results [2] .....	40
Figure 36: Steel (ER70S-6) Tensile Test Results [2].....	41
Figure 37: Stainless Steel (ER308) Tensile Test Results [2] .....	41
Figure 38: Voids Found between Layers in Steel (ER70S-6) Parts [2].....	42
Figure 39: (Left) Microstructure of Steel (ER70S-6) Sample before Heat Treatment (Right) Microstructure of Steel (ER70S-6) Sample after Heat Treatment [2].....	42
Figure 40: Grain Size Comparison Varying Shielding Gas Composition of Helium and Argon Mix A) 30% He B) 50% He C) 70% He [38].....	45

Figure 41: Predicted First Order 3D Response Surface Model for the Effective Wall Width Response as a function of the Wire Diameter and WFS, for a Constant WFS/TS Ratio of 20 [38].....	46
Figure 42: A) CAD Model of Part and Injection Molds B) Near-Net Shape Molds C) Finished Molds [39].....	47
Figure 43: Depositions Made at Different Combinations of Process Parameters [39].....	48
Figure 44: Predicted vs. Measured <i>Yield</i> using Equation 1 [39].....	49
Figure 45: Temperature Verification of Transient and Steady-State Models [40].....	51
Figure 46: Stress Verification of Transient and Steady-State Models [40].....	51
Figure 47: Stress along the Z-Direction Before and After Clamping [40].....	51
Figure 48: CMT-WAAM Experimental System [41].....	53
Figure 49: Porosity of WAAM 2319 deposited by A) CMT-PADV process, WFS=6m/min, TS=0.6m/min, Heat Input (HI)=112.2 J/mm, B) CMT-P process, WFS=6m/min, TS=0.8m/min, HI=189.1 J/mm [41].....	54
Figure 50: Application of the Pinning Ability [42].....	55
Figure 51: Error for Predicted and Actual Area of Weld Bead Cross Section [44].....	57
Figure 52: Varying Travel Speed with a Constant WFS/TS Ratio of 30 m/min [3].....	59
Figure 53: Range of Orientations Achievable by the CMT Process [46].....	59
Figure 54: Flow Chart for Various Parameters Based on Material Choice and Diameter	65
Figure 55: Effect of Interpass Temperature on Tensile Strength for Steel Weld [52].....	70
Figure 56: Previous Version of WAAM Printer [2].....	78
Figure 57: WAAM Printer Bed/Plate [2].....	79
Figure 58: Mach3 CNC Software.....	80
Figure 59: Fronius Weld System [56].....	81
Figure 60: Fronius CMT Advanced 4000 MV R Power Source [49].....	82
Figure 61: Fronius VR 7000 CMT Wire Feeder [49].....	83

Figure 62: Fronius Robacta 5000 Drive/Torch [54] .....	84
Figure 63: Fronius Wire Buffer [49].....	85
Figure 64: Fronius RCU 5000i [49].....	86
Figure 65: Sealevel RS-485 Modbus RTU (left), Sealevel RS-485 I/O (right).....	88
Figure 66: Fronius Welder Interface.....	92
Figure 67: Cincinnati CNC .....	94
Figure 68: Bridgeport Series I 2 HP Vertical Milling Machine.....	94
Figure 69: Southbend 450 Lathe.....	95
Figure 70: Do All 2013-V Vertical Band Saw (L) Wellsaw 1118 Horizontal Band Saw (R) .....	96
Figure 71: Wilton Belt Sander.....	96
Figure 72: Model HR-150 Rockwell Hardness Tester .....	97
Figure 73: MTS Q-Test 100.....	98
Figure 74: Keyence VHX 1000 E 3D microscope.....	99
Figure 75: MTS Landmark Servo Hydraulic Load Frame.....	100
Figure 76: Mitutoyo 6” Dial Calipers Model Number 505-675 .....	100
Figure 77: Omega Universal Temperature Process Controller CN245 .....	101
Figure 78: ASTM E8 Subsize Tensile Testing Standard [55] .....	105
Figure 79: Test Orientation for Samples Produced Perpendicular to Deposition.....	107
Figure 80: Test Orientation for Samples Produced Parallel to Deposition.....	109
Figure 81: Initial Thermocouple Position in Relation to Printed Wall.....	124
Figure 82: Second Thermocouple Position to Maintain Proper Distance.....	124
Figure 83: Third Thermocouple Position to Maintain Proper Distance .....	125
Figure 84: Final Thermocouple Position to Maintain Proper Distance .....	125

Figure 85: Arc Length Correction Setting [49].....	129
Figure 86: Welder Setup Heading.....	129
Figure 87: Arc Force (Dynamic) Correction [49].....	129
Figure 88: 2-Step Welding Mode with Crater Fill (I-E) [49] .....	130
Figure 89: GMAW Block Diagram .....	131
Figure 90: GMAW Block Diagram with CTWD Feedback .....	132
Figure 91: Fronius CMT DSP + $\mu$ P Block Diagram [49].....	133
Figure 92: CMT-GMAW Block Diagram with CTWD Feedback .....	133
Figure 93: CMT-GMAW Block Diagram with CTWD and Temperature Monitoring Feedback .....	135
Figure 94: Main Effects Plot for ER70S-6 for CTWD Control for Hardness .....	138
Figure 95: Main Effects Plot for ER70S-6 for CTWD Control for UTS.....	139
Figure 96: Main Effects Plot for ER70S-6 for CTWD Control for Yield .....	139
Figure 97: Residual Plots for ER70S-6 for CTWD Control for Yield .....	140
Figure 98: Residual Plots for ER70S-6 for CTWD Control for Hardness .....	140
Figure 99: Residual Plots for ER70S-6 for CTWD Control for UTS.....	141
Figure 100: Interval Plot for ER70S-6 for CTWD Control for Hardness.....	142
Figure 101: Tukey Analysis for ER70S-6 for CTWD Control for Hardness .....	142
Figure 102: Interval Plot for ER70S-6 for CTWD Control for Yield.....	143
Figure 103: Tukey Analysis for ER70S-6 for CTWD Control for Yield .....	143
Figure 104: Interval Plot for ER70S-6 for CTWD Control for UTS .....	144
Figure 105: Tukey Analysis for ER70S-6 for CTWD Control for UTS.....	144
Figure 106: Interval Plot for ER70S-6 for CTWD Control for Hardness.....	145
Figure 107: Tukey Analysis for ER70S-6 for CTWD Control for Hardness .....	145



Figure 108: Interval Plot for ER70S-6 for CTWD Control for Yield.....	146
Figure 109: Tukey Analysis for ER70S-6 for CTWD Control for Yield .....	146
Figure 110: Tukey Analysis for ER70S-6 for CTWD Control for UTS.....	147
Figure 111: Interval Plot for ER70S-6 for CTWD Control for UTS .....	147
Figure 112: Main Effects Plot for ER308L for CTWD Control for Yield .....	149
Figure 113: Main Effects Plot for ER308L for CTWD Control for Hardness .....	149
Figure 114: Residual Plots for ER308L for CWTD Control for Hardness.....	150
Figure 115: Main Effects Plot for ER308L for CTWD Control for UTS.....	150
Figure 116: Residual Plots for ER308L for CWTD Control for Yield.....	151
Figure 117: Residual Plots for ER308L for CWTD Control for UTS .....	151
Figure 118: Interval Plot for ER308L for CWTD Control for Hardness.....	152
Figure 119: Tukey Analysis for ER308L for CWTD Control for Hardness .....	152
Figure 120: Interval Plot for ER308L for CWTD Control for Yield.....	153
Figure 121: Tukey Analysis for ER308L for CWTD Control for Yield .....	153
Figure 122: Interval Plot for ER308L for CWTD Control for UTS .....	154
Figure 123: Tukey Analysis for ER308L for CWTD Control for UTS.....	154
Figure 124: Interval Plot for ER308L for CWTD Control for Hardness.....	155
Figure 125: Tukey Analysis for ER308L for CWTD Control for Hardness .....	155
Figure 126: Interval Plot for ER308L for CWTD Control for Yield.....	156
Figure 127: Tukey Analysis for ER308L for CWTD Control for Yield .....	156
Figure 128: Interval Plot for ER308L for CWTD Control for UTS .....	157
Figure 129: Tukey Analysis for ER308L for CWTD Control for UTS.....	157
Figure 130: ER70S-6 CTWD Control Scheme Evaluation .....	158

Figure 131: ER308L CTWD Control Scheme Evaluation .....	159
Figure 132: ER70S-6 without CTWD Control Layer Interface.....	161
Figure 133: ER70S-6 without CTWD Control Representative Structure.....	161
Figure 134: Top to Bottom View of ER70S-6 without CTWD Control.....	162
Figure 135: ER70S-6 with CTWD Control Layer Interface.....	163
Figure 136: ER70S-6 with CTWD Control Representative Structure.....	163
Figure 137: ER308L Typical Layer Interface with Noticeable Boundary .....	164
Figure 138: ER308L Typical Microstructure .....	164
Figure 139: Main Effects Plot for ER70S-6 for Hardness .....	168
Figure 140: Main Effects Plot for ER70S-6 for Yield.....	168
Figure 141: Residual Plots for ER70S-6 for Hardness .....	169
Figure 142: Main Effects Plot for ER70S-6 for UTS .....	169
Figure 143: Residual Plots for ER70S-6 for Yield .....	170
Figure 144: Residual Plots for ER70S-6 for UTS .....	170
Figure 145: Tukey Analysis for ER70S-6 for Hardness.....	171
Figure 146: Interval Plot for ER70S-6 for Hardness .....	171
Figure 147: Interval Plot for ER70S-6 for Yield .....	172
Figure 148: Tukey Analysis for ER70S-6 for Yield.....	172
Figure 149: Interval Plots for ER70S-6 for UTS .....	173
Figure 150: Tukey Analysis for ER70S-6 for UTS .....	173
Figure 151: Tukey Analysis for ER70S-6 for Hardness.....	174
Figure 152: Interval Plot for ER70S-6 for Hardness .....	174
Figure 153: Interval Plot for ER70S-6 for Yield .....	175

Figure 154: Tukey Analysis for ER70S-6 for Yield.....	175
Figure 155: Interval Plot for ER70S-6 for UTS.....	176
Figure 156: Tukey Analysis for ER70S-6 for UTS .....	176
Figure 157: Main Effects Plot for ER308L for Hardness .....	177
Figure 158: Main Effects Plot for ER308L for UTS .....	178
Figure 159: Main Effects Plot for ER308L for Yield.....	178
Figure 160: Residual Plots for ER308L for Yield .....	179
Figure 161: Residual Plots for ER308L for Hardness .....	179
Figure 162: Residual Plots for ER308L for UTS.....	180
Figure 163: Interval Plot for ER308L for Hardness .....	181
Figure 164: Tukey Analysis for ER308L for Hardness .....	181
Figure 165: Interval Plot for ER308L for Yield .....	182
Figure 166: Tukey Analysis for ER308L for Yield.....	182
Figure 167: Tukey Analysis for ER308L for UTS .....	183
Figure 168: Interval Plot for ER308L for UTS.....	183
Figure 169: Tukey Analysis for ER308L for Hardness .....	184
Figure 170: Interval Plot for ER308L for Hardness .....	184
Figure 171: Tukey Analysis for ER308L for Yield.....	185
Figure 172: Interval Plot for ER308L for Yield .....	185
Figure 173: Tukey Analysis for ER308L for UTS .....	186
Figure 174: Interval Plot for ER308L for UTS.....	186
Figure 175: ER70S-6 CMT Control Scheme Evaluation .....	188
Figure 176: ER308L CMT Control Scheme Evaluation.....	188

Figure 177: Standard Mode Voltage and Current Plot .....	191
Figure 178: CMT Mode Voltage and Current Plot.....	191
Figure 179: ER70S-6 with CMT Control Layer Interface.....	193
Figure 180: ER70S-6 with CMT Control Representative Structure.....	193
Figure 181: ER70S-6 with Previous Standard Welder Layer Interfaces [2] .....	194
Figure 182: ER70S-6 with Standard Control Layer Interfaces.....	194
Figure 183: ER308L with CMT Control Typical Microstructure .....	195
Figure 184: ER308L with CMT Control Layer Interface Boundary .....	195
Figure 185: ER308L with Standard Control.....	196
Figure 186: Main Effects Plot for Yield for ER70S-6 with Temp Control .....	198
Figure 187: Main Effects Plot for Hardness for ER70S-6 with Temp Control .....	198
Figure 188: Residual Plots for Hardness for ER70S-6 for Temp Control.....	199
Figure 189: Main Effects Plot for UTS for ER70S-6 with Temp Control.....	199
Figure 190: Residual Plots for UTS for ER70S-6 for Temp Control .....	200
Figure 191: Residual Plots for Yield for ER70S-6 for Temp Control.....	200
Figure 192: Tukey Analysis for Hardness for ER70S-6 for Temp Control.....	202
Figure 193: Interval Plot for Hardness for ER70S-6 for Temp Control.....	202
Figure 194: Tukey Analysis for Yield for ER70S-6 for Temp Control.....	203
Figure 195: Interval Plot for Yield for ER70S-6 for Temp Control.....	203
Figure 196: Tukey Analysis for UTS for ER70S-6 for Temp Control.....	204
Figure 197: Interval Plot for UTS for ER70S-6 for Temp Control .....	204
Figure 198: Tukey Analysis for Hardness for ER70S-6 for Temp Control.....	205
Figure 199: Interval Plot for Hardness for ER70S-6 for Temp Control.....	205

Figure 200: Tukey Analysis for Yield for ER70S-6 for Temp Control.....	206
Figure 201: Interval Plot for Yield for ER70S-6 for Temp Control.....	206
Figure 202: Tukey Analysis for UTS for ER70S-6 for Temp Control.....	207
Figure 203: Interval Plot for UTS for ER70S-6 for Temp Control .....	207
Figure 204: Graph of ER70S-6 Temp Control Measurables with Accuracy.....	209
Figure 205: Temperature v. UTS for ER70S-6 with Accuracy .....	209
Figure 206: Temperature v. Yield Strength for ER70S-6 with Accuracy .....	210
Figure 207: Main Effects Plot for Hardness for ER308L for Temp Control.....	211
Figure 208: Main Effects Plot for UTS for ER308L for Temp Control .....	212
Figure 209: Main Effects Plot for Yield for ER308L for Temp Control.....	212
Figure 210: Residual Plots for Yield for ER308L for Temp Control.....	213
Figure 211: Residual Plots for Hardness for ER308L for Temp Control .....	213
Figure 212: Residual Plots for UTS for ER308L for Temp Control .....	214
Figure 213: Interval Plot for Hardness for ER308L for Temp Control .....	215
Figure 214: Tukey Analysis for Hardness for ER308L for Temp Control.....	215
Figure 215: Interval Plot for Yield for ER308L for Temp Control .....	216
Figure 216: Tukey Analysis for Yield for ER308L for Temp Control.....	216
Figure 217: Interval Plot for UTS for ER308L for Temp Control .....	217
Figure 218: Tukey Analysis for UTS for ER308L for Temp Control .....	217
Figure 219: Tukey Analysis for Hardness for ER308L for Temp Control.....	218
Figure 220: Interval Plot for Hardness for ER308L for Temp Control .....	218
Figure 221: Interval Plot for Yield for ER308L for Temp Control .....	219
Figure 222: Tukey Analysis for Yield for ER308L for Temp Control.....	219

Figure 223: Interval Plot for UTS for ER308L for Temp Control .....	220
Figure 224: Tukey Analysis for UTS for ER308L for Temp Control .....	220
Figure 225: Temperature v. UTS for ER308L with Accuracy .....	221
Figure 226: Graph of ER308L Temp Control Measurables with Accuracy .....	221
Figure 227: Yield Strength v. Temperature for ER308L with Accuracy .....	222
Figure 228: ER70S-6 without Temperature Control Representative Structure .....	224
Figure 229: ER70S-6 without Temperature Control Layer Interface .....	225
Figure 230: ER70S-6 with Temperature Control at 232°C .....	225
Figure 231: ER70S-6 with Temperature Control at 288°C .....	226
Figure 232: ER70S-6 with Temperature Control at 260°C .....	226
Figure 233: ER308L without Temperature Control Layer Interface Boundary .....	227
Figure 234: ER308L without Temperature Control Typical Microstructure.....	227
Figure 235: ER308L with Temperature Control at 150°C .....	228
Figure 236: ER308L with Temperature Control at 150°C Layer Interface .....	228
Figure 237: ER308L with Temperature Control at 205°C Layer Interface .....	229
Figure 238: ER308L with Temperature Control at 205°C .....	229
Figure 239: ER308L with Temperature Control at 260°C Layer Interface .....	230
Figure 240: ER308L with Temperature Control at 260°C .....	230
Figure 241: Control Encumulator Wiring Diagram.....	499
Figure 242. HSMWorks Toolpath Generation Shown for Stainless Geometries .....	502
Figure 243. Starting G-Code as Output (left) and as Post Processed (right). .....	503
Figure 244. Layer Change G-Code as Output (left) and as Post Processed (right). .....	505

## **I. Introduction**

Commercial metal additive manufacturing machines currently provide users fair to high resolution and the ability to produce complex geometries which traditional manufacturing techniques simply cannot produce. These machines are slow, limited in scalability, and expensive. Auburn University's Wire 3D machine offers a highly modular, open frame design that utilizes the Wire + Arc Additive Manufacturing (WAAM) technique. The WAAM process utilizes a modified welder to melt feed wire layer by layer to produce metal 'prints.'

To date, most researchers have studied the WAAM process utilizing modified Gas Metal Arc Welders (GMAW). Short Circuit Transfer and Cold Metal Transfer (CMT) are the two main techniques used for the GMAW WAAM technique. Previous research at Auburn University focused on applying the Short Circuit Transfer process to WAAM, while this research focuses on CMT-WAAM.

The lack of control over the process has been identified by researchers as a prevalent root issue for decades. Nearly all researchers have added rudimentary techniques to monitor one or two in-process parameters; however, none have successfully implemented an actual closed-loop feed-back control loop for the many parameters in the process. The use of CMT-GMAW has been acknowledged to provide greater control over the voltage/current/wire feed relationship; however, many more process variables play a

significant role during the 'printing' process. This research attempts to close the gap on the control issue prevalent in the field.



## II. Literature Review

### Metal Additive Manufacturing

Manufacturing systems used for the additive manufacturing of metals can be generalized into three broad categories: powder bed systems, powder feed systems and wire feed systems [1]. Each system comes with its own drawbacks and advantages, while the end-user must decide what meets the needs.

“A powder bed is created by raking powder across the work area. The energy source (electron beam or laser beam) is programmed to deliver energy to the surface of the bed melting or sintering the powder into the desired shape. Additional powder is raked across the work area, and the process is repeated to create a solid three-dimensional component. The advantages of this system include its ability to produce high resolution features, internal passages, and maintain dimensional control” [1]. Powder bed systems are not without their drawbacks; they are costly to purchase and operate. This is partly because currently “all the powder bed systems are manufactured by companies located outside the United States” [1]. For example, “ARCAM , a Swedish company, manufactures the only powder bed electron beam system, the ARCAM A2” [1]. Additionally, since the entire machine is filled with material, powder bed systems often waste a large amount of un-sintered powder. Even if the excess powder is reclaimed, there is still a portion that is partially sintered that cannot be reused. Additionally, powder bed

systems have low material deposition rates due to the repeated process of dispersing powder over the bed and ensuring it is flat and level for the next layer. Figure 1 shows a generalized illustration of a powder bed system.

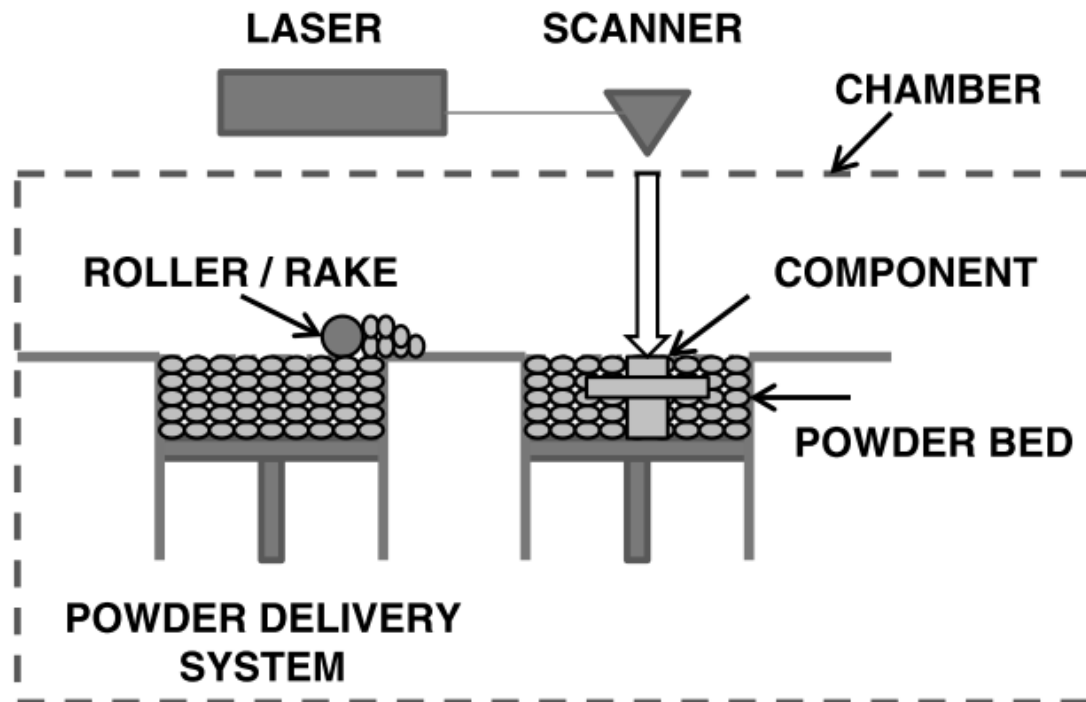


Figure 1: Typical Powder Bed System Setup [1]

Powder feed systems work on a similar concept to powder bed systems. “The build volumes of these systems are generally larger (e.g.,  $>1.2 \text{ m}^3$  for the Optomec LENS 850-R unit). Further, the powder feed systems lend themselves more readily to build volume scale up than do the powder bed units. In these systems, powders are conveyed through a nozzle onto the build surface. A laser is used to melt a monolayer or more of the powder into the shape desired. This process is repeated to create a solid three-dimensional component. There are two dominate types of systems in the market. 1. The work piece remains stationary, and deposition head moves. 2. The deposition head remains stationary, and the

work piece is moved. The advantages of this type of system include its larger build volume and its ability to be used to refurbish worn or damaged components” [1]. While powder fed systems seem superior to powder bed, they still have relatively low deposition rates and are incapable of producing fine internal passages and features quite like powder bed systems can due to the excess powder acting as a support structure. Figure 2 shows a generalized illustration of a powder feed system.

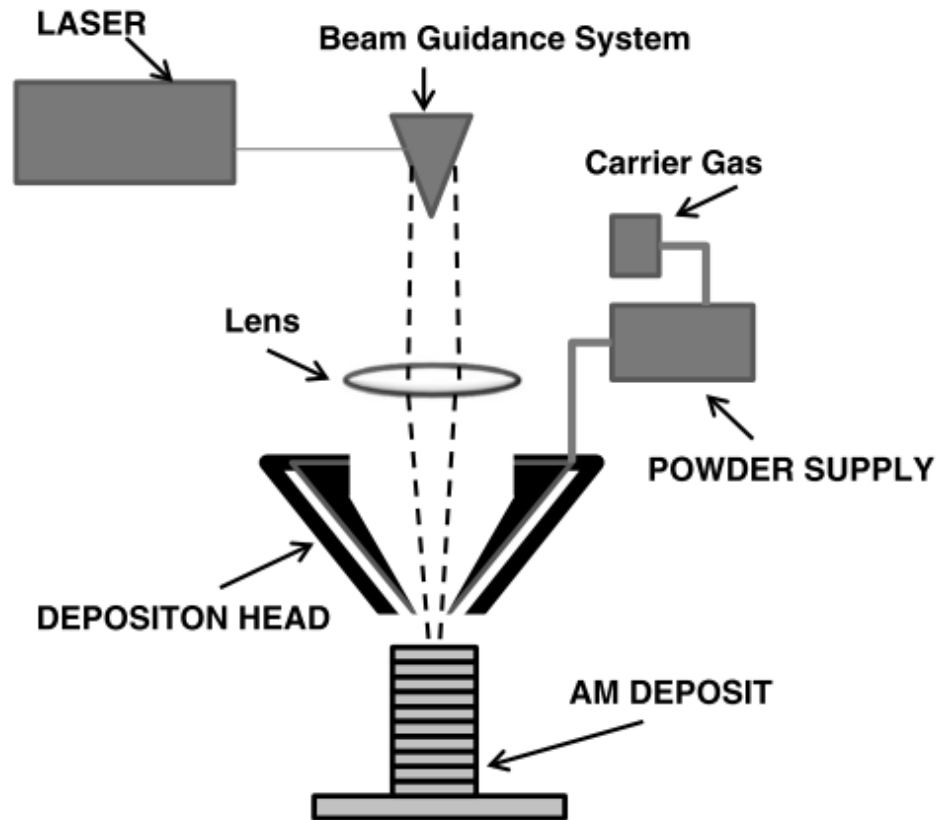


Figure 2: Typical Powder Fed System Setup [1]

Wire feed systems use wire feed stock to deposit and build subsequent layers. “The feed stock is wire, and the energy source for these units can include electron beam, laser beam, and plasma arc. Initially, a single bead of material is deposited and upon subsequent passes is built upon to develop a three-dimensional structure. In general, wire feed systems are well suited for high deposition rate processing and have large build volumes; however,

the fabricated product usually requires more extensive machining than the powder bed or powder fed systems do” [1]. “Another advantage of wire fed machines is the economic use of material. Wire feed systems only deposit object material, without any waste and have low raw material costs when compared to powders. This makes wire fed machines ideal for near net shape manufacturing of large structural objects with low material waste. Additionally, wire feed systems do not require complex powder distribution hardware and are easily integrated into a gantry style CNC machine” [2]. Figure 3 shows a generalized illustration of a wire feed system; however, in the illustration an electron beam as energy source is being used.

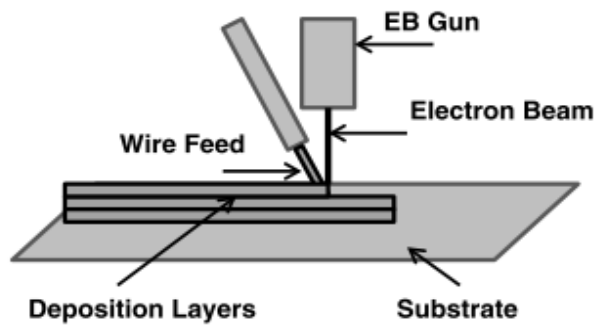


Figure 3: Typical Wire Feed System Setup (E-Beam Energy Source Process) [1]

### **Wire and Arc Additive Manufacturing**

"The wire fed additive manufacturing process can be further classified into multiple types dependent upon the wire melting method. The two types of wire fed additive manufacturing systems use a repurposed and modified Tungsten Inert Gas (TIG/GTAW) or Metal Inert Gas (MIG/GMAW) welding power source [3]. The GTAW process uses an energy source (laser, electron beam, or electricity) to melt a fed wire in an inert gas environment. The GMAW process uses a consumable wire electrode that is melted by electricity and deposited in an inert gas environment.

Both the GMAW deposition process and the GTAW deposition process have advantages. The GMAW process results in an easier control because it requires less moving components than the GTAW process. The GTAW process requires movement of an electrode and the deposited metal wire in coordination. The GMAW process only has one moving component because the deposited metal wire is the electrode. Additionally, the GMAW process does not require orientation of the deposited metal wire. The GTAW process requires appropriate orientation of the wire as well as the arc source which results in complicated toolpath generation. The GTAW process, however, is less prone to electric arc wandering and a better surface finish is consequently easier to achieve [3]” [2].

### **GMAW Deposition Processes**

“Whenever possible, GMAW is the process of choice: the wire is the consumable electrode, and its coaxiality with the welding torch results in easier tool path” [3]. GMAW welding has multiple methods of deposition based on the controls available. Metal transfer is accomplished by feed wire being melted and deposited on a substrate. These methods of deposition include Short Circuit Transfer, Globular Transfer, Spray Arc Transfer, and Cold Metal Transfer (CMT) [4, 5].

“Short Circuit Transfer is the traditional GMAW process as illustrated in Figure 4. During the Short Circuit Transfer process, the welding wire contacts the base metal between 90-200 times per second. While Short Circuit Transfer is not capable of as high deposition rates as Spray Arc Transfer, it does have several advantages. Short Circuit Transfer requires relatively low voltages and consequently lower heat is put into the welded object. A potentially negative consequence of this behavior is a lack of complete weld fusion when attempting to weld thick metals [4]. However, the additive manufacturing

process requires less heat input than a traditional weld which requires full heating and penetration of two pieces of base metal. In the additive manufacturing process, only enough energy to penetrate the relatively thin previously deposited layer is required. This makes the Short Circuit Transfer mechanism capable of high deposition rates.

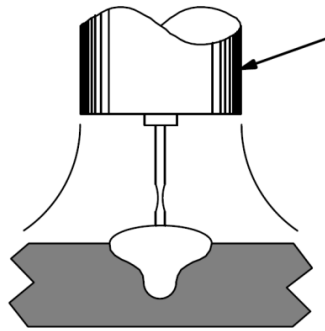


Figure 4: GMAW Short Circuit Transfer [4]

An intermittent mode of transfer between Short Circuit Transfer and Spray Arc Transfer is Globular Transfer. Shown in Figure 5, Globular Transfer occurs when globs of hot metal accumulate on the feed wire electrode and are discharged onto the base metal. Instead of a small amount of metal being deposited during a brief Short Circuit, a large amount of metal accumulates on the electrode before it is deposited. Globular Transfer is not a preferred mode because it creates large amounts of spatter, a large weld, and a poor weld appearance [4]. This makes it a poor choice for application in additive manufacturing.

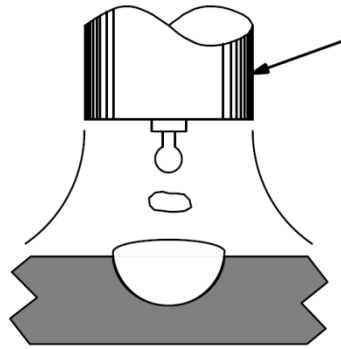


Figure 5: GMAW Globular Transfer [4]

As shown in Figure 6, Spray Arc Transfer occurs when a stream of tiny drops flow from the feed wire electrode to the base metal. Spray Arc Transfer has the advantage of a high deposition rate and good weld penetration. However, Spray Arc Transfer does require higher power input to the weld and consequently adds more heat to the deposit [4]. This behavior makes Spray Arc Transfer not conducive to the ideally low thermal input additive manufacturing process.

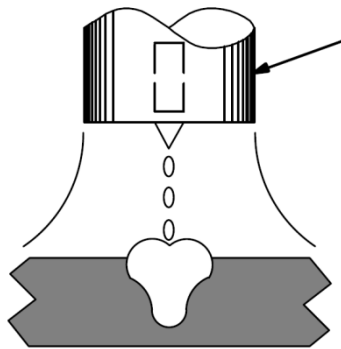


Figure 6: GMAW Spray Arc Transfer [4]

The final GMAW welding technique is Cold Metal Transfer (CMT) as illustrated in Figure 7. Developed by the Austrian company Fronius, CMT is a relatively novel welding technique which involves a controlled dip transfer. During the CMT process, wire electrode is fed towards the base metal [3]” [2]. “It uses a peak current lower than the

transition current to prevent accidental detachment and takes advantage of the downward momentum of the oscillating droplet to enhance the detachment. When the droplet moves toward the weld pool, the current is switched to peak level and the combination of increased electromagnetic detaching force and downward momentum ensures detachment. Hence, the metal transfer process becomes controllable and robust against variations in welding parameters” [6]. However, this process requires proprietary and relatively expensive equipment (as compared to other GMAW processes) [2].

Previous research conducted at Auburn University, focused on the Short Circuit Transfer and its application to Additive Manufacturing; while this research will primarily focus only on Cold Metal Transfers its application in Additive Manufacturing.

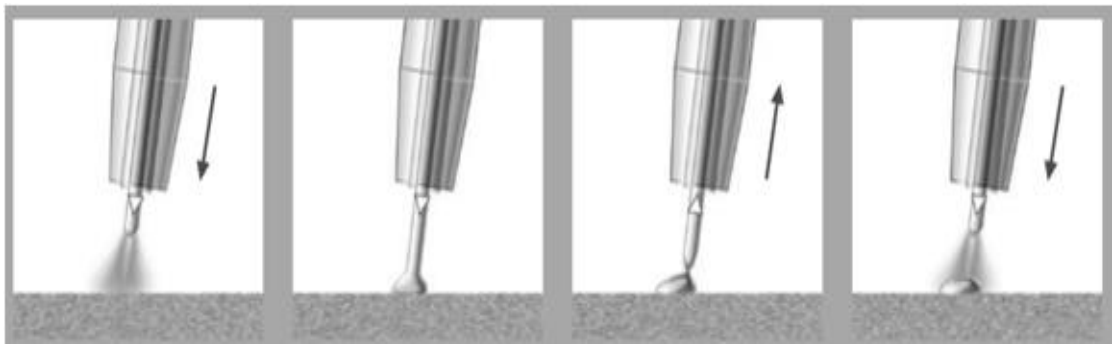


Figure 7: GMAW Cold Metal Transfer [5]

### **Wire and Arc Additive Manufacturing using Short Circuit Transfer GMAW**

Short Circuit transfer GMAW welding has been applied to additive manufacturing in several research attempts; including researchers at Cranfield University, UK, University of Nottingham, UK, University of Minho, Portugal, and Southern Methodist University, Dallas, Texas [7]. Wire and arc additive manufacturing was first recorded in a patent by Baker in 1925, entitled Method of Making Decorative Articles. The patent presented a technique of creating objects using a metal electrode and electricity to deposit material in layers to form an object. The patent included drawings of two objects and a close-up of



built up layers as shown in Figure 8. Baker identified that the current was related to the speed of the moving electrode and the thickness of the layer. Baker focused on creating decorative objects that did not have any mechanical value. The process was manually actuated for movement of the welding tip [2, 8].

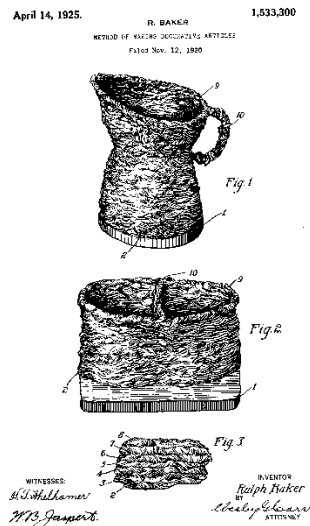


Figure 8: Baker's Patent [8]

Additional research in the field is evidenced by the filing of several patents. In 1925, Eschholz deposited single layers of metal to form ornamental letters. Eschholz determined that the important process parameters were substrate material, arc current, travel speed, bead width, bead height, and penetration depth [2, 9].

Shockey in 1932 used a novel wire and arc deposition method in his patent for *Machine for Reclaiming Worn Brake Drums*. In the patent, one-layer tall weld beads were deposited on worn brake drums, so they could be reserviced. After depositing the material, the brake drum was post-machined to size. The deposition process was mechanized, instead of manually operated, and was a major improvement in this patented method. As

a result, Shockey noted the impact of travel speed and electrical current on the geometry of the deposited bead. Shockey's technique was determined to not be economically viable due to the fact that the process was more costly than the cost of a new brake rotor [2, 10].

In 1933, Noble filed a patent for an economical method of enlarging shaft diameters. Noble proposed near net shape manufacturing technique of placing a collar on a shaft and welding it in place, instead of machining a large diameter shaft down in steps with great material waste [2, 11].

In 1943, Carpenter and Kerr made a significant development by patenting an invention that utilized the relatively new, high deposition rate Submerged Arc Welding (SAW) process to deposit alloys with a significant percentage of chromium (24-27%) and nickel (19-22%). Their goal was to manufacture large shafts with increased strength when compared to traditionally manufactured objects. It was determined that the substrate must be preheated to permit a high rate of metal deposition. Preheating seemed to allow a greater feed rate [2, 12].

The use of the SAW process was more refined in a 1962 patent, by White, in which rollers were used to press the previously deposited layer. White observed large variance in the process which prevented its application in the food processing industry. The pressure roller improved the surface of the layer creating a more repeatable process. For future work, White proposed that pre-heating the roller improved the deposit quality and recommended a post process of gradual cooling for internal stress relief [2, 13].

Ujiiie filed patents in 1967 and 1970, where large thick-walled pressure vessels were created. In addition to the SAW process, Ujiiie used an inert shielding gas and multiple welding nozzles. To achieve a high deposition rate, three simultaneous parallel wire

electrodes were used. This created a larger weld pool than previous researchers. However, the larger weld pool, when compared to the single wire electrode objects using a smaller weld pool, had degraded grain structure and voids. Ujiie hypothesized that the pressure vessel's more desirable mechanical properties resulted from the tempering effects of subsequent layer deposition [2, 14].

Brandi and Luckow filed a patent, in 1974, featuring fabrication of large shafts and rotors for turbines and electric generator applications requiring high strength and durability. They compared the near net shape process to the traditional forging process and concluded that the novel method had near isotropic mechanical properties. They additionally determined that the welding power and temperature of the substrate, and subsequent layers, were interrelated factors that could be controlled [2, 15].

“The SAW additive manufacturing process continued to be developed and studied with multiple welding heads and steel alloys. Significant improvements in mechanical properties were observed with comparing deposited parts to forged and rolled objects. Prior to the Chernobyl disaster in 1986, German researchers at the large steelmaker *Thyssen-Hutte AG* were focused on applying near net shape additive manufacturing techniques to produce nuclear boilers or pressure vessels. After 1986, the rapid SAW additive manufacturing research powered by a high market demand for nuclear energy was refocused on production of pressure vessels for the chemical industry or heavy turbine shafts. However, funding for these industries was not sufficient for the previous research rate” and the research was ended [2, 16].

In 1990, Acheson's patent, titled *Automatic Welding Apparatus for Weld Build-up and Method of Achieving Weld Build-up*, included a nozzle for a shielding gas that moved

with the feed wire in a process like Gas Metal Arc Welding (GMAW), also known as Metal Inert Gas (MIG) welding. Acheson focused on the mechanical design of a shielding gas nozzle in relation to additive manufacturing but did not provide any testing or evaluation of his invention. However, this patent marked the beginning of the current trend of focused research of the GMAW based wire and arc additive manufacturing process [2, 17].

With the advancement of Computer Numerical Control (CNC), wire and arc additive manufacturing process has been increasingly researched and developed with focus on the GMAW process. Recognizing the potential of this, Rolls-Royce internally investigated the application of this technique to the aerospace industry in the early 1990s. The focus of the research was on lowering cost by producing near net shape high performance alloys with low waste [2, 16, 18].

At the University of Nottingham in 1992, UK, Dickens *et al.* conducted a preliminary study of additive manufacturing using GMAW based methods. A commercially available welding robot was used allowing the researchers noted improvement due to robotic control and automation, consistent material properties, rapid manufacturing times, and material efficiency. The team used mild steel welding wire based on Fe-C (0.08%) – Si (0.9%) Mn (1.5%). As shown in Figure 9 and 10 the authors achieved production of a square box and a truncated pyramid [2, 18].

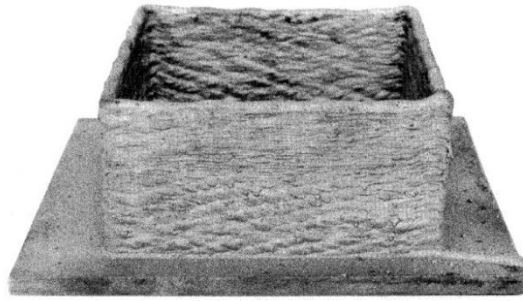


Figure 9: Box Produced using GMAW Process [18]

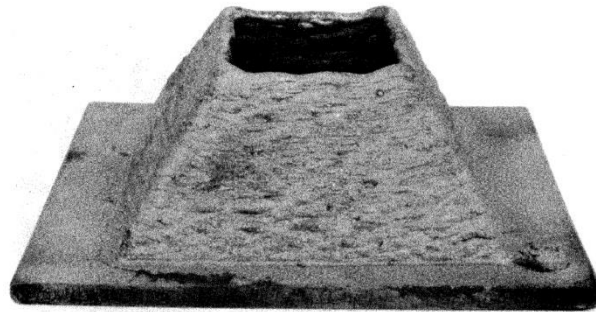


Figure 10: Truncated Hollow Pyramid using GMAW Process [18]

Dickens *et al.* emphasized the importance of geometry of the produced weld bead and conducted numerous trials of singular weld beads with varying parameters. The authors observed that the geometry of the weld bead was dependent upon several factors such as: voltage, wire feed rate, wire stick out distance from the nozzle, wire diameter, and welding velocity. They observed their effect on: arc voltage, arc current, layer width, and layer height. The general observed trends are presented in Table 1. It was observed that the shape of the weld bead could be modified from a wide and flat bead to a narrow bead when producing vertical walls by varying the velocity of the welder [2, 18].

Dickens *et al.* also conducted a brief, post process mechanical and microstructural evaluation of the square box wall sections. Hardness tests showed an increase in hardness from the base of the wall to the top of the wall. They hypothesized that this was the result of tempering of the lower layers due to heating during deposit of subsequent layers, as did

Ujiie. Tensile tests were conducted parallel and orthogonally to the layers. There was very little difference in ultimate tensile strength in the two directions; however, a statistical study was not performed [2, 14, 18].

Table 1: Interactions observed by Dickens et al. [18]

Increasing Variable	Effect on Measured Variable			
	Arc Voltage	Current	Bead Width	Bead Height
Voltage	↑	=/↑	↑	↓
Wire Feed	↓	↑	↑	↑
Stickout	↑	↓	↓	↑
Wire Diameter	↓	↑	↑	↑
Velocity	=	=	↓	↓

“When examining the microstructure, the wall was largely equiaxed ferrite and perlite with a grain size of approximately  $60\mu m$ . It was observed that the structure was much less equiaxed and more columnar in the top layers of the wall that were not subjected to reheating during the additive manufacturing process. As subsequent layers are deposited, the previous layers are repetitiously reheated and consequently tempered during the process. The researchers recommended heat treating the object to ensure a uniform microstructure, but they did not test this hypothesis. Additionally, there were no voids or cavities in the material when a sample was polished and observed under a microscope. The part was concluded to have good mechanical properties.

Dickens *et al.* concluded that to further develop the GMAW based additive manufacturing technique there must be significant software development. Additionally, a sensing feed-back loop between the welder and the robot controller was identified as necessary to improve the consistency of the process and create surface finishes similar in quality to cast objects. The authors recommended that the sensing feed-back loop provide

the wire offset distance to the controller. The controller would then maintain the wire offset distance to a constant value” [2, 18].

“Further research at the University of Nottingham of the GMAW additive manufacturing technique was published by Spencer *et al.* in 1997. The team used a commercially available three axis GMAW welder with a Siemens controller to build layers on a platform that could tilt and rotate. The platform was manually moved before the additive manufacturing operation. This allowed orientation of the part at different angles to the welder so geometries could be made without supports” [2, 19].

“Three test parts, a hollow box, a vertical wall, and a horizontal slab, were studied and are shown in Figure 11. The geometries consisted of 82 layers totaling 100 mm high. The test parts were made from a copper coated mild steel wire that was 1 mm in diameter. The parts were manufactured on a 12mm thick mild steel build plate. The layer width of the resulting weld bead was 3.5mm. It was found that layer widths between 3 and 6 mm were possible. Attempting to build walls of thicknesses greater than 6mm resulted in excessive heat input and poor bead profile due to insufficient cooling of built up heat” [2, 19].

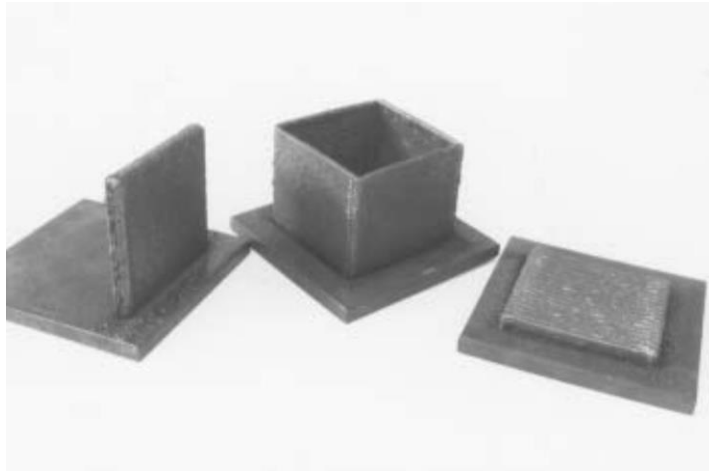


Figure 11: Geometries studied by Spencer et al [19]

“Spencer *et al.* attempted to manufacture thicker walls by placing multiple beads beside each other. However, there was incomplete penetration of the substrate and neighboring bead. Attempts to angle the welding torch to deposit multiple adjacent beads were unsuccessful due to an unpredictable bead profile. The dye penetrant test shown in Figure 12 demonstrated the lack of fusion when attempting to deposit adjacent beads. Instead of attempting to deposit the beads directly next to each other, the authors deposited beads at a pitch approximately double the width of the weld bead crest. As illustrated in Figure 13, material was then deposited in the root channel formed by the two beads separated by the pitch distance. According to tensile tests, the researchers concluded that this method of adjacent layer deposition created excellent (at/near manufacturer’s specs) mechanical properties. The tensile test standard used was not recorded” [2].



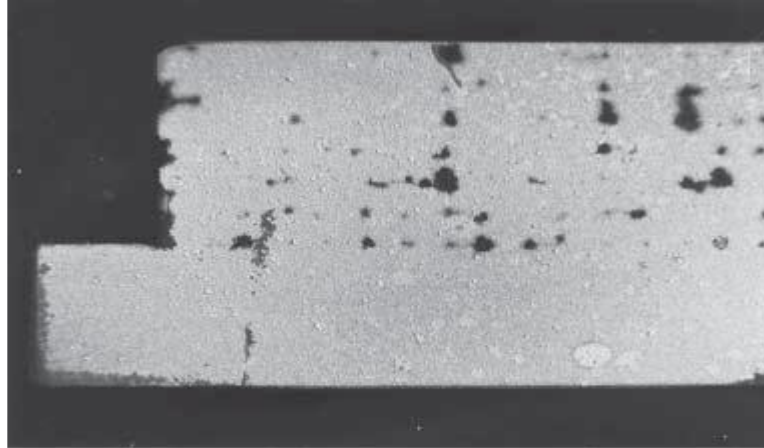


Figure 12: Procedure for depositing adjacent layers by Spencer et al. [19]

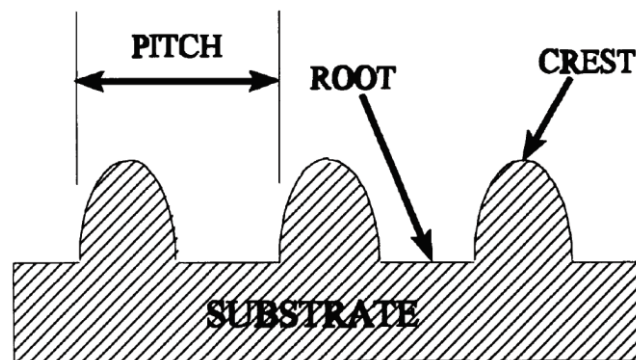


Figure 13: Voids in adjacent beads as shown in dye penetrant test by Spencer et al. [19]

Spencer *et al.* also implemented temperature control loop to ensure the previous layer had adequately cooled before depositing the next layer. The operators set a maximum allowable temperature at which welding was to be performed, and an if-else loop prevented welding until the part reached an acceptable temperature read as by an infra-red sensor. After implementing temperature control, the authors achieved an improved surface finish at the cost of more than double the build time [19].

When examining the microstructure of a cut, polished, and chemically etched sample, Spencer *et al.* observed that the upper surface had a martensitic structure due to rapid cooling; however, the recrystallization and slower cooling of the lower layers resulted

in a finer ferrite/pearlite grain structure. Aside from the top layer, Spencer *et al.* achieved uniform grain structure and fusion between layers throughout the created sample [2, 19].

Additionally, Spencer *et al.* conducted stress tests on the finished parts to determine residual stresses and compared the results to the layer temperatures. The residual stress measurements were performed using the center hole method [20]. A three-strain gauge rosette was used to measure the change in stress when the material was removed by drilling a whole through the sample. The results varied greatly between the different geometries and the sample size was small so there was no significant conclusion [19].

The work of Dickens *et al.* and Spencer *et al.* did not include Computer Aided Manufacturing (CAM) integration [21]. The researchers coded the machine by hand and only created rather simple objects. Ribeiro *et al.* at Canfield University in 1994 developed a process for transferring a CAD drawing to the GMAW technology based additive manufacturing equipment. Their proprietary, unpublished software package translated a CAD file created with AutoCAD into movements interpreted by the software controlling the industrial robotic arm welder. The weld parameters were kept at predefined constants and were controlled by the internal circuitry of the welding robot. Ribeiro *et al.* successfully produced a circular metal vase out of mild steel with this process as shown in Figure 14 [2, 22, 23].

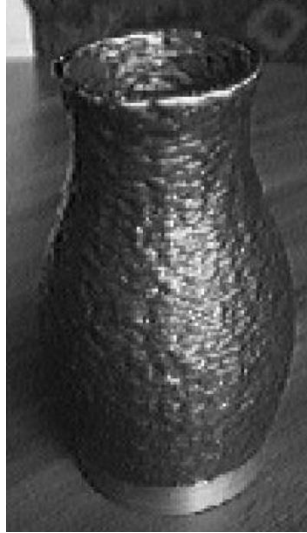


Figure 14: First successful integration of CAD and welder controls [22]

Although his main goal was to perform a software process evaluation, Ribeiro *et al.* recorded various conclusions from the experiment unrelated to the software. The authors identified that the splined geometry of the vase created a varying distance between the arcing wire and the previous layer while being deposited. Additionally, it was observed that the quality declined with time which was likely due to latent heat buildup as well as scale error due to the layering process. Finally, Ribeiro, *et al* recommended weighing the substrate plate before ‘printing’ an object to calculate how much material was deposited during the process [2, 22, 24].

“To illustrate the software capabilities and evaluate the geometric accuracy, an additional hollow object was created with refined software by Ribeiro, *et al* in 1996 and is shown in Figure 15. The authors concluded that bead geometry (layer height and width) was of utmost importance and must be properly estimated for the slicing parameters to function correctly. Additionally, during the build process, the distance between the arcing wire and the previous layer was variable and required manual adjustment during the

process. The inward taper of the component was considered to be the cause of this issue and closed-loop control was recommended as the solution [25, 26]” [2].



Figure 15: Complex geometry produced by Ribeiro *et al.* [26]

To increase control of the GMAW welding process, Ribeiro *et al.* developed a mathematical model to determine the appropriate parameters to input into the previously developed unpublished software. The input welding parameters were layer width, layer height, welding current, and welding voltage. To evaluate the feasibility of creating a ‘schedule’ for additive manufacturing, Ribeiro *et al.* created cylindrical test pieces ten layers high. The machine travel speed was varied between 500 and 2500 mm/min, and the welding current was varied between 120 and 160 Amps [2, 21]. The robotic welding arm utilized by the authors used a synergic algorithm to control the pulsing of the power source and the wire feed speed. The synergic algorithm was a control scheme internal to the welder that varied the welding power based upon the wire feed rate. The robotic welding

arm used a Short Circuit GMAW process with a synergic algorithm and the internal controls were not studied. Therefore, the wire feed speed was not considered [2, 21, 27].

Ribeiro *et al.* performed their experiments with 1.0 mm diameter Inconel 718 wire and used argon shielding gas. During the experiments, the layer width varied between 3.8 and 10 mm and the layer height varied between 0.44 and 1.24 mm. The authors observed a relationship between welding speed and layer width as shown in Figure 16 [2, 21].

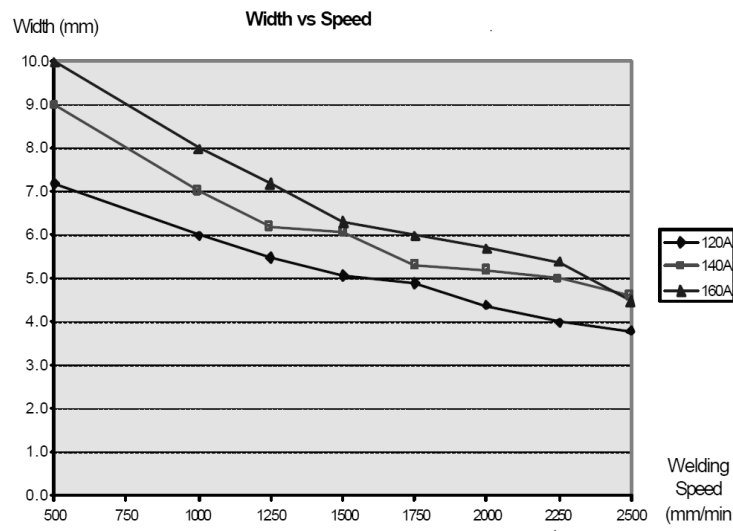


Figure 16: Relationship between layer width and travel speed by Ribeiro et al. [21]

“To develop the parameter input algorithm for the slicing software, Ribeiro *et al.* used empirical results as inputs for a regression analysis to determine the relationship between four measurable coefficients of welding speed, welding current, layer height, and layer width. The created mathematical model was incorporated into the software, so the user could input a desired layer height, and the computer would automatically set the welding speed and current. To evaluate the software, three test objects of desired layer width were manufactured. The greatest observed absolute layer width error was 0.4mm

with an expected layer width of 8.0 mm. The authors considered this layer width error to be relatively small [21]” [2].

While Ribeiro *et al.* were successful in creating an appropriately sized geometry, their preliminary study failed to consider many parameters (*e.g.* wire feed speed, weld characteristics, wire offset, wire diameter) identified as important factors by other researchers [16]. Additionally, the authors did not study the influence of the internal controls of the welder. Finally, the model was purely based upon empirical data for Inconel 718 deposited by the studied welder and was not applied to other materials and setups.

“In 1998, Kovacevic *et al.* at Southern Methodist University used a high-speed vision system to study the formation of droplet parameters and resulting weld penetration of GMAW based additive manufacturing. Additionally, the researchers performed a finite element analysis to simulate the cooling characteristics of the process. The end goal of the research was to create a sensing system that could improve the process consistency; however, the research was not completed [28].

Kovacevic *et al.* used a 24 Volt GMAW welder with ER70S-6 mild steel wire. A shielding gas of 95% Argon and 5% CO<sub>2</sub> was used and the machine traveled at a constant speed of 6.4 mm/sec. The researchers proposed controlling the metal transfer process by turning the electrical current to the welder on and off based upon the size of the metal droplet formed at the end of the electrode. To observe the metal transfer process, a high speed digital camera capable of 800 frames per second with a resolution of 128X128 pixels was used [28]. Kovacevic *et al.* determined that the deposited metal bead size and penetration could be controlled by the pulsing electrical current. Therefore, this strategy could be used for increased control and consistency during the deposition process [28]”[2].

In 1999, Kmecko *et al.* continued to research the GMAW based additive manufacturing technique at Southern Methodist University by applying real time image processing to the system to reduce weld spatter. The developed system measured the voltage and current used by the welder and featured an infrared pyrometer and a light sensor. While the system was capable of real time image capture, no demonstration of successful closed-loop control was presented. Kmecko *et al.* were convinced that the closed-loop control was necessary to improve the process and reducing welding spatter [2, 29].

In 2002, Zhang *et al.* at the University of Kentucky published an improved GMAW based additive manufacturing process utilizing a more sophisticated CAD model slicing strategy. The team developed unpublished software that could vary the infill method and vary the layer height throughout different regions of the model. Additionally, the author's software can vary the start point of each deposited layer.

Zhang, *et al* used two different steel-based wires of E70S-6 and SS308 to evaluate the novel CAD model slicing software. For both materials, the wire was fed at a speed of 160 in/min and the machine travel speed was 0.2 in/sec. The welding voltage was 25 Volts for both materials and the welding current was 125 Amps for the E70S-6 wire and 110 Amps for the SS308 wire. The shielding gas was an argon and CO<sub>2</sub> mix; with 25% CO<sub>2</sub> for the E70S-6 wire and 5% CO<sub>2</sub> for the SS308 wire.

To study the software's varying start point capability, Zhang *et al.* created cylindrical parts with and without varying start points. As shown in Figure 17, the scale error from buildup at the start point of the deposited layer path is significant. Figure 18 presents a cylindrical part with a varied layer start point. As a result, the effects of the scale error are mitigated [2, 30].

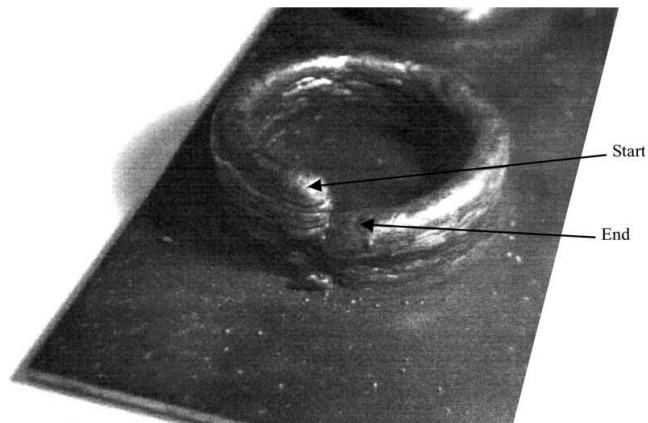


Figure 17: Tube shaped part with the same layer start point by Zhang et al. [30]

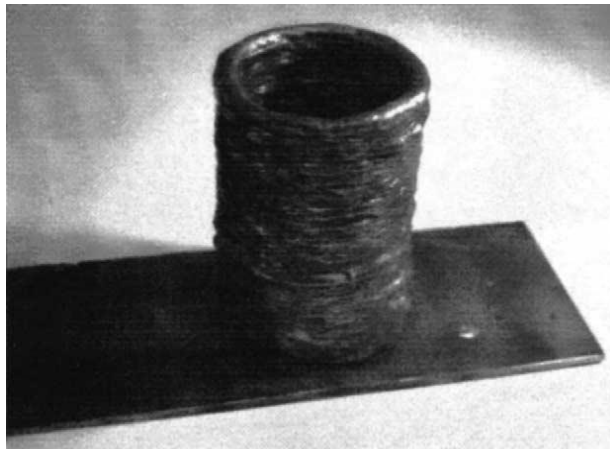


Figure 18: Tube shaped part with varied layer start point by Zhang et al. [30]

The software was also capable of lead-in and lead-out speed control of a deposited line. The researchers observed buildup of the layer at the start of the path and a decreased amount of material at the end of the path. To counteract this, the authors increased the machine travel speed at the beginning of the path and slowed the machine travel speed at



the end of the path while the wire feed speed was kept constant as shown in Figure 19. Additionally, a second pass was added to the end region of the path to further level the deposited layer [2, 30].

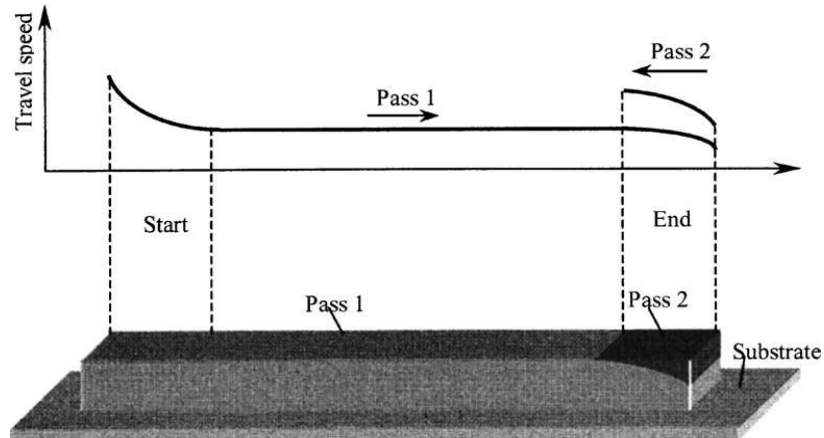


Figure 19: Speed control for the start and stop of the path by Zhang *et al.* [30]

To evaluate this linking strategy, Zhang *et al.* deposited a sample wall section with and without lead control. As shown in Figure 20, the wall is not level with buildup at the start point of the path and lacking material at the end of the path. Figure 21 presents a wall section with lead control. As a result, the wall section is much more even [30].

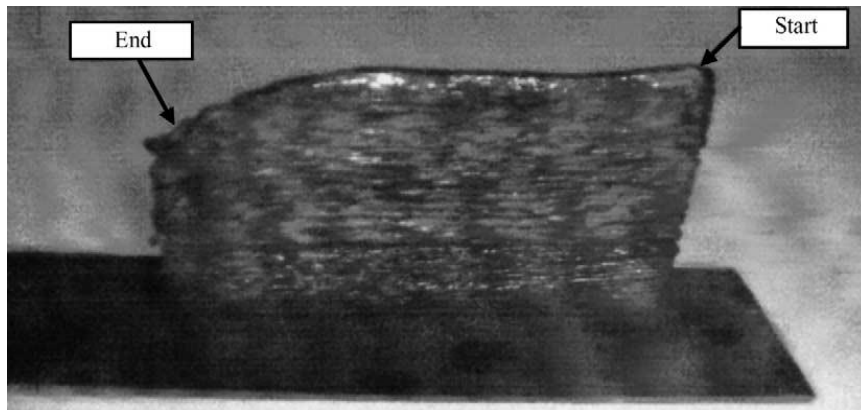


Figure 20: Wall section without start and end-point control by Zhang *et al.* [30]

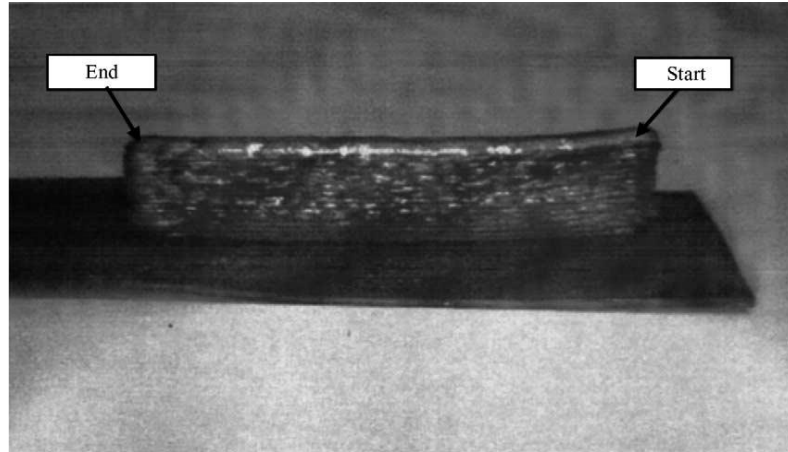


Figure 21: Wall section with start and end-point control by Zhang *et al.* [30]

While successful in implementing effective slicing software with linking parameter control, Zhang *et al.* identified future work was still necessary to manage the heat input to the deposited part [2, 30].

In 2004, Song *et al.* published a technique combining GMAW additive manufacturing coupled with a subtractive manufacturing milling machine [31]. The authors proposed a machining post process after each layer was deposited. As shown in Figure 22, the research was performed on a 3-axis CNC machine with an added laser welding unit and two arc welding guns. Additionally, the build plate was heated to 200°C with a built-in heater. The researchers hypothesized that preheating the build plate would reduce thermal stress build up during deposition but did nothing to validate the hypothesis. Song *et al.* confirmed that several factors greatly influenced the process. These factors were layer height, layer width, welding speed, welding voltage, welding current, and distance between adjacent layers [2, 32].



Figure 22: Integrated welding and milling machine created by Song et al. [32]

To evaluate the welding/milling process, the authors constructed test parts with a constant welding voltage of 19 volts and a constant welding current of 120 amps with a welding speed of 1.2 m/min. The material used in the experiments was mild steel wire 0.9 mm in diameter. During the process, the authors deposited layers and machined the surfaces as shown in Figure 23. The object had a layer height of 0.8 mm, a layer width of 4 mm, and a surface roughness of  $R_a=150 \mu m$ . After machining, the object had a wall thickness of 1 mm and a surface roughness of  $R_a=2 \mu m$ . The layers shown in Figure are uneven from poor control of the process [2, 32].

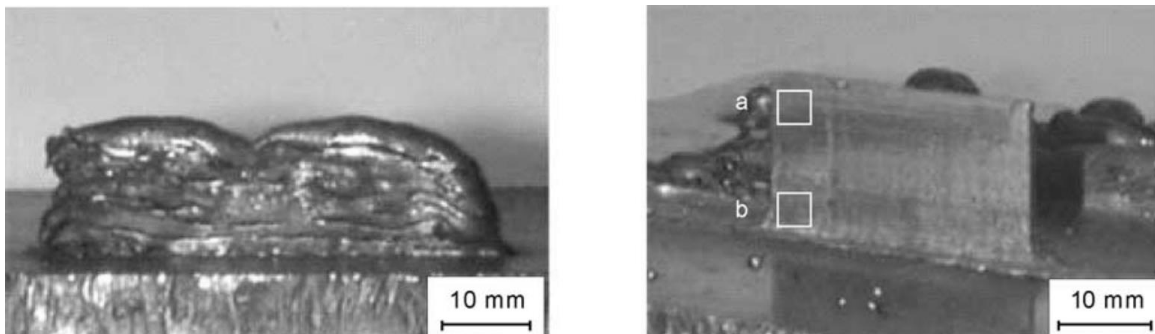


Figure 23: Thin-walled part before and after machining by Song et al. [32]

Song *et al.* examined the microstructure of a sample; as shown in Figure 24, the sample had large grains in the upper region of the wall (region a) and fine grains in the lower region of the wall (region b). This is consistent with the observations of Ribeiro *et al.* [32].

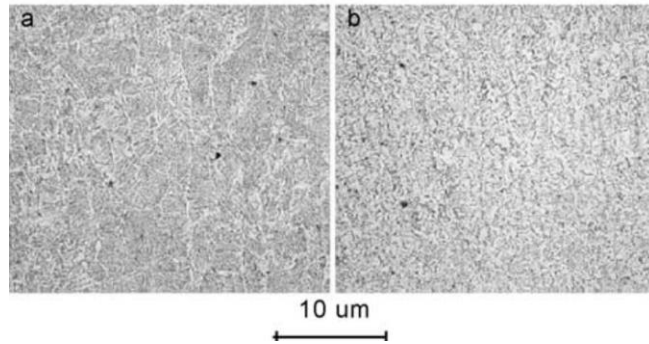


Figure 24: (A) Upper Region of the Wall; (B) Lower Region of the Wall [32]

In addition to a thin wall, Song *et al.* manufactured a rectangular object as shown in Figure 25. The object had a layer height of 0.8 mm and a deposited layer offset of 2.8 mm. The solid test object was measured to have a dimensional accuracy of  $\pm 0.5$  mm before machining. When examining the microstructure, the solid part had similar results as the thin wall part with a microstructure that was finer at the base due to the reheating effects [2, 32].

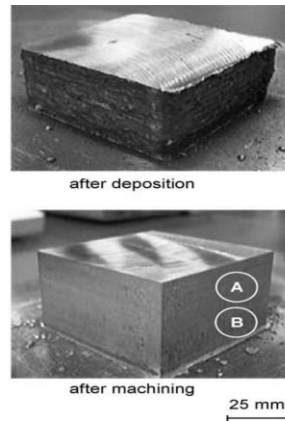


Figure 25: Solid part before and after machining by Song *et al.* [32]

Song *et al.* also performed a tensile test parallel to the layers of the deposited material and observed that the object had a tensile strength of 620 MPa which was compared to the deposited wire material which had a tensile strength of 550 MPa; however, Song *et al.* did not perform a tensile test normal to the direction of deposited layers of material [2, 32].

In a continuation, Song *et al.* published an additional paper in which the authors optimized their welding and milling technique using statistical methods. The authors chose to optimize four parameters which were the voltage, wire feed speed, wire stick out and shielding gas composition. The welding voltage was varied between 14 and 26 volts. The wire feed speed was varied between 3 and 8 m/min. The wire offset was varied between 6 and 8 mm. The shielding gas was composed of CO<sub>2</sub> and argon with the amount of CO<sub>2</sub> varying from 30 to 10%. The weld spatter and deposited layer width were chosen as the two main results of the welding parameters [2, 33]. To quantify the weld spatter, a ‘spatter index’ was created; which was the ratio of the mass of the spatter divided by the mass of the welded wire. The mass of the spatter was determined by collecting and measuring the spatter beads after completing the bead. The mass of feed wire was determined based upon the feed wire speed and assuming no slip [2, 33].

Performing an analysis of variance (ANOVA), Song *et al.* determined that the welding voltage, wire feed speed, and wire offset have a high impact on the spatter formation; however, the shielding had a negligible effect on spatter formation. When examining deposited layer width, the welding voltage and wire feed speed had significant impact; however, the wire offset and shielding gas composition have a small impact on the deposited layer width [2, 33].

From these results, the authors concluded it was best to use the least expensive shielding gas with a CO<sub>2</sub> composition of 30%. Additionally, the wire offset only had a small impact on layer width, so the wire offset was reduced to the minimum of 6 mm to reduce spatter. In addition to studying the factors' effects on weld spatter and deposited width, Song *et al.* studied the distance between layers (bead offset), the direction of layer deposition, and alternating the direction of layer deposition. The direction of layer deposition options studied are shown in Figure 26. To measure the studied factors, tensile tests and hardness tests were performed to see which build strategy performed the best [2, 33].

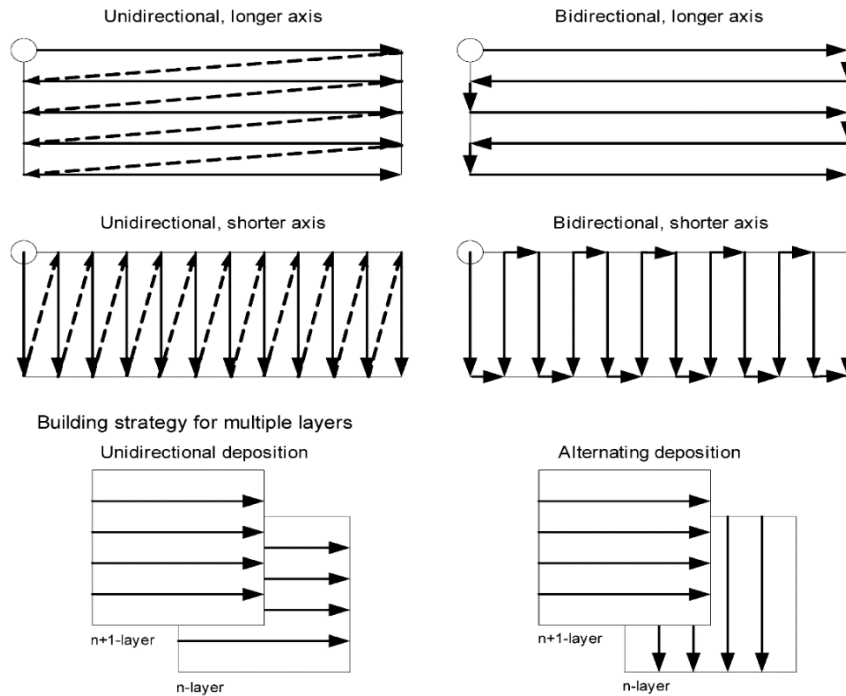


Figure 26: Build Strategies for Solid Layers [33]

Performing an ANOVA indicated that the deposition parameters have a negligible effect on the surface hardness; however, the team did not examine the surface hardness along the height of the object. The researchers concluded that the orientation of the deposited layer determines the tensile strength and alternating the deposition direction between layers increased the tensile strength. The authors proposed that the method of alternating deposition direction was stronger due to voids being filled in the subsequent layer and increased the surface quality and density of the layer [2, 33].

In 2007, Clark *et al.* with Rolls-Royce researched the feasibility of GMAW based additive manufacturing of a nickel-based polycrystalline super alloy, Inconel Alloy 718, for aerospace engine applications. The researchers used a synergetic GMAW power source with argon shielding gas. The welder was set to 35 volts, the wire sickout was 20 mm, the travel speed was 10 mm/s, and the wire feed speed was 10 mm/s. The deposited layers had a nominal width of 12.8 mm and nominal height of 1.7 mm [2, 34].

“Clark *et al.* performed multiple deposition geometries and examined the polished and etched samples with a scanning electron microscope for microstructural analysis and x-ray for chemical analysis. The first deposition trial was construction of a thin wall of multiple layers. The second deposition trial was construction of two adjacent beads of a single layer. The final deposition trial was construction of two adjacent beads for multiple layers. When performing the trials, the authors waited until the previous layer had cooled to 80°C before deposited the subsequent layer. This was to prevent latent heat buildup in the deposited object and created approximately a 10-minute cooling duration between welds. The resulted in lengthy build times because each deposited layer required over 10 minutes.

When examining the microstructure, Clark *et al.* concluded that the results were highly dependent upon the deposition factors. The authors concluded that controlling the cooling rate was necessary for a uniform part and the prevention of crack formation. Additionally, the authors recommend further study of the GMAW additive manufacturing process to further qualify the mechanical properties of the process for aerospace applications [34]” [2].

In 2013, Anzalone *et al.* at Michigan Technological University developed a low cost (less than \$2000) open-source metal ‘printer’ that used the GMAW based additive manufacturing process. The machine used open-source controls and is shown in Figure 27. The machine utilized a three-axis delta-style robot that was designed for Fused Deposition Modeling (FDM) plastic extrusion 3-D printing without any feed-back. The authors used readily available open-sourced Cura software created for Fused Deposition Modeling (FDM) additive manufacturing. The system used a shielding gas composed of



75% Argon and 25% CO<sub>2</sub> at a rate of 20 CFH. The distance between the build surface and the welding tip was 6 mm. The wire used was 0.024 in. diameter ER70S-6 wire [35]. As a proof of concept, the sprocket shown in Figure 28 was created by the authors. The object had a layer height of 1.75mm and was created with a wire feed rate of 3.5 cm/s [2, 35].

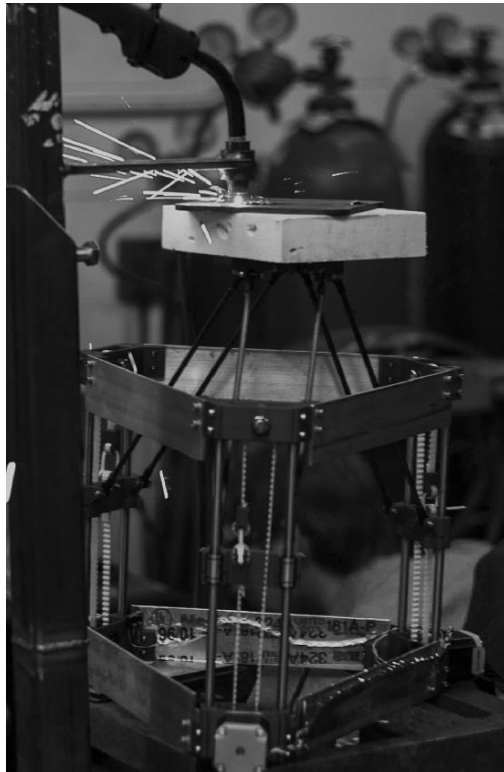


Figure 27: Low-Cost Open-Source GMAW Printer by Anzalone et al. [35]



Figure 28: Sprocket manufactured by Anzalone et al. [35]

Additionally, Anzalone *et al.* examined the microstructure of a polished and etched sample. Like previous researchers, Anzalone *et al.* concluded that the microstructure was finer at lower region layers when compared to upper regions. Once again, this was due to reheating of the subsequent layers during the deposition process. The researchers concluded their results proved that this was a feasible process for the economical production of metal parts [2, 35].

“Researchers at Michigan Technological University also created a voltage and current monitor for use with the GMAW based additive manufacturing process. This low-cost, open-source monitor was used to measure and record the welder’s current and voltage. An Arduino Uno microcontroller was used to record the information measured by the monitor. The researchers concluded that the voltage and current monitor would be useful for further evaluation of the GMAW based additive manufacturing process [36]” [2].

Recent research performed at Auburn University in 2015, sought to produce a low-cost metal additive machine, using off-the-shelf components, and to measure parameters and validate their importance as a way to validate the machine’s capabilities [2]. These components included a standard Miller welder, Mach3 CNC control software, gantry style

80/20 framing, Probotix CNC motor controller and stepper motors, along with standard linear rails and ball screws. Figure 29 shows the finished machined Gaddes produced at Auburn University.



Figure 29: WAAM Machined Produced at Auburn University [2]

Gaddes' first study was a geometry evaluation. Test prints were created to evaluate infill strategies (zigzag patterns vs. parallel patterns), step-over, ability to “bridge” parts, overhangs, layer heights, as well as post processing.

For infill strategies tested, Gaddes found that making a parallel infill part or a spiral shape where the material was swept across the geometry produced a better result than having an infill with bordering “shells.” Figure 30 shows two parts produce by Gaddes with and without “shells” [2].

The machine's ability to perform more complicated geometries was also tested.

Figure 31 & 32 show parts that were produced to test these capabilities [2].

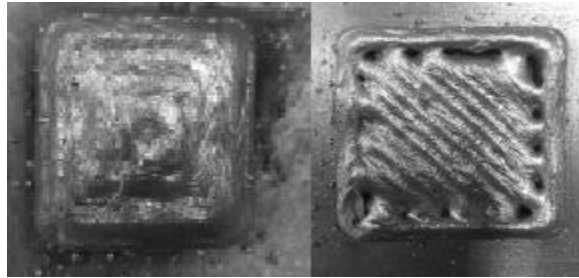


Figure 30: Solid Infill vs. Infill with Shells [2]



Figure 31: Outward and Inward Facing Geometry Test [2]



Figure 32: Bridge Geometry Test [2]

Gaddes concluded that having the layer height helix along the parts vertical axis produced the best results due to the start and end of each layer being slightly different thickness than the steady-state layer height. He noted that randomizing start points did help but the error was still existent due to starting and ending build-up [2].

“As a demonstration of a useful part, two stainless steel printed nozzles are shown in Figure 33. The part on the right was turned on a lathe. The surface finish after turning was excellent and no voids were observed. Before turning, the large diameter of the part was 1.770 in. with a wall thickness of 0.172 in. After turning, the part was 1.667 in. diameter with a wall thickness of 0.087 in” [2].

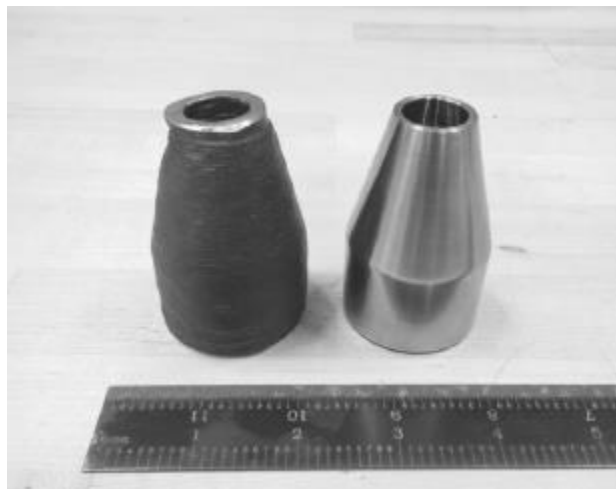


Figure 33: Stainless Steel Nozzle as Printed and Post Processed [2]

Gaddes next studied the effect of varying feed wire diameters on the voltage and current required by the machine to produce the same geometries. Figures 34 and 35 show the results of his study [2]. The varying wire diameters had no effect on the power input required by the machine even for the different materials. This was because the process being used was Constant Current/Constant Voltage (CC/CV) GMAW Short Circuit Transfer (off-the-shelf unit).

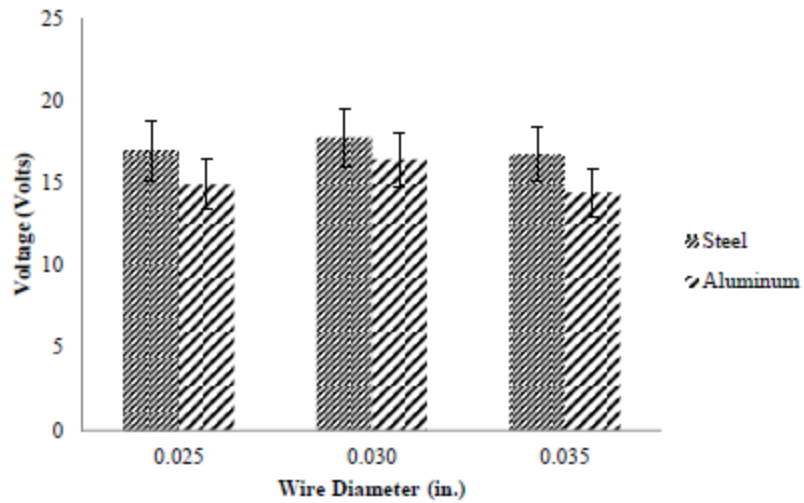


Figure 34: Wire Diameter Study Voltage Results [2]

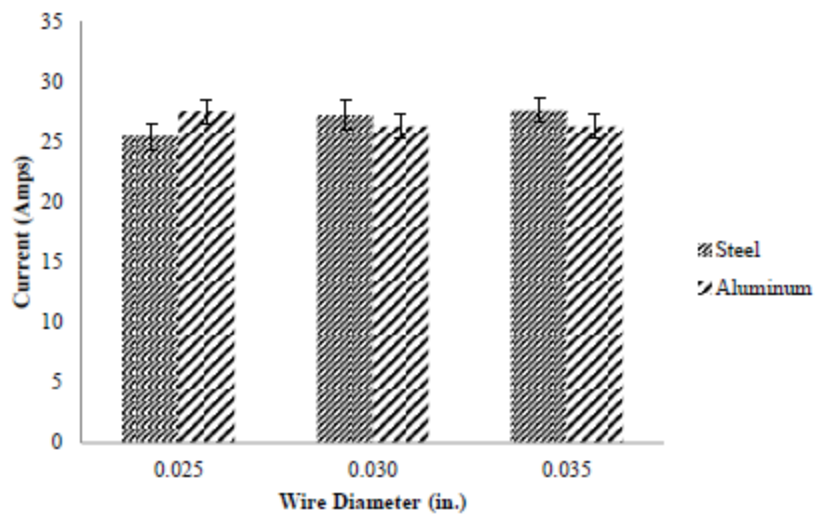


Figure 35: Wire Diameter Study Current Results [2]

The next study performed by Gaddes was a comparison of layer strength vs. material strength by comparing tensile tests at different deposition orientations. By producing prints and machining dog bones parallel and perpendicular to the deposition

direction, tensile tests could be performed to compare parts' properties in orthonormal planes. Figure 36 shows the results of part of this study [2]. The material was orthotropic in behavior, but also to be noted is the repeatability issues between walls in the vertical specimens. Figure 37 shows the same study's results for stainless steel material [2]. The repeatability greatly improved here, although the desired strength decreased while the orthotropic behavior persisted.

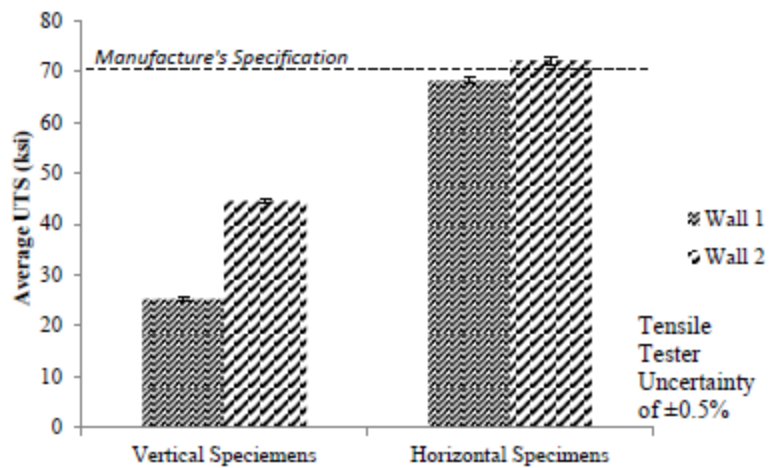


Figure 36: Steel (ER70S-6) Tensile Test Results [2]

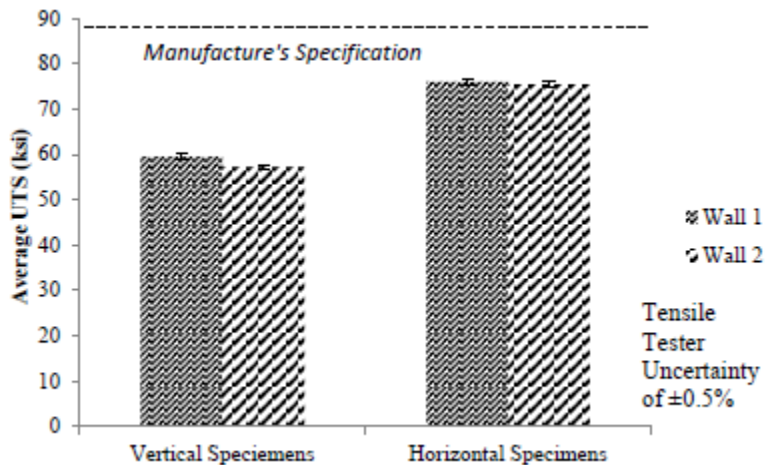


Figure 37: Stainless Steel (ER308) Tensile Test Results [2]

The cause behind these issues (orthotropic, repeatability, low strength) was believed to be primarily due to lack of control over the GMAW transfer process (being CC/CV) which created porosity in the prints. Figure 38 shows voids between layers that were experienced. Gaddes noted that post process heat treatment did improve the microstructural voids. Figure 39 shows the microstructural results of a Steel Specimen before and after a heat treatment cycle [2].

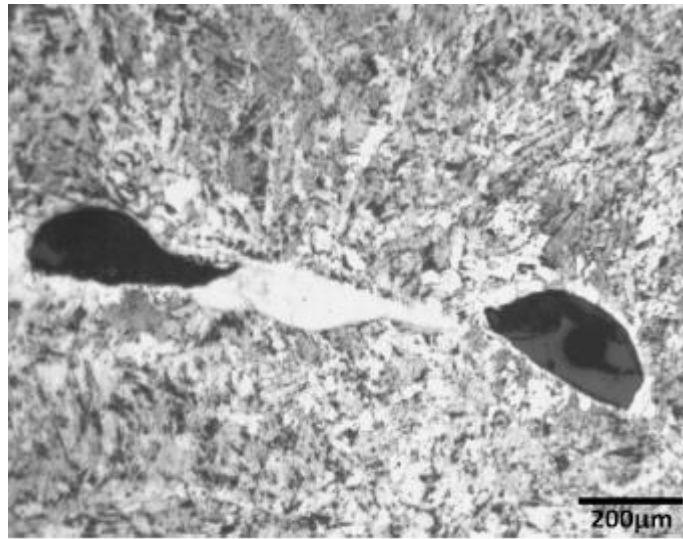


Figure 38: Voids Found between Layers in Steel (ER70S-6) Parts [2]

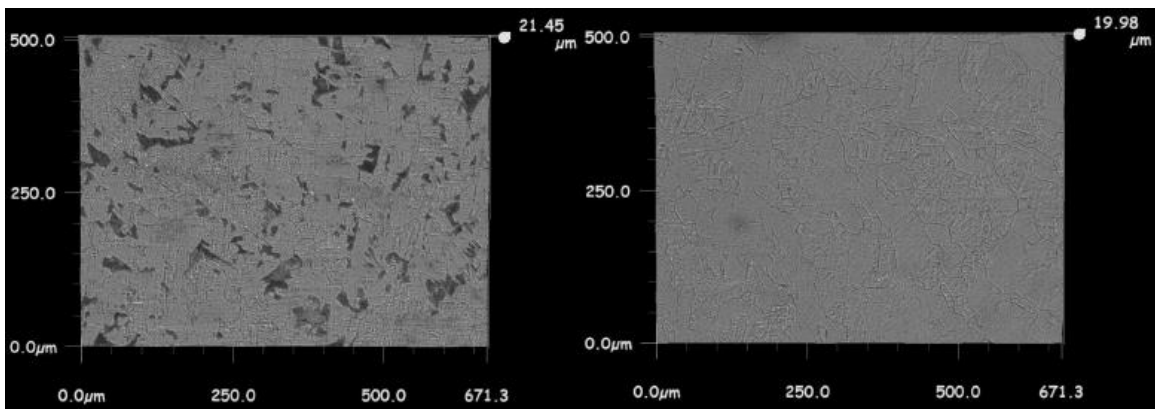


Figure 39: (Left) Microstructure of Steel (ER70S-6) Sample before Heat Treatment  
(Right) Microstructure of Steel (ER70S-6) Sample after Heat Treatment [2]



A few of Gaddes' listed suggestions for future work to "provide greater control of the process" were as follows:

- "A cold-water tip cooled GMAW gun would assist in the deposition of aluminum and copper.
- A pulsed GMAW gun would assist in controlling the heat buildup in the deposit.
- A Cold Metal Transfer GMAW process would result in greater control of the weld bead" [2].

### **Wire and Arc Additive Manufacturing using Cold Metal Transfer GMAW**

One of the common themes from the researchers utilizing Short Circuit Transfer GMAW for additive purposes, is the lack of control in the process. Changing over to a Cold Metal Transfer GMAW (CMT-GMAW, CMT) process was suggested to provide better control by several authors.

Hasselberg completed a metallurgical and structural characterization feasibility study of nickel base superalloy Inconel 718TM welded via CMT in 2009. "According to the parameter optimization study it was noted that the key attribute of the CMT-GMAW process is its electronically controlled short circuit droplet detachment method, which is dictated by the weld synergic line. The synergic line is a linear mathematical relationship, proprietary to Fronius International LLC, which incorporates voltage and amperage process controls into the wire feed speed." Hasselberg also noted his samples "showed little evidence of the porosity that is commonly inherent when using a conventional GMAW process. Macro and micro-analysis of the CMT-GMAW weldments exhibited a columnar grain microstructure similar to those obtained with conventional GTAW with the

exception of a reduced substrate consumption, Heat Affected Zone (HAZ), and less” distorted welds [37]. Some of the material properties discovered with the samples were that tensile strength and hardness characteristics proved to be like that of traditional processes; however, Hasselberg noted there was a 200% increase of Reduction in Area (RA) at not only room temperatures, but also at elevated temperature (1100°F). “It was concluded that CMT-GMAW provides the following benefits: excellent weld quality on wrought Inconel 718™; comparable metallographic structure to those commonly seen in fusion welded deposits; increased deposition rates when compared to GTAW; a reduction in overall thermal input by achieving almost current-free metal transfer; virtually spatter-free metal transfer by controlling the short circuiting; comparable material hardness to GTAW weldments; and analogous tensile strength with increased RA when compared to GTAW” [37].

Researchers at Cranfield University conducted a process model study of additive layer manufacturing using CMT with Ti-6Al-4V. The researchers noted that the CMT process provided better results due to the “extremely controlled dip transfer mode regime of the CMT assures that no free flight droplet is transferred during the arcing period. Thus, the repulsion of filler metal caused by the acting momentum of external electromagnetic “pinch” forces, or issuing cathode jets, on incorporated droplets is prevented. Moreover, the metal transfer to the molten pool occurs by the surface tension mechanism at low current levels, where a back-drawing force assists the liquid bridge fracture” [38]. The group also conducted a small study on the effect of different shielding gasses on the grain structure of the ‘prints.’ Figure 40 shows the results of varying the amount of helium in the shielding gas. The researchers believe the reasons behind the grain

refinement when using higher He contents is due to: “1) higher T gradients promote intensive force convection and mass transport, breaking primary columnar grains near the S/L interface or promoting a globular structure by spherical growth; 2) fine solid nuclei will work as “seeds” or nucleation sites within the liquid and therefore decrease the energy barrier for heterogeneous nucleation; 3) the CMT dip transfer mechanism induces a stirring effect reducing energy barrier for homogeneous nucleation; 4) augment of the cooling rate due to the larger specific weld bead contact areas” [38].

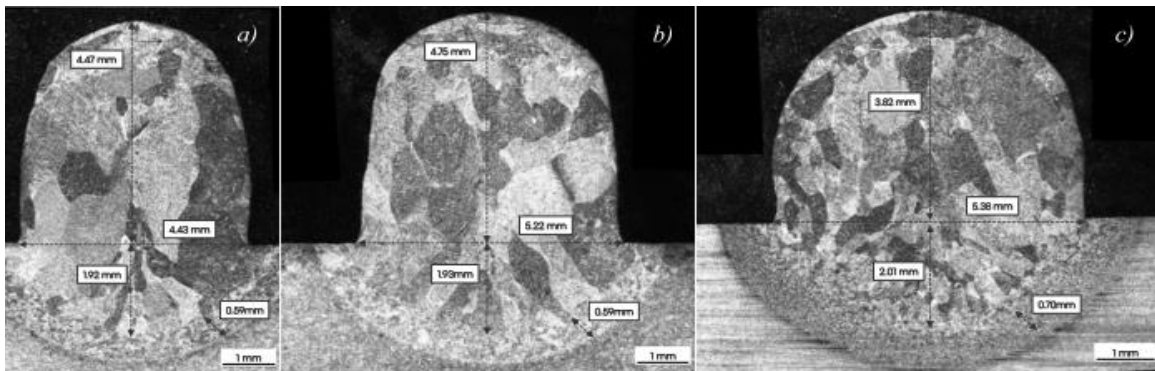


Figure 40: Grain Size Comparison Varying Shielding Gas Composition of Helium and Argon Mix A) 30% He B) 50% He C) 70% He [38]

The researchers controlled three parameters to develop an empirically predictive model. “The controllable variables included the solid wire diameter, wire feed speed (WFS) and WFS/travel speed (TS) ratios. Ti-6Al-4V 0.9 and 1.2mm wire diameters were used and the WFS settings for each individual wire ranged from 2 to 12m/min, in a unit basis. The WFS/TS ratios were 15, 20 and 25. It should be noted that the WFS/TS ratio was selected as an independent factor, rather than TS, guaranteeing good welding conditions and high-quality deposits all over the design space. Data was fed into a least squares regression analysis software and the main effects and interactions between controllable variables and responses were estimated. Several responses were selected and

measured, although only the effective wall width and the deposition efficiency are reported here. The effective wall width is defined in the present context as the target wall width dimension, after undergoing the post processing machining stage. On the other hand, the deposition efficiency estimates the ratio between the effective volume of metal utilized to net shape the component over the total delivered metal volume. A typical first order 3D response surface output, namely the effective wall width, is represented in Figure 41 as a function of the wire diameter and the WFS, for constant WFS/TS of 20. It can be seen that larger effective wall widths are achieved with thicker wires for constant WFS and WFS/TS ratio” [38].

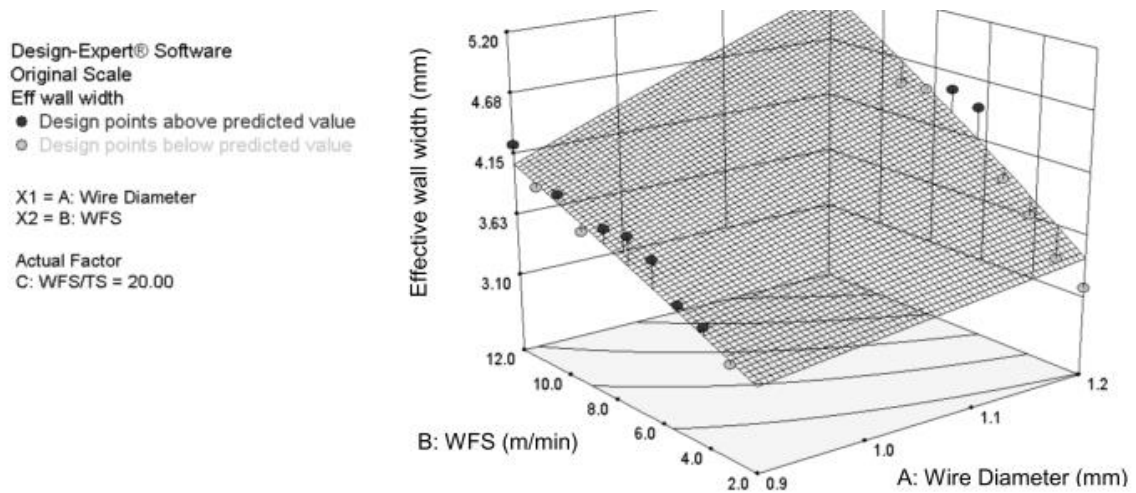


Figure 41: Predicted First Order 3D Response Surface Model for the Effective Wall Width Response as a function of the Wire Diameter and WFS, for a Constant WFS/TS Ratio of 20 [38]

Researchers at the Indian Institute of Technology conducted a weld bead modeling and process optimization study of WAAM using the CMT process. Their goal was to understand the weld bead formation and the interface between overlapping bead, to produce alternative injection molds via the CMT-GMAW WAAM process. Figure 42 shows the process from conceptual design, to ‘as printed,’ to post processed.

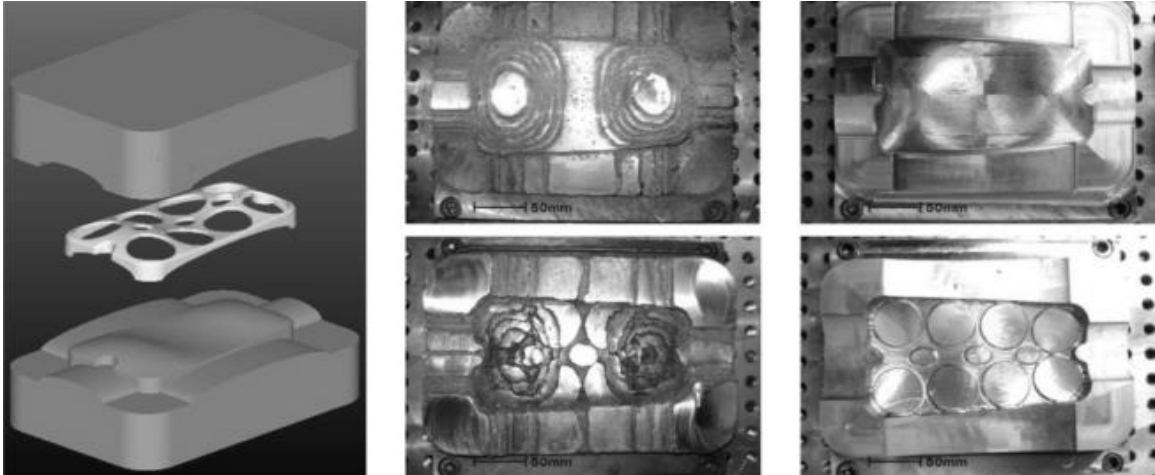


Figure 42: A) CAD Model of Part and Injection Molds B) Near-Net Shape Molds C) Finished Molds [39]

The group, like many others, utilized a synergic process “in which the process parameters are grouped based on their interdependence and their relationships stored; when one parameter in any group is changed the other parameters are automatically modified to maintain a stable arc. For instance, filler wire speed increases monotonously with the welding current. In this closely controlled deposition process, only the following parameters influence the beads:

- i. Filler wire diameter ( $d$ ).
- ii. Filler wire speed ( $v_w$ ).
- iii. Welding torch speed ( $v_t$ ) and
- iv. The distance between consecutive beads called step over increment ( $p$ ).” [39]

They also noted that many have already produced welding process models; however, “most of these models study single bead formation and hence do not explain the behavior of the overlapping material in multi-bead deposition” [39]. By assuming the weld bead to be a parabolic geometry, the group developed a predictive model to optimize the

parts' geometry. The smoother the surfaces were the less time and effort went into post processing. Figure 43 shows where the group made multiple samples at various parameter combinations ( $v_w$ ,  $v_t$ , and  $p$ ) to study the effect on the surfaces. The group concluded “minimum rate of heat input, wider heat distribution, higher resolution and optimum yield are the most desired criteria in weld-deposition. Minimum possible wire speed, maximum possible torch speed and a step over increment of two-thirds of the bead's width are thus recommended” [39].

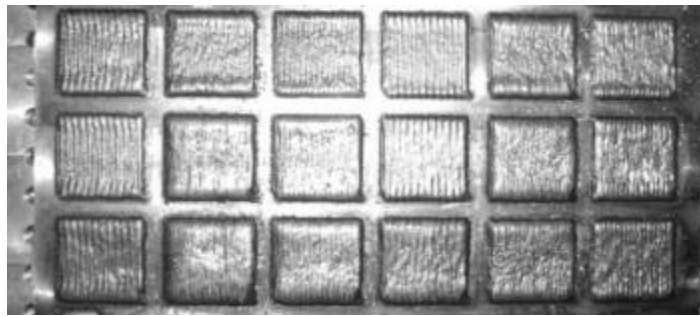


Figure 43: Depositions Made at Different Combinations of Process Parameters [39]

The group also developed an equation to measure the *yield* ( $\eta$ ) of a ‘print’ to quantify the ratio of material remaining in the object after post processing to the material originally deposited. Equation 1 shows the group’s predictive *yield* model, while Figure 44 shows their results from experimentation [39].

$$\eta = \frac{\text{Area of Layer} * \text{Layer Thickness}}{\left(\frac{\text{Length of Path}}{v_t}\right) v_w \left(\frac{\pi}{4} d^2\right)} \times 100\% \quad [39] \quad \text{Equation 1}$$

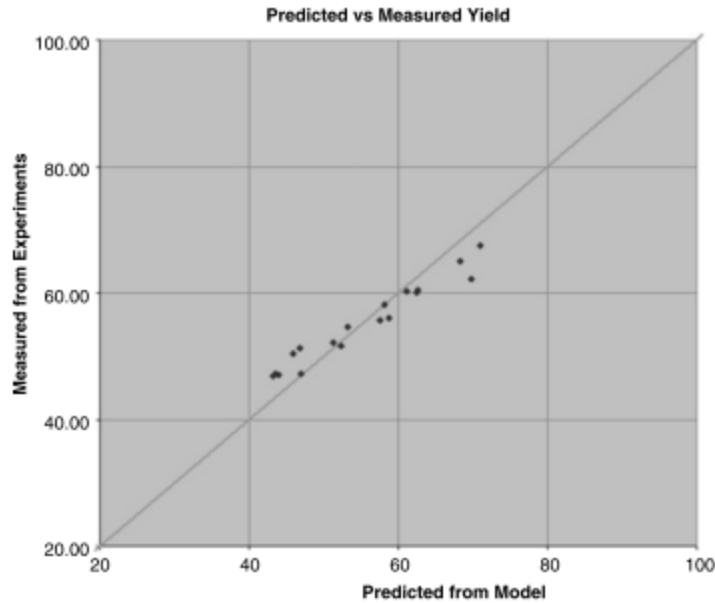


Figure 44: Predicted vs. Measured *Yield* using Equation 1 [39]

Cranfield University researcher, Ding, performed a thermo-mechanical analysis of the WAAM process and its effect on larger parts. They recognized that the high heat input leads to distortion and residual stresses. They also noted that while many others have produced Finite Element (FE) models to predict this behavior, the model size is usually small due to computational limitations and the time it takes to produce the actual parts to compare the model to. “Unlike the conventional transient method which uses a time increment scheme to model the moving welding torch, the steady state method attaches an Eulerian reference frame to the welding torch and the material ‘flows’ through the mesh. Therefore, the problem can be solved for a single time step saving a large amount of computational time. Moreover, the model using the Eulerian frame does not need to use a high-density mesh uniformly along the weld line, saving additional computational time. While the steady state solution of the thermal problem is relatively trivial, application to the mechanical problem is more difficult” [40].

The researcher added thermocouples and used a strain scanner along the part to get empirical data; while for the FE model they used ABAQUS software. The walls were deposited along the center of the base plates with a width of 5mm and a height of 2mm. CMT-GMAW was used as the heat source with a wire diameter of 1.2mm and torch speed of 8.33 mm/s. This equated to a heat input of 269.5 J/mm, assuming a 90% efficiency. A water-cooled plate was used to cool the parts faster as well as a 400 second wait time between layers. The trial included 5 specimens of one, two, three, four, and 20 layers. Figure 45 shows the results of the transient and steady-state model and how close they are to the empirical data for temperature. Figure 46 shows the results of the transient and steady-state model and how close they are to the empirical data for stress in the y-direction for three layers. The group concluded that with their steady-state model there was a total time saving of 80.21% in simulating the thermo-mechanical model versus the transient method. The group also concluded that both FE models can accurately predict the heating and cooling cycles during the WAAM process. The stress across the deposit is very uniform with very little influence of the preceding layers on the following layers according to the numerical model. Lastly the researchers stated that a “significant stress redistribution is observed after unclamping. The stress at the top of the deposited wall has a much lower value than at the interface due to the bending distortion of the sample.” Figure 47 shows the stress distribution along the z-direction before and after clamping [40].



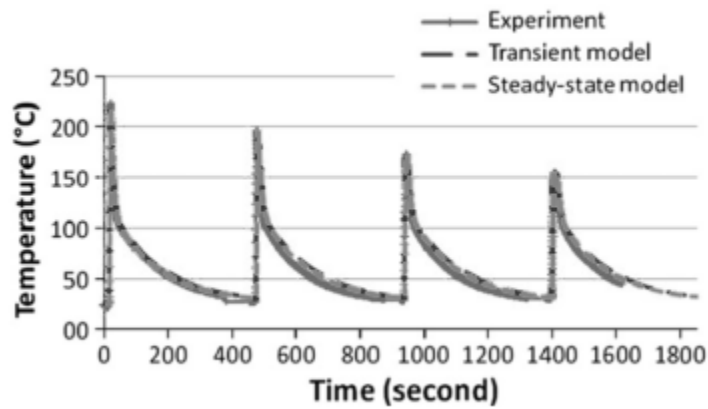


Figure 45: Temperature Verification of Transient and Steady-State Models [40]

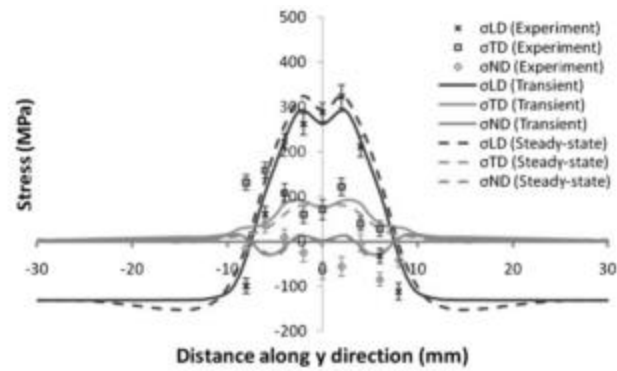


Figure 46: Stress Verification of Transient and Steady-State Models [40]

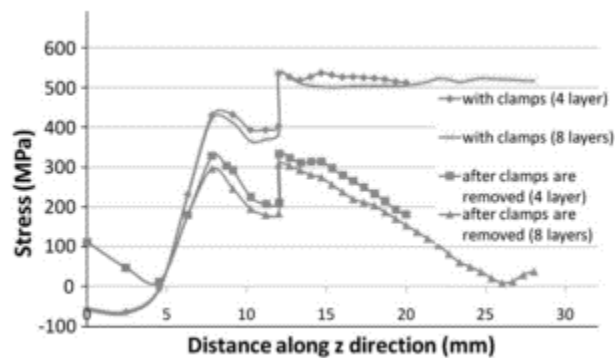


Figure 47: Stress along the Z-Direction Before and After Clamping [40]

A collaborative study of researchers from Cranfield, Northeastern, and Beihang University studied the use of WAAM with Aluminum alloys using the CMT-GMAW process. The group makes a distinction between different types of CMT-GMAW with one variant being “where conventional spray is mixed with the dip transfer mode and this is referred to as CMT pulsed (CMT-P). A further development is the advanced variant of both these processes (CMT-ADV and CMT-PADV). This variant allows for polarity reversal and therefore AC operation” [41].

“ER2319 aluminum alloy wire [walls were created] by the WAAM fabrication system which is shown in Figure 48. 2219-T851 aluminum plates were used as substrates. A Fronius CMT Advanced 4000 R was employed as the power source, which was connected to the ABB robot IRB2400. Pure argon (99.99%) was used as the shielding gas with a constant flow rate of 25 L/min. The contact tip to work distance (CTWD) was kept constant at 15mm. Walls dimensions were 500mm long and 200mm high and were built by the CMT process using variable wire feed speed (WFS) and deposition travel speed (TS)” [41]. Figure 49 shows the results of a porosity study performed by the group using CMT-PADV and CMT-P processes. The CMT-PADV process produced much better results. The group also noted that they naturally aged the specimens for 30 days prior to tests. “The experimentally evaluated vertical and horizontal tensile properties of WAAM deposited 2319 aluminum alloy and wrought 2219 alloy are presented in Table 1. The vertical (V) direction refers to samples taken across the build layers whilst the horizontal (H) direction refers to those taken along the layers. Yield strength (YS), ultimate tensile strength (UTS) and elongation of the WAAM alloy are evenly distributed in the whole as-deposited wall. Average YS and UTS are 110 MPa and 260 MPa respectively. Although

the strength values are lower than those of the T851-tempered alloy, they are 50% higher than those of the O-tempered alloy. Meanwhile, the excellent 17% plastic elongation is higher than the T-tempered alloy” [41]. The group concluded that with additional processing (such as cold working, aging, or solution treatment) the WAAM produced parts would induce grain refinement as well as increased hardness. In doing so, the strength of the material would approach those of the T851-tempered alloy even more.

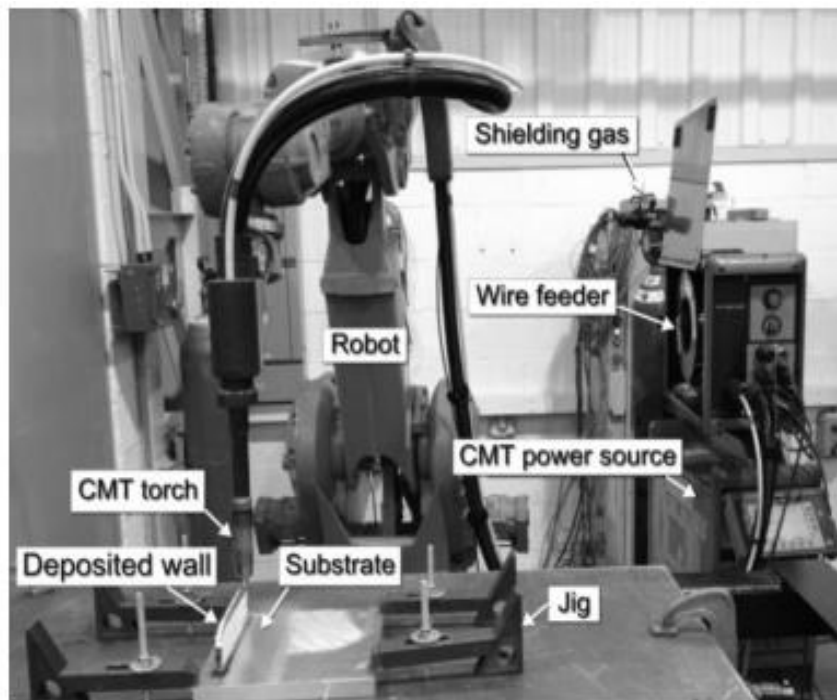


Figure 48: CMT-WAAM Experimental System [41]

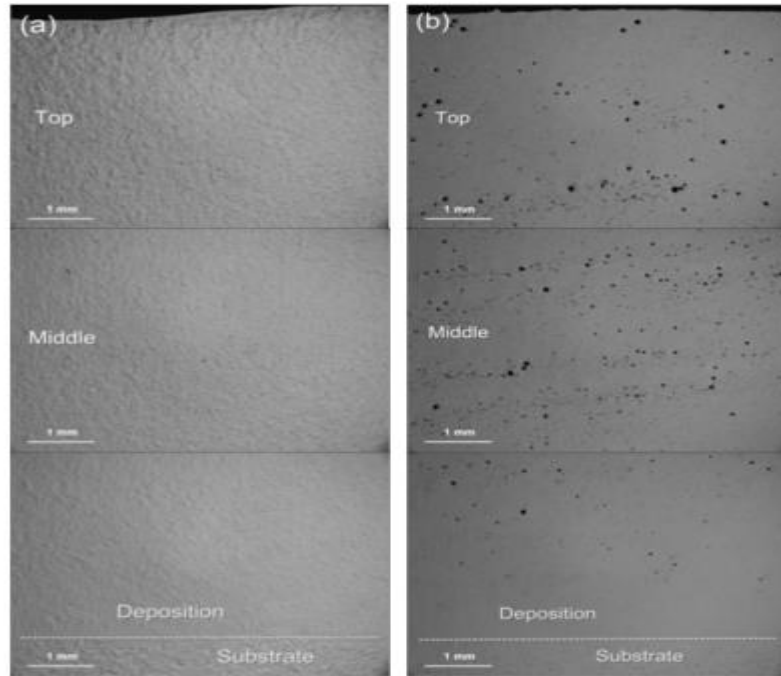


Figure 49: Porosity of WAAM 2319 deposited by A) CMT-PADV process, WFS=6m/min, TS=0.6m/min, Heat Input (HI)=112.2 J/mm, B) CMT-P process, WFS=6m/min, TS=0.8m/min, HI=189.1 J/mm [41]

Table 2: Tensile Properties of Deposited 2319 Alloy and Wrought 2219 Alloy [41]

Property	WAAM alloy						Wrought alloy	
	V1	V2	V3	H1	H2	H3	2219-O	2219-T851
Yield strength /MPa	105	106	107	112	110	121	76	350
Ultimate tensile Strength/MPa	257	261	256	262	263	263	172	455
Elongation /%	15.4	16.8	14.4	18.3	19.0	17.8	18	10

(V-Vertical; H-Horizontal)

In 2014, Posch, noted the use of the WAAM process by a different name, “MicroGuss™,” where in the early 1990s the company ANDRITZ HYDRO produced Pelton runners by adding forged runner tips (high stress concentration area) to cast sub-structures, instead of trying to cast a more complex and weaker/inferior product. Posch

introduced the idea to apply CMT-GMAW for the process due to its precise dip transfer method. He discusses the ‘CMT Pinning’ ability where tiny parts of filler wire can be welded to a substrate, depending on power and forces at hand, different pin structures can be created such as ball, cone, or a flat shape. Figure 50 shows how this ability can be utilized to create small features [42].

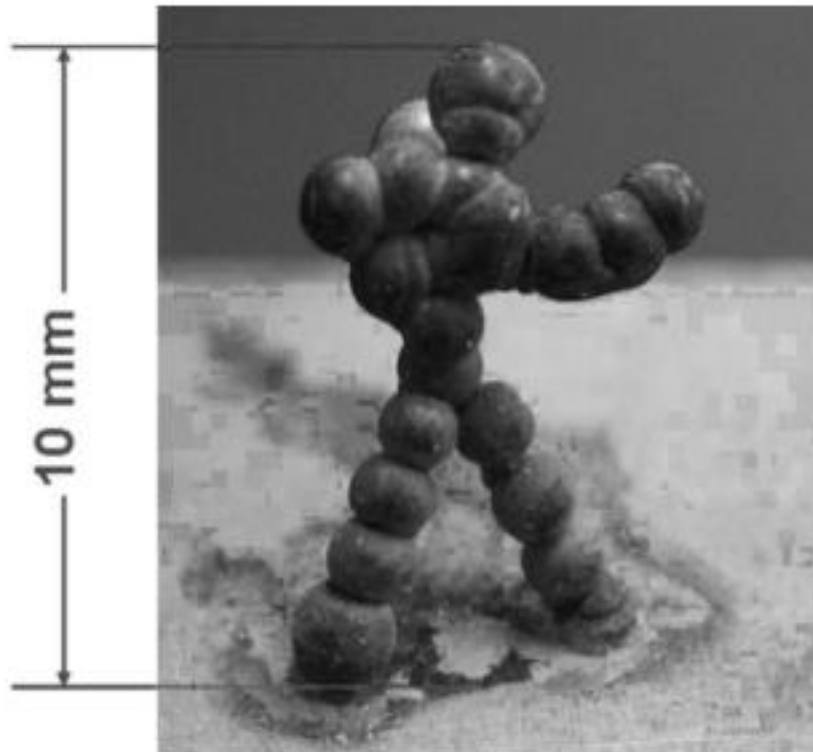


Figure 50: Application of the Pinning Ability [42]

Posch, who works for Fronius, states “minimum achievable thickness thereby depends mainly on the diameter of the filler metal which is used – and the standard wire diameter for the CMT process in general is 1.2mm. In this combination, minimum wall thicknesses of around 4-5 mm can be realized, depending on the wetting characteristics during the metal transfer from the wire tip to the weld pool. Broader cross sections can be realized by torch weaving during welding and/or putting a certain number of welds side by side – up to establishing complete overlays. Best results can be achieved when the electric

arc is in a vertical position. If inclined three-dimensional planes [must] be made, only a limited sideward offset of the actual welding torch position to the previous one can be done. If the base is fixed, planes with a decline up to 15% from the vertical can be established. But if the base is mounted on a commercial turntable very complex 3D planes can be produced – nevertheless the programming effort for the robot and turntable movement increases rapidly. A realistic deposition rate for a single layer pile up by CMT/MAM using stainless steel is around 1.5 – 2 kg/h metal. The thicker the cross section, the higher the deposition rate can be – up to approximately 5 kg/h as it is for CMT joining and CMT cladding. For very thick cross sections also a CMT Twin process (2 wires) could be taken into account – then the process could go to its theoretical limit of about 10 kg/h as it is for real cladding applications” [42]. These parameter limitations are invaluable to know beforehand in the research community looking to use CMT-GMAW as a process for WAAM. Posch later noted that the microstructure was comparable to traditional GMAW weld metals: “An austenite/ $\delta$ -ferrite microstructure was revealed with a  $\delta$ -ferrite content of 30FN. The  $\delta$ -ferrite grains showed a preferred crystallographic orientation in [001] direction, whereas the austenite grains were bloc wise, randomly oriented. No indication for porosity and lack of fusion could be observed by the metallographic investigations. The mechanical properties were [comparable] to the values given in the filler metal data sheet” [43].

Researchers at the University of Wollongong sought out to develop a model for a multi bead geometry using the CMT process. The group approached the problem similarly to the Indian Institute of Technology researchers; however, the group looked at modeling the single bead as not only a parabolic model but also as cosine and arc model. Figure 51 shows the group’s results of model geometry vs. actual weld bead cross-sectional area as percent error (for a single bead). The group also states that based on their calculations a step-over distance of  $2/3$  the wire diameter is not optimal (while typically researchers agree it is) as it would create “an unstable overlapping process.” The group then discusses that  $0.738$  times the wire diameter ( $0.738*w$ ) is the “critical distance” calculated for their mathematical model. The group then shows the results of the two step-overs, with  $2/3*w$  producing better results than their calculated  $0.738*w$  [44].

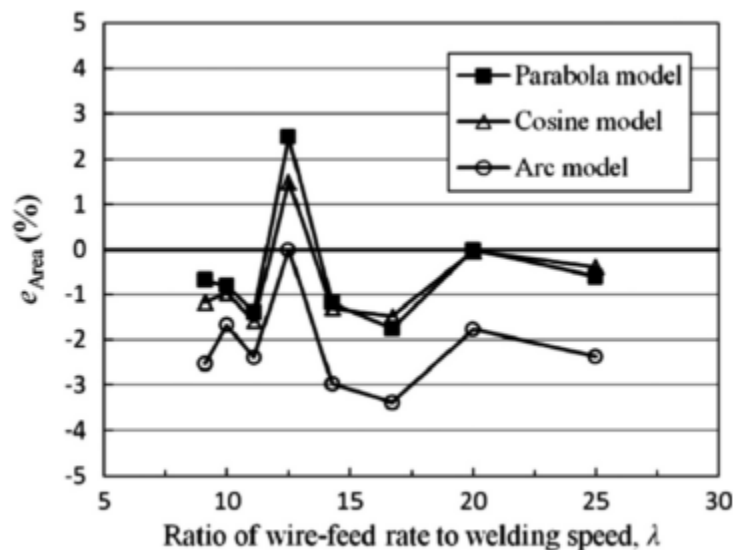


Figure 51: Error for Predicted and Actual Area of Weld Bead Cross Section [44]

Pinto, from Tecnico Lisboa, sought to study the effects of varying current and travel speed on “deposition rate, deposition efficiency, build-up average width, final useful area, hardness and, finally, the surface texture” in the final results of a Nickel alloy. The

researcher’s results are presented in Table 3 below. One peculiar note is that the research found the deposition efficiency to be directly proportional up to 110 amps and inversely proportional afterwards. The study never mentioned any thought on this phenomenon [45].

Table 3: Directly Proportional (X) and Inversely Proportional (1/X) Responses to Current and Travel Speed [45]

Response:	Current Effect:	Travel Speed:
Deposition Rate	X	1/X
Deposition Efficiency	X up to 110 Amps	1/X
Poor Fusion Effect	1/X	X
Width	X	1/X
Area	X	1/X
Average Hardness	Insignificant	Insignificant

Williams *et al.* found for CMT “the travel speed (TS) has the largest effect on deposits quality. Figure 52 shows that, for a given wire feed speed/TS ratio of 30 (keeping the WFS/TS ratio constant ensures that both the amount of material per unit of length and the heat input are kept constant), the lowest TS of 0.2 m/min resulted in the best deposit; the quality progressively deteriorated for increasing TS, and finally, deposits were unacceptable for a TS of 0.5 m/min” [3].



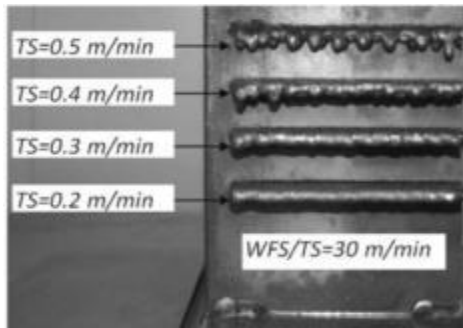


Figure 52: Varying Travel Speed with a Constant WFS/TS Ratio of 30 m/min [3]

Recently a group from The Welding Institute (TWI), performed a small case study on the CMT process’s capability at performing angular parts, particularly in aluminum alloy 5183 components. Figure 53 shows some of the samples the group could achieve as well as the torch’s orientation in relation to the sample. The group concluded that for bead height and width between 1-3mm and 1-5mm respectively, the technique was “capable of producing good quality deposits free of porosity, showing good inter-layer fusion, and with an impressive regularity when performed even at an angle as shown in Figure 53” [46].

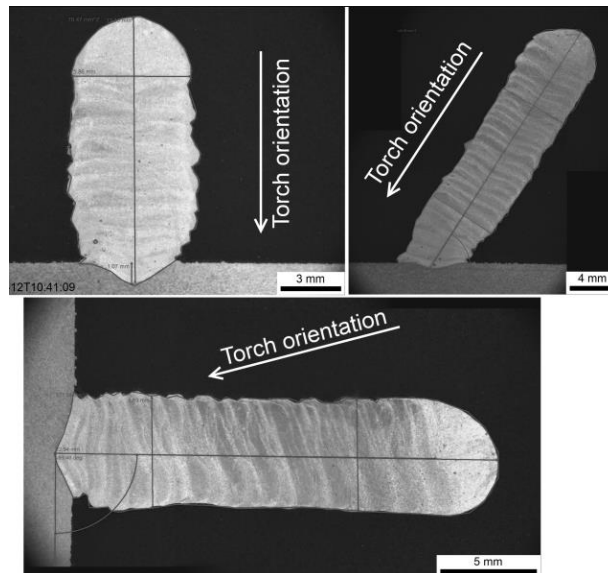


Figure 53: Range of Orientations Achievable by the CMT Process [46]

## Process Control

Dickens *et al.* concluded that to further develop the GMAW based additive manufacturing technique, a feed-back loop to provide the wire offset distance to the controller was necessary. The controller would then maintain the wire offset distance to a constant [18].

Spencer *et al.* implemented a temperature control loop to ensure adequate cooling between layers. A temperature set-point in an if-else type loop prevented welding until the part reached an acceptable temperature read by an infra-red sensor. The group noted the recrystallization and slower cooling of the lower layers resulted in a finer ferrite/pearlite grain structure, as well as an improved surface finish [19].

In 1992, Xie discussed the synergic control system to control the current, thus allowing prediction of wire melting rate. “In the synergic control system, the current pulse parameters are automatically generated by an electronic control unit or a computer system for a given wire feed rate, based on predetermined parametric relationships. The parametric relationships relate the four pulse parameters to wire feed rate for a stable welding operation. A square waveform of current is normally desired since with this waveform the amplitude of the current can be exactly controlled. To obtain a stable pulsed current welding process there are three essential criteria that must be satisfied:

1. *Burn-off Criterion*: The wire feed rate must be matched by the burn-off rate of the wire to keep a constant arc length.
2. *Metal Transfer Criterion*: The metal must be transferred in a spray mode and controlled by the current pulse.

3. *Arc Stability Criterion*: The welding arc must be stable during the background current duration” [47].

Xie also breaks down the quality control process for welding into three groups with five fundamental functions: Prior, During, and Post Welding. In the Prior to Welding category, he states that (I) a proper analysis of product design and weld procedure must be carried out; (II) the correct implementation of the weld procedure and optimization of the welding process must be performed. This would correlate to the proper input parameters for the process for the ‘printed’ part, being selected based on the part. For example, a hollow part should have different parameters than a solid part. In the During Weld category, he states (III) proper manipulation of the weld arc must be controlled; (IV) real-time closed-loop control must be utilized. Most importantly, in the After-Weld category, he states (V) diagnosis of quality issues. This means that the process should be adaptively learning from mistakes and have continuous improvement [47].

Xie then states that feed-back control for welding “can be classified into two main groups: geometrical and technological feed-back control. The geometrical feed-back control automatically adjusts the position of the welding arc relative to the joint path. Without this technique, the robot moves the welding torch in a predetermined trajectory regardless where the joint is located. Using this technique, the robot trajectory is consistently adjusted to the joint path. Another advantage of this technique is that the demand on the geometrical accuracy of the workpiece and on the repeatability of the fixture is reduced. The technological feed-back control automatically adjusts the welding parameters in response to the variations in the welding process” [47]. The advantage to

this technique, is that weld quality parameters can be maintained; such as: arc length, proper gas flow, etc.

Ribeiro *et al.* noted, much like Dickens *et al.*, that during the build process, the wire offset distance was variable and required manual adjustment during the process. The part geometry was considered to be the cause of their issue and closed-loop control was recommended as the solution [25, 26]. To increase control of the GMAW welding process, Ribeiro *et al.* developed a mathematical model for layer width. The input parameters were layer height, welding current, and welding voltage. Wire feed speed was not considered as it was an internal parameter to the welder. The group noted a max layer width (output of model) error of 5% utilizing their method; however, many important parameters noted by other researchers were ignored [21].

In 1997, Carvalho, applied multiple control schemes to the welding process to try and improve the system. One method of control that was utilized was a touch sensing scheme in which the welding head would approach the part, sense the joint to be welded, and set its offset distance accordingly. The author did so by measuring the resistance on the voltage leads until the value read zero (when the wire touched the surface). Voltage control was also implemented, as well as a combination of the control schemes. One suggestion made by Carvalho was that “control of deposition rate by adjusting wire feed speed and/or travel speed could be introduced if sensor(s) for measuring gap and bead geometry were available” [48]. While this study held much promise from a control standpoint, much of this is internally controllable via a synergic process or Fronius’ CMT process. The touch sensing scheme to maintain offset distance was an approach to solve

the issue both Dickens and Ribeiro noted; however, the author did not implement it in a way to maintain the offset distance throughout the weld process.

In 1998, Kovacevic *et al.* used a high-speed vision system to study the formation of droplet parameters and weld penetration of GMAW based additive manufacturing. The goal of the research was to create a sensing system that could improve the process consistency; however, the research was not completed [28]. The researchers proposed controlling the metal transfer process by turning the current to the welder on and off (pulsing, similarly to the CMT-GMAW process). The group determined that the deposited bead size and penetration could be controlled by the pulsing; therefore, this strategy could be used for increased control [28].

In 1999, Kmecko *et al.* applied real time image processing to the system to reduce weld spatter. The system measured the voltage and current used by the welder and featured an infrared pyrometer and a light sensor. The system was capable of real time image capture; however, no reference of successful closed-loop control was presented. Kmecko *et al.* were convinced that the closed-loop control was necessary to improve the process [2, 29].

In 2012, Almeida, went into detail parameterizing the WAAM process and discussed controls, yet did nothing in actual implementation of control into the process. Some of the suggestions for future work did however include the need for the development of process control using algorithms developed for the specific process (GMAW, GTAW, etc.), as well as the need for a method to control residual stresses and distortion [16].

When examining the microstructure, Clark *et al.* concluded that the results were highly dependent upon the deposition factors. The authors concluded that controlling the cooling rate was necessary for a uniform part and the prevention of crack formation [34].

One common reoccurring theme in literature is the lack of process control in the WAAM process. While the introduction of CMT-GMAW has improved this with better control over the current/voltage/wire feed relationship, there is still a lack of control in the ‘During Weld’ group, as Xie categorized.

### **Fronius CMT Welding**

The Fronius CMT welding process utilizes a synergic line with presets for various materials, wire diameters, and gas compositions. Previous research studied many parameters that factors in the system, however with the Fronius CMT controls many of these factors are closed-loop controlled and/or set by the material selection and wire diameter. Figure 54 is a flow chart showing that once an operator selects a material and the appropriate wire diameter based on the feed rollers in use, many parameters are set based on these choices.

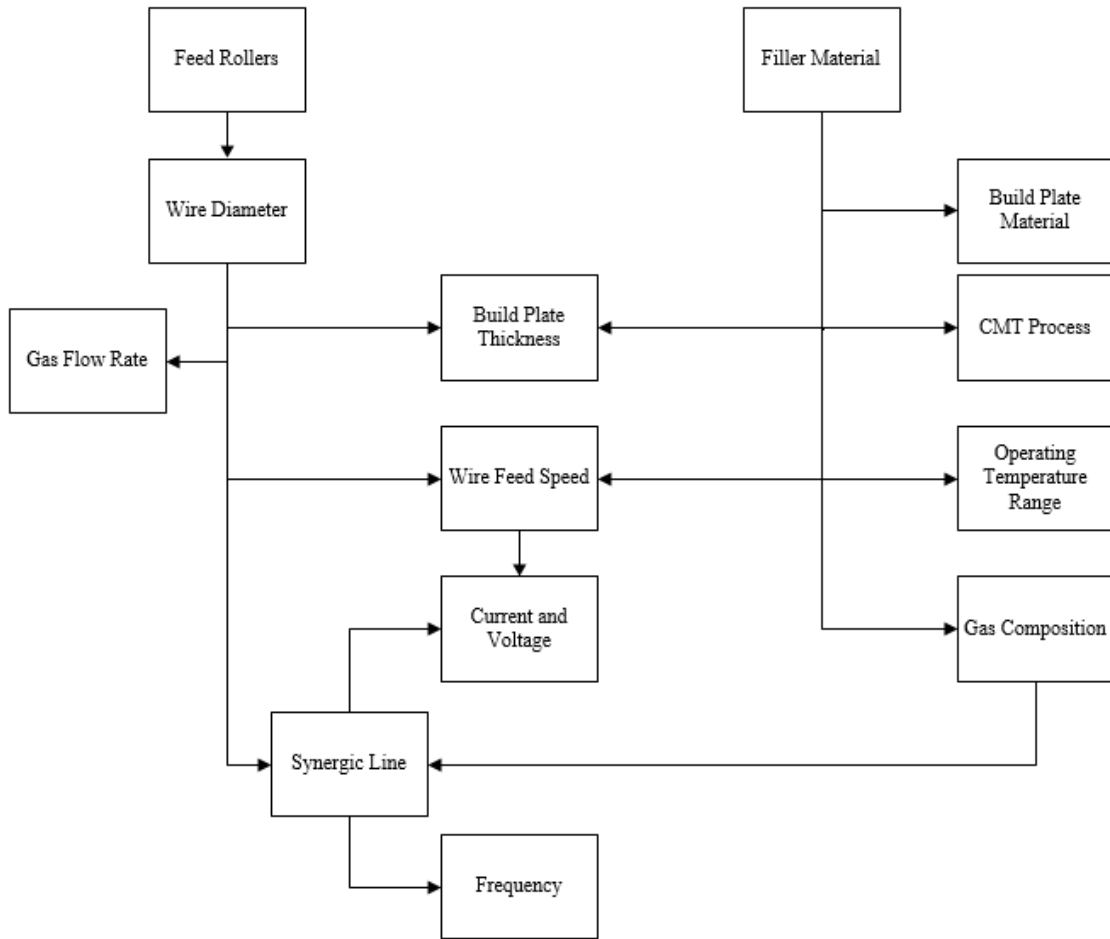


Figure 54: Flow Chart for Various Parameters Based on Material Choice and Diameter

Following the flow chart from Figure 54, the feed rollers used are for set diameter of wire. This sets the wire diameter choice for the weld process. The gas flow rate is based off of the wire diameter according to Equation 2 below [49]. The welder's digital gas sensor regulates, monitors, and reports back specific gas flow data to the proprietary closed-loop controls. The filler material is chosen by the operator based on their needs or requirements. The filler material manufacturer specs the material the filler should be used with (build plate material). Fronius specs what process (CMT, CMT Pulsed, CMT Advanced, etc.) should be used for the filler material chosen. The material properties choose what operating range the material should be maintained at (melt temp,

recrystallization temp, etc.). The material properties also determine what gas composition should be used; whether it be a fully inert environment or have active gases. The wire manufacturer specs how thick of a plate should be used for the specific material and diameter combination chosen as well as a suggested wire feed speed. The wire diameter, gas composition, and de facto material chosen, set the synergic line for the Fronius welder. Based on Fronius' proprietary synergic line process parameterizations and controls, the operating frequency is set. The wire feed speed and the synergic line maintain the operating current and voltage in the process via Fronius' proprietary closed-loop feedback control schemes. The operator chooses a material (based on whatever criteria for the part they wish to produce) and a wire diameter (based on the feed rollers available) and many parameters are in effect set or at least set to within a good operating range.

$$\text{Gas Flow Rate } \left(\frac{L}{\text{min}}\right) = \text{Wire Diameter} \times (10 \text{ to } 12) \quad [49] \quad \text{Equation 2}$$

## **Weld Temperature**

A part's mechanical properties are highly reliant upon the temperatures the part is exposed to and the duration of those temperatures in the WAAM process, much like with many other processes in manufacturing. The temperatures of interest in the WAAM process can be broken into three groups: before, during, and post weld. Prior to producing a part via WAAM, one must determine if a pre-heat is appropriate for the end purpose, geometry, and material. If a part's mechanical properties are not of interest (prototype), then temperatures do not matter as much pre-weld. Preheating can be beneficial when used appropriately; however, one risks wasting time and the integrity of the part without proper use. "There are four primary reasons to utilize preheat: it slows the cooling rate in the weld metal and base metal, producing a more ductile metallurgical structure with greater



resistance to cracking; the slower cooling rate provides an opportunity for hydrogen that may be present to diffuse out harmlessly, reducing the potential for cracking; it reduces the shrinkage stresses in the weld and adjacent base metal, which is especially important in highly restrained joints; and it raises some steels above the temperature at which brittle fracture would occur in fabrication. Additionally, preheat can be used to help ensure specific mechanical properties, such as weld metal notch toughness.” [50]. Typically for welding applications a preheat is more necessary for thicker sections, as more mass requires more heat input to reach a desired temperature. For the WAAM process, the build plates tend to be thinner and a preheat is generally not as necessary. For low carbon steels (ER70s-6) a preheat is not required for build plates “less than 1 inch thick” [50]. For other materials, a preheat is generally treated to the same manor; however, it is noted that if the presence of cracking occurs or if hydrogen in the weld is not given enough time to sufficiently diffuse out, a preheat is recommended.

During the WAAM process the previous layers produced get reheated by the current layer being deposited. The temperature of the ‘print’ before the next layer is deposited atop it, is known as the interpass temperature. The temperatures of the weld process will greatly affect the mechanical properties of the produced part. Higher temperatures typically give a finer grain structure and higher toughness. According to Funderburk, from Lincoln Electric, this trend may be reversed above temperatures of 500°F (260°C) for steel [50]. According to the American Welding Society, interpass temperature should not exceed 550°F (290°C) for steel. Adding a maximum interpass temperature control over the process would be ideal to maintain desired mechanical properties. When recording temperature to maintain a maximum interpass temperature, Funderburk

recommends measuring 1 inch from the weld. For maintaining the minimum interpass temperature throughout the part the American Welding Society states to record temperature “for a distance at least equal to the thickness [of the part]” but not more than 3 inches [50, 51]. “Although there is some debate as to where the interpass temperature should be measured, most experts agree that it must be maintained for some reasonable distance away from the welded joint. Since this decision may greatly influence the fabrication cost, a reasonable and practical location must be determined. One foot away from the joint is probably excessive, while a tenth of an inch, or on the weld itself, is probably excessively conservative” [50]. Within 3 inches of the weld pool seems to be considered reasonable by all accords. Gaddes recorded temperature of a base plate roughly one inch away and noted a steady state temperature of ~500°F after a given amount of time. This falls in line with Funderburk’s peak strength temperature curve. “The objectives of controlling the interpass temperature are

- (1) to minimize the risk of hydrogen cracking for carbon, carbon-manganese, and ferritic alloy steels, in which the minimum interpass temperature is specified to be the same as the minimum preheating temperature
- (2) to prevent deterioration of mechanical properties for carbon, carbon-manganese, and ferritic alloy steels, in which the maximum interpass temperature is specified
- (3) to minimize the risk of solidification or liquation cracking for austenitic stainless steel, nickel and nickel alloys, and aluminum and aluminum alloys, in which the maximum interpass temperature is specified
- (4) to maintain good wetting of the molten pool onto the base metal for copper

and copper alloys, in which the minimum interpass temperature is specified to be the same as the minimum preheating temperature” [52]

For the WAAM application, a minimum interpass temperature to prevent hydrogen cracking (objectives 1 and 4) is not much of an issue. A maximum interpass temperature to prevent mechanical property deterioration and solidification cracking (objectives 2 and 3) are the main concern for WAAM purposes. Figure 55 below shows the results of a study of the effects of interpass maximum temperature on the tensile strength of a steel weld. At above  $\sim 250^{\circ}\text{C}$  the tensile strength begins to dramatically decrease. This is closely in agreement with Funderburk’s recommendation of  $260^{\circ}\text{C}$ . Kobe Steel also states that “maximum interpass temperatures of  $150^{\circ}\text{C}$  for austenitic stainless steel and nickel-base alloys, and  $70^{\circ}\text{C}$  for aluminum alloys are generally required to prevent hot cracks” [52]. This is in agreement with the NORSOK (‘Norsk Søkkel Konkuranseposisjon’ - Norwegian shelf Competition Position) Standard on ‘Welding and Inspection of Piping;’ which also states that stainless steels shall not exceed a maximum interpass temperature of  $150^{\circ}\text{C}$  [53].

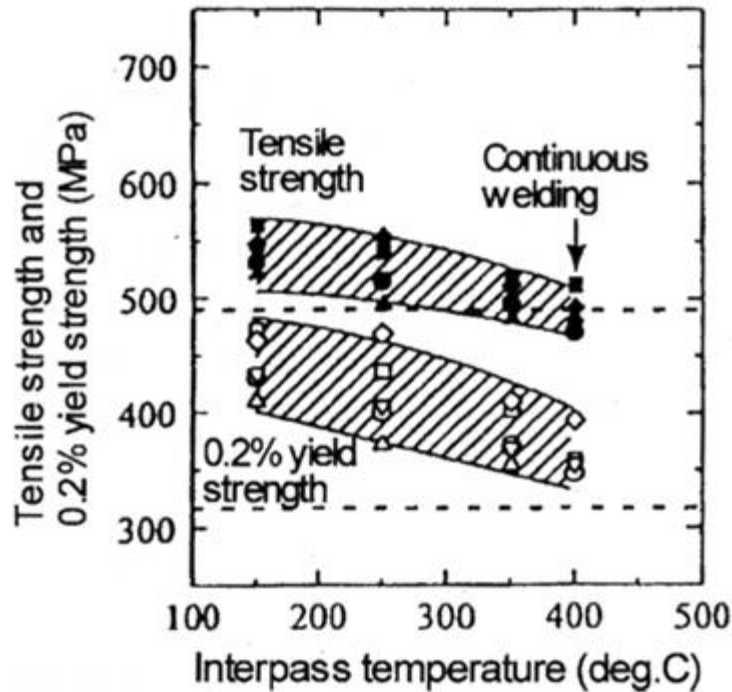


Figure 55: Effect of Interpass Temperature on Tensile Strength for Steel Weld [52]

After a part is produced via WAAM, the next step is to determine the proper post treatment for the part. Post weld heat treatment (PWHT) is typically prescribed to improve mechanical properties. “In general, when PWHT is required, the goal is to increase the resistance to brittle fracture and relaxing residual stresses. Other desired results from PWHT may include hardness reduction, and material strength enhancements” [50]. PWHT is used to minimize hydrogen cracking. For this to occur, one of the following must be present: “a sensitive microstructure, a sufficient level of hydrogen, or a high level of stress (e.g., because of highly constrained connections). In structural steels, hydrogen embrittlement occurs at temperatures close to the ambient temperature. Therefore, it is possible to avoid cracking in a susceptible microstructure by diffusing hydrogen from the welded area before it cools. After welding has been completed, the steel must not be allowed to cool to room temperature; instead, it should be immediately heated from the

interpass temperature to the post heat temperature and held at this temperature for some minimum amount of time. Although various code and service requirements can dictate a variety of temperatures and hold times, 450°F (230°C) is a common post heating temperature to be maintained for 1 hour per inch (25 mm) of thickness. The need for post heating assumes a potential hydrogen cracking problem exists due to a sensitive base metal microstructure, high levels of hydrogen, and/or high stresses, and is not necessary for most applications” [50]. For the WAAM process, stress relieving PWHT are probably more useful if hydrogen induced cracking is not an issue. For carbon steels, stress relief PWHT are “typically held at 1100-1250°F (600-675°F) for 1 hour per inch (25 mm) of thickness. For stress relieving PWHT the part must be allowed to sufficiently cool to room temperature to have the residual stresses to be relieved. Some of the issues that can occur due to PWHT are stress relief cracking, where the part fractures during the process, and a loss of material strength due to exceeding tempering temperatures. Typically for filler metals [(those typically used in the WAAM process)] the material strength decreases after a PWHT” [50].

### **Wire Offset Distance**

Dickens and Ribeiro *et al.* noted, that during the process, the wire offset distance varied and required manual adjustment during the process. This is due to scale error as well as other issues. The part geometry was considered to be the cause of their issue and closed-loop control was recommended as the solution [25, 26]. For the CMT welder being used in this research Fronius recommends a wire offset distance of 14 mm (0.551 inches) be maintained [54]. Having the machine maintain this distance between layers as the part

is built vertically is thought to be a key aspect to control in the WAAM process by multiple researchers.

### **Evaluation Techniques for CMT-GMAW Additive Manufacturing**

The American Society for Testing and Materials (ASTM) has published the *Standard Guide for Evaluating Mechanical Properties of Metal Materials Made via Additive Manufacturing Process* in 2014. The standard outlines applicable procedures for measuring deformation and fatigue properties. When measuring deformation and fatigue properties, the specimen's properties are to be measured using conventional processes for measurement as traditionally manufactured materials [55].

When results are reported, ASTM requires the above guidelines be followed; however, additional information about construction procedure for the additive manufactured part must be reported. The information reported must include location and orientation of the part within the build volume. This is due to the typical orthotropic behavior of additively manufactured specimen [55].

Previous researchers of GMAW based Additive Manufacturing have used tensile tests machined from manufactured wall sections to measure strength. Multiple researchers measured the surface hardness. The microstructure of a polished and etched sample was examined via multiple technologies. Each researcher additionally visually assessed the quality an appearance of the each 'printed' piece.

### **Summary of Research Opportunities**

While the WAAM process has been considered since 1925, there are many opportunities for process improvement. Nearly every researcher noted the lack of, or little control during the WAAM process for both Short Circuit and CMT-GMAW processes.

While the CMT process has been noted to give the operators/researchers better control over the voltage/current/wire feed relationship, a closed-loop control process has yet to be fully implemented. Many researchers have added a sensor or two and monitored variables, and a few have even added these sensors to a loop; however, none have fully implemented multiple control sensors that constantly monitor the process with the capability to stop/modify the WAAM 'print' process either in a geometrical or technological feedback loop. The main reoccurring areas noted for the need of control in the WAAM process by the researchers are process temperature, wire offset distance, and the voltage/current/speed relationship (with gas control included in this relationship noted by a couple of researchers).

### **III. Scope and Objectives**

The comprehensive literature review indicates a lack of control in the Wire Arc Additive Manufacturing (WAAM) Process amongst experimentalists. The need for control is reported from various researchers. While the introduction of a synergic weld line algorithm and Cold Metal Transfer-Gas Metal Arc Welding (CMT-GMAW) have been noted to improve the process with better control over the current/voltage/wire feed relationship and heat input, there is still a lack of control throughout the process. Specific areas noted in the literature that were suggested to be key areas to control are the voltage/current/wire feed speed relationship, process temperature, and the wire offset distance. The control of these specified areas will be incorporated within the scope of this dissertation.

I. Specific primary objectives for the dissertation include:

- Adapt existing 3 axis WAAM printer previously operating using short-circuit transfer components, with the new Cold Metal Transfer (CMT) components.
- Document the printer's adaptation (drawings, bill of materials, wiring diagrams, etc.).
- Demonstrate the ability to create standard geometric shapes (cylinder, wall, hollow structure, etc.)
- Establish a statistical design of experiments (DOE) with different factor levels under observations, such as travel speed, wire feed speed, material, etc.



- Study and compare the tensile strength of specimen made with different materials to that of the machine in its previous configuration. Specimen will be made parallel and perpendicular to the direction of deposition.
  - Study and compare the hardness of specimen made with different materials to that of the machine in its previous configuration. Specimen will be made parallel and perpendicular to the direction of deposition.
  - Study the macrostructure and microstructure of specimen made with different materials to that of the machine in its previous configuration. Specimen will be made parallel and perpendicular to the direction of deposition.
  - Investigate the development of a closed-loop process control method for maintaining wire offset distance throughout the process, as noted in the literature review to be a significant aspect to control.
  - Investigate the development of a closed-loop process control method for maintaining the voltage/current/wire feed speed relationship throughout the process per given parameters (material, wire diameter, etc.), as noted in the literature review to be a significant aspect to control.
  - Investigate the development of a closed-loop process control method for maintaining process temperatures based on deposition materials, as noted in the literature review to be a significant aspect to control.
  - Evaluate control schemes and verify their significance.
- II. Specific secondary objectives for the dissertation include:
- Investigate the use of a wire mesh raft to aid in removability of ‘printed’ parts from their build plates.

- Develop an operator's manual for subsequent Auburn University researchers.
- Develop easy to 'print' files/programs to create traditional standard test specimen for subsequent Auburn University researchers.
- Investigate the development of a g-code post (machine specific m-codes, g-codes, etc.) for the machine to produce future 'prints' more readily.

## **IV. Design and Construction of Equipment**

Previous research conducted by Gaddes at Auburn University on WAAM involved construction of a purpose built, 3-axis, gantry-style CNC machine. A build volume of 18” x 18” x 18” was specified to meet the requirement of evaluating the construction of large objects while providing room for future expansion. “Cartesian style machine was chosen with a build plate that traversed horizontally (y) and not vertically (z)” [2]. Gaddes chose to integrate a commercially available and reliable Miller model 190 welder via a custom-built wire feeder head attached to the x-axis carriage. A Fronius CMT 4000 Advanced welder was specified for advancing the research and integrated into the printer for this study. A complete overview of the equipment and retrofitting procedure is included in the following section.

### **Previous Machine Design**

Auburn University’s WAAM printer was previously configured for research utilizing an off the shelf welder. This machine is used as a base for the current research. Figure 56 shows the printer in its previous configuration. The frame of the machine is constructed from 80/20 aluminum extrusions that allow for easy modification. The build plate travels on two linear guide rails via four ball bearing carriages in the y-axis and is driven by a single ball screw and ball nut. The z-axis moves along four linear rails and carriages and is driven by two ball screws connected by an L-series belt and timing pulley.

The welding torch is carried upon the x-axis and is driven by a single ball screw between two linear rails and carriages. The custom ball screws are 16 mm in diameter and the linear rails are 20 mm wide. Repeatability studies performed by the previous researchers show that the machine is accurate to  $\pm 0.0005$  in.

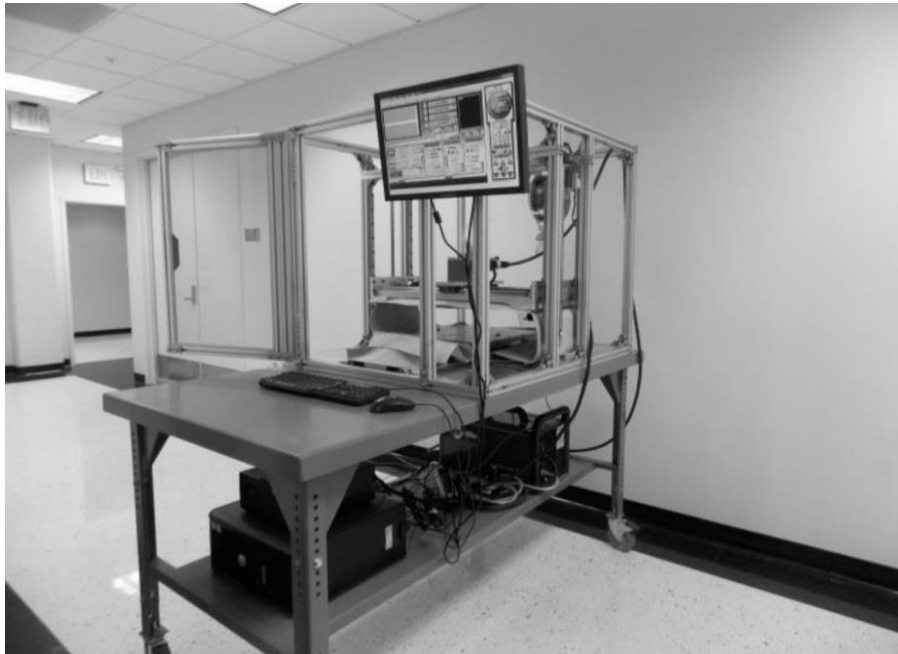


Figure 56: Previous Version of WAAM Printer [2]

The axes are driven by stepper motors. The stepper motors used are NEMA 23 with 1.8°/200 steps per Rev. and have 420 oz-in. of holding torque. The stepper motors are connected to the ball screws by an elastomer coupler to minimize possible binding.

The build plate assembly (Figure 57) consists of multiple layers to provide thermal and electrical isolation. The first layer is a piece of machined aluminum plate that connects to the carriages and the ball screw nut. Next is a 1 in. thick ceramic fiber electrical and thermal insulation board called Duraboard 3000. In addition to being an electrical insulator, this ceramic board has a maximum operating temperature of 3000°F and a very low thermal conductivity of 0.8 at 1000°F. The thermal insulation is important to protect

the mechanism beneath from the heat generated during the WAAM process. The electrical insulation is important to protect the operator and the machines electronics. Above the ceramic insulator is an 18 x 18 x 0.5 in. steel plate which is bolted to the aluminum plate with counter-bored ceramic inserts to maintain isolation. The steel plate features threaded holes (1/2-13 UNC) in a 4-inch spacing pattern to allow attachment of build plates.

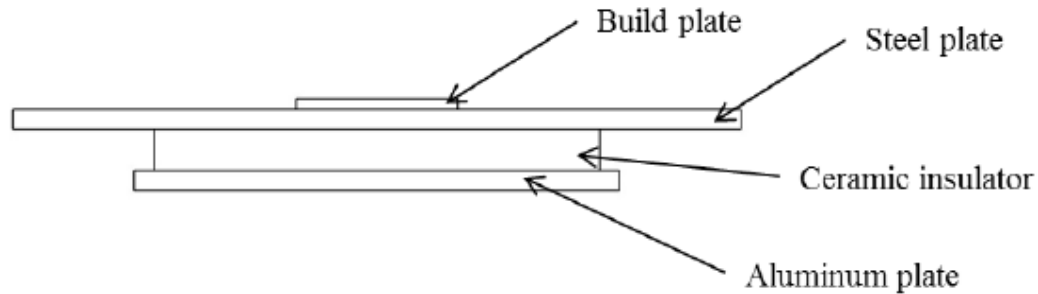


Figure 57: WAAM Printer Bed/Plate [2]

The machine is controlled by the inexpensive CNC control software Mach3 as shown in Figure 58. The software runs on a dedicated computer and accepts standard G-codes and M-codes; it also has its own post for most CAM packages. The Mach3 software is configured to control the three axes. Originally, the wire feed mechanism was configured as a variable speed spindle, and later changed to be driven by a stepper motor with a direct drive feed gear. Now the Fronius VR 7000 CMT Wire Feeder is utilized. Mach3 communicates with the machine via a standard parallel port breakout board. The breakout board distributes signals to stepper motor drivers to control the motors as described later in the Robot – Welder Integration section.

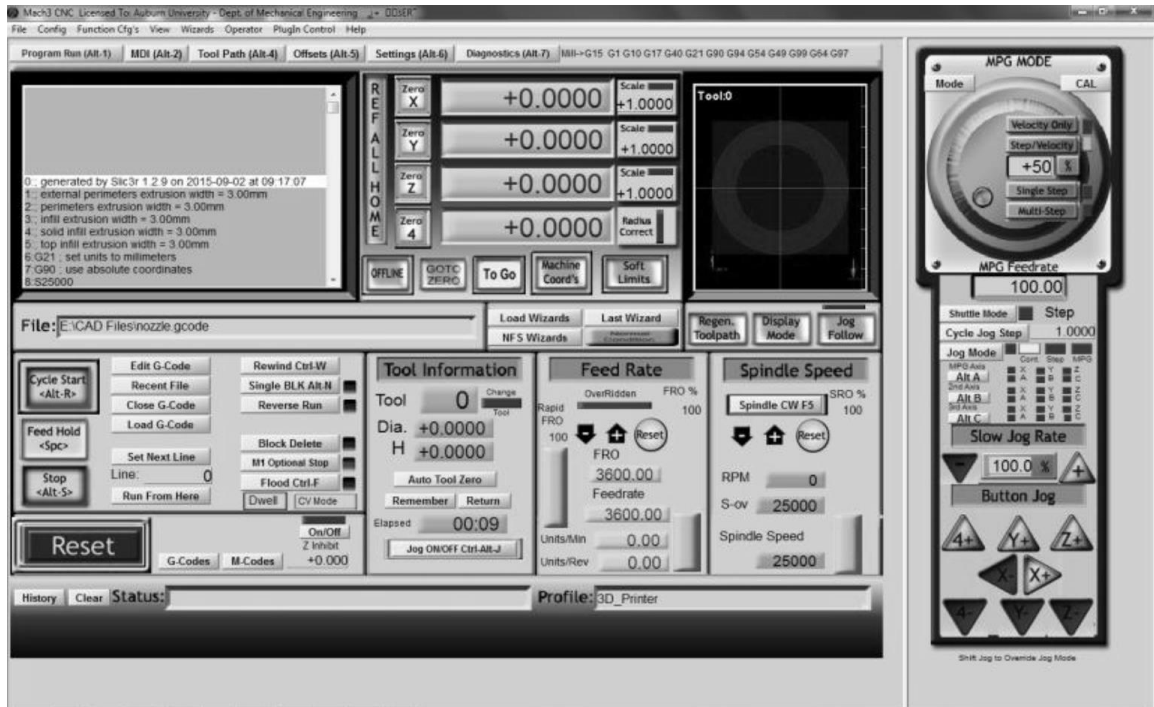


Figure 58: Mach3 CNC Software

## CMT Weld System

The equipment listed below encompasses the Fronius weld system as shown in Figure 59 [56].

- Fronius CMT Advanced 4000 MV R Power Source
- Fronius VR 7000 CMT Wire Feeder
- Robacta 5000 Welding Torch
- Robacta Drive CMT W
- FK 4000 Cooling unit
- Wire Buffer
- RCU 5000i
- Shielding Gases

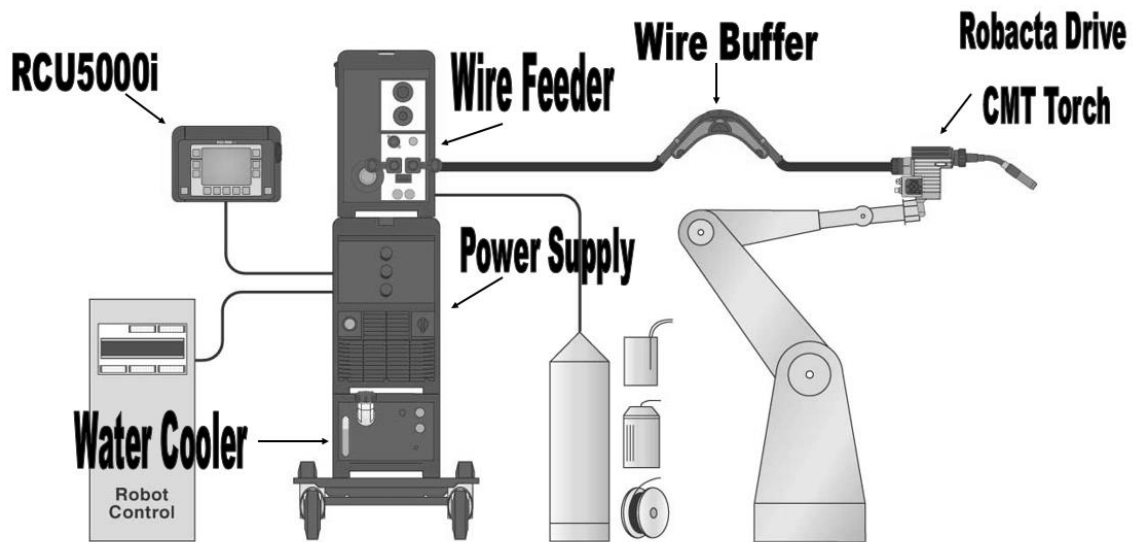


Figure 59: Fronius Weld System [56]

#### Fronius CMT Advanced 4000 MV R Power Source

The Fronius CMT Advanced 4000 MV R Welder shown in Figure 60 below was used to produce specimens via CMT-GMAW process [49]. The accuracy of the machine with respect to displayed values is noted at a max of +/- 8 % of the load for voltage, and a max of +/- 10 % of the load for current. Table 4 shows the specs for the welder. The power source transforms energy into the appropriate form for use in the welding process. The digital process control ensures quality and repeatable welding results [57].



Figure 60: Fronius CMT Advanced 4000 MV R Power Source [49]

Table 4: Fronius CMT Advance 4000 MV R Power Source Specs [57]

Welding Current Range	MIG	3-400 A
Welding Voltage Range	MIG	14.2-34.0 V
Max Welding Voltage		n/a
Open Circuit Voltage		90 V
Duty Cycle (77°F)		85% @ 400 A
		100% @ 380 A
Duty Cycle (104°F)		40% @ 400 A
		60% @ 350 A
		100% @ 290 A

#### Fronius VR 7000 CMT Wire Feeder

The VR 7000 (Figure 61) was created specifically for the CMT welding process. The feeder can utilize large spool sizes as well as drums for higher production jobs. Being as that the feeder is designed for CMT it can operate with a push/pull process torch or a normal push only torch [49]. The wire feeder unit uses a 4-roller drive for feeding the filler



metal from the wire feeder to the torch. The two profiles for the feed rollers are U-Groove and H-Groove. The U-Groove profile is a semicircular shape and is good for most materials, but specifically for steel and stainless wire. These rollers have four points of contact and are to be set to a tension of  $\sim 2.5 - 3$  on the tensioner. The H-Groove profile is a trapezoidal geometry that creates a hexagon when used in conjunction with another roller. This profile is best for aluminum and CuSi. These rollers have two points of contact and the tension is to be set at  $\sim 1.5 - 2$  on the tensioner [Fronius].



Figure 61: Fronius VR 7000 CMT Wire Feeder [49]

#### Robacta 5000 Welding Torch and Drive CMT W

The Robacta 5000 is a “water-cooled” drive/torch unit for the CMT welding system. The term “water-cooled” is misleading as it utilizes proprietary coolant from Fronius. This unit is designed to be mounted to a CNC control unit and not be used manually. The unit does have the capability to feed and retract wire as well as test gas

flow. The torch uses either a conical or counter bored tip. The conical tips allow the filler wire to be guided to the center of the tip for welding purposes. The counter bore tips allow the wire liner to be directly in the tip and have no need for guidance. This allows softer materials to not be deformed by the tip [54]. Figure 62 shows the Robacta Drive with the Robacta Torch attached.



Figure 62: Fronius Robacta 5000 Drive/Torch [54]

#### FK 4000 Cooling unit

The FK 4000 cooling unit is the standard cooling unit for most of Fronius' MIG and TIG packages. It has an internal reservoir and a closed-loop system that flows to the Robacta Drive for cooling purposes. The unit is fuse protected for over-voltage damage [49].

#### Wire Buffer

The wire buffer provides tension in the wire when the drive motors switch from push to pull operation during the CMT process. This prevents binding in the system and

insures the torch's dynamic functions are not hindered. The unit is to be mounted no more than 1.6 m from the Robacta Drive [49]. Figure 63 shows the wire buffer.



Figure 63: Fronius Wire Buffer [49]

#### RCU 5000*i*

The RCU 5000*i* is a universal remote unit for the Fronius welder. It is required for the CMT process and allows the operator to choose between the different operating modes (CMT, Pulse, or Standard). The unit also allows the user to adjust and set the weld parameters prior to and during the welding process [49]. Figure 64 shows the RCU 5000*i* unit.



Figure 64: Fronius RCU 5000i [49]

### Shielding Gases

Shielding gases for the welding process provide a stable environment for the weld pool. Gases are acquired through Airgas. Depending on the specific material being welded, a different composition of gases it to be selected to produce quality specimens. The Fronius welder controls the flow rate based on the diameter of the wire. Fronius states that the flow rate in cubic feet per hour (CFH) of gas flow for the weld process should be 21 – 25.2 times the diameter of the wire (or 10 – 12 liters per minute) [49].

### Robot – Welder Integration

The equipment and instruments listed below were used together to create the CMT based WAAM printer and interface the welder into the existing setup. The equipment listed includes the gantry-based CNC, the welder, upgrades to the machine, software and hardware, and machine I/O logic interface.

- Auburn University's WAAM Printer

- Fronius Weld System (outlined in previous section)
- Fronius RCU 5000i
- Fronius ROB 5000
- Fronius Xplorer Software
- Sealevel RS-485 ModBus RTU Interface (Seal/O-410M-OEM)
- RS-485 PCI Express Card
- Probotix 3-Axis Monster Mill Stepper Motor Driver Kit
- Mach3 CNC Control Software
- LocalNet RS-232 PC Connection Cable
- Passive Splitter
- LocalNet Cables
- Mean Well 12 Volt DIN Rail Power Supply
- Dell Optiplex 755 PC (Windows XP)

Integrating the Fronius CMT welder into Auburn University's WAAM machine was accomplished via the ROB 5000 Discrete I/O interfaced to Mach3 with the RS-485 Modbus protocol. The ROB 5000 features interface signals that are individually wired for connection to the robot automation controller to provide communication between the welding system and the robot controller. Figure 65 (left) below shows the Sealevel RS-485 Modbus RTU interface. It utilizes 16 I/O ports to communicate between the welder's ROB 5000 controller and Mach3. Figure 65 (right) shows the I/O setup on the Seal/O-410M-OEM Modbus.

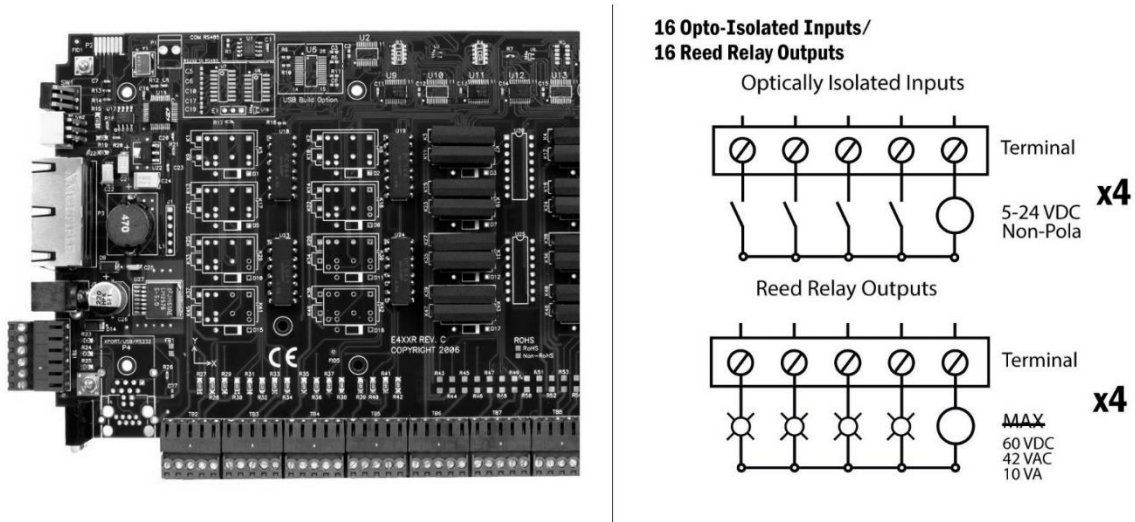


Figure 65: Sealevel RS-485 Modbus RTU (left), Sealevel RS-485 I/O (right).

The Fronius LocalNet interface, connects the welder as a slave to the controller, in our case Mach3 CNC software. Digital input signals to the welder (output signals from Mach3), are accomplished and actuated using machine codes (m-codes) that were created in Mach3 to activate/deactivate the various output signals to the welder and activate hi/lo status. These outputs were designated to ports & pins in Mach3 to control the various signals available. Table 5 shows the setup coming from Mach3 to the ROB 5000 with the designated m-codes assigned. In Mach3 m-codes above 100 are designated for user functions, therefore m-codes begin with M1XX. The second number in the designation indicates what output pin the function is on the Modbus board. The third number in the designation indicates the relay status as high/low (1/0, I/O). Appendix III details the specifics of each m-code.

Table 5: Machine Codes used to Operate the Welder

<b>M-Code</b>	<b>Function</b>
M111/M110	Welding Start/Welding Stop
M121	Quick Stop
M120	Robot Ready (Active Low)
M131/M130	Gas Test Start/Stop
M141	Touch Sensing
M151/M150	Wire Retract Start/Stop
M161	Source Error Reset
M171	Blow Through
M181/M180	Wire Feed Start/Stop

The robot ready signal, M120, indicates that the robot is communicating, functioning and ready to weld. This is one of two signals required for any sort of operation of the welding system. The signal is active low and therefore unless disabled using the quick stop command, M121, Mach3 will send a high signal to Output 2 signaling the robot is ready. The source error reset signal, M161, is designed to clear any error state the welder is in. For proper use, this signal should be toggled on and then off again, therefore the signal does not have a corresponding M160 command to deactivate the signal. The M161 command activates the signal, pauses, and deactivates the signal without additional operator action. The welding start signal, M111, will start the welding process, beginning with pre-welding (gas pre-flow, hot start) and then automatically move to the welding process. When this signal goes low, M110, the post welding process (crater fill, and gas post-flow) will start automatically. The gas test signal, M131 is used to purge gas. It can be used as a gas pre-flow or post-flow as necessary. Wire inching and wire retract, M181 and M151 respectively, is used to move the wire forward or backward. The blow through signal, M171, actuates a compressed gas purge blow through to clean the welding nozzle

to remove any spatter that may have accumulated. Like the source error reset signal, this signal is actuated for 5 seconds and then automatically turned off [Fronius].

The ROB 5000 allows for the selection of welding modes via the robot interface using a combination of three signals, X2:6, X8:1, X8:2. This allows for the selection between standard program, pulsed arc program, job mode, parameter selection internal, manual, CC/CV, TIG, or CMT/special process. For our application, parameter selection internal was hardwired by wiring X2:6 High, X8:1 High, and X8:2 Low. This allowed process selection using the RCU 5000i. Welding jobs can be called in a similar way, with several bits joined together to form a binary number between 0-99. The set of bits used tells the welder what weld schedule to use. This feature was deemed unnecessary for our application and not used [49].

Digital input signals (output from the welder) to the robot controller are read via the assigned ports & pins designated in Mach3. The inputs from the ROB 5000 to Mach3 are arc stable, power source ready, and process active; and are connected to pins 1,2, and 4 respectively. Arc stable is a signal sent from the ROB 5000 “once an arc has been started and that arc is within acceptable parameters as determined by the welding power source.” Arc stable functions as the touch sensing input signal, with the input going high once contact has been made between the electrode and the base. The power source ready signal is sent from the ROB 5000 “when the power source has established successful communication and there are no errors that will interfere with the function of the welder.” The process active signal is sent from the ROB 5000 “once the welding process has started (after a “welding start” signal) beginning with the gas pre-flow if set by the welder (note this signal will not go high if the gas is controlled by the robot instead)” [49].



The ROB 5000 features analog outputs for welding voltage, welding current, wire drive current, wire feed speed, and arc length via a 0 – 10V signal. These outputs are used for displaying and documenting the process parameters and monitoring the weld. The decision was made to forgo using these signals and to instead use the Fronius Xplorer software for monitoring and logging of all weld data. The welder interfaces with the computer, RCU 5000*i* handheld controller, and ROB 5000 via the LocalNet. Figure 66 shows the complete layout of the interface.

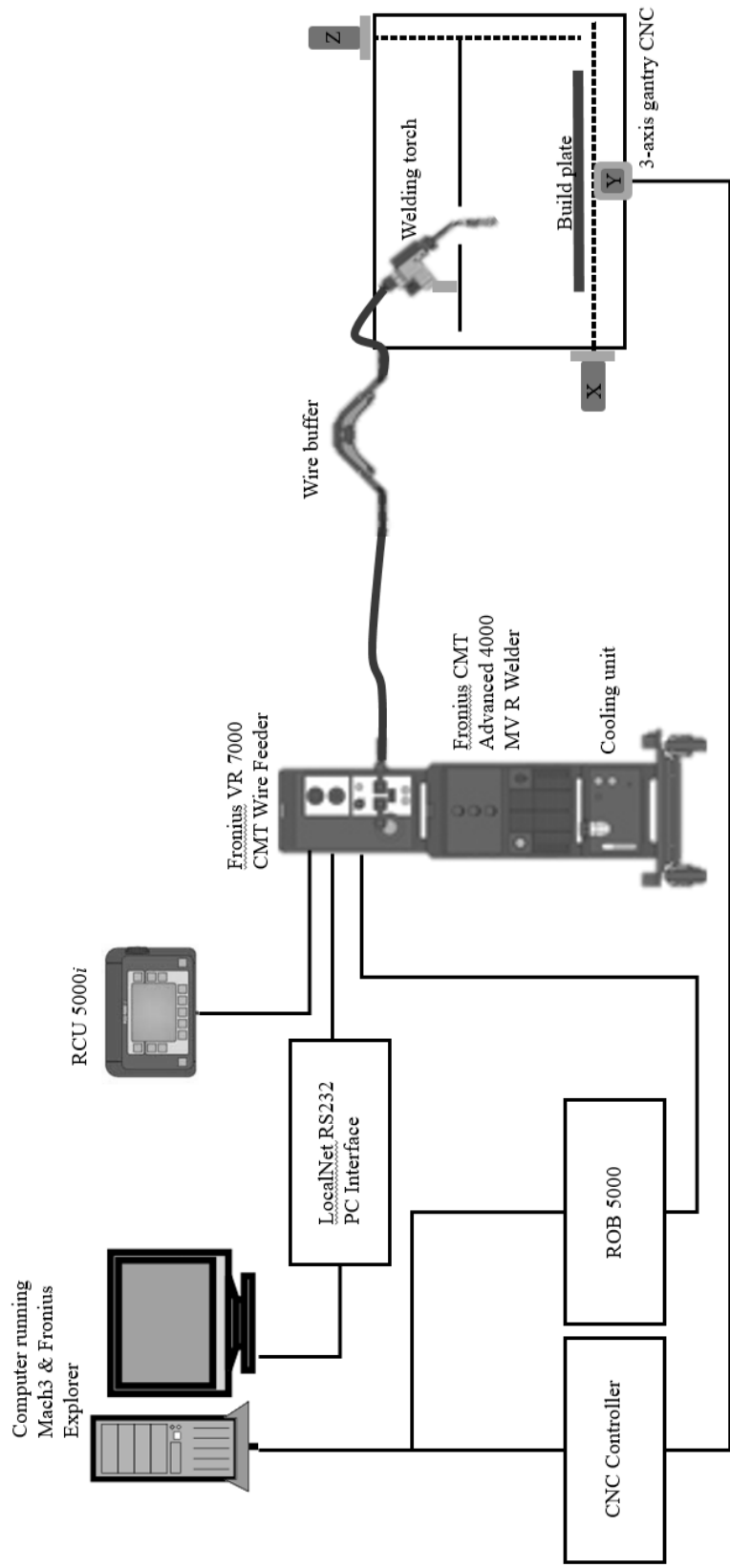


Figure 66: Fronius Welder Interface.

## **Instruments**

The following equipment was used in this research to prepare or test specimens and create any custom fixtures or tooling required. The material testing equipment used to obtain the material properties of the final specimens is included in this section. Software used for design and post processing of data is also listed.

- Cincinnati Arrow VMC-750 CNC Mill
- Bridgeport Series I 2 HP Vertical Milling Machine
- Southbend 450 Lathe
- Do All 2013-V Vertical Band Saw
- Wellsaw 1118 Horizontal Band Saw
- Wilton Belt Sander
- Model HR-150 Rockwell Hardness Tester
- MTS Q-Test 100 Tensile Tester
- Keyence VHX 1000 E 3D Microscope
- Dassault Systems Solidworks Modeling Software
- Autodesk HSMWorks CAM Software
- Mathworks MatLab 2016b
- Microsoft Excel 2016
- Microsoft Word 2016
- Minitab 17 Statistical Analysis Software
- Slic3r Slicing Software
- MTS/661.20H-03 Tensile Tester
- Mitutoyo 6" Dial Calipers 505-675

- Omega Universal Temperature Process Controller CN245

The Cincinnati CNC milling machine shown in Figure 67 was used to machine the tensile samples from each sample as well as prepare fixtures, jigs, and components for/of the machine. G-code was generated on a separate PC and then loaded via USB stick onto the CNC machine.



Figure 67: Cincinnati CNC

The Bridgeport milling machine shown in Figure 68 below was used to create machine components as well as prepare fixtures/jigs.



Figure 68: Bridgeport Series I 2 HP Vertical Milling Machine

The Southbend 450 lathe, Figure 69 below, was used to create machine components as well as prepare fixtures/jigs/specimen.



Figure 69: Southbend 450 Lathe.

The vertical band saw seen in Figure 70 (left) was used to rough cut machine components and fixtures/jigs. The horizontal band saw seen in Figure 70 (right) was used to separate the specimens from the build plates, as well as rough cut machine components and fixtures/jigs.



Figure 70: Do All 2013-V Vertical Band Saw (L) Wellsaw 1118 Horizontal Band Saw (R)

The belt sander, shown in Figure 71, was used to for various purposes including the removal of burrs from specimens generated during the machining process. The belt sander was also used for initial sanding of the samples after coming out of the mill.



Figure 71: Wilton Belt Sander.

Figure 72 shows the HR-150A Rockwell hardness tester used to test the samples. The appropriate tip was placed in the tester for a Rockwell B test. The screw handle was turned to raise the sample to be tested into the testing tip. The lever on the side is then pulled which applies the load required for the test. Once the load has been fully applied another lever is pulled which removes the initial force and the resulting hardness value is shown on the dial on the front of the machine. Accuracy and repeatability of the tester is  $\pm 2$  Rockwell.



Figure 72: Model HR-150 Rockwell Hardness Tester

The MTS Q-Test 100 tensile testing machine used can be seen in Figure 73. The tensile testing machine moves at a constant displacement rate and records the forces applied to the load cell. The jaws used for the tensile testing of the metal samples were of the screw clamping type. A screw collar is tightened which clamps down on the piece. The jaws are designed so that as the pulling force increases the clamping force does as well.

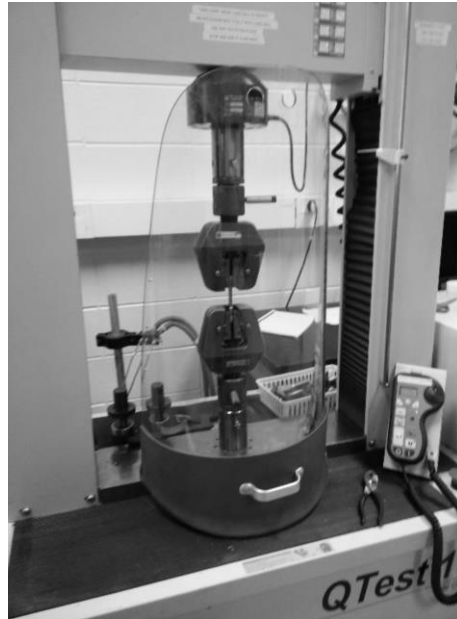


Figure 73: MTS Q-Test 100

A Keyence VHX 1000 E 3D microscope, shown in Figure 74, was used in the study of weld specimen microstructure. It is a two-stage microscope with the first stage having a magnification range of 100x to 1000x and the second stage magnification range of 500x to 5000x. The resolution of this microscope is +/- 0.05 microns and a repeatability of +/- 0.5 microns.





Figure 74: Keyence VHX 1000 E 3D microscope

An MTS Landmark Servohydraulic load frame Model 370.10, shown in Figure 75, was used for tensile testing. The tensile testing machine moves at a constant displacement rate and records the forces applied to the load cell. Featuring a high-resolution force transducer with a range of 100 kN (22 kip), the MTS Landmark provides highly accurate force measurements with a maximum error in tension of 0.05 % of the load. The jaws used for the tensile testing of the metal samples are hydraulically actuated grips. When combined with precision alignment fixtures the machine delivers tightly controlled and constant zero specimen loading [58, 59].



Figure 75: MTS Landmark Servo Hydraulic Load Frame

Mitutoyo dial calipers, as shown in Figure 76, were used to measure specimen before and after tensile testing. They have an accuracy of  $\pm 0.001$  inches.

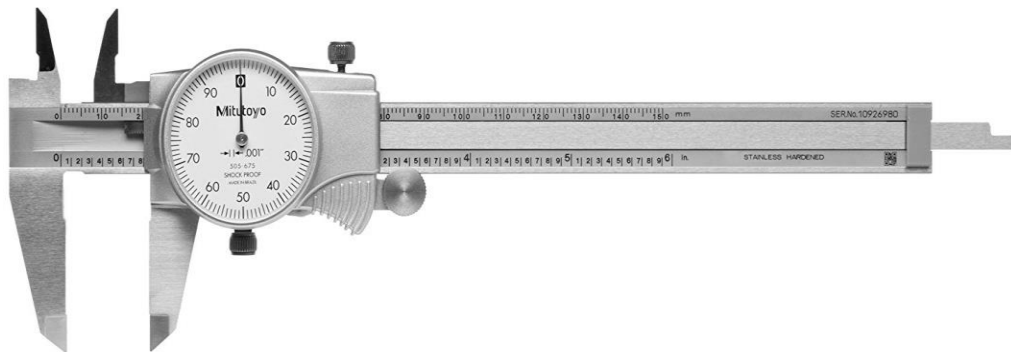


Figure 76: Mitutoyo 6" Dial Calipers Model Number 505-675

Omega's universal temperature process controller (Model CN245) was used to monitor temperatures during the WAAM process and send signals to the Modbus for control purposes. The unit has RS485 capabilities for future communication possibilities.

The unit has a wide range of voltage inputs, so it is adaptable to future modifications to the system. Its accuracy is  $\pm 0.5^{\circ}\text{C}$  or 0.2% of the reading. The unit is also capable of using many different temperature inputs. Currently a K-type thermocouple is used; however, for future purposes it is capable of utilizing: K, J, S, or R-thermocouples; Pt100, Pt500, Pt1000, or Ni100 RTDs; PTC 1K, NTC 10L, or NTC 2252 $\Omega$  thermistors. For output, the unit has two resistive relays and a DC 12V pulse. As shown in Figure 77 the unit has simple operator inputs for easy programming by future users/researchers [60].



Figure 77: Omega Universal Temperature Process Controller CN245

## Materials

The materials chosen for this experiment are listed below in Tables 6 and 7 documenting the material properties.

ER308L [61]:

- Stainless steel consumable
- Westward 0.045” diameter 30lb spool
- Balanced chromium and nickel levels provide enough ferrite in the weld for high resistance to hot cracking
- Dual classification ensures the maximum carbon content is 0.03%
- 0.03% carbon content increases resistance to intergranular corrosion

Table 6: ER308L filler material properties

<b>ER308/308L Wire Properties and Chemistry</b>				
Tensile Strength (As Deposited)				87,000 psi
Yield Strength (As Deposited)				57,000 psi
Shielding Gas (% Ar / % CO <sub>2</sub> )				98% / 2%
% C	% Cr	% Ni	% Mo	% Mn
0.08 Max	19.5-22	9.0-11.0	0.75 Max	1.0-2.5
% Si	% P	% S	% Cu	
0.3-0.65	0.03 Max	0.03 Max	0.75 Max	

ER70S-6 [62]:

- Mild steel consumable
- National Standard 0.045” diameter NS-115 Copperfree [63]
- High levels of manganese and silicon deoxidizers tolerate medium to heavy mill scale surfaces
- More puddle fluidity due to higher silicon content (lower surface tension)

- Excellent wetting action

Table 7: ER70S-6 filler material properties [National Standard]

<b>ER70S-6 Wire Properties and Chemistry</b>				
Tensile Strength (As Deposited)				70,000 psi
Yield Strength (As Deposited)				58,000 psi
Shielding Gas (% Ar / % CO <sub>2</sub> )				90% / 10%
% C	% Mn	% S	% Si	% P
0.09	1.52	0.011	0.91	0.012
% Cu	% Cr	% Ni	% Mo	% V
0.07	0.06	0.06	0.01	0.01

## **V. Methodology and Statistical Design of Experiments**

The methodology for the design and testing of CMT-GMAW WAAM specimen and control evaluation based on mechanical testing and microstructural examination is proposed in the following sections.

### **Tensile Strength Evaluation**

Tensile test specimens are to be created using ER70S-6 and ER308L filler wire at 0.045 inches. To determine the validity of the data collected from the machine for experimentation, a repeatability study is required. As with the research performed previously on Auburn's WAAM machine, four walls are to be produced per material and dog bones are to be machined out of the walls parallel and perpendicular to the deposited layers (2 walls per direction). Six samples are to be produced per wall, giving a total of 24 tensile samples per material to study. The tensile test specimens are to be created according to the ASTM E8 standard which dictates a specimen with a gauge length of  $1.000 \pm 0.003$  inches, a neck width of  $0.250 \pm 0.005$  inches, and a thickness of  $0.250 \pm 0.005$  inches, as shown in Figure 78 [55]. After machining, the samples will be sanded and polished using the following schedule: 80-grit, followed by 120, 180, 240, 320, 400, 500, 600, 800, 1000, 1200, then polished with Mother's MAG and Aluminum Metal Polish. Prior to pulling the specimens, the precise dimensions of the tensile test bars are to be verified and recorded using Mitutoyo calipers. The pull rate for the tensile test is to be 0.15 ipm.

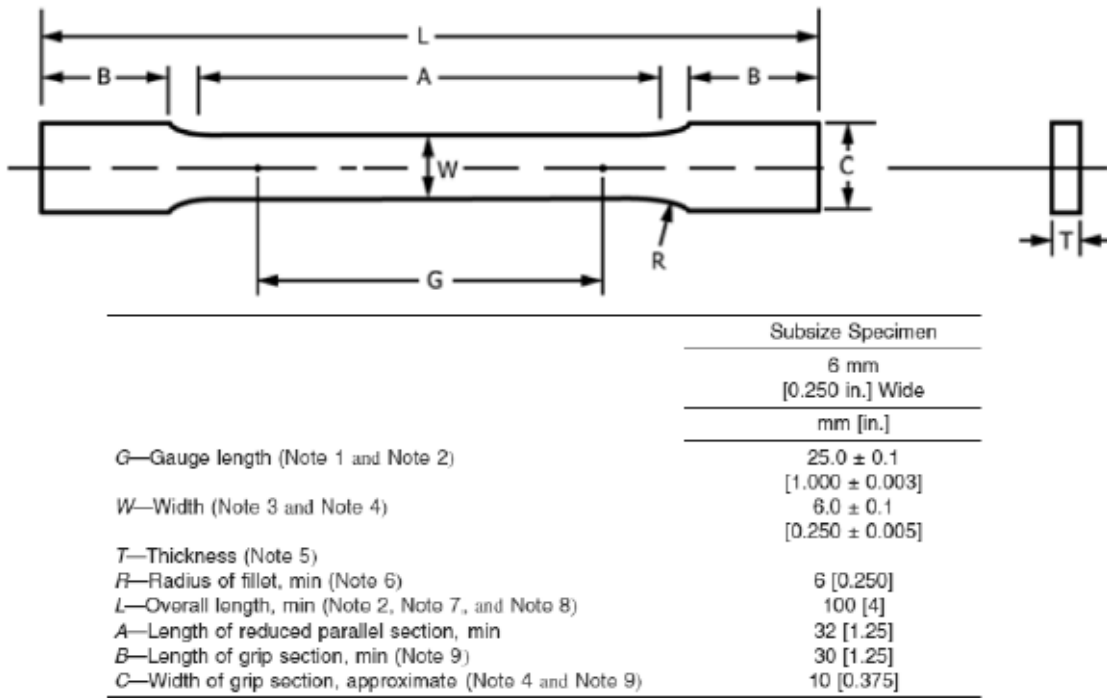


Figure 78: ASTM E8 Subsize Tensile Testing Standard [55]

Appropriate t-tests (paired or unpaired) are to be performed to compare the results of each wall to itself (outer samples to the inner sample or the top layer samples to the bottom), as well as to compare each wall to each other (wall one to wall two). For each t-test performed the null hypothesis will be that the mean difference between samples tested is equal to zero; while the alternative hypothesis is that they are not equal to zero. A confidence of 95% is to be used, giving an alpha of 0.05. If the p-values produced are above 0.05 the tests have failed to reject the null hypothesis. This means that the samples in that test are statistically equal with 95% confidence. If the results of the study show that two identical walls are statistically the same, then further research shall commence. Otherwise, if the study shows that two identically produced walls are not statistically the same in tension then things must be adjusted to get useable data for research. This was not

performed in past research and the results of past research show inconsistent tensile data that possibly could have been prevented had this not been overlooked.

For the repeatability study, the synergic line from Fronius is to be selected accordingly to the material. For ER70S-6, per Fronius' recommendations, a wire feed speed of 90 inches per minute (ipm), burnback correction of -0.5 seconds, arc length correction of -15%, dynamic correction of 1.2%, crater fill for 0.7 seconds at 45% current, with a gas composition of 90% argon and 10% carbon dioxide at 25.4 cubic feet per hour (CFH) is to be used at a travel speed of 29.5 ipm. The geometry produced is to be a wall that is 8 mm wide, 120 mm long, 111 mm tall. Per Fronius' recommendation a weave pattern is to be used in a zig zag profile with a wavelength of 2.5 mm and an amplitude of half the width with a 0.2 second pause at each peak and a layer height of 2.4 mm. On the subsequent pass (next layer) a phase shift is utilized equal to one period to try to cross-hatch the deposition for better heat input. All while a one-minute pause between layers is utilized to allow the part to not receive excess heat.

Table 8 below shows the results of the tensile tests for specimen produced perpendicular to the deposition layers. The samples are listed left to right of the wall as shown in Figure 79. Table 9 shows the results of each t-test for ultimate tensile strength (UTS) and yield strength. The p-values are all above 0.05 and therefore the tensile tests for ER70S-6 are all statistically repeatable with 95% confidence and further research can be implemented with this machine for this material.



Table 8: ER70S-6 Repeatability Perpendicular Tensile Results

<b>Perpendicular</b>	<b>Wall 1</b>	<b>Wall 2</b>	<b>Wall 1</b>	<b>Wall 2</b>
<b>Sample</b>	<b>UTS (psi)</b>	<b>UTS (psi)</b>	<b>Yield (psi)</b>	<b>Yield (psi)</b>
1	67898	67198	51801	51712
2	67507	67484	57237	53355
3	67938	67829	54569	54366
4	68099	67915	52908	53357
5	68227	67681	52382	52655
6	67731	67432	51115	47599

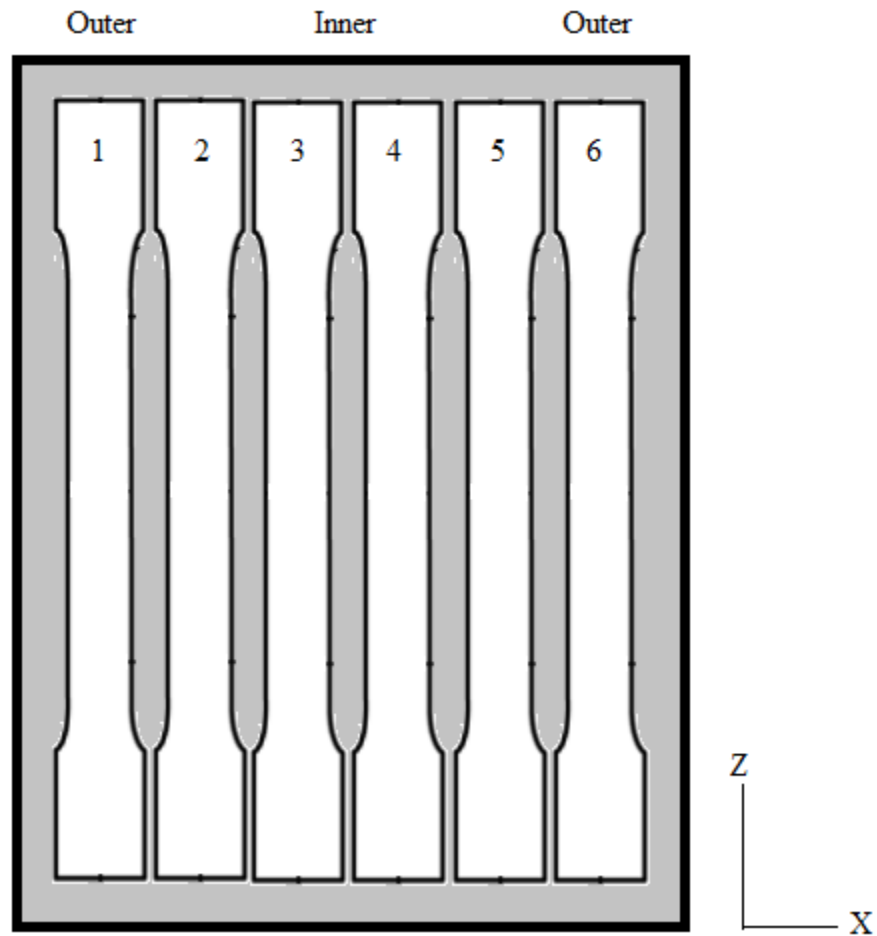


Figure 79: Test Orientation for Samples Produced Perpendicular to Deposition

Table 9: ER70S-6 Perpendicular Repeatability T-Test Results

<b>Perpendicular</b>		
<b>Test</b>	<b>Measurable</b>	<b>P-Value</b>
Wall 1 Outer to Inner	UTS	0.430
Wall 2 Outer to Inner	UTS	0.084
Wall 1 to Wall 2	UTS	0.068
Wall 1 Outer to Inner	Yield Strength	0.134
Wall 2 Outer to Inner	Yield Strength	0.225
Wall 1 to Wall 2	Yield Strength	0.407

Table 10 below shows the results of the tensile tests for specimen produced parallel to the deposition layers. The samples are listed top to bottom of the wall as shown in Figure 80. Table 11 shows the results of each t-test for ultimate tensile strength (UTS) and yield strength. The p-values are all above 0.05 and therefore the tensile tests for ER70S-6 are all statistically repeatable with 95% confidence and further research can be implemented with this machine for this material.

Table 10: ER70S-6 Repeatability Parallel Tensile Results

<b>Parallel</b>	<b>Wall 1</b>	<b>Wall 2</b>	<b>Wall 1</b>	<b>Wall 2</b>
<b>Sample</b>	<b>UTS (psi)</b>	<b>UTS (psi)</b>	<b>Yield (psi)</b>	<b>Yield (psi)</b>
1	69881	69297	57052	48327
2	68739	68285	49444	50805
3	68499	68582	50706	50679
4	68272	68645	50795	50524
5	69941	69626	50999	51831
6	71230	70493	51871	51229

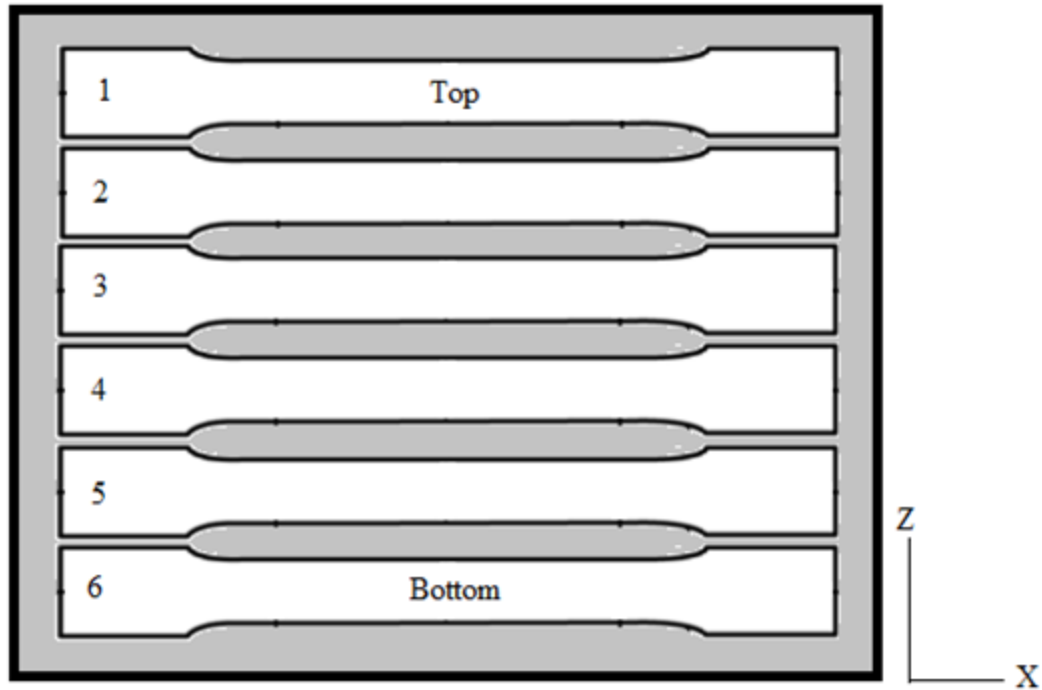


Figure 80: Test Orientation for Samples Produced Parallel to Deposition

Table 11: ER70S-6 Parallel Repeatability T-Test Results

Parallel		
Test	Measurable	P-Value
Wall 1 Top to Bottom	UTS	0.485
Wall 2 Top to Bottom	UTS	0.406
Wall 1 to Wall 2	UTS	0.643
Wall 1 Top to Bottom	Yield Strength	0.743
Wall 2 Top to Bottom	Yield Strength	0.424
Wall 1 to Wall 2	Yield Strength	0.323

To compare the parallel and perpendicularly produced samples, t-tests are to be performed comparing the walls. Table 12 shows the results of these t-tests. The p-value is above 0.05 for yield strength; however, it is below 0.05 for ultimate tensile strength. This means that walls produced in ER70S-6 have statistically the same yield strength regardless of orientation; however, they do have different UTS and therefore both

orientations must be studied as separate independent factors for UTS. When looking at the means of the populations compared to the manufacturer’s specifications; the parallelly and perpendicularly produced walls are 99% and 97% of the manufacturer’s UTS spec respectively. For yield strength, the parallelly and perpendicularly produced walls are 90% of the spec (listed as one value since statistically the same). While not the manufacturer’s specs, these values are an improvement on previous research in value and/or repeatability. This study is not to try and meet or exceed the manufacturer’s spec, just simply to compare to identically produced parts to each other and it is considered ok to not meet the spec at this point.

Table 12: Parallel Vs Perpendicular T-Test Results

<b>Parallel Vs Perpendicular</b>		
<b>Test</b>	<b>Measurable</b>	<b>P-Value</b>
Parallel to Perpendicular	UTS	0.00002
Parallel to Perpendicular	Yield Strength	0.094

Now that there is known information about the material and how repeatable it is; a power analysis is to be performed to determine the minimum number of samples to be taken to detect an effect with 95% confidence. This will be completed using Equation 3 below. Here  $n$  is the sample size,  $z$  is the z-score (equals 1.959964, based on 95% confidence),  $\sigma$  is the standard deviation of the population, and  $E$  is the margin of error. The standard deviations of the groups are presented below in Table 13. Once completed the power analysis shows to be within one standard deviation of the population that 3.8414 samples are to be taken for UTS and yield strength specimen produced both in parallel and perpendicular orientations. Since .84 samples cannot be taken, we round up to the nearest whole number of four samples. Therefore, for tensile tests in ER70S-6, samples are to be

produced parallel and perpendicular to deposition with four samples each. One thing to note is for all the tensile tests, the specimens failed ductility with typical cup-and-cone fracture.

$$\eta = \left(\frac{z\sigma}{E}\right)^2 \quad \text{Equation 3}$$

Table 13: Tensile Standard Deviations ( $\sigma$ )

Test	$\sigma$ (psi)
Perpendicular UTS	299
Parallel UTS	953
Yield Strength	2290

### Hardness Evaluation

Hardness tests are to be performed on ER70S-6 and ER308L samples using the Rockwell Scale due to the availability of the equipment. To determine the validity of the data collected from the machine for experimentation, a repeatability study is performed. As with the research performed previously on Auburn’s WAAM machine, four walls are to be produced per material and dog bones are to be machined out of the walls parallel and perpendicular to the deposited layers (2 walls per direction). Six samples are to be produced per wall, giving a total of 24 tensile samples per material to study. The hardness tests will be performed in the grip regions of these tensile specimen to save time, material, and to directly compare hardness to tensile data from the same sample. Two hardness tests will be performed on each end of the tensile specimens’ grip region.

Table 14 below shows the results of the hardness tests for specimens produced perpendicular to the deposition layers. The samples are listed left to right of the wall (sample 3 and 4 being the middle of the wall). Table 15 shows the results of each t-test for

hardness. The p-values are all above 0.05 and therefore the hardness tests for ER70S-6 are all statistically repeatable with 95% confidence and further research can be implemented with this machine for this material.

Table 14: ER70S-6 Repeatability Perpendicular Hardness Results Rockwell B

Perpendicular Sample	Wall 1		Wall 1		Wall 2		Wall 2	
	Top of Wall	Bottom of Wall	Top of Wall	Bottom of Wall	Top of Wall	Bottom of Wall	Top of Wall	Bottom of Wall
1	77.5	77.5	75.5	76	77.5	77	75	77
2	76	77	76	76.5	76.5	77	74.5	75
3	74.5	77.5	75	77	76	76	74	74
4	77.5	76	77	76.5	76.5	77.5	77	77
5	77.5	77.5	75.5	77	76.5	75.5	76	77
6	78	76	75	78	76.5	77	77	76

Table 15: ER70S-6 Perpendicular Repeatability T-Test Results

Perpendicular	
Test	P-Value
Wall 1 Top to Bottom Averages	0.087
Wall 2 Top to Bottom Averages	0.114
Wall 1 Outer to Inner Averages	0.496
Wall 2 Outer to Inner Averages	0.439
Wall 1 Top to Wall 2 Top	0.475
Wall 1 Bottom to Wall 2 Bottom	0.313
Wall 1 to Wall 2	0.236

Table 16 below shows the results of the hardness tests for specimen produced parallel to the deposition layers. The samples are listed top to bottom of the wall (sample 3 and 4 being the middle of the wall). Table 17 shows the results of each t-test for hardness. The p-values are all above 0.05 and therefore the hardness tests for ER70S-6 are all statistically repeatable with 95% confidence and further research can be implemented with this machine for this material.

Table 16: ER70S-6 Repeatability Parallel Hardness Results Rockwell B

Perpendicular Sample	Wall 1		Wall 1		Wall 2		Wall 2	
	Left of Wall		Right of Wall		Left of Wall		Right of Wall	
1	77	77	76	76.5	74.5	75	77.5	77.5
2	75.5	75.5	75	76	75.5	76.5	75.5	75.5
3	75.5	75	76	75.5	74.5	75.5	75	75
4	75.5	75	77	75.5	75.5	76	74.5	76
5	77	75.5	76	75.5	74.5	76.5	75.5	76.5
6	76.5	76	75	76.75	77	77.5	76	76

Table 17: ER70S-6 Parallel Repeatability T-Test Results

Parallel	
Test	P-Value
Wall 1 Left to Right	0.936
Wall 2 Left to Right	0.689
Wall 1 Top to Bottom	0.920
Wall 2 Top to Bottom	0.582
Wall 1 Top to Wall 2 Top	0.795
Wall 1 Bottom to Wall 2 Bottom	0.707
Wall 1 to Wall 2	0.635

Since the hardness values are independent of deposition direction, parallel and perpendicular is not to be compared; however, the location of the measurement is to be compared (top, bottom). To compare the hardness values of produced samples, t-tests are to be performed comparing the average hardness values of the walls. Table 18 shows the results of these t-tests. The p-values are above 0.05 and therefore the hardness tests for ER70S-6 are statistically the same with 95% confidence in both locations and further research can be implemented with this machine for this material.

Table 18: Average Hardness T-Test Results

<b>Perpendicular Wall 1, 2 Vs. Parallel Wall 1, 2</b>	
<b>Test</b>	<b>P-Value</b>
Perpendicular Walls' Top to Parallel Walls' Top	0.031
Perpendicular Walls' Bottom to Parallel Walls' Bottom	0.797
Perpendicular and Parallel Top to Bottom	0.107

Now that there is known information about the material and how repeatable it is; a power analysis is to be performed to determine the minimum number of samples to be taken to detect an effect with 95% confidence. This will be completed using Equation 3 **Error! Reference source not found.** again. The standard deviations of the groups are presented below in Table 19. Once completed the power analysis shows to be within one standard deviation of the population that 3.8414 samples are to be taken for hardness specimen produced. Since .84 samples cannot be taken, we round up to the nearest whole number of four samples. Therefore, for hardness tests in ER70S-6, four samples are to be taken per factor level. Since four tensile specimens also are to be produced and to make research simpler; one hardness will be performed in the grip region of each tensile sample (double the amount required).

Table 19: Hardness Tests Standard Deviations ( $\sigma$ )

<b>Location</b>	<b><math>\sigma</math> (Rockwell B)</b>
Top of Walls	0.781
Bottom of Walls	0.726
All Samples	0.770

### **Macrostructure & Microstructure Evaluation**

Once a wall is complete, test specimens are to be cut out for tensile tests. The parts will undergo visual inspection during the milling/sanding process to identify large defects, if any. The metallurgical details of the deposited materials are to be examined using an optical microscope. The samples to be examined are to be cut from the walls manufactured for the tensile/hardness test specimens. Samples are to be selected in the



top, middle, and bottom of a wall and at the interface between layers to get a representative view of the deposited material. The samples are to be polished, using the same schedule as for the tensile samples, and etched for 90 seconds with the appropriate solution per material per the ASTM E 407 guidelines [64]. 3% Nital etchant mixed as shown below in Table 20 is to be used for the ER70S-6 samples. Kroll's Reagent etchant mixed as shown in

Table 21 is to be used for the ER308L samples. Any leftover etchant is to be properly disposed of after a maximum of one week from manufacture. Storage of the etchant is to be in an appropriate non-reactive plastic container. The samples are then to be examined under an optical microscope and the grain structure evaluated. Images of the microstructure are to be taken and examined to study interlayer bonding, grain structure, and the effect of heat throughout the 'print.'

Table 20: Mixing Solution for %3 Nital Etchant, ASTM No. 74a

3% Nital Etchant Solution	
Nitric Acid	Ethanol
HNO <sub>3</sub>	C <sub>2</sub> H <sub>6</sub> O
3 mL	97 mL

Table 21: Mixing Solution for Kroll's Reagent Etchant, ASTM No. 88

Etchant Solution		
Hydrochloric Acid	Nitric Acid	Water
HCl	HNO <sub>3</sub>	H <sub>2</sub> O
20 mL	10 mL	30 mL

### Wire Offset Distance Control

Before one can discuss the controls schemes to alleviate the issues of inconsistent wire offset distance, the types of systematic errors that exist due to this must be discussed.

There are two types of systematic error that occur during the WAAM process that are related to the wire offset distance; offset error, scale error. Random error, or unsystematic error, can also occur in the WAAM process.

Offset error is where initialization protocols are not met and there is an error that is carried out throughout the process. This is related to the WAAM process via wire offset distance through the machine not properly being zeroed on the build plate at the start of a 'print,' or the proper amount of wire is not feed out of the nozzle before the zeroing process is initialized. This error is entirely due to operator error in the case of WAAM and can be avoided if protocols are followed. To follow said protocols, one must ensure that a proper zero is set based off the origin of the part being created.

Scale error is where values are recorded proportional to the true measurement. This is related to the WAAM process via wire offset distance through compounding error due to improper layer step-up distance. This is where the program is designed to create layers at a certain height and step up in increments of that height every layer; however, the layers created are actually a different size and a compounding error is created as the part is 'printed.' This compounding error can greatly offset the part to the point of having to cease production and start over. A control scheme is to be developed and evaluated to eliminate or alleviate the WAAM scale error.

Random error is exactly as the title states. Random error occurs randomly throughout a process for unknown or unforeseen reasons, thus is hard/to impossible to predict and/or prevent. This is related to the WAAM process via wire offset distance through issues that may occur due to slip in the feed gears causing the wire stick out to be offset, slumping in the geometry due to various reasons causing layer heights to be offset,

and many more unpredictable reasons. Due to the literally ‘random’ nature of random error, a control scheme to alleviate this type of error will not be looked at in this research experiment. If random errors do occur during the WAAM process, proper procedures would be to take an average of the data or increase the sample size of the data. If the data point can be proven to be a statistical outlier, then that data point can be eliminated. Good engineering discretion should be utilized by the operators in this event to maintain sound research data or adequate part quality depending on the issue.

One of the biggest issues in practically all additive process is maintaining the layer heights. Having the head of the machine maintain the appropriate distance from the last layer is increasingly difficult when the layer heights change constantly due to various issues. A control scheme to maintain the offset distance throughout the ‘print’ is thought to be a key aspect in the WAAM process’ success by multiple researchers. Fronius recommends a wire offset distance of 14 mm (0.551 inches) be maintained. Having the WAAM machine constantly maintain this distance regardless of variations in layer height would essentially eliminate scale error. By creating a m-code to maintain the distance, the WAAM machine has the capability to do exactly this. Since the welder stops welding after every layer via a m-code (M110, weld stop), this would be an opportune time to check the wire offset distance and see if the layer deposited was created to the spec programmed. By compensating for variations every layer, the compounding scale error is essentially eliminated thus leading to better and easier to produce parts.

An experiment is planned to test the development, as well as advantage, of a wire offset control scheme. If the control scheme proves to overcomplicate the process, while not providing statistically beneficial properties (strength, time savings, etc.), the control

scheme should not be utilized. After a control scheme is created, it is to be tested against not using the protocol. Evaluation of the protocol is to be based on the materials' UTS, yield strength, hardness, as well micro and macrostructure. Walls are to be produced in both ER70S-6 and ER308L where tensile specimen are to be manufactured in both the parallel and perpendicular directions to deposition. Table 22 shows the proposed data to be collected and compared. There are to be two walls per material (parallel and perpendicular) for both with and without the control scheme utilized. This accounts for four walls per material in total. Since the wire offset distance is to be maintained at a set value according to Fronius, different offset distances are not to be varied on purpose. For the tests without control, the user will manually try to maintain the wire offset distance every layer as in past research.

Table 22: Wire Offset Distance Control Scheme Combinations

Materials:	ER70S-6, ER308L
Directions of Test:	Parallel, Perpendicular to Deposition
Control Schemes:	With, Without Offset Control
Measurables (Quantitative/Qualitative):	Ultimate Tensile Strength, Yield Strength, Hardness, Microstructure, Macrostructure, Time Spent to Produce Part

### **Wire Feed Speed/Voltage/Current Control**

Originally, researchers maintained wire feed speed, voltage, and/or current (WFS/V/C) manually throughout the WAAM process. Most of these researchers noted difficulty in controlling the process, as the three are related and having them controlled independently leads to excessive trial and error. Later in the '90s, the synergic welding

control scheme was introduced and utilized in the WAAM process. The synergic control greatly improved the reliability, repeatability, and ease of use in the process for the researchers.

“In the synergic control system, the current pulse parameters are automatically generated by an electronic control unit or a computer system for a given wire feed rate, based on predetermined parametric relationships. The parametric relationships relate the four pulse parameters to wire feed rate for a stable welding operation. A square waveform of current is normally desired since with this wave-form the amplitude of the current can be exactly controlled. To obtain a stable pulsed current welding process there are three essential criteria that must be satisfied:

1. *Burn-off Criterion*: The wire feed rate must be matched by the burn-off rate of the wire to keep a constant arc length.
2. *Metal Transfer Criterion*: The metal must be transferred in a spray mode and controlled by the current pulse.
3. *Arc Stability Criterion*: The welding arc must be stable during the background current duration” [47].

For the Fronius CMT welding process, a synergic line is utilized with presets for various materials, wire diameters, and gas compositions. Previous research studied many parameters that factor into the system. However, the Fronius CMT process controls many of these factors in closed-loop system and/or are set by the material selection and wire diameter. Figure 54, from the literature review, is a flow chart showing that once an operator selects a material and the appropriate wire diameter based on the feed rollers in use, many parameters are set based on these choices.

Since the CMT process is a closed-loop control method, an experiment is purposed not to create a control scheme, but to evaluate the control scheme already created via the CMT process. If the control scheme proves to overcomplicate the process, while not providing statistically beneficial properties (strength, time savings, etc.), the control scheme should not be utilized. The CMT process is to be tested against not using the protocol (CC/CV, standard mode), as well as against original research data from Gaddes. Evaluation of the protocol is to be based on the materials' UTS, yield strength, hardness, as well micro and macrostructure. Walls are to be produced in both ER70S-6 and ER308L where tensile specimen are to be manufactured in both the parallel and perpendicular directions to deposition. Table 23 shows the proposed data to be collected and compared. There are to be two walls per material (parallel and perpendicular) with and without the CMT control scheme utilized. This accounts for four walls per material in total. The results will also be cross referenced and compared to the results from Gaddes' research which also used a standard CC/CV synergic control scheme, but with a different machine (Miller instead of Fronius).

Table 23: WFS/Voltage/Current Control Scheme Combinations

Materials:	ER70S-6, ER308L
Directions of Test:	Parallel, Perpendicular to Deposition
Control Schemes:	Fronius CMT, Fronius Standard Mode, Original Data from Gaddes' Research
Measurables (Quantitative/Qualitative):	Ultimate Tensile Strength, Yield Strength, Hardness, Microstructure, Macrostructure, Time Spent to Produce Part

## Temperature Control

Material properties of the ‘printed’ part are highly reliant upon the temperatures the part is exposed to and the duration it is exposed to those temperatures throughout the WAAM process, much like with many other manufacturing processes. As with the weld quality control noted by Xie, the WAAM temperatures of interest can be broken into three groups: before, during, and post weld. According to Funderburk, for build plates less than 1 inch, a preheat is not required before the weld [50]. Since the build plates for the WAAM process are much smaller than 1 inch, a preheat will not be considered; unless the presence of cracking or hydrogen precipitation issues occur.

For post weld, heat treatment is the typical solution to improve mechanical properties of a part. Typical goals of a post weld heat treatment (PWHT) are to reduce hardness, relax residual stresses, and/or to increase resistance to brittle fracture. During the repeatability study, it was noted that the materials failed in a very ductile manner. It was also noted that the hardness values maintained a nice correlation to the tensile strengths of the materials as is typical with commercial metals. Due to these facts, PWHT will not be considered for the reduction of hardness or brittle fracture. The material’s manufacturers list PWHT schedule for the materials as well as expected properties in doing so. For residual stresses, if it is noted that high amounts of warpage occur during the process, or if the material properties indicate undesirable results (when compared to manufacturer specs) then a PWHT is to be investigated.

For the during weld category of the WAAM process, the main concern is the reheating of previous layers by the layer being deposited. This interpass temperature, as it known, is the main area of concern. According to Funderburk and the American Welding

Society, the toughness and grain structure are negatively affected after interpass temperatures exceed 500°F (260°C) and should not exceed 550°F (290°C) [50].

An experiment is planned to maintain the parts' mechanical properties via interpass temperature. A temperature monitoring system will be used to monitor the parts' temperature and send a signal to pause production if temperatures exceed a set point. The system is to constantly measure temperature in a closed-loop system and send feedback to the computer. The temperature measuring device is to be a K-type thermocouple due to availability, ease of use, and the temperature ranges expected. The temperature set point will be 500°F initially (as according to literature), then will be varied 50° above and below the initial setpoint to test the sensitivity of the process temperature for steel. For stainless, literature states a set point of 150°C but little else is mentioned. Therefore, the other setpoints are to be at 260°C (initial point for steel) and 205°C (in between the two). Table 24 shows the proposed data to be collected and compared. There are to be two walls per material (parallel and perpendicular) for both with and without the control scheme utilized. As well as three set points within the group for with the control scheme. This accounts for eight total walls per material to be produced and studied. If the control scheme proves to overcomplicate the process, while not providing statistically beneficial properties (strength, time savings, etc.), the control scheme should not be utilized. For placement of the thermocouple, according to literature, the probe should be placed 1-3 inches from the weld pool. Since the weld pool is moving in all three axes throughout the process, it is noted that the probe will need to be maintained at this distance throughout; however, not necessarily follow the weld pool. Figure 81-84 show the locations for the thermocouple probe to be positioned to maintain the 3-inch (76.2 mm) distance from the weld pool. This



considers the diameter of the probe as well as the trigonometric relationship between the probe and the max distance the weld pool will travel during a 100 mm tall print.

Table 24: Temperature Control Scheme Combinations

Materials:	ER70S-6, ER308L
Directions of Test:	Parallel, Perpendicular to Deposition
Control Schemes:	With and Without Temperature Monitoring System
Control Set Points:	500°F (260°C), 550°F (288°C), 450°F (232°C) [Steel]/ 302°F (150°C), 401°F (205°C), 500°F (260°C) [Stainless]
Measurables (Quantitative/Qualitative):	Ultimate Tensile Strength, Yield Strength, Hardness, Microstructure, Macrostructure, Time Spent to Produce Part

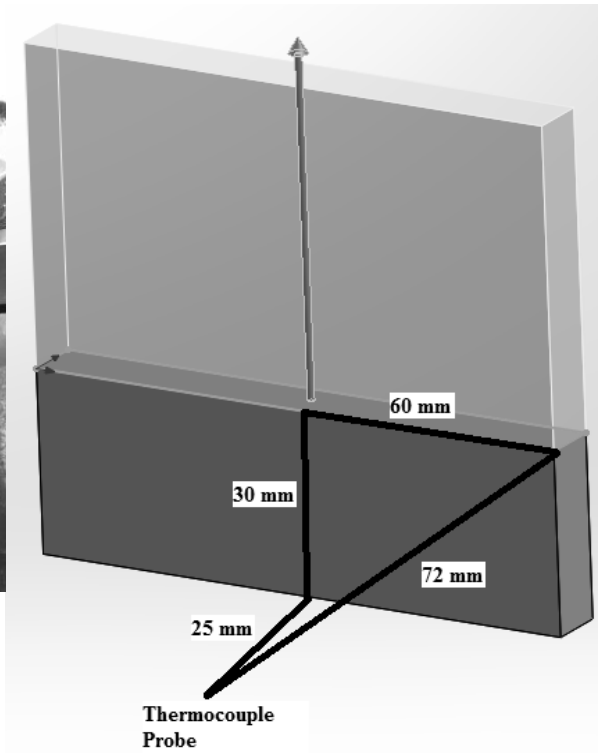


Figure 81: Initial Thermocouple Position in Relation to Printed Wall

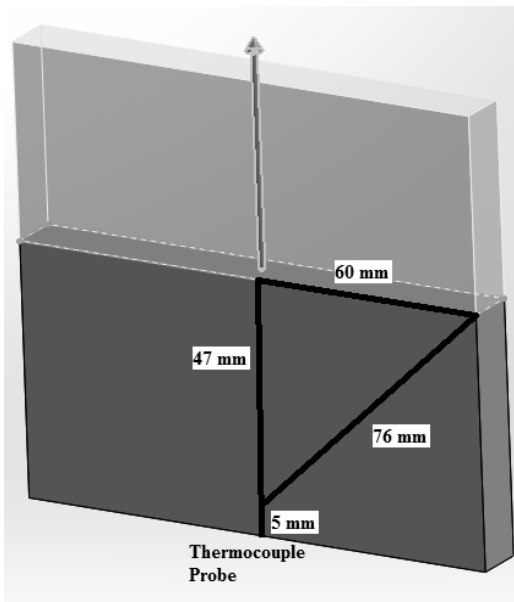


Figure 82: Second Thermocouple Position to Maintain Proper Distance

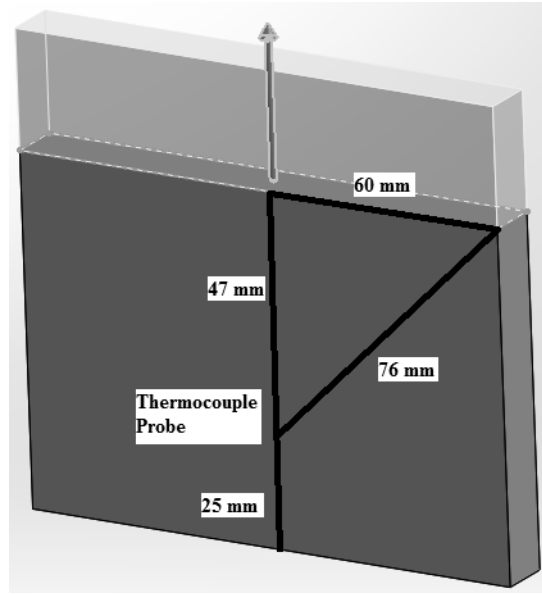
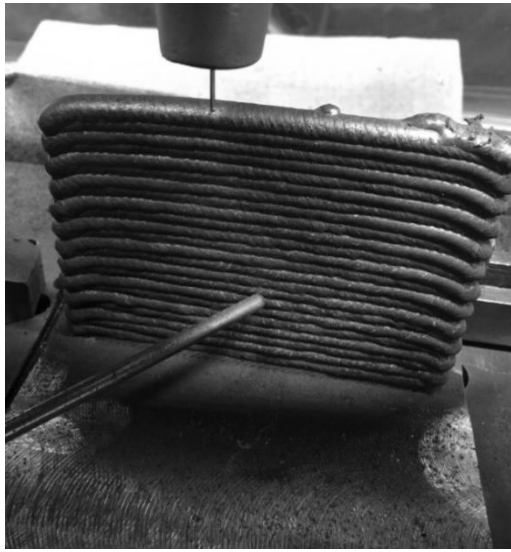


Figure 83: Third Thermocouple Position to Maintain Proper Distance

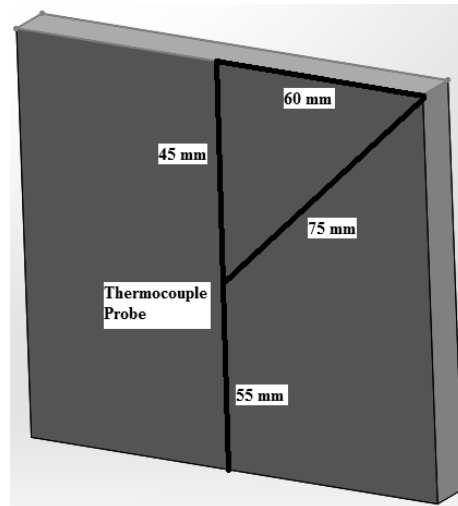


Figure 84: Final Thermocouple Position to Maintain Proper Distance

## **Operators' Manual**

To carry on research with the machine for further investigations in the future, an operators' manual is to be created. The machine can be broken down into three categories: hardware, software, and operation. The hardware category refers to the machine's mechanics, the welder, the wire feed mechanism, the computer, etc. Much of this category is detailed in the Design and Construction of Equipment portion of this research; where it is detailed on the conversion of the machine from the old setup to the new one. The key aspects from this section will be laid out as to not include too much redundancy, yet still give the necessary information in the manual. The software category includes the Fronius Xplorer, Mach3, etc. Details on these software packages will be included in the manual where appropriate, otherwise a base understanding of the software will be assumed, and information can be found in the original software documentation for basic features. The operation portion will be the main attribute of the manual as it will detail the process for routine operation to create a 'print.' A fundamental understanding of the base machine will be assumed, and information can be found in the manufacturers' manuals for basic functions.

## **Summary**

In summary, there are three factors to be studied: contact tip to work distance (CTWD) control, cold metal transfer (CMT) control, and temperature control. Each factor will be tested in the parallel and perpendicular direction with four replicates per direction per material. For CTWD and CMT control there are two levels to be studied (with or without the control scheme). For temperature control there are four levels to be studied

(three temperature set points and a baseline). This equates to a total of 128 permutations.

Tables 22-24 detail this in tabular format.

## **VI. Results**

### **Standard Specimen Data Sheet**

A data collection sheet heading was created to record relevant data for each experiment setup as shown in Figure 85. The data sheet details the information needed to setup the Fronius welder to produce the ‘print’ as there are numerous settings to adjust that will greatly affect the characteristics of the weld. In the heading, the specific wire material is to be specified along with the chosen gas composition. Next the specific synergic line should be specified from the list of empirically derived options available on the welder. While the wire feed speed is directly related and set by other variables; there is a small range that it can be adjusted within and should be noted to ensure repeatable results. Arc length correction (ALC) adjusts weld parameters based off the contact tip to work distance (CTWD) as shown in Figure 86 [49]. The value is adjustable from -30 to 30%, with -30% being very close to the weld pool and 30% being far away. This affects the penetration, bead width, and heat input to the weld pool greatly and should therefore be noted. The arc force correction (dynamic correction) adjusts the current wave geometry. It is adjustable from -5 to 5% with characteristics of these adjustments shown in Figure 87 [49]. Burn back correction changes how much wire stick out is present at the end of a weld seam and is adjustable +/- 0.20 seconds [49]. Crater fill is part of the 2-step automated welding system where the amperage is adjusted at the end of a weld seam for a specified

amount of time. This helps with the weld pool falling off (drooping) at the end of a weld such as that found in Figure 20 of the literature review. This makes for less complicated g-code as the machine is not having to slow down/speed up travel speeds at the end of the weld as in Figure 19 in the Literature Review, instead the welder is independently controlling the parameters to accomplish the same task. Figure 88 shows the crater fill phase in the 2-step welding mode, where the section labeled I-E is the crater fill [49].

Material	Gas	Synergic Line	WFS (ipm)	ALC (%)	Dyn Cor (%)	Burn Back (s)	Crater Fill

Figure 85: Welder Setup Heading

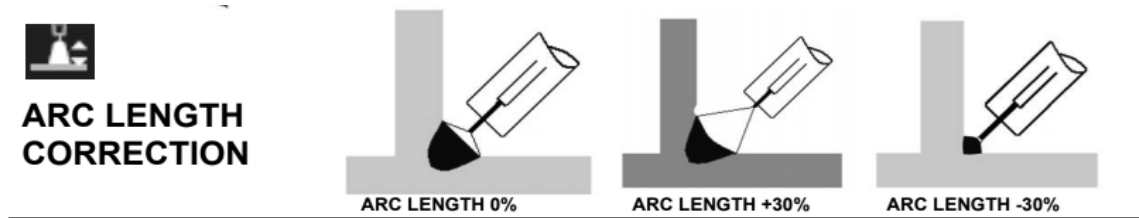


Figure 86: Arc Length Correction Setting [49]

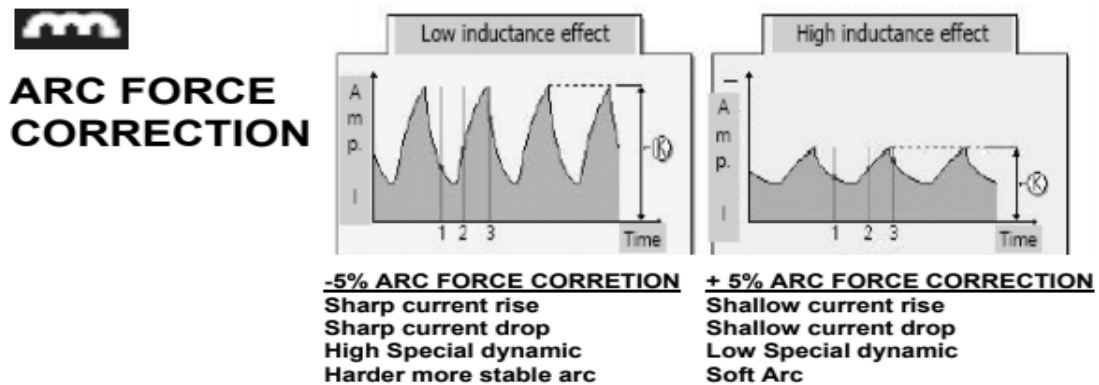


Figure 87: Arc Force (Dynamic) Correction [49]

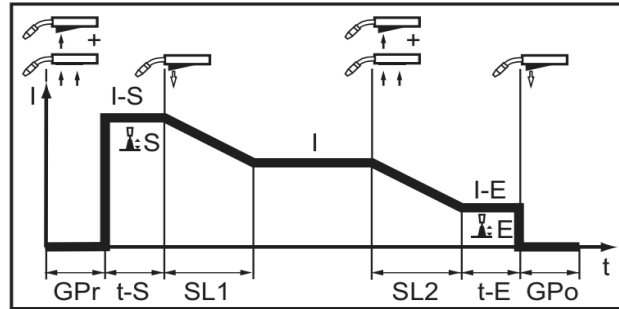


Figure 88: 2-Step Welding Mode with Crater Fill (I-E) [49]

### Closed-Loop Process Control

Figure 89 shows the basic block diagram of a standard GMAW welder. Any error that exists will be cumulative throughout the build due to scale error. Early testing and setup of the welder revealed issues with starting the weld. The welder would begin movement before the welder initiated an arc. This led to issues as those found in Figure 20 of the literature review, as well as issues with getting a good, repeatable, and stable arc to commence. A pause could be programmed as others have done in the literature review. However, this method does not account for the varying time to create a stable arc, only the time for the signal to try to begin an arc [65]. A closed-loop control scheme was developed to get repeatable results starting a weld seam. The Fronius ROB 5000 features an output (Arc Stable) that goes high when the arc is initiated. Custom VB Scripts in Mach3 which are detailed in Appendix III show the logic behind using the output signal to initiate movement. Once a M111 command is established, the CNC program is paused until the Arc Stable signal is received. This script runs in the background and is unnoticeable in practice.



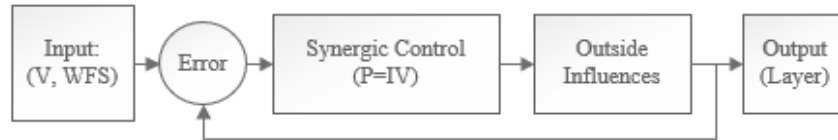


Figure 89: GMAW Block Diagram

One of the three main issues noted in the literature review related to process control, was the contract tip to work distance (CTWD). The issue lies in the layering characteristic of additive manufacturing. A set layer height is programmed (step up); however, due to outside influences (heat, lack of fusion, humidity, etc.) the part's layer height is inconsistent and variable. This issue leads to scale error where the CTWD either increases or decreases each layer and is magnified over many layers to the point that the 'print' must be stopped and either scraped or reset. In the past, operators would adjust the step up as they noticed the CTWD was getting too close or too far away. This requires a skilled operator and is inconsistent throughout the 'print.' A better solution is to have the desired step up height programmed and step up each layer based on whatever the actual previous layer height was. Doing so eliminates the scale error throughout the process. A probing program was created that utilizes the touch sensing function of the Fronius welder and is assigned to the M141 command. Once the M141 code is executed, touch sensing is activated on the welder, and the z-axis moves down until contact is made with the previous layer. Once contact has been made the ROB 5000 outputs an arc stable signal high. A VB script was created (Appendix III) that contains the entire program and involves multiple loops and checks of initial conditions to make sure that the command is not initiated during a weld. The program first checks to see if contact is already made, if not it will begin to lower the z-axis at a low feed rate of 100 mm/min until contact is made. Prior to changing the feed rate, the program reads the current feed rate and stores that to a variable, this allows

the feed rate to be reverted at the end of the program. Once contact is made, the machine is commanded to move up relative to this point by a set distance and re-zero at that level. For a desired CTWD of 14 mm, the z-axis is to be lifted 8mm when probing on the edge of a part due to the burn back feature of the wire [54]. Figure 90 shows the welding block diagram with the probing feedback to maintain a consistent CTWD between layers.

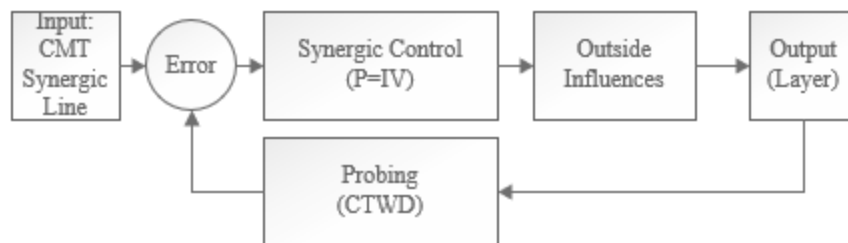


Figure 90: GMAW Block Diagram with CTWD Feedback

The second issue noted in the literature review, was the lack of control over the general welding process. As one can see in Figure above, there is feedback in the typical Synergic GMAW process but only the current is adjusted as the voltage and wire feed speed are set independently by the operator. These parameters, and many others, are interrelated and affect the weld process. The CMT-GMAW welding process monitors and controls many of these parameters based on the users desired wire feed speed. Figure 91 shows the block diagram for the proprietary CMT-GMAW welding process [49]. While little is disclosed on the proprietary process, it does have the basics of a standard inverter type welder. The difference here, according to Fronius, is their Digital Signal Processing and Microcontroller Processor (DSP +  $\mu$ P). The current and voltage are monitored throughout the process digitally, and adjustments are made at the switching transistor and secondary rectifier to control the complex wave forms of the CMT process to meet all the user-specified settings. The DSP regulates the parameters/variables while the

microprocessor executes controls. This results in a highly repeatable and controllable process, as many parameters are adjusted and monitored throughout the process instead of only adjusting current as with standard synergic lines. Figure 92 shows the CMT-GMAW addition to the process block diagram. Here the CMT process shown in Figure 91 is just a simple block for simplicity. The CMT portion of the control scheme is based off fundamental electrical engineering equations as well as empirical data collected by Fronius to ensure a high quality, repeatable welding process.

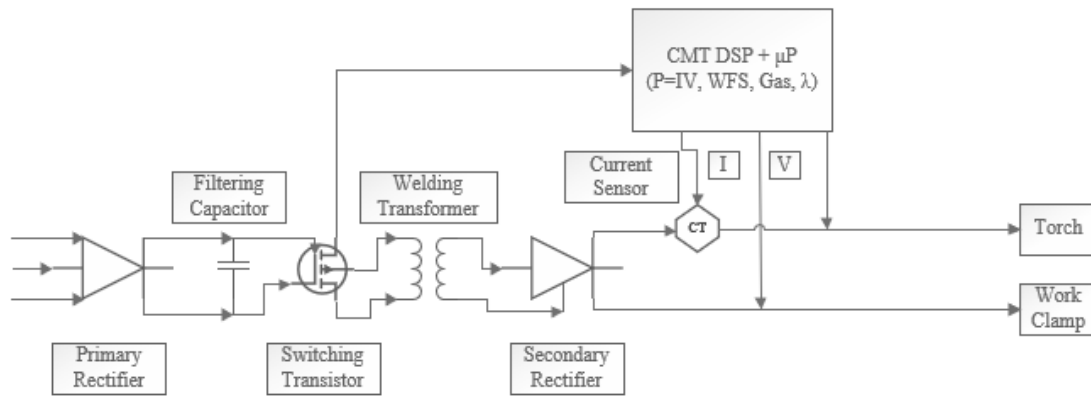


Figure 91: Fronius CMT DSP +  $\mu$ P Block Diagram [49]

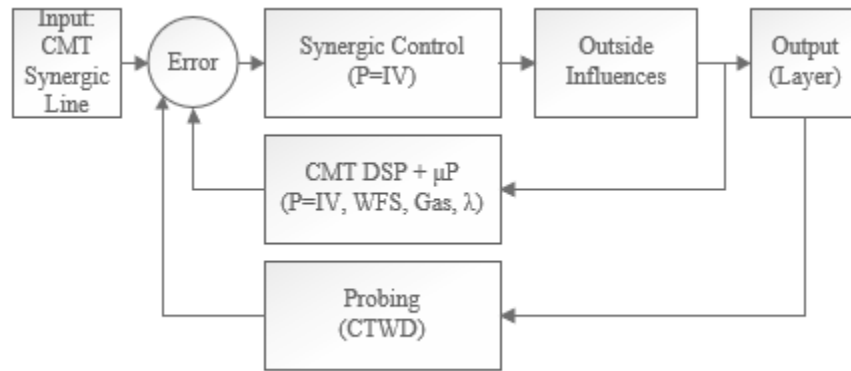


Figure 92: CMT-GMAW Block Diagram with CTWD Feedback

The last main issue noted from the Literature Review is the lack of control over the weld process temperature. This issue is common among most additive manufacturing processes and is detrimental in producing reliable parts. Since each layer needs to be

bonded to the previous, some form of heat must be used; however, too much heat and the part melts or penetrates the weld pool into too many previous layers causing errors. On the other hand, too little heat will cause delamination later in the process or simply lack of fusion at all to the previous layer. With thermoplastics, this issue is less of a problem as there is a nice range of glass transition temperatures for the material that it can melt and re-melt at and still give representative material properties. This is not the case for metals. Metals' material properties are highly dependent upon the time/temperature 'heat treating' schedule they undergo. This makes the case for a closed-loop feedback of the temperature of the weld highly pertinent in this additive process. Once a weld bead is started it is best to continue that bead until it is finished. If the bead is too hot, or too cold, adjustments should be made after the profile is deposited [Fronius]. Therefore, a control scheme to monitor the weld temperature was created and waits for the temperature to drop before starting another layer. The VB script for this command is in Appendix III and is combined in the welding command. Figure 93 shows the process block diagram with the addition of temperature monitoring. Temperatures are monitored throughout the weld process at locations noted in the Literature and Methodology and Statistical Design of Experiments. The process pauses for the specified amount of time found to be optimal in the coinciding research with this project (90 seconds) [66].

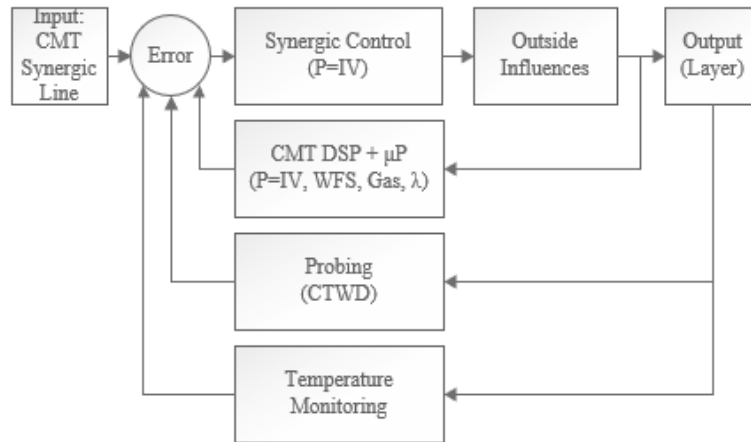


Figure 93: CMT-GMAW Block Diagram with CTWD and Temperature Monitoring Feedback

### Contact Tip to Work Distance Control Evaluation

Table 25 shows the results of comparing walls ‘printed’ with the contact tip to work distance (CTWD) control to those ‘printed’ without the control scheme (operator manually adjusts distance as needed) for ER70S-6. A P-Value greater than 0.05 indicates no significant difference between the means of the group and they are statistically equal with 95% confidence. If the parallel and perpendicular directions for both sub-groups were statistically equal, they were treated as a single grouping for comparison to each other. Appendix IV has the statistical outputs for these tests.

The walls created with the CTWD control were statistically equal in both parallel and perpendicular directions for UTS, yield, and hardness measurables. The walls created without the CTWD control were statistically the same for yield strength and hardness but were not for ultimate tensile strength. Since the two directions were not statistically equal for UTS, they were treated independently when compared to the walls that did utilize the CTWD control scheme.

Table 25: ER70S-6 With v. Without CTWD Control P-Values

	UTS	Yield	Hardness
With CTWD Control: Parallel v. Perpendicular	0.396	0.543	0.801
Without CTWD Control: Parallel v. Perpendicular	0.020	0.530	0.054
Parallel v. Parallel	0.04	n/a	n/a
Perpendicular v. Perpendicular	0.00009	n/a	n/a
With v. Without CTWD Control	n/a	0.201	0.204

When evaluating the control scheme for ER70S-6, both yield strength and hardness values were statistically equal; however, the UTS in both the parallel and perpendicular directions were not statistically the same. When looking at the values of the tests, it shows that the UTS of the walls with the CTWD control were higher than without the control method. When looking at the values of UTS for the comparison of parallel to perpendicular deposition without the CTWD control, the parallel direction had higher values.

Table 26 shows the results of comparing walls ‘printed’ with the contact tip to work distance (CTWD) control to those ‘printed’ without the control scheme (operator manually adjusts distance as needed) for ER308L. A P-Value greater than 0.05 indicates no significant difference between the means of the group and they are statistically equal with 95% confidence. If the parallel and perpendicular directions for both sub-groups were statistically equal, they were treated as a single grouping for comparison to each other. Appendix IV has the statistical outputs for these tests.

Table 26: ER308L With v. Without CTWD Control P-Values

	UTS	Yield	Hardness
With CTWD Control: Parallel v. Perpendicular	0.014	0.002	0.003
Without CTWD Control: Parallel v. Perpendicular	0.028	0.493	0.015
With CTWD Control v. Without: Parallel	0.013	0.00057	0.004
With CTWD Control v. Without: Perpendicular	0.008	0.330	0.052

The walls created with the CTWD control were not statistically equal in both parallel and perpendicular directions for UTS, yield, or hardness measurables. The walls created without the CTWD control were statistically the same for yield strength but were not for ultimate tensile strength or hardness. Since the two directions were not statistically equal for the combinations, they were treated independently when compared to the walls that did, or did not, utilize the CTWD control scheme.

When evaluating the control scheme for ER308L, the yield strength and hardness values were statistically equal in the perpendicular direction; however, the other values in both the parallel and perpendicular directions were not statistically the same. When looking at the values of the tests, it shows that the UTS, yield, and hardness of the walls with the CTWD control were higher than without the control method (when they were not statistically equal). When looking at the values of UTS, yield, and hardness for the

comparison of parallel to perpendicular deposition, the parallel direction had higher values for all measurables for all cases except for the hardness without the CTWD control.

Figures 94-96 show the main effects plots for the hardness, yield strength, and UTS for ER70S-6. Figures 97-99 show the residual plots for hardness, yield strength, and UTS for ER70S-6. Figures 100-111 show the Tukey-Kramer analysis and interval plots for hardness, yield strength, and UTS for ER70S-6. Note values for hardness are in HRB, and for yield strength and UTS; kips.

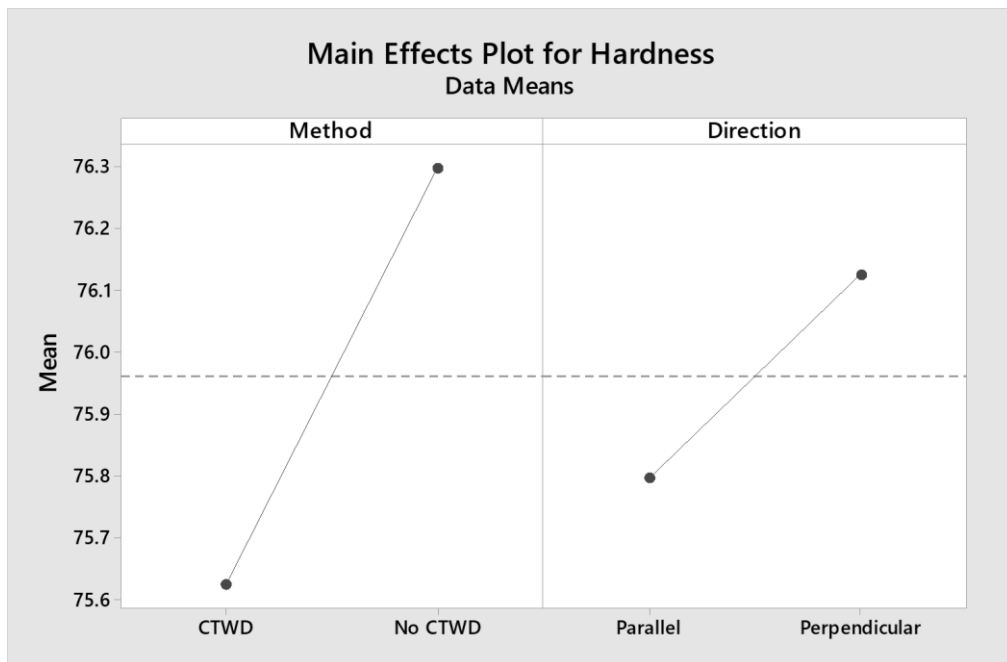


Figure 94: Main Effects Plot for ER70S-6 for CTWD Control for Hardness



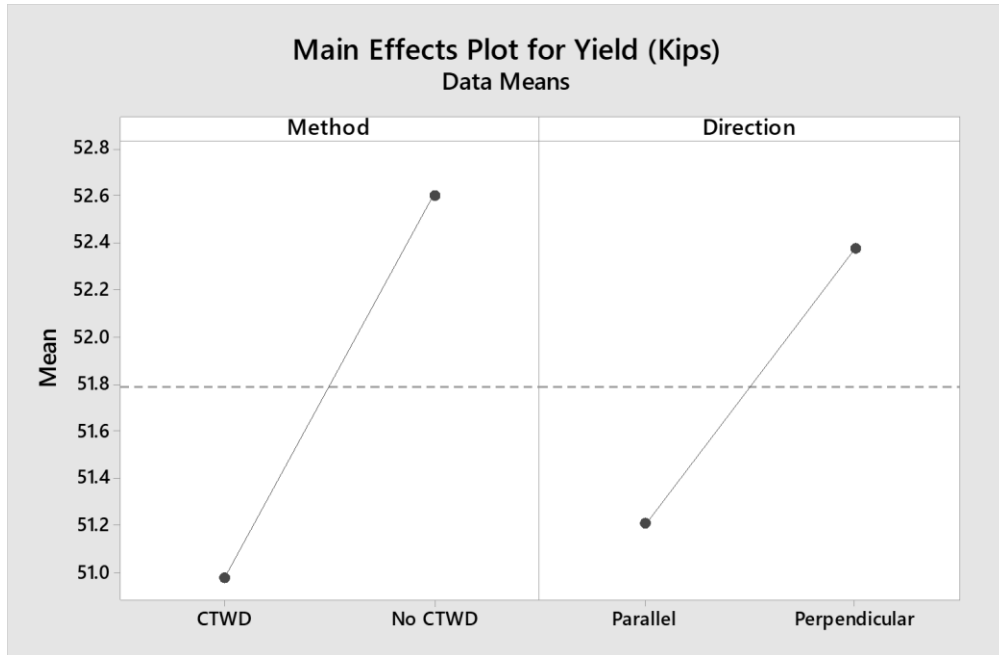


Figure 95: Main Effects Plot for ER70S-6 for CTWD Control for Yield

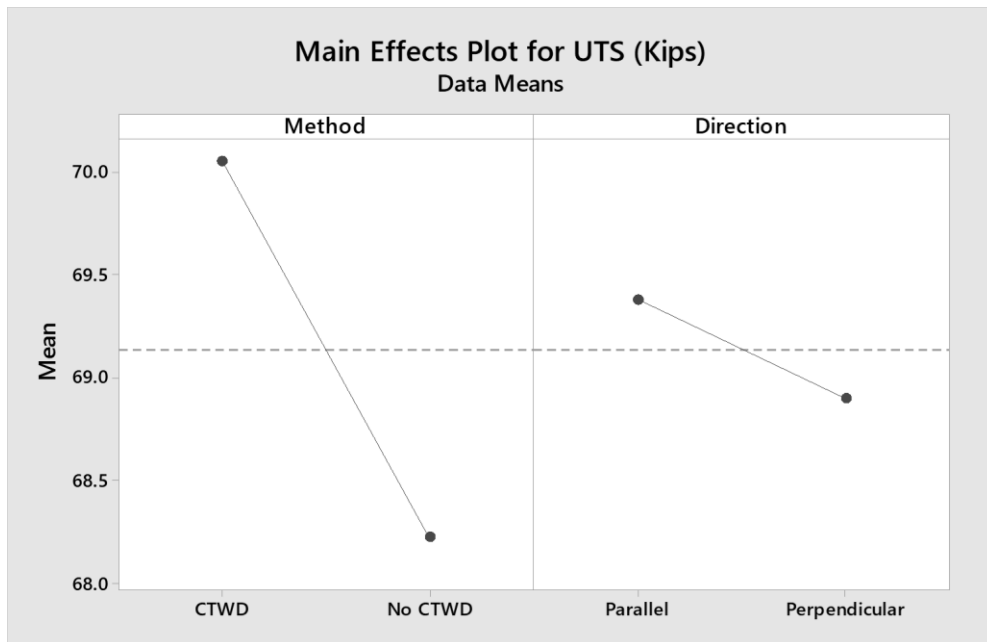


Figure 96: Main Effects Plot for ER70S-6 for CTWD Control for UTS

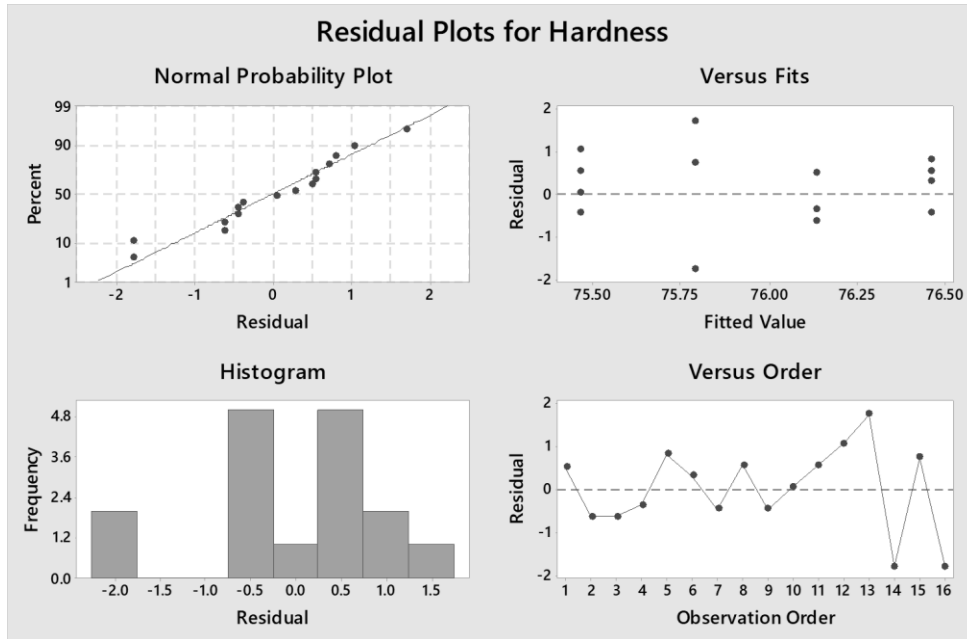


Figure 97: Residual Plots for ER70S-6 for CTWD Control for Hardness

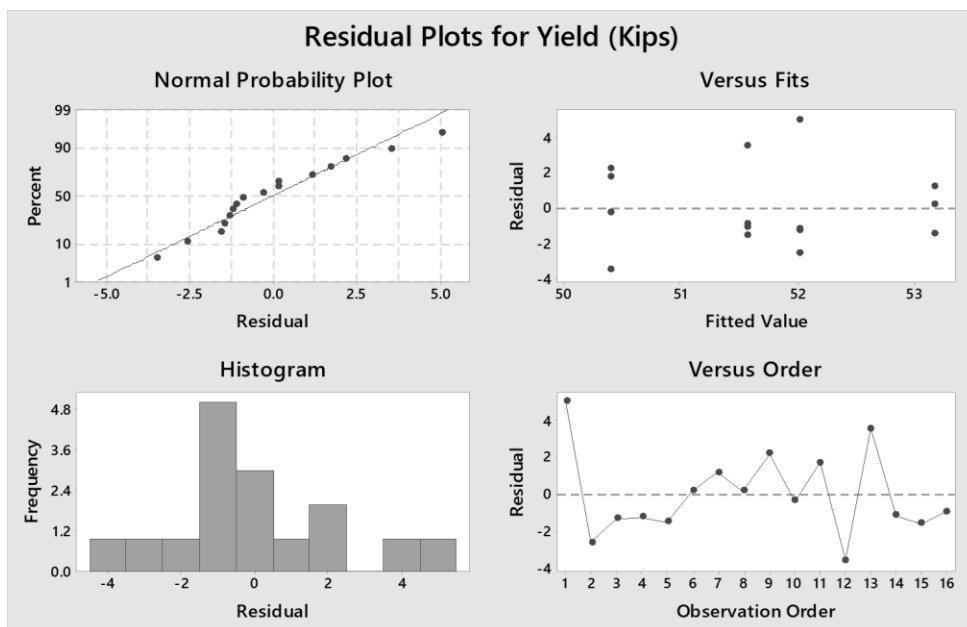


Figure 98: Residual Plots for ER70S-6 for CTWD Control for Yield

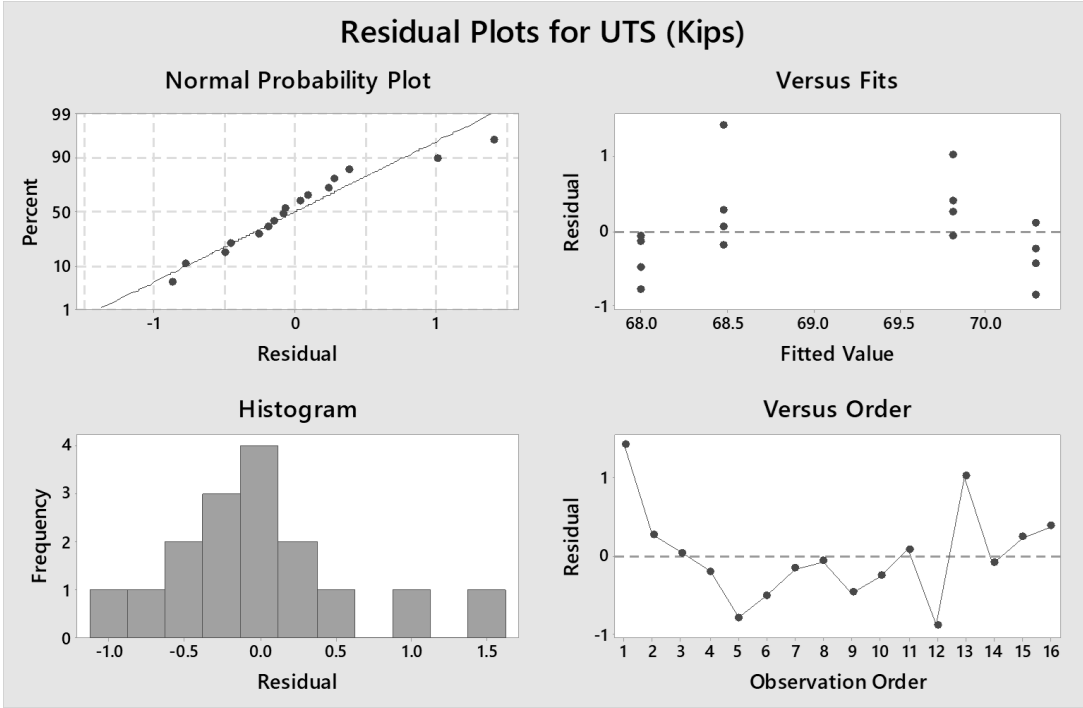


Figure 99: Residual Plots for ER70S-6 for CTWD Control for UTS

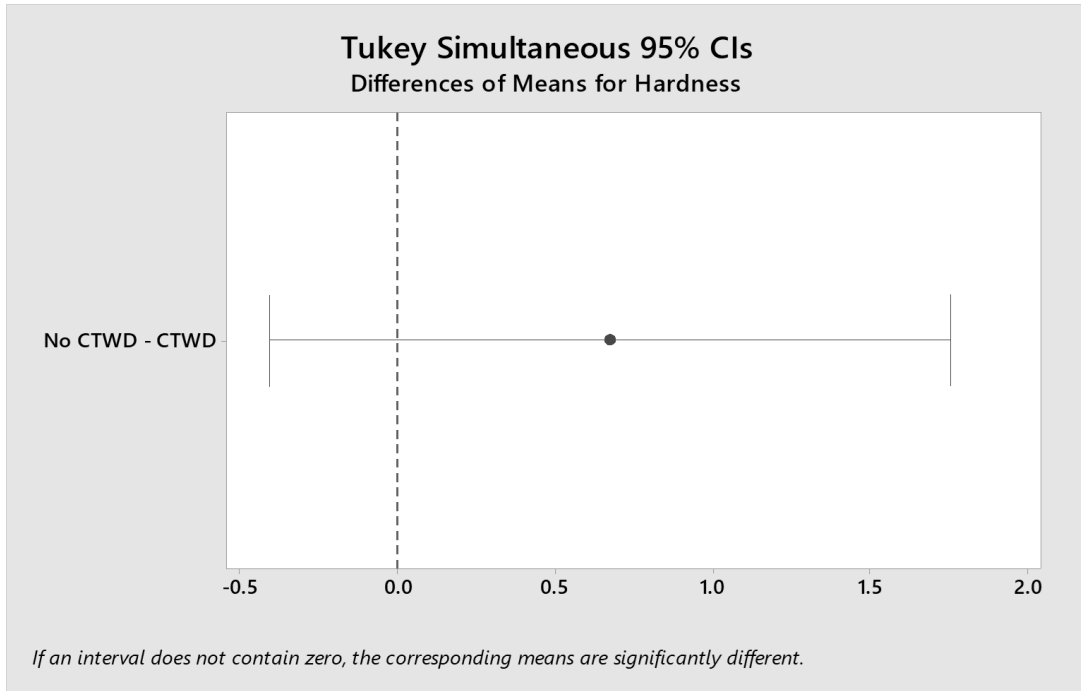


Figure 100: Tukey Analysis for ER70S-6 for CTWD Control for Hardness

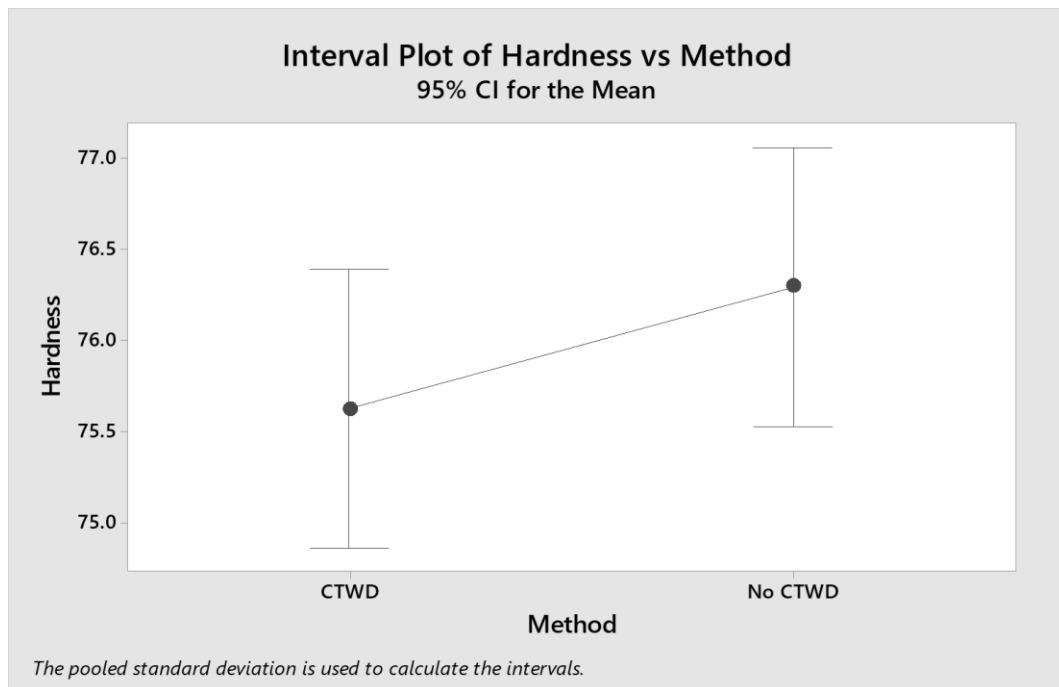


Figure 101: Interval Plot for ER70S-6 for CTWD Control for Hardness

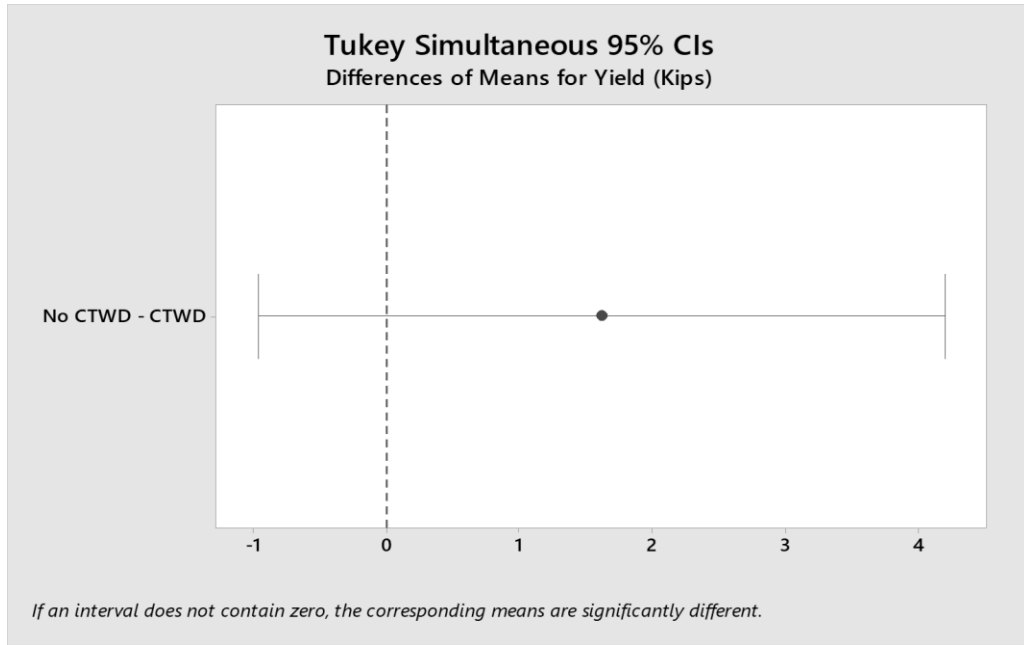


Figure 102: Tukey Analysis for ER70S-6 for CTWD Control for Yield

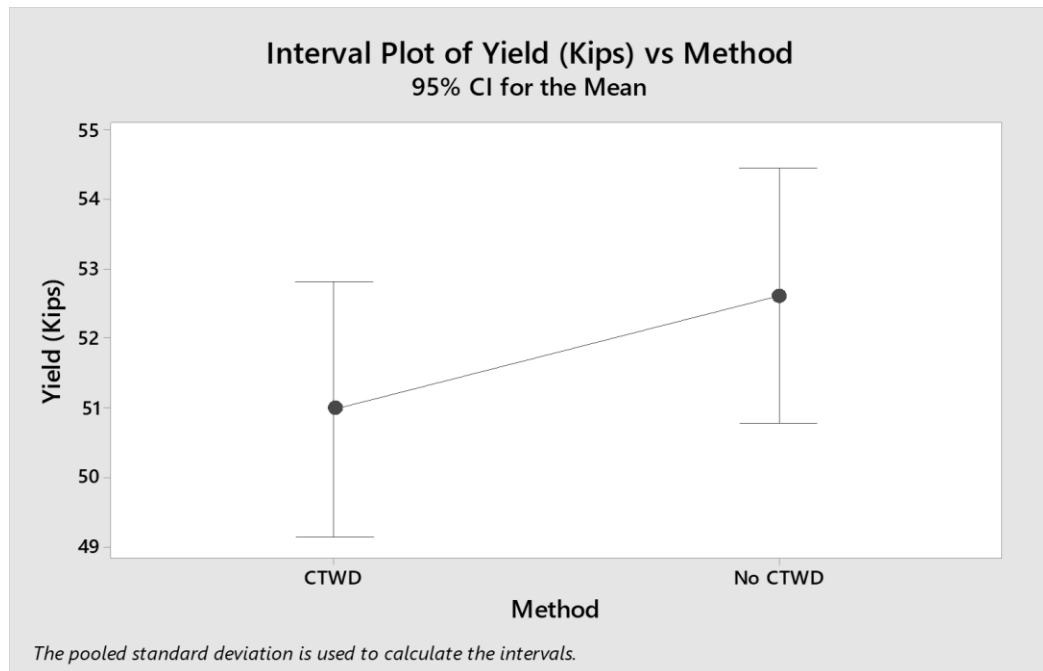


Figure 103: Interval Plot for ER70S-6 for CTWD Control for Yield

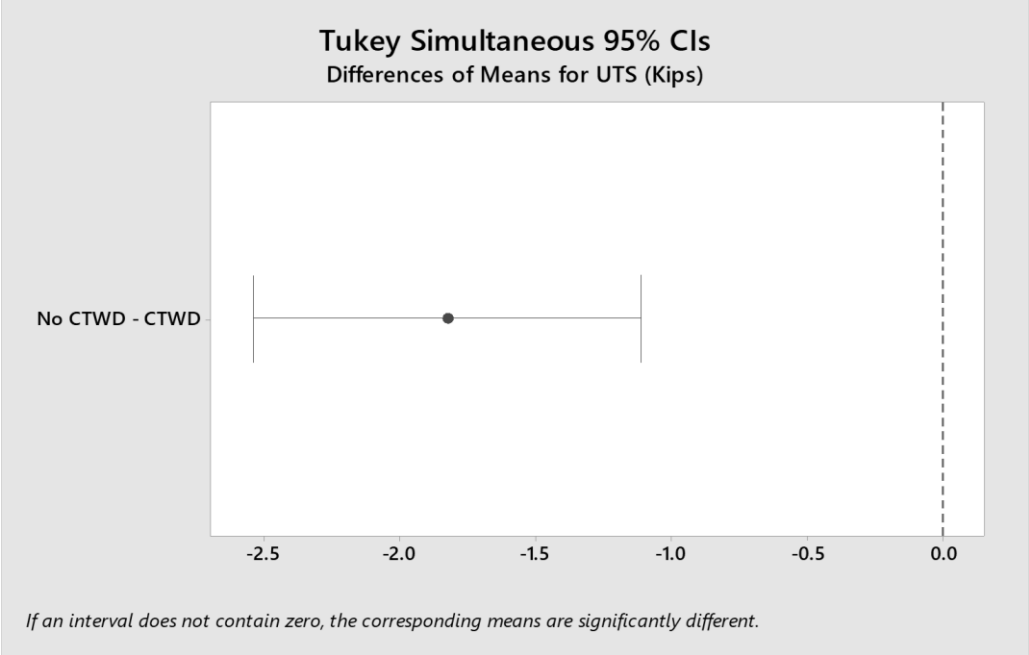


Figure 104: Tukey Analysis for ER70S-6 for CTWD Control for UTS

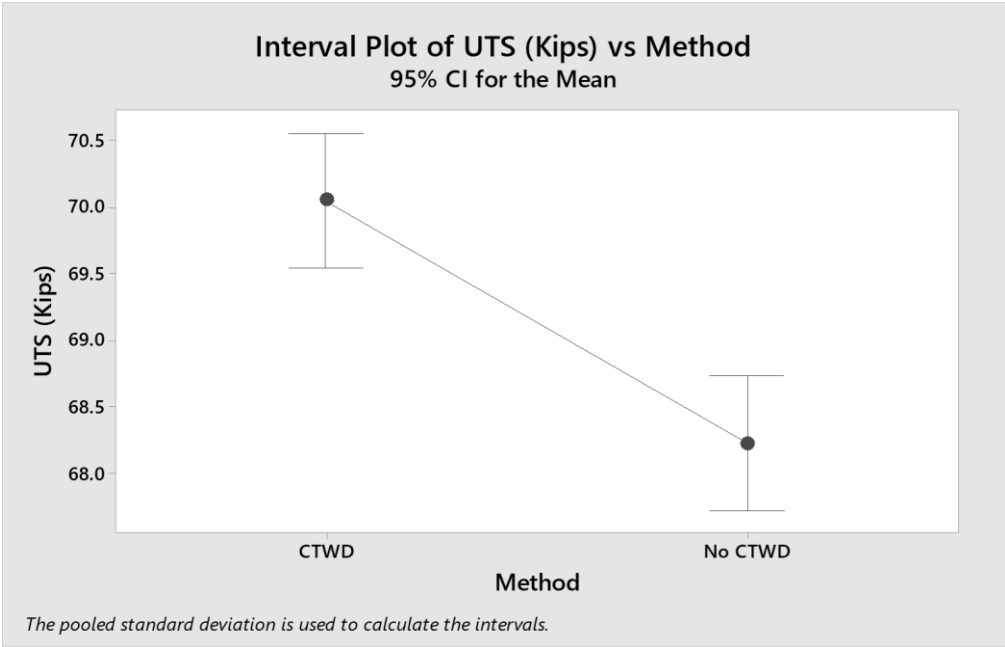


Figure 105: Interval Plot for ER70S-6 for CTWD Control for UTS

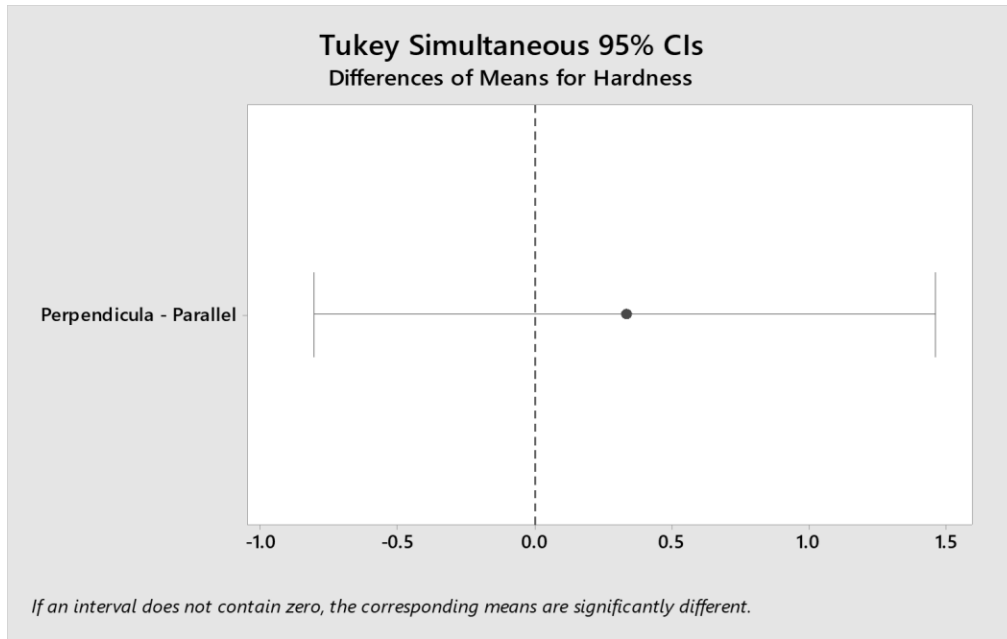


Figure 106: Tukey Analysis for ER70S-6 for CTWD Control for Hardness

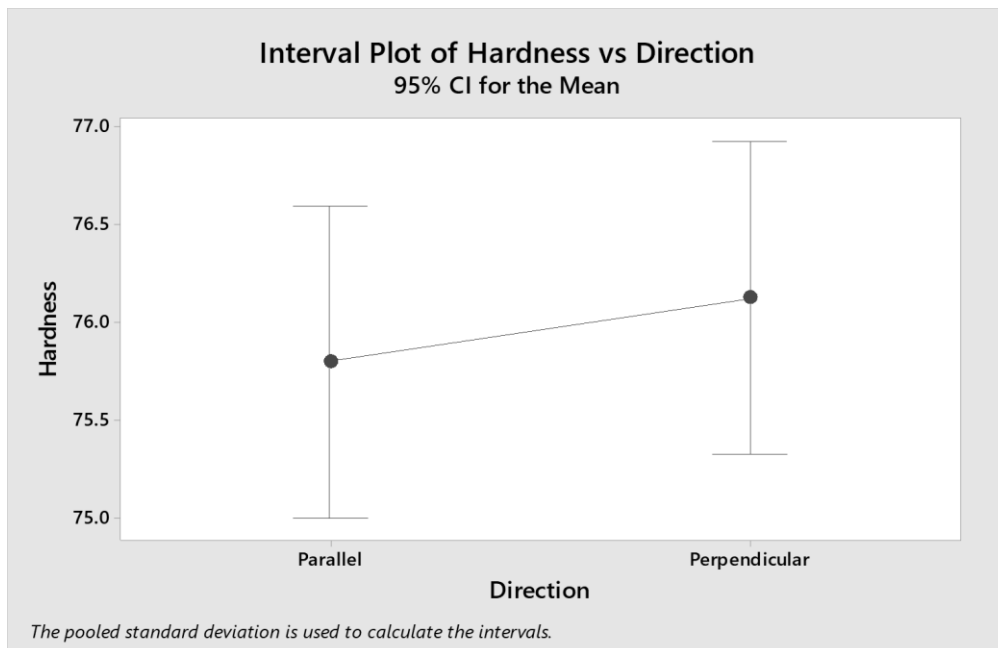


Figure 107: Interval Plot for ER70S-6 for CTWD Control for Hardness

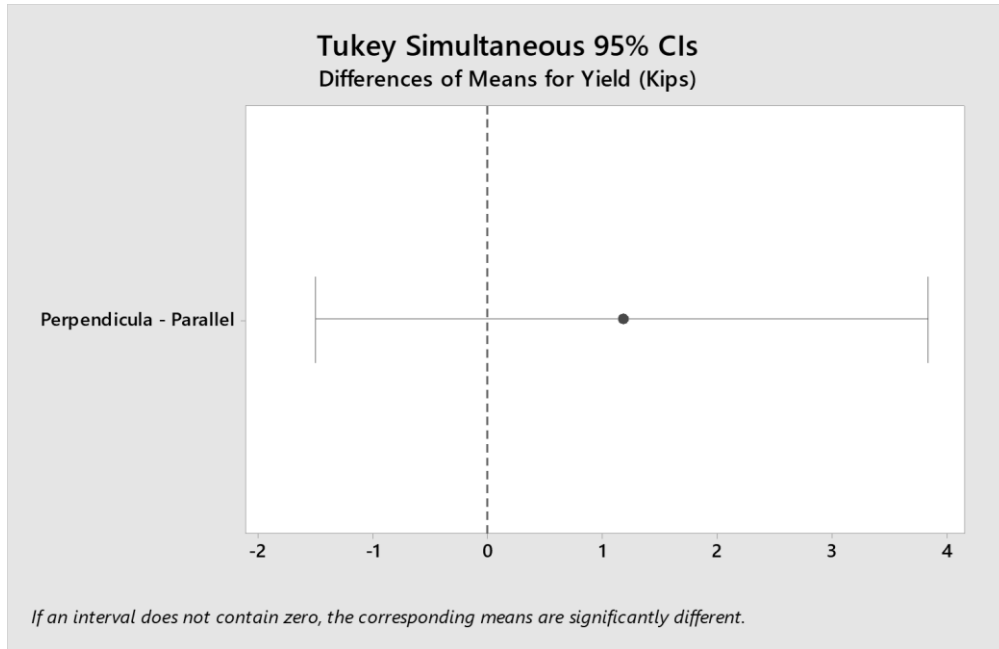


Figure 108: Tukey Analysis for ER70S-6 for CTWD Control for Yield

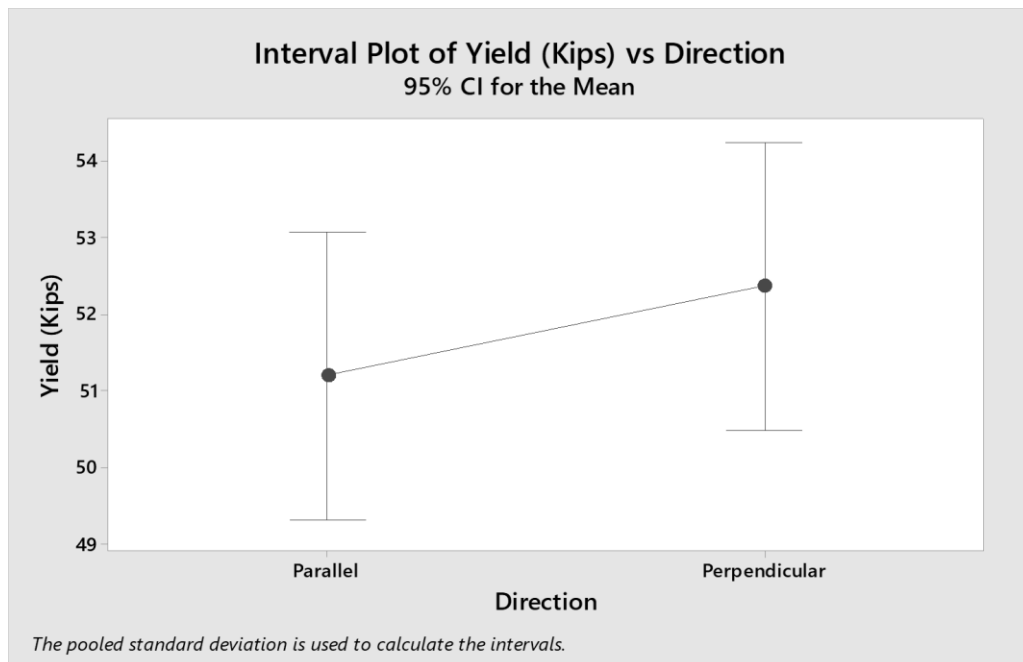


Figure 109: Interval Plot for ER70S-6 for CTWD Control for Yield



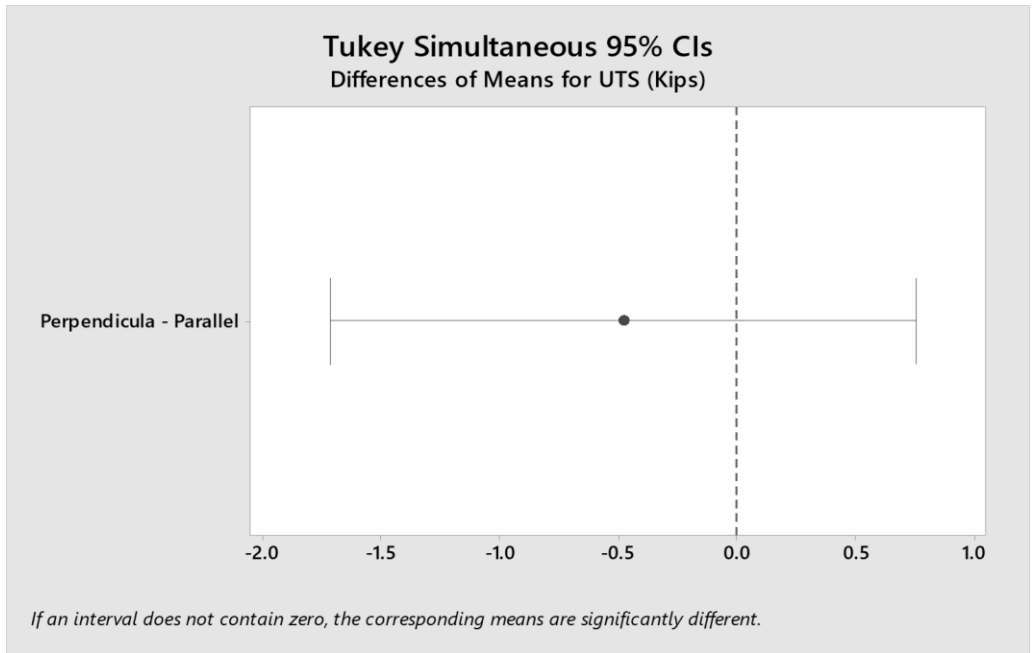


Figure 110: Tukey Analysis for ER70S-6 for CTWD Control for UTS

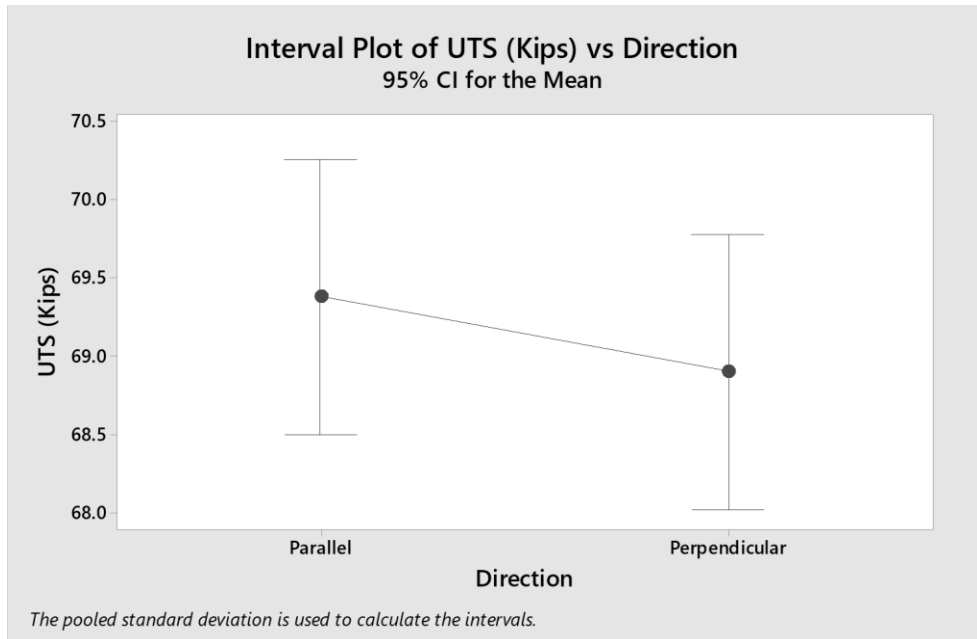


Figure 111: Interval Plot for ER70S-6 for CTWD Control for UTS

Figures 112-114 show the main effects plots for the hardness, yield strength, and UTS for ER308L. Figures 115-117 show the residual plots for hardness, yield strength, and UTS for ER308L. Figures 118-129 show the Tukey-Kramer analysis and interval plots for hardness, yield strength, and UTS for ER308L. Note values for hardness are in HRB, and for yield strength and UTS; kips.

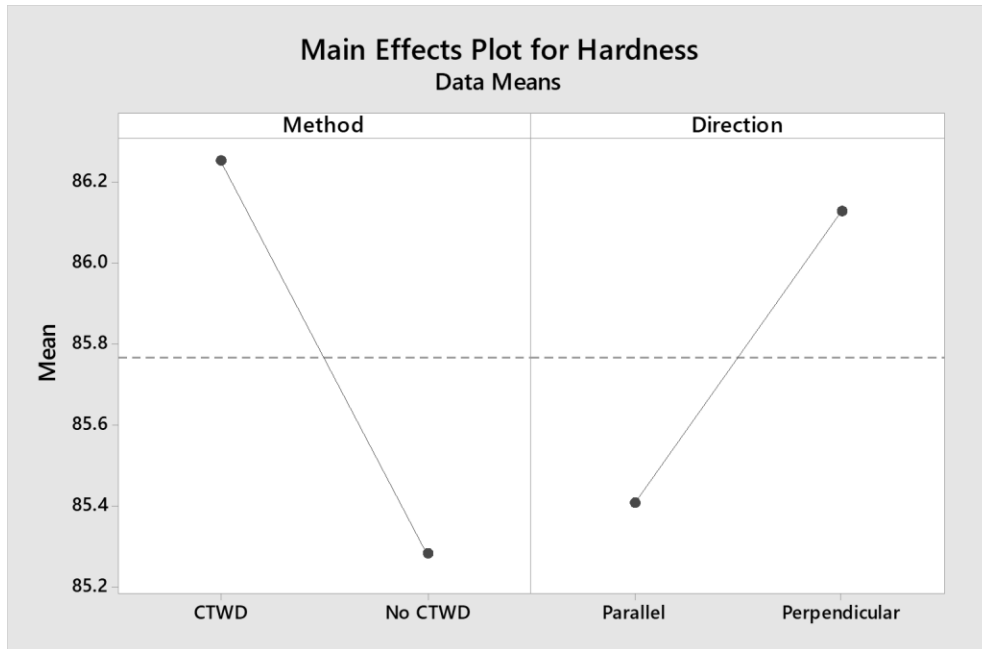


Figure 112: Main Effects Plot for ER308L for CTWD Control for Hardness

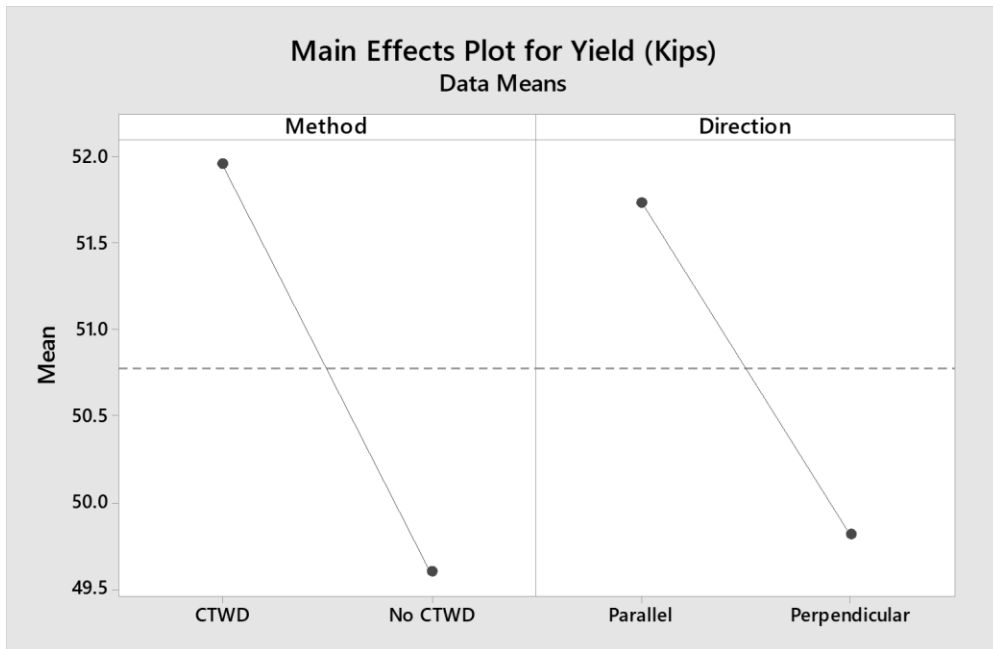


Figure 113: Main Effects Plot for ER308L for CTWD Control for Yield

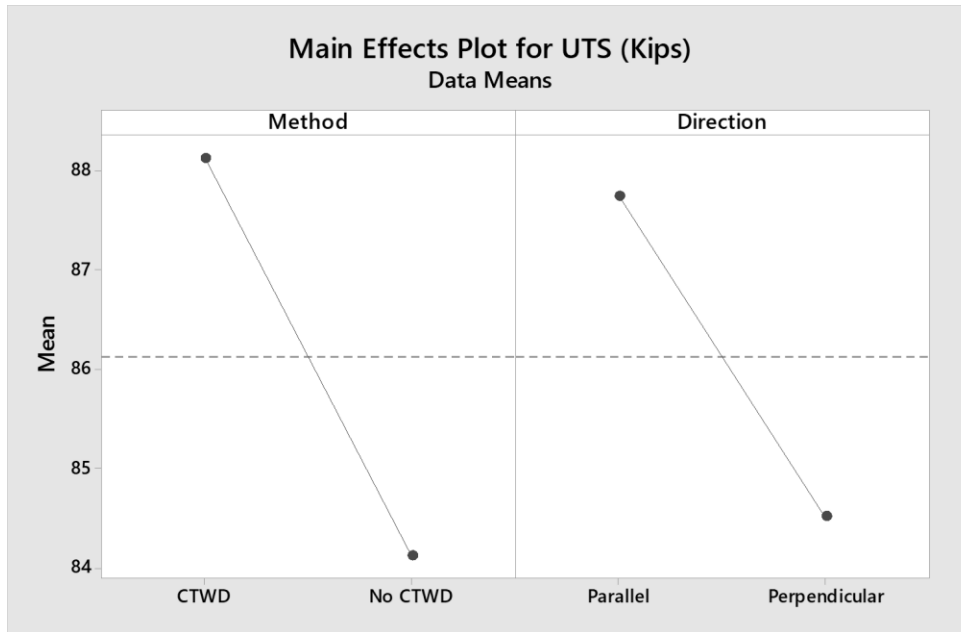


Figure 114: Main Effects Plot for ER308L for CTWD Control for UTS

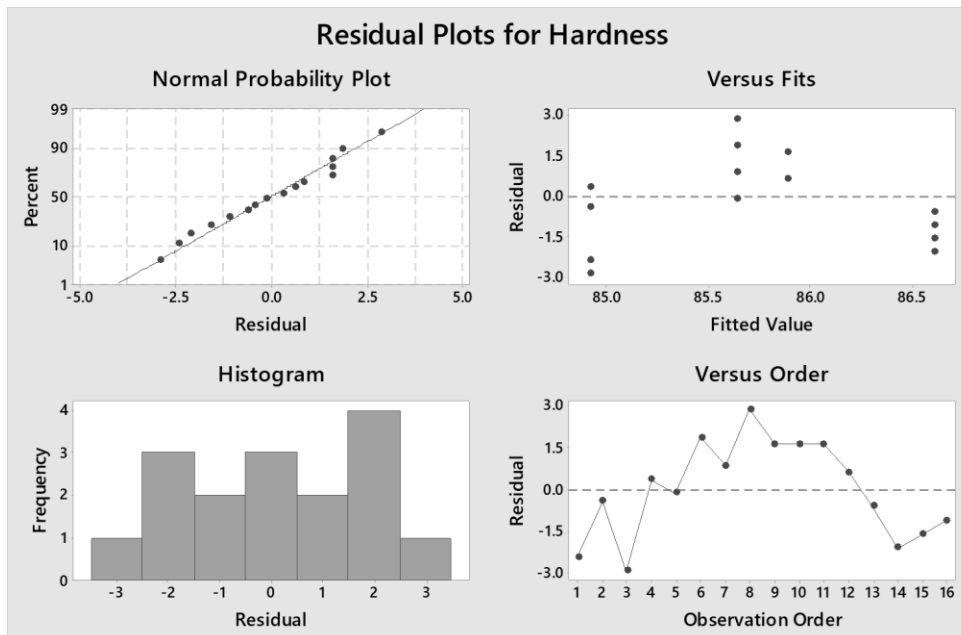


Figure 115: Residual Plots for ER308L for CWTD Control for Hardness

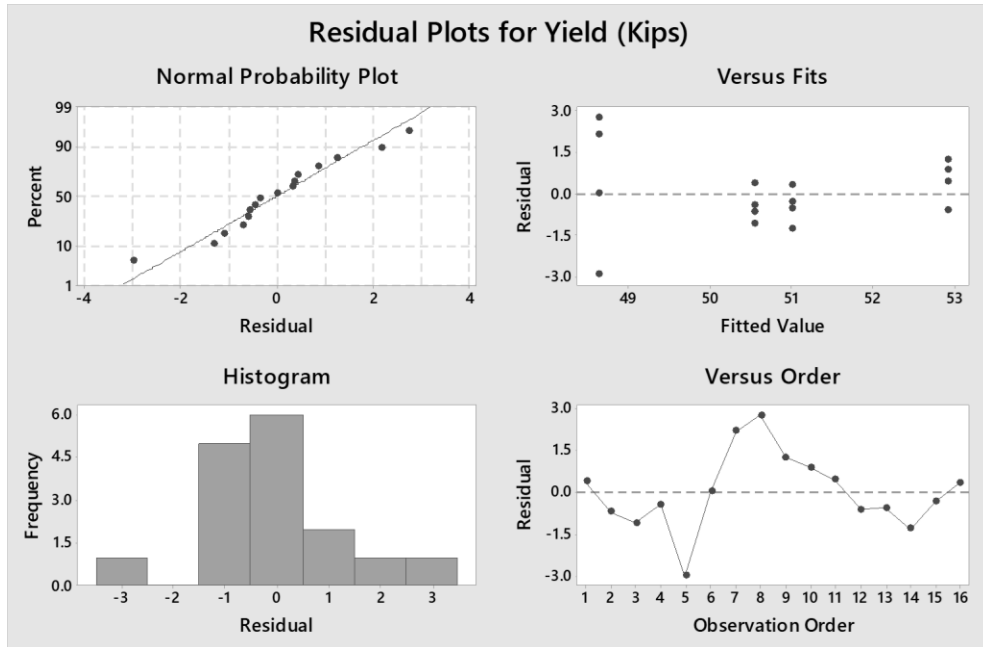


Figure 116: Residual Plots for ER308L for CWTD Control for Yield

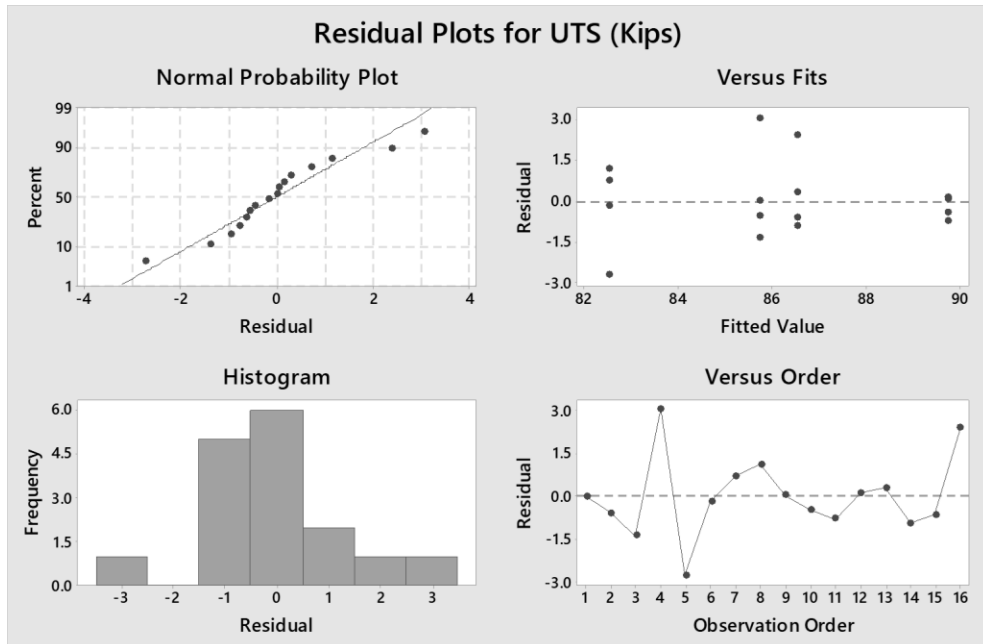


Figure 117: Residual Plots for ER308L for CWTD Control for UTS

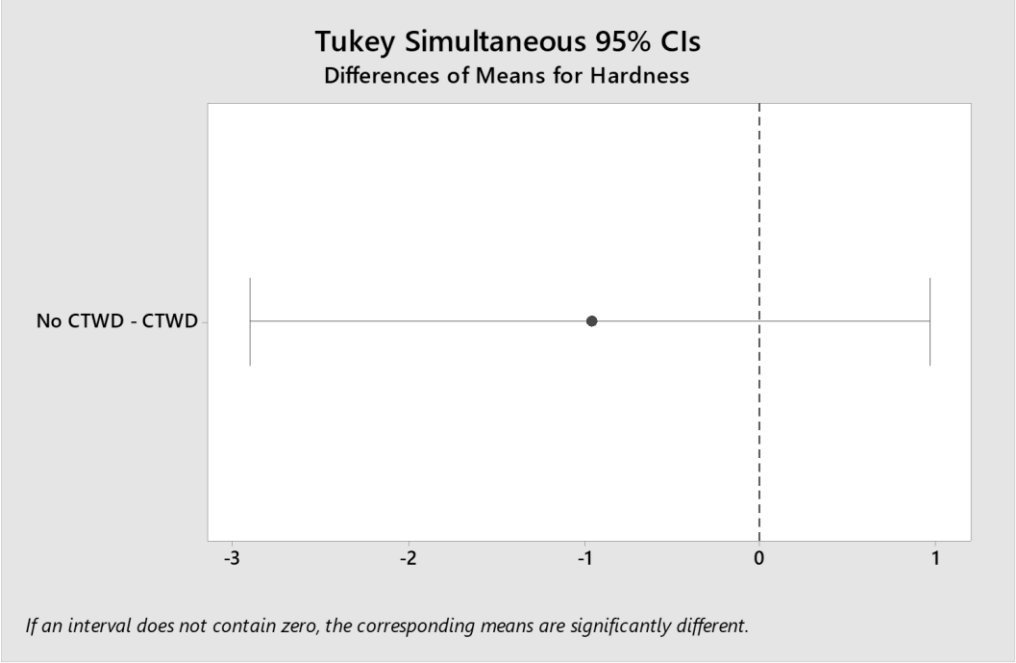


Figure 118: Tukey Analysis for ER308L for CWTD Control for Hardness

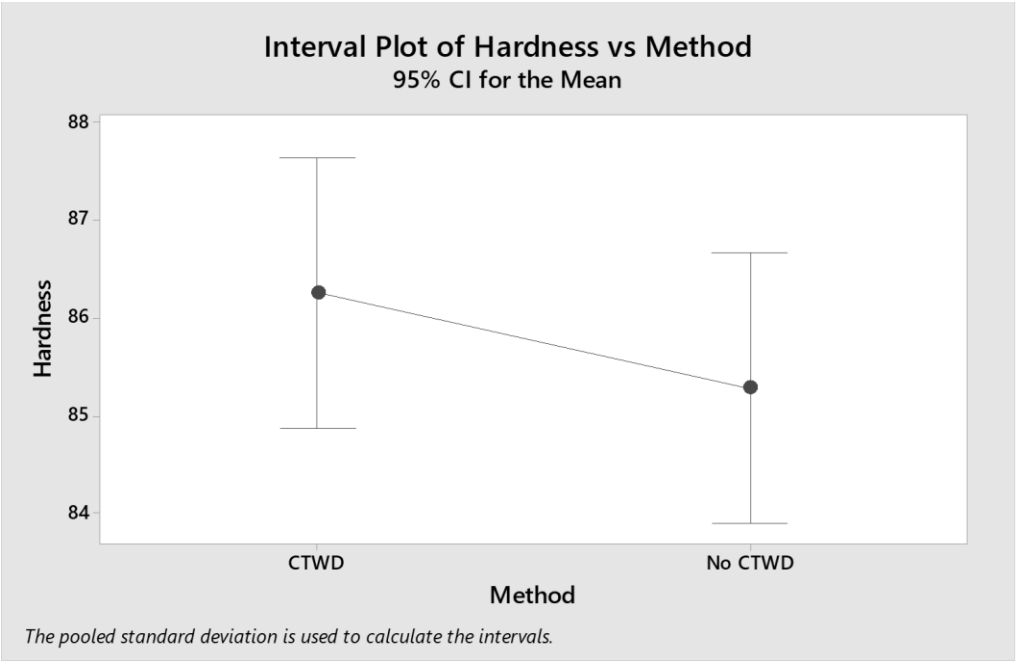


Figure 119: Interval Plot for ER308L for CWTD Control for Hardness

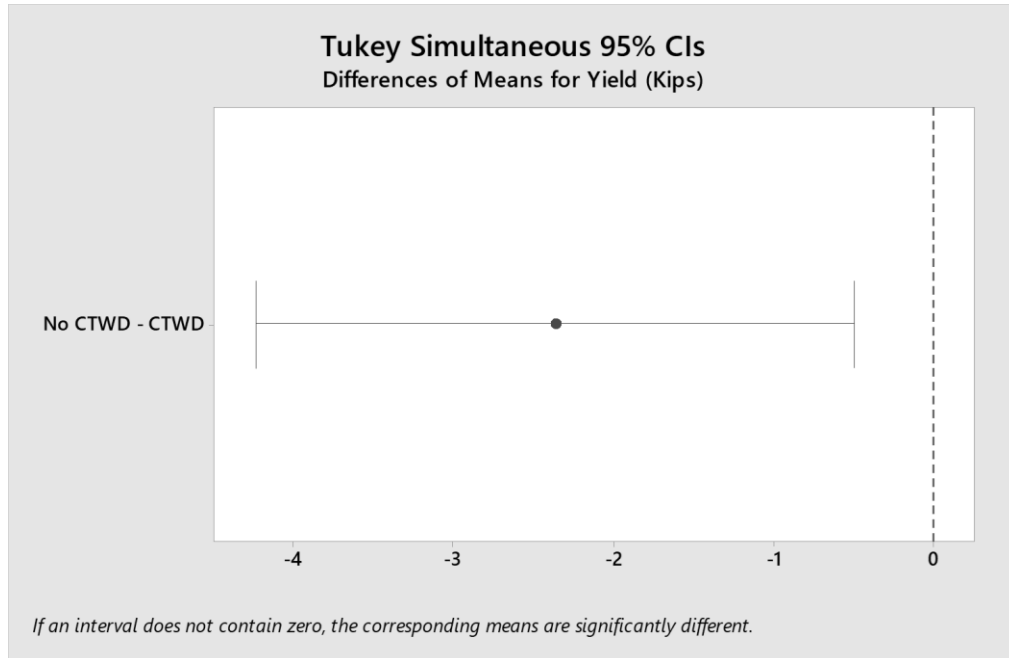


Figure 120: Tukey Analysis for ER308L for CWTD Control for Yield

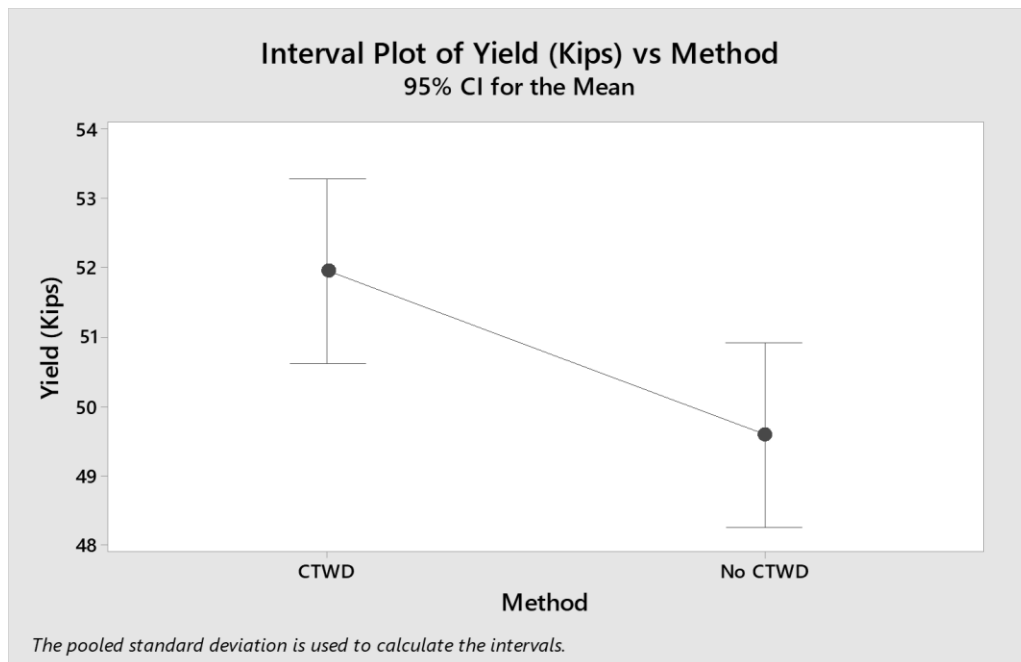


Figure 121: Interval Plot for ER308L for CWTD Control for Yield

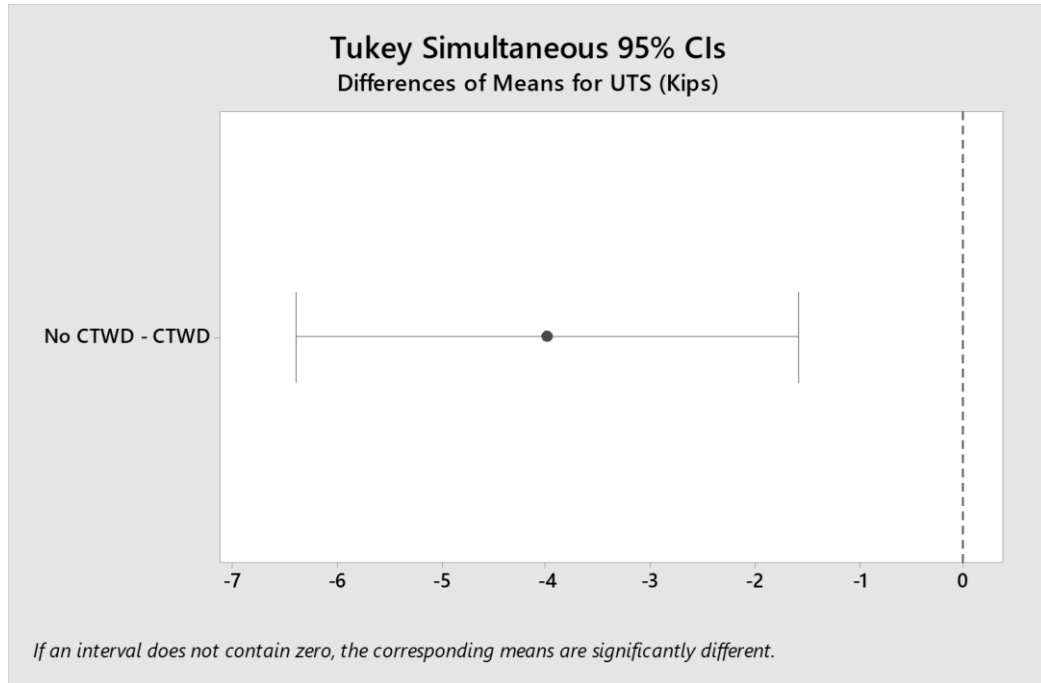


Figure 122: Tukey Analysis for ER308L for CWTD Control for UTS

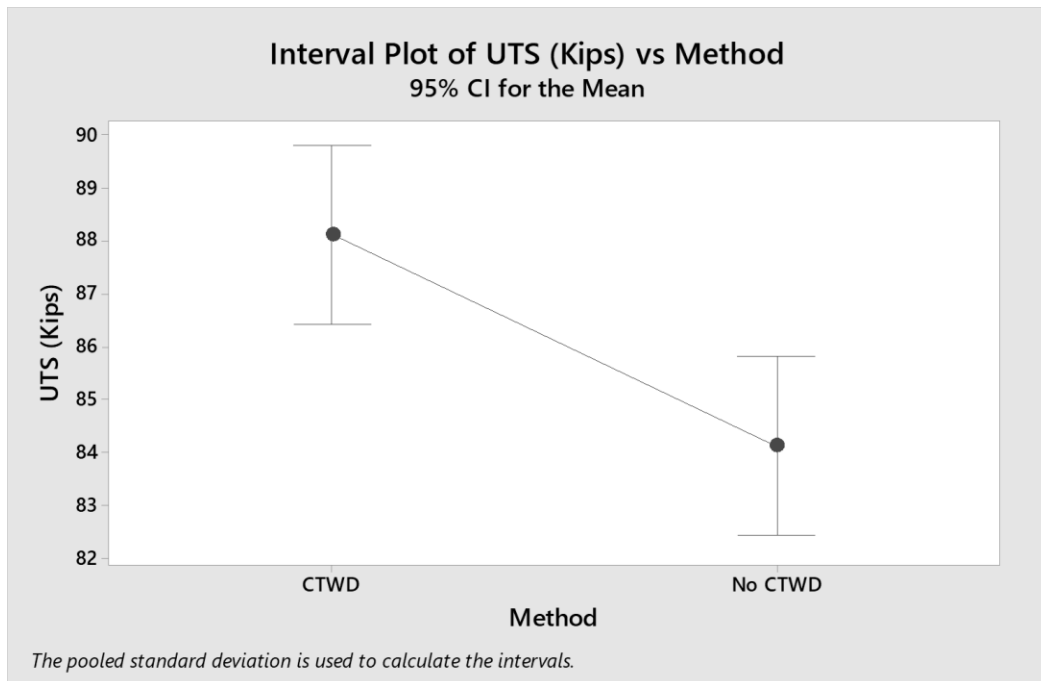


Figure 1123: Interval Plot for ER308L for CWTD Control for UTS



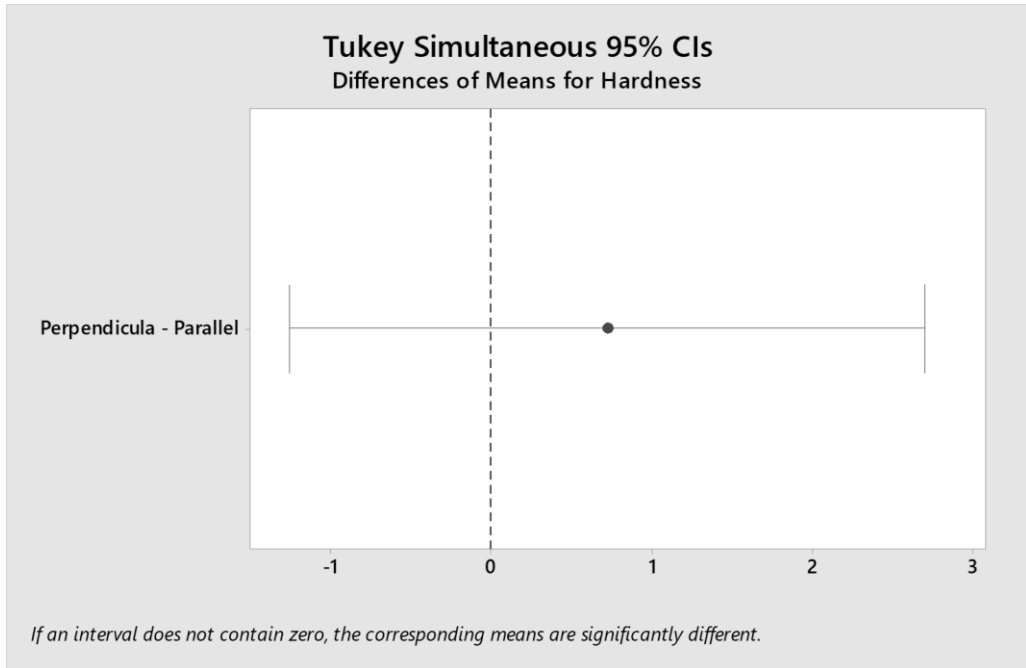


Figure 124: Tukey Analysis for ER308L for CWTD Control for Hardness

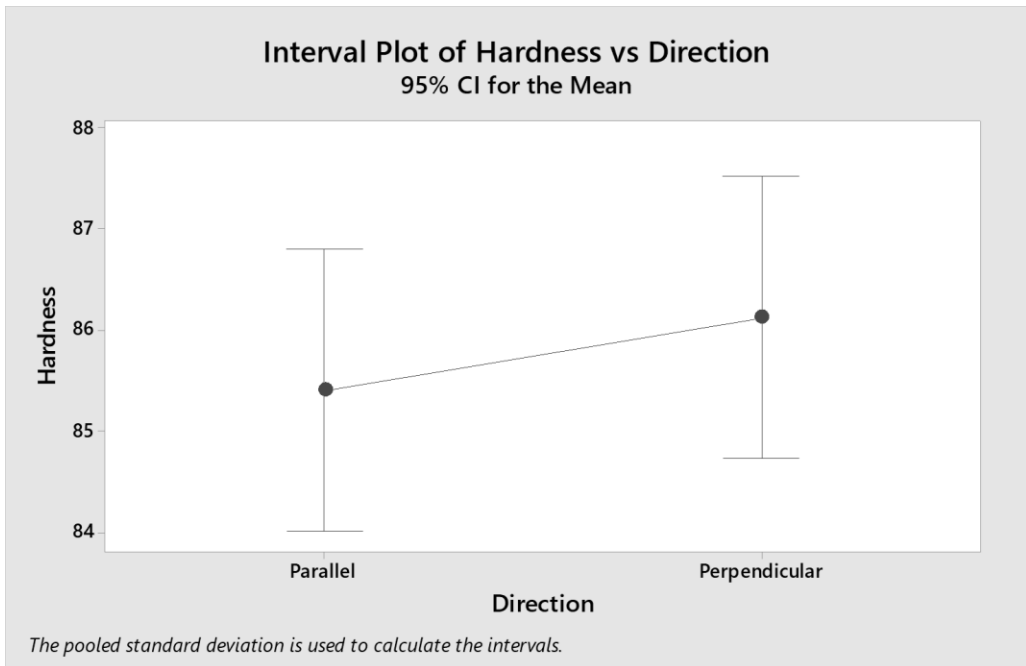


Figure 125: Interval Plot for ER308L for CWTD Control for Hardness

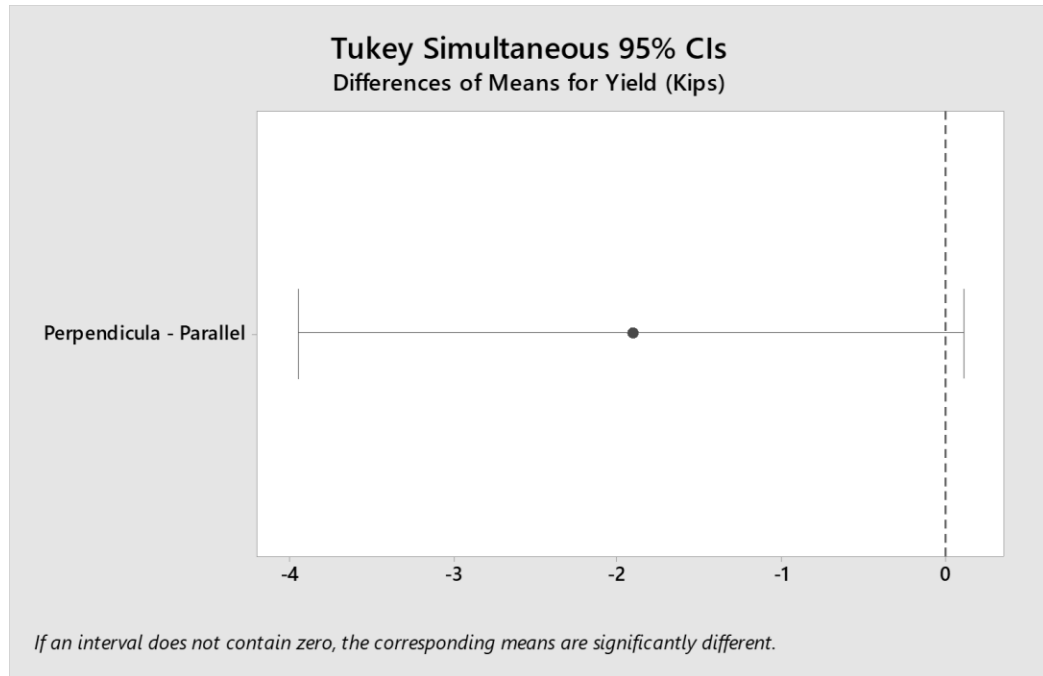


Figure 126: Tukey Analysis for ER308L for CWTD Control for Yield

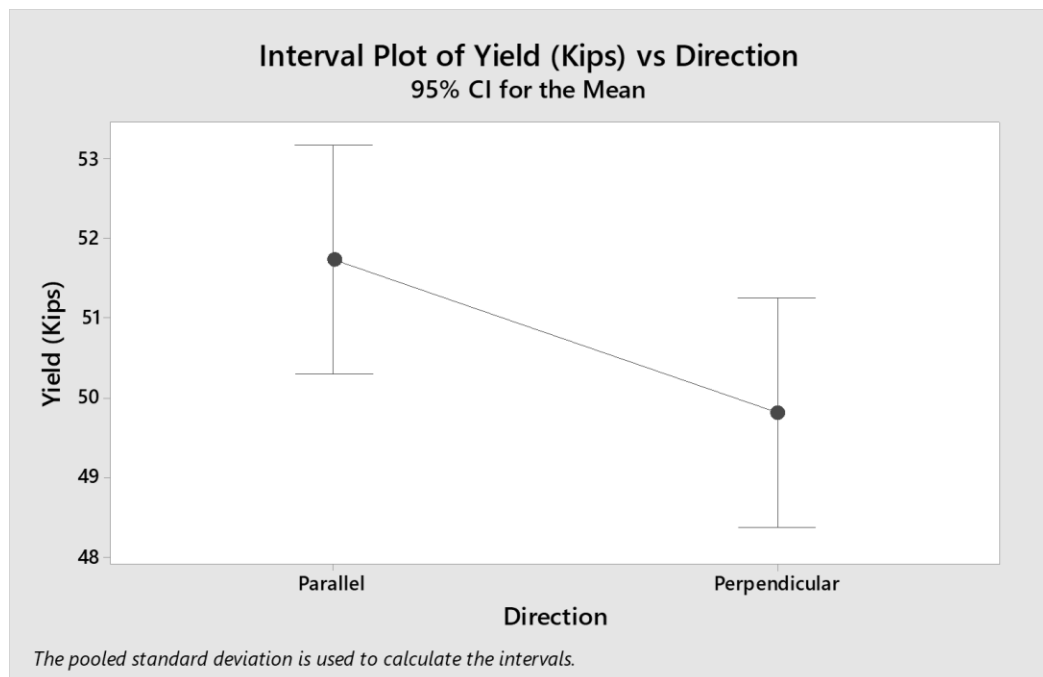


Figure 127: Interval Plot for ER308L for CWTD Control for Yield

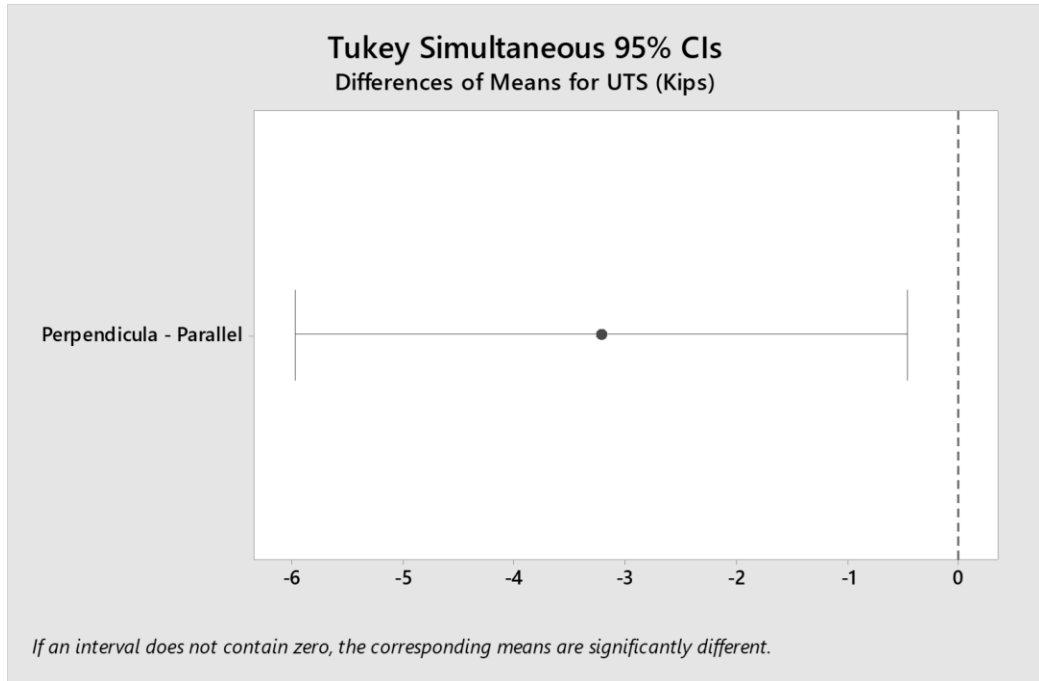


Figure 128: Tukey Analysis for ER308L for CWTD Control for UTS

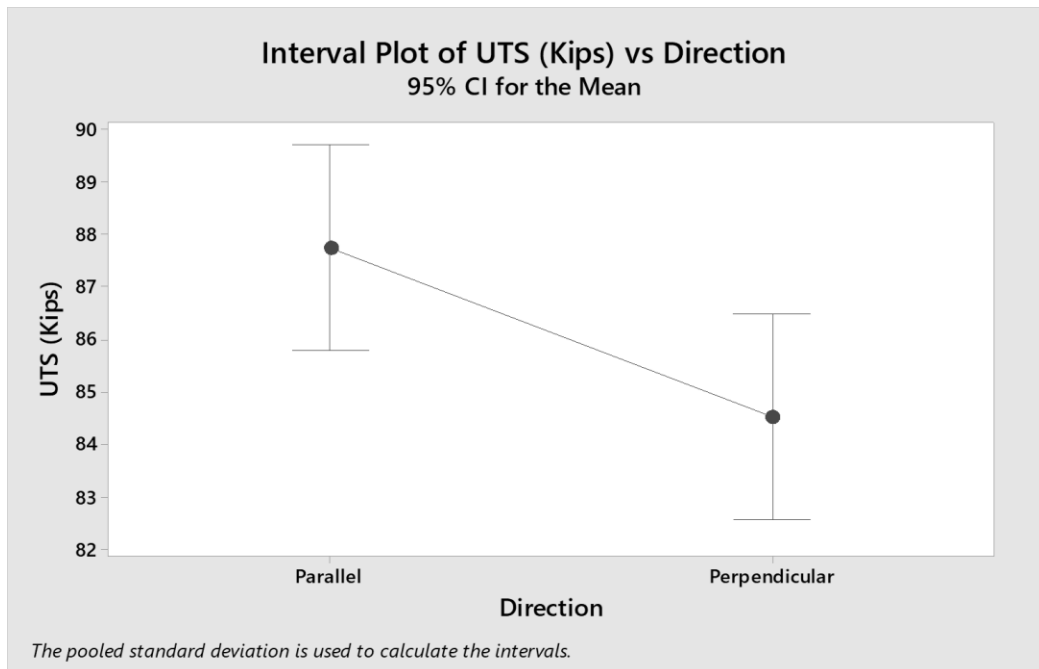


Figure 129: Interval Plot for ER308L for CWTD Control for UTS

When considering the accuracy of the measurements (combined accuracies of all the instruments used to acquire the data), the results of UTS, yield, and hardness are presented in Figures 130-131 for ER70S-6 and ER308L. Reevaluating the statistics with machine accuracy considered, the only statistically unequal combination for ER70S-6 is the UTS in the perpendicular direction when comparing with or without the CTWD control scheme. For ER308L with machine accuracy taken into consideration, the only combinations that change are the comparisons for hardness. With machine accuracy taken into consideration the hardness values for all ER308L combinations with or without the CTWD control are equal.

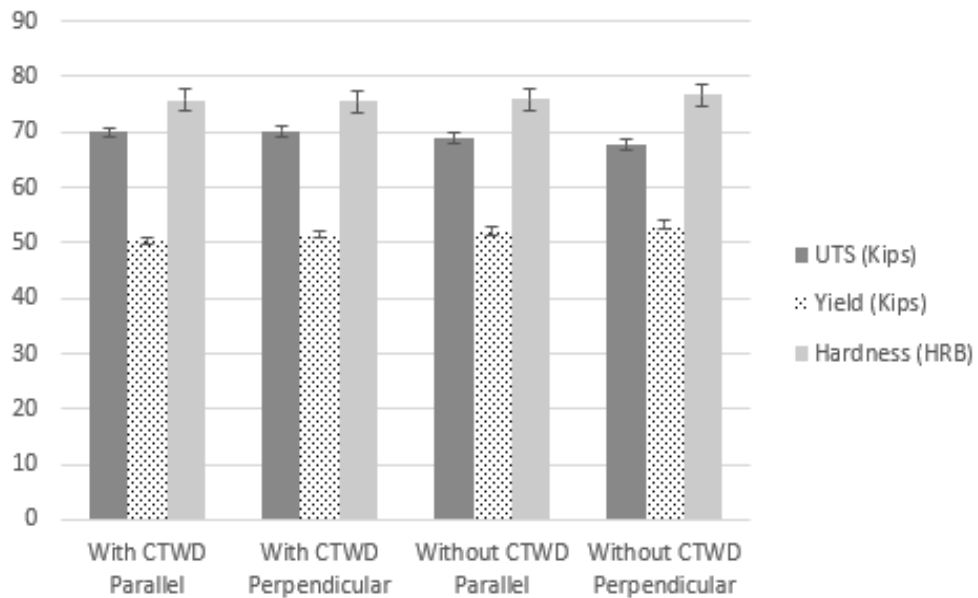


Figure 1302: ER70S-6 CTWD Control Scheme Evaluation

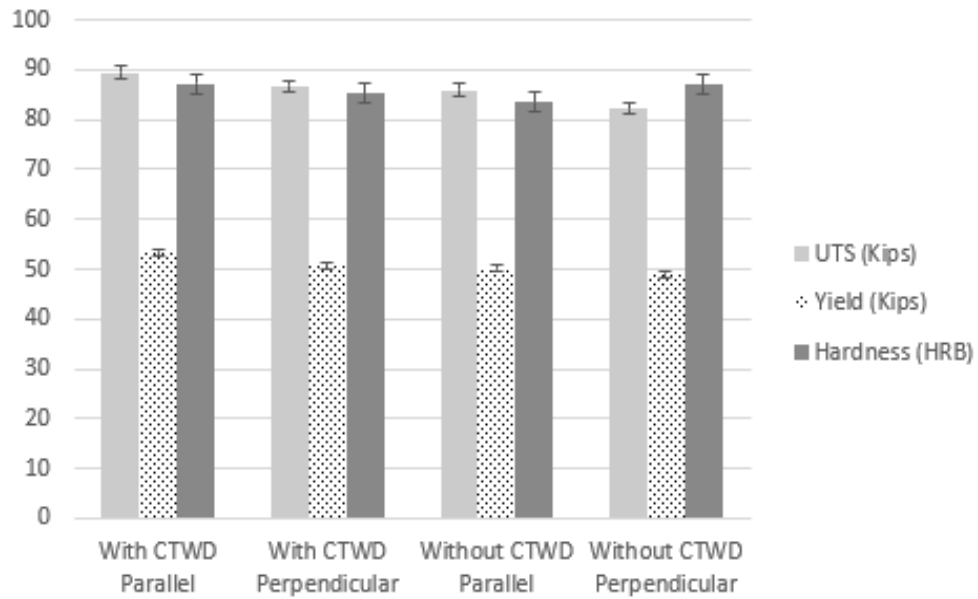


Figure 1313: ER308L CTWD Control Scheme Evaluation

Other measurables evaluating the CTWD control scheme were taken; however, they were single points (print time, etc.) and statistical analysis cannot truly be taken on this data. The print times for the samples were recorded from the machine run time. This includes the time it takes for the operator to stop the program and other arbitrary tasks; therefore, there is some discrepancy between identically produced walls (parallel v. perpendicular) of a few minutes. The amount of material removed from each wall on each side was also recorded. This is the total amount of material needed to have a smooth flat surface on both sides. Table 27 shows the data for both ER70S-6 and ER308L. The values are similar within reason and very little discrepancies are noted.

Table 27: CTWD Control Print Time and Machining Evaluation

	Print Time:	Machined til Flat (in):
With CTWD Control: Parallel	2:00 ER70S-6	0.055 ER70S-6
	1:23 ER308L	0.067 ER308L
With CTWD Control: Perpendicular	2:05 ER70S-6	0.060 ER70S-6
	1:20 ER308L	0.080 ER308L
W/O CTWD Control: Parallel	2:10 ER70S-6	0.054 ER70S-6
	1:24 ER308L	0.071 ER308L
W/O CTWD Control: Perpendicular	2:08 ER70S-6	0.058 ER70S-6
	1:23 ER308L	0.075 ER308L

Metallographic analysis of the microstructure of ER70S-6 and ER308L samples were studied with guidance from the ASM Handbook -Vol 9 [67]. Figure 132 shows the typical microstructure observed in ER70S-6 without the CTWD control. Figure 133 shows the layer boundary of ER70S-6 without the CTWD control. The dark area of the image is where the edges of the sample meet the mounting polymer and is not a void. The grain structure was evaluated at the top and the bottom of the wall to see the effect of repeated reheating and cooling. The results show this produced a non-uniform grain structure with the top of the weld exhibiting acicular ferrite with some regions of pearlite and bainite. This region was observed to only extend for the first few millimeters. The layer interface was noted to have no distinct boundary, unlike previous research [2]. Figure 134 shows a stitched image of the top to bottom of the wall. At the top of the image, Widmanstatten ferrite can be clearly seen along with some acicular ferrite. Grain size starts to decrease and become uniform as you get closer to the bottom.

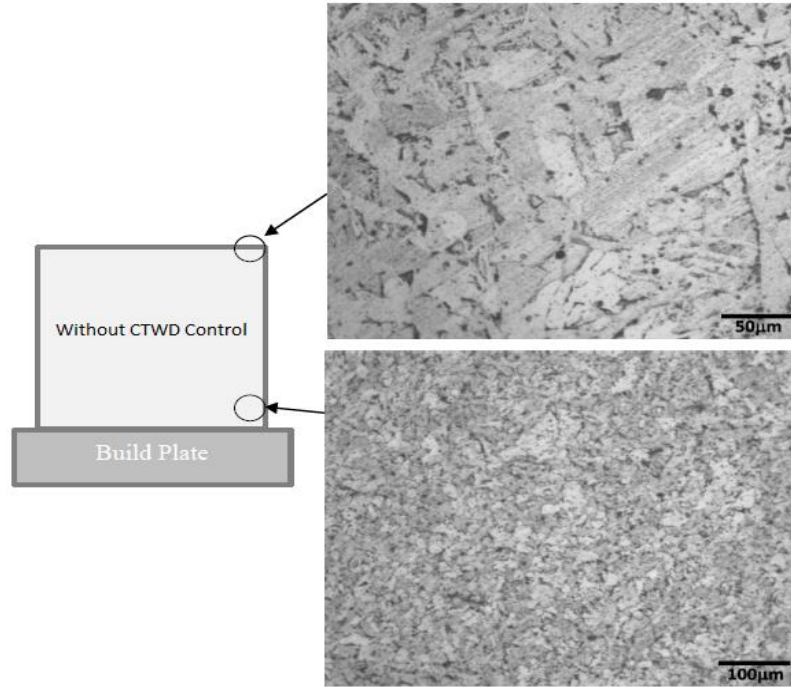


Figure 132: ER70S-6 without CTWD Control Representative Structure

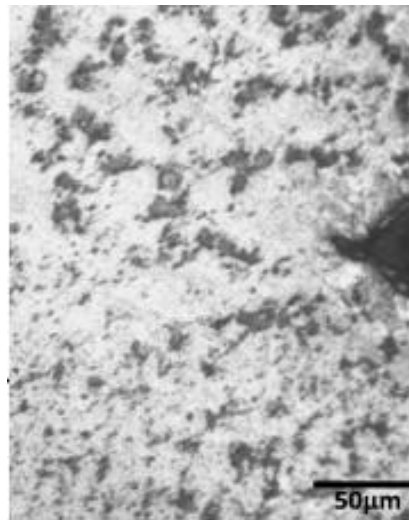


Figure 133: ER70S-6 without CTWD Control Layer Interface

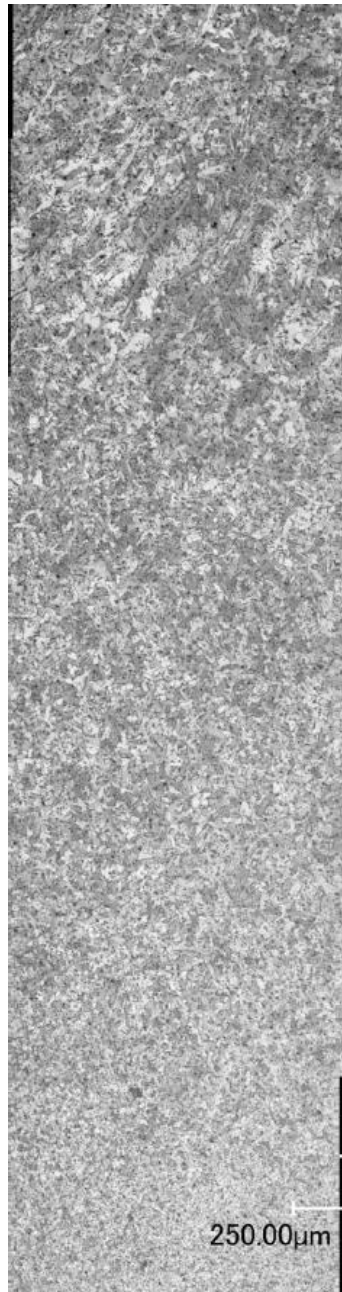


Figure 134: Top to Bottom View of ER70S-6 without CTWD Control

Figure 135 shows the typical microstructure observed in ER70S-6 with the CTWD control. Figure 136 shows the layer boundary of ER70S-6 with the CTWD control. Again, the dark area of the image is where the edges of the sample meet the mounting polymer and is not a void. A uniform grain structure was noted throughout the wall and the layer interface was once again noted to have no distinct boundary.



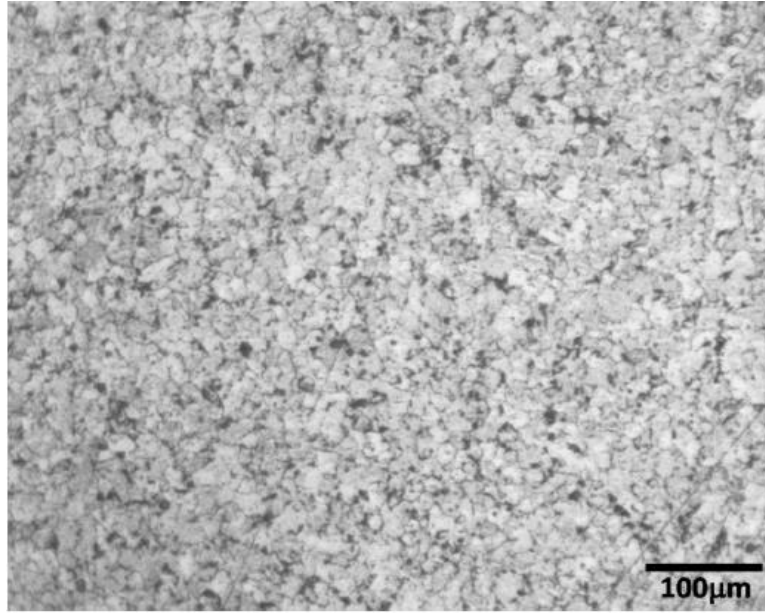


Figure 135: ER70S-6 with CTWD Control Representative Structure

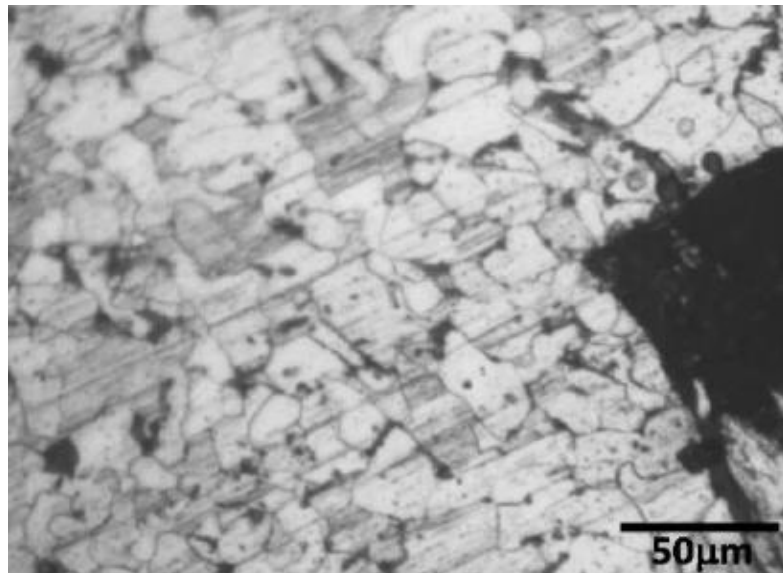


Figure 136: ER70S-6 with CTWD Control Layer Interface

For ER308L there was no notable difference in microstructures either with and without the CTWD control. Figure 137 shows the typical microstructure found in ER308L. Figure 138 shows the layer interface. A clear boundary layer is present like that found in previous research [2]. The general microstructure is comprised of skeletal  $\delta$ -ferrite in an austenitic matrix.

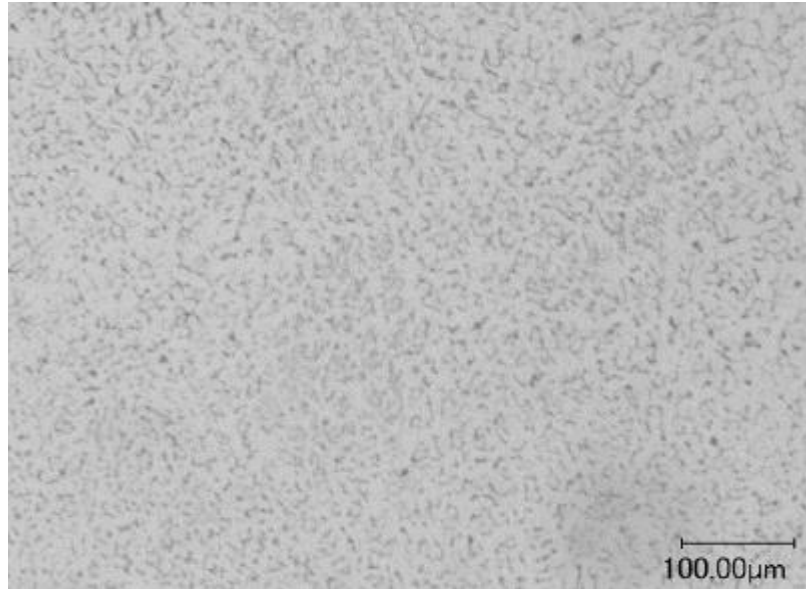


Figure 137: ER308L Typical Microstructure

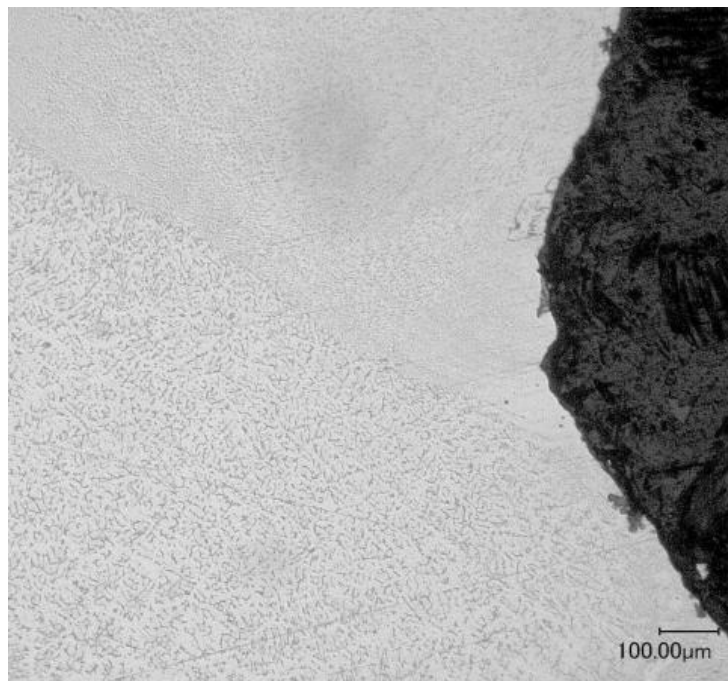


Figure 138: ER308L Typical Layer Interface with Noticeable Boundary

One of the issues noted during the production of samples without the CTWD control scheme was that the ‘print’ constantly needed to be monitored to ensure that the proper CTWD was maintained or at least visually sound. If the operator noticed the CTWD was too close at the end of a layer, the distance was manually adjusted, and the program

restarted at that height. This occurred 2-3 times per wall which would also account for the slightly longer print times without the CTWD control. Measurables such as voltage, current, and wire feed speed were unaffected by the CTWD control as it only took place at the end of a layer and not during a layer.

### **Cold Metal Transfer Control Evaluation**

Table 28 shows the results of comparing walls ‘printed’ with the standard synergic control to those ‘printed’ with the CMT control scheme for ER70S-6. A P-Value above 0.05 indicates no significant difference between the means of the group and they are statistically equal with 95% confidence. Appendix IV has the statistical outputs for these tests.

Table 28: ER70S-6 CMT v. Standard Control P-Values

	UTS	Yield	Hardness
With CMT Control: Parallel v. Perpendicular	0.396	0.543	0.801
With Standard Control: Parallel v. Perpendicular	0.862	0.458	0.038
CMT v. Standard Control	0.00019	0.685	0.010

The walls created with the CMT control were statistically equal in both parallel and perpendicular directions for UTS, yield, and hardness measurables. The walls created with the standard control were statistically the same for UTS and yield strength but were not for hardness. Since the hardness is not a directional measurable, the two directions were not treated independently when compared to the walls that did utilize the CMT control scheme.

When evaluating the CMT control scheme for ER70S-6, the yield strength was statistically equal; however, the UTS and hardness in both the parallel and perpendicular directions was not statistically the same. When looking at the values of the tests, it shows that the UTS of the walls with the CMT control were higher than with the standard method. When looking at the values of the tests, it shows that the hardness of the walls with the standard control were higher than with the CMT method; but not as repeatable.

Table 29 shows the results of comparing walls ‘printed’ with the CMT control to those ‘printed’ with the standard scheme for ER308L. A P-Value above 0.05 indicates no significant difference between the means of the group and they are statistically equal with 95% confidence. If the parallel and perpendicular directions for both sub-groups were statistically equal, they were treated as a single grouping for comparison to each other. Appendix IV has the statistical outputs for these tests.

Table 29: ER308L CMT v. Standard Control P-Values

	UTS	Yield	Hardness
With CMT Control: Parallel v. Perpendicular	0.014	0.002	0.003
With Standard Control: Parallel v. Perpendicular	0.443	0.556	0.708
CMT v. Standard: Parallel	0.000001	0.002	0.0002
CMT v. Standard: Perpendicular	0.002	0.00004	0.000004

The walls created with the CMT control were not statistically equal in both parallel and perpendicular directions for UTS, yield, or hardness measurables. The walls created with the standard control were statistically the same for UTS, yield strength, and hardness.

When evaluating the CMT control scheme for ER308L, the UTS, yield strength, and hardness in both the parallel and perpendicular directions were not statistically the same. When looking at the values of the tests, it shows that the UTS of the walls with the CMT control were higher than with the standard method in both directions. When looking at the values of the tests, it shows that the yield strength and hardness of the walls with the standard control were higher than with the CMT control in both directions. For the CMT control both the UTS and yield strength values were higher for the parallel deposition direction.

Figures 139-141 show the main effects plots for the hardness, yield strength, and UTS for ER70S-6. Figures 142-144 show the residual plots for hardness, yield strength, and UTS for ER70S-6. Figures 145-156 show the Tukey-Kramer analysis and interval plots for hardness, yield strength, and UTS for ER70S-6. Note values for hardness are in HRB, and for yield strength and UTS; kips.

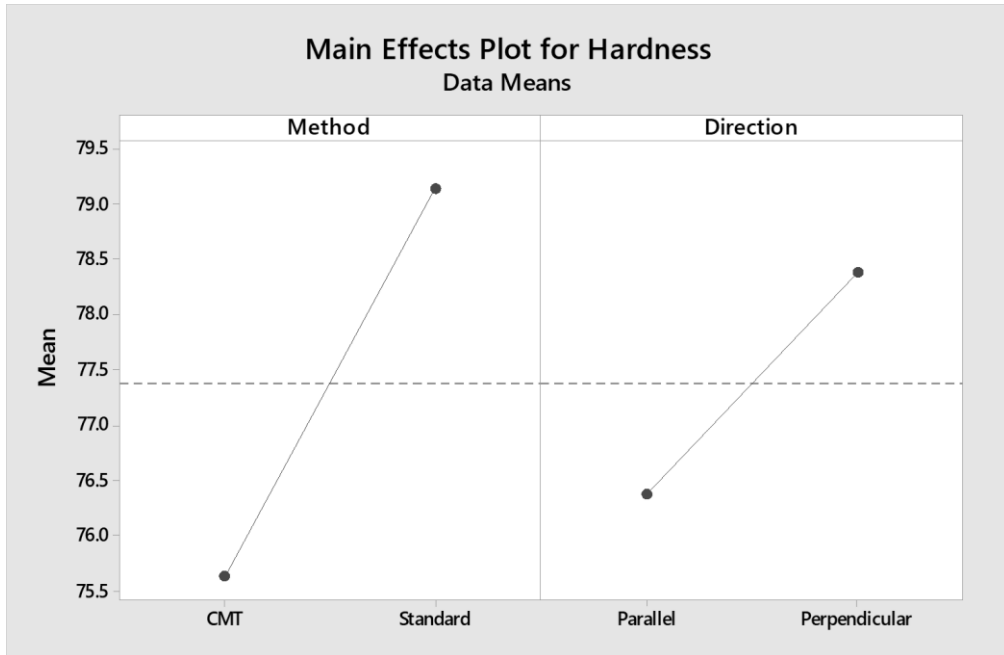


Figure 139: Main Effects Plot for ER70S-6 for Hardness

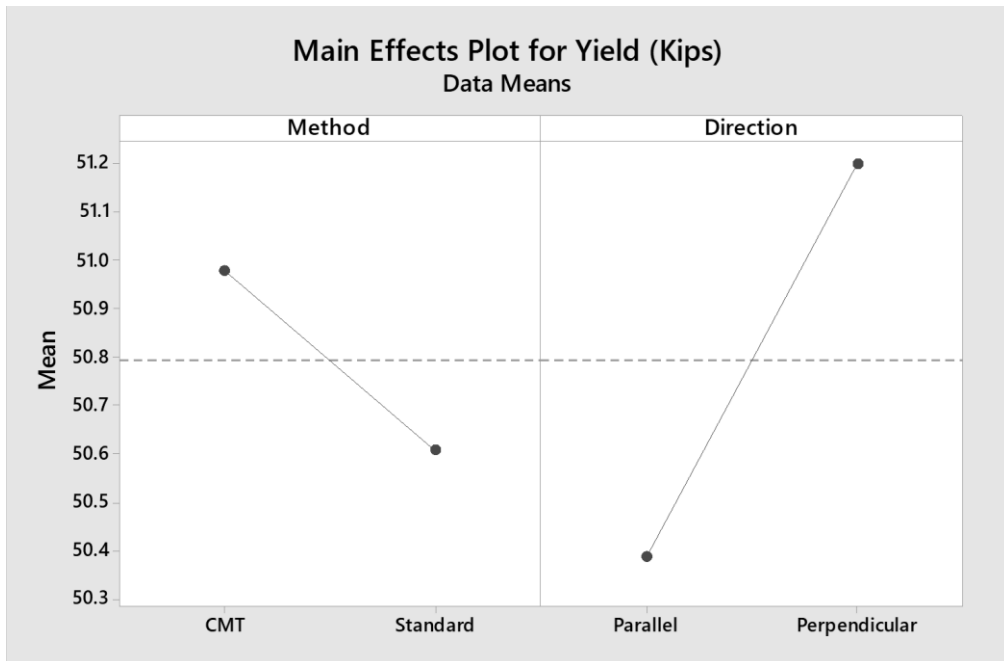


Figure 140: Main Effects Plot for ER70S-6 for Yield

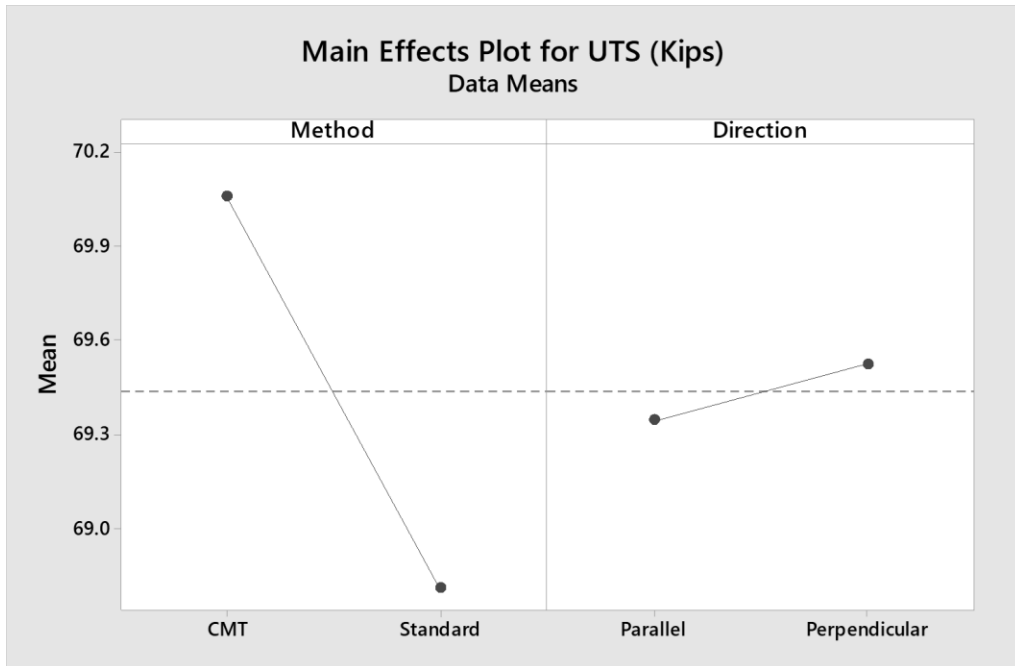


Figure 141: Main Effects Plot for ER70S-6 for UTS

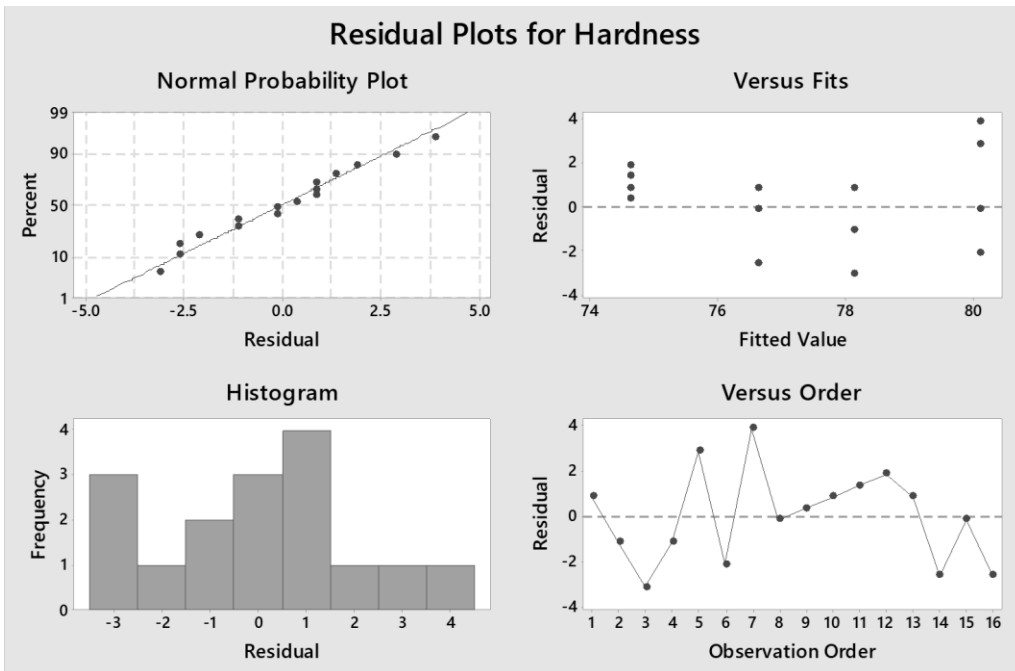


Figure 142: Residual Plots for ER70S-6 for Hardness

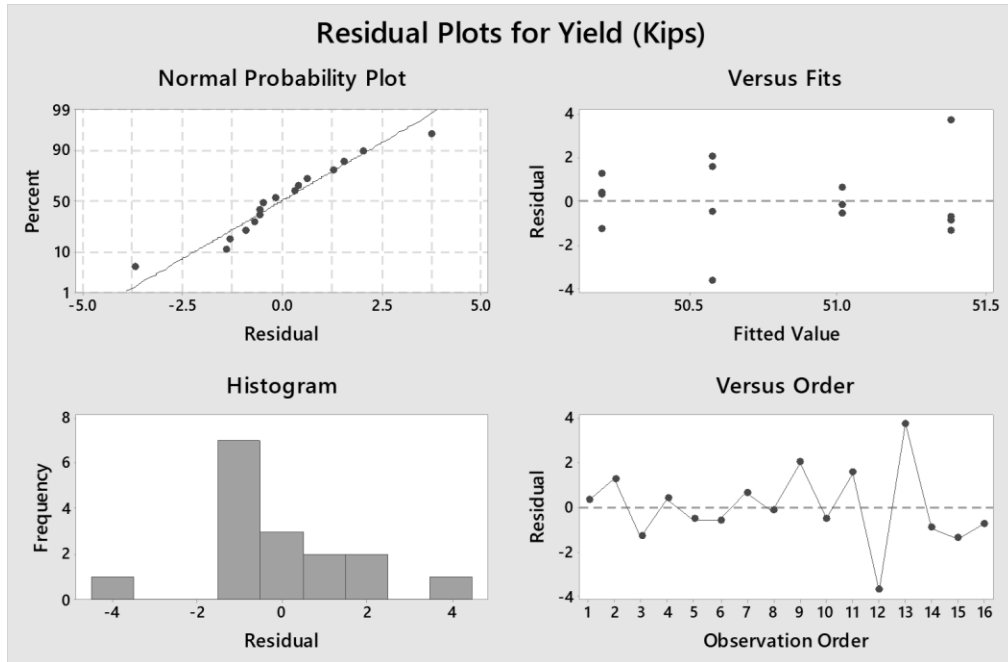


Figure 143: Residual Plots for ER70S-6 for Yield

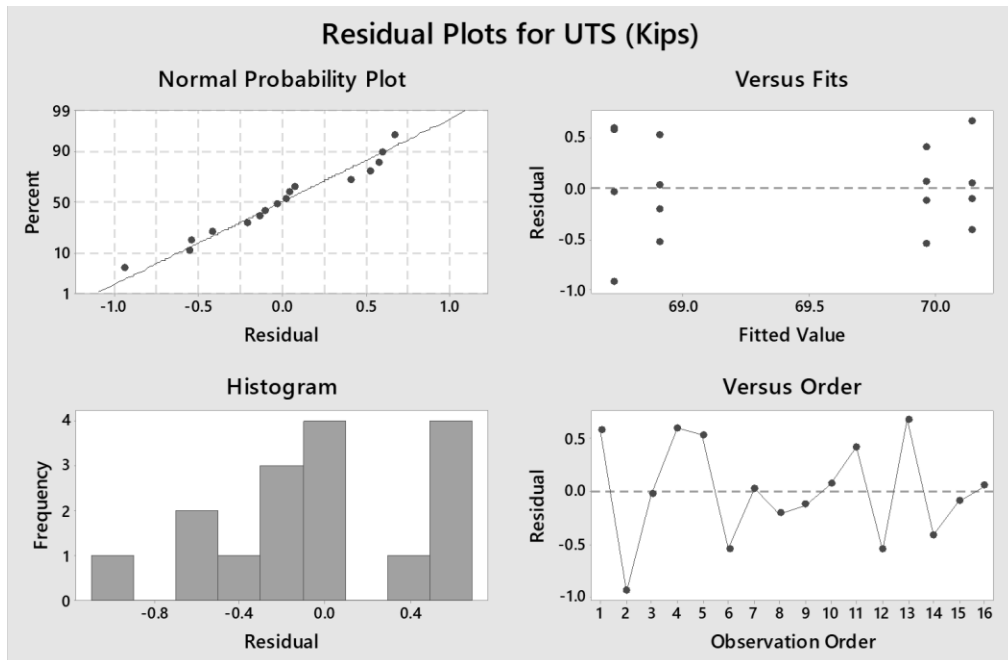


Figure 144: Residual Plots for ER70S-6 for UTS



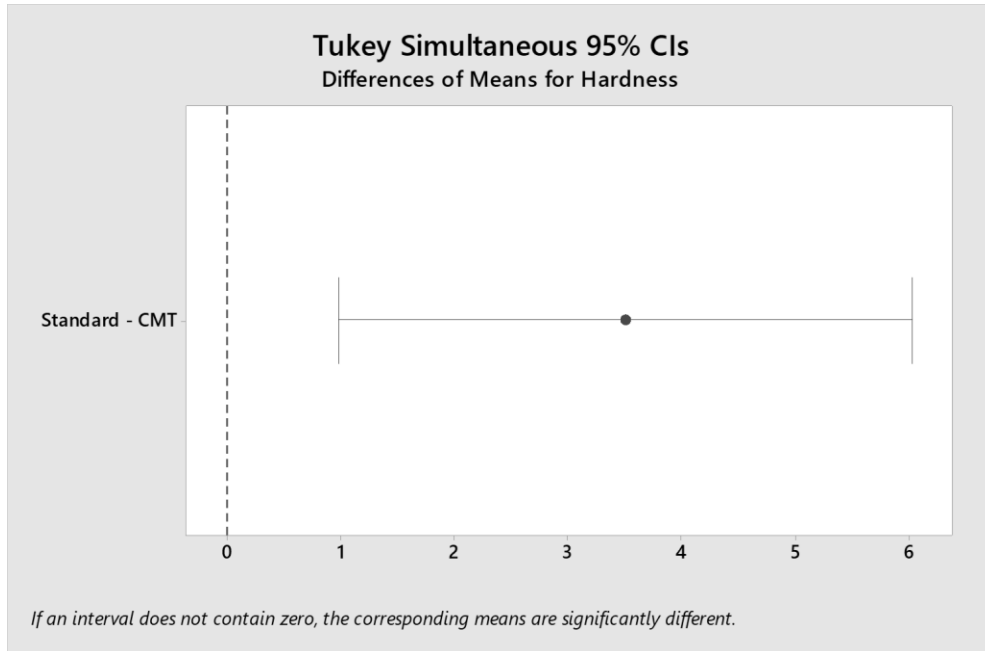


Figure 145: Tukey Analysis for ER70S-6 for Hardness

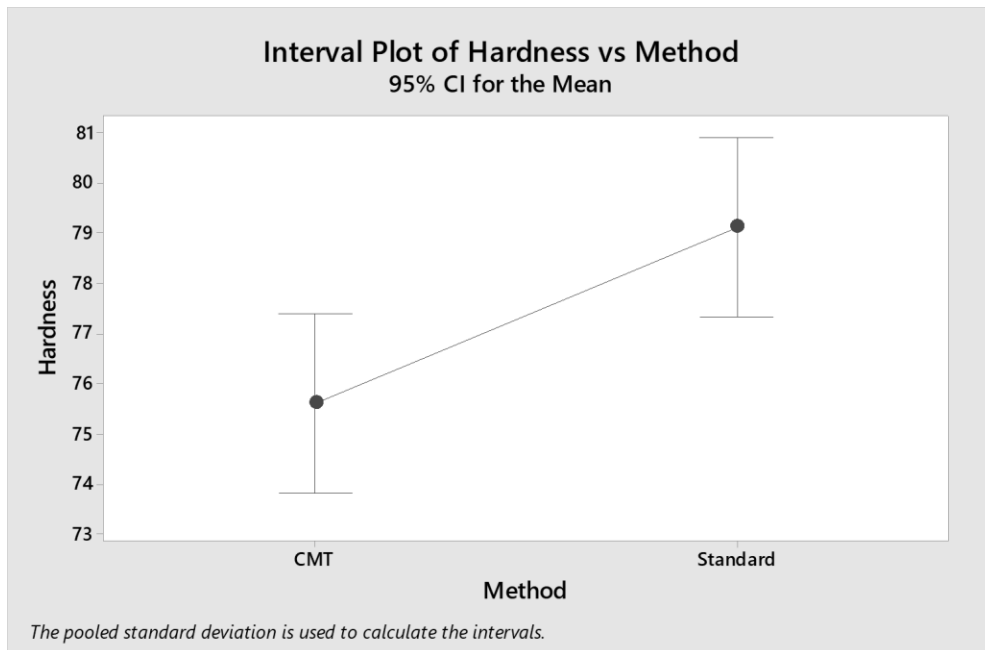


Figure 146: Interval Plot for ER70S-6 for Hardness

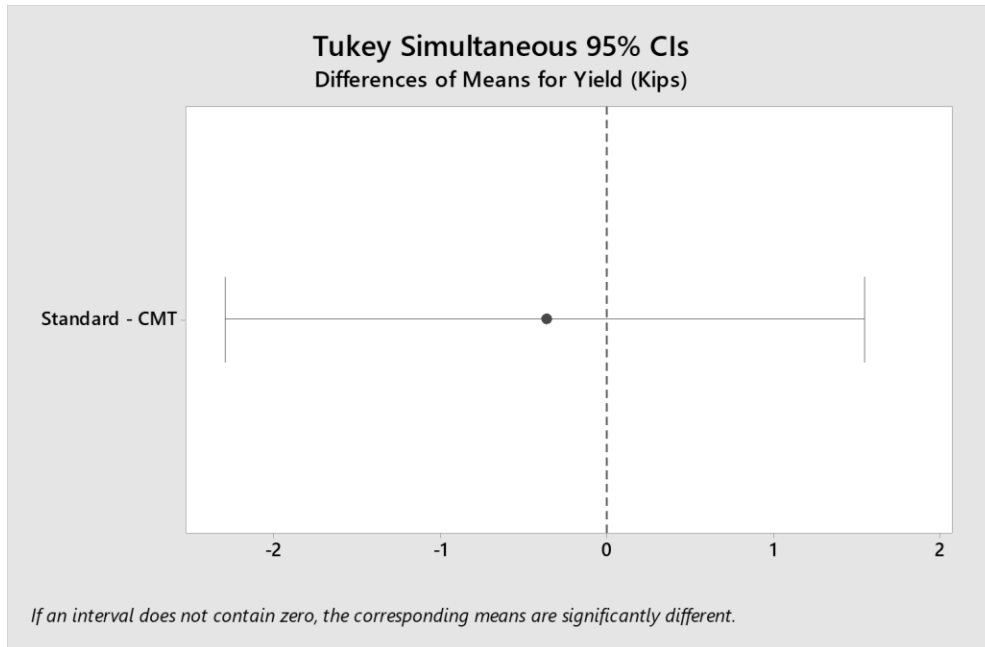


Figure 147: Tukey Analysis for ER70S-6 for Yield

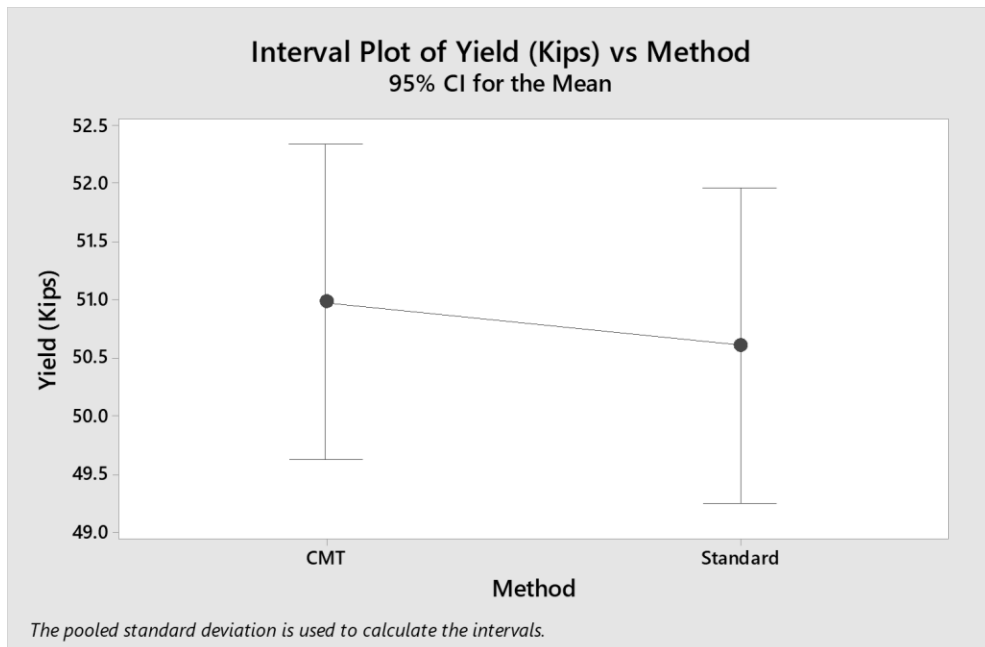


Figure 148: Interval Plot for ER70S-6 for Yield

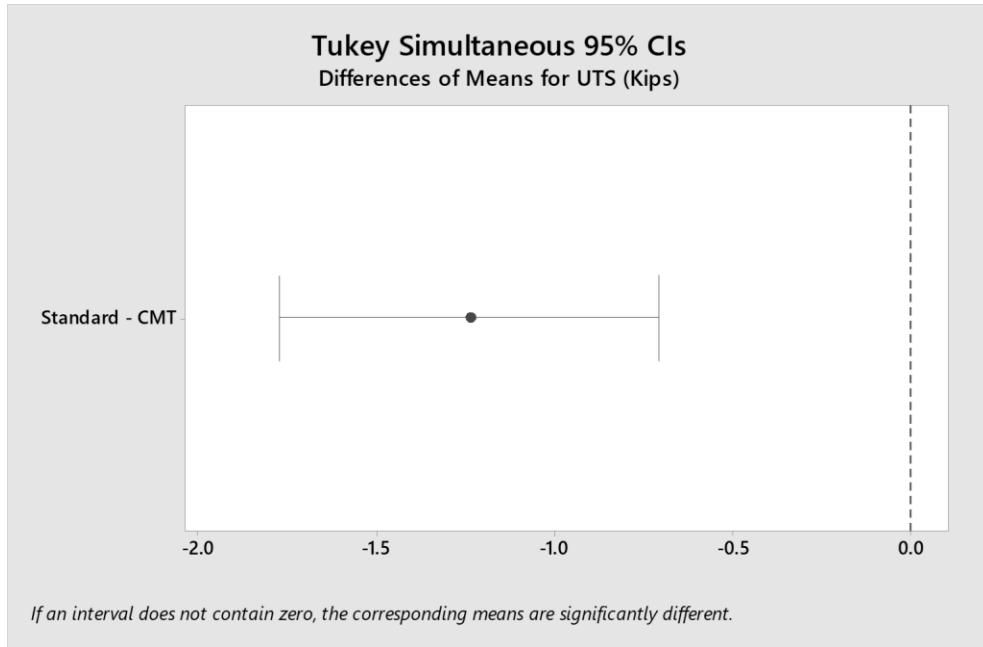


Figure 149: Tukey Analysis for ER70S-6 for UTS

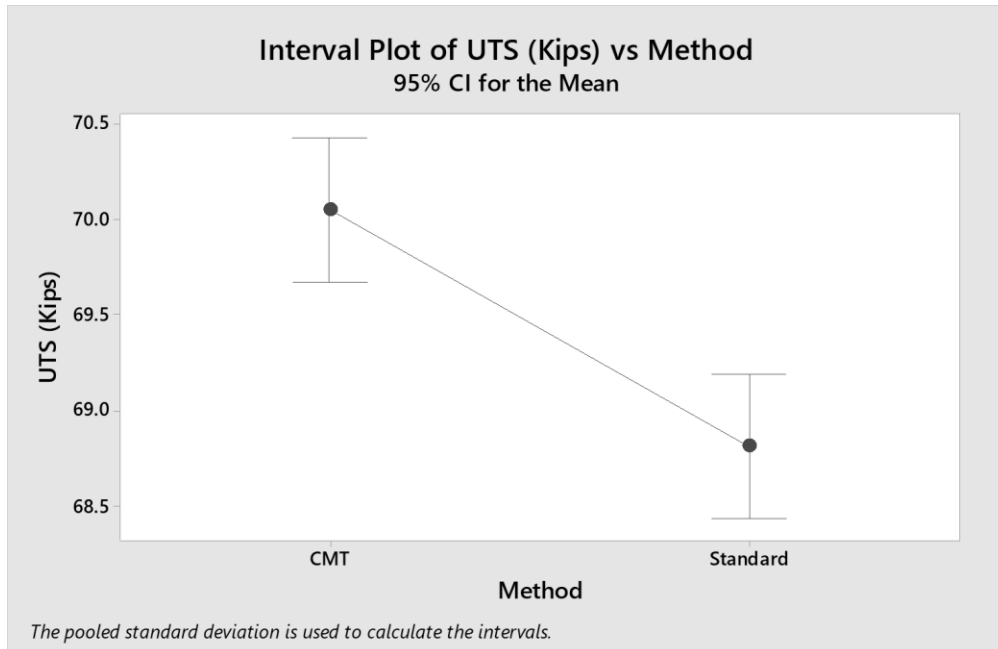


Figure 150: Interval Plots for ER70S-6 for UTS

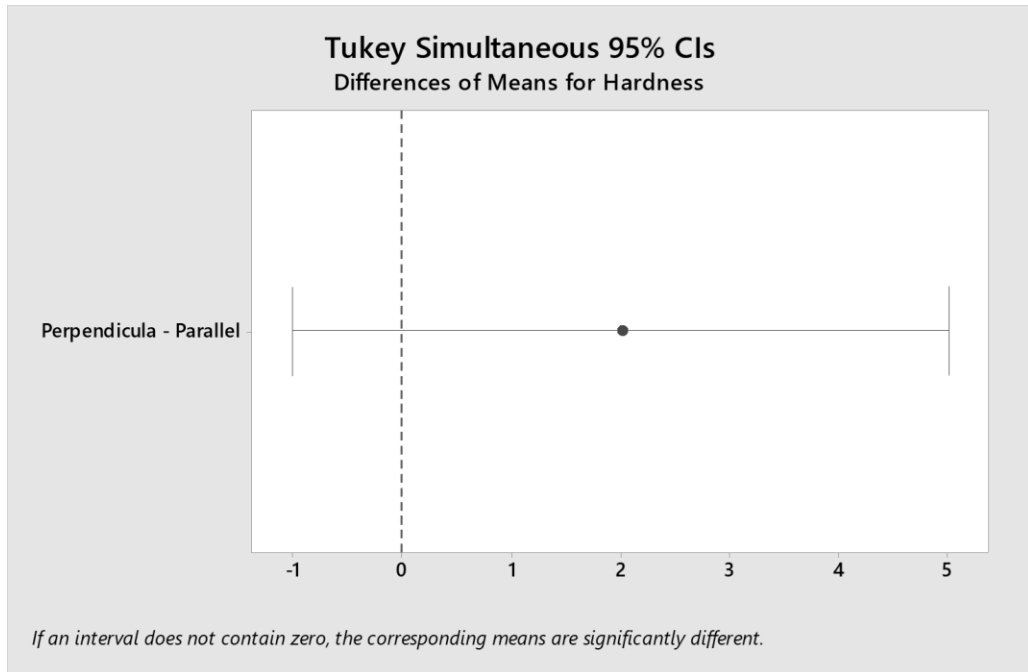


Figure 151: Tukey Analysis for ER70S-6 for Hardness

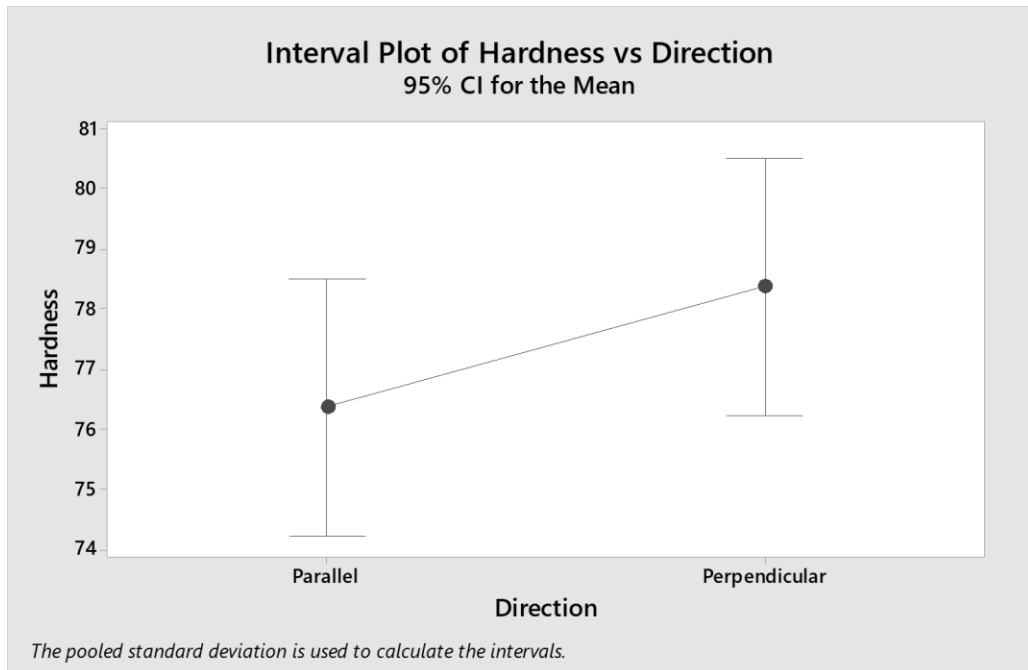


Figure 152: Interval Plot for ER70S-6 for Hardness

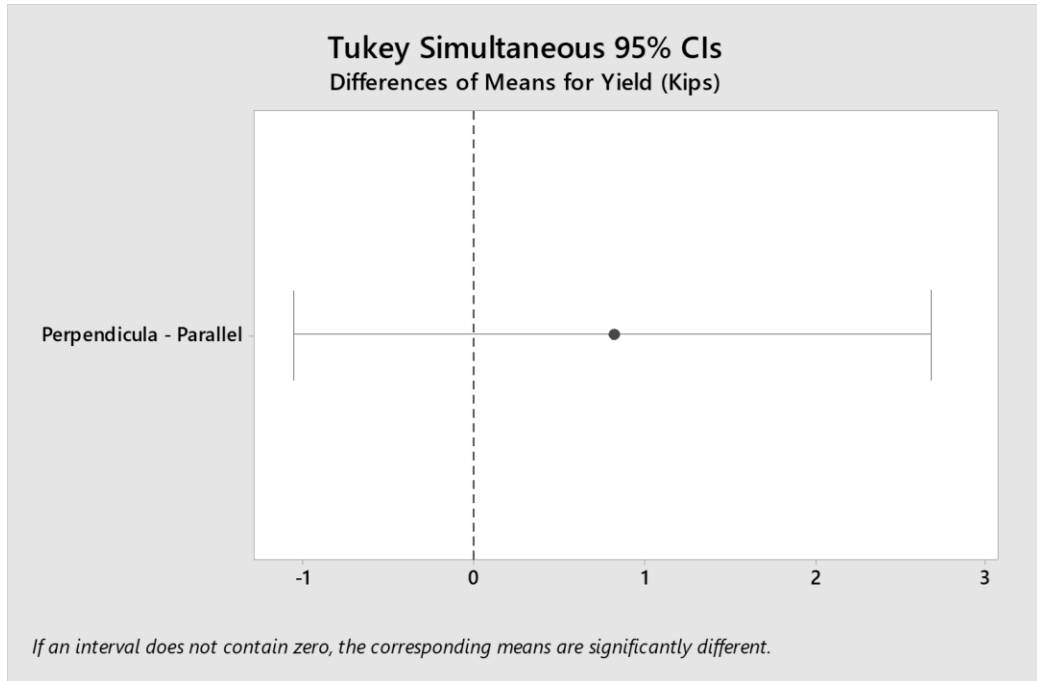


Figure 153: Tukey Analysis for ER70S-6 for Yield

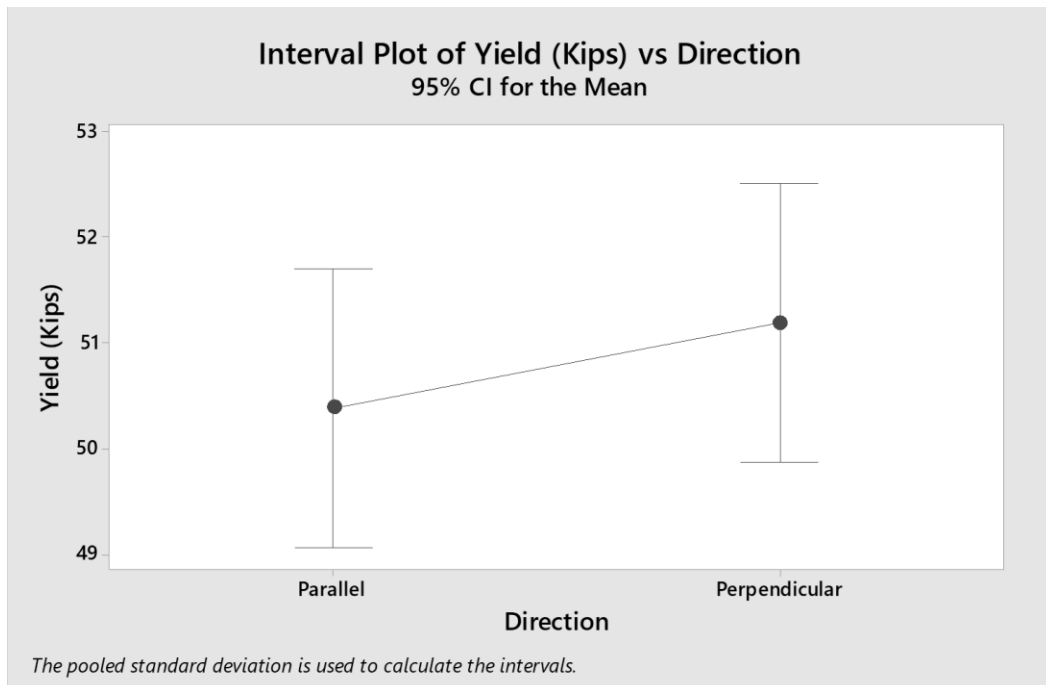


Figure 154: Interval Plot for ER70S-6 for Yield

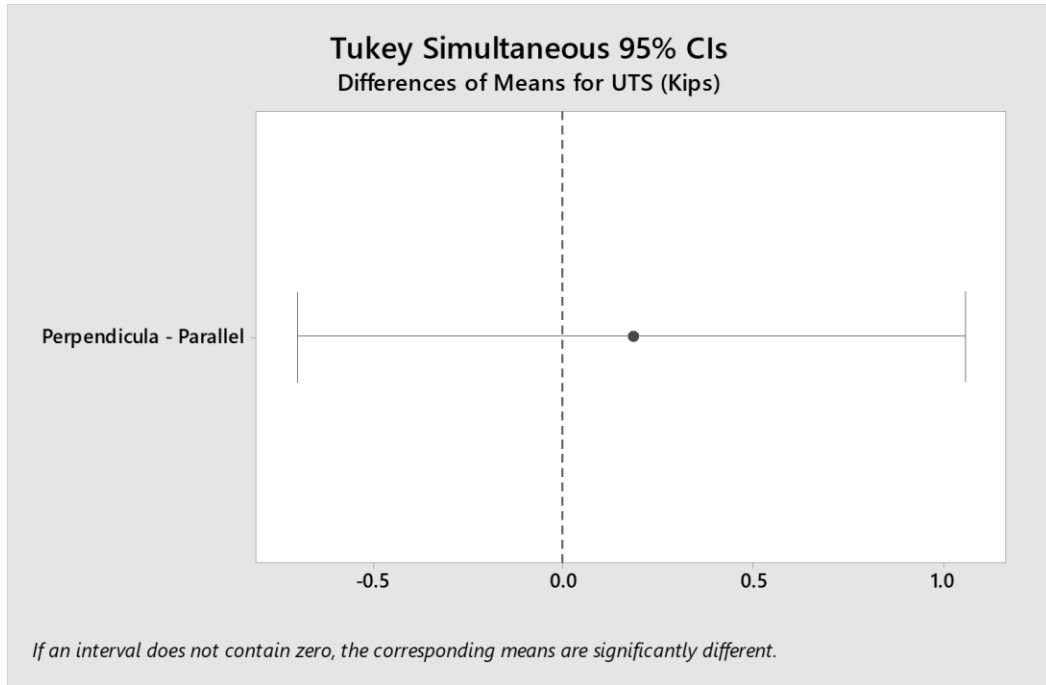


Figure 155: Tukey Analysis for ER70S-6 for UTS

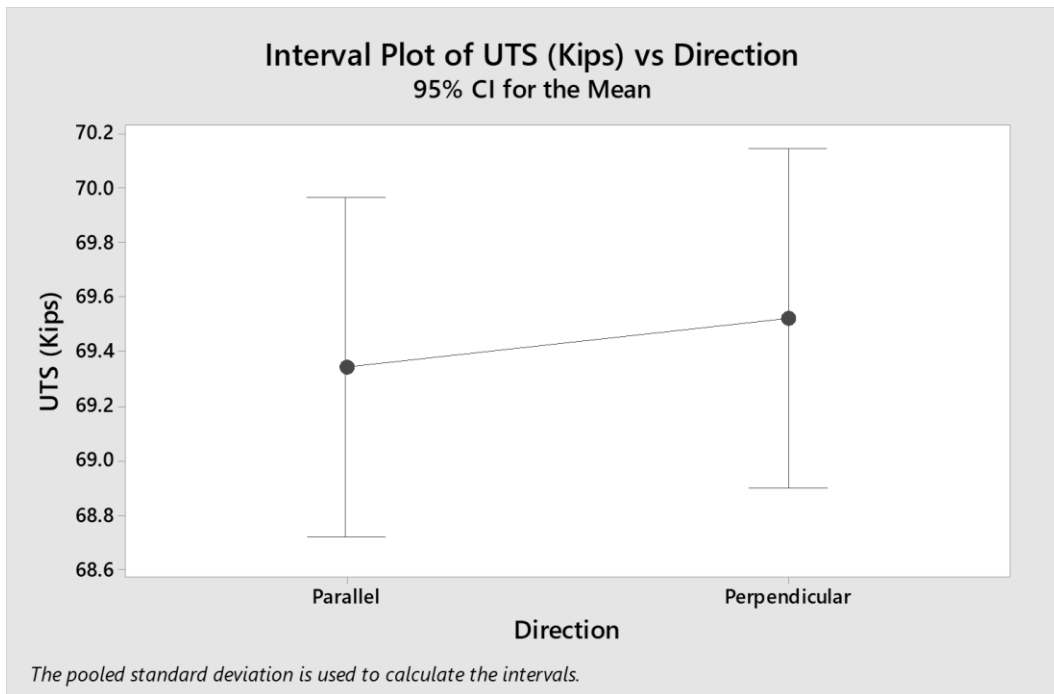


Figure 156: Interval Plot for ER70S-6 for UTS

Figures 157-159 show the main effects plots for the hardness, yield strength, and UTS for ER308L. Figures 160-162 show the residual plots for hardness, yield strength, and UTS for ER308L. Figures 163-174 show the Tukey-Kramer analysis and interval plots for hardness, yield strength, and UTS for ER308L. Note values for hardness are in HRB, and for yield strength and UTS; kips.

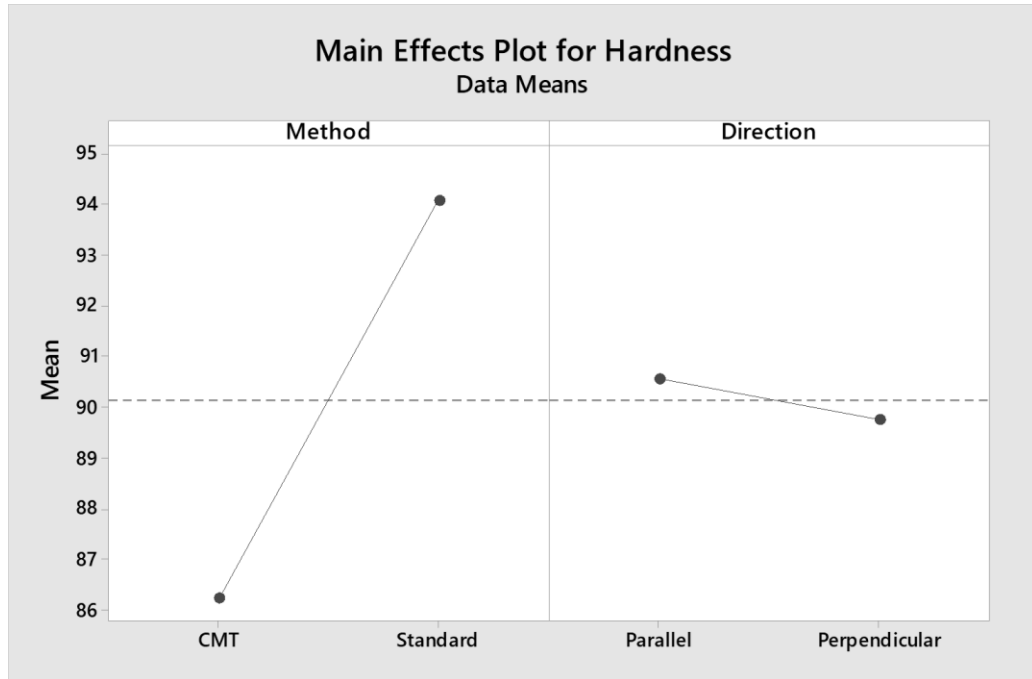


Figure 157: Main Effects Plot for ER308L for Hardness

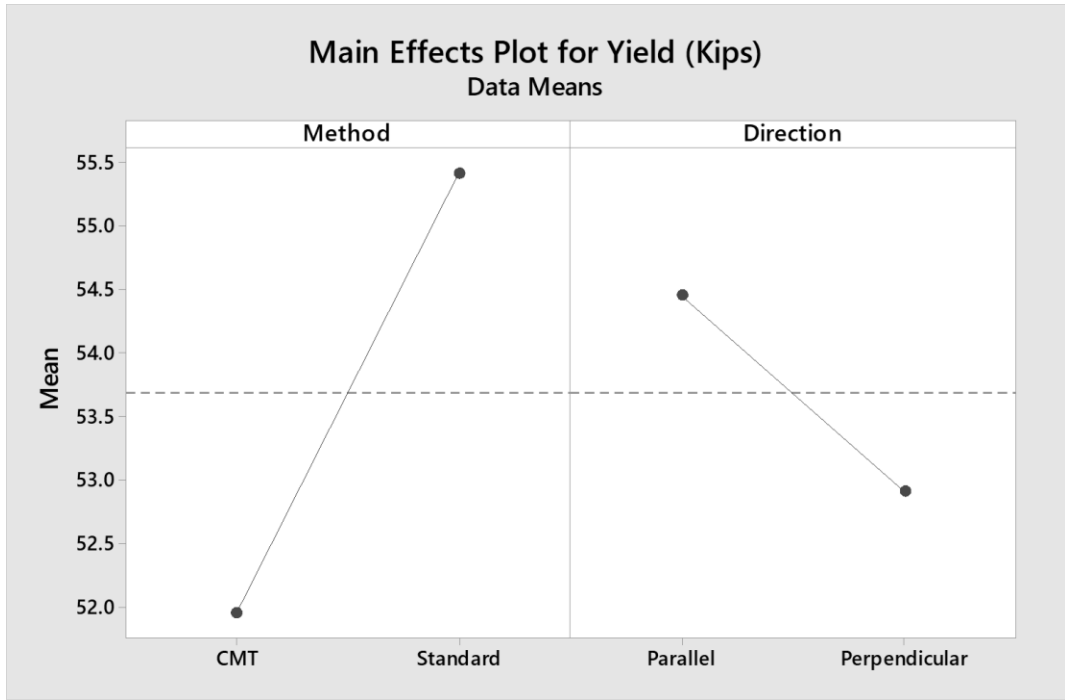


Figure 158: Main Effects Plot for ER308L for Yield

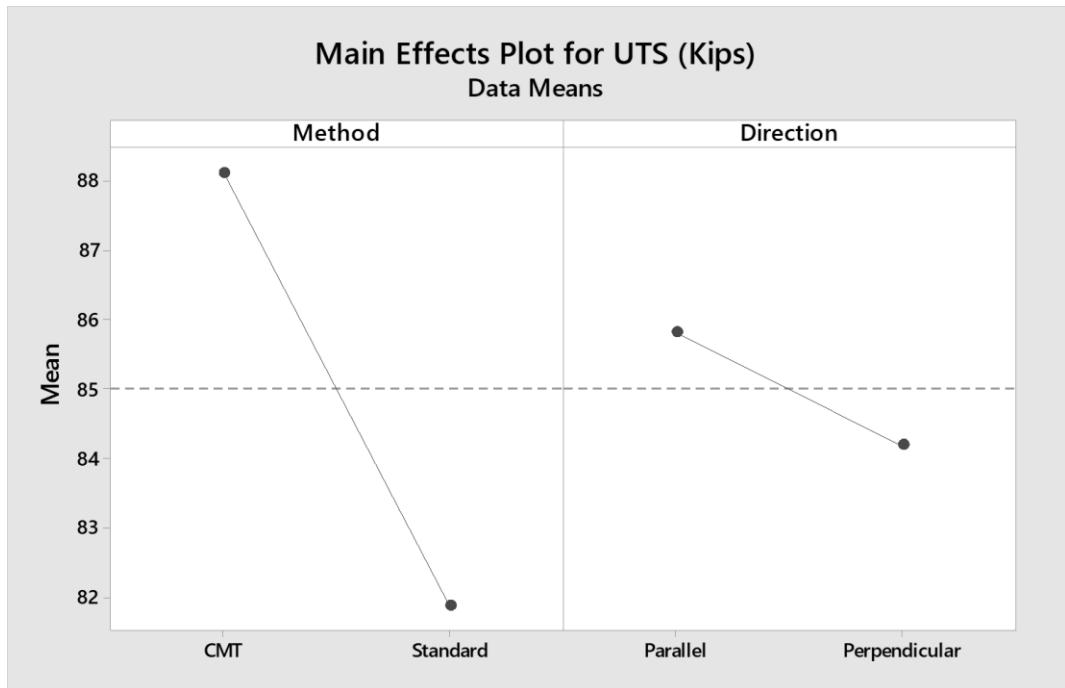


Figure 159: Main Effects Plot for ER308L for UTS



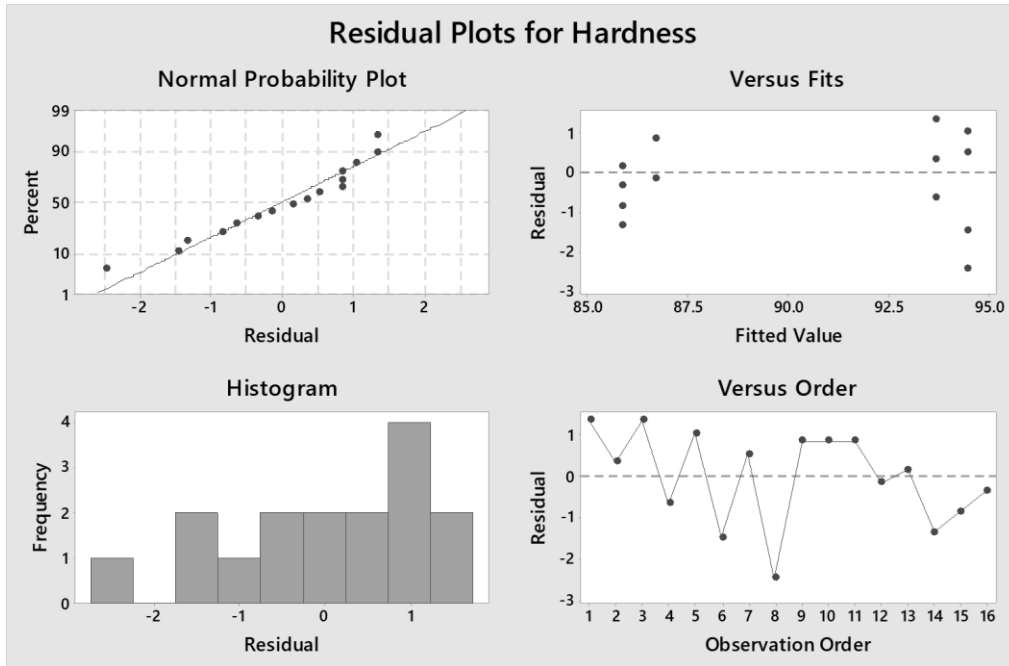


Figure 160: Residual Plots for ER308L for Hardness

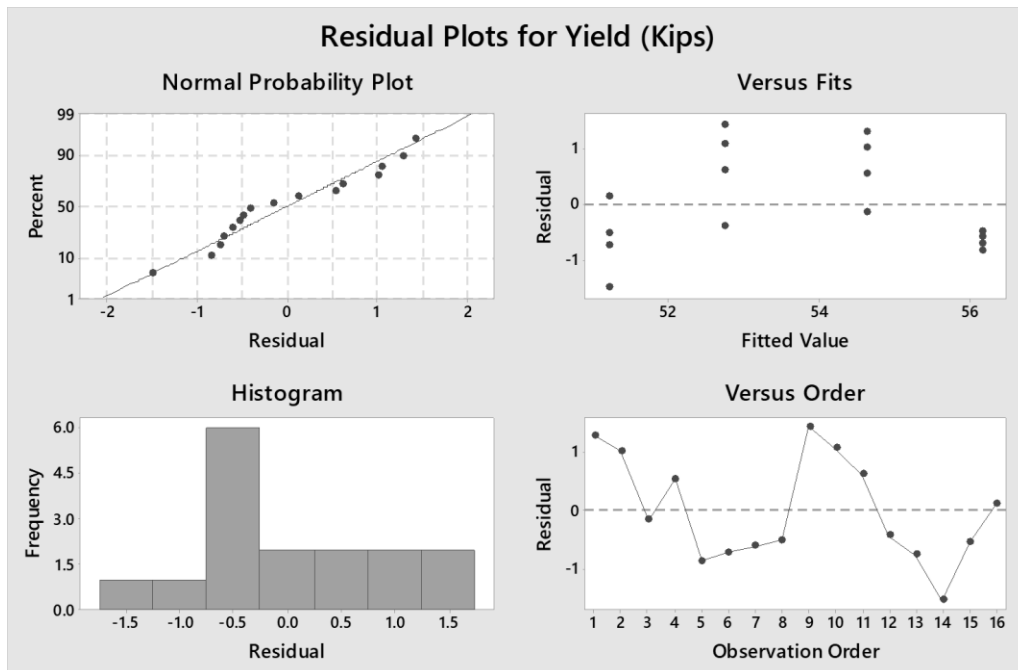


Figure 161: Residual Plots for ER308L for Yield

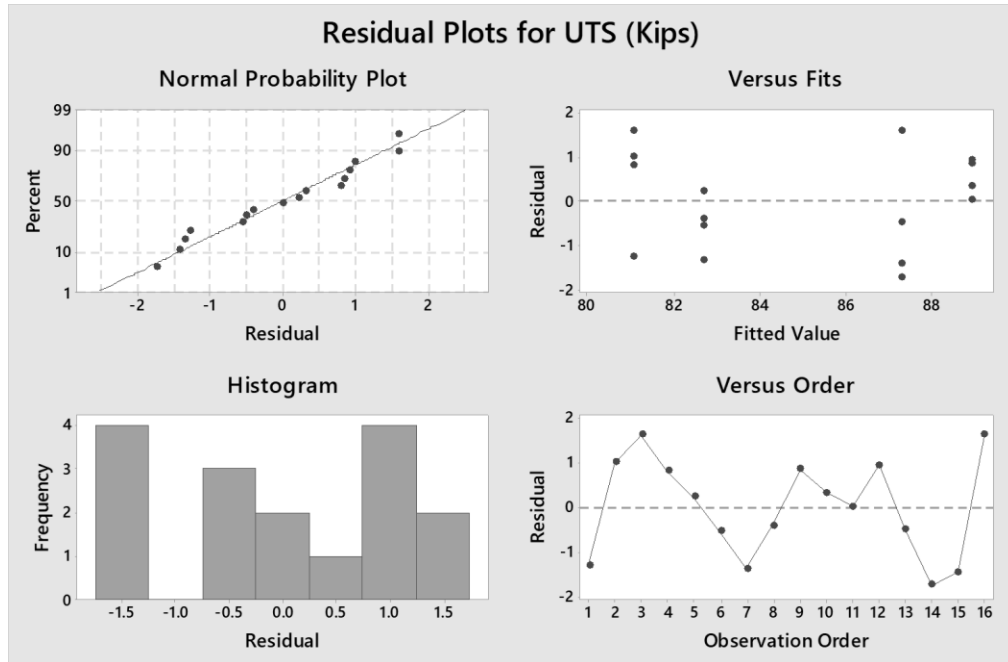


Figure 162: Residual Plots for ER308L for UTS

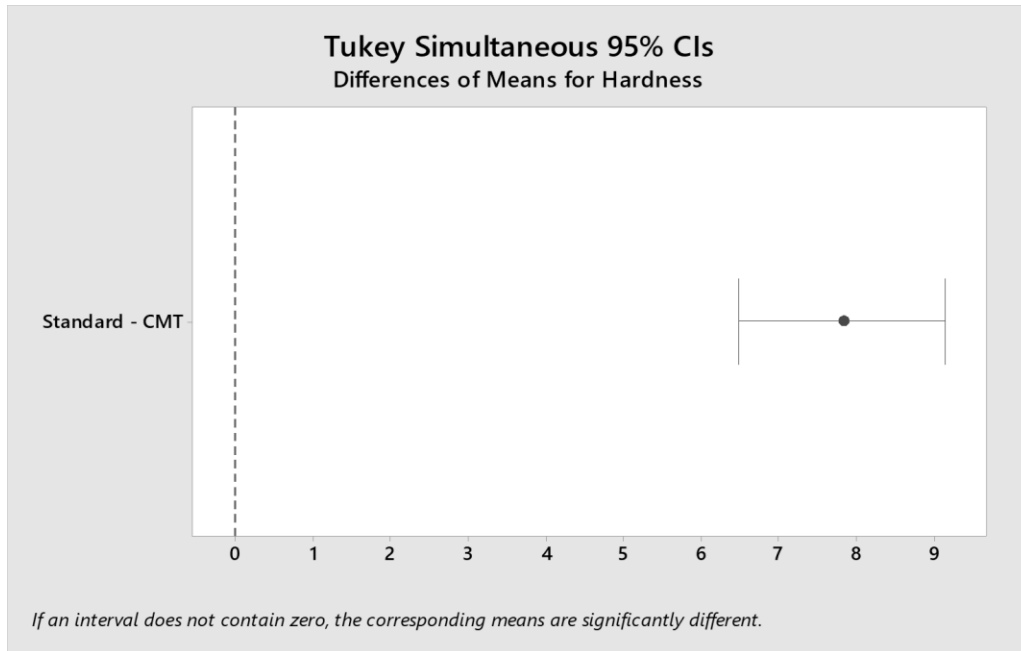


Figure 163: Tukey Analysis for ER308L for Hardness

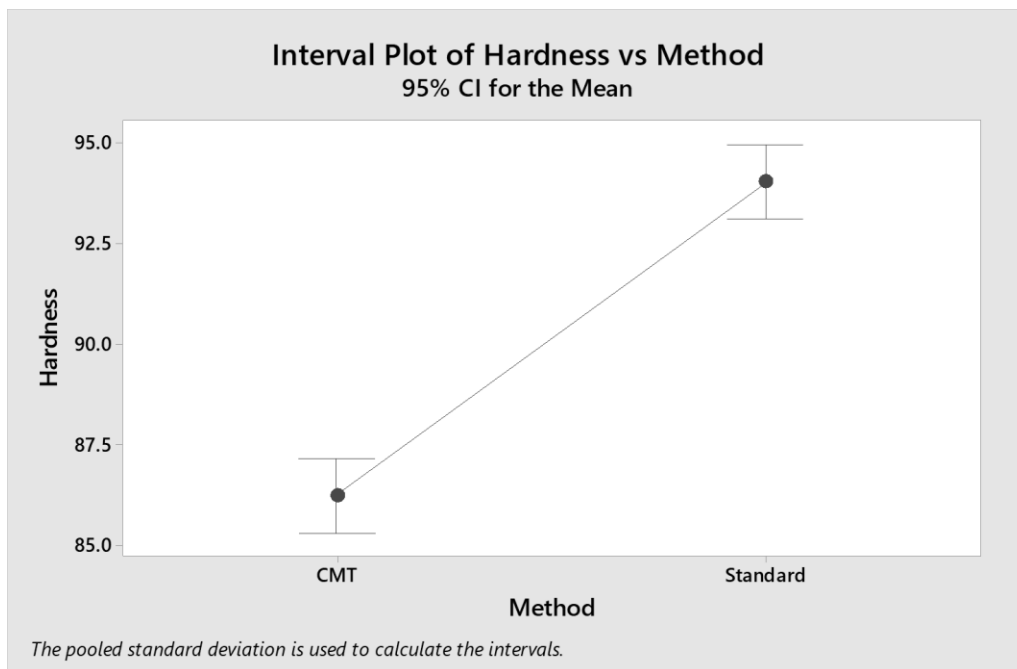


Figure 164: Interval Plot for ER308L for Hardness

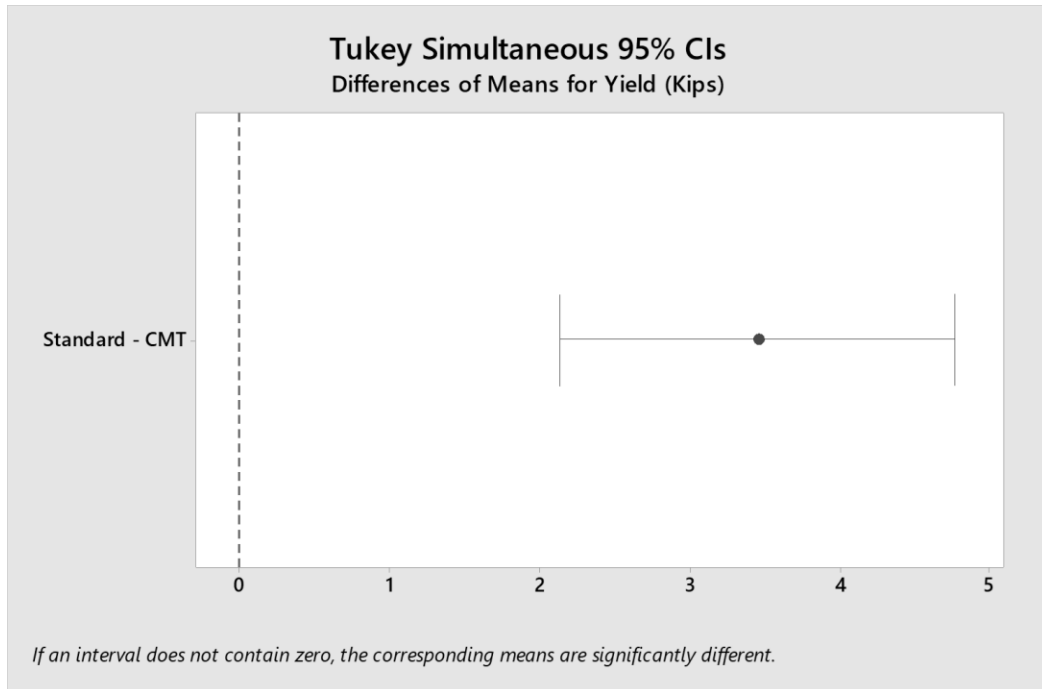


Figure 165: Tukey Analysis for ER308L for Yield

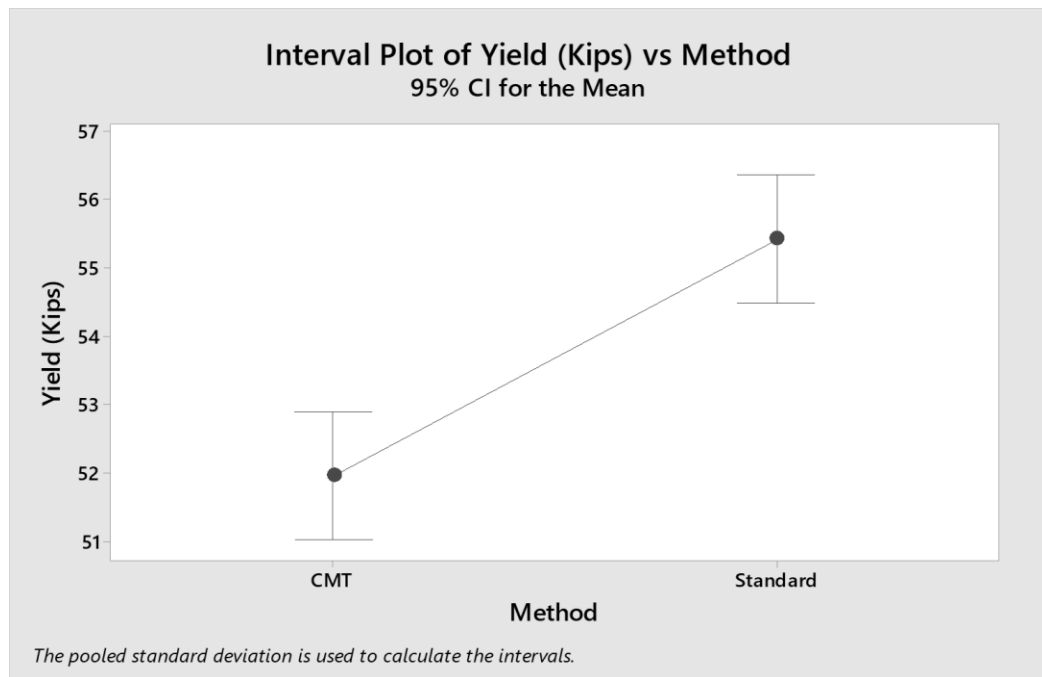


Figure 166: Interval Plot for ER308L for Yield

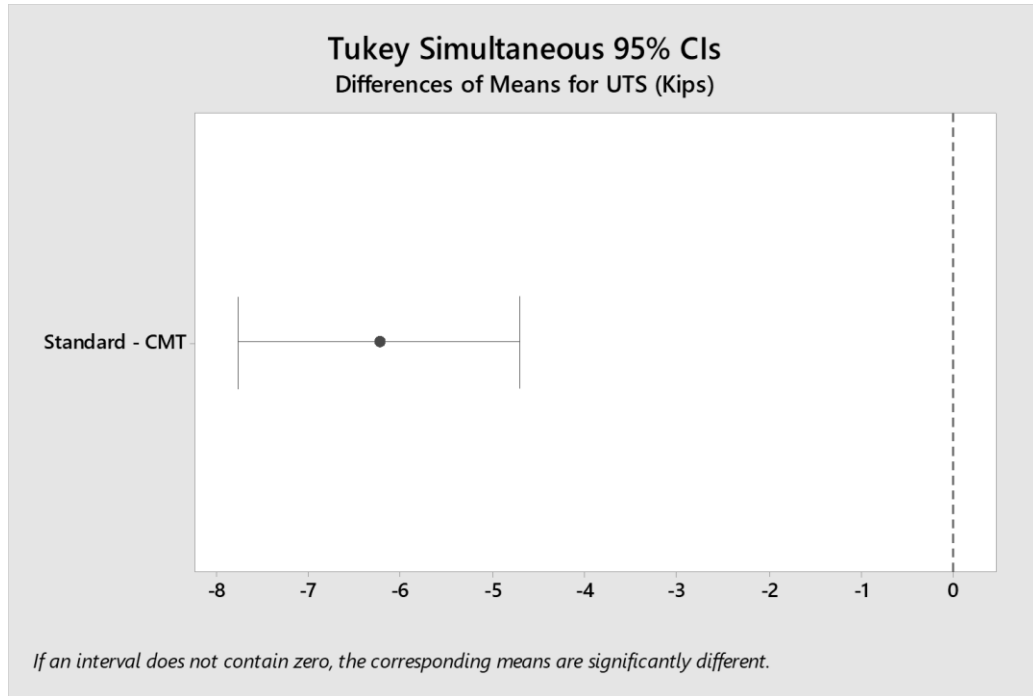


Figure 167: Tukey Analysis for ER308L for UTS

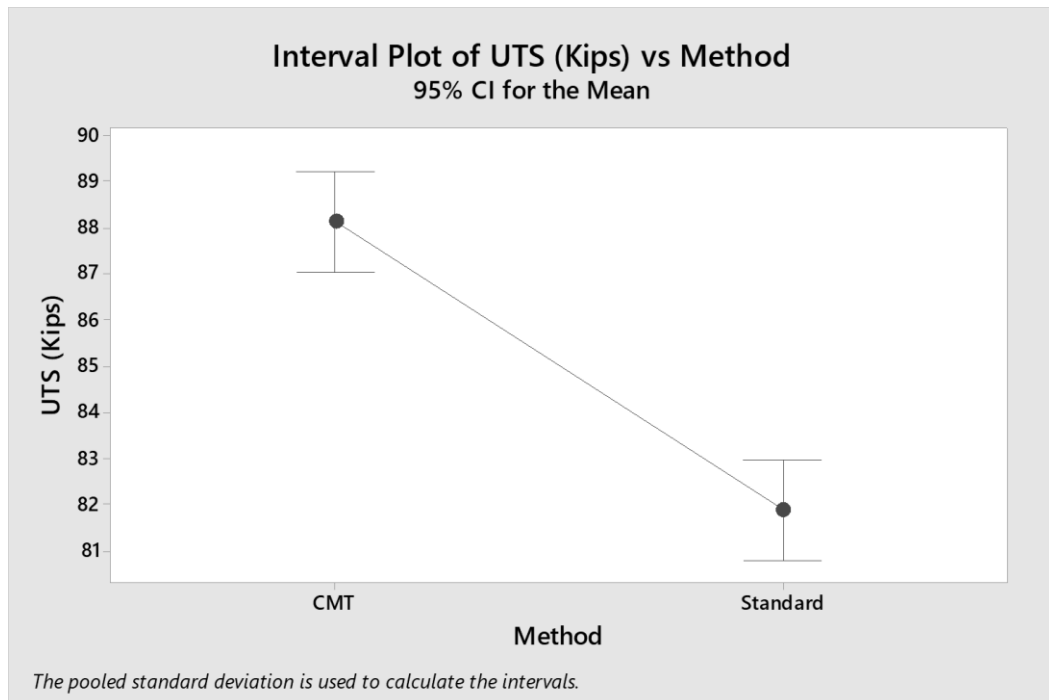


Figure 168: Interval Plot for ER308L for UTS

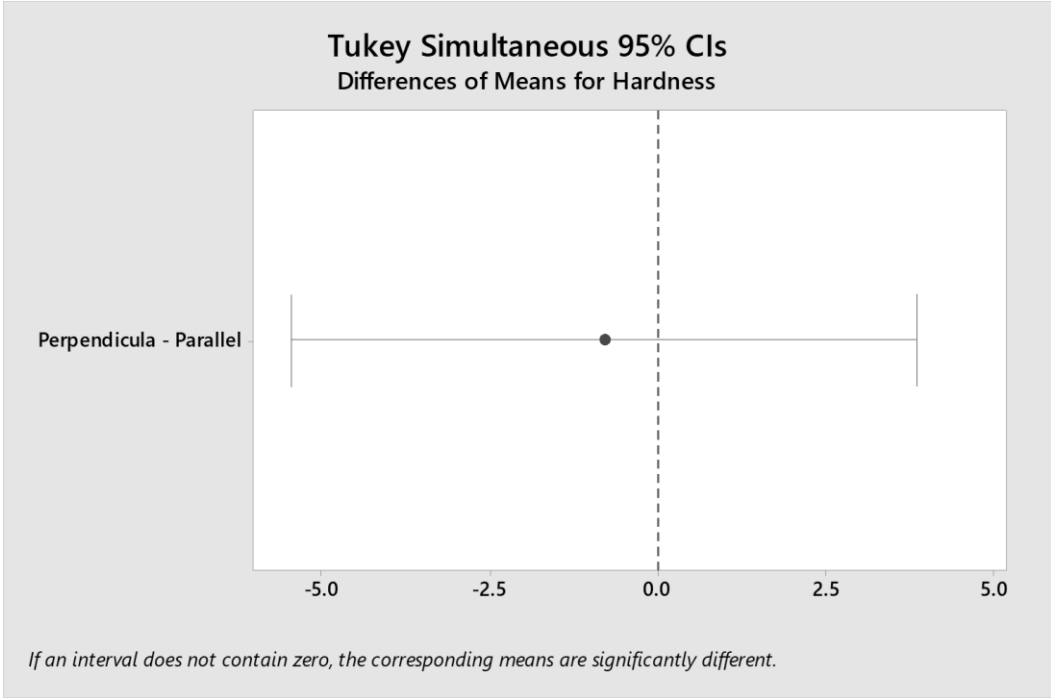


Figure 169: Tukey Analysis for ER308L for Hardness

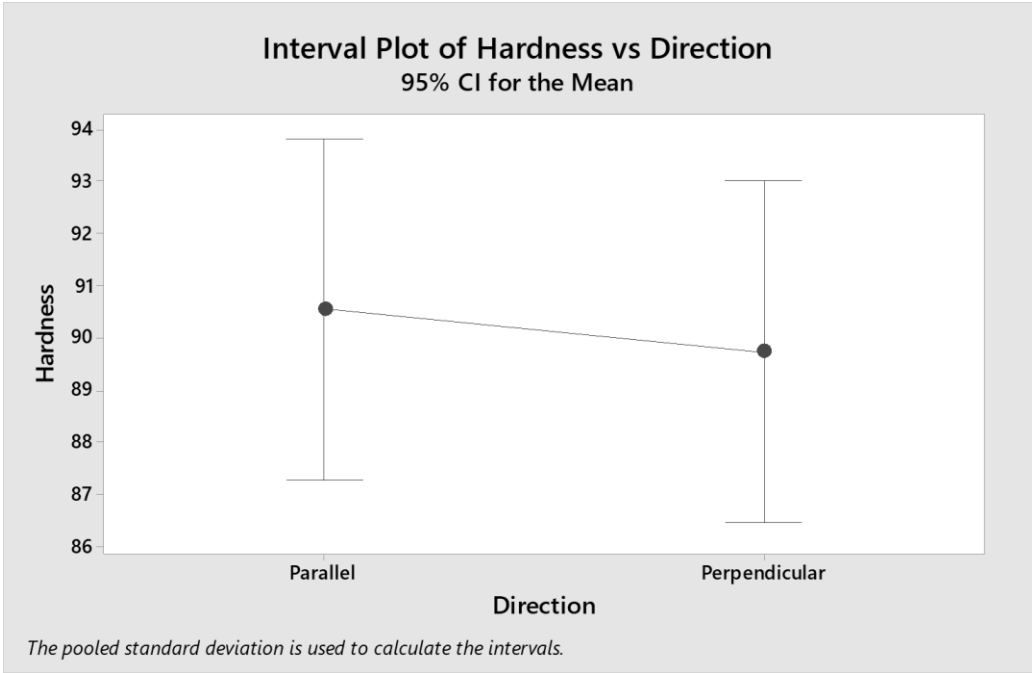


Figure 170: Interval Plot for ER308L for Hardness

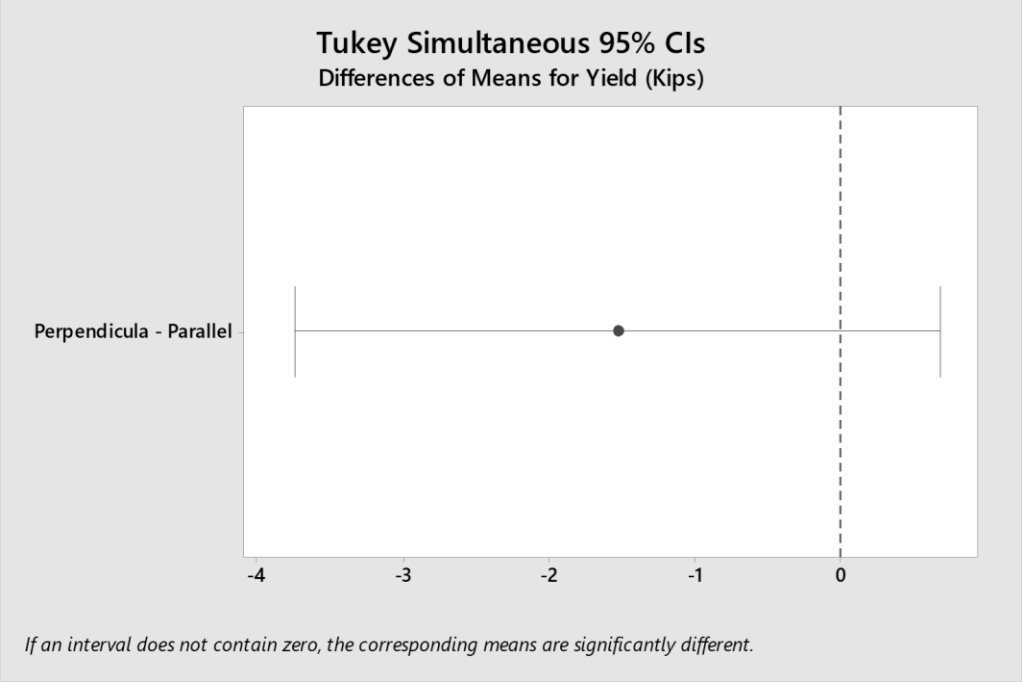


Figure 171: Tukey Analysis for ER308L for Yield

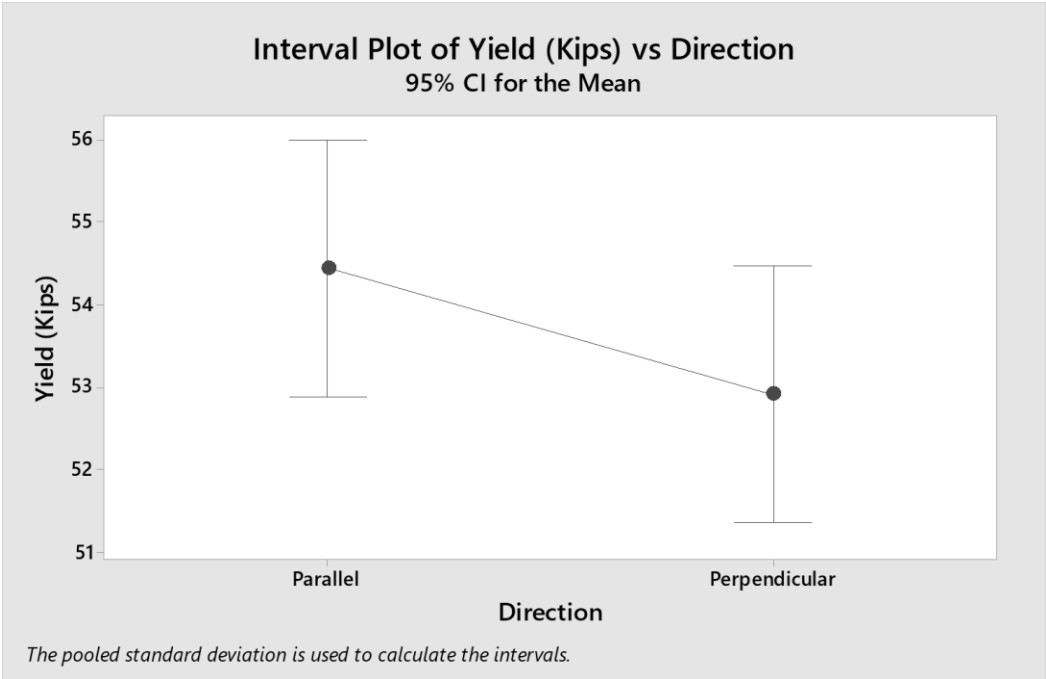


Figure 172: Interval Plot for ER308L for Yield

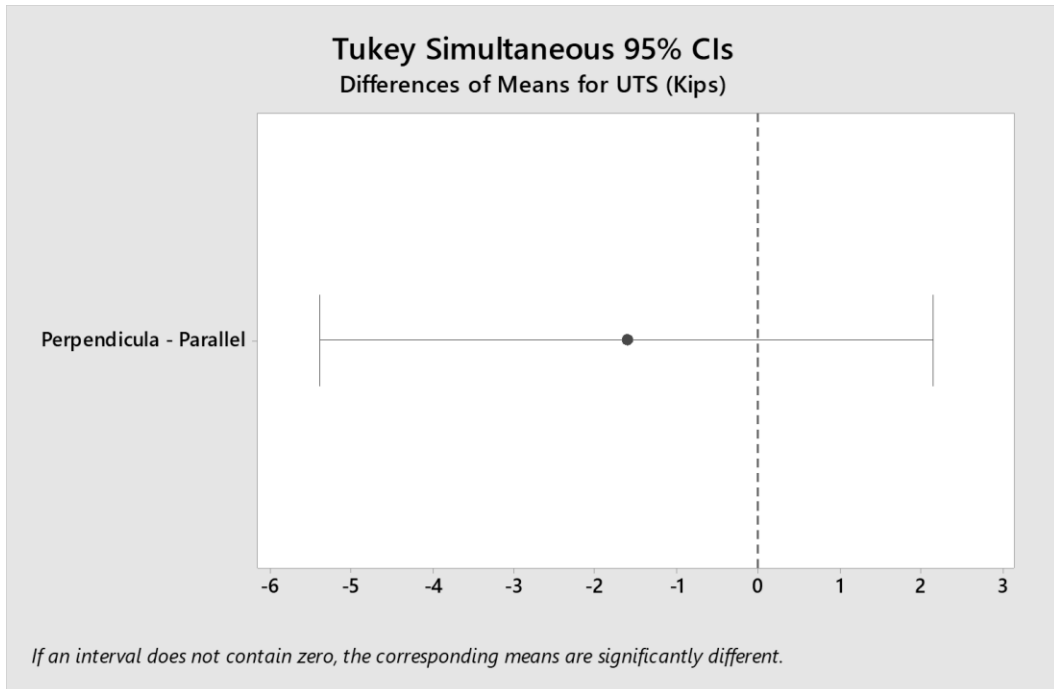


Figure 173: Tukey Analysis for ER308L for UTS

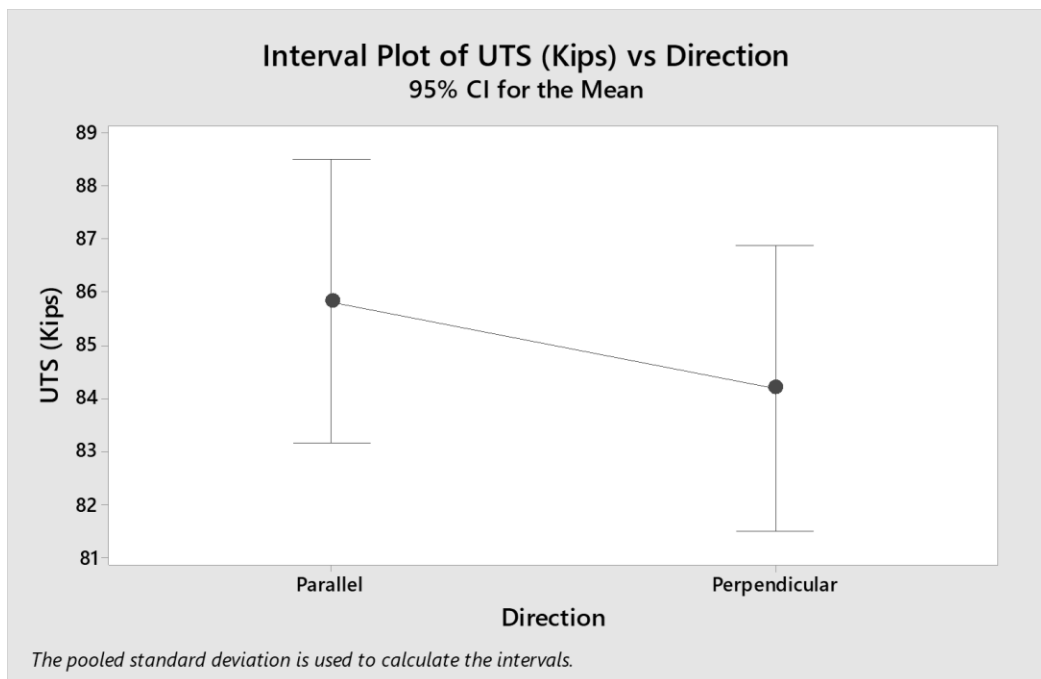


Figure 174: Interval Plot for ER308L for UTS



When considering the accuracy of the measurements (combined accuracies of all the instruments used to acquire the data), the results of UTS, yield, and hardness are presented in Figures 175-176 for ER70S-6 and ER308L. Reevaluating the statistics with machine accuracy considered, the only statistically unequal combination for ER70S-6 is the hardness in the different directions for the walls created with the standard control scheme. For ER308L with machine accuracy taken into consideration, the only combinations that change is the hardness for CMT control. With machine accuracy taken into consideration the hardness values for ER308L with CMT or standard control are equal in both directions (repeatable, since non-directional quantity).

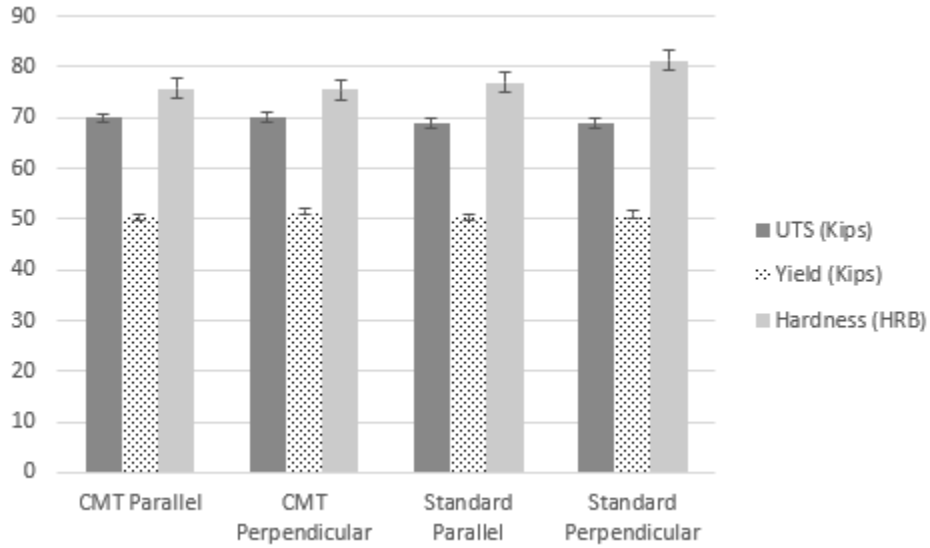


Figure 175: ER70S-6 CMT Control Scheme Evaluation

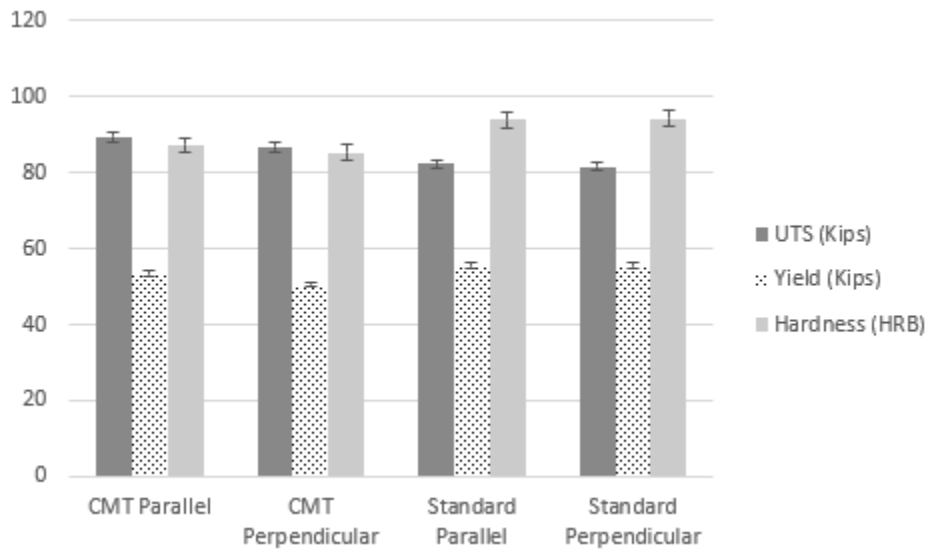


Figure 176: ER308L CMT Control Scheme Evaluation

Other measurables evaluating the CTWD control scheme were taken; however, they were single points (deposition rate, etc.) and statistical analysis cannot truly be taken on this data. The print times for the samples were recorded from the machine run time; however, since the standard mode does not pulse the wire back and forth the deposition rate is compared instead. This includes the time it takes for the operator to stop the program

and other arbitrary tasks; therefore, there is some discrepancy between identically produced walls (parallel v. perpendicular) of a few minutes. The weight of the sample was then divided by the total time to calculate the deposition rate. The amount of material removed from each wall on each side was also recorded. This is the total amount of material needed to have a smooth flat surface on both sides. The average layer height of each wall was also recorded. Table 30 shows the data for both ER70S-6 and ER308L. The values are similar within reason and very little discrepancies are noted for the deposition rates of both materials. The layer heights for the ER70S-6 walls are also considerably the same between control methods. The total material machined for both materials is considerably more for the standard control method. The layer height for the standard control method for ER308L is not only higher than the CMT method, but also more inconsistent. Another noted occurrence during the production of the perpendicular wall for ER308L, there were two 'no arc error' faults from the machine on layers 2 and 11.

Table 30: CMT Control Deposition Rate, Machining, and Layer Height Evaluation

	Deposition Rate (kg/hr):	Total Machined (in):	Layer Height (mm):
CMT Control: Parallel	0.6 ER70S-6	0.055 ER70S-6	2.9
	0.58 ER308L	0.067 ER308L	3.5
CMT Control: Perpendicular	0.6 ER70S-6	0.060 ER70S-6	2.9
	0.58 ER308L	0.080 ER308L	3.5
Standard Control: Parallel	0.61 ER70S-6	0.145 ER70S-6	2.9
	0.58 ER308L	0.224 ER308L	4.4
Standard Control: Perpendicular	0.62 ER70S-6	0.195 ER70S-6	2.9
	0.55 ER308L	0.222 ER308L	3.8

The current, voltage, and wire feed speed was also recorded for the two methods due to the fundamentally different control methods. Figure 177 shows a sample plot for ER70S-6 in standard mode at the start of a layer. The current and voltage vary proportionally and inversely, and voltage reaches a steady state at around 1.5 seconds. Figure 178 shows a sample plot for ER70S-6 in CMT mode at the start of a layer. The current reaches steady state almost instantly and the voltage is modulated to maintain the current throughout. Also note the much tighter range while at steady state for both current and voltage when compared to standard mode. ER308L shows the same trend with voltage and current. When in the standard mode the voltage and wire feed speed are set by the operator and the synergic control varies the current to meet these demands. For CMT control the wire feed speed is set and all parameters are modulated to try and maintain a steady state phenomenon for all variables (arc stable).

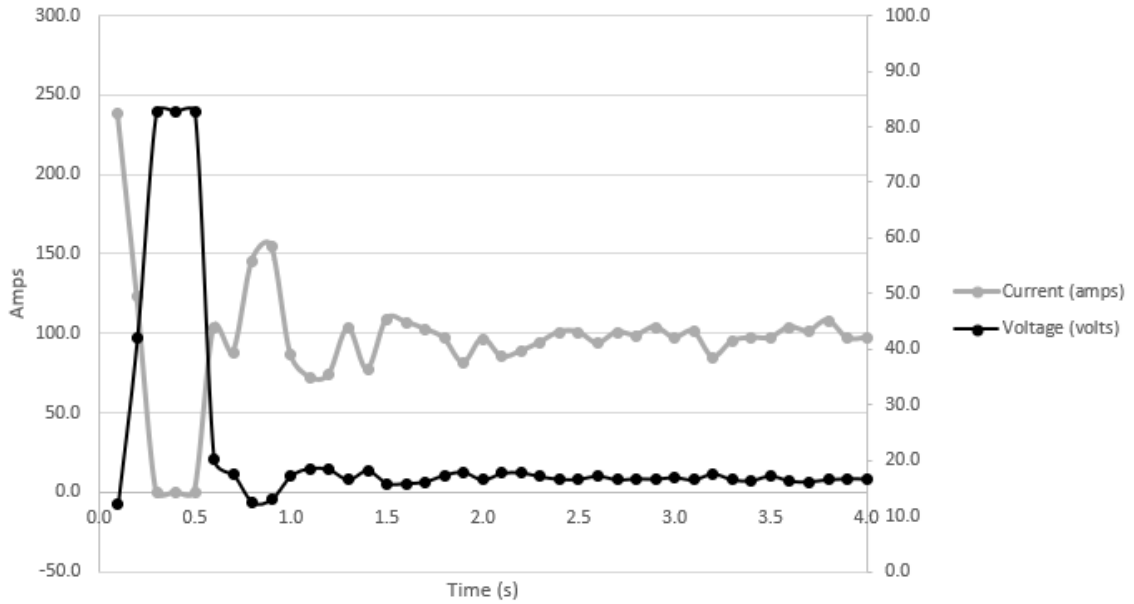


Figure 177: Standard Mode Voltage and Current Plot

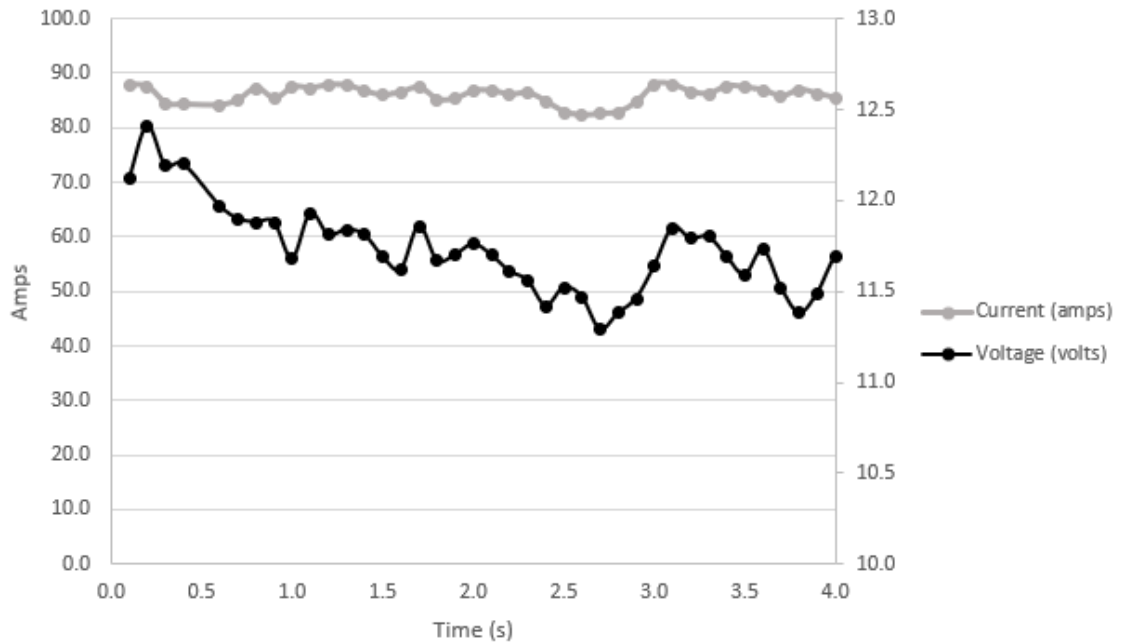


Figure 178: CMT Mode Voltage and Current Plot

Table 31 shows the average voltage, current, and wire feed speed for representative walls with CMT and standard mode in ER70S-6 and ER308L. The average wire feed speed was independent of material and the voltage and current (power) was lower for the CMT

mode even with an arguably the same deposition rate. This equates to the lower heat input of the CMT method ('Cold' – Cold Metal Transfer).

Table 31: Average WFS, V, C for Representative Wall for Different Modes

	Wire Feed Speed (ipm)	Voltage (volts)	Current (amps)
Standard Mode: ER70S-6	118.11	16	104
CMT Mode: ER70S-6	78.74	12	86
Standard Mode: ER308L	118.11	20	92
CMT Mode: ER308L	78.74	10	65

Metallographic analysis of the microstructure of ER70S-6 and ER308L samples were studied with guidance from the ASM Handbook -Vol 9 [67]. Figure 179 shows the typical microstructure observed in ER70S-6 with the CMT control. Figure 180 shows the layer boundary of ER70S-6 with the CMT control. Again, the dark area of the image is where the edges of the sample meet the mounting polymer and is not a void. A uniform grain structure was noted throughout the wall and the layer interface was once again noted to have no distinct boundary.

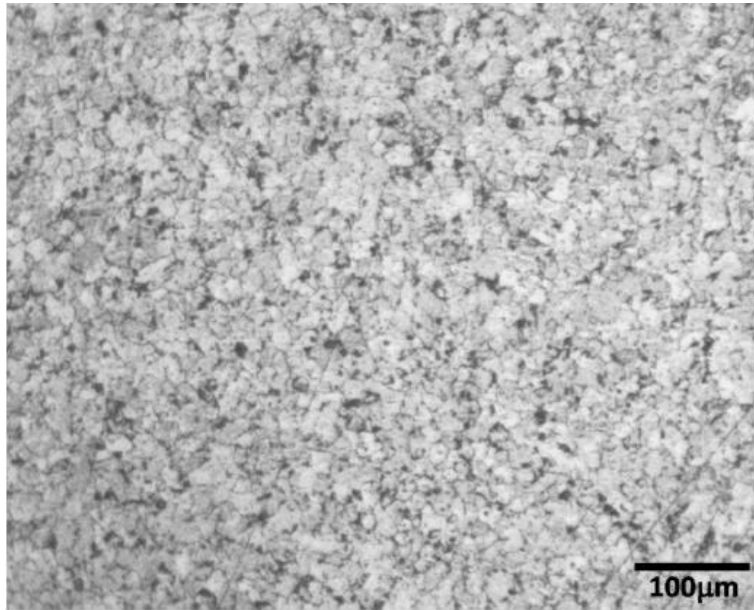


Figure 179: ER70S-6 with CMT Control Representative Structure

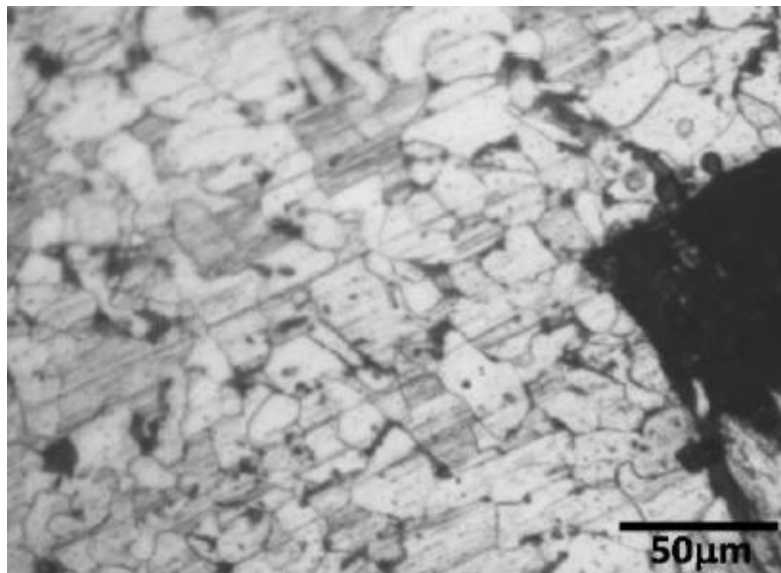


Figure 180: ER70S-6 with CMT Control Layer Interface

Figure 181 shows some of the layer boundaries of ER70S-6 with the standard Fronius control. Acicular ferrite is noted in the structure, while Widmanstatten ferrite is found at the interfaces. Figure 182 shows a sample image of the layer interfaces with ER70S-6 with the previous standard synergic welder from Miller [2]. Acicular ferrite is

found in these samples as well, and there is a clear white region at the interface which could be the onset of Widmanstatten ferrite as that found with the Fronius welder.

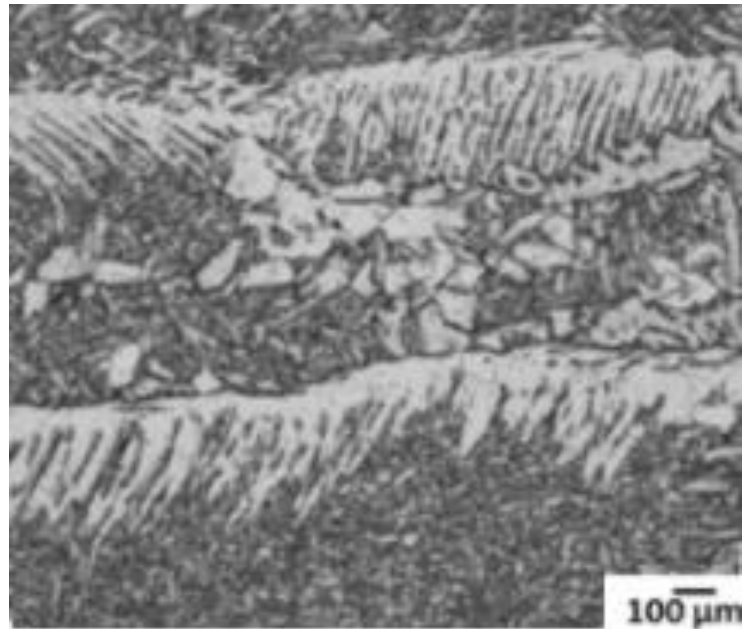


Figure 181: ER70S-6 with Standard Control Layer Interfaces

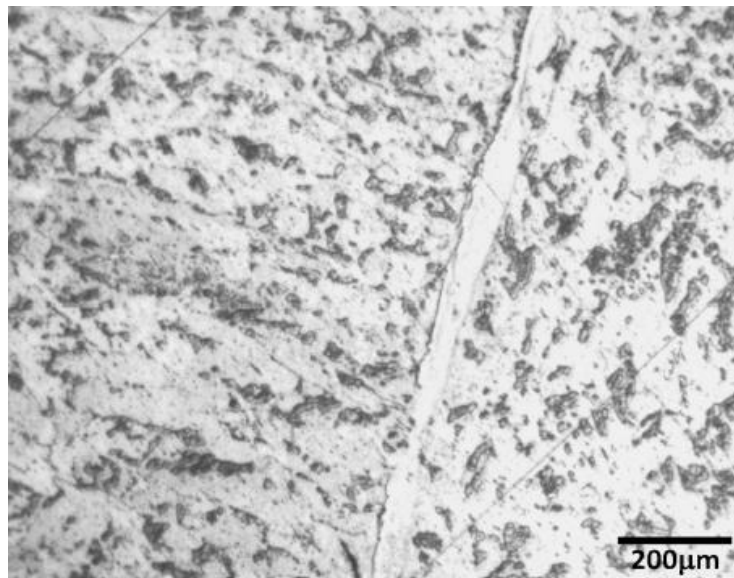


Figure 182: ER70S-6 with Previous Standard Welder Layer Interfaces [2]

Figure 183 shows the typical microstructure found in ER308L with CMT control.

Figure 184 shows the layer interface and a clear boundary layer is present like that found



in previous research [2]. The general microstructure is comprised of skeletal  $\delta$ -ferrite in an austenitic matrix.

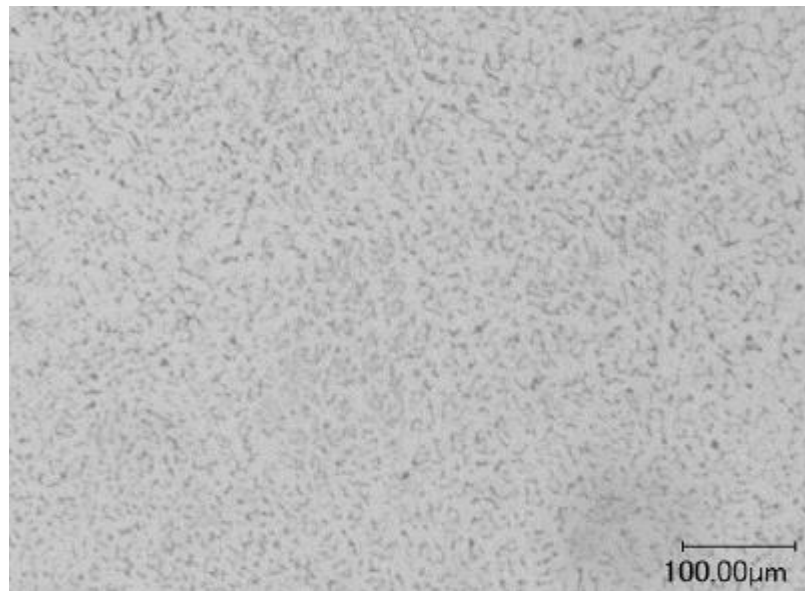


Figure 183: ER308L with CMT Control Typical Microstructure

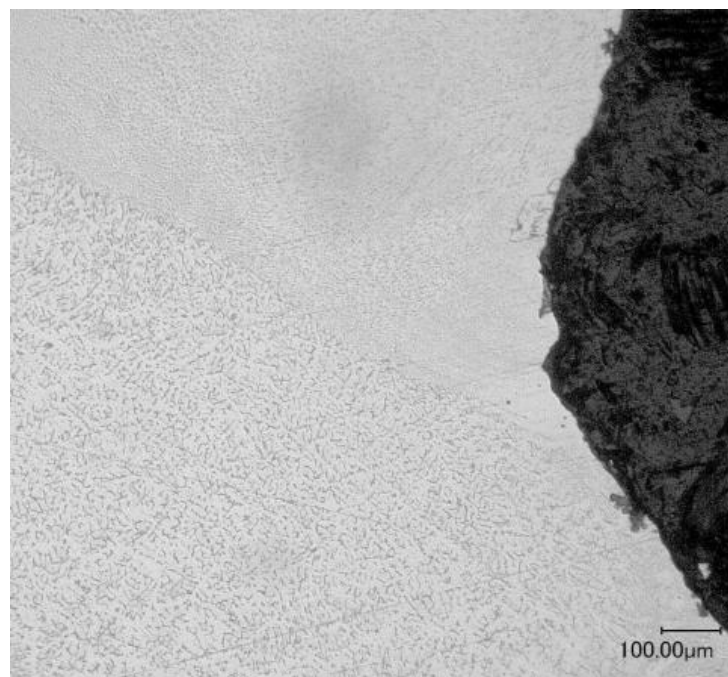


Figure 184: ER308L with CMT Control Layer Interface Boundary

Figure 185 shows the typical ER308L microstructure with standard control to once again have  $\delta$ -ferrite present in an austenitic matrix (although more distinct). The layer boundaries do not exhibit any noticeable difference to those with CMT control.

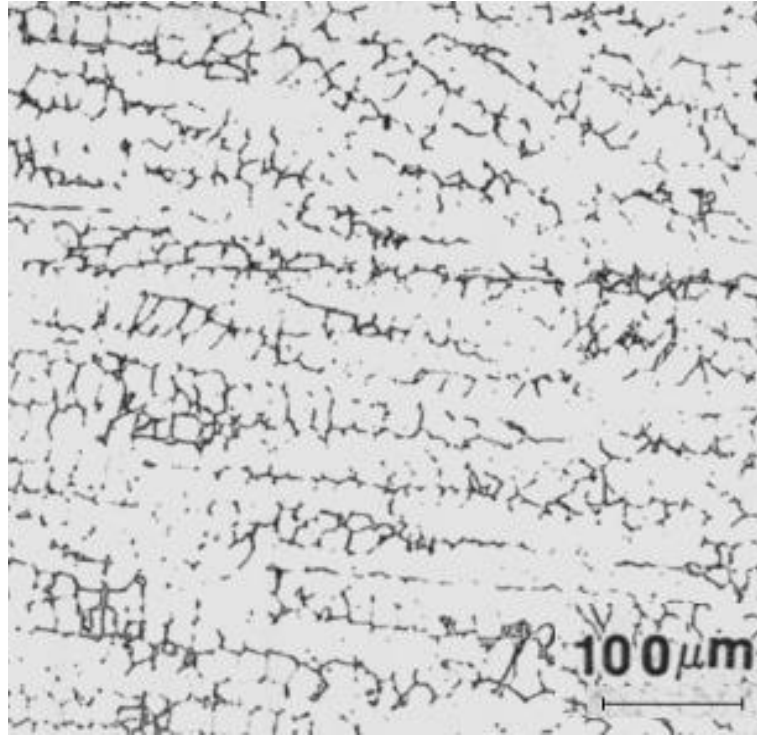


Figure 185: ER308L with Standard Control

One of the issues noted during the production of samples with the standard control scheme was that the ‘print’ constantly needed to be monitored to ensure that the spatter from the welding process did not damage anything. The standard print also had two errors occur (both on the same wall) that cause production to cease until corrected.

### **Temperature Monitoring Control Evaluation**

Table 32 shows the results of comparing walls ‘printed’ without temperature monitoring (baseline, at 205°C, 401°F) to those ‘printed’ with the temperature control scheme for ER70S-6. A P-Value above 0.05 indicates no significant difference between

the means of the group and they are statistically equal with 95% confidence. Appendix IV has the complete statistical outputs for these tests.

Table 32: ER70S-6 With v. Without Temperature Control P-Values

	UTS	Yield	Hardness
With Temp Control @ 232°C: Parallel v. Perpendicular	0.149	0.519	0.012
With Temp Control @ 260°C: Parallel v. Perpendicular	0.228	0.105	0.235
With Temp Control @ 288°C: Parallel v. Perpendicular	.00043	0.013	0.570
Baseline (@ 205°C): Parallel v. Perpendicular	0.396	0.543	0.801

The UTS and yield strength were statistically equal directionally until 288°C (550°F). The hardness, while not a directional quantity, was not statistically equal at 232°C (450°F). Comparison between factors are displayed via main effects, residual, Tukey analysis, and interval plots. Figures 186-191 show the main effects and residual plots for ER70S-6.

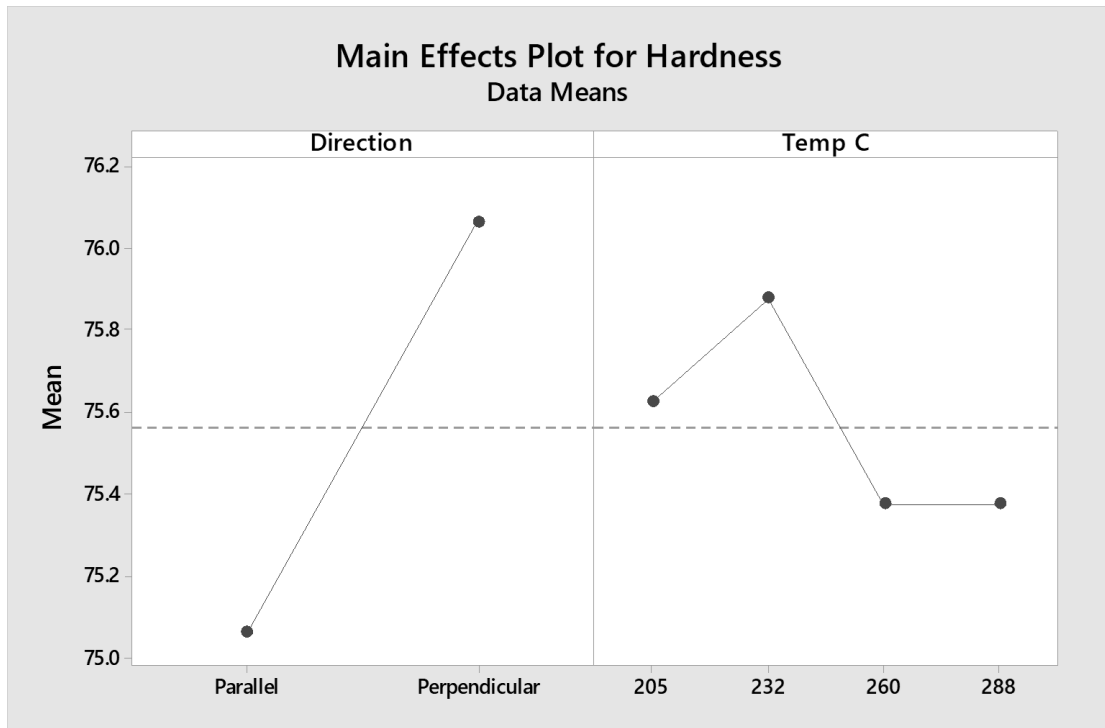


Figure 186: Main Effects Plot for Hardness for ER70S-6 with Temp Control

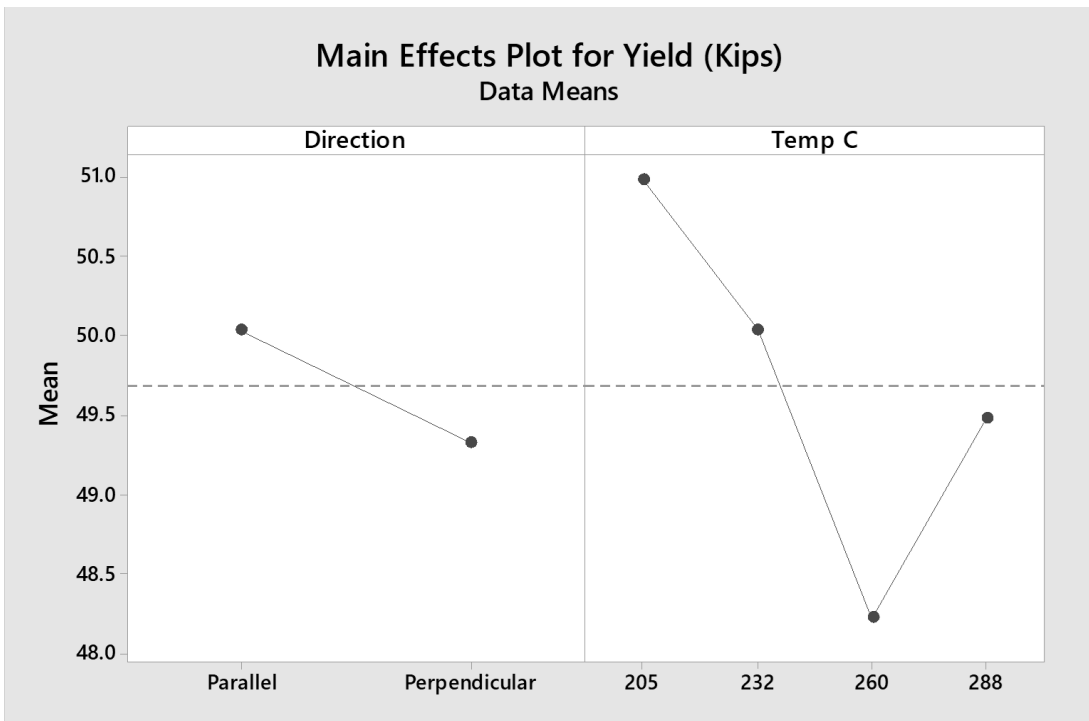


Figure 187: Main Effects Plot for Yield for ER70S-6 with Temp Control

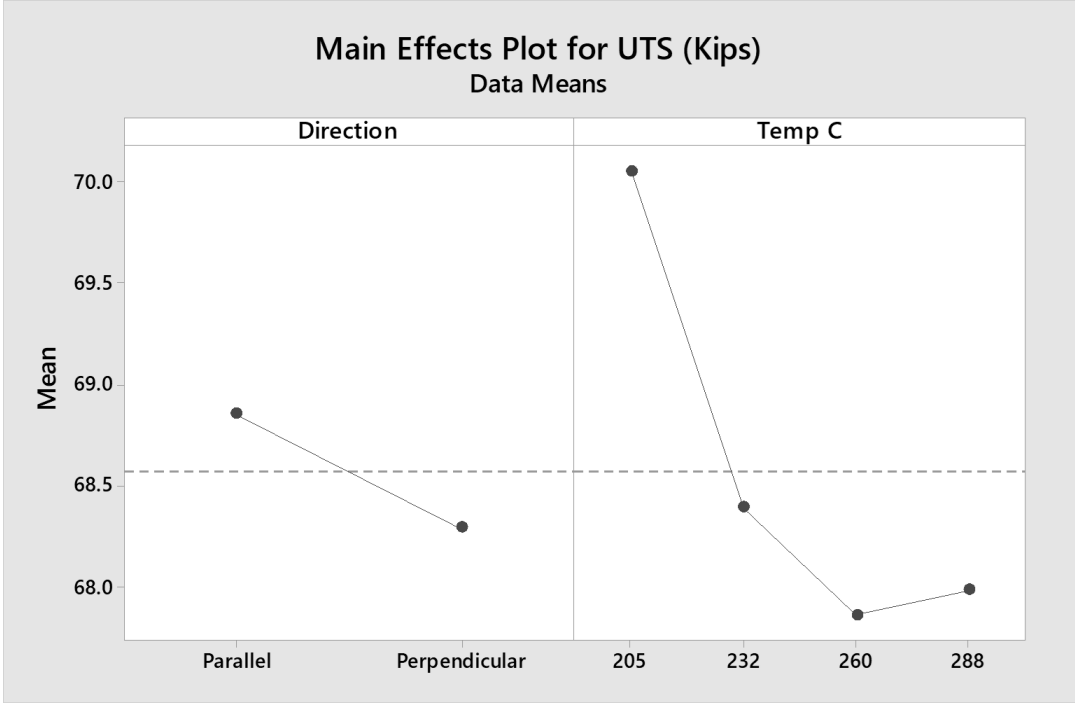


Figure 188: Main Effects Plot for UTS for ER70S-6 with Temp Control

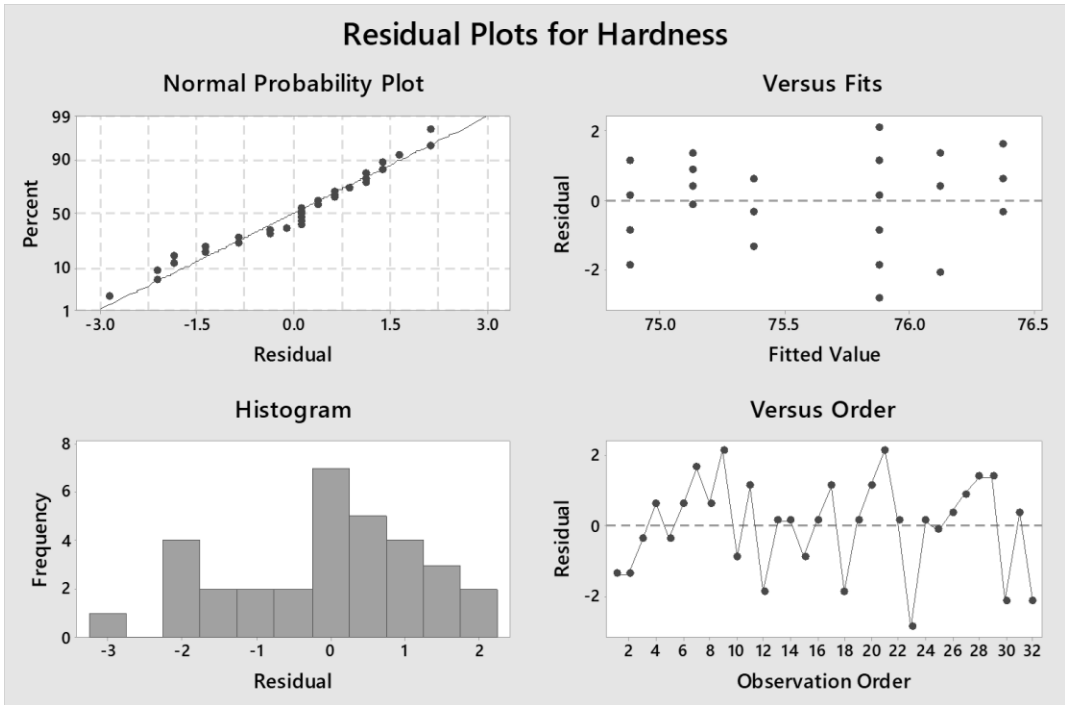


Figure 189: Residual Plots for Hardness for ER70S-6 for Temp Control

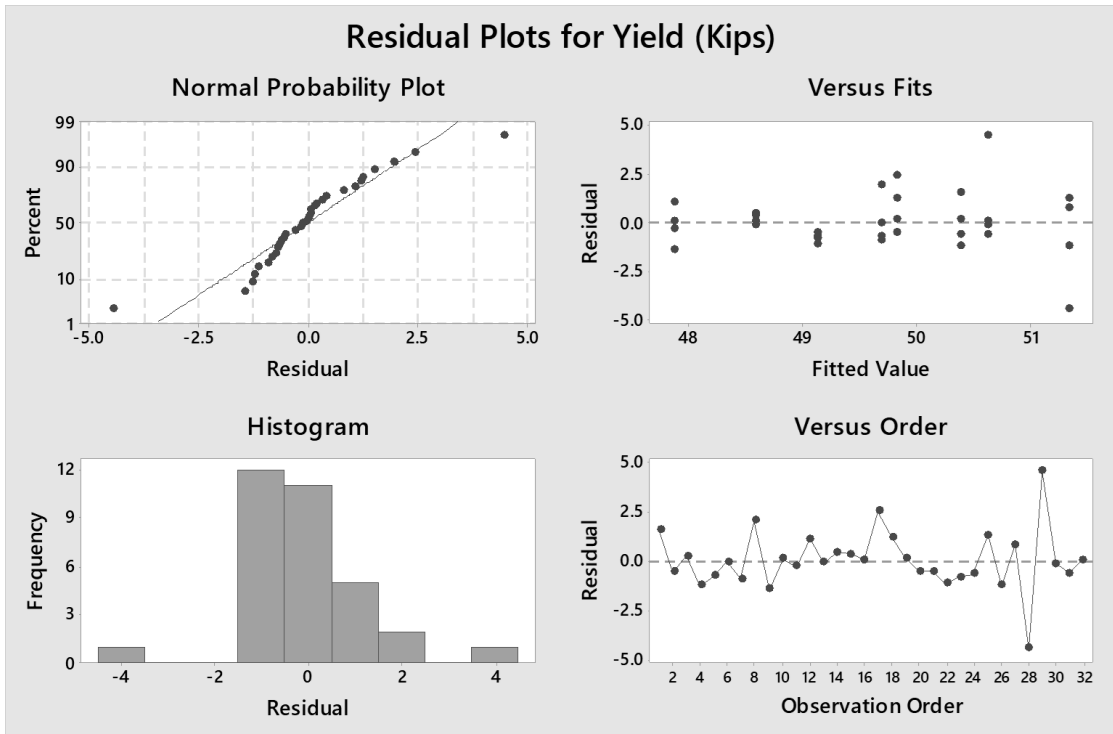


Figure 190: Residual Plots for Yield for ER70S-6 for Temp Control

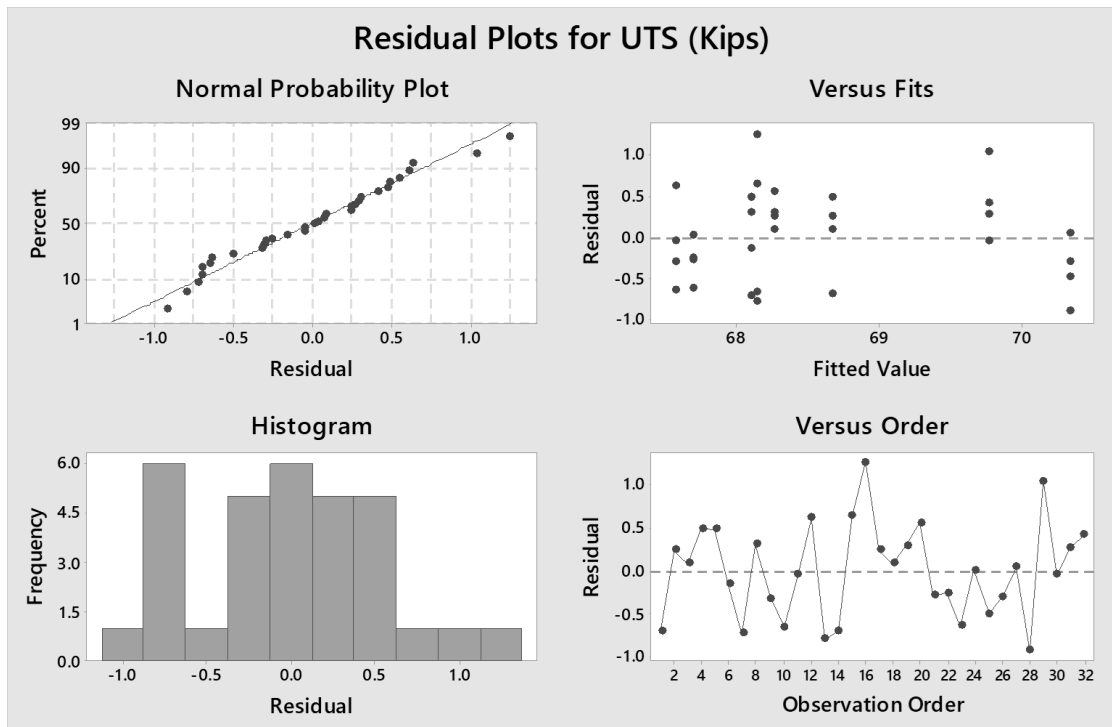


Figure 191: Residual Plots for UTS for ER70S-6 for Temp Control

The yield strength and UTS decrease with increasing temperature control limit up to a point. It should be noted that the upper values of temperature are at continuous welding and therefore the temperature cannot be increased without secondary means (laser, heated bed, etc.). The UTS and yield strength were also slightly lower in the perpendicular direction when compared to the parallel direction of deposition. The hardness appears to be consistent throughout tests, noting that it is not a directional quantity and any difference found between directions is due to measurement accuracy, material repeatability, or outside influences. Figures 192-203 show the Tukey analysis and interval plots for the temperature control scheme for ER70S-6.

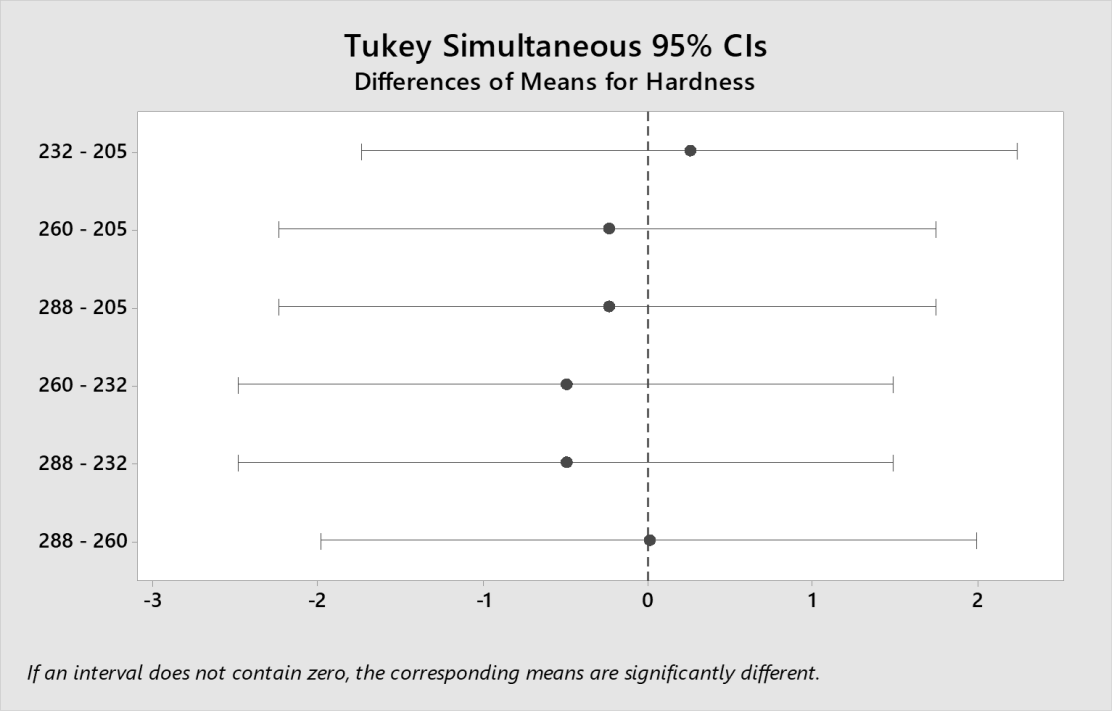


Figure 192: Tukey Analysis for Hardness for ER70S-6 for Temp Control

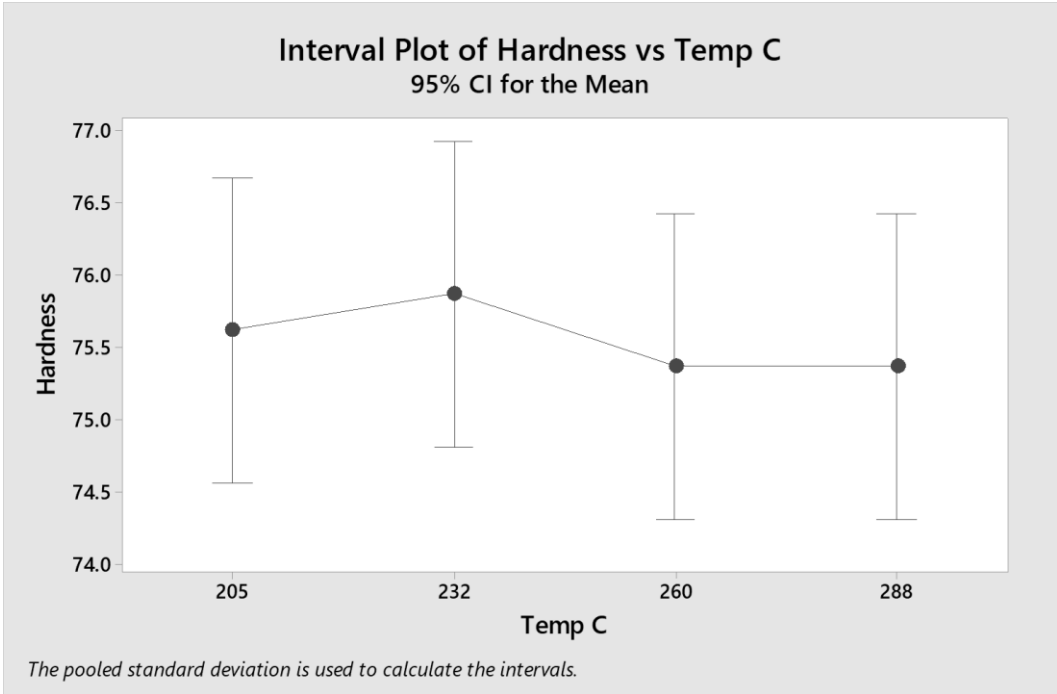


Figure 193: Interval Plot for Hardness for ER70S-6 for Temp Control



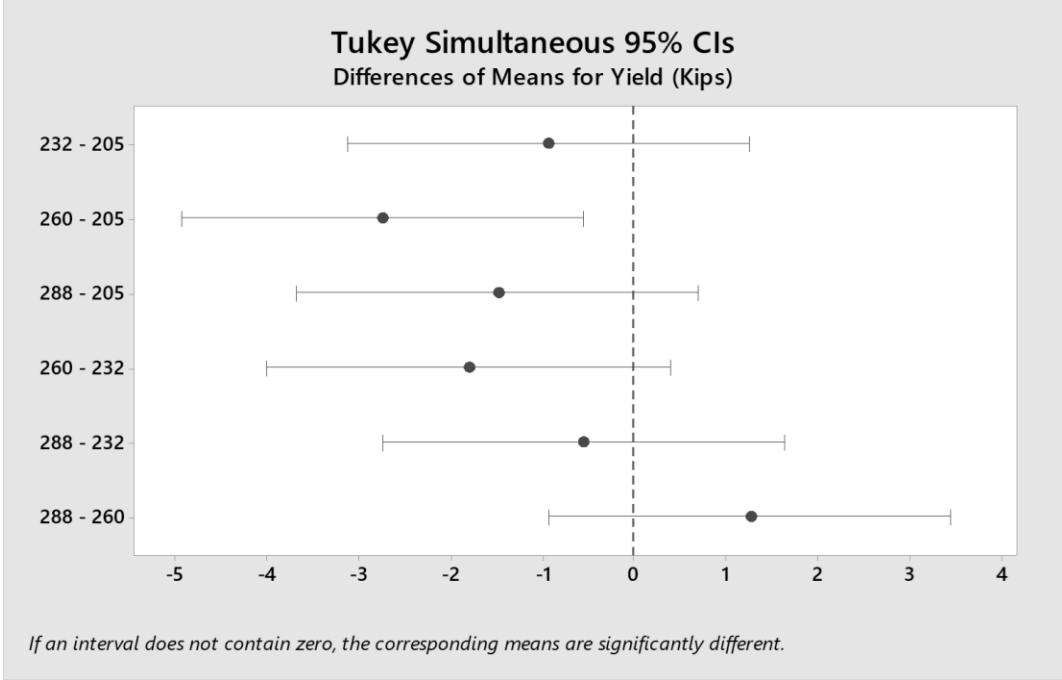


Figure 194: Tukey Analysis for Yield for ER70S-6 for Temp Control

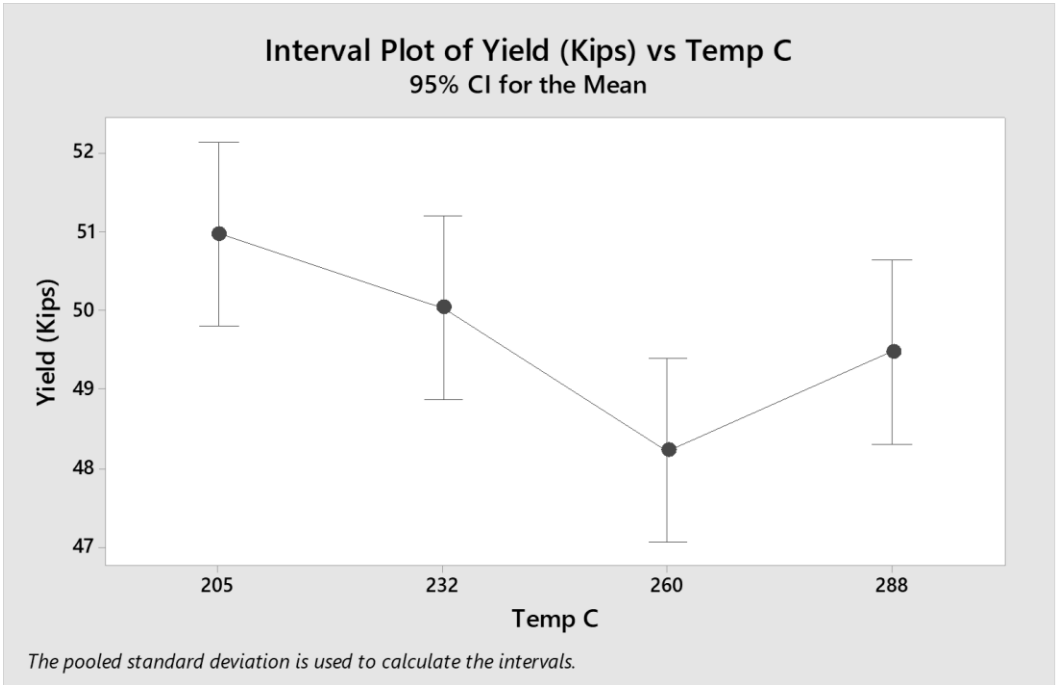


Figure 195: Interval Plot for Yield for ER70S-6 for Temp Control

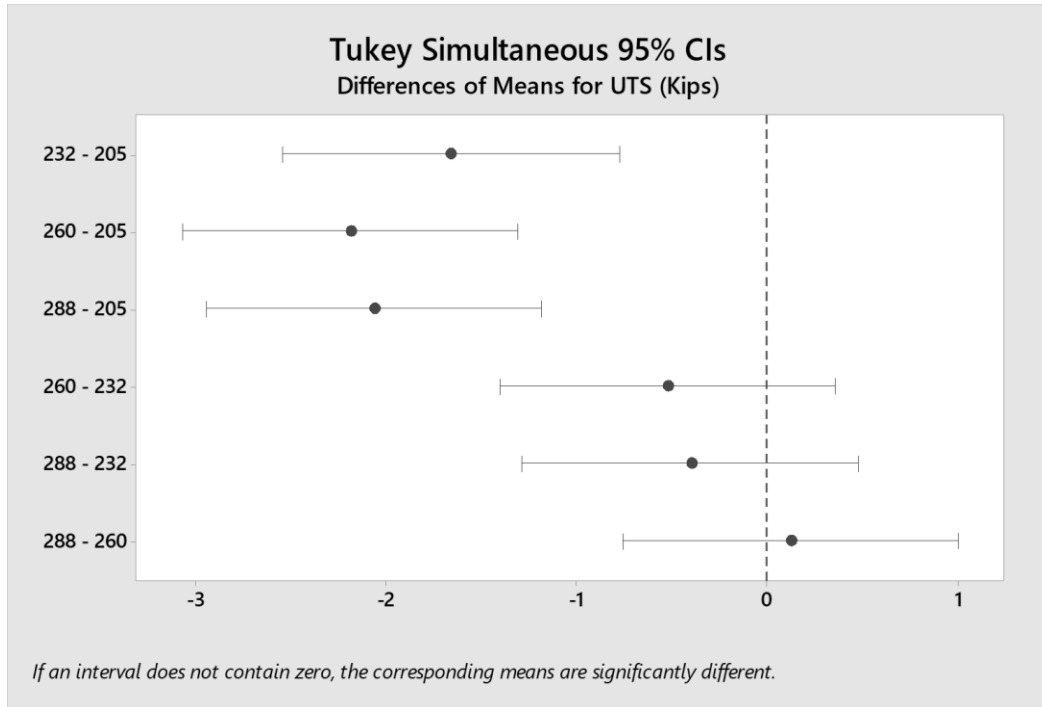


Figure 196: Tukey Analysis for UTS for ER70S-6 for Temp Control

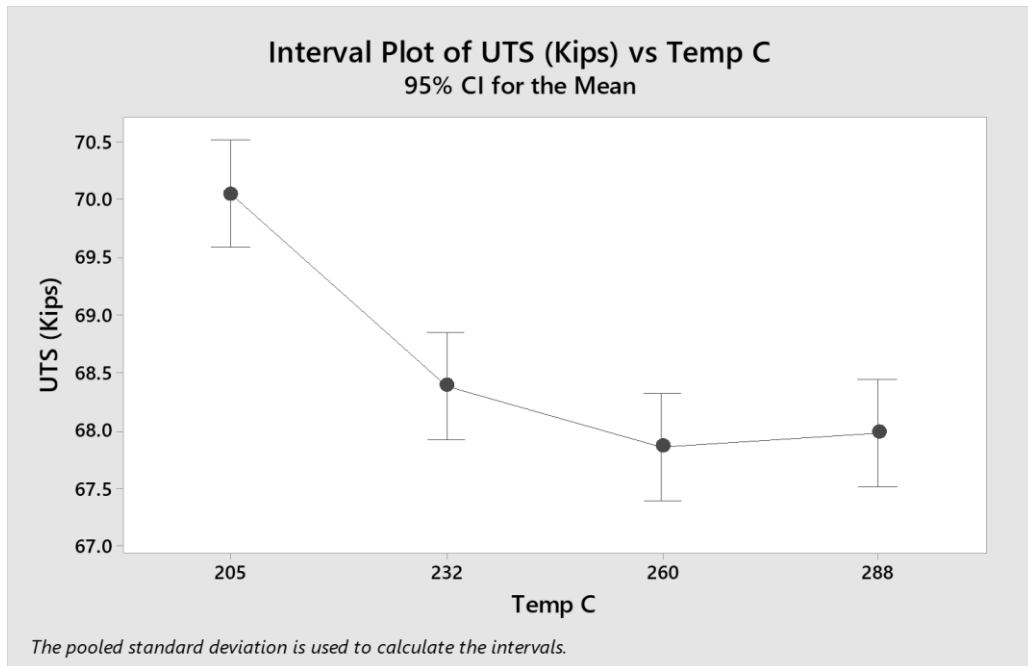


Figure 197: Interval Plot for UTS for ER70S-6 for Temp Control

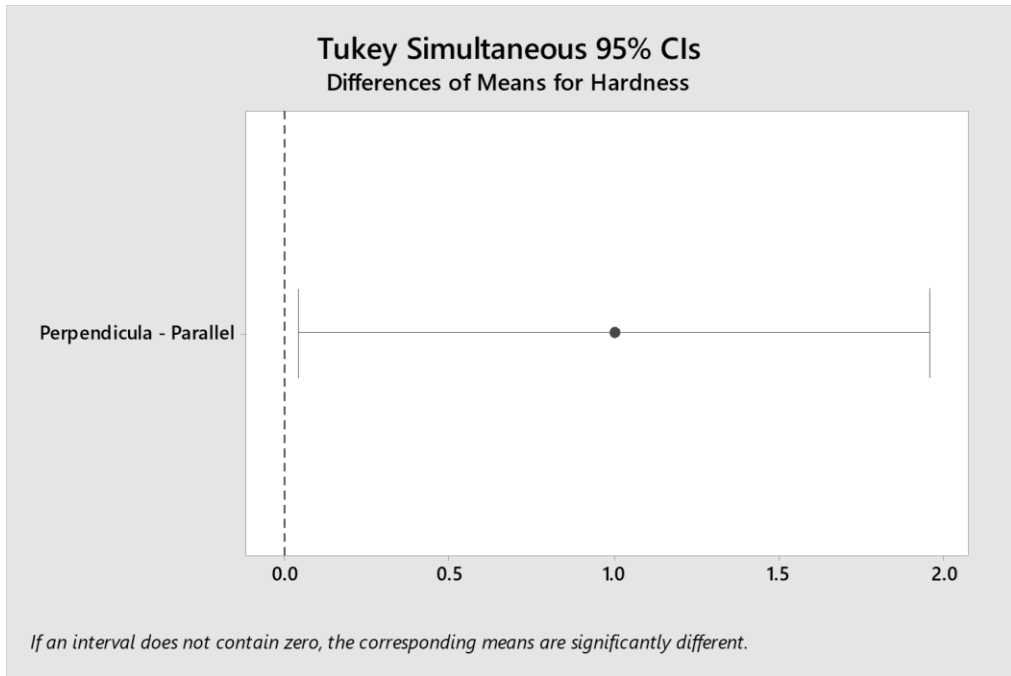


Figure 198: Tukey Analysis for Hardness for ER70S-6 for Temp Control

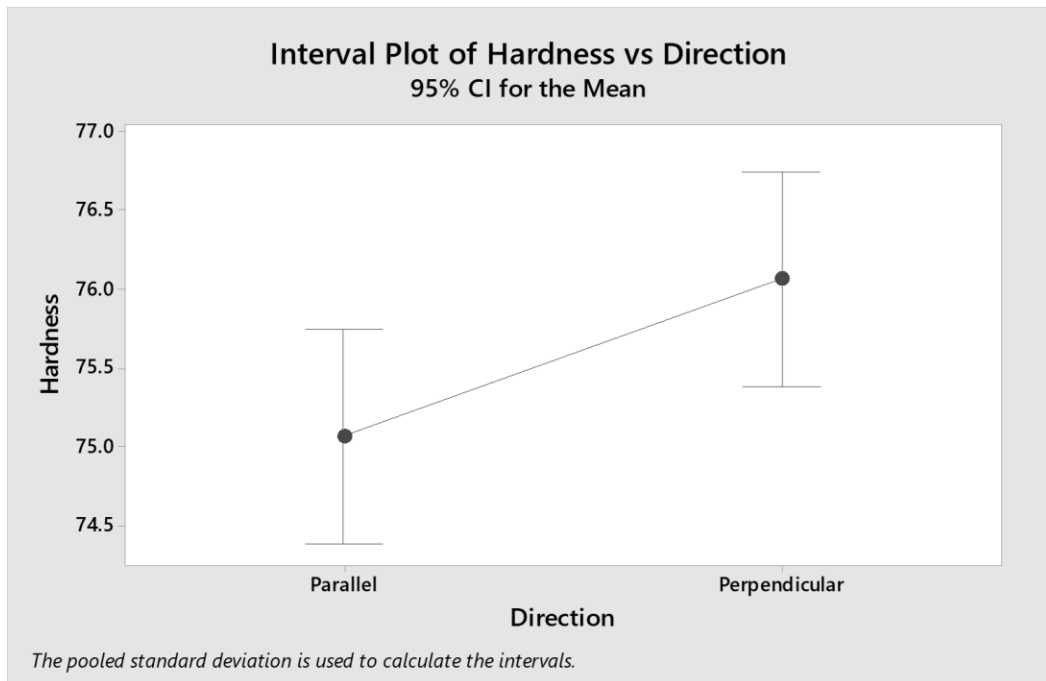


Figure 199: Interval Plot for Hardness for ER70S-6 for Temp Control

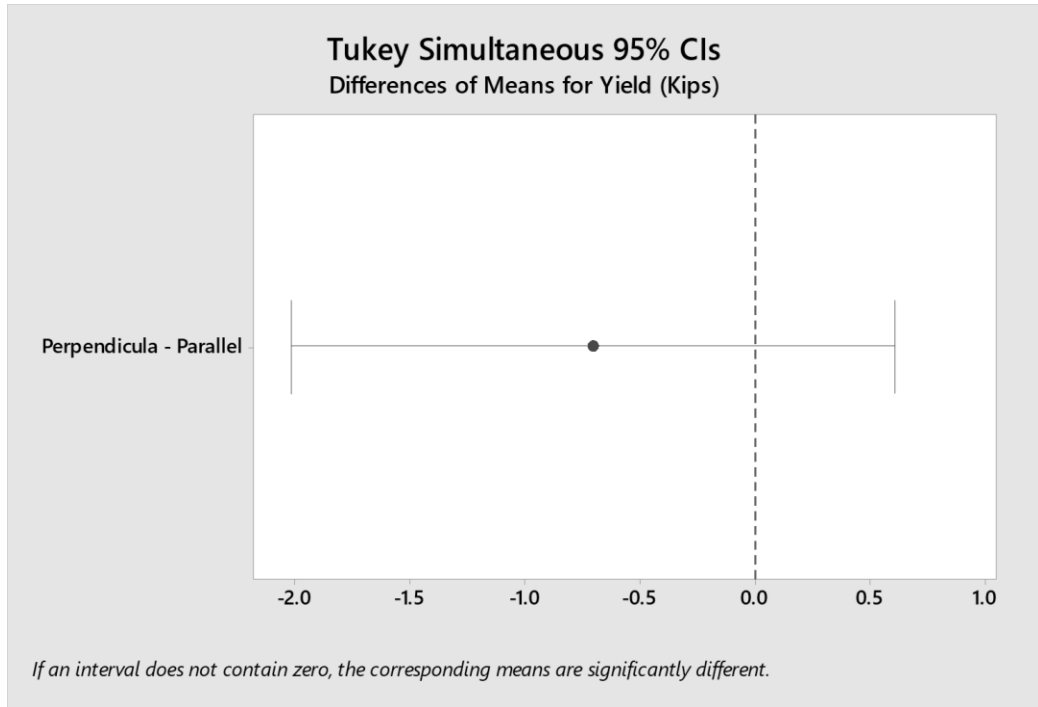


Figure 200: Tukey Analysis for Yield for ER70S-6 for Temp Control

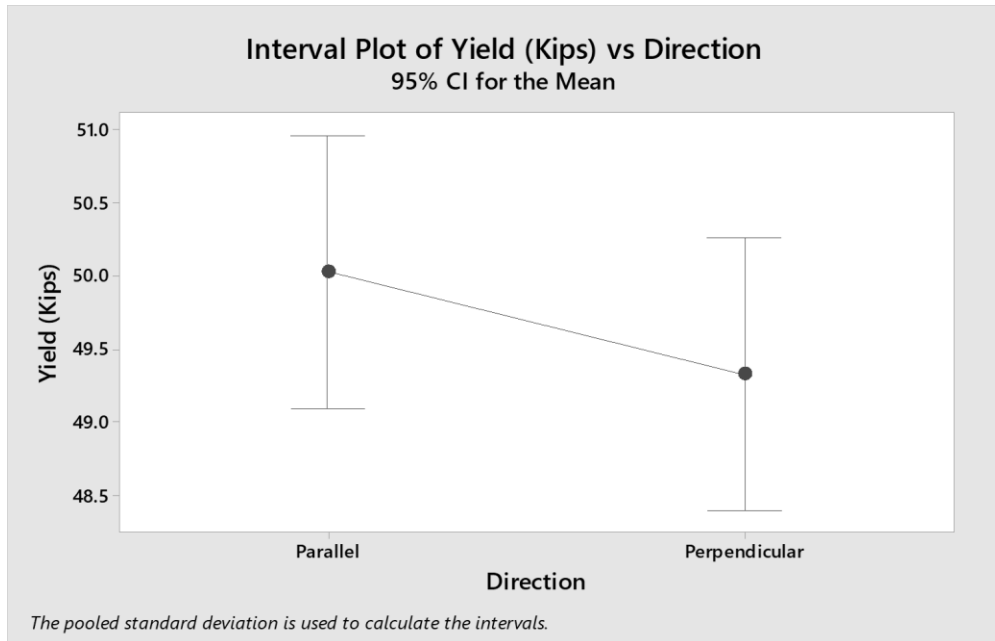


Figure 201: Interval Plot for Yield for ER70S-6 for Temp Control

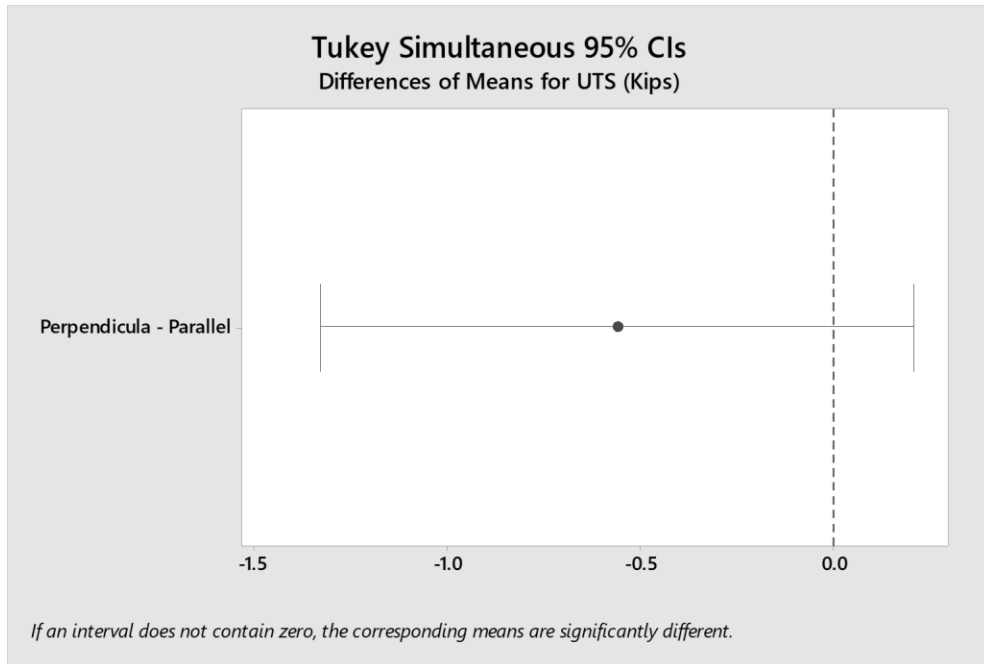


Figure 202: Tukey Analysis for UTS for ER70S-6 for Temp Control

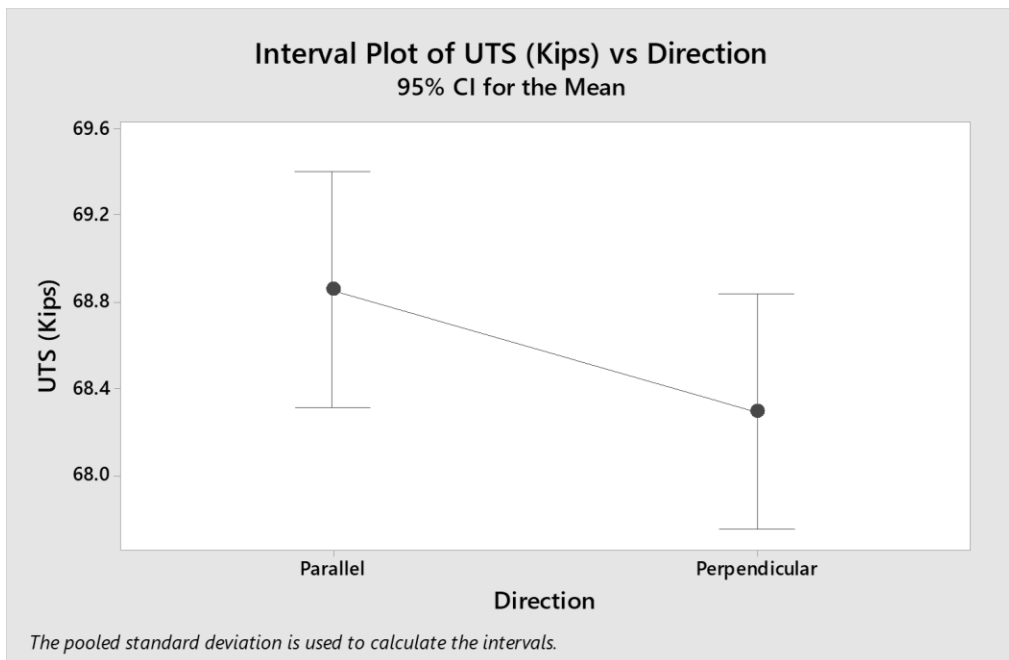


Figure 203: Interval Plot for UTS for ER70S-6 for Temp Control

The hardness is statistically the same for all combinations per temperature. The yield strength is equal for all combinations except for 260°C (500°F) compared to the baseline, 205°C (401°F). The UTS is equal for all combinations except for those compared to the baseline (205°C). Directionally the hardness is not statistically equal for all combinations, while the UTS and yield strength are. Figures 204-206 show the results of the UTS, yield strength, and hardness with the accuracy (total combined accuracy of measurable) taken into consideration. With the accuracy taken into consideration, the UTS is equal for all combinations except for those compared to the baseline (205°C, 401°F) in the perpendicular direction.

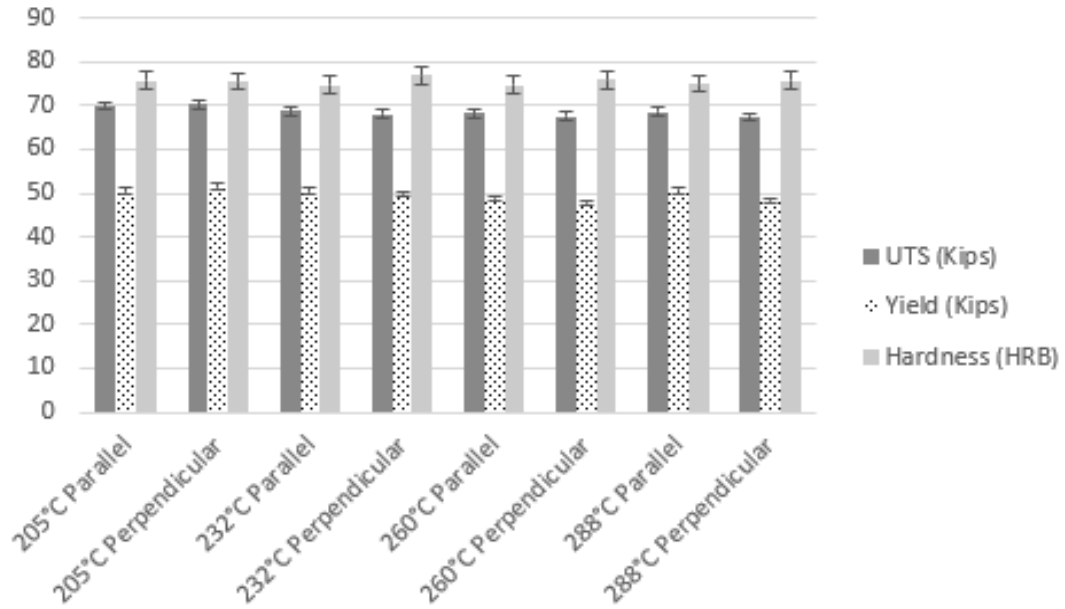


Figure 204: Graph of ER70S-6 Temp Control Measurables with Accuracy

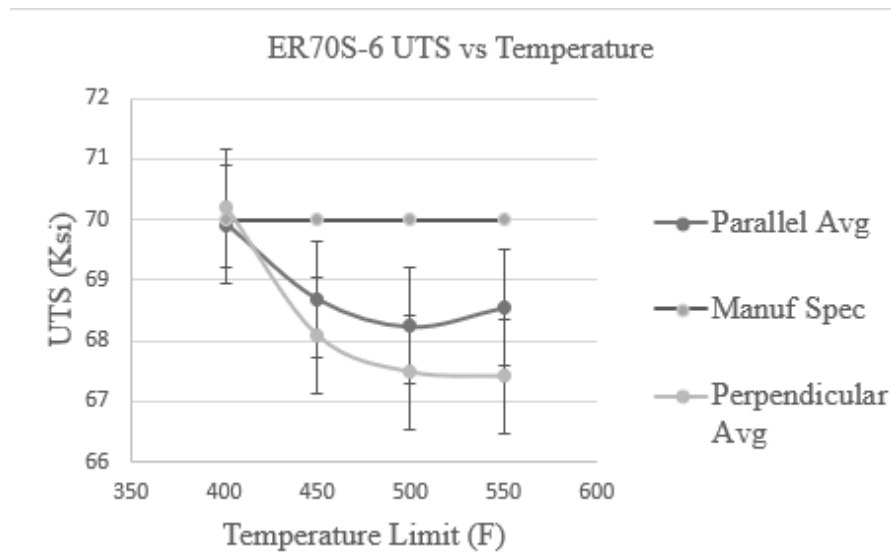


Figure 205: Temperature v. UTS for ER70S-6 with Accuracy

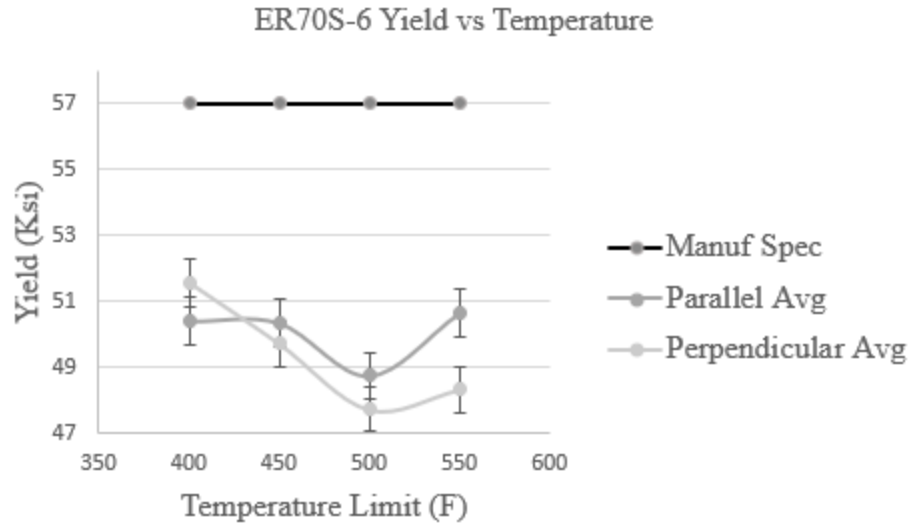


Figure 206: Temperature v. Yield Strength for ER70S-6 with Accuracy

Table 33 shows the results of comparing walls ‘printed’ without temperature monitoring (baseline, at 125°C (257°F)) to those ‘printed’ with the temperature control scheme for ER308L. A P-Value above 0.05 indicates no significant difference between the means of the group and they are statistically equal with 95% confidence. Appendix IV has the complete statistical outputs for these tests.

The yield strength was statistically equal directionally at 150°C (302°F). The hardness, while not a directional quantity, was statistically equal at 150°C (302°F) and 260°C (500°F). The UTS was statistically equal at 205°C (401°F). Comparison between factors are displayed via main effects, residual, Tukey analysis, and interval plots. Figures 207-212 show the main effects and residual plots for ER308L.



Table 33: With V. Without Temperature Control for ER308L P-Values

	UTS	Yield	Hardness
With Temp Control @ 150°C: Parallel v. Perpendicular	0.021	0.875	0.083
With Temp Control @ 205°C: Parallel v. Perpendicular	0.088	0.030	0.037
With Temp Control @ 260°C: Parallel v. Perpendicular	0.002	0.002	0.159
Baseline (@ 125°C): Parallel v. Perpendicular	0.014	0.002	0.003

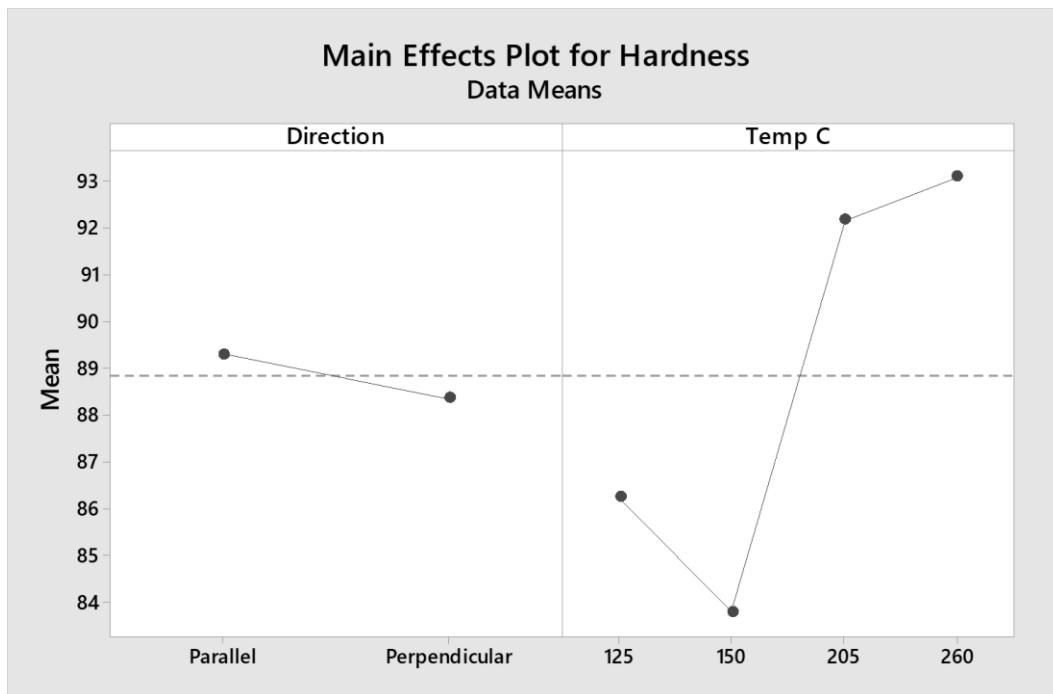


Figure 207: Main Effects Plot for Hardness for ER308L for Temp Control

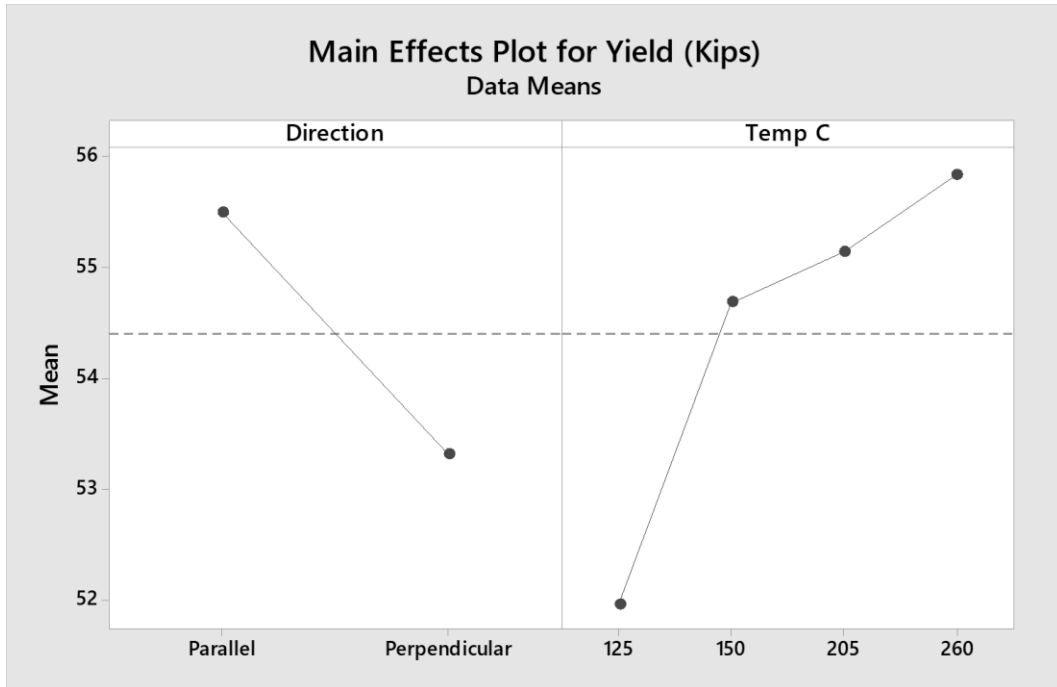


Figure 208: Main Effects Plot for Yield for ER308L for Temp Control

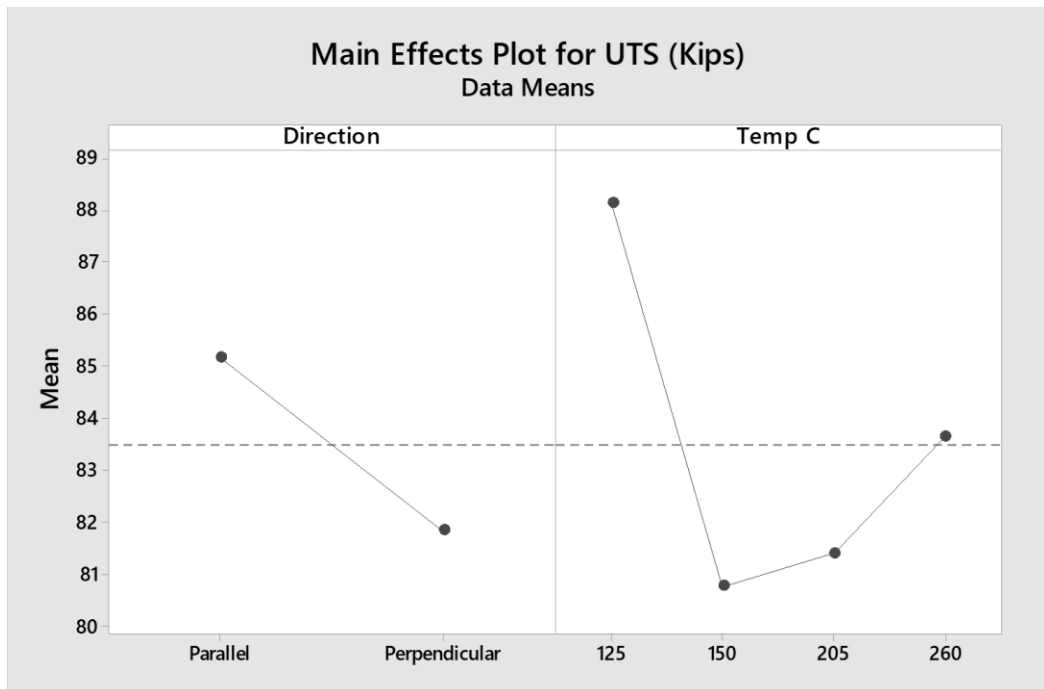


Figure 209: Main Effects Plot for UTS for ER308L for Temp Control

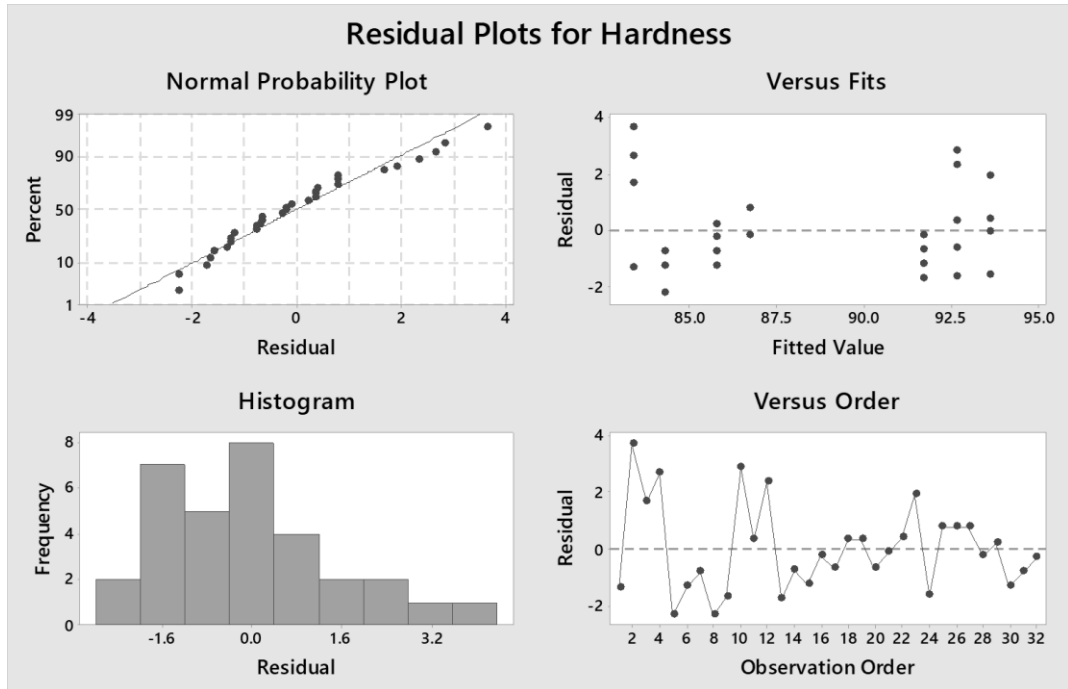


Figure 210: Residual Plots for Hardness for ER308L for Temp Control

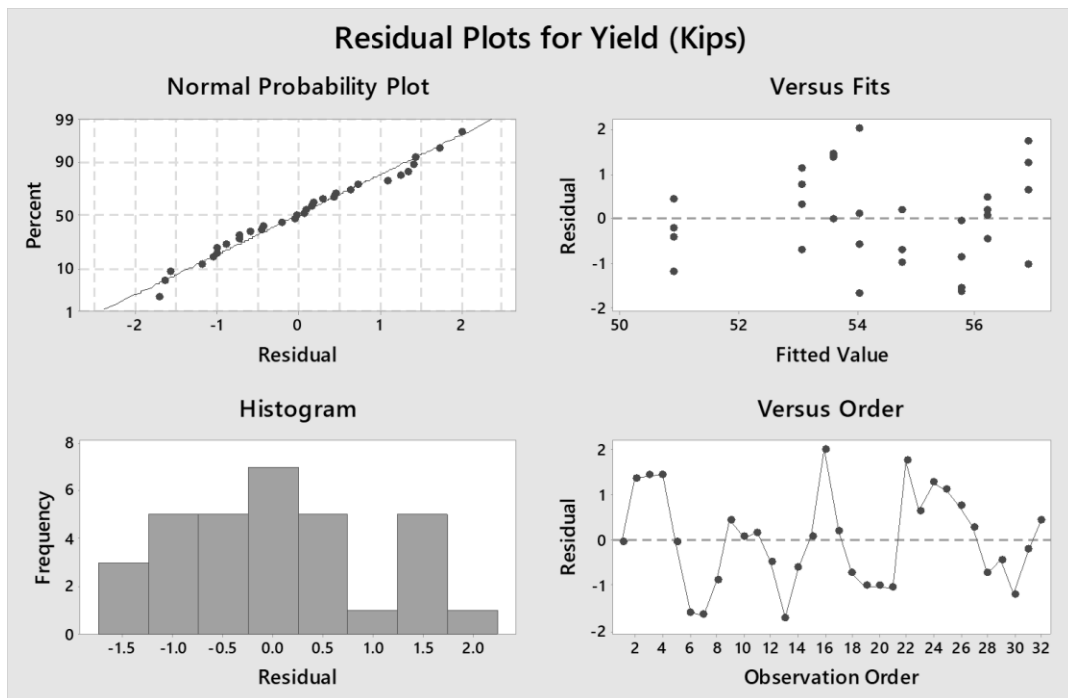


Figure 211: Residual Plots for Yield for ER308L for Temp Control

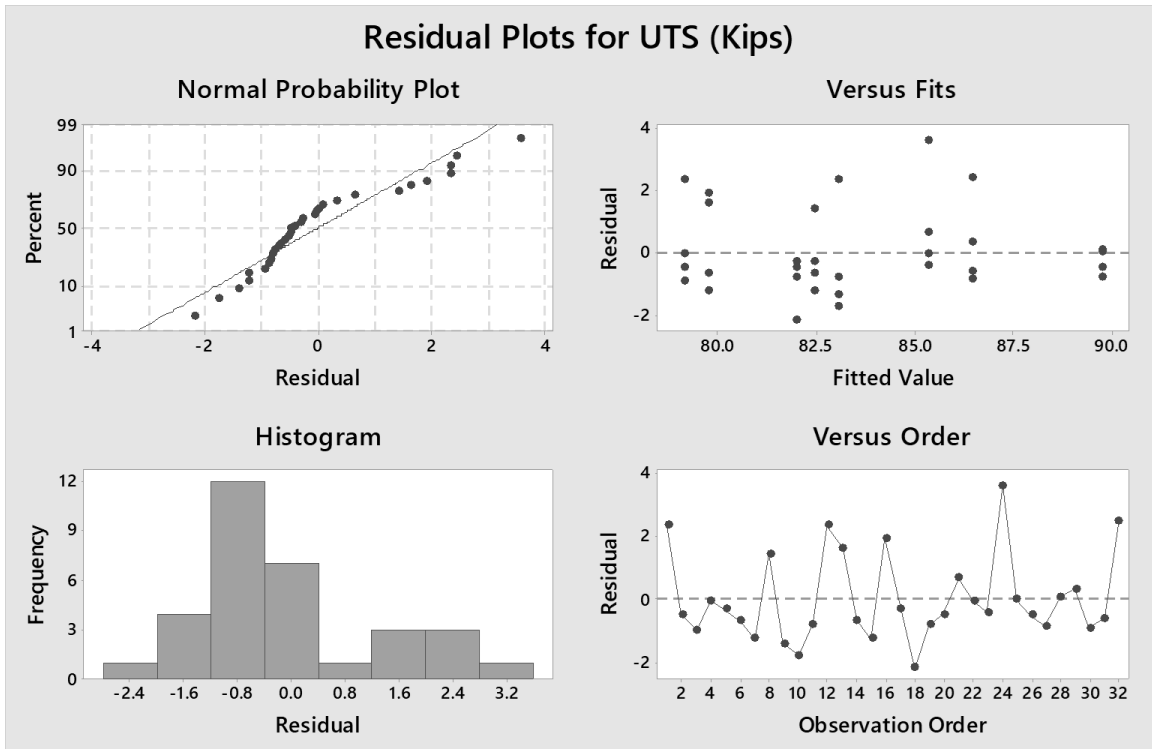


Figure 212: Residual Plots for UTS for ER308L for Temp Control

The yield strength increases with increasing temperature control limit. It should be noted that the upper values of temperature are at continuous welding and therefore the temperature cannot be increased without secondary means (laser, heated bed, etc.). The UTS and hardness hit an inflection point, then increase with increasing temperature. The UTS, yield strength, and hardness were slightly lower in the perpendicular direction when compared to the parallel direction of deposition. Noting that hardness is not a directional quantity and any difference found between directions is due to measurement accuracy, material repeatability, or outside influences. Figures 213-224 show the Tukey analysis and interval plots for the temperature control scheme for ER308L.

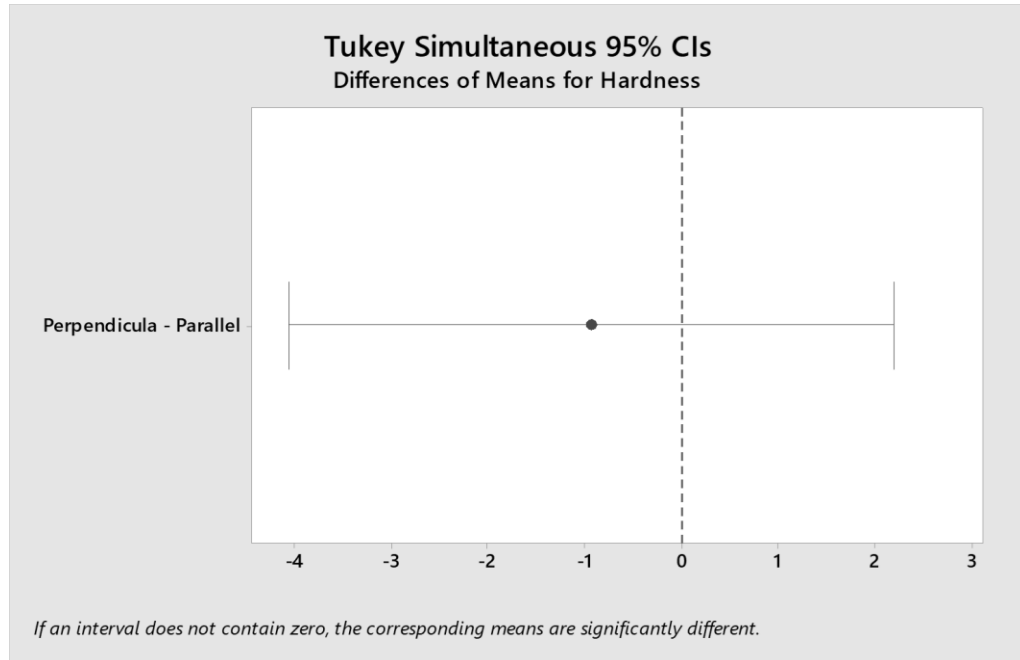


Figure 213: Tukey Analysis for Hardness for ER308L for Temp Control

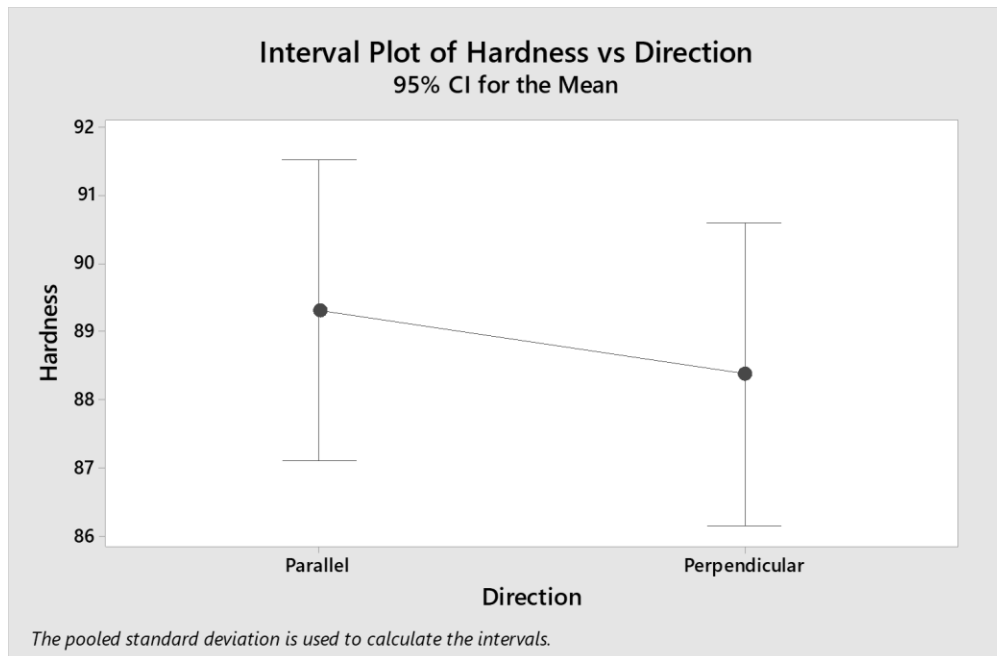


Figure 214: Interval Plot for Hardness for ER308L for Temp Control

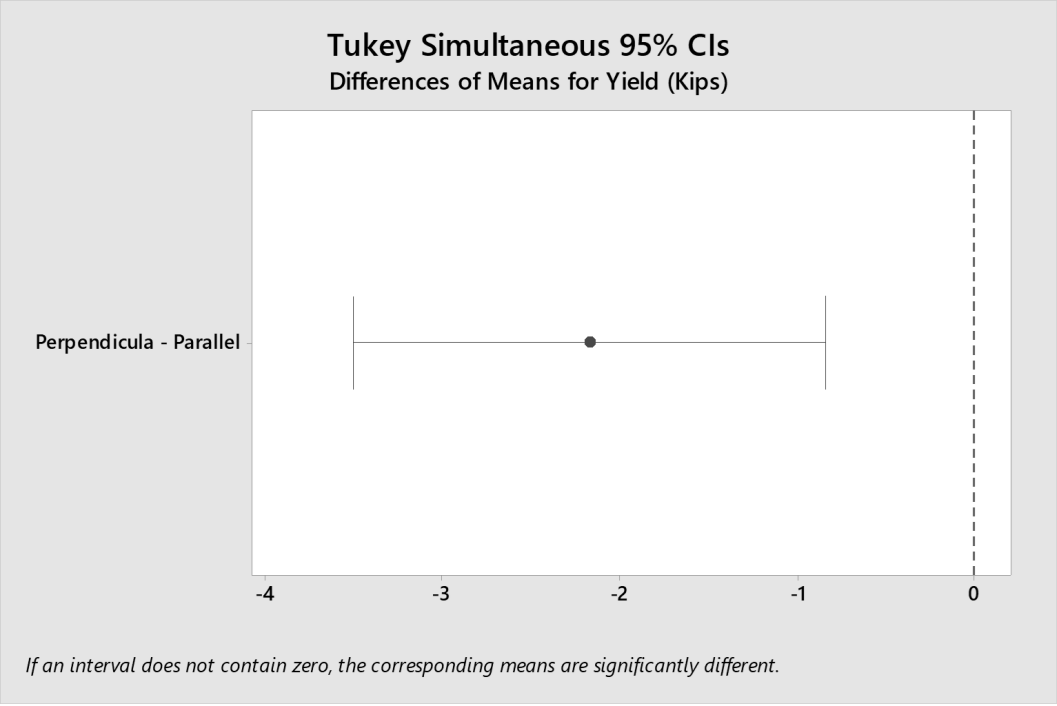


Figure 215: Tukey Analysis for Yield for ER308L for Temp Control

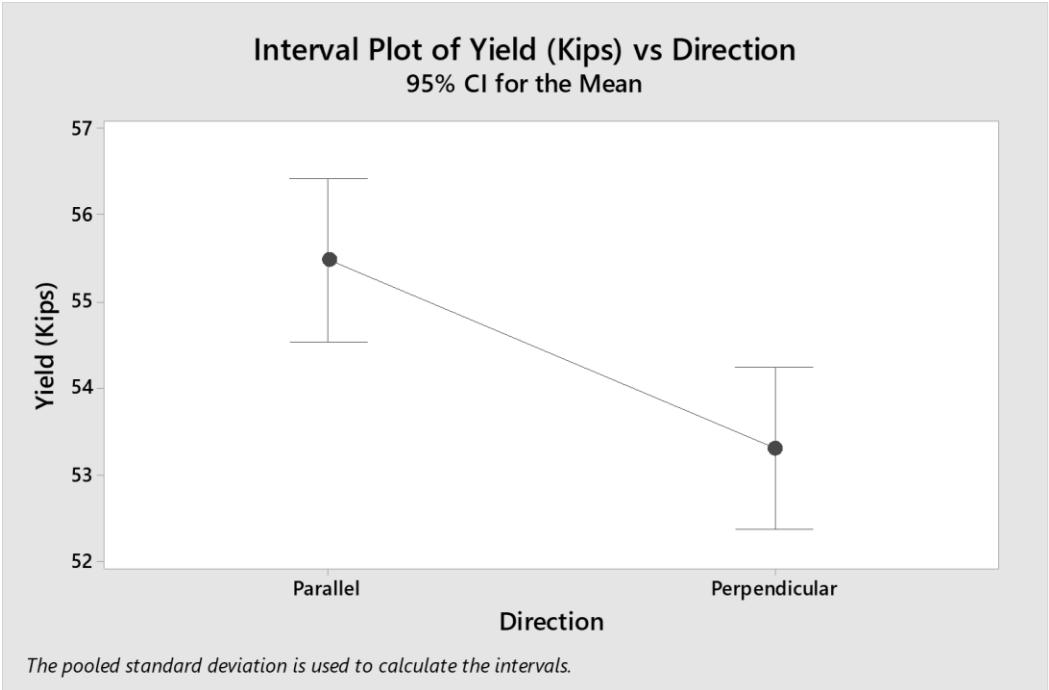


Figure 216: Interval Plot for Yield for ER308L for Temp Control

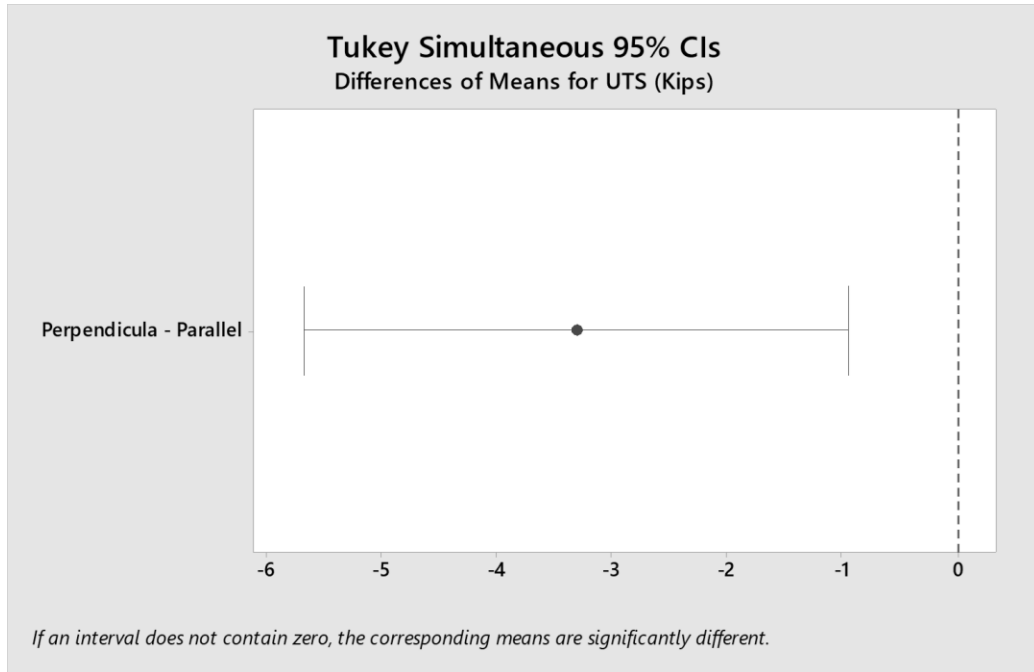


Figure 217: Tukey Analysis for UTS for ER308L for Temp Control

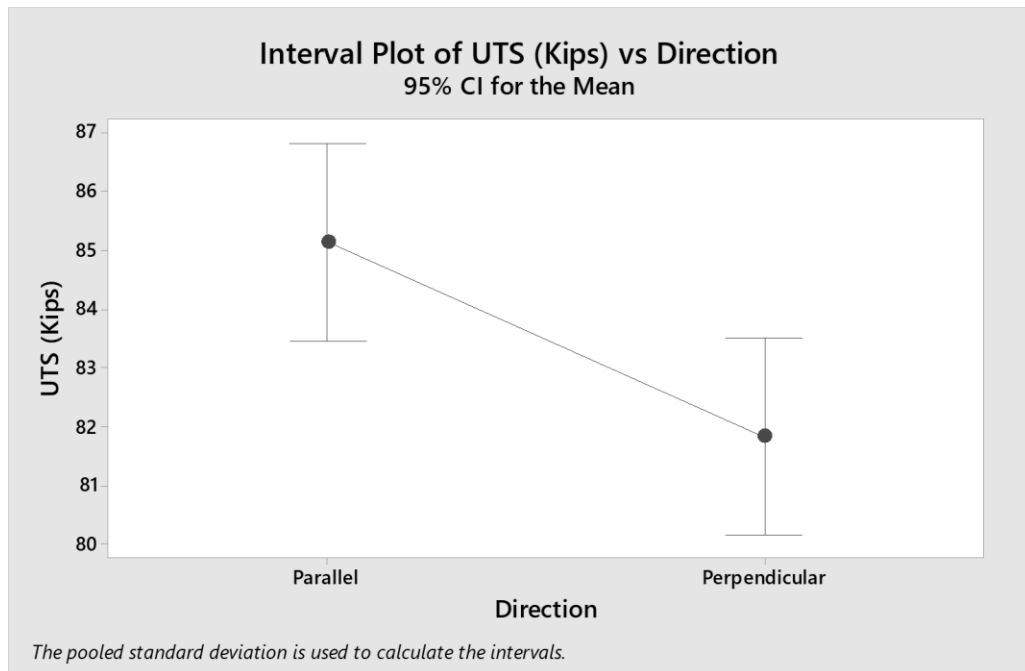


Figure 218: Interval Plot for UTS for ER308L for Temp Control

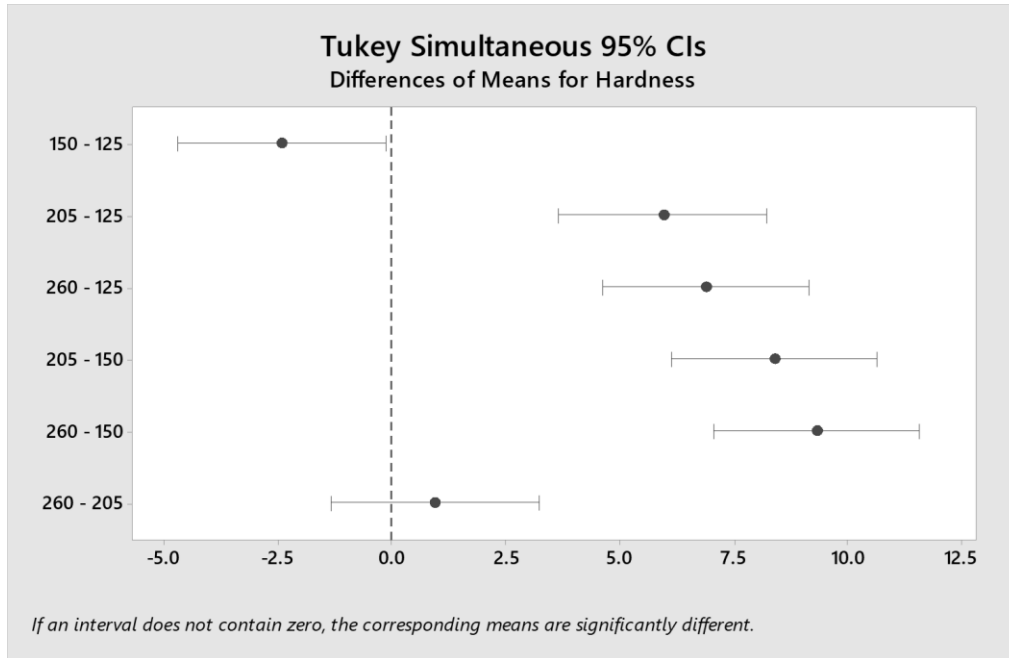


Figure 219: Tukey Analysis for Hardness for ER308L for Temp Control

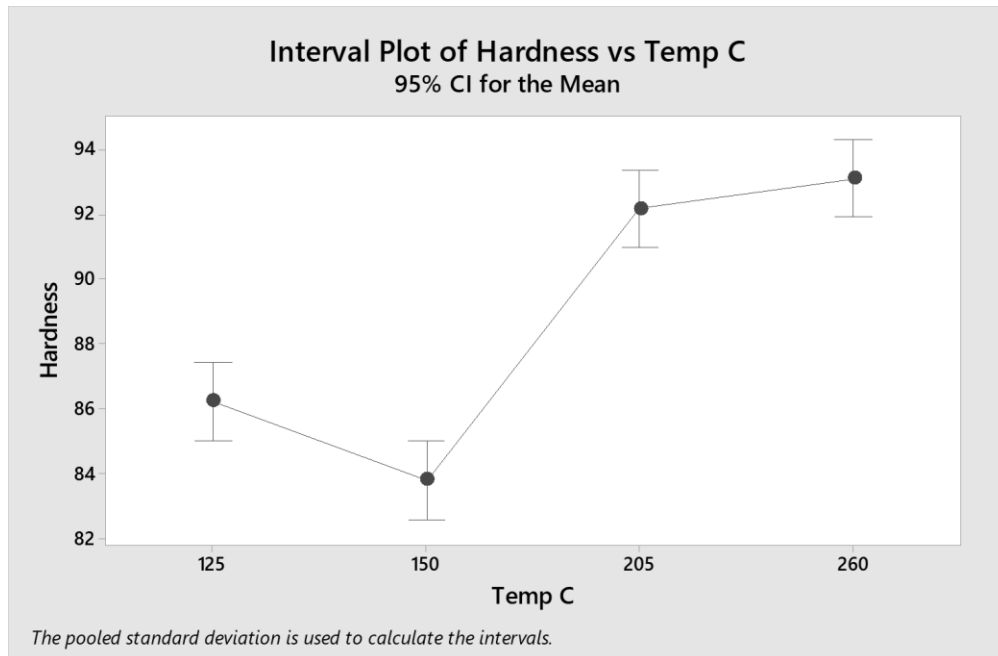


Figure 220: Interval Plot for Hardness for ER308L for Temp Control



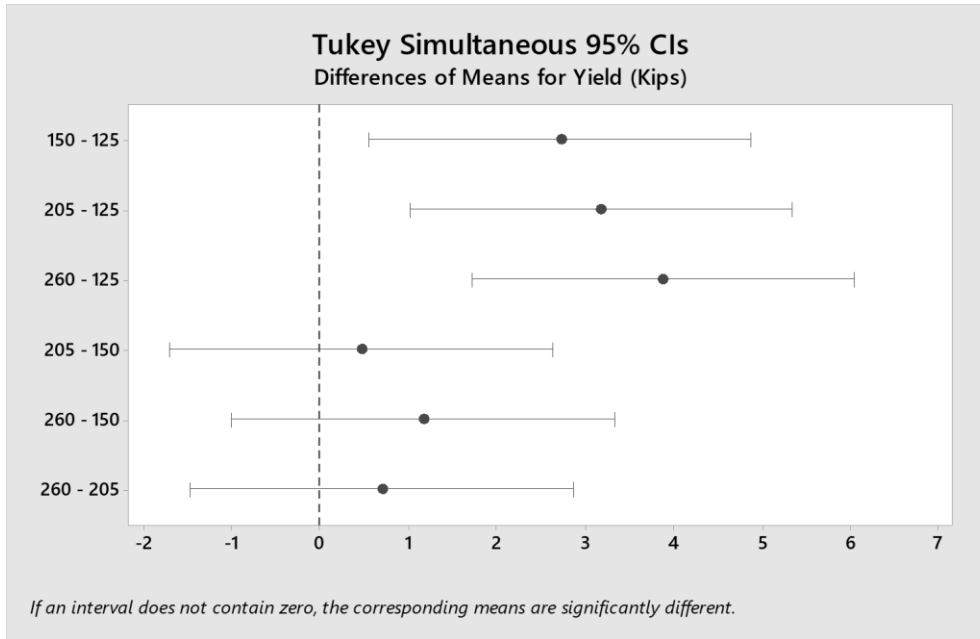


Figure 221: Tukey Analysis for Yield for ER308L for Temp Control

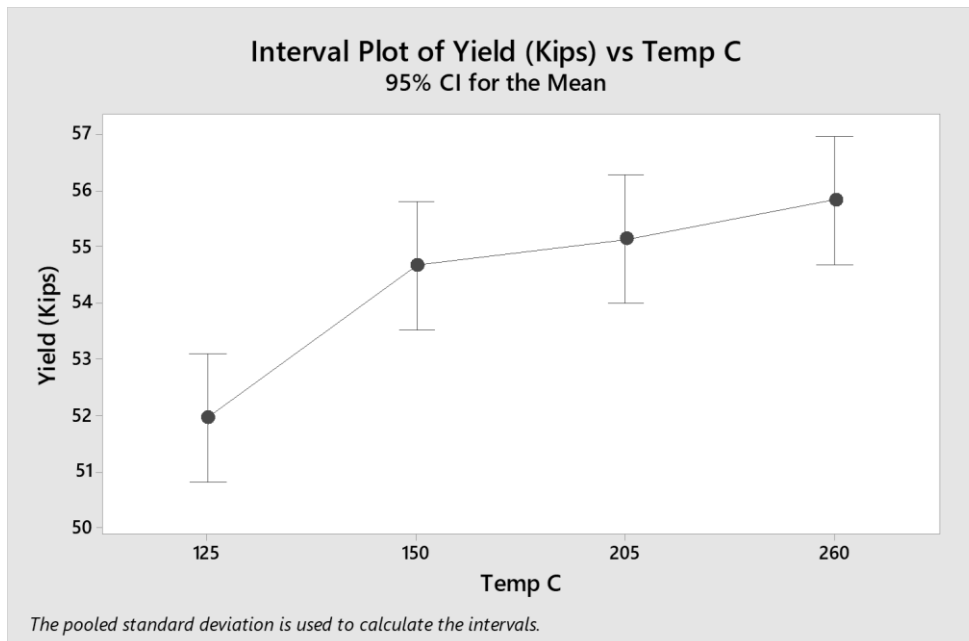


Figure 222: Interval Plot for Yield for ER308L for Temp Control

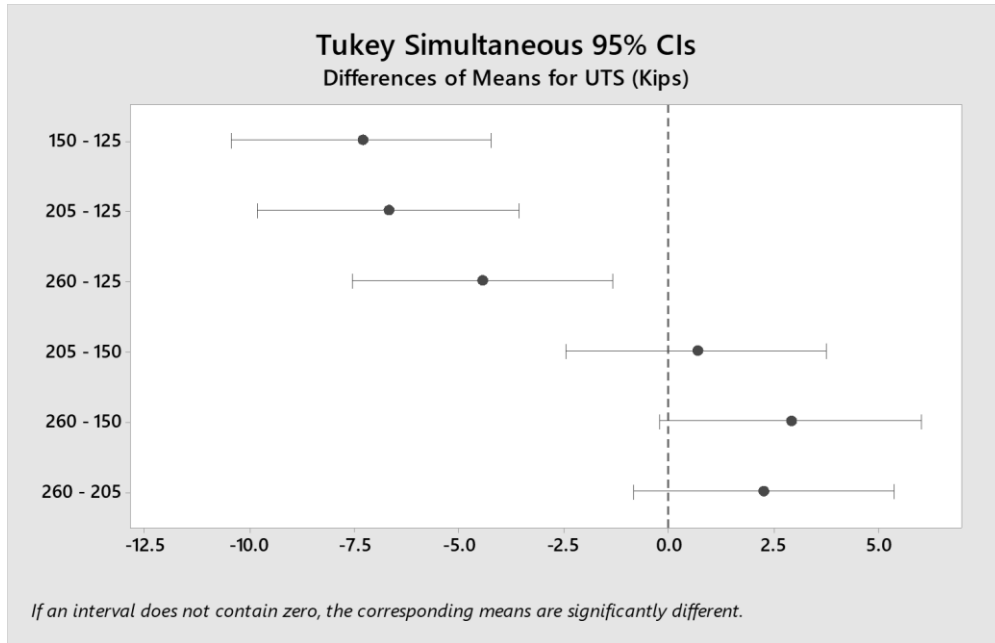


Figure 223: Tukey Analysis for UTS for ER308L for Temp Control

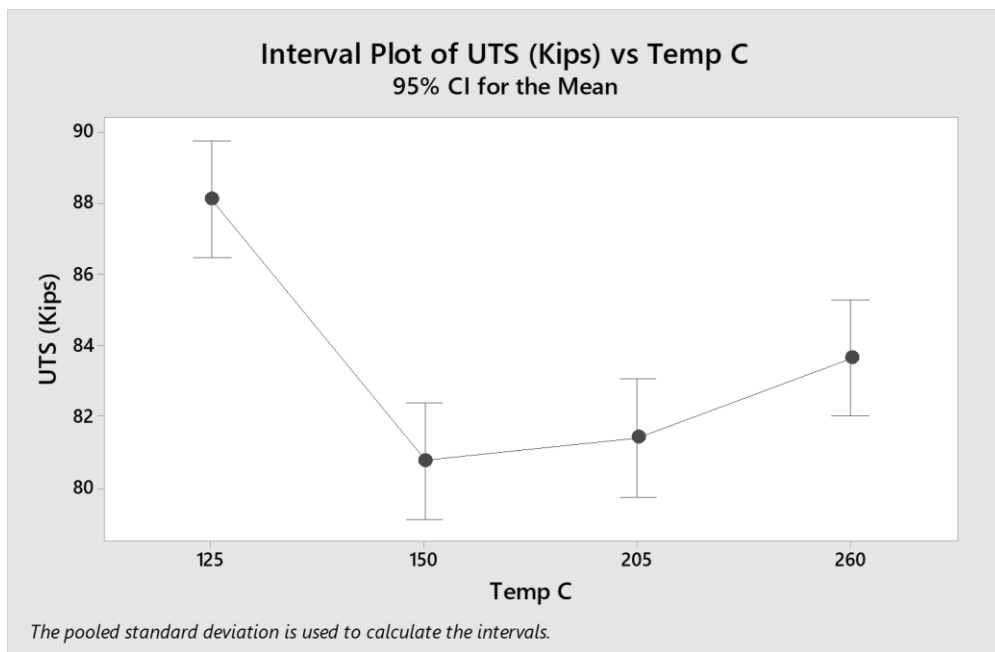


Figure 224: Interval Plot for UTS for ER308L for Temp Control

As one can see the hardness is statistically the same directionally (as it should be since it is not a directional component). The yield strength and UTS are not equal directionally, with the parallel direction being higher. The hardness is not statistically

equal for all combinations except for combination 205°C & 260°C (401°F & 500°F). The yield strength and UTS are statistically equal for all combinations except for those combined with the baseline (125°C). Figures 225-227 show the results of the UTS, yield strength, and hardness with the accuracy (total combined accuracy of measurable) taken into consideration.

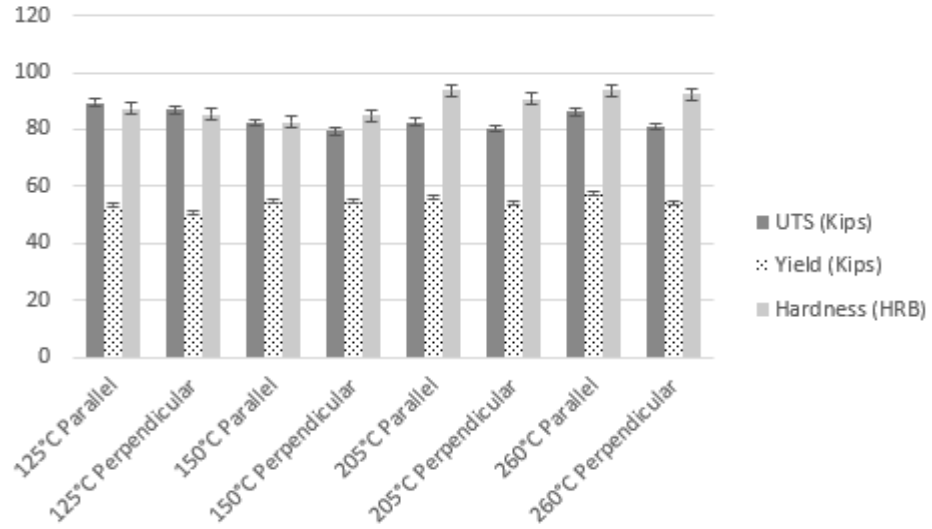


Figure 225: Graph of ER308L Temp Control Measurables with Accuracy

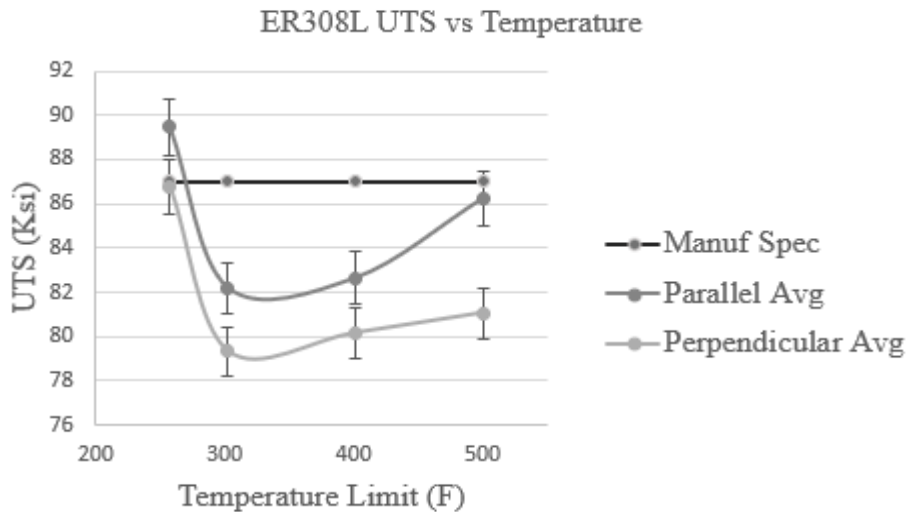


Figure 226: Temperature v. UTS for ER308L with Accuracy

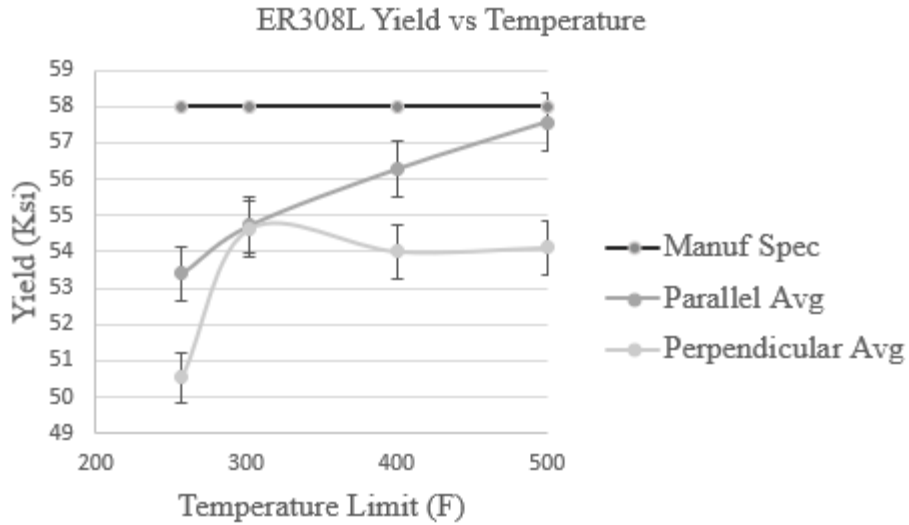


Figure 227: Yield Strength v. Temperature for ER308L with Accuracy

With the accuracy taken into consideration, the yield strength at 150°C (302°F) is equal directionally. The hardness for the combination of 150°C (302°F) and the baseline are equal. The UTS in the parallel direction at 260°C (500°F) is equal to the UTS at 125°C (257°F) in the perpendicular direction. The yield strength for the baseline in the parallel direction is equal to the yield strengths for the other temperature points in the perpendicular direction and in the parallel direction at 150°C (302°F).

Other measurables evaluating the temperature control scheme were taken; however, they were single points (deposition rate, etc.) and statistical analysis cannot be analyzed on this data. The print times for the samples were recorded from the machine run time; this was converted into deposition rate and compared instead. This includes the time it takes for the operator to stop the program and other arbitrary tasks; therefore, there is some discrepancy between identically produced walls (parallel v. perpendicular) of a minute or so. The weight of the sample was then divided by the total time to calculate the deposition rate. The amount of material removed from each wall on each side was also recorded. This is the total amount of material needed to have a smooth flat surface on both sides. The

average layer height of each wall was also recorded. Table 34 shows the data for both ER70S-6 and ER308L. As one can see the values are similar and very few discrepancies are noted directionally for all measurables for both materials independently. The layer heights for both materials are also considerably the same between temperature limits. The total material machined for both materials is considerably more for both materials with the temperature control and is reasonably the same between temperature limits. The deposition rate for both materials is considerably higher for both materials with the temperature control and is arguably the same between the temperature limits.

Table 34: Temp Control Deposition Rate, Machining, and Layer Height Evaluation

	Deposition Rate (kg/hr):	Machined til flat (in):	Layer Height (mm):
Baseline Control: ER70S-6	0.6 / 0.6	0.055 / 0.060	2.9 / 2.9
Baseline Control: ER308L	0.58 / 0.58	0.067 / 0.080	3.5 / 3.5
First Limit: ER70S-6	0.81 / 0.78	0.122 / 0.133	2.9 / 2.9
First Limit: ER308L	0.716 / 0.677	0.090 / 0.088	3.6 / 3.5
Secondary Limit: ER70S-6	0.86 / 0.88	0.121 / 0.123	2.9 / 2.9
Secondary Limit: ER308L	0.861 / 0.863	0.090 / 0.092	3.6 / 3.6
Upper Limit: ER70S-6	0.86 / 0.88	0.124 / 0.141	2.9 / 2.9
Upper Limit: ER308L	0.762 / 0.811	0.104 / 0.109	3.3 / 3.3

The WFS, voltage, and current did not change between tests as the same program was executed during the layers. The temperature control only took effect at the end of layers; therefore, any discrepancies noted with these measurables are not due to the temperature control and are not noted here.

Metallographic analysis of the microstructure of ER70S-6 and ER308L samples were studied with guidance from the ASM Handbook -Vol 9 [67]. Figure 228 shows the typical microstructure observed in ER70S-6 without the temperature control (baseline). Figure 229 shows the layer boundary of ER70S-6 without the temperature control. Again, the dark area of the image is where the edges of the sample meet the mounting polymer and is not a void. A uniform grain structure was noted throughout the wall and the layer interface was once again noted to have no distinct boundary.

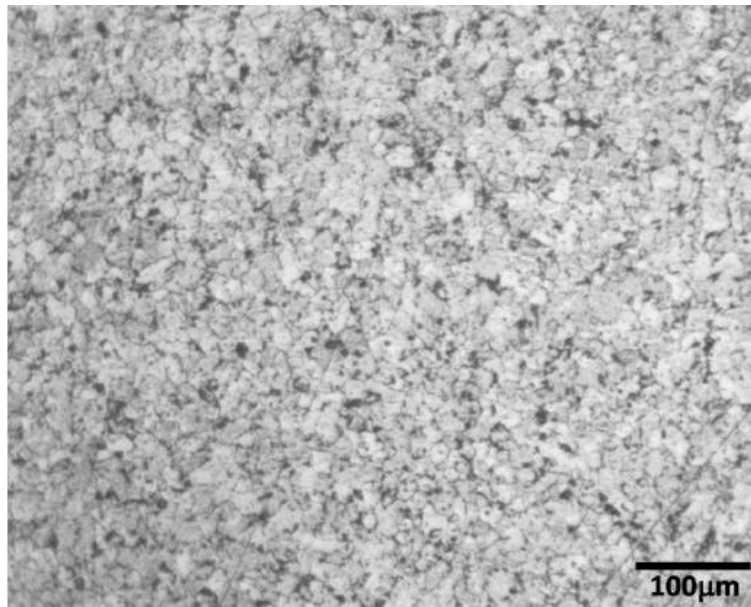


Figure 228: ER70S-6 without Temperature Control Representative Structure

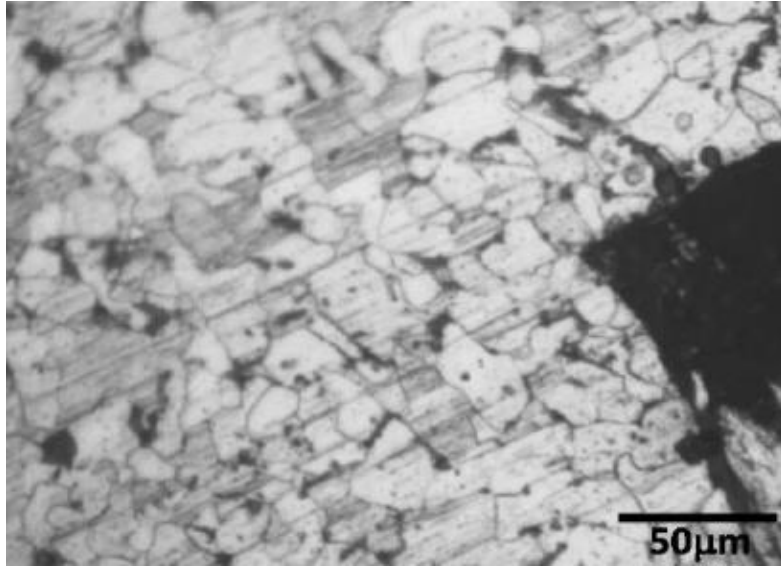


Figure 229: ER70S-6 without Temperature Control Layer Interface

Figure 230-234 show the microstructure found in ER70S-6 with the temperature control at each of the factor levels. At the layer boundaries there was no distinct layer interface noted as was also the case without the temperature control. A uniform ferrite grain structure was noted throughout in all cases with some hard oxides present (from sanding).

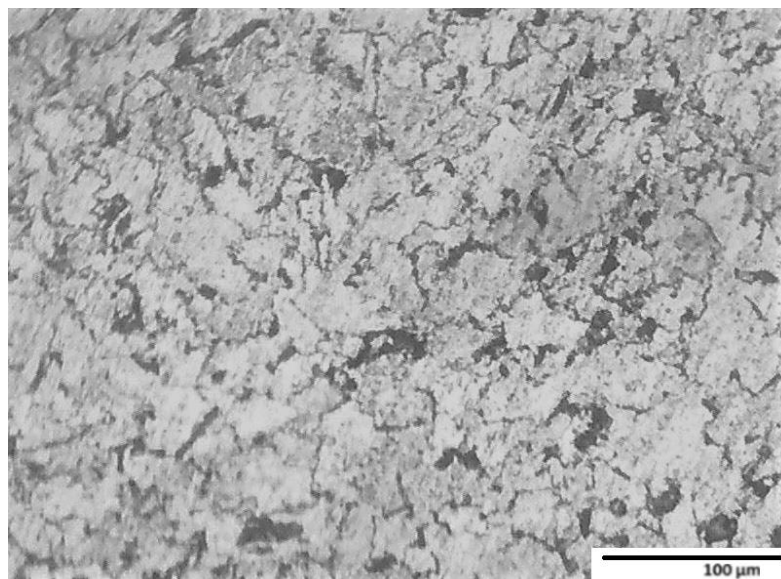


Figure 230: ER70S-6 with Temperature Control at 232°C

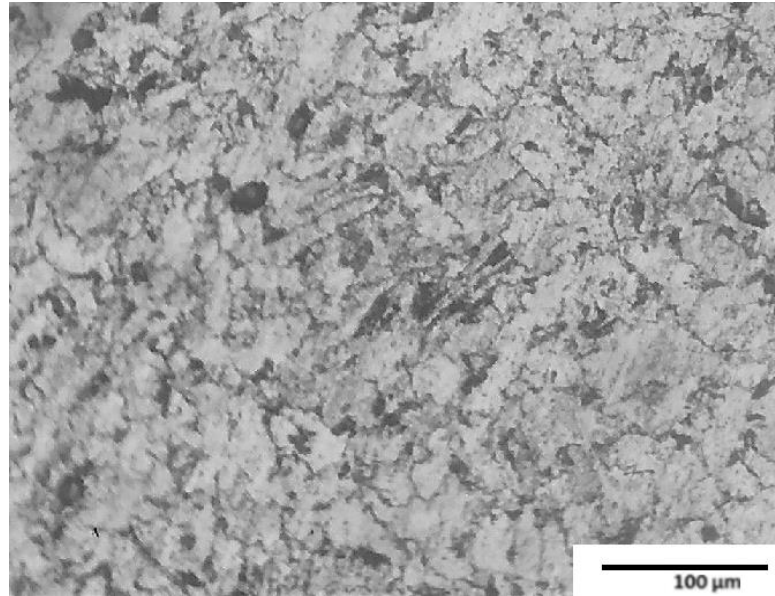


Figure 231: ER70S-6 with Temperature Control at 260°C

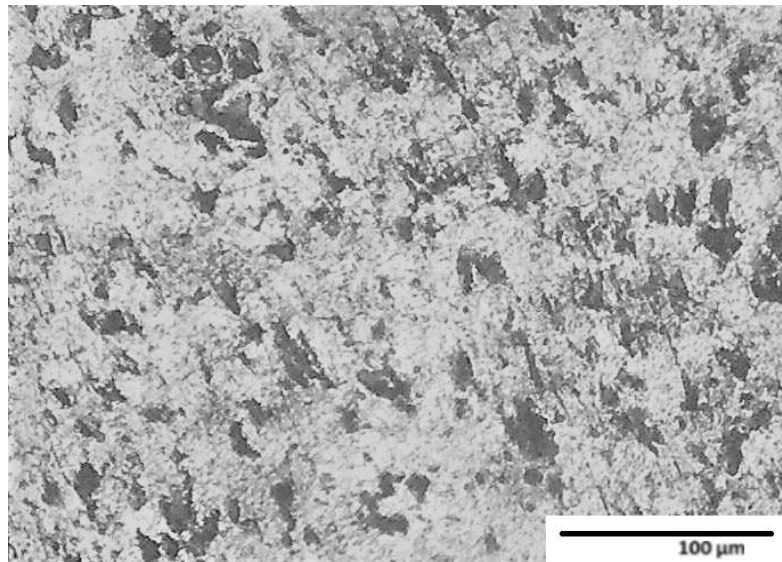


Figure 232: ER70S-6 with Temperature Control at 288°C

Figure 233 shows the typical microstructure found in ER308L without the temperature control. Figure 234 shows the layer interface and a clear boundary layer is present like that found in previous research [2]. The general microstructure is comprised of skeletal  $\delta$ -ferrite in an austenitic matrix.



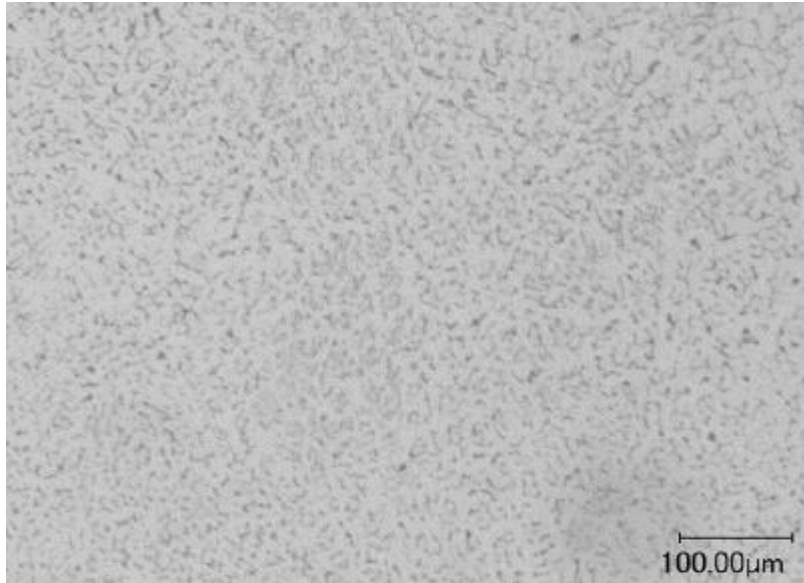


Figure 233: ER308L without Temperature Control Typical Microstructure

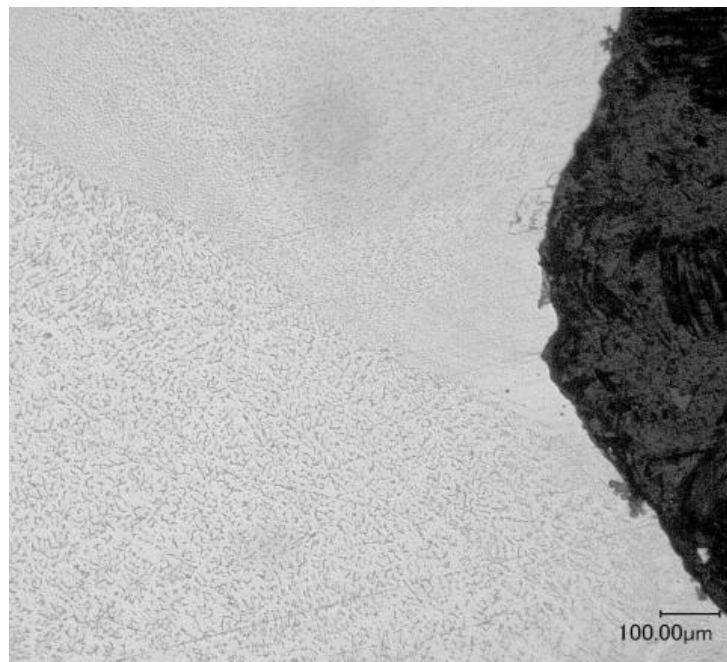


Figure 234: ER308L without Temperature Control Layer Interface Boundary

Figures 235-242 show the microstructure found in ER308L with the temperature control at each of the factor levels. At 150°C skeletal  $\delta$ -ferrite can be seen along with lathy  $\delta$ -ferrite (Figure 235). At the layer interface, a similar structure is found as without the temperature control (Figure 236).

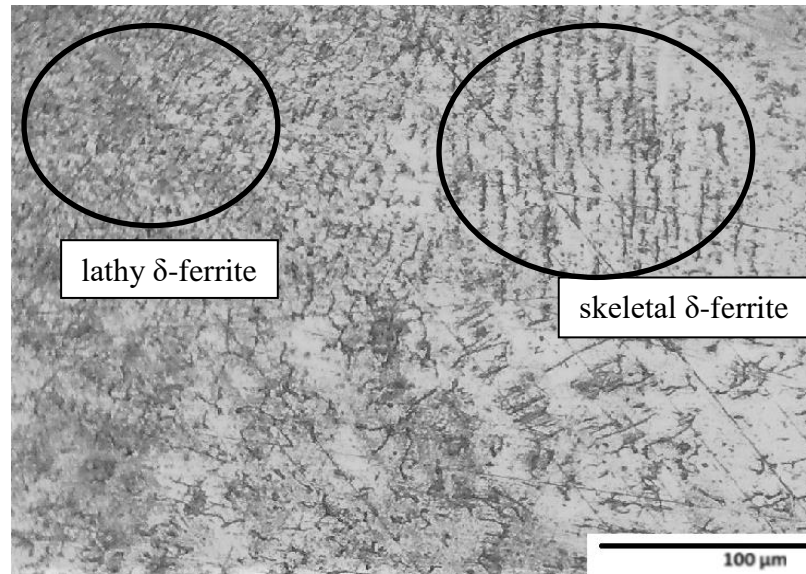


Figure 235: ER308L with Temperature Control at 150°C

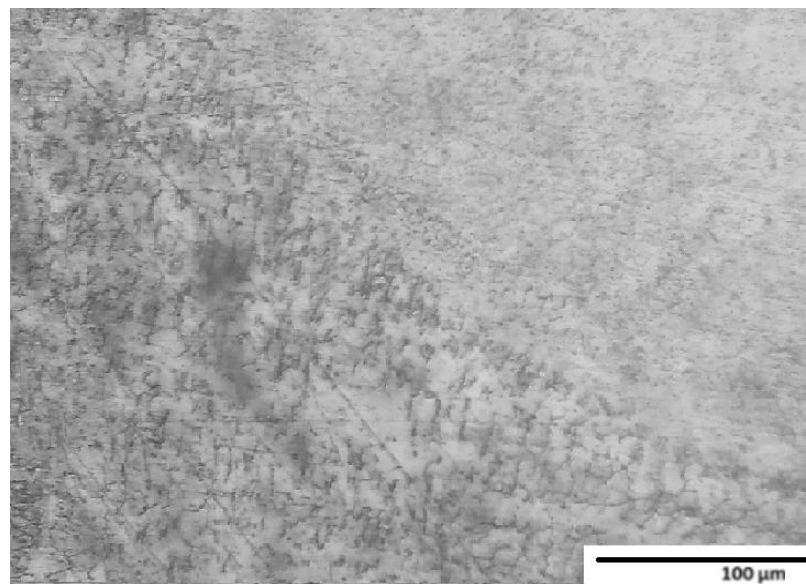


Figure 236: ER308L with Temperature Control at 150°C Layer Interface

Figure 237 shows the microstructure with temperature control at 205°C. Skeletal  $\delta$ -ferrite can be seen once again; however, no lathy  $\delta$ -ferrite was noticed. At the layer interface, a similar structure is found as before; however, a less distinguishable interface is noticed (Figure 238).

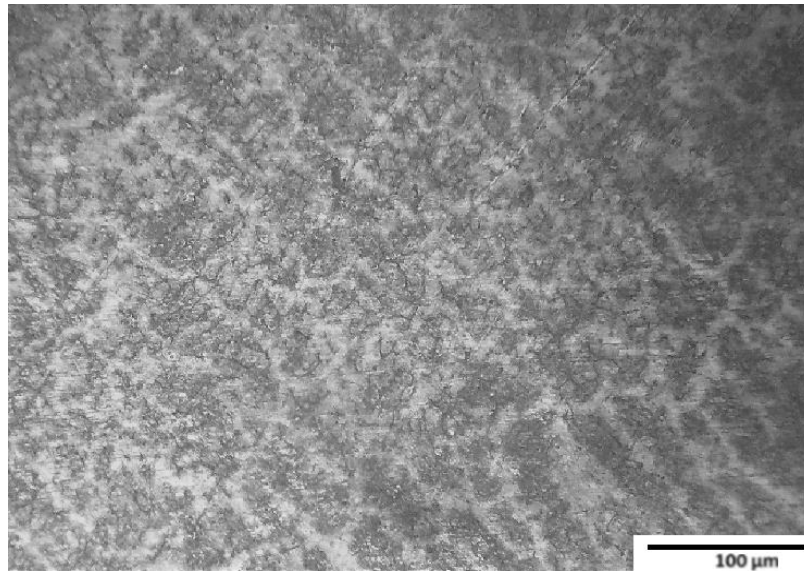


Figure 237: ER308L with Temperature Control at 205°C

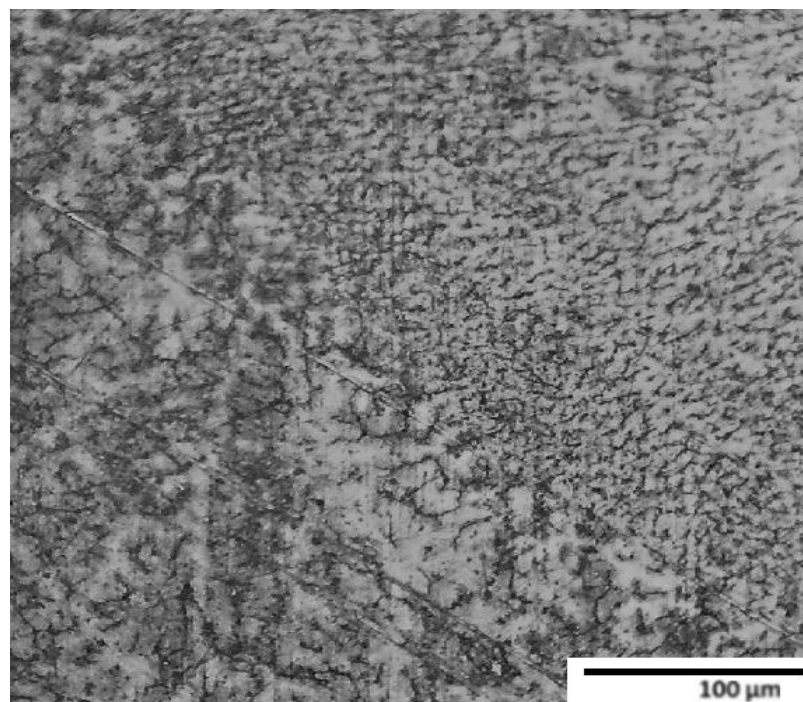


Figure 238: ER308L with Temperature Control at 205°C Layer Interface

Figure 239 shows the microstructure with temperature control at 260°C. A uniform skeletal  $\delta$ -ferrite can be seen. At the layer interface, a similar structure is found as before; however, an almost undistinguishable interface is noticed (Figure 240). A few spots of hard oxide, from sanding, are also noticed.

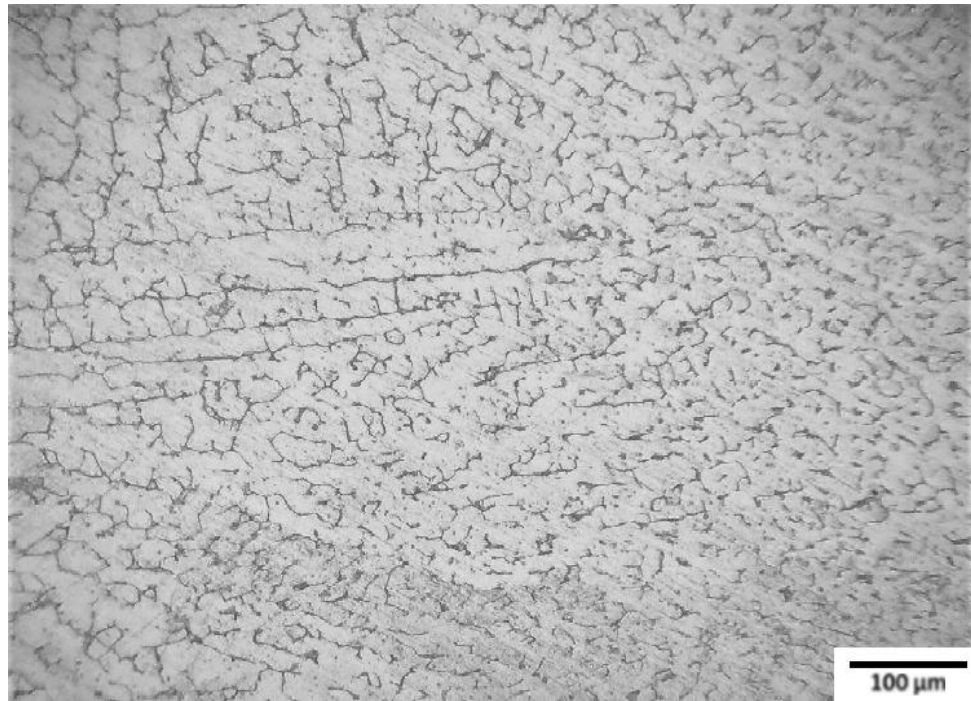


Figure 239: ER308L with Temperature Control at 260°C

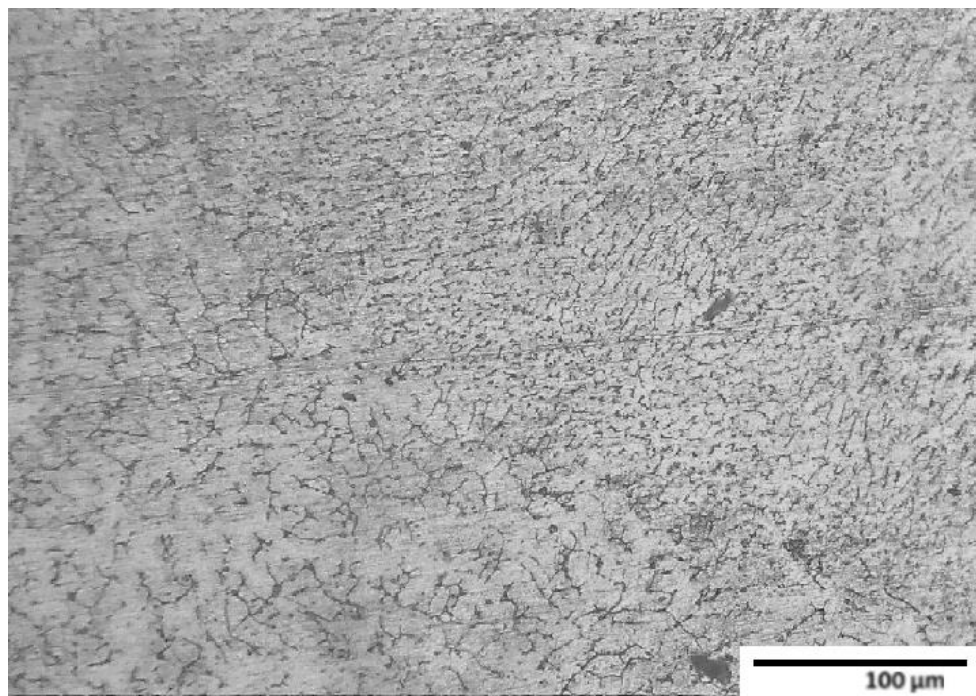


Figure 240: ER308L with Temperature Control at 260°C Layer Interface

## **VII. Discussion**

Analysis of the results found in the previous chapter allows a greater understanding of the process, its advantages, and improvement opportunities. A discussion of the results from each aspect of the project is found below.

### **Closed-Loop Process Control Discussion**

The need for a closed-loop process control scheme in additive manufacturing processes has been noted as a must to take the technology to the next step. For Wire + Arc Additive Manufacturing (WAAM), the three specific areas found to be in the most need of better process control were maintaining proper contact tip to work distance, controlling weld parameters, and preserving thermal affects throughout the process.

### **Contact Tip to Work Distance Control Discussion**

While maintaining proper CTWD did little for improving mechanical properties, the benefits found in easing production were very notable. Since the control scheme works to eliminate scale error. It is believed that any discrepancies found in this research would only be amplified as the part is scaled up. These samples only attributed to roughly 0.1% of the total build volume available in the machine. This leads to a great potential for scale error to completely alter a part geometrically, metallurgically, or even mechanically. This also increases the production time potential as the operator will have to constantly monitor the production and adjust continuously. With the CTWD control there is little to no need for the operator to adjust offsets throughout the process to maintain CTWD.

## **Cold Metal Transfer Control Discussion**

While the synergic control line is a great improvement on the GMAW process, it does leave much to be desired. Synergic control simply augments amperage to try and maintain voltage requirements at a set wire feed speed. The CMT control produced parts with less heat input, less total energy used, practically zero spatter, and less post process machining required. While there was no noted difference in yield strength for ER70S-6, the UTS was higher for CMT in both ER70S-6 and ER308L. Figure 55 shows this could be remedied by simply using a different brand of ER308L wire. The CMT process also makes using the machine easier as so many parameters are interrelated that there are few things that a novice user needs to set to begin a 'print.' The microstructure for both control schemes produced similar results, minus that of ER70S-6. The CMT process produced indistinguishable layer boundaries in ER70S-6.

## **Temperature Monitoring Control Discussion**

Once again looking at Figure 55, one can see the dramatic effect of interpass temperature on strength. Figure 205-6 closely agree with the results found in Figure 55, showing the trend of decreasing strength with increasing interpass temperature for ER70S-6. Interestingly, there really is not much information on the effects of interpass temperature for stainless welded alloys. Figures 226-227 show the results of this phenomenon found in this study. As one can see, UTS decreases with increasing interpass temperature up to a certain point and the trends changes, but eventually levels off below manufacturer's specs. The yield strength increases with increasing interpass temperature until it levels off below manufacturer's specs. One thing to note here is the effect of interlayer bonding (deposition direction) is magnified as interpass temperature is increased for both yield

strength and UTS. This is possibly due to the chromium precipitates that become more prevalent at the surface (sugaring) as more time is allowed for resolidification of the weld pool to commence (hotter). Looking at the microstructure; however, this does not appear to be the case. As the temperature increases it appears to achieve a more uniform grain structure at layer boundaries as grains are closer to the same size with all of them becoming larger. After 150°C, this becomes more noticeable; which is also where the inflection points occur in both the UTS and yield strength graphs. The more uniform grain structure helps to explain why yield strength is increasing with increasing temperature. Logically, the microstructural change that occurs after 150°C at the boundaries, is the reason behind the increasing interlayer effects on both UTS and yield strength.

The increased deposition rate utilizing the temperature monitoring scheme more than makes up for the slight post processing that needed to occur. With a 'print' time savings of roughly 60% using the control scheme at any temperature set point, having to make a few extra passes in post processing is miniscule. When this is scaled, the time savings has enormous potential, while the increased post processing remains unknown. If a different, harder to machine material was used (Inconel, titanium), the extra post processing would be more detrimental but still nothing compared to traditional manufacturing. The time savings in either case, is still much greater than other metal additive processes with or without the temperature control.

## **General Discussion**

The control schemes developed to improve the overall control of the WAAM process, were a success. Maintaining a consistent CTWD throughout the print successfully eliminated the scale error that occurs from discrepancies in actual layer height produced

versus layer height programmed. The CMT-GMAW process proved to be a better welding control scheme than the previously used standard synergic control in not only producing better quality ‘prints,’ but also in providing more reliable and repeatable results. A temperature monitoring system, like that of Spencer *et al.*, was successfully created and evaluated to monitor/maintain weld temperature throughout a ‘print’ to achieve desired mechanical properties. The use of all these controls in conjunction is recommended highly for future users.

The parts produced dimensionally resulted in about 1 mm (~0.040”) of excess material all around. This means the user does not need to scale models to allow for post process machining as the allowance is built-in. This WAAM-BAM (built-in allowance for machining) feature aids in allowing the user room to remove layering ‘humps’ for the surface finish without the pre-processing of other additive processes.

The Fronius weld parameter control logic operates on a 0-10 volt DC system. The rest of the controls operate at 12, 24 VDC or 120 AC. To have I/O communication with the welder a controllable 0-10 volt system needs to be created if further closed-loop control is to be implemented to control weld parameters live (during ‘print’). Multiple MOSFET chipsets were made and left with the welder for future researchers use [68].

## **Summary**

In additive manufacturing the need for optimal mechanical properties is not always necessary. Often a simple working prototype for proof of concept is all that is necessary. In this case the fastest method, without compromising the machine, is best. The use of all the control schemes in conjunction with each other is highly recommended for all future users for all occasions. This not only benefits the user and the ‘printed’ part, but also the



machine. If a high UTS is desired, the lowest temperature set point is recommended for both materials. If a good yield strength is desired, the second lowest temperature set point is recommended for both materials.

## VII. Conclusion and Future Work

A comprehensive literature review was conducted to address the state of process controls in additive manufacture, specifically in WAAM. From the literature review, the need for closed-loop control was noted to improve areas of CTWD, weld parameters, and thermal management. Controls were developed and evaluated experimentally to improve the WAAM process. The results of the experiments are listed below.

- A Fronius CMT welder was integrated into the existing 3-axis, gantry-style CNC 3D printer.
- New machine code was developed, adding greater functionality to the robot.
- An experimental record sheet header was created for future researchers to use.
- Four feedback control loops were created and implemented to improve on process stability.
- These controls were successfully used in concurrence with each other producing a unique multiple closed-loop control process for geometrical and technological control of the WAAM process.
- A loop was created to improve the ease of use of the machine, by having the ‘robot ready’ and not arc until actual movement commenced.
- A control scheme to maintain CTWD was developed and evaluated to remove scale error from the WAAM process.
- The CMT welding process was compared to the traditional synergic welding process in the WAAM process qualitatively and quantifiably.

- The effect of interpass temperature on mechanical properties has been studied for multilayer deposition
- An operating manual was created for future users to understand the machine and to improve upon it.
- A graph was developed to evaluate the mechanical property effects of interpass temperature on ER308L (stainless) which has yet to be found elsewhere (227-8).
- A flow chart was developed to help future users understand weld parameterization and the available user defined characteristics of the WAAM process (Figure 54).
- A wiring diagram of the robot integration with the CNC controls was created for future additions or maintenance (Appendix VI).
- Near isotropic characteristics were found in ER70S-6 (steel), which is a significant find in the additive manufacturing community.
- MOSFET regulator chipsets were created for future users to have the ability to control weld parameters in process in a closed-loop system [68].
- Files for producing walls to create tensile specimen were left behind for future users.

### **Recommendations for Future Work**

As always, further analysis is necessary to continually refine and improve the process. This future work can be divided into improvements in the control, improvements in the machine, and improvements in process.

Methods of improving and furthering control:

- Implementing a closed-loop control of user definable weld parameters.

Methods of improving and furthering the machine:

- The addition of more axes will aid in geometrical capabilities of the machine.
- A controllable cooled bed can aid in certain materials and help maintain desired weld temperature.
- Develop a dedicated post processor for the machine.

Methods of improving and furthering the process:

- Further analysis of ER308L to achieve near isotropic characteristics like those found with ER70S-6. Starting with changing brand of ER308L to Lincoln Electric® Blue Max® ER308LSi. The additional silicone will improve the layer boundary definition via better wetting action. The variance in AWS class wire will also improve yield strength and UTS results.
- Expansion of analysis with other materials. Based on experience, these materials would be not only other stainless and steel wires, but also materials such as Inconel or titanium. These metals are traditionally notorious for being difficult to machine as well as very expensive. Producing them via the WAAM-BAM method would cut manufacturing costs significantly. Materials such as aluminum are not recommended for further application, as the tensile properties are significantly lower than those found with traditional methods. Aluminum is also known for its machinability which leads to less need to ‘print’ it, especially with its high level of difficulty to ‘print’ due to its high thermal conductivity.

- A well-mapped material properties database should be developed for ER70S-6 and other well-developed material in the WAAM-BAM process. This goes beyond UTS, yield strength, and hardness; and into properties such as modulus, Poisson's ratio, etc.
- Scaling prints up to larger scale and restudying the effects found here would be beneficial to the research community and is deemed almost necessary as a next step for future research.
- With the CMT welder, one can weld aluminum to steel. The ability to 'print' multi-material metal parts would be a very unique area to research with a plethora of opportunity for advancement.

### **Outstanding Objectives**

The use of a raft to aid in removability of 'printed' parts was omitted from the research. It was found that the parts were not difficult or lavishly time consuming to remove from the build plates and that the build plates were reusable. More importantly, the first layer is widely considered to be the most important layer in additive processes as it is the least stable and 'steady-state' layer. Any flaws in this layer will be carried out throughout the rest of the part (humps, undercuts, etc.). If different materials were used in the future, the use of a raft may become more suitable or necessary.

Development of a g-code post was started with machine specific m-codes and g-codes; however, a dedicated post processor was not created. Since most of the codes needed were needed at the end or beginning of a layer (z-movement), a simple control + f for a z-movement in the code was quick enough to modify machine code. For a much

larger print than was produced in this research or if more axes were implemented, this would simply be unsuitable, and a dedicated post processor would be required.

## References

- [1] Frazier, W. E., 2014, "Metal Additive Manufacturing: A Review," *Journal of Materials Engineering and Performance*, 23(6), pp. 1917-1928.
- [2] Gaddes, J. S., 2015, "Parametric Development of Wire 3D Printing," Master of Science, Auburn University.
- [3] Williams, S. W., Martina, F., Addison, A. C., Ding, J., Pardal, G., and Colegrove, P., 2016, "Wire + Arc Additive Manufacturing," *Materials Science and Technology*, 32(7), pp. 641-647.
- [4] Miller, "Guidelines For Gas Metal Arc Welding (GMAW)," Miller Welding, millerwelds.com, ed.
- [5] Fronius, "Cold Metal Transfer. The Technology.," Fronius USA LLC, Perfect Welding(fronius-usa.com).
- [6] LI, Y. M. Z. A. P. J., 2001, "Modified Active Control of Metal Transfer and Pulsed GMAW of Titanium," American Welding Society, AWS, WELDING RESEARCH SUPPLEMENT.
- [7] Mufti, R. A., 2008, "Mechanical and Microstructural Investigation of Weld Based Rapid Prototyping," PhD, Ghulam Ishaq Khan Institute of Engineering Sciences and Technology.
- [8] Baker, R., 1925, "Method of Making Decorative Articles "U.S. Patent 1533300.

- [9] Eschholz, O. H., 1925, "Ornamental Arc Welding,"U.S. Patent 1533239.
- [10] Shockey, H. K., 1932, "Machine for Reclaiming Worn Brake Drums,"U.S. Patent 1886503.
- [11] Noble, P., 1933, "Method and Apparatus for Electric Arc Welding,"U.S. Patent 1898060.
- [12] R. Carpenter Otis, H. J. K., 1947, "Method and Apparatus for Metal Coating Metal Pipes by Electric Fusion,"U.S. Patent 2427350.
- [13] White, J. W. D., 1964, "Pressure Roller and Method of Manufacture,"U.S. Patent 3156968.
- [14] Ujiie, A., 1971, "Method of and Apparatus for Constructing Substantially Circular Cross Section Vessel by Welding,"U.S. Patent 3558846.
- [15] H. Brandi, H. L., 1976, "Method of Making Large Structural One-Piece Parts of Metal, Particularly One-Piece Shafts,"U.S. Patent 3985995.
- [16] ALMEIDA, P. M. S., 2012, "Process Control and Development in Wire and Arc Additive Manufacturing," PhD, Cranfield University.
- [17] Acheson, R., 1990, "Automatic Welding Apparatus for Weld Build-Up and Method of Achieving Weld Build-Up,"U.S. Patent 4952769.
- [18] Dr P M Dickens, D. M. S. P., Dr R C Cobb, Dr I Gibson and Mr G Dixon, 1992, "Rapid Prototyping Using 3-D Welding," Annual International Solid Freeform Fabrication Symposium, U. o. N. Department of Manufacturing Engineering and Operations Management, UK., ed.University of Texas at Austin.



- [19] J D Spencer, P. M. D. a. C. M. W., 1998, "Rapid Prototyping of Metal Parts by Three-Dimensional Welding," Department of Manufacturing Engineering and Operations Management, The University of Nottingham, 212(Part B).
- [20] Rossini, N. S., Dassisti, M., Benyounis, K. Y., and Olabi, A. G., 2012, "Methods of Measuring Residual Stresses in Components," *Materials & Design*, 35, pp. 572-588.
- [21] Ribeiro, F., Ogunbiyi, B., and Norrish, J., 1997, "Mathematical Model of Welding Parameters for Rapid Prototyping Using Robot Welding," *Science and Technology of Welding and Joining*, 2(5), pp. 185-190.
- [22] Ribeiro, F., Norrish, J., and McMaster, R. S., 1994, "Practical Case of Rapid Prototyping Using Gas Metal Arc Welding," Cranfield University.
- [23] Ribeiro, F., 1998, "3D Printing with Metals," *COMPUTING & CONTROL ENGINEERING JOURNAL*, Rapid Prototyping.
- [24] Ribeiro, A. F., and Norrish, J., 1996, "Rapid Prototyping Using Robot Welding - Slicing System Development," *DEI - Artigos em atas de congressos internacionais*.
- [25] Norrish, F. R. a. P. J., 1996, "Case Study of Rapid Prototyping using Robot Welding - Second 'Square to Round' Shape."
- [26] Fernando Ribeiro, P. J. N., 1996, "Metal Based Rapid Prototyping for More Complex Shapes," The Welding Institute.
- [27] Norrish, J., 2006, *Advanced Welding Processes: Technologies and Process Control*, Woodhead Publishing.
- [28] Beardsley, R. K. a. H., 1998, "Process Control of 3D Welding as a Droplet-Based Rapid Prototyping Technique," *Annual International Solid Freeform Fabrication Symposium*, Southern Methodist University, Dallas, TX, University of Texas at Austin.

- [29] I. Kmecko, D. H. a. R. K., 1999, "Controlling Heat Input Spatter and Weld Penetration in GMA Welding for Solid Freeform Fabrication," Annual International Solid Freeform Fabrication Symposium, D. Southern Methodist University, TX, ed. University of Texas at Austin.
- [30] YuMing Zhang, Y. C., Pengjiu Li, Alan T. Male, 2003, "Weld Deposition-Based Rapid Prototyping: A Preliminary Study," Journal of Materials Processing Technology, 135, pp. 347–357.
- [31] Yong-Ak Song, S. P., Kyunghyun Hwang, Doosun Choi, Haeseong Jee, 1998, "3D Welding and Milling for Direct Prototyping of Metallic Parts," Annual International Solid Freeform Fabrication Symposium, Korea Institute of Science and Technology KIST, CAD/CAM Research Center; Korea Institute of Machinery and Metals KIMM; Hongik University, Dept. of Mechanical Engineering, University of Texas at Austin.
- [32] Song, Y.-A., Park, S., Choi, D., and Jee, H., 2005, "3D Welding and Milling: Part I—A Direct Approach for Freeform Fabrication of Metallic Prototypes," International Journal of Machine Tools and Manufacture, 45(9), pp. 1057-1062.
- [33] Song, Y.-A., Park, S., and Chae, S.-W., 2005, "3D Welding and Milling: Part II—Optimization of the 3D Welding Process Using an Experimental Design Approach," International Journal of Machine Tools and Manufacture, 45(9), pp. 1063-1069.
- [34] Clark, D., Bache, M. R., and Whittaker, M. T., 2008, "Shaped metal deposition of a nickel alloy for aero engine applications," Journal of Materials Processing Technology, 203(1-3), pp. 439-448.
- [35] Anzalone, G. C., Chenlong, Z., Wijnen, B., Sanders, P. G., and Pearce, J. M., 2013, "A Low-Cost Open-Source Metal 3-D Printer," IEEE Access, 1, pp. 803-810.

- [36] Pinar, A., Wijnen, B., Anzalone, G. C., Havens, T. C., Sanders, P. G., and Pearce, J. M., 2015, "Low-Cost Open-Source Voltage and Current Monitor for Gas Metal Arc Weld 3D Printing," *Journal of Sensors*, 2015, pp. 1-8.
- [37] Hasselberg, T. P., 2009, "A Feasibility Study of "Cold Metal Transfer" – Gas Metal Arc Welding (CMT-GMAW) Nickel Base Superalloy Inconel 718™," MASTER OF SCIENCE, Rensselaer Polytechnic Institute, Hartford, Connecticut.
- [38] P. M. Sequeira Almeida, S. W., 2010, "Innovative Process Model of Ti-6Al-4V Additive Layer Manufacturing Using Cold Metal Transfer (CMT)," Annual International Solid Freeform Fabrication Symposium University of Texas at Austin.
- [39] Suryakumar, S., Karunakaran, K. P., Bernard, A., Chandrasekhar, U., Raghavender, N., and Sharma, D., 2011, "Weld Bead Modeling and Process Optimization in Hybrid Layered Manufacturing," *Computer-Aided Design*, 43(4), pp. 331-344.
- [40] DING, J., 2012, "Thermo-Mechanical Analysis of Wire and Arc Additive Manufacturing Process," PhD, CRANFIELD UNIVERSITY.
- [41] Jianglong Gu, B. C., Jialuo Ding, Stewart W. Williams, Yuchun Zhai, 2014, "Wire+Arc Additive Manufacturing of Aluminum," Annual International Solid Freeform Fabrication Symposium, Welding Engineering and Laser Processing Centre, Cranfield University, UK; School of Materials and Metallurgy, Northeastern University, China; School of Mechanical Engineering and Automation, Beihang University, China, University of Texas at Austin.
- [42] Gerhard Posch, K. F., Hackl Heinz, Chladil Harald, 2014, "Manufacturing of Turbine Blades by Shape Giving CMT-Welding," Metal Additive Manufacturing Conference Vienna.

- [43] Gerhard Posch, K. C., Harald Chladil, 2017, "Material Properties of CMT-Metal Additive Manufactured Duplex Stainless Steel Blade-Like Geometries," Weld World, International Institute of Welding.
- [44] Ding, D., Pan, Z., Cuiuri, D., and Li, H., 2015, "A Multi-Bead Overlapping Model for Robotic Wire and Arc Additive Manufacturing (WAAM)," Robotics and Computer-Integrated Manufacturing, 31, pp. 101-110.
- [45] Pinto, I. P. M. S., 2015, "Additive Manufacturing of Nickel Components Using CMT Process," Master of Science in Mechanical Engineering, Tecnico Lisboa.
- [46] Institute, T. W., 2017, "Additive Manufacture of Aluminium Alloy Components Using the Cold Metal Transfer (CMT) Process," TWI Ltd, Granta Park, Great Abington, Cambridge CB21 6AL, United Kingdom.
- [47] Xie, M., 1992, "Quality Assurance and Control for Robotic GMA Welding," PhD, Lund University, Sweden.
- [48] Carvalho, G. C., 1997, "An Adaptive Control System for Off-Line Programming in Robotic Gas Metal Arc Welding," PhD, Cranfield University.
- [49] USA, F., 2015, "MIG Welding Equipment: Operations Guide."
- [50] Funderburk, R. S., 2000, "Taking Your Weld's Temperature," North American Steel Construction Conference, Modern Steel Construction.
- [51] Society, A. W., 1999, "Structural Welding Code-Steel," aws.d1.1:2000.
- [52] Kobe Steel, L., 2017, "The ABC's of Arc Welding: How Interpass Temperature Affects the Quality of Welds," [kobelco-welding.jp/education-center/abc/ABC\\_2001-01.html](http://kobelco-welding.jp/education-center/abc/ABC_2001-01.html).

- [53] Standard, N., 1994, "Common Requirements: Welding and Inspection of Piping," M-CR-601 p. 14.
- [54] Fronius, "Robacta 5000/Robacta 5000 CT."
- [55] International, A., 2014, "Standard Guide for Evaluating Mechanical Properties of Metal Materials Made via Additive Manufacturing Processes."
- [56] Fronius, 2017, "CMT – Shifting the Limits," Technology Center Fronius USA.
- [57] GmbH, F. I., 2017, "Calibration Protocol."
- [58] MTS, 2017, "Certificate of Calibration: 39-075-103," M. S. C. C. Laboratory, ed.
- [59] MTS, 2016, "Certificate of Calibration: MTS/661.20H-03," M. S. C. C. Laboratory, ed.
- [60] Omega, 2017, "DIN Rail Mountable Universal Temperature Process Controller: CN245-R1-R2-F3-C4," O. Engineering, ed.
- [61] AWS, 2017, "AWS A5.9 ER308L," [weldingwarehouseinc.com/products/aws/a5-9/er308l](http://weldingwarehouseinc.com/products/aws/a5-9/er308l).
- [62] AWS, 2017, "AWS A5.18 ER70S-6," [weldingwarehouseinc.com/products/aws/a5-18/er70s-6/](http://weldingwarehouseinc.com/products/aws/a5-18/er70s-6/).
- [63] Standard, N., 2014, "NS-115 Copperfree™ AWS ER70S-6."
- [64] ASTM International, A. S. f. T. a. M., "Standard Practice for Microetching Metals and Alloys," Designation: E 407 – 99ASTM, 100 Barr Harbor Drive, West Conshohocken, PA 19428-2959, United States.
- [65] Ding, D., Pan, Z., Cuiuri, D., and Li, H., 2015, "A Practical Path Planning Methodology for Wire and Arc Additive Manufacturing of Thin-Walled Structures," Robotics and Computer-Integrated Manufacturing, 34, pp. 8-19.

[66] Coupland, C., 2017, "Parametric Development of Cold Metal Transfer Wire Arc Additive Manufacturing " Master's of Science, Auburn University.

[67] International, A., 1985, ASM Handbook - Metallography and Microstructures.

[68] Instruments, T., SNVS769J –MARCH 2000–REVISED DECEMBER 2014, "LM2940x 1-A Low Dropout Regulator," Copyright © 2017, Texas Instruments Incorporated, p. 35.

[69] Hackl, H., "Digitally Controlled GMA Power Sources," W. Fronius International GmbH, Austria, ed.

## **Appendix I – Data Results**

## Synergic 'Standard Mode' Data

### Standard Synergic ER70S-6

		hardness	uts (kips)	yield (kips)
<b>parallel</b>	<i>std-1-1</i>	79	69.30220388	50.50796813
	<i>std-1-2</i>	77	67.7865873	51.46849206
	<i>std-1-3</i>	75	68.69315357	48.89285714
	<i>std-1-4</i>	77	69.32091166	50.60002545
<b>perpendicular</b>	<i>std-2-1</i>	83	69.43143568	50.44922224
	<i>std-2-2</i>	78	68.36302981	50.44067905
	<i>std-2-3</i>	84	68.9276471	51.64854657
	<i>std-2-4</i>	80	68.68923312	50.85609103

### Standard Synergic ER308L

		hardness	uts (kips)	yield (kips)
<b>perpendicular</b>	std-1-1	95	79.787	55.92905805
	std-1-2	94	82.05722	55.65311803
	std-1-3	95	82.66927	54.48489043
	std-1-4	93	81.87348	55.18139177
<b>parallel</b>	std-2-1	95.5	82.92876	55.32963853
	std-2-2	93	82.1496	55.46818664
	std-2-3	95	81.33621	55.57547688
	std-2-4	92	82.29498	55.68568097



## CTWD Control Data

### CTWD Control ER70S-6

		uts (kips)	yield (kips)	hardness
<b>parallel</b>	1	69.88093657	57.05163473	76.625
	2	68.73894821	49.44352191	75.5
	3	68.49859526	50.70640149	75.5
	4	68.27227598	50.794631	75.75
<b>perpendicular</b>	1	67.1983501	51.71244852	77.25
	2	67.48378141	53.35541631	76.75
	3	67.82920538	54.36595459	76
	4	67.91516606	53.35651479	77

### CTWD Control ER308L

		uts (kips)	yield (kips)	hardness
<b>parallel</b>	1	85.74	50.9	82.5
	2	85.16	49.85	84.5
	3	84.35	49.46	82
	4	88.78	50.11	85.25
<b>perpendicular</b>	1	79.76	45.66	85.5
	2	82.34	48.64	87.5
	3	83.23	50.79	86.5
	4	83.65	51.36	88.5

## Temperature Control ER70S-6

		hardness	uts (kips)	yield (kips)
<b>parallel</b>	232-1-1	74	67.97181	51.8854784
	232-1-2	74	68.91035	49.7915363
	232-1-3	75	68.74959	50.5868601
	232-1-4	76	69.15626	49.1167293
<b>perpendicular</b>	232-2-1	76	68.58413	48.91462
	232-2-2	77	67.95713	49.6210082
	232-2-3	78	67.38552	48.7383805
	232-2-4	77	68.41133	51.653041
<b>perpendicular</b>	260-1-1	78	67.26318	46.4157883
	260-1-2	75	66.93426	47.9315057
	260-1-3	77	67.53863	47.5758487
	260-1-4	74	68.19387	48.9406515
<b>parallel</b>	260-2-1	75	67.35284	48.4544687
	260-2-2	75	67.45454	48.9979719
	260-2-3	74	68.78148	48.9100955
	260-2-4	75	69.39654	48.5941456
<b>parallel</b>	288-1-1	76	68.50653	52.283828
	288-1-2	73	68.35024	51.0161083
	288-1-3	75	68.55935	49.9723061
	288-1-4	76	68.817	49.2841122
<b>perpendicular</b>	288-2-1	78	67.41031	48.5724111
	288-2-2	76	67.44876	47.971266
	288-2-3	73	67.06759	48.3024638
	288-2-4	76	67.71556	48.4369109

## Temperature Control ER308L

		<b>hardness</b>	<b>uts (kips)</b>	<b>yield (kips)</b>
<b>perpendicular</b>	150-1-1	82	81.45122	53.56235
	150-1-2	87	78.63155	54.94002
	150-1-3	85	78.16559	55.00099
	150-1-4	86	79.08601	55.02749
<b>parallel</b>	150-2-1	82	82.11439	55.70433
	150-2-2	83	81.72828	54.1807
	150-2-3	83.5	81.18123	54.11125
	150-2-4	82	83.84933	54.87267
<b>parallel</b>	205-1-1	91	81.67578	56.67682
	205-1-2	95.5	81.29318	56.29179
	205-1-3	93	82.28238	56.38147
	205-1-4	95	85.40547	55.7557
<b>perpendicular</b>	205-2-1	90	81.37398	52.34273
	205-2-2	91	79.09714	53.45033
	205-2-3	90.5	78.52816	54.14691
	205-2-4	91.5	81.67402	56.05438
<b>perpendicular</b>	260-1-1	92	81.7268	54.92734
	260-1-2	93	79.83117	54.02253
	260-1-3	93	81.1758	53.73916
	260-1-4	92	81.51942	53.7395
<b>parallel</b>	260-2-1	93.5	85.96573	55.86187
	260-2-2	94	85.26515	58.65639
	260-2-3	95.5	84.91063	57.55431
	260-2-4	92	88.89756	58.17254

## Baseline Comparison Data

### Baseline ER70S-6

	sample	hardness	uts (kips)	yield (kips)
<b>P90 parallel</b>	1	75	69.83348	52.580046
	2	75.5	70.03435	50.072339
	3	76	70.3778	52.1083824
	4	76.5	69.41475	46.8781671
<b>P90 perpendicular</b>	1	77.5	70.81538	55.1111041
	2	74	69.72644	50.4446515
	3	76.5	70.04291	49.9750185
	4	74	70.18998	50.6577123

### Baseline ER308L

	sample	hardness	uts (kips)	yield (kips)
<b>P90 parallel</b>	1	87.5	89.78	54.15
	2	87.5	89.26	53.79
	3	87.5	88.95	53.34
	4	86.5	89.86	52.31
<b>P90 perpendicular</b>	1	86	86.8	50.45
	2	84.5	85.57	49.68
	3	85	85.87	50.66
	4	85.5	88.9	51.32

## Repeatability Study in ER70S-6 - Tensile

	Sample	UTS (psi)	Upper Yield (psi)	Lower Yield (psi)	Modulus (psi)
Wall 1	1	67897.58	51800.93946	46748.08371	6483364.891
	2	67507.32	57237.40224	46477.79993	6863495.148
	3	67937.98	54569.14476	47259.98033	7039881.257
	4	68098.87	52907.99298	47846.54422	6699953.943
	5	68227.26	52382.48052	46750.51804	6817356.244
	6	67731.23	51115.29286	46733.554	6779935.325
Wall 2	1	67198.35	51712.44852	47000.37791	6165013.1
	2	67483.78	53355.41631	47324.88543	6827066.896
	3	67829.21	54365.95459	48227.35016	6791331.558
	4	67915.17	53356.51479	47286.76776	6804412.551
	5	67680.52	52655.40628	48132.98302	6789842.924
	6	67432.11	47599.03083	47084.41666	6099108.574
Wall 3	1	69880.94	57051.63473		
	2	68738.95	49443.52191		
	3	68498.6	50706.40149		
	4	68272.28	50794.631		
	5	69941.1	50999.2		
	6	71229.98	51871.392		
Wall 4	1	69297.17	48327.14286		
	2	68284.72	50805.4502		
	3	68581.63	50678.78884		
	4	68645.23	50524		
	5	69626.43	51831.232		
	6	70492.75	51228.544		

### Repeatability Study in ER70S-6 - Hardness

	Top 1	Top 2	Avg Top	Bottom 1	Bottom 2	Avg Bot
Wall 1-1	77.5	77.5	77.5	75.5	76	75.75
2	76	77	76.5	76	76.5	76.25
3	74.5	77.5	76	75	77	76
4	77.5	76	76.75	77	76.5	76.75
5	77.5	77.5	77.5	75.5	77	76.25
6	78	76	77	75	78	76.5
Wall 2-1	77.5	77	77.25	75	77	76
2	76.5	77	76.75	74.5	75	74.75
3	76	76	76	74	74	74
4	76.5	77.5	77	77	77	77
5	76.5	75.5	76	76	77	76.5
6	76.5	77	76.75	77	76	76.5

	Left 1	Left 2	Avg. Left	Right 1	Right 2	Avg. Left
	77	77	77	76	76.5	76.25
Wall 1-1	75.5	75.5	75.5	75	76	75.5
2	75.5	75	75.25	76	75.5	75.75
3	75.5	75	75.25	77	75.5	76.25
4	77	75.5	76.25	76	75.5	75.75
5	76.5	76	76.25	75	76.75	75.875
6	74.5	75	74.75	77.5	77.5	77.5
Wall 2-1	75.5	76.5	76	75.5	75.5	75.5
2	74.5	75.5	75	75	75	75
3	75.5	76	75.75	74.5	76	75.25
4	74.5	76.5	75.5	75.5	76.5	76
5	77	77.5	77.25	76	76	76
6						

## **Appendix II – Experiment Sheets/Notes**

Material	Gas	Synergic Line	WFS (ipm)	ALC (%)	Dyn. Cor (%)	Burn Back (s)	Crater Fill
ER70S- 6	90/10	Standard ER70S-6	110	-7	0	0	off

Parallel

Print Time: 88

Unclamped Temp: 54

Deposition Rate: 0.61 kg/hr

Width: 123

Height: 77

Layer Height: 2.944

Material	Gas	Synergic Line	WFS (ipm)	ALC (%)	Dyn. Cor (%)	Burn Back (s)	Crater Fill
ER70S- 6	90/10	Standard ER70S-6	110	-7	0	0	off

Perpendicular

Print Time: 103

Unclamped Temp: 54

Deposition Rate: 0.62 kg/hr

Width: 123

Height: 88

Layer Height: 2.944



Material	Gas	Synergic Line	WFS (ipm)	ALC (%)	Dyn. Cor (%)	Burn Back (s)	Crater Fill
ER70S- 6	90/10	CMT ER70S-6	95	15	-1.2	-.05	.7 @ 60%

Print Time: 105, 120

Unclamped Temp: 54

Deposition Rate: 0.6 kg/hr

Width: 123, 123

Height: 95, 106

Layer Height: 2.944

Material	Gas	Synergic Line	WFS (ipm)	ALC (%)	Dyn Cor (%)	Burn Back (s)	Crater Fill
ER308L	98/2	Standard ER308L	110	15	0	0	0

Perpendicular

Print Time: 103

Unclamped Temp: 54

Deposition Rate: 0.545 kg/hr

Width: 123

Height: 88

Layer Height: 3.8

Layer 2 no arc error

Layer 12 (really 11 since 2 failed) no arc error

Material	Gas	Synergic Line	WFS (ipm)	ALC (%)	Dyn Cor (%)	Burn Back (s)	Crater Fill
ER308L	98/2	Standard ER308L	110	15	0	0	0

Parallel

Print Time: 94

Unclamped Temp: 54

Deposition Rate: 0.58 kg/hr

Width: 124

Height: 90

Layer Height: 4.4

Material	Gas	Synergic Line	WFS (ipm)	ALC (%)	Boost Cor (%)	Burn Back (s)	Crater Fill
ER308L	98/2	cmt ER308L	95	15	-1.2	-0.05	0.7 @ 50%

Print Time: 83, 80

Unclamped Temp: 54

Deposition Rate: 0.58 kg/hr

Width: 126, 124

Height: 84,106

Layer Height: 3.5

Material	Gas	Synergic Line	WFS (ipm)	ALC (%)	Dyn. Cor (%)	Burn Back (s)	Crater Fill
ER70S-6	90/10	CMT ER70S-6	95	15	-1.2	-0.05	0.7 @ 60%

Temperature Limit: 260

Perpendicular

Right	Temperature	Left	Temperature	Notes
L1	40	L2	69	Probe position issue due to height
L3	107	L4	125	Probe position issue due to height
L5	237	L6	266	Triggered @ 12 min, dropped to 183
L7	235	L8	238	
L9	230	L10	236	Moved to touch base of wall
L11	237	L12	264	Triggered @ 27 min, dropped to 215
L13	235	L14	245	
L15	253	L16	248	
L17	251	L18	241	
L19	236	L20	238	Moved to 25 mm up wall
L21	238	L22	210	
L23	215	L24	209	
L25	205	L26	235	
L27	247	L28	225	
L29	229	L30	203	
L31	185	L32	165	
L33	166	L34	162	
L35	160	L36	142	

Print Time: 84

Unclamped Temp: 54

Deposition Rate: 0.88 kg/hr

Width: 123

Height: 106

Layer Height: 2.944

Temperature Limit: 260

Parallel

Right	Temperature	Left	Temperature	Notes
L1	52	L2	154	
L3	172	L4	205	
L5	212	L6	216	
L7	218	L8	207	
L9	217	L10	222	Moved to touch base of wall
L11	270	L12	254	Triggered @ 25 min, dropped to 236
L13	251	L14	264	Triggered @ 31 min, dropped to 195
L15	202	L16	218	
L17	234	L18	225	
L19	230	L20	220	Moved to 25 mm up wall
L21	241	L22	225	
L23	230	L24	214	
L25	217	L26	219	
L27	227	L28	213	
L29	219	L30	202	
L31	200	L32	201	
L33	186	L34	182	
L35	173	L36	170	

Print Time: 84

Unclamped Temp: 54

Deposition Rate: 0.86

Width: 125

Height: 105

Layer Height: 2.916

Temperature Limit: 288

Parallel

Right	Temperature	Left	Temperature	Notes
L1	56	L2	95	
L3	178	L4	202	
L5	209	L6	216	
L7	219	L8	220	
L9	216	L10	219	Moved to touch base of wall
L11	285	L12	280	Would've Triggered both times
L13	267	L14	266	Would've Triggered both times
L15	257	L16	257	
L17	243	L18	230	
L19	226	L20	218	Moved to 25 mm up wall
L21	252	L22	222	
L23	211	L24	209	
L25	215	L26	212	Moved to 55 mm up wall
L27	221	L28	238	
L29	224	L30	210	
L31	209	L32	195	
L33	189	L34	172	
L35	174	L36	164	

Print Time: 81

Unclamped Temp: 54

Deposition Rate: 0.92

Width: 124

Height: 105

Layer Height: 2.916

Temperature Limit: 288

Perpendicular

Right	Temperature	Left	Temperature	Notes
L1	121	L2	172	
L3	192	L4	210	
L5	219	L6	235	
L7	233	L8	241	
L9	240	L10	240	Moved to touch base of wall
L11	300	L12	254	Triggered @ 25 min, dropped to 250
L13	269	L14	275	Would've Triggered both times
L15	278	L16	271	Would've Triggered both times
L17	262	L18	255	Would've Triggered
L19	250	L20	245	Moved to 25 mm up wall
L21	260	L22	232	Would've Triggered
L23	233	L24	225	
L25	219	L26	210	Moved to 55 mm up wall
L27	223	L28	238	
L29	245	L30	235	
L31	221	L32	215	
L33	210	L34	185	
L35	183	L36	167	

Print Time: 82

Unclamped Temp: 54

Deposition Rate: 0.89

Width: 126

Height: 105

Layer Height: 2.916

Temperature Limit: 232

Parallel

Right	Temperature	Left	Temperature	Notes
L1	90	L2	158	
L3	181	L4	193	
L5	205	L6	212	
L7	219	L8	221	
L9	222	L10	225	Moved to touch base of wall
L11	290	L12	247	Triggered @ 25/28, dropped 232/205
L13	234	L14	218	Triggered @ 32 min, dropped to 199
L15	242	L16	214	Triggered @ 38 min, dropped to 210
L17	232	L18	203	Triggered @ 44 min, dropped to 203
L19	217	L20	240	Moved to 25 mm up wall
L21	204	L22	222	
L23	225	L24	225	
L25	223	L26	216	Moved to 55 mm up wall
L27	227	L28	230	
L29	252	L30	219	Triggered @ 74 min, dropped to 220
L31	206	L32	203	
L33	198	L34	193	
L35	187	L36	176	

Print Time: 92

Unclamped Temp: 54

Deposition Rate: 0.81

Width: 124

Height: 104

Layer Height: 2.888



Temperature Limit: 232

Perpendicular

Right	Temperature	Left	Temperature	Notes
L1	130	L2	180	
L3	214	L4	220	
L5	223	L6	265	Triggered @ 13 min, dropped to 180
L7	226	L8	260	Triggered @ 19 min, dropped to 186
L9	222	L10	244	Moved to touch base of wall Triggered @ 25, dropped to 231
L11	267	L12	260	Triggered @ 29/32, dropped 226/215
L13	238	L14	236	Triggered @ 37/40, dropped 209/202
L15	219	L16	251	Triggered @ 46 min, dropped to 214
L17	218	L18	233	Triggered @ 54 min, dropped to 205
L19	206	L20	204	Moved to 25 mm up wall
L21	222	L22	217	
L23	219	L24	216	
L25	218	L26	208	Moved to 55 mm up wall
L27	219	L28	209	
L29	208	L30	196	
L31	190	L32	179	
L33	183	L34	173	
L35	170	L36	161	

Print Time: 93

Unclamped Temp: 54

Deposition Rate: 0.78

Width: 124

Height: 104

Layer Height: 2.888

Material	Gas	Synergic Line	WFS (ipm)	ALC (%)	Boost Cor (%)	Burn Back (s)	Crater Fill
ER308L	98/2	CMT ER308L	95	15	-1.2	-0.05	0.7 @ 50%

Temperature Limit: 260

Perpendicular

Right	Temperature	Left	Temperature	Notes
L1	78	L2	115	
L3	134	L4	150	
L5	156	L6	163	
L7	160	L8	164	
L9	163	L10	164	Moved to touch base of wall
L11	217	L12	224	
L13	215	L14	210	
L15	200	L16	192	
L17	189	L18	188	
L19	177	L20	176	Moved to 25 mm up wall
L21	196	L22	184	
L23	180	L24	170	
L25	158	L26	154	Moved to 55 mm up wall
L27	206	L28	208	
L29	195	L30	198	
L31	178	L32	176	
L33	164	L34	160	
L35	151	L36	145	

Print Time: 78

Unclamped Temp: 54

Deposition Rate: 0.811 kg/hr

Width: 124

Height: 117

Layer Height: 3.25

Temperature Limit: 260

Parallel

Right	Temperature	Left	Temperature	Notes
L1	97	L2	138	
L3	152	L4	162	
L5	165	L6	174	
L7	167	L8	169	
L9	165	L10	165	Moved to touch base of wall
L11	212	L12	215	
L13	210	L14	207	
L15	197	L16	192	
L17	184	L18	182	
L19	172	L20	167	Moved to 25 mm up wall
L21	179	L22	180	
L23	182	L24	172	
L25	167	L26	158	Moved to 55 mm up wall
L27	193	L28	182	
L29	187	L30	181	
L31	171	L32	157	
L33	153	L34	143	
L35	142	L36	138	

Print Time: 78

Unclamped Temp: 54

Deposition Rate: 0.762 kg/hr

Width: 123

Height: 117

Layer Height: 3.25

Temperature Limit: 205

Parallel

Right	Temperature	Left	Temperature	Notes
L1	73	L2	99	
L3	123	L4	122	
L5	142	L6	138	
L7	144	L8	142	
L9	140	L10	147	Moved to touch base of wall
L11	201	L12	212	26:20 - cooled 160
L13	174	L14	188	
L15	176	L16	179	
L17	173	L18	167	
L19	158	L20	145	Moved to 25 mm up wall
L21	169	L22	169	
L23	156	L24	149	
L25	140	L26	137	Moved to 55 mm up wall
L27	161	L28	158	
L29	150	L30	143	
L31	134	L32	132	
L33	115	L34	119	
L35	107	L36	109	

Print Time: 81

Unclamped Temp: 54

Deposition Rate: 0.861 kg/hr

Width: 123

Height: 128

Layer Height: 3.555

Temperature Limit: 205

Perpendicular

Right	Temperature	Left	Temperature	Notes
L1	69	L2	104	
L3	115	L4	121	
L5	126	L6	131	
L7	142	L8	151	
L9	150	L10	153	Moved to touch base of wall
L11	205	L12	184	24:20 - cooled 163
L13	188	L14	198	
L15	184	L16	177	
L17	170	L18	163	
L19	154	L20	150	Moved to 25 mm up wall
L21	169	L22	163	
L23	160	L24	149	
L25	135	L26	134	Moved to 55 mm up wall
L27	152	L28	152	
L29	145	L30	144	
L31	142	L32	135	
L33	129	L34	124	
L35	114	L36	109	

Print Time: 81

Unclamped Temp: 54

Deposition Rate: 0.863 kg/hr

Width: 123

Height: 129

Layer Height: 3.58

Temperature Limit: 150

Perpendicular

Right	Temperature	Left	Temperature	Notes
L1	61	L2	152	4:30 - cooled 84
L3	128	L4	158	9:50 - cooled 90
L5	126	L6	156	16:00 - cooled 99
L7	131	L8	156	21:50 - cooled 106
L9	135	L10	152	Moved to touch base of wall 27:50 - cooled 107
L11	162	L12	154	31:40 - cooled 133 35:20 - cooled 127
L13	154	L14	142	39:00 - cooled 124
L15	154	L16	133	45:00 - cooled 125
L17	142	L18	140	
L19	138	L20	134	Moved to 25 mm up wall
L21	152	L22	133	1:00:00 - cooled 136
L23	150	L24	127	1:06:00 - cooled 126
L25	127	L26	124	Moved to 55 mm up wall
L27	145	L28	147	
L29	153	L30	128	1:20:45 - cooled 134
L31	132	L32	126	
L33	121	L34	112	
L35	111	L36	106	

Print Time: 98

Unclamped Temp: 54

Deposition Rate: 0.677 kg/hr

Width: 123

Height: 128

Layer Height: 3.55

Temperature Limit: 150

Parallel

Right	Temperature	Left	Temperature	Notes
L1	100	L2	140	
L3	146	L4	164	8:30 - cooled 103
L5	132	L6	169	14:20 - cooled 111
L7	141	L8	164	20:20 - cooled 113
L9	137	L10	154	Moved to touch base of wall 26:20 - cooled 114
L11	163	L12	160	30:10 - cooled 134 33:45 - cooled 127
L13	148	L14	163	39:45 - cooled 132
L15	143	L16	151	45:45 - cooled 120
L17	133	L18	140	
L19	145	L20	137	Moved to 25 mm up wall
L21	149	L22	157	1:00:00 - cooled 125
L23	138	L24	133	
L25	129	L26	137	Moved to 55 mm up wall
L27	154	L28	140	1:13:20 - cooled 129
L29	129	L30	128	
L31	131	L32	130	
L33	120	L34	123	
L35	108	L36	107	

Print Time: 95

Unclamped Temp: 54

Deposition Rate: 0.716 kg/hr

Width: 123

Height: 131

Layer Height: 3.63

## **Appendix III – Machine Codes**



**M111 – Welding Start**

```
ActivateSignal(OUTPUT1) ; Activate signal, X2:4 on ROB 5000
Do Until IsActive(Input1) ; Until Arc Stable signal received
DoOEMButton(1001) ;Feedhold
Sleep(50) ;Pause for 50 ms
Loop ; Loop
DoOEMButton(1000) ;Cycle Start to resume program
```

**M110 – Welding Stop**

```
DeactivateSignal(OUTPUT1) ; Deactivate signal, X2:4 on ROB 5000

WhileIsActive(Input1) ; While Arc Stable is High, do nothing
Wend ; While Loop end

Code("G4 P1") ; Pause for 1 second

If Not IsActive(Input3) ; If Temperature Probe Signal is Fault
Then Code("G4 P0.5") ; Pause 0.5 second
End If ; End If Loop
```

**M121 – Quick Stop (Active Low)**

```
ActivateSignal(OUTPUT2) ; Activate signal, X2:5 on ROB 5000
```

**M120 – Robot Ready**

```
DeactivateSignal(OUTPUT2) ; Deactivate signal, X2:5 on ROB 5000
```

**M131 – Gas Test Start**

```
ActivateSignal(OUTPUT3) ; Activate signal, X2:7 on ROB 5000
```

**M130 – Gas Test Stop**

```
DeactivateSignal(OUTPUT3) ; Deactivate signal, X2:7 on ROB 5000
```

**M141 – Touch Sensing**

```
ActivateSignal(OUTPUT4) ; Activate signal, X8:7 on ROB 5000

CurrentFeed = GetOEMDRO(818) ; Get current feed rate of program

If Not IsActive(Input1) Then ; If arc stable is not active (not touching)
Code("G31 Z0 F100") ; G-code probing cycle, feed rate 100
mm/min
While IsMoving() ; While probing, do nothing
Wend ; While loop end
ZProbePos = GetVar(2002) ; Probed Z value where probe touched
Code("G0 Z" &ZProbePos) ; Move z-axis to that position, rapid
While IsMoving() ; While moving, do nothing
Wend ; While loop end
```

```

Code("G92 Z0")           ; Zero the z-axis at the probed position
Code("G4 P0.25")        ; Pause for 0.25 seconds
Code("F" &CurrentFeed)  ; Reset the feed rate to the prior feed rate
Code("G1 Z3")           ; Move the z-axis up 3 mm
End If                   ; End the probing loop

DeactivateSignal(OUTPUT4) ; Deactivate signal, X8:7 on ROB 5000

M151 – Wire Retract Start
  ActivateSignal(OUTPUT5) ; Activate signal, X14:6 on ROB 5000

M150 – Wire Retract Stop
  DeactivateSignal(OUTPUT5) ; Deactivate signal, X14:6 on ROB 5000

M161 – Source Error Reset
  ActivateSignal(OUTPUT6) ; Activate signal, X8:5 on ROB 5000

  Sleep(1000)             ; Pause for 1 second

  DeactivateSignal(OUTPUT6) ; Deactivate signal to reset welder

M171 – Blow Through
  ActivateSignal(OUTPUT7) ; Activate signal, X14:5 on ROB 5000

  Sleep(5000)            ; Pause for 5 seconds

  DeactivateSignal(OUTPUT7) ; Deactivate signal, X14:5 on ROB 5000

M181 – Wire Feed Start
  ActivateSignal(OUTPUT8) ; Activate signal, X2:11 on ROB 5000

M180 – Wire Feed Stop
  DeactivateSignal(OUTPUT8) ; Deactivate signal, X2:11 on ROB 5000

```

## **Appendix IV – Statistics**

## Repeatability Stats for Hardness for ER70S-6

### Perpendicular Walls Hardness T-Tests

Perpendicular Wall 1 Average Hardness Top to Bottom T-Test

### Paired T-Test and CI: top, bottom

#### Descriptive Statistics

Sample	N	Mean	StDev	SE Mean
top	6	76.875	0.586	0.239
bottom	6	76.250	0.354	0.144

#### Estimation for Paired Difference

Mean	StDev	SE Mean	95% CI for $\mu_{\text{difference}}$
0.625	0.720	0.294	(-0.131, 1.381)

$\mu_{\text{difference}}$ : mean of (top - bottom)

#### Test

Null hypothesis  $H_0: \mu_{\text{difference}} = 0$   
Alternative hypothesis  $H_1: \mu_{\text{difference}} \neq 0$

T-Value	P-Value
2.13	0.087

## Perpendicular Wall 2 Average Hardness Top to Bottom T-Test

### Paired T-Test and CI: top2, bottom2

#### Descriptive Statistics

Sample	N	Mean	StDev	SE Mean
top2	6	76.625	0.518	0.212
bottom2	6	75.792	1.166	0.476

#### Estimation for Paired Difference

Mean	StDev	SE Mean	95% CI for $\mu_{\text{difference}}$
0.833	1.068	0.436	(-0.288, 1.955)

$\mu_{\text{difference}}$ : mean of (top2 - bottom2)

#### Test

Null hypothesis  $H_0: \mu_{\text{difference}} = 0$   
Alternative hypothesis  $H_1: \mu_{\text{difference}} \neq 0$

T-Value	P-Value
1.91	0.114

## Perpendicular Wall 1 Average Hardness Outer to Inner T-Test

### Two-Sample T-Test and CI: outer, inner

#### Method

$\mu_1$ : mean of outer

$\mu_2$ : mean of inner

Difference:  $\mu_1 - \mu_2$

*Equal variances are assumed for this analysis.*

#### Descriptive Statistics

Sample	N	Mean	StDev	SE Mean
outer	4	76.688	0.747	0.37
inner	4	76.375	0.433	0.22

#### Estimation for Difference

Difference	Pooled StDev	95% CI for Difference
0.313	0.610	(-0.743, 1.368)

#### Test

Null hypothesis  $H_0: \mu_1 - \mu_2 = 0$

Alternative hypothesis  $H_1: \mu_1 - \mu_2 \neq 0$

T-Value	DF	P-Value
0.72	6	0.496

## Perpendicular Wall 2 Average Hardness Outer to Inner T-Test

### Two-Sample T-Test and CI: outer2, inner2

#### Method

$\mu_1$ : mean of outer2

$\mu_2$ : mean of inner2

Difference:  $\mu_1 - \mu_2$

*Equal variances are assumed for this analysis.*

#### Descriptive Statistics

Sample	N	Mean	StDev	SE Mean
outer2	4	76.625	0.520	0.26
inner2	4	76.00	1.41	0.71

#### Estimation for Difference

Difference	Pooled StDev	95% CI for Difference
0.625	1.066	(-1.219, 2.469)

#### Test

Null hypothesis  $H_0: \mu_1 - \mu_2 = 0$

Alternative hypothesis  $H_1: \mu_1 - \mu_2 \neq 0$

T-Value	DF	P-Value
0.83	6	0.439

## Perpendicular Wall 1 Top to Wall 2 Top Hardness T-Test

### Two-Sample T-Test and CI: top1, top2

#### Method

$\mu_1$ : mean of top1

$\mu_2$ : mean of top2

Difference:  $\mu_1 - \mu_2$

*Equal variances are assumed for this analysis.*

#### Descriptive Statistics

Sample	N	Mean	StDev	SE Mean
top1	12	76.88	1.03	0.30
top2	12	76.625	0.608	0.18

#### Estimation for Difference

Difference	Pooled StDev	95% CI for Difference
0.250	0.843	(-0.464, 0.964)

#### Test

Null hypothesis  $H_0: \mu_1 - \mu_2 = 0$

Alternative hypothesis  $H_1: \mu_1 - \mu_2 \neq 0$

T-Value	DF	P-Value
0.73	22	0.475



## Perpendicular Wall 1 Bottom to Wall 2 Bottom Hardness T-Test

### Two-Sample T-Test and CI: bottom1, bottom2

#### Method

$\mu_1$ : mean of bottom1

$\mu_2$ : mean of bottom2

Difference:  $\mu_1 - \mu_2$

*Equal variances are assumed for this analysis.*

#### Descriptive Statistics

Sample	N	Mean	StDev	SE Mean
bottom1	12	76.250	0.917	0.26
bottom2	12	75.79	1.23	0.36

#### Estimation for Difference

Difference	Pooled StDev	95% CI for Difference
0.458	1.087	(-0.462, 1.378)

#### Test

Null hypothesis  $H_0: \mu_1 - \mu_2 = 0$

Alternative hypothesis  $H_1: \mu_1 - \mu_2 \neq 0$

T-Value	DF	P-Value
1.03	22	0.313

## Perpendicular Wall 1 to Wall 2 Hardness T-Test

### Two-Sample T-Test and CI: wall 1, wall 2

#### Method

$\mu_1$ : mean of wall 1

$\mu_2$ : mean of wall 2

Difference:  $\mu_1 - \mu_2$

*Equal variances are assumed for this analysis.*

#### Descriptive Statistics

Sample	N	Mean	StDev	SE Mean
wall 1	24	76.56	1.00	0.20
wall 2	24	76.21	1.04	0.21

#### Estimation for Difference

Difference	Pooled StDev	95% CI for Difference
0.354	1.023	(-0.240, 0.948)

#### Test

Null hypothesis  $H_0: \mu_1 - \mu_2 = 0$

Alternative hypothesis  $H_1: \mu_1 - \mu_2 \neq 0$

T-Value	DF	P-Value
1.20	46	0.236

## Parallel Walls Tensile T-Tests

Parallel Wall 1 Hardness Left to Right T-Test

### Paired T-Test and CI: Left, Right

#### Descriptive Statistics

Sample	N	Mean	StDev	SE Mean
Left	12	75.917	0.764	0.220
Right	12	75.896	0.635	0.183

#### Estimation for Paired Difference

Mean	StDev	SE Mean	95% CI for $\mu_{\text{difference}}$
0.021	0.882	0.255	(-0.540, 0.581)

$\mu_{\text{difference}}$ : mean of (Left - Right)

#### Test

Null hypothesis  $H_0: \mu_{\text{difference}} = 0$   
Alternative hypothesis  $H_1: \mu_{\text{difference}} \neq 0$

T-Value	P-Value
0.08	0.936

## Parallel Wall 2 Hardness Left to Right T-Test

### Paired T-Test and CI: Left, Right

#### Descriptive Statistics

Sample	N	Mean	StDev	SE Mean
Left	12	75.708	1.010	0.292
Right	12	75.875	0.932	0.269

#### Estimation for Paired Difference

Mean	StDev	SE Mean	95% CI for $\mu_{\text{difference}}$
-0.167	1.403	0.405	(-1.058, 0.725)

$\mu_{\text{difference}}$ : mean of (Left - Right)

#### Test

Null hypothesis  $H_0: \mu_{\text{difference}} = 0$

Alternative hypothesis  $H_1: \mu_{\text{difference}} \neq 0$

T-Value	P-Value
-0.41	0.689

## Parallel Wall 1 Hardness Top to Bottom T-Test

### Paired T-Test and CI: Top, Bottom

#### Descriptive Statistics

Sample	N	Mean	StDev	SE Mean
Top	8	76.063	0.729	0.258
Bottom	8	76.031	0.687	0.243

#### Estimation for Paired Difference

Mean	StDev	SE Mean	95% CI for $\mu_{\text{difference}}$
0.031	0.850	0.300	(-0.679, 0.742)

$\mu_{\text{difference}}$ : mean of (Top - Bottom)

#### Test

Null hypothesis  $H_0: \mu_{\text{difference}} = 0$   
Alternative hypothesis  $H_1: \mu_{\text{difference}} \neq 0$

T-Value	P-Value
0.10	0.920

## Parallel Wall 2 Hardness Top to Bottom T-Test

### Paired T-Test and CI: Top, Bottom

#### Descriptive Statistics

Sample	N	Mean	StDev	SE Mean
Top	8	75.938	1.116	0.395
Bottom	8	76.188	0.923	0.326

#### Estimation for Paired Difference

Mean	StDev	SE Mean	95% CI for $\mu_{\text{difference}}$
-0.250	1.225	0.433	(-1.274, 0.774)

$\mu_{\text{difference}}$ : mean of (Top - Bottom)

#### Test

Null hypothesis  $H_0: \mu_{\text{difference}} = 0$   
Alternative hypothesis  $H_1: \mu_{\text{difference}} \neq 0$

T-Value	P-Value
-0.58	0.582

## Parallel Wall 1 Top to Wall 2 Top Hardness T-Test

### Two-Sample T-Test and CI: Top 1, Top 2

#### Method

$\mu_1$ : mean of Top 1

$\mu_2$ : mean of Top 2

Difference:  $\mu_1 - \mu_2$

*Equal variances are assumed for this analysis.*

#### Descriptive Statistics

Sample	N	Mean	StDev	SE Mean
Top 1	8	76.063	0.729	0.26
Top 2	8	75.94	1.12	0.39

#### Estimation for Difference

Difference	Pooled StDev	95% CI for Difference
0.125	0.943	(-0.886, 1.136)

#### Test

Null hypothesis  $H_0: \mu_1 - \mu_2 = 0$

Alternative hypothesis  $H_1: \mu_1 - \mu_2 \neq 0$

T-Value	DF	P-Value
0.27	14	0.795

## Parallel Wall 1 Top to Wall 2 Bottom Hardness T-Test

### Two-Sample T-Test and CI: Bottom 1, Bottom 2

#### Method

$\mu_1$ : mean of Bottom 1

$\mu_2$ : mean of Bottom 2

Difference:  $\mu_1 - \mu_2$

*Equal variances are assumed for this analysis.*

#### Descriptive Statistics

Sample	N	Mean	StDev	SE Mean
Bottom 1	8	76.031	0.687	0.24
Bottom 2	8	76.188	0.923	0.33

#### Estimation for Difference

Difference	Pooled StDev	95% CI for Difference
-0.156	0.814	(-1.029, 0.717)

#### Test

Null hypothesis  $H_0: \mu_1 - \mu_2 = 0$

Alternative hypothesis  $H_1: \mu_1 - \mu_2 \neq 0$

T-Value	DF	P-Value
-0.38	14	0.707



## Parallel Wall 1 to Wall 2 Hardness T-Test

### Two-Sample T-Test and CI: Wall 1, Wall 2

#### Method

$\mu_1$ : mean of Wall 1

$\mu_2$ : mean of Wall 2

Difference:  $\mu_1 - \mu_2$

*Equal variances are assumed for this analysis.*

#### Descriptive Statistics

Sample	N	Mean	StDev	SE Mean
Wall 1	24	75.906	0.687	0.14
Wall 2	24	75.792	0.955	0.19

#### Estimation for Difference

Difference	Pooled StDev	95% CI for Difference
0.115	0.832	(-0.369, 0.598)

#### Test

Null hypothesis  $H_0: \mu_1 - \mu_2 = 0$

Alternative hypothesis  $H_1: \mu_1 - \mu_2 \neq 0$

T-Value	DF	P-Value
0.48	46	0.635

## Perpendicular Vs. Parallel Walls Hardness T-Tests

Parallel Walls' Tops Vs. Perpendicular Walls' Tops Hardness T-Test

### Two-Sample T-Test and CI: Perpendicular Tops, Parallel Tops

#### Method

$\mu_1$ : mean of Perpendicular Tops

$\mu_2$ : mean of Parallel Tops

Difference:  $\mu_1 - \mu_2$

*Equal variances are assumed for this analysis.*

#### Descriptive Statistics

Sample	N	Mean	StDev	SE Mean
Perpendicular Tops	12	76.750	0.544	0.16
Parallel Tops	8	76.000	0.896	0.32

#### Estimation for Difference

Difference	Pooled StDev	95% CI for Difference
0.750	0.702	(0.077, 1.423)

#### Test

Null hypothesis  $H_0: \mu_1 - \mu_2 = 0$

Alternative hypothesis  $H_1: \mu_1 - \mu_2 \neq 0$

T-Value	DF	P-Value
2.34	18	0.031

## Parallel Walls' Bottoms Vs. Perpendicular Walls' Bottoms Hardness T-Test

### Two-Sample T-Test and CI: Perpendicular Bottoms, Parallel Bottoms

#### Method

$\mu_1$ : mean of Perpendicular Bottoms

$\mu_2$ : mean of Parallel Bottoms

Difference:  $\mu_1 - \mu_2$

*Equal variances are assumed for this analysis.*

#### Descriptive Statistics

Sample	N	Mean	StDev	SE Mean
Perpendicular Bottoms	12	76.021	0.856	0.25
Parallel Bottoms	8	76.109	0.524	0.19

#### Estimation for Difference

Difference	Pooled StDev	95% CI for Difference
-0.089	0.745	(-0.802, 0.625)

#### Test

Null hypothesis  $H_0: \mu_1 - \mu_2 = 0$

Alternative hypothesis  $H_1: \mu_1 - \mu_2 \neq 0$

T-Value	DF	P-Value
-0.26	18	0.797

## Parallel Walls Vs. Perpendicular Walls Hardness T-Test

### Two-Sample T-Test and CI: All Tops, All Bottoms

#### Method

$\mu_1$ : mean of All Tops

$\mu_2$ : mean of All Bottoms

Difference:  $\mu_1 - \mu_2$

*Equal variances are assumed for this analysis.*

#### Descriptive Statistics

Sample	N	Mean	StDev	SE Mean
All Tops	20	76.450	0.781	0.17
All Bottoms	20	76.056	0.726	0.16

#### Estimation for Difference

Difference	Pooled StDev	95% CI for Difference
0.394	0.754	(-0.089, 0.876)

#### Test

Null hypothesis  $H_0: \mu_1 - \mu_2 = 0$

Alternative hypothesis  $H_1: \mu_1 - \mu_2 \neq 0$

T-Value	DF	P-Value
1.65	38	0.107

## Hardness Power Analysis

All Samples Hardness Power Analysis

### Sample Size for Estimation

#### Method

Parameter	Mean
Distribution	Normal
Standard deviation	0.77 (population value)
Confidence level	95%
Confidence interval	Two-sided

#### Results

Margin of Error	Sample Size
0.77	4

## Repeatability Stats for Tensile for ER70S-6

### Perpendicular Walls Tensile T-Tests

Perpendicular Wall 1 Ultimate Tensile Strength Outer to Inner T-Test

## Paired T-Test and CI: Outer UTS, Inner UTS

### Descriptive Statistics

Sample	N	Mean	StDev	SE Mean
Outer UTS	2	67814.4	117.6	83.2
Inner UTS	2	68018.4	113.8	80.4

### Estimation for Paired Difference

Mean	StDev	SE Mean	95% CI for $\mu_{\text{difference}}$
-204	231	164	(-2283, 1875)

$\mu_{\text{difference}}$ : mean of (Outer UTS - Inner UTS)

### Test

Null hypothesis  $H_0: \mu_{\text{difference}} = 0$   
Alternative hypothesis  $H_1: \mu_{\text{difference}} \neq 0$

T-Value	P-Value
-1.25	0.430

## Perpendicular Wall 2 Ultimate Tensile Strength Outer to Inner T-Test

### Paired T-Test and CI: Outer UTS, Inner UTS

#### Descriptive Statistics

Sample	N	Mean	StDev	SE Mean
Outer UTS	2	67315	165	117
Inner UTS	2	67872	61	43

#### Estimation for Paired Difference

Mean	StDev	SE Mean	95% CI for $\mu_{\text{difference}}$
-557.0	104.5	73.9	(-1496.0, 382.0)

$\mu_{\text{difference}}$ : mean of (Outer UTS - Inner UTS)

#### Test

Null hypothesis  $H_0: \mu_{\text{difference}} = 0$   
Alternative hypothesis  $H_1: \mu_{\text{difference}} \neq 0$

T-Value	P-Value
-7.54	0.084

## Perpendicular Wall 1 to Wall 2 Ultimate Tensile Strength T-Test

### Two-Sample T-Test and CI: Wall 1, Wall 2

#### Method

$\mu_1$ : mean of Wall 1

$\mu_2$ : mean of Wall 2

Difference:  $\mu_1 - \mu_2$

*Equal variances are assumed for this analysis.*

#### Descriptive Statistics

Sample	N	Mean	StDev	SE Mean
Wall 1	6	67900	257	105
Wall 2	6	67590	269	110

#### Estimation for Difference

Difference	Pooled StDev	95% CI for Difference
310	263	(-28, 648)

#### Test

Null hypothesis  $H_0: \mu_1 - \mu_2 = 0$

Alternative hypothesis  $H_1: \mu_1 - \mu_2 \neq 0$

T-Value	DF	P-Value
2.04	10	0.068



## Perpendicular Wall 1 Yield Strength Outer to Inner T-Test

### Paired T-Test and CI: Outer, Inner

#### Descriptive Statistics

Sample	N	Mean	StDev	SE Mean
Outer	2	51458	485	343
Inner	2	53739	1175	831

#### Estimation for Paired Difference

Mean	StDev	SE Mean	95% CI for $\mu_{\text{difference}}$
-2280	690	488	(-8478, 3917)

$\mu_{\text{difference}}$ : mean of (Outer - Inner)

#### Test

Null hypothesis  $H_0: \mu_{\text{difference}} = 0$   
Alternative hypothesis  $H_1: \mu_{\text{difference}} \neq 0$

T-Value	P-Value
-4.68	0.134

## Perpendicular Wall 2 Yield Strength Outer to Inner T-Test

### Paired T-Test and CI: Outer 2, Inner 2

#### Descriptive Statistics

Sample	N	Mean	StDev	SE Mean
Outer 2	2	49656	2909	2057
Inner 2	2	53861	714	505

#### Estimation for Paired Difference

Mean	StDev	SE Mean	95% CI for $\mu_{\text{difference}}$
-4205	2195	1552	(-23925, 15514)

$\mu_{\text{difference}}$ : mean of (Outer 2 - Inner 2)

#### Test

Null hypothesis  $H_0: \mu_{\text{difference}} = 0$

Alternative hypothesis  $H_1: \mu_{\text{difference}} \neq 0$

T-Value	P-Value
-2.71	0.225

## Perpendicular Wall 1 to Wall 2 Yield Strength T-Test

### Two-Sample T-Test and CI: Wall 1, Wall 2

#### Method

$\mu_1$ : mean of Wall 1

$\mu_2$ : mean of Wall 2

Difference:  $\mu_1 - \mu_2$

*Equal variances are assumed for this analysis.*

#### Descriptive Statistics

Sample	N	Mean	StDev	SE Mean
Wall 1	6	53336	2242	915
Wall 2	6	52174	2407	983

#### Estimation for Difference

Difference	Pooled StDev	95% CI for Difference
1161	2326	(-1831, 4153)

#### Test

Null hypothesis  $H_0: \mu_1 - \mu_2 = 0$

Alternative hypothesis  $H_1: \mu_1 - \mu_2 \neq 0$

T-Value	DF	P-Value
0.86	10	0.407

## Parallel Walls Tensile T-Tests

Parallel Wall 1 Ultimate Tensile Strength Top to Bottom T-Test

### Paired T-Test and CI: UTS Top, UTS Bottom

#### Descriptive Statistics

Sample	N	Mean	StDev	SE Mean
UTS Top	2	69310	808	571
UTS Bottom	2	70586	911	644

#### Estimation for Paired Difference

Mean	StDev	SE Mean	95% CI for $\mu_{\text{difference}}$
-1276	1719	1215	(-16719, 14168)

$\mu_{\text{difference}}$ : mean of (UTS Top - UTS Bottom)

#### Test

Null hypothesis  $H_0: \mu_{\text{difference}} = 0$   
Alternative hypothesis  $H_1: \mu_{\text{difference}} \neq 0$

T-Value	P-Value
-1.05	0.485

Parallel Wall 2 Ultimate Tensile Strength Top to Bottom T-Test

## Paired T-Test and CI: UTS Top 2, UTS Bottom 2

### Descriptive Statistics

Sample	N	Mean	StDev	SE Mean
UTS Top 2	2	68791	716	506
UTS Bottom 2	2	70060	613	433

### Estimation for Paired Difference

Mean	StDev	SE Mean	95% CI for $\mu_{\text{difference}}$
-1269	1328	939	(-13204, 10667)

$\mu_{\text{difference}}$ : mean of (UTS Top 2 - UTS Bottom 2)

### Test

Null hypothesis  $H_0: \mu_{\text{difference}} = 0$   
Alternative hypothesis  $H_1: \mu_{\text{difference}} \neq 0$

T-Value	P-Value
-1.35	0.406

## Parallel Wall 1 to Wall 2 Ultimate Tensile Strength T-Test

### Two-Sample T-Test and CI: Wall 1, Wall 2

#### Method

$\mu_1$ : mean of Wall 1

$\mu_2$ : mean of Wall 2

Difference:  $\mu_1 - \mu_2$

*Equal variances are assumed for this analysis.*

#### Descriptive Statistics

Sample	N	Mean	StDev	SE Mean
Wall 1	6	69427	1130	462
Wall 2	6	69155	822	336

#### Estimation for Difference

Difference	Pooled StDev	95% CI for Difference
272	988	(-999, 1544)

#### Test

Null hypothesis  $H_0: \mu_1 - \mu_2 = 0$

Alternative hypothesis  $H_1: \mu_1 - \mu_2 \neq 0$

T-Value	DF	P-Value
0.48	10	0.643

## Parallel Wall 1 Yield Strength Top to Bottom T-Test

### Paired T-Test and CI: Top 1, Bottom 1

#### Descriptive Statistics

Sample	N	Mean	StDev	SE Mean
Top 1	2	53248	5380	3804
Bottom 1	2	51435	617	436

#### Estimation for Paired Difference

Mean	StDev	SE Mean	95% CI for $\mu_{\text{difference}}$
1812	5996	4240	(-52064, 55689)

$\mu_{\text{difference}}$ : mean of (Top 1 - Bottom 1)

#### Test

Null hypothesis  $H_0: \mu_{\text{difference}} = 0$

Alternative hypothesis  $H_1: \mu_{\text{difference}} \neq 0$

T-Value	P-Value
0.43	0.743

## Parallel Wall 2 Yield Strength Top to Bottom T-Test

### Paired T-Test and CI: Top 2, Bottom 2

#### Descriptive Statistics

Sample	N	Mean	StDev	SE Mean
Top 2	2	49566	1752	1239
Bottom 2	2	51530	426	301

#### Estimation for Paired Difference

Mean	StDev	SE Mean	95% CI for $\mu_{\text{difference}}$
-1964	2179	1540	(-21537, 17610)

$\mu_{\text{difference}}$ : mean of (Top 2 - Bottom 2)

#### Test

Null hypothesis  $H_0: \mu_{\text{difference}} = 0$   
Alternative hypothesis  $H_1: \mu_{\text{difference}} \neq 0$

T-Value	P-Value
-1.27	0.424



## Parallel Wall 1 to Wall 2 Yield Strength T-Test

### Two-Sample T-Test and CI: Wall 1, Wall 2

#### Method

$\mu_1$ : mean of Wall 1

$\mu_2$ : mean of Wall 2

Difference:  $\mu_1 - \mu_2$

*Equal variances are assumed for this analysis.*

#### Descriptive Statistics

Sample	N	Mean	StDev	SE Mean
Wall 1	6	51811	2683	1095
Wall 2	6	50566	1194	487

#### Estimation for Difference

Difference	Pooled StDev	95% CI for Difference
1245	2076	(-1426, 3916)

#### Test

Null hypothesis  $H_0: \mu_1 - \mu_2 = 0$

Alternative hypothesis  $H_1: \mu_1 - \mu_2 \neq 0$

T-Value	DF	P-Value
1.04	10	0.323

## Perpendicular Vs. Parallel Walls Tensile T-Tests

Parallel Vs. Perpendicular Ultimate Tensile Strength T-Test

### Two-Sample T-Test and CI: Parallel, Perpendicular

#### Method

$\mu_1$ : mean of Parallel

$\mu_2$ : mean of Perpendicular

Difference:  $\mu_1 - \mu_2$

*Equal variances are assumed for this analysis.*

#### Descriptive Statistics

Sample	N	Mean	StDev	SE Mean
Parallel	12	69291	953	275
Perpendicular	12	67745	299	86

#### Estimation for Difference

Difference	Pooled StDev	95% CI for Difference
1546	706	(948, 2144)

#### Test

Null hypothesis  $H_0: \mu_1 - \mu_2 = 0$

Alternative hypothesis  $H_1: \mu_1 - \mu_2 \neq 0$

T-Value	DF	P-Value
5.36	22	0.00002

## Parallel Vs. Perpendicular Yield Strength T-Test

### Two-Sample T-Test and CI: Parallel, Perpendicular

#### Method

$\mu_1$ : mean of Parallel

$\mu_2$ : mean of Perpendicular

Difference:  $\mu_1 - \mu_2$

*Equal variances are assumed for this analysis.*

#### Descriptive Statistics

Sample	N	Mean	StDev	SE Mean
Parallel	12	51188	2084	602
Perpendicular	12	52755	2299	664

#### Estimation for Difference

Difference	Pooled StDev	95% CI for Difference
-1566	2194	(-3424, 291)

#### Test

Null hypothesis  $H_0: \mu_1 - \mu_2 = 0$

Alternative hypothesis  $H_1: \mu_1 - \mu_2 \neq 0$

T-Value	DF	P-Value
-1.75	22	0.094

## Tensile Power Analysis

Perpendicular Ultimate Tensile Strength Power Analysis

### Sample Size for Estimation

#### Method

Parameter	Mean
Distribution	Normal
Standard deviation	299 (population value)
Confidence level	95%
Confidence interval	Two-sided

#### Results

Margin of Error	Sample Size
299	4

## Parallel Ultimate Tensile Strength Power Analysis

### Sample Size for Estimation

#### Method

Parameter	Mean
Distribution	Normal
Standard deviation	953 (population value)
Confidence level	95%
Confidence interval	Two-sided

#### Results

Margin of Error	Sample Size
953	4

## Parallel and Perpendicular Yield Strength Power Analysis

### Sample Size for Estimation

#### Method

Parameter	Mean
Distribution	Normal
Standard deviation	2290 (population value)
Confidence level	95%
Confidence interval	Two-sided

#### Results

Margin of Error	Sample Size
2290	4

## CTWD Control Stats for ER70S-6

Standard Parallel vs Perpendicular Samples (UTS)

### Two-Sample T-Test and CI: Std Par, Std Per

#### Method

$\mu_1$ : mean of Std Par

$\mu_2$ : mean of Std Per

Difference:  $\mu_1 - \mu_2$

*Equal variances are assumed for this analysis.*

#### Descriptive Statistics

Sample	N	Mean	StDev	SE Mean
Std Par	4	69.915	0.402	0.20
Std Per	4	70.194	0.457	0.23

#### Estimation for Difference

Difference	Pooled StDev	95% CI for Difference
-0.279	0.431	(-1.024, 0.467)

#### Test

Null hypothesis  $H_0: \mu_1 - \mu_2 = 0$

Alternative hypothesis  $H_1: \mu_1 - \mu_2 \neq 0$

T-Value	DF	P-Value
-0.91	6	0.396

No Contact Tip to Work Distance (CTWD) Control Parallel vs Perpendicular (UTS)

## Two-Sample T-Test and CI: No CTWD Par, No CTWD Per

### Method

$\mu_1$ : mean of No CTWD Par

$\mu_2$ : mean of No CTWD Per

Difference:  $\mu_1 - \mu_2$

*Equal variances are assumed for this analysis.*

### Descriptive Statistics

Sample	N	Mean	StDev	SE Mean
No CTWD Par	4	68.848	0.715	0.36
No CTWD Per	4	67.607	0.330	0.16

### Estimation for Difference

Difference	Pooled StDev	95% CI for Difference
1.241	0.557	(0.278, 2.204)

### Test

Null hypothesis  $H_0: \mu_1 - \mu_2 = 0$

Alternative hypothesis  $H_1: \mu_1 - \mu_2 \neq 0$

T-Value	DF	P-Value
3.15	6	0.020



Standard vs No CTWD Control Parallel (UTS)

## Two-Sample T-Test and CI: No CTWD Par, Std Par

### Method

$\mu_1$ : mean of No CTWD Par

$\mu_2$ : mean of Std Par

Difference:  $\mu_1 - \mu_2$

*Equal variances are assumed for this analysis.*

### Descriptive Statistics

Sample	N	Mean	StDev	SE Mean
No CTWD Par	4	68.848	0.715	0.36
Std Par	4	69.915	0.402	0.20

### Estimation for Difference

Difference	Pooled StDev	95% CI for Difference
-1.067	0.580	(-2.071, -0.064)

### Test

Null hypothesis  $H_0: \mu_1 - \mu_2 = 0$

Alternative hypothesis  $H_1: \mu_1 - \mu_2 \neq 0$

T-Value	DF	P-Value
-2.60	6	0.040

Standard vs No CTWD Control Perpendicular (UTS)

## Two-Sample T-Test and CI: Std Per, No CTWD Per

### Method

$\mu_1$ : mean of Std Per

$\mu_2$ : mean of No CTWD Per

Difference:  $\mu_1 - \mu_2$

*Equal variances are assumed for this analysis.*

### Descriptive Statistics

Sample	N	Mean	StDev	SE Mean
Std Per	4	70.194	0.457	0.23
No CTWD Per	4	67.607	0.330	0.16

### Estimation for Difference

Difference	Pooled StDev	95% CI for Difference
2.587	0.399	(1.897, 3.277)

### Test

Null hypothesis  $H_0: \mu_1 - \mu_2 = 0$

Alternative hypothesis  $H_1: \mu_1 - \mu_2 \neq 0$

T-Value	DF	P-Value
9.17	6	0.0000944

## Two-Sample T-Test and CI: Std Per, Std Par

### Method

$\mu_1$ : mean of Std Per

$\mu_2$ : mean of Std Par

Difference:  $\mu_1 - \mu_2$

*Equal variances are assumed for this analysis.*

### Descriptive Statistics

Sample	N	Mean	StDev	SE Mean
Std Per	4	51.55	2.39	1.2
Std Par	4	50.41	2.59	1.3

### Estimation for Difference

Difference	Pooled StDev	95% CI for Difference
1.14	2.50	(-3.18, 5.45)

### Test

Null hypothesis  $H_0: \mu_1 - \mu_2 = 0$

Alternative hypothesis  $H_1: \mu_1 - \mu_2 \neq 0$

T-Value	DF	P-Value
0.64	6	0.543

No Contact Tip to Work Distance (CTWD) Control Parallel vs Perpendicular (Yield)

## Two-Sample T-Test and CI: No CTWD Per, No CTWD Par

### Method

$\mu_1$ : mean of No CTWD Per

$\mu_2$ : mean of No CTWD Par

Difference:  $\mu_1 - \mu_2$

*Equal variances are assumed for this analysis.*

### Descriptive Statistics

Sample	N	Mean	StDev	SE Mean
No CTWD Per	4	53.20	1.10	0.55
No CTWD Par	4	52.00	3.42	1.7

### Estimation for Difference

Difference	Pooled StDev	95% CI for Difference
1.20	2.54	(-3.20, 5.60)

### Test

Null hypothesis  $H_0: \mu_1 - \mu_2 = 0$

Alternative hypothesis  $H_1: \mu_1 - \mu_2 \neq 0$

T-Value	DF	P-Value
0.67	6	0.530

Standard vs No CTWD Control (Yield)

## Two-Sample T-Test and CI: No CTWD, Std

### Method

$\mu_1$ : mean of No CTWD

$\mu_2$ : mean of Std

Difference:  $\mu_1 - \mu_2$

*Equal variances are assumed for this analysis.*

### Descriptive Statistics

Sample	N	Mean	StDev	SE Mean
No CTWD	8	52.60	2.44	0.86
Std	8	50.98	2.39	0.84

### Estimation for Difference

Difference	Pooled StDev	95% CI for Difference
1.62	2.41	(-0.97, 4.21)

### Test

Null hypothesis  $H_0: \mu_1 - \mu_2 = 0$

Alternative hypothesis  $H_1: \mu_1 - \mu_2 \neq 0$

T-Value	DF	P-Value
1.34	14	0.201

## Two-Sample T-Test and CI: Std Par, Std Per

### Method

$\mu_1$ : mean of Std Par

$\mu_2$ : mean of Std Per

Difference:  $\mu_1 - \mu_2$

*Equal variances are assumed for this analysis.*

### Descriptive Statistics

Sample	N	Mean	StDev	SE Mean
Std Par	4	75.750	0.645	0.32
Std Per	4	75.50	1.78	0.89

### Estimation for Difference

Difference	Pooled StDev	95% CI for Difference
0.250	1.339	(-2.066, 2.566)

### Test

Null hypothesis  $H_0: \mu_1 - \mu_2 = 0$

Alternative hypothesis  $H_1: \mu_1 - \mu_2 \neq 0$

T-Value	DF	P-Value
0.26	6	0.801

No Contact Tip to Work Distance (CTWD) Control Parallel vs Perpendicular (Hardness)

## Two-Sample T-Test and CI: No CTWD Par, No CTWD Per

### Method

$\mu_1$ : mean of No CTWD Par

$\mu_2$ : mean of No CTWD Per

Difference:  $\mu_1 - \mu_2$

*Equal variances are assumed for this analysis.*

### Descriptive Statistics

Sample	N	Mean	StDev	SE Mean
No CTWD Par	4	75.844	0.534	0.27
No CTWD Per	4	76.750	0.540	0.27

### Estimation for Difference

Difference	Pooled StDev	95% CI for Difference
-0.906	0.537	(-1.835, 0.023)

### Test

Null hypothesis  $H_0: \mu_1 - \mu_2 = 0$

Alternative hypothesis  $H_1: \mu_1 - \mu_2 \neq 0$

T-Value	DF	P-Value
-2.39	6	0.054

Standard vs No CTWD Control (Hardness)

## Two-Sample T-Test and CI: Std, No CTWD

### Method

$\mu_1$ : mean of Std

$\mu_2$ : mean of No CTWD

Difference:  $\mu_1 - \mu_2$

*Equal variances are assumed for this analysis.*

### Descriptive Statistics

Sample	N	Mean	StDev	SE Mean
Std	8	75.63	1.25	0.44
No CTWD	8	76.297	0.694	0.25

### Estimation for Difference

Difference	Pooled StDev	95% CI for Difference
-0.672	1.009	(-1.754, 0.410)

### Test

Null hypothesis  $H_0: \mu_1 - \mu_2 = 0$

Alternative hypothesis  $H_1: \mu_1 - \mu_2 \neq 0$

T-Value	DF	P-Value
-1.33	14	0.204



## CTWD Control Stats for ER308L

Standard Parallel vs Perpendicular Samples (UTS)

### Two-Sample T-Test and CI: STD Par, STD Per

#### Method

$\mu_1$ : mean of STD Par

$\mu_2$ : mean of STD Per

Difference:  $\mu_1 - \mu_2$

*Equal variances are assumed for this analysis.*

#### Descriptive Statistics

Sample	N	Mean	StDev	SE Mean
STD Par	4	89.463	0.433	0.22
STD Per	4	86.78	1.50	0.75

#### Estimation for Difference

Difference	Pooled StDev	95% CI for Difference
2.678	1.107	(0.763, 4.592)

#### Test

Null hypothesis  $H_0: \mu_1 - \mu_2 = 0$

Alternative hypothesis  $H_1: \mu_1 - \mu_2 \neq 0$

T-Value	DF	P-Value
3.42	6	0.014

No Contact Tip to Work Distance (CTWD) Control Parallel vs Perpendicular (UTS)

## Two-Sample T-Test and CI: No CTWD Par, No CTWD Per

### Method

$\mu_1$ : mean of No CTWD Par

$\mu_2$ : mean of No CTWD Per

Difference:  $\mu_1 - \mu_2$

*Equal variances are assumed for this analysis.*

### Descriptive Statistics

Sample	N	Mean	StDev	SE Mean
No CTWD Par	4	86.01	1.93	0.97
No CTWD Per	4	82.25	1.74	0.87

### Estimation for Difference

Difference	Pooled StDev	95% CI for Difference
3.76	1.84	(0.58, 6.95)

### Test

Null hypothesis  $H_0: \mu_1 - \mu_2 = 0$

Alternative hypothesis  $H_1: \mu_1 - \mu_2 \neq 0$

T-Value	DF	P-Value
2.89	6	0.028

Standard vs No CTWD Control Parallel (UTS)

## Two-Sample T-Test and CI: STD Par, No CTWD Par

### Method

$\mu_1$ : mean of STD Par

$\mu_2$ : mean of No CTWD Par

Difference:  $\mu_1 - \mu_2$

*Equal variances are assumed for this analysis.*

### Descriptive Statistics

Sample	N	Mean	StDev	SE Mean
STD Par	4	89.463	0.433	0.22
No CTWD Par	4	86.01	1.93	0.97

### Estimation for Difference

Difference	Pooled StDev	95% CI for Difference
3.455	1.402	(1.030, 5.880)

### Test

Null hypothesis  $H_0: \mu_1 - \mu_2 = 0$

Alternative hypothesis  $H_1: \mu_1 - \mu_2 \neq 0$

T-Value	DF	P-Value
3.49	6	0.013

Standard vs No CTWD Control Perpendicular (UTS)

## Two-Sample T-Test and CI: STD Per, No CTWD Per

### Method

$\mu_1$ : mean of STD Per

$\mu_2$ : mean of No CTWD Per

Difference:  $\mu_1 - \mu_2$

*Equal variances are assumed for this analysis.*

### Descriptive Statistics

Sample	N	Mean	StDev	SE Mean
STD Per	4	86.78	1.50	0.75
No CTWD Per	4	82.25	1.74	0.87

### Estimation for Difference

Difference	Pooled StDev	95% CI for Difference
4.54	1.63	(1.72, 7.36)

### Test

Null hypothesis  $H_0: \mu_1 - \mu_2 = 0$

Alternative hypothesis  $H_1: \mu_1 - \mu_2 \neq 0$

T-Value	DF	P-Value
3.94	6	0.008

## Standard Parallel vs Perpendicular Samples (Yield)

### Two-Sample T-Test and CI: STD Per, STD Par

#### Method

$\mu_1$ : mean of STD Per

$\mu_2$ : mean of STD Par

Difference:  $\mu_1 - \mu_2$

*Equal variances are assumed for this analysis.*

#### Descriptive Statistics

Sample	N	Mean	StDev	SE Mean
STD Per	4	50.527	0.676	0.34
STD Par	4	53.398	0.797	0.40

#### Estimation for Difference

Difference	Pooled StDev	95% CI for Difference
-2.870	0.739	(-4.149, -1.591)

#### Test

Null hypothesis  $H_0: \mu_1 - \mu_2 = 0$

Alternative hypothesis  $H_1: \mu_1 - \mu_2 \neq 0$

T-Value	DF	P-Value
-5.49	6	0.002

No Contact Tip to Work Distance (CTWD) Control Parallel vs Perpendicular (Yield)

## Two-Sample T-Test and CI: No CTWD Par, No CTWD Per

### Method

$\mu_1$ : mean of No CTWD Par

$\mu_2$ : mean of No CTWD Per

Difference:  $\mu_1 - \mu_2$

*Equal variances are assumed for this analysis.*

### Descriptive Statistics

Sample	N	Mean	StDev	SE Mean
No CTWD Par	4	50.080	0.608	0.30
No CTWD Per	4	49.11	2.58	1.3

### Estimation for Difference

Difference	Pooled StDev	95% CI for Difference
0.97	1.88	(-2.28, 4.21)

### Test

Null hypothesis  $H_0: \mu_1 - \mu_2 = 0$

Alternative hypothesis  $H_1: \mu_1 - \mu_2 \neq 0$

T-Value	DF	P-Value
0.73	6	0.493

## Standard vs No CTWD Control Perpendicular (Yield)

### Two-Sample T-Test and CI: STD Per, No CTWD Per

#### Method

$\mu_1$ : mean of STD Per

$\mu_2$ : mean of No CTWD Per

Difference:  $\mu_1 - \mu_2$

*Equal variances are assumed for this analysis.*

#### Descriptive Statistics

Sample	N	Mean	StDev	SE Mean
STD Per	4	50.527	0.676	0.34
No CTWD Per	4	49.11	2.58	1.3

#### Estimation for Difference

Difference	Pooled StDev	95% CI for Difference
1.41	1.89	(-1.85, 4.68)

#### Test

Null hypothesis  $H_0: \mu_1 - \mu_2 = 0$

Alternative hypothesis  $H_1: \mu_1 - \mu_2 \neq 0$

T-Value	DF	P-Value
1.06	6	0.330

## Standard vs No CTWD Control Parallel (Yield)

### Two-Sample T-Test and CI: STD Par, No CTWD Par

#### Method

$\mu_1$ : mean of STD Par

$\mu_2$ : mean of No CTWD Par

Difference:  $\mu_1 - \mu_2$

*Equal variances are assumed for this analysis.*

#### Descriptive Statistics

Sample	N	Mean	StDev	SE Mean
STD Par	4	53.398	0.797	0.40
No CTWD Par	4	50.080	0.608	0.30

#### Estimation for Difference

Difference	Pooled StDev	95% CI for Difference
3.318	0.709	(2.091, 4.544)

#### Test

Null hypothesis  $H_0: \mu_1 - \mu_2 = 0$

Alternative hypothesis  $H_1: \mu_1 - \mu_2 \neq 0$

T-Value	DF	P-Value
6.62	6	0.00057



## Standard Parallel vs Perpendicular Samples (Hardness)

### Two-Sample T-Test and CI: STD Par, STD Per

#### Method

$\mu_1$ : mean of STD Par

$\mu_2$ : mean of STD Per

Difference:  $\mu_1 - \mu_2$

*Equal variances are assumed for this analysis.*

#### Descriptive Statistics

Sample	N	Mean	StDev	SE Mean
STD Par	4	87.250	0.500	0.25
STD Per	4	85.250	0.645	0.32

#### Estimation for Difference

Difference	Pooled StDev	95% CI for Difference
2.000	0.577	(1.001, 2.999)

#### Test

Null hypothesis  $H_0: \mu_1 - \mu_2 = 0$

Alternative hypothesis  $H_1: \mu_1 - \mu_2 \neq 0$

T-Value	DF	P-Value
4.90	6	0.003

No Contact Tip to Work Distance (CTWD) Control Parallel vs Perpendicular (Hardness)

## Two-Sample T-Test and CI: No CTWD Per, No CTWD Par

### Method

$\mu_1$ : mean of No CTWD Per

$\mu_2$ : mean of No CTWD Par

Difference:  $\mu_1 - \mu_2$

*Equal variances are assumed for this analysis.*

### Descriptive Statistics

Sample	N	Mean	StDev	SE Mean
No CTWD Per	4	87.00	1.29	0.65
No CTWD Par	4	83.56	1.56	0.78

### Estimation for Difference

Difference	Pooled StDev	95% CI for Difference
3.44	1.43	(0.96, 5.91)

### Test

Null hypothesis  $H_0: \mu_1 - \mu_2 = 0$

Alternative hypothesis  $H_1: \mu_1 - \mu_2 \neq 0$

T-Value	DF	P-Value
3.40	6	0.015

## Standard vs No CTWD Control Perpendicular (Hardness)

### Two-Sample T-Test and CI: No CTWD Per, STD Per

#### Method

$\mu_1$ : mean of No CTWD Per

$\mu_2$ : mean of STD Per

Difference:  $\mu_1 - \mu_2$

*Equal variances are assumed for this analysis.*

#### Descriptive Statistics

Sample	N	Mean	StDev	SE Mean
No CTWD Per	4	87.00	1.29	0.65
STD Per	4	85.250	0.645	0.32

#### Estimation for Difference

Difference	Pooled StDev	95% CI for Difference
1.750	1.021	(-0.016, 3.516)

#### Test

Null hypothesis  $H_0: \mu_1 - \mu_2 = 0$

Alternative hypothesis  $H_1: \mu_1 - \mu_2 \neq 0$

T-Value	DF	P-Value
2.42	6	0.052

Standard vs No CTWD Control Parallel (Hardness)

## Two-Sample T-Test and CI: No CTWD Par, STD Par

### Method

$\mu_1$ : mean of No CTWD Par

$\mu_2$ : mean of STD Par

Difference:  $\mu_1 - \mu_2$

*Equal variances are assumed for this analysis.*

### Descriptive Statistics

Sample	N	Mean	StDev	SE Mean
No CTWD Par	4	83.56	1.56	0.78
STD Par	4	87.250	0.500	0.25

### Estimation for Difference

Difference	Pooled StDev	95% CI for Difference
-3.688	1.158	(-5.691, -1.684)

### Test

Null hypothesis  $H_0: \mu_1 - \mu_2 = 0$

Alternative hypothesis  $H_1: \mu_1 - \mu_2 \neq 0$

T-Value	DF	P-Value
-4.50	6	0.004

## CMT Control Stats for ER70S-6

CMT Mode Parallel vs Perpendicular Samples (UTS)

### Two-Sample T-Test and CI: CMT Parallel, CMT Perpendicular

#### Method

$\mu_1$ : mean of CMT Parallel

$\mu_2$ : mean of CMT Perpendicular

Difference:  $\mu_1 - \mu_2$

*Equal variances are assumed for this analysis.*

#### Descriptive Statistics

Sample	N	Mean	StDev	SE Mean
CMT Parallel	4	69.915	0.402	0.20
CMT Perpendicular	4	70.194	0.457	0.23

#### Estimation for Difference

Difference	Pooled StDev	95% CI for Difference
-0.279	0.431	(-1.024, 0.467)

#### Test

Null hypothesis  $H_0: \mu_1 - \mu_2 = 0$

Alternative hypothesis  $H_1: \mu_1 - \mu_2 \neq 0$

T-Value	DF	P-Value
-0.91	6	0.396

## Standard Mode Parallel vs Perpendicular (UTS)

### Two-Sample T-Test and CI: Std Parallel, Std Perpendicular

#### Method

$\mu_1$ : mean of Std Parallel

$\mu_2$ : mean of Std Perpendicular

Difference:  $\mu_1 - \mu_2$

*Equal variances are assumed for this analysis.*

#### Descriptive Statistics

Sample	N	Mean	StDev	SE Mean
Std Parallel	4	68.776	0.721	0.36
Std Perpendicular	4	68.853	0.450	0.22

#### Estimation for Difference

Difference	Pooled StDev	95% CI for Difference
-0.077	0.601	(-1.117, 0.963)

#### Test

Null hypothesis  $H_0: \mu_1 - \mu_2 = 0$

Alternative hypothesis  $H_1: \mu_1 - \mu_2 \neq 0$

T-Value	DF	P-Value
-0.18	6	0.862

Standard vs CMT mode (UTS)

## Two-Sample T-Test and CI: Std, CMT

### Method

$\mu_1$ : mean of Std

$\mu_2$ : mean of CMT

Difference:  $\mu_1 - \mu_2$

*Equal variances are assumed for this analysis.*

### Descriptive Statistics

Sample	N	Mean	StDev	SE Mean
Std	8	68.814	0.558	0.20
CMT	8	70.054	0.426	0.15

### Estimation for Difference

Difference	Pooled StDev	95% CI for Difference
-1.240	0.496	(-1.772, -0.708)

### Test

Null hypothesis  $H_0: \mu_1 - \mu_2 = 0$

Alternative hypothesis  $H_1: \mu_1 - \mu_2 \neq 0$

T-Value	DF	P-Value
-5.00	14	0.0001950

## CMT Mode Parallel vs Perpendicular (Yield)

### Two-Sample T-Test and CI: CMT Parallel, CMT Perpendicular

#### Method

$\mu_1$ : mean of CMT Parallel

$\mu_2$ : mean of CMT Perpendicular

Difference:  $\mu_1 - \mu_2$

*Equal variances are assumed for this analysis.*

#### Descriptive Statistics

Sample	N	Mean	StDev	SE Mean
CMT Parallel	4	50.41	2.59	1.3
CMT Perpendicular	4	51.55	2.39	1.2

#### Estimation for Difference

Difference	Pooled StDev	95% CI for Difference
-1.14	2.50	(-5.45, 3.18)

#### Test

Null hypothesis  $H_0: \mu_1 - \mu_2 = 0$

Alternative hypothesis  $H_1: \mu_1 - \mu_2 \neq 0$

T-Value	DF	P-Value
-0.64	6	0.543



## Standard Mode Parallel Vs Perpendicular (Yield)

### Two-Sample T-Test and CI: Std Parallel, Std Perpendicular

#### Method

$\mu_1$ : mean of Std Parallel

$\mu_2$ : mean of Std Perpendicular

Difference:  $\mu_1 - \mu_2$

*Equal variances are assumed for this analysis.*

#### Descriptive Statistics

Sample	N	Mean	StDev	SE Mean
Std Parallel	4	50.37	1.07	0.54
Std Perpendicular	4	50.849	0.567	0.28

#### Estimation for Difference

Difference	Pooled StDev	95% CI for Difference
-0.481	0.859	(-1.967, 1.005)

#### Test

Null hypothesis  $H_0: \mu_1 - \mu_2 = 0$

Alternative hypothesis  $H_1: \mu_1 - \mu_2 \neq 0$

T-Value	DF	P-Value
-0.79	6	0.458

Standard vs CMT Mode (Yield)

## Two-Sample T-Test and CI: Std, CMT

### Method

$\mu_1$ : mean of Std

$\mu_2$ : mean of CMT

Difference:  $\mu_1 - \mu_2$

*Equal variances are assumed for this analysis.*

### Descriptive Statistics

Sample	N	Mean	StDev	SE Mean
Std	8	50.608	0.836	0.30
CMT	8	50.98	2.39	0.84

### Estimation for Difference

Difference	Pooled StDev	95% CI for Difference
-0.370	1.790	(-2.290, 1.549)

### Test

Null hypothesis  $H_0: \mu_1 - \mu_2 = 0$

Alternative hypothesis  $H_1: \mu_1 - \mu_2 \neq 0$

T-Value	DF	P-Value
-0.41	14	0.685

## CMT Mode Parallel vs Perpendicular (Hardness)

### Two-Sample T-Test and CI: CMT Parallel, CMT Perpendicular

#### Method

$\mu_1$ : mean of CMT Parallel

$\mu_2$ : mean of CMT Perpendicular

Difference:  $\mu_1 - \mu_2$

*Equal variances are assumed for this analysis.*

#### Descriptive Statistics

Sample	N	Mean	StDev	SE Mean
CMT Parallel	4	75.750	0.645	0.32
CMT Perpendicular	4	75.50	1.78	0.89

#### Estimation for Difference

Difference	Pooled StDev	95% CI for Difference
0.250	1.339	(-2.066, 2.566)

#### Test

Null hypothesis  $H_0: \mu_1 - \mu_2 = 0$

Alternative hypothesis  $H_1: \mu_1 - \mu_2 \neq 0$

T-Value	DF	P-Value
0.26	6	0.801

## Standard Mode Parallel Vs Perpendicular (Hardness)

### Two-Sample T-Test and CI: Std Parallel, Std Perpendicular

#### Method

$\mu_1$ : mean of Std Parallel

$\mu_2$ : mean of Std Perpendicular

Difference:  $\mu_1 - \mu_2$

*Equal variances are assumed for this analysis.*

#### Descriptive Statistics

Sample	N	Mean	StDev	SE Mean
Std Parallel	4	77.00	1.63	0.82
Std Perpendicular	4	81.25	2.75	1.4

#### Estimation for Difference

Difference	Pooled StDev	95% CI for Difference
-4.25	2.26	(-8.17, -0.33)

#### Test

Null hypothesis  $H_0: \mu_1 - \mu_2 = 0$

Alternative hypothesis  $H_1: \mu_1 - \mu_2 \neq 0$

T-Value	DF	P-Value
-2.65	6	0.038

Standard vs CMT Mode (Hardness)

## Two-Sample T-Test and CI: Std, CMT

### Method

$\mu_1$ : mean of Std

$\mu_2$ : mean of CMT

Difference:  $\mu_1 - \mu_2$

*Equal variances are assumed for this analysis.*

### Descriptive Statistics

Sample	N	Mean	StDev	SE Mean
Std	8	79.13	3.09	1.1
CMT	8	75.63	1.25	0.44

### Estimation for Difference

Difference	Pooled StDev	95% CI for Difference
3.50	2.36	(0.97, 6.03)

### Test

Null hypothesis  $H_0: \mu_1 - \mu_2 = 0$

Alternative hypothesis  $H_1: \mu_1 - \mu_2 \neq 0$

T-Value	DF	P-Value
2.97	14	0.010

## CMT Control Stats for ER308L

CMT Mode Parallel vs Perpendicular Samples (UTS)

### Two-Sample T-Test and CI: CMT Par, CMT Per

#### Method

$\mu_1$ : mean of CMT Par

$\mu_2$ : mean of CMT Per

Difference:  $\mu_1 - \mu_2$

*Equal variances are assumed for this analysis.*

#### Descriptive Statistics

Sample	N	Mean	StDev	SE Mean
CMT Par	4	89.463	0.433	0.22
CMT Per	4	86.78	1.50	0.75

#### Estimation for Difference

Difference	Pooled StDev	95% CI for Difference
2.678	1.107	(0.763, 4.592)

#### Test

Null hypothesis  $H_0: \mu_1 - \mu_2 = 0$

Alternative hypothesis  $H_1: \mu_1 - \mu_2 \neq 0$

T-Value	DF	P-Value
3.42	6	0.014

## Standard Mode Parallel vs Perpendicular (UTS)

### Two-Sample T-Test and CI: STD Par, STD Per

#### Method

$\mu_1$ : mean of STD Par

$\mu_2$ : mean of STD Per

Difference:  $\mu_1 - \mu_2$

*Equal variances are assumed for this analysis.*

#### Descriptive Statistics

Sample	N	Mean	StDev	SE Mean
STD Par	4	82.177	0.655	0.33
STD Per	4	81.60	1.25	0.63

#### Estimation for Difference

Difference	Pooled StDev	95% CI for Difference
0.581	1.000	(-1.150, 2.311)

#### Test

Null hypothesis  $H_0: \mu_1 - \mu_2 = 0$

Alternative hypothesis  $H_1: \mu_1 - \mu_2 \neq 0$

T-Value	DF	P-Value
0.82	6	0.443

Standard vs CMT mode Perpendicular (UTS)

## Two-Sample T-Test and CI: CMT Per, STD Per

### Method

$\mu_1$ : mean of CMT Per

$\mu_2$ : mean of STD Per

Difference:  $\mu_1 - \mu_2$

*Equal variances are assumed for this analysis.*

### Descriptive Statistics

Sample	N	Mean	StDev	SE Mean
CMT Per	4	86.78	1.50	0.75
STD Per	4	81.60	1.25	0.63

### Estimation for Difference

Difference	Pooled StDev	95% CI for Difference
5.188	1.384	(2.793, 7.584)

### Test

Null hypothesis  $H_0: \mu_1 - \mu_2 = 0$

Alternative hypothesis  $H_1: \mu_1 - \mu_2 \neq 0$

T-Value	DF	P-Value
5.30	6	0.002



Standard vs CMT mode Parallel (UTS)

## Two-Sample T-Test and CI: CMT Par, STD Par

### Method

$\mu_1$ : mean of CMT Par

$\mu_2$ : mean of STD Par

Difference:  $\mu_1 - \mu_2$

*Equal variances are assumed for this analysis.*

### Descriptive Statistics

Sample	N	Mean	StDev	SE Mean
CMT Par	4	89.463	0.433	0.22
STD Par	4	82.177	0.655	0.33

### Estimation for Difference

Difference	Pooled StDev	95% CI for Difference
7.285	0.555	(6.325, 8.246)

### Test

Null hypothesis  $H_0: \mu_1 - \mu_2 = 0$

Alternative hypothesis  $H_1: \mu_1 - \mu_2 \neq 0$

T-Value	DF	P-Value
18.56	6	0.0000016

## CMT Mode Parallel vs Perpendicular (Yield)

### Two-Sample T-Test and CI: CMT Par, CMT Per

#### Method

$\mu_1$ : mean of CMT Par

$\mu_2$ : mean of CMT Per

Difference:  $\mu_1 - \mu_2$

*Equal variances are assumed for this analysis.*

#### Descriptive Statistics

Sample	N	Mean	StDev	SE Mean
CMT Par	4	53.398	0.797	0.40
CMT Per	4	50.527	0.676	0.34

#### Estimation for Difference

Difference	Pooled StDev	95% CI for Difference
2.870	0.739	(1.591, 4.149)

#### Test

Null hypothesis  $H_0: \mu_1 - \mu_2 = 0$

Alternative hypothesis  $H_1: \mu_1 - \mu_2 \neq 0$

T-Value	DF	P-Value
5.49	6	0.002

## Standard Mode Parallel Vs Perpendicular (Yield)

### Two-Sample T-Test and CI: STD Per, STD Par

#### Method

$\mu_1$ : mean of STD Per

$\mu_2$ : mean of STD Par

Difference:  $\mu_1 - \mu_2$

*Equal variances are assumed for this analysis.*

#### Descriptive Statistics

Sample	N	Mean	StDev	SE Mean
STD Per	4	55.312	0.632	0.32
STD Par	4	55.515	0.152	0.076

#### Estimation for Difference

Difference	Pooled StDev	95% CI for Difference
-0.203	0.460	(-0.998, 0.593)

#### Test

Null hypothesis  $H_0: \mu_1 - \mu_2 = 0$

Alternative hypothesis  $H_1: \mu_1 - \mu_2 \neq 0$

T-Value	DF	P-Value
-0.62	6	0.556

## Standard vs CMT Mode Parallel (Yield)

### Two-Sample T-Test and CI: CMT Par, STD Par

#### Method

$\mu_1$ : mean of CMT Par

$\mu_2$ : mean of STD Par

Difference:  $\mu_1 - \mu_2$

*Equal variances are assumed for this analysis.*

#### Descriptive Statistics

Sample	N	Mean	StDev	SE Mean
CMT Par	4	53.398	0.797	0.40
STD Par	4	55.515	0.152	0.076

#### Estimation for Difference

Difference	Pooled StDev	95% CI for Difference
-2.117	0.574	(-3.110, -1.124)

#### Test

Null hypothesis  $H_0: \mu_1 - \mu_2 = 0$

Alternative hypothesis  $H_1: \mu_1 - \mu_2 \neq 0$

T-Value	DF	P-Value
-5.22	6	0.002

## Standard vs CMT Mode Perpendicular (Yield)

### Two-Sample T-Test and CI: CMT Per, STD Per

#### Method

$\mu_1$ : mean of CMT Per

$\mu_2$ : mean of STD Per

Difference:  $\mu_1 - \mu_2$

*Equal variances are assumed for this analysis.*

#### Descriptive Statistics

Sample	N	Mean	StDev	SE Mean
CMT Per	4	50.527	0.676	0.34
STD Per	4	55.312	0.632	0.32

#### Estimation for Difference

Difference	Pooled StDev	95% CI for Difference
-4.785	0.654	(-5.917, -3.653)

#### Test

Null hypothesis  $H_0: \mu_1 - \mu_2 = 0$

Alternative hypothesis  $H_1: \mu_1 - \mu_2 \neq 0$

T-Value	DF	P-Value
-10.34	6	0.0000478

## CMT Mode Parallel vs Perpendicular (Hardness)

### Two-Sample T-Test and CI: CMT Per, CMT Par

#### Method

$\mu_1$ : mean of CMT Per

$\mu_2$ : mean of CMT Par

Difference:  $\mu_1 - \mu_2$

*Equal variances are assumed for this analysis.*

#### Descriptive Statistics

Sample	N	Mean	StDev	SE Mean
CMT Per	4	85.250	0.645	0.32
CMT Par	4	87.250	0.500	0.25

#### Estimation for Difference

Difference	Pooled StDev	95% CI for Difference
-2.000	0.577	(-2.999, -1.001)

#### Test

Null hypothesis  $H_0: \mu_1 - \mu_2 = 0$

Alternative hypothesis  $H_1: \mu_1 - \mu_2 \neq 0$

T-Value	DF	P-Value
-4.90	6	0.003

## Standard Mode Parallel Vs Perpendicular (Hardness)

### Two-Sample T-Test and CI: STD Per, STD Par

#### Method

$\mu_1$ : mean of STD Per

$\mu_2$ : mean of STD Par

Difference:  $\mu_1 - \mu_2$

*Equal variances are assumed for this analysis.*

#### Descriptive Statistics

Sample	N	Mean	StDev	SE Mean
STD Per	4	94.250	0.957	0.48
STD Par	4	93.88	1.65	0.83

#### Estimation for Difference

Difference	Pooled StDev	95% CI for Difference
0.375	1.350	(-1.961, 2.711)

#### Test

Null hypothesis  $H_0: \mu_1 - \mu_2 = 0$

Alternative hypothesis  $H_1: \mu_1 - \mu_2 \neq 0$

T-Value	DF	P-Value
0.39	6	0.708

## Standard vs CMT Mode Parallel (Hardness)

### Two-Sample T-Test and CI: CMT Par, STD Par

#### Method

$\mu_1$ : mean of CMT Par

$\mu_2$ : mean of STD Par

Difference:  $\mu_1 - \mu_2$

*Equal variances are assumed for this analysis.*

#### Descriptive Statistics

Sample	N	Mean	StDev	SE Mean
CMT Par	4	87.250	0.500	0.25
STD Par	4	93.88	1.65	0.83

#### Estimation for Difference

Difference	Pooled StDev	95% CI for Difference
-6.625	1.220	(-8.737, -4.513)

#### Test

Null hypothesis  $H_0: \mu_1 - \mu_2 = 0$

Alternative hypothesis  $H_1: \mu_1 - \mu_2 \neq 0$

T-Value	DF	P-Value
-7.68	6	0.0002556



## Standard vs CMT Mode Perpendicular (Hardness)

### Two-Sample T-Test and CI: STD Per, CMT Per

#### Method

$\mu_1$ : mean of STD Per  
 $\mu_2$ : mean of CMT Per  
Difference:  $\mu_1 - \mu_2$

*Equal variances are assumed for this analysis.*

#### Descriptive Statistics

Sample	N	Mean	StDev	SE Mean
STD Per	4	94.250	0.957	0.48
CMT Per	4	85.250	0.645	0.32

#### Estimation for Difference

Difference	Pooled StDev	95% CI for Difference
9.000	0.816	(7.587, 10.413)

#### Test

Null hypothesis  $H_0: \mu_1 - \mu_2 = 0$   
Alternative hypothesis  $H_1: \mu_1 - \mu_2 \neq 0$

T-Value	DF	P-Value
15.59	6	0.0000044

## Temperature Control Stats for ER70S-6

232 Parallel vs. Perpendicular (UTS)

### Two-Sample T-Test and CI: 232 Parallel, 232 Perpendicular

#### Method

$\mu_1$ : mean of 232 Parallel

$\mu_2$ : mean of 232 Perpendicular

Difference:  $\mu_1 - \mu_2$

*Equal variances are assumed for this analysis.*

#### Descriptive Statistics

Sample	N	Mean	StDev	SE Mean
232 Parallel	4	68.697	0.512	0.26
232 Perpendicular	4	68.085	0.536	0.27

#### Estimation for Difference

Difference	Pooled StDev	95% CI for Difference
0.612	0.524	(-0.294, 1.519)

#### Test

Null hypothesis  $H_0: \mu_1 - \mu_2 = 0$

Alternative hypothesis  $H_1: \mu_1 - \mu_2 \neq 0$

T-Value	DF	P-Value
1.65	6	0.149

## 260 Parallel vs. Perpendicular (UTS)

### Two-Sample T-Test and CI: 260 Parallel, 260 Perpendicular

#### Method

$\mu_1$ : mean of 260 Parallel

$\mu_2$ : mean of 260 Perpendicular

Difference:  $\mu_1 - \mu_2$

*Equal variances are assumed for this analysis.*

#### Descriptive Statistics

Sample	N	Mean	StDev	SE Mean
260 Parallel	4	68.25	1.01	0.50
260 Perpendicular	4	67.482	0.535	0.27

#### Estimation for Difference

Difference	Pooled StDev	95% CI for Difference
0.764	0.805	(-0.630, 2.157)

#### Test

Null hypothesis  $H_0: \mu_1 - \mu_2 = 0$

Alternative hypothesis  $H_1: \mu_1 - \mu_2 \neq 0$

T-Value	DF	P-Value
1.34	6	0.228

## 288 Parallel vs. Perpendicular (UTS)

### Two-Sample T-Test and CI: 288 Parallel, 288 Perpendicular

#### Method

$\mu_1$ : mean of 288 Parallel

$\mu_2$ : mean of 288 Perpendicular

Difference:  $\mu_1 - \mu_2$

*Equal variances are assumed for this analysis.*

#### Descriptive Statistics

Sample	N	Mean	StDev	SE Mean
288 Parallel	4	68.558	0.194	0.097
288 Perpendicular	4	67.411	0.266	0.13

#### Estimation for Difference

Difference	Pooled StDev	95% CI for Difference
1.148	0.233	(0.745, 1.550)

#### Test

Null hypothesis  $H_0: \mu_1 - \mu_2 = 0$

Alternative hypothesis  $H_1: \mu_1 - \mu_2 \neq 0$

T-Value	DF	P-Value
6.97	6	0.00043

Baseline vs. 232 (UTS)

## Two-Sample T-Test and CI: Baseline, 232

### Method

$\mu_1$ : mean of Baseline

$\mu_2$ : mean of 232

Difference:  $\mu_1 - \mu_2$

*Equal variances are assumed for this analysis.*

### Descriptive Statistics

Sample	N	Mean	StDev	SE Mean
Baseline	8	70.054	0.426	0.15
232	8	68.391	0.585	0.21

### Estimation for Difference

Difference	Pooled StDev	95% CI for Difference
1.664	0.512	(1.115, 2.212)

### Test

Null hypothesis  $H_0: \mu_1 - \mu_2 = 0$

Alternative hypothesis  $H_1: \mu_1 - \mu_2 \neq 0$

T-Value	DF	P-Value
6.50	14	0.000014

Baseline vs. 260 (UTS)

## Two-Sample T-Test and CI: Baseline, 260

### Method

$\mu_1$ : mean of Baseline

$\mu_2$ : mean of 260

Difference:  $\mu_1 - \mu_2$

*Equal variances are assumed for this analysis.*

### Descriptive Statistics

Sample	N	Mean	StDev	SE Mean
Baseline	8	70.054	0.426	0.15
260	8	67.864	0.850	0.30

### Estimation for Difference

Difference	Pooled StDev	95% CI for Difference
2.190	0.672	(1.469, 2.911)

### Test

Null hypothesis  $H_0: \mu_1 - \mu_2 = 0$

Alternative hypothesis  $H_1: \mu_1 - \mu_2 \neq 0$

T-Value	DF	P-Value
6.51	14	0.000014

Baseline vs. 288 (UTS)

## Two-Sample T-Test and CI: Baseline, 288

### Method

$\mu_1$ : mean of Baseline

$\mu_2$ : mean of 288

Difference:  $\mu_1 - \mu_2$

*Equal variances are assumed for this analysis.*

### Descriptive Statistics

Sample	N	Mean	StDev	SE Mean
Baseline	8	70.054	0.426	0.15
288	8	67.984	0.650	0.23

### Estimation for Difference

Difference	Pooled StDev	95% CI for Difference
2.070	0.550	(1.481, 2.659)

### Test

Null hypothesis  $H_0: \mu_1 - \mu_2 = 0$

Alternative hypothesis  $H_1: \mu_1 - \mu_2 \neq 0$

T-Value	DF	P-Value
7.53	14	0.000003

232 vs. 260 (UTS)

## Two-Sample T-Test and CI: 232, 260

### Method

$\mu_1$ : mean of 232

$\mu_2$ : mean of 260

Difference:  $\mu_1 - \mu_2$

*Equal variances are assumed for this analysis.*

### Descriptive Statistics

Sample	N	Mean	StDev	SE Mean
232	8	68.391	0.585	0.21
260	8	67.864	0.850	0.30

### Estimation for Difference

Difference	Pooled StDev	95% CI for Difference
0.526	0.730	(-0.256, 1.309)

### Test

Null hypothesis  $H_0: \mu_1 - \mu_2 = 0$

Alternative hypothesis  $H_1: \mu_1 - \mu_2 \neq 0$

T-Value	DF	P-Value
1.44	14	0.171



232 vs. 288 (UTS)

## Two-Sample T-Test and CI: 232, 288

### Method

$\mu_1$ : mean of 232

$\mu_2$ : mean of 288

Difference:  $\mu_1 - \mu_2$

*Equal variances are assumed for this analysis.*

### Descriptive Statistics

Sample	N	Mean	StDev	SE Mean
232	8	68.391	0.585	0.21
288	8	67.984	0.650	0.23

### Estimation for Difference

Difference	Pooled StDev	95% CI for Difference
0.406	0.619	(-0.257, 1.070)

### Test

Null hypothesis  $H_0: \mu_1 - \mu_2 = 0$

Alternative hypothesis  $H_1: \mu_1 - \mu_2 \neq 0$

T-Value	DF	P-Value
1.31	14	0.210

260 vs. 288 (UTS)

## Two-Sample T-Test and CI: 260, 288

### Method

$\mu_1$ : mean of 260

$\mu_2$ : mean of 288

Difference:  $\mu_1 - \mu_2$

*Equal variances are assumed for this analysis.*

### Descriptive Statistics

Sample	N	Mean	StDev	SE Mean
260	8	67.864	0.850	0.30
288	8	67.984	0.650	0.23

### Estimation for Difference

Difference	Pooled StDev	95% CI for Difference
-0.120	0.757	(-0.932, 0.692)

### Test

Null hypothesis  $H_0: \mu_1 - \mu_2 = 0$

Alternative hypothesis  $H_1: \mu_1 - \mu_2 \neq 0$

T-Value	DF	P-Value
-0.32	14	0.756

## 232 Parallel vs. Perpendicular (Yield)

### Two-Sample T-Test and CI: 232 Parallel, 232 Perpendicular

#### Method

$\mu_1$ : mean of 232 Parallel

$\mu_2$ : mean of 232 Perpendicular

Difference:  $\mu_1 - \mu_2$

*Equal variances are assumed for this analysis.*

#### Descriptive Statistics

Sample	N	Mean	StDev	SE Mean
232 Parallel	4	50.35	1.19	0.59
232 Perpendicular	4	49.73	1.34	0.67

#### Estimation for Difference

Difference	Pooled StDev	95% CI for Difference
0.613	1.265	(-1.576, 2.803)

#### Test

Null hypothesis  $H_0: \mu_1 - \mu_2 = 0$

Alternative hypothesis  $H_1: \mu_1 - \mu_2 \neq 0$

T-Value	DF	P-Value
0.69	6	0.519

## 260 Parallel vs. Perpendicular (Yield)

### Two-Sample T-Test and CI: 260 Parallel, 260 Perpendicular

#### Method

$\mu_1$ : mean of 260 Parallel

$\mu_2$ : mean of 260 Perpendicular

Difference:  $\mu_1 - \mu_2$

*Equal variances are assumed for this analysis.*

#### Descriptive Statistics

Sample	N	Mean	StDev	SE Mean
260 Parallel	4	48.739	0.257	0.13
260 Perpendicular	4	47.72	1.04	0.52

#### Estimation for Difference

Difference	Pooled StDev	95% CI for Difference
1.023	0.759	(-0.290, 2.336)

#### Test

Null hypothesis  $H_0: \mu_1 - \mu_2 = 0$

Alternative hypothesis  $H_1: \mu_1 - \mu_2 \neq 0$

T-Value	DF	P-Value
1.91	6	0.105

## 288 Parallel vs. Perpendicular (Yield)

### Two-Sample T-Test and CI: 288 Parallel, 288 Perpendicular

#### Method

$\mu_1$ : mean of 288 Parallel

$\mu_2$ : mean of 288 Perpendicular

Difference:  $\mu_1 - \mu_2$

*Equal variances are assumed for this analysis.*

#### Descriptive Statistics

Sample	N	Mean	StDev	SE Mean
288 Parallel	4	50.64	1.31	0.65
288 Perpendicular	4	48.321	0.258	0.13

#### Estimation for Difference

Difference	Pooled StDev	95% CI for Difference
2.318	0.942	(0.688, 3.949)

#### Test

Null hypothesis  $H_0: \mu_1 - \mu_2 = 0$

Alternative hypothesis  $H_1: \mu_1 - \mu_2 \neq 0$

T-Value	DF	P-Value
3.48	6	0.013

Baseline vs. 232 (Yield)

## Two-Sample T-Test and CI: Baseline, 232

### Method

$\mu_1$ : mean of Baseline

$\mu_2$ : mean of 232

Difference:  $\mu_1 - \mu_2$

*Equal variances are assumed for this analysis.*

### Descriptive Statistics

Sample	N	Mean	StDev	SE Mean
Baseline	8	50.98	2.39	0.84
232	8	50.04	1.22	0.43

### Estimation for Difference

Difference	Pooled StDev	95% CI for Difference
0.940	1.896	(-1.093, 2.973)

### Test

Null hypothesis  $H_0: \mu_1 - \mu_2 = 0$

Alternative hypothesis  $H_1: \mu_1 - \mu_2 \neq 0$

T-Value	DF	P-Value
0.99	14	0.338

Baseline vs. 260 (Yield)

## Two-Sample T-Test and CI: Baseline, 260

### Method

$\mu_1$ : mean of Baseline

$\mu_2$ : mean of 260

Difference:  $\mu_1 - \mu_2$

*Equal variances are assumed for this analysis.*

### Descriptive Statistics

Sample	N	Mean	StDev	SE Mean
Baseline	8	50.98	2.39	0.84
260	8	48.228	0.890	0.31

### Estimation for Difference

Difference	Pooled StDev	95% CI for Difference
2.751	1.803	(0.818, 4.684)

### Test

Null hypothesis  $H_0: \mu_1 - \mu_2 = 0$

Alternative hypothesis  $H_1: \mu_1 - \mu_2 \neq 0$

T-Value	DF	P-Value
3.05	14	0.009

Baseline vs. 288 (Yield)

## Two-Sample T-Test and CI: Baseline, 288

### Method

$\mu_1$ : mean of Baseline

$\mu_2$ : mean of 288

Difference:  $\mu_1 - \mu_2$

*Equal variances are assumed for this analysis.*

### Descriptive Statistics

Sample	N	Mean	StDev	SE Mean
Baseline	8	50.98	2.39	0.84
288	8	49.48	1.52	0.54

### Estimation for Difference

Difference	Pooled StDev	95% CI for Difference
1.50	2.00	(-0.65, 3.64)

### Test

Null hypothesis  $H_0: \mu_1 - \mu_2 = 0$

Alternative hypothesis  $H_1: \mu_1 - \mu_2 \neq 0$

T-Value	DF	P-Value
1.50	14	0.156



232 vs. 260 (Yield)

## Two-Sample T-Test and CI: 232, 260

### Method

$\mu_1$ : mean of 232

$\mu_2$ : mean of 260

Difference:  $\mu_1 - \mu_2$

*Equal variances are assumed for this analysis.*

### Descriptive Statistics

Sample	N	Mean	StDev	SE Mean
232	8	50.04	1.22	0.43
260	8	48.228	0.890	0.31

### Estimation for Difference

Difference	Pooled StDev	95% CI for Difference
1.811	1.066	(0.668, 2.954)

### Test

Null hypothesis  $H_0: \mu_1 - \mu_2 = 0$

Alternative hypothesis  $H_1: \mu_1 - \mu_2 \neq 0$

T-Value	DF	P-Value
3.40	14	0.004

232 vs. 288 (Yield)

## Two-Sample T-Test and CI: 232, 288

### Method

$\mu_1$ : mean of 232

$\mu_2$ : mean of 288

Difference:  $\mu_1 - \mu_2$

*Equal variances are assumed for this analysis.*

### Descriptive Statistics

Sample	N	Mean	StDev	SE Mean
232	8	50.04	1.22	0.43
288	8	49.48	1.52	0.54

### Estimation for Difference

Difference	Pooled StDev	95% CI for Difference
0.559	1.374	(-0.915, 2.032)

### Test

Null hypothesis  $H_0: \mu_1 - \mu_2 = 0$

Alternative hypothesis  $H_1: \mu_1 - \mu_2 \neq 0$

T-Value	DF	P-Value
0.81	14	0.430

260 vs. 288 (Yield)

## Two-Sample T-Test and CI: 260, 288

### Method

$\mu_1$ : mean of 260

$\mu_2$ : mean of 288

Difference:  $\mu_1 - \mu_2$

*Equal variances are assumed for this analysis.*

### Descriptive Statistics

Sample	N	Mean	StDev	SE Mean
260	8	48.228	0.890	0.31
288	8	49.48	1.52	0.54

### Estimation for Difference

Difference	Pooled StDev	95% CI for Difference
-1.252	1.243	(-2.585, 0.080)

### Test

Null hypothesis  $H_0: \mu_1 - \mu_2 = 0$

Alternative hypothesis  $H_1: \mu_1 - \mu_2 \neq 0$

T-Value	DF	P-Value
-2.02	14	0.063

## 232 Parallel vs. Perpendicular (Hardness)

### Two-Sample T-Test and CI: 232 Parallel, 232 Perpendicular

#### Method

$\mu_1$ : mean of 232 Parallel

$\mu_2$ : mean of 232 Perpendicular

Difference:  $\mu_1 - \mu_2$

*Equal variances are assumed for this analysis.*

#### Descriptive Statistics

Sample	N	Mean	StDev	SE Mean
232 Parallel	4	74.750	0.957	0.48
232 Perpendicular	4	77.000	0.816	0.41

#### Estimation for Difference

Difference	Pooled StDev	95% CI for Difference
-2.250	0.890	(-3.789, -0.711)

#### Test

Null hypothesis  $H_0: \mu_1 - \mu_2 = 0$

Alternative hypothesis  $H_1: \mu_1 - \mu_2 \neq 0$

T-Value	DF	P-Value
-3.58	6	0.012

## 260 Parallel vs. Perpendicular (Hardness)

### Two-Sample T-Test and CI: 260 Parallel, 260 Perpendicular

#### Method

$\mu_1$ : mean of 260 Parallel  
 $\mu_2$ : mean of 260 Perpendicular  
Difference:  $\mu_1 - \mu_2$

*Equal variances are assumed for this analysis.*

#### Descriptive Statistics

Sample	N	Mean	StDev	SE Mean
260 Parallel	4	74.750	0.500	0.25
260 Perpendicular	4	76.00	1.83	0.91

#### Estimation for Difference

Difference	Pooled StDev	95% CI for Difference
-1.250	1.339	(-3.566, 1.066)

#### Test

Null hypothesis  $H_0: \mu_1 - \mu_2 = 0$   
Alternative hypothesis  $H_1: \mu_1 - \mu_2 \neq 0$

T-Value	DF	P-Value
-1.32	6	0.235

## 288 Parallel vs. Perpendicular (Hardness)

### Two-Sample T-Test and CI: 288 Parallel, 288 Perpendicular

#### Method

$\mu_1$ : mean of 288 Parallel  
 $\mu_2$ : mean of 288 Perpendicular  
Difference:  $\mu_1 - \mu_2$

*Equal variances are assumed for this analysis.*

#### Descriptive Statistics

Sample	N	Mean	StDev	SE Mean
288 Parallel	4	75.00	1.41	0.71
288 Perpendicular	4	75.75	2.06	1.0

#### Estimation for Difference

Difference	Pooled StDev	95% CI for Difference
-0.75	1.77	(-3.81, 2.31)

#### Test

Null hypothesis  $H_0: \mu_1 - \mu_2 = 0$   
Alternative hypothesis  $H_1: \mu_1 - \mu_2 \neq 0$

T-Value	DF	P-Value
-0.60	6	0.570

Baseline vs. 232 (Hardness)

## Two-Sample T-Test and CI: Baseline, 232

### Method

$\mu_1$ : mean of Baseline

$\mu_2$ : mean of 232

Difference:  $\mu_1 - \mu_2$

*Equal variances are assumed for this analysis.*

### Descriptive Statistics

Sample	N	Mean	StDev	SE Mean
Baseline	8	75.63	1.25	0.44
232	8	75.88	1.46	0.52

### Estimation for Difference

Difference	Pooled StDev	95% CI for Difference
-0.250	1.356	(-1.704, 1.204)

### Test

Null hypothesis  $H_0: \mu_1 - \mu_2 = 0$

Alternative hypothesis  $H_1: \mu_1 - \mu_2 \neq 0$

T-Value	DF	P-Value
-0.37	14	0.718

Baseline vs. 260 (Hardness)

## Two-Sample T-Test and CI: Baseline, 260

### Method

$\mu_1$ : mean of Baseline

$\mu_2$ : mean of 260

Difference:  $\mu_1 - \mu_2$

*Equal variances are assumed for this analysis.*

### Descriptive Statistics

Sample	N	Mean	StDev	SE Mean
Baseline	8	75.63	1.25	0.44
260	8	75.38	1.41	0.50

### Estimation for Difference

Difference	Pooled StDev	95% CI for Difference
0.250	1.330	(-1.176, 1.676)

### Test

Null hypothesis  $H_0: \mu_1 - \mu_2 = 0$

Alternative hypothesis  $H_1: \mu_1 - \mu_2 \neq 0$

T-Value	DF	P-Value
0.38	14	0.713



Baseline vs. 288 (Hardness)

## Two-Sample T-Test and CI: Baseline, 288

### Method

$\mu_1$ : mean of Baseline

$\mu_2$ : mean of 288

Difference:  $\mu_1 - \mu_2$

*Equal variances are assumed for this analysis.*

### Descriptive Statistics

Sample	N	Mean	StDev	SE Mean
Baseline	8	75.63	1.25	0.44
288	8	75.38	1.69	0.60

### Estimation for Difference

Difference	Pooled StDev	95% CI for Difference
0.250	1.482	(-1.339, 1.839)

### Test

Null hypothesis  $H_0: \mu_1 - \mu_2 = 0$

Alternative hypothesis  $H_1: \mu_1 - \mu_2 \neq 0$

T-Value	DF	P-Value
0.34	14	0.741

232 vs. 260 (Hardness)

## Two-Sample T-Test and CI: 232, 260

### Method

$\mu_1$ : mean of 232

$\mu_2$ : mean of 260

Difference:  $\mu_1 - \mu_2$

*Equal variances are assumed for this analysis.*

### Descriptive Statistics

Sample	N	Mean	StDev	SE Mean
232	8	75.88	1.46	0.52
260	8	75.38	1.41	0.50

### Estimation for Difference

Difference	Pooled StDev	95% CI for Difference
0.500	1.433	(-1.037, 2.037)

### Test

Null hypothesis  $H_0: \mu_1 - \mu_2 = 0$

Alternative hypothesis  $H_1: \mu_1 - \mu_2 \neq 0$

T-Value	DF	P-Value
0.70	14	0.497

232 vs. 288 (Hardness)

## Two-Sample T-Test and CI: 232, 288

### Method

$\mu_1$ : mean of 232

$\mu_2$ : mean of 288

Difference:  $\mu_1 - \mu_2$

*Equal variances are assumed for this analysis.*

### Descriptive Statistics

Sample	N	Mean	StDev	SE Mean
232	8	75.88	1.46	0.52
288	8	75.38	1.69	0.60

### Estimation for Difference

Difference	Pooled StDev	95% CI for Difference
0.500	1.575	(-1.190, 2.190)

### Test

Null hypothesis  $H_0: \mu_1 - \mu_2 = 0$

Alternative hypothesis  $H_1: \mu_1 - \mu_2 \neq 0$

T-Value	DF	P-Value
0.63	14	0.536

260 vs. 288 (Hardness)

## Two-Sample T-Test and CI: 260, 288

### Method

$\mu_1$ : mean of 260

$\mu_2$ : mean of 288

Difference:  $\mu_1 - \mu_2$

*Equal variances are assumed for this analysis.*

### Descriptive Statistics

Sample	N	Mean	StDev	SE Mean
260	8	75.38	1.41	0.50
288	8	75.38	1.69	0.60

### Estimation for Difference

Difference	Pooled StDev	95% CI for Difference
0.000	1.553	(-1.665, 1.665)

### Test

Null hypothesis  $H_0: \mu_1 - \mu_2 = 0$

Alternative hypothesis  $H_1: \mu_1 - \mu_2 \neq 0$

T-Value	DF	P-Value
0.00	14	1.0000000000000000

## Temperature Control Stats for ER308L

150 Parallel vs. Perpendicular (UTS)

### Two-Sample T-Test and CI: 150 Per, 150 Par

#### Method

$\mu_1$ : mean of 150 Per

$\mu_2$ : mean of 150 Par

Difference:  $\mu_1 - \mu_2$

*Equal variances are assumed for this analysis.*

#### Descriptive Statistics

Sample	N	Mean	StDev	SE Mean
150 Per	4	79.33	1.46	0.73
150 Par	4	82.22	1.15	0.58

#### Estimation for Difference

Difference	Pooled StDev	95% CI for Difference
-2.885	1.316	(-5.162, -0.608)

#### Test

Null hypothesis  $H_0: \mu_1 - \mu_2 = 0$

Alternative hypothesis  $H_1: \mu_1 - \mu_2 \neq 0$

T-Value	DF	P-Value
-3.10	6	0.021

## 205 Parallel vs. Perpendicular (UTS)

### Two-Sample T-Test and CI: 205 Per, 205 Par

#### Method

$\mu_1$ : mean of 205 Per

$\mu_2$ : mean of 205 Par

Difference:  $\mu_1 - \mu_2$

*Equal variances are assumed for this analysis.*

#### Descriptive Statistics

Sample	N	Mean	StDev	SE Mean
205 Per	4	80.17	1.59	0.79
205 Par	4	82.66	1.87	0.94

#### Estimation for Difference

Difference	Pooled StDev	95% CI for Difference
-2.50	1.74	(-5.50, 0.51)

#### Test

Null hypothesis  $H_0: \mu_1 - \mu_2 = 0$

Alternative hypothesis  $H_1: \mu_1 - \mu_2 \neq 0$

T-Value	DF	P-Value
-2.03	6	0.088

## 260 Parallel vs. Perpendicular (UTS)

### Two-Sample T-Test and CI: 260 Per, 260 Par

#### Method

$\mu_1$ : mean of 260 Per

$\mu_2$ : mean of 260 Par

Difference:  $\mu_1 - \mu_2$

*Equal variances are assumed for this analysis.*

#### Descriptive Statistics

Sample	N	Mean	StDev	SE Mean
260 Per	4	81.063	0.852	0.43
260 Par	4	86.26	1.81	0.91

#### Estimation for Difference

Difference	Pooled StDev	95% CI for Difference
-5.20	1.42	(-7.65, -2.75)

#### Test

Null hypothesis  $H_0: \mu_1 - \mu_2 = 0$

Alternative hypothesis  $H_1: \mu_1 - \mu_2 \neq 0$

T-Value	DF	P-Value
-5.19	6	0.002

Baseline vs. 150 Parallel (UTS)

## Two-Sample T-Test and CI: 150 Par, Baseline Par

### Method

$\mu_1$ : mean of 150 Par

$\mu_2$ : mean of Baseline Par

Difference:  $\mu_1 - \mu_2$

*Equal variances are assumed for this analysis.*

### Descriptive Statistics

Sample	N	Mean	StDev	SE Mean
150 Par	4	82.22	1.15	0.58
Baseline Par	4	89.463	0.433	0.22

### Estimation for Difference

Difference	Pooled StDev	95% CI for Difference
-7.244	0.871	(-8.751, -5.738)

### Test

Null hypothesis  $H_0: \mu_1 - \mu_2 = 0$

Alternative hypothesis  $H_1: \mu_1 - \mu_2 \neq 0$

T-Value	DF	P-Value
-11.77	6	0.0000228



Baseline vs. 205 Parallel (UTS)

## Two-Sample T-Test and CI: 205 Par, Baseline Par

### Method

$\mu_1$ : mean of 205 Par

$\mu_2$ : mean of Baseline Par

Difference:  $\mu_1 - \mu_2$

*Equal variances are assumed for this analysis.*

### Descriptive Statistics

Sample	N	Mean	StDev	SE Mean
205 Par	4	82.66	1.87	0.94
Baseline Par	4	89.463	0.433	0.22

### Estimation for Difference

Difference	Pooled StDev	95% CI for Difference
-6.798	1.359	(-9.149, -4.447)

### Test

Null hypothesis  $H_0: \mu_1 - \mu_2 = 0$

Alternative hypothesis  $H_1: \mu_1 - \mu_2 \neq 0$

T-Value	DF	P-Value
-7.08	6	0.0003996

Baseline vs. 260 Parallel (UTS)

## Two-Sample T-Test and CI: 260 Par, Baseline Par

### Method

$\mu_1$ : mean of 260 Par

$\mu_2$ : mean of Baseline Par

Difference:  $\mu_1 - \mu_2$

*Equal variances are assumed for this analysis.*

### Descriptive Statistics

Sample	N	Mean	StDev	SE Mean
260 Par	4	86.26	1.81	0.91
Baseline Par	4	89.463	0.433	0.22

### Estimation for Difference

Difference	Pooled StDev	95% CI for Difference
-3.203	1.318	(-5.482, -0.923)

### Test

Null hypothesis  $H_0: \mu_1 - \mu_2 = 0$

Alternative hypothesis  $H_1: \mu_1 - \mu_2 \neq 0$

T-Value	DF	P-Value
-3.44	6	0.014

150 Parallel vs. 205 Parallel (UTS)

## Two-Sample T-Test and CI: 150 Par, 205 Par

### Method

$\mu_1$ : mean of 150 Par

$\mu_2$ : mean of 205 Par

Difference:  $\mu_1 - \mu_2$

*Equal variances are assumed for this analysis.*

### Descriptive Statistics

Sample	N	Mean	StDev	SE Mean
150 Par	4	82.22	1.15	0.58
205 Par	4	82.66	1.87	0.94

### Estimation for Difference

Difference	Pooled StDev	95% CI for Difference
-0.45	1.55	(-3.14, 2.24)

### Test

Null hypothesis  $H_0: \mu_1 - \mu_2 = 0$

Alternative hypothesis  $H_1: \mu_1 - \mu_2 \neq 0$

T-Value	DF	P-Value
-0.41	6	0.699

150 Parallel vs. 260 Parallel (UTS)

## Two-Sample T-Test and CI: 150 Par, 260 Par

### Method

$\mu_1$ : mean of 150 Par

$\mu_2$ : mean of 260 Par

Difference:  $\mu_1 - \mu_2$

*Equal variances are assumed for this analysis.*

### Descriptive Statistics

Sample	N	Mean	StDev	SE Mean
150 Par	4	82.22	1.15	0.58
260 Par	4	86.26	1.81	0.91

### Estimation for Difference

Difference	Pooled StDev	95% CI for Difference
-4.04	1.52	(-6.67, -1.41)

### Test

Null hypothesis  $H_0: \mu_1 - \mu_2 = 0$

Alternative hypothesis  $H_1: \mu_1 - \mu_2 \neq 0$

T-Value	DF	P-Value
-3.76	6	0.009

205 Parallel vs. 260 Parallel (UTS)

## Two-Sample T-Test and CI: 205 Par, 260 Par

### Method

$\mu_1$ : mean of 205 Par

$\mu_2$ : mean of 260 Par

Difference:  $\mu_1 - \mu_2$

*Equal variances are assumed for this analysis.*

### Descriptive Statistics

Sample	N	Mean	StDev	SE Mean
205 Par	4	82.66	1.87	0.94
260 Par	4	86.26	1.81	0.91

### Estimation for Difference

Difference	Pooled StDev	95% CI for Difference
-3.60	1.84	(-6.78, -0.41)

### Test

Null hypothesis  $H_0: \mu_1 - \mu_2 = 0$

Alternative hypothesis  $H_1: \mu_1 - \mu_2 \neq 0$

T-Value	DF	P-Value
-2.76	6	0.033

## Baseline Perpendicular vs. 150 Perpendicular (UTS)

### Two-Sample T-Test and CI: 150 Per, Baseline Per

#### Method

$\mu_1$ : mean of 150 Per  
 $\mu_2$ : mean of Baseline Per  
Difference:  $\mu_1 - \mu_2$

*Equal variances are assumed for this analysis.*

#### Descriptive Statistics

Sample	N	Mean	StDev	SE Mean
150 Per	4	79.33	1.46	0.73
Baseline Per	4	86.78	1.50	0.75

#### Estimation for Difference

Difference	Pooled StDev	95% CI for Difference
-7.45	1.48	(-10.02, -4.89)

#### Test

Null hypothesis  $H_0: \mu_1 - \mu_2 = 0$   
Alternative hypothesis  $H_1: \mu_1 - \mu_2 \neq 0$

T-Value	DF	P-Value
-7.11	6	0.0003898

## Baseline Perpendicular vs. 205 Perpendicular (UTS)

### Two-Sample T-Test and CI: 205 Per, Baseline Per

#### Method

$\mu_1$ : mean of 205 Per

$\mu_2$ : mean of Baseline Per

Difference:  $\mu_1 - \mu_2$

*Equal variances are assumed for this analysis.*

#### Descriptive Statistics

Sample	N	Mean	StDev	SE Mean
205 Per	4	80.17	1.59	0.79
Baseline Per	4	86.78	1.50	0.75

#### Estimation for Difference

Difference	Pooled StDev	95% CI for Difference
-6.62	1.55	(-9.29, -3.94)

#### Test

Null hypothesis  $H_0: \mu_1 - \mu_2 = 0$

Alternative hypothesis  $H_1: \mu_1 - \mu_2 \neq 0$

T-Value	DF	P-Value
-6.05	6	0.00092

## Baseline Perpendicular vs. 260 Perpendicular (UTS)

### Two-Sample T-Test and CI: 260 Per, Baseline Per

#### Method

$\mu_1$ : mean of 260 Per

$\mu_2$ : mean of Baseline Per

Difference:  $\mu_1 - \mu_2$

*Equal variances are assumed for this analysis.*

#### Descriptive Statistics

Sample	N	Mean	StDev	SE Mean
260 Per	4	81.063	0.852	0.43
Baseline Per	4	86.78	1.50	0.75

#### Estimation for Difference

Difference	Pooled StDev	95% CI for Difference
-5.722	1.222	(-7.837, -3.607)

#### Test

Null hypothesis  $H_0: \mu_1 - \mu_2 = 0$

Alternative hypothesis  $H_1: \mu_1 - \mu_2 \neq 0$

T-Value	DF	P-Value
-6.62	6	0.00057



150 Perpendicular vs. 205 Perpendicular (UTS)

## Two-Sample T-Test and CI: 150 Per, 205 Per

### Method

$\mu_1$ : mean of 150 Per

$\mu_2$ : mean of 205 Per

Difference:  $\mu_1 - \mu_2$

*Equal variances are assumed for this analysis.*

### Descriptive Statistics

Sample	N	Mean	StDev	SE Mean
150 Per	4	79.33	1.46	0.73
205 Per	4	80.17	1.59	0.79

### Estimation for Difference

Difference	Pooled StDev	95% CI for Difference
-0.83	1.53	(-3.47, 1.80)

### Test

Null hypothesis  $H_0: \mu_1 - \mu_2 = 0$

Alternative hypothesis  $H_1: \mu_1 - \mu_2 \neq 0$

T-Value	DF	P-Value
-0.77	6	0.468

150 Perpendicular vs. 260 Perpendicular (UTS)

## Two-Sample T-Test and CI: 150 Per, 260 Per

### Method

$\mu_1$ : mean of 150 Per

$\mu_2$ : mean of 260 Per

Difference:  $\mu_1 - \mu_2$

*Equal variances are assumed for this analysis.*

### Descriptive Statistics

Sample	N	Mean	StDev	SE Mean
150 Per	4	79.33	1.46	0.73
260 Per	4	81.063	0.852	0.43

### Estimation for Difference

Difference	Pooled StDev	95% CI for Difference
-1.730	1.196	(-3.799, 0.340)

### Test

Null hypothesis  $H_0: \mu_1 - \mu_2 = 0$

Alternative hypothesis  $H_1: \mu_1 - \mu_2 \neq 0$

T-Value	DF	P-Value
-2.05	6	0.087

205 Perpendicular vs. 260 Perpendicular (UTS)

## Two-Sample T-Test and CI: 205 Per, 260 Per

### Method

$\mu_1$ : mean of 205 Per

$\mu_2$ : mean of 260 Per

Difference:  $\mu_1 - \mu_2$

*Equal variances are assumed for this analysis.*

### Descriptive Statistics

Sample	N	Mean	StDev	SE Mean
205 Per	4	80.17	1.59	0.79
260 Per	4	81.063	0.852	0.43

### Estimation for Difference

Difference	Pooled StDev	95% CI for Difference
-0.895	1.274	(-3.099, 1.309)

### Test

Null hypothesis  $H_0: \mu_1 - \mu_2 = 0$

Alternative hypothesis  $H_1: \mu_1 - \mu_2 \neq 0$

T-Value	DF	P-Value
-0.99	6	0.359

## 150 Parallel vs. Perpendicular (Yield)

### Two-Sample T-Test and CI: 150 Per, 150 Par

#### Method

$\mu_1$ : mean of 150 Per

$\mu_2$ : mean of 150 Par

Difference:  $\mu_1 - \mu_2$

*Equal variances are assumed for this analysis.*

#### Descriptive Statistics

Sample	N	Mean	StDev	SE Mean
150 Per	4	54.633	0.715	0.36
150 Par	4	54.717	0.742	0.37

#### Estimation for Difference

Difference	Pooled StDev	95% CI for Difference
-0.085	0.729	(-1.345, 1.176)

#### Test

Null hypothesis  $H_0: \mu_1 - \mu_2 = 0$

Alternative hypothesis  $H_1: \mu_1 - \mu_2 \neq 0$

T-Value	DF	P-Value
-0.16	6	0.875

## 205 Parallel vs. Perpendicular (Yield)

### Two-Sample T-Test and CI: 205 Per, 205 Par

#### Method

$\mu_1$ : mean of 205 Per

$\mu_2$ : mean of 205 Par

Difference:  $\mu_1 - \mu_2$

*Equal variances are assumed for this analysis.*

#### Descriptive Statistics

Sample	N	Mean	StDev	SE Mean
205 Per	4	54.00	1.56	0.78
205 Par	4	56.276	0.384	0.19

#### Estimation for Difference

Difference	Pooled StDev	95% CI for Difference
-2.278	1.135	(-4.242, -0.314)

#### Test

Null hypothesis  $H_0: \mu_1 - \mu_2 = 0$

Alternative hypothesis  $H_1: \mu_1 - \mu_2 \neq 0$

T-Value	DF	P-Value
-2.84	6	0.030

## 260 Parallel vs. Perpendicular (Yield)

### Two-Sample T-Test and CI: 260 Per, 260 Par

#### Method

$\mu_1$ : mean of 260 Per

$\mu_2$ : mean of 260 Par

Difference:  $\mu_1 - \mu_2$

*Equal variances are assumed for this analysis.*

#### Descriptive Statistics

Sample	N	Mean	StDev	SE Mean
260 Per	4	54.107	0.563	0.28
260 Par	4	57.56	1.22	0.61

#### Estimation for Difference

Difference	Pooled StDev	95% CI for Difference
-3.454	0.950	(-5.097, -1.811)

#### Test

Null hypothesis  $H_0: \mu_1 - \mu_2 = 0$

Alternative hypothesis  $H_1: \mu_1 - \mu_2 \neq 0$

T-Value	DF	P-Value
-5.14	6	0.002

## Baseline Parallel vs. 150 Parallel (Yield)

### Two-Sample T-Test and CI: 150 Par, Baseline Par

#### Method

$\mu_1$ : mean of 150 Par  
 $\mu_2$ : mean of Baseline Par  
Difference:  $\mu_1 - \mu_2$

*Equal variances are assumed for this analysis.*

#### Descriptive Statistics

Sample	N	Mean	StDev	SE Mean
150 Par	4	54.717	0.742	0.37
Baseline Par	4	53.398	0.797	0.40

#### Estimation for Difference

Difference	Pooled StDev	95% CI for Difference
1.320	0.770	(-0.013, 2.652)

#### Test

Null hypothesis  $H_0: \mu_1 - \mu_2 = 0$   
Alternative hypothesis  $H_1: \mu_1 - \mu_2 \neq 0$

T-Value	DF	P-Value
2.42	6	0.052

## Baseline Parallel vs. 205 Parallel (Yield)

### Two-Sample T-Test and CI: 205 Par, Baseline Par

#### Method

$\mu_1$ : mean of 205 Par

$\mu_2$ : mean of Baseline Par

Difference:  $\mu_1 - \mu_2$

*Equal variances are assumed for this analysis.*

#### Descriptive Statistics

Sample	N	Mean	StDev	SE Mean
205 Par	4	56.276	0.384	0.19
Baseline Par	4	53.398	0.797	0.40

#### Estimation for Difference

Difference	Pooled StDev	95% CI for Difference
2.879	0.626	(1.796, 3.962)

#### Test

Null hypothesis  $H_0: \mu_1 - \mu_2 = 0$

Alternative hypothesis  $H_1: \mu_1 - \mu_2 \neq 0$

T-Value	DF	P-Value
6.51	6	0.00063



## Baseline Parallel vs. 260 Parallel (Yield)

### Two-Sample T-Test and CI: 260 Par, Baseline Par

#### Method

$\mu_1$ : mean of 260 Par

$\mu_2$ : mean of Baseline Par

Difference:  $\mu_1 - \mu_2$

*Equal variances are assumed for this analysis.*

#### Descriptive Statistics

Sample	N	Mean	StDev	SE Mean
260 Par	4	57.56	1.22	0.61
Baseline Par	4	53.398	0.797	0.40

#### Estimation for Difference

Difference	Pooled StDev	95% CI for Difference
4.164	1.030	(2.381, 5.946)

#### Test

Null hypothesis  $H_0: \mu_1 - \mu_2 = 0$

Alternative hypothesis  $H_1: \mu_1 - \mu_2 \neq 0$

T-Value	DF	P-Value
5.72	6	0.00124

150 Parallel vs. 205 Parallel (Yield)

## Two-Sample T-Test and CI: 150 Par, 205 Par

### Method

$\mu_1$ : mean of 150 Par

$\mu_2$ : mean of 205 Par

Difference:  $\mu_1 - \mu_2$

*Equal variances are assumed for this analysis.*

### Descriptive Statistics

Sample	N	Mean	StDev	SE Mean
150 Par	4	54.717	0.742	0.37
205 Par	4	56.276	0.384	0.19

### Estimation for Difference

Difference	Pooled StDev	95% CI for Difference
-1.559	0.591	(-2.582, -0.536)

### Test

Null hypothesis  $H_0: \mu_1 - \mu_2 = 0$

Alternative hypothesis  $H_1: \mu_1 - \mu_2 \neq 0$

T-Value	DF	P-Value
-3.73	6	0.010

150 Parallel vs. 260 Parallel (Yield)

## Two-Sample T-Test and CI: 150 Par, 260 Par

### Method

$\mu_1$ : mean of 150 Par

$\mu_2$ : mean of 260 Par

Difference:  $\mu_1 - \mu_2$

*Equal variances are assumed for this analysis.*

### Descriptive Statistics

Sample	N	Mean	StDev	SE Mean
150 Par	4	54.717	0.742	0.37
260 Par	4	57.56	1.22	0.61

### Estimation for Difference

Difference	Pooled StDev	95% CI for Difference
-2.844	1.010	(-4.591, -1.097)

### Test

Null hypothesis  $H_0: \mu_1 - \mu_2 = 0$

Alternative hypothesis  $H_1: \mu_1 - \mu_2 \neq 0$

T-Value	DF	P-Value
-3.98	6	0.0072

205 Parallel vs. 260 Parallel (Yield)

## Two-Sample T-Test and CI: 205 Par, 260 Par

### Method

$\mu_1$ : mean of 205 Par

$\mu_2$ : mean of 260 Par

Difference:  $\mu_1 - \mu_2$

*Equal variances are assumed for this analysis.*

### Descriptive Statistics

Sample	N	Mean	StDev	SE Mean
205 Par	4	56.276	0.384	0.19
260 Par	4	57.56	1.22	0.61

### Estimation for Difference

Difference	Pooled StDev	95% CI for Difference
-1.285	0.904	(-2.849, 0.279)

### Test

Null hypothesis  $H_0: \mu_1 - \mu_2 = 0$

Alternative hypothesis  $H_1: \mu_1 - \mu_2 \neq 0$

T-Value	DF	P-Value
-2.01	6	0.091

Baseline Perpendicular vs. 150 Perpendicular (Yield)

## Two-Sample T-Test and CI: 150 Per, Baseline Per

### Method

$\mu_1$ : mean of 150 Per

$\mu_2$ : mean of Baseline Per

Difference:  $\mu_1 - \mu_2$

*Equal variances are assumed for this analysis.*

### Descriptive Statistics

Sample	N	Mean	StDev	SE Mean
150 Per	4	54.633	0.715	0.36
Baseline Per	4	50.527	0.676	0.34

### Estimation for Difference

Difference	Pooled StDev	95% CI for Difference
4.105	0.695	(2.902, 5.308)

### Test

Null hypothesis  $H_0: \mu_1 - \mu_2 = 0$

Alternative hypothesis  $H_1: \mu_1 - \mu_2 \neq 0$

T-Value	DF	P-Value
8.35	6	0.0001605

## Baseline Perpendicular vs. 205 Perpendicular (Yield)

### Two-Sample T-Test and CI: 205 Per, Baseline Per

#### Method

$\mu_1$ : mean of 205 Per

$\mu_2$ : mean of Baseline Per

Difference:  $\mu_1 - \mu_2$

*Equal variances are assumed for this analysis.*

#### Descriptive Statistics

Sample	N	Mean	StDev	SE Mean
205 Per	4	54.00	1.56	0.78
Baseline Per	4	50.527	0.676	0.34

#### Estimation for Difference

Difference	Pooled StDev	95% CI for Difference
3.471	1.201	(1.392, 5.550)

#### Test

Null hypothesis  $H_0: \mu_1 - \mu_2 = 0$

Alternative hypothesis  $H_1: \mu_1 - \mu_2 \neq 0$

T-Value	DF	P-Value
4.09	6	0.0065

## Baseline Perpendicular vs. 260 Perpendicular (Yield)

### Two-Sample T-Test and CI: 260 Per, Baseline Per

#### Method

$\mu_1$ : mean of 260 Per

$\mu_2$ : mean of Baseline Per

Difference:  $\mu_1 - \mu_2$

*Equal variances are assumed for this analysis.*

#### Descriptive Statistics

Sample	N	Mean	StDev	SE Mean
260 Per	4	54.107	0.563	0.28
Baseline Per	4	50.527	0.676	0.34

#### Estimation for Difference

Difference	Pooled StDev	95% CI for Difference
3.580	0.622	(2.504, 4.656)

#### Test

Null hypothesis  $H_0: \mu_1 - \mu_2 = 0$

Alternative hypothesis  $H_1: \mu_1 - \mu_2 \neq 0$

T-Value	DF	P-Value
8.14	6	0.0001847

150 Perpendicular vs. 205 Perpendicular (Yield)

## Two-Sample T-Test and CI: 150 Per, 205 Per

### Method

$\mu_1$ : mean of 150 Per

$\mu_2$ : mean of 205 Per

Difference:  $\mu_1 - \mu_2$

*Equal variances are assumed for this analysis.*

### Descriptive Statistics

Sample	N	Mean	StDev	SE Mean
150 Per	4	54.633	0.715	0.36
205 Per	4	54.00	1.56	0.78

### Estimation for Difference

Difference	Pooled StDev	95% CI for Difference
0.634	1.213	(-1.464, 2.732)

### Test

Null hypothesis  $H_0: \mu_1 - \mu_2 = 0$

Alternative hypothesis  $H_1: \mu_1 - \mu_2 \neq 0$

T-Value	DF	P-Value
0.74	6	0.487



150 Perpendicular vs. 260 Perpendicular (Yield)

## Two-Sample T-Test and CI: 150 Per, 260 Per

### Method

$\mu_1$ : mean of 150 Per

$\mu_2$ : mean of 260 Per

Difference:  $\mu_1 - \mu_2$

*Equal variances are assumed for this analysis.*

### Descriptive Statistics

Sample	N	Mean	StDev	SE Mean
150 Per	4	54.633	0.715	0.36
260 Per	4	54.107	0.563	0.28

### Estimation for Difference

Difference	Pooled StDev	95% CI for Difference
0.526	0.643	(-0.587, 1.638)

### Test

Null hypothesis  $H_0: \mu_1 - \mu_2 = 0$

Alternative hypothesis  $H_1: \mu_1 - \mu_2 \neq 0$

T-Value	DF	P-Value
1.16	6	0.292

205 Perpendicular vs. 260 Perpendicular (Yield)

## Two-Sample T-Test and CI: 205 Per, 260 Per

### Method

$\mu_1$ : mean of 205 Per

$\mu_2$ : mean of 260 Per

Difference:  $\mu_1 - \mu_2$

*Equal variances are assumed for this analysis.*

### Descriptive Statistics

Sample	N	Mean	StDev	SE Mean
205 Per	4	54.00	1.56	0.78
260 Per	4	54.107	0.563	0.28

### Estimation for Difference

Difference	Pooled StDev	95% CI for Difference
-0.109	1.172	(-2.136, 1.919)

### Test

Null hypothesis  $H_0: \mu_1 - \mu_2 = 0$

Alternative hypothesis  $H_1: \mu_1 - \mu_2 \neq 0$

T-Value	DF	P-Value
-0.13	6	0.900

## 150 Parallel vs. Perpendicular (Hardness)

### Two-Sample T-Test and CI: 150 Par, 150 Per

#### Method

$\mu_1$ : mean of 150 Par

$\mu_2$ : mean of 150 Per

Difference:  $\mu_1 - \mu_2$

*Equal variances are assumed for this analysis.*

#### Descriptive Statistics

Sample	N	Mean	StDev	SE Mean
150 Par	4	82.625	0.750	0.38
150 Per	4	85.00	2.16	1.1

#### Estimation for Difference

Difference	Pooled StDev	95% CI for Difference
-2.38	1.62	(-5.17, 0.42)

#### Test

Null hypothesis  $H_0: \mu_1 - \mu_2 = 0$

Alternative hypothesis  $H_1: \mu_1 - \mu_2 \neq 0$

T-Value	DF	P-Value
-2.08	6	0.083

## 205 Parallel vs. Perpendicular (Hardness)

### Two-Sample T-Test and CI: 205 Per, 205 Par

#### Method

$\mu_1$ : mean of 205 Per

$\mu_2$ : mean of 205 Par

Difference:  $\mu_1 - \mu_2$

*Equal variances are assumed for this analysis.*

#### Descriptive Statistics

Sample	N	Mean	StDev	SE Mean
205 Per	4	90.750	0.645	0.32
205 Par	4	93.63	2.06	1.0

#### Estimation for Difference

Difference	Pooled StDev	95% CI for Difference
-2.88	1.52	(-5.51, -0.24)

#### Test

Null hypothesis  $H_0: \mu_1 - \mu_2 = 0$

Alternative hypothesis  $H_1: \mu_1 - \mu_2 \neq 0$

T-Value	DF	P-Value
-2.67	6	0.037

## 260 Parallel vs. Perpendicular (Hardness)

### Two-Sample T-Test and CI: 260 Per, 260 Par

#### Method

$\mu_1$ : mean of 260 Per

$\mu_2$ : mean of 260 Par

Difference:  $\mu_1 - \mu_2$

*Equal variances are assumed for this analysis.*

#### Descriptive Statistics

Sample	N	Mean	StDev	SE Mean
260 Per	4	92.500	0.577	0.29
260 Par	4	93.75	1.44	0.72

#### Estimation for Difference

Difference	Pooled StDev	95% CI for Difference
-1.250	1.099	(-3.152, 0.652)

#### Test

Null hypothesis  $H_0: \mu_1 - \mu_2 = 0$

Alternative hypothesis  $H_1: \mu_1 - \mu_2 \neq 0$

T-Value	DF	P-Value
-1.61	6	0.159

## Baseline Parallel vs. 150 Parallel (Hardness)

### Two-Sample T-Test and CI: 150 Par, Baseline Par

#### Method

$\mu_1$ : mean of 150 Par

$\mu_2$ : mean of Baseline Par

Difference:  $\mu_1 - \mu_2$

*Equal variances are assumed for this analysis.*

#### Descriptive Statistics

Sample	N	Mean	StDev	SE Mean
150 Par	4	82.625	0.750	0.38
Baseline Par	4	87.250	0.500	0.25

#### Estimation for Difference

Difference	Pooled StDev	95% CI for Difference
-4.625	0.637	(-5.728, -3.522)

#### Test

Null hypothesis  $H_0: \mu_1 - \mu_2 = 0$

Alternative hypothesis  $H_1: \mu_1 - \mu_2 \neq 0$

T-Value	DF	P-Value
-10.26	6	0.0000500

## Baseline Parallel vs. 205 Parallel (Hardness)

### Two-Sample T-Test and CI: 205 Par, Baseline Par

#### Method

$\mu_1$ : mean of 205 Par

$\mu_2$ : mean of Baseline Par

Difference:  $\mu_1 - \mu_2$

*Equal variances are assumed for this analysis.*

#### Descriptive Statistics

Sample	N	Mean	StDev	SE Mean
205 Par	4	93.63	2.06	1.0
Baseline Par	4	87.250	0.500	0.25

#### Estimation for Difference

Difference	Pooled StDev	95% CI for Difference
6.38	1.50	(3.79, 8.96)

#### Test

Null hypothesis  $H_0: \mu_1 - \mu_2 = 0$

Alternative hypothesis  $H_1: \mu_1 - \mu_2 \neq 0$

T-Value	DF	P-Value
6.02	6	0.00094

## Baseline Parallel vs. 260 Parallel (Hardness)

### Two-Sample T-Test and CI: 260 Par, Baseline Par

#### Method

$\mu_1$ : mean of 260 Par

$\mu_2$ : mean of Baseline Par

Difference:  $\mu_1 - \mu_2$

*Equal variances are assumed for this analysis.*

#### Descriptive Statistics

Sample	N	Mean	StDev	SE Mean
260 Par	4	93.75	1.44	0.72
Baseline Par	4	87.250	0.500	0.25

#### Estimation for Difference

Difference	Pooled StDev	95% CI for Difference
6.500	1.080	(4.631, 8.369)

#### Test

Null hypothesis  $H_0: \mu_1 - \mu_2 = 0$

Alternative hypothesis  $H_1: \mu_1 - \mu_2 \neq 0$

T-Value	DF	P-Value
8.51	6	0.0001441



150 Parallel vs. 205 Parallel (Hardness)

## Two-Sample T-Test and CI: 150 Par, 205 Par

### Method

$\mu_1$ : mean of 150 Par

$\mu_2$ : mean of 205 Par

Difference:  $\mu_1 - \mu_2$

*Equal variances are assumed for this analysis.*

### Descriptive Statistics

Sample	N	Mean	StDev	SE Mean
150 Par	4	82.625	0.750	0.38
205 Par	4	93.63	2.06	1.0

### Estimation for Difference

Difference	Pooled StDev	95% CI for Difference
-11.00	1.55	(-13.68, -8.32)

### Test

Null hypothesis  $H_0: \mu_1 - \mu_2 = 0$

Alternative hypothesis  $H_1: \mu_1 - \mu_2 \neq 0$

T-Value	DF	P-Value
-10.05	6	0.0000563

## 150 Parallel vs. 260 Parallel (Hardness)

### Two-Sample T-Test and CI: 150 Par, 260 Par

#### Method

$\mu_1$ : mean of 150 Par

$\mu_2$ : mean of 260 Par

Difference:  $\mu_1 - \mu_2$

*Equal variances are assumed for this analysis.*

#### Descriptive Statistics

Sample	N	Mean	StDev	SE Mean
150 Par	4	82.625	0.750	0.38
260 Par	4	93.75	1.44	0.72

#### Estimation for Difference

Difference	Pooled StDev	95% CI for Difference
-11.125	1.150	(-13.115, -9.135)

#### Test

Null hypothesis  $H_0: \mu_1 - \mu_2 = 0$

Alternative hypothesis  $H_1: \mu_1 - \mu_2 \neq 0$

T-Value	DF	P-Value
-13.68	6	0.0000095

## 205 Parallel vs. 260 Parallel (Hardness)

### Two-Sample T-Test and CI: 205 Par, 260 Par

#### Method

$\mu_1$ : mean of 205 Par

$\mu_2$ : mean of 260 Par

Difference:  $\mu_1 - \mu_2$

*Equal variances are assumed for this analysis.*

#### Descriptive Statistics

Sample	N	Mean	StDev	SE Mean
205 Par	4	93.63	2.06	1.0
260 Par	4	93.75	1.44	0.72

#### Estimation for Difference

Difference	Pooled StDev	95% CI for Difference
-0.13	1.78	(-3.20, 2.95)

#### Test

Null hypothesis  $H_0: \mu_1 - \mu_2 = 0$

Alternative hypothesis  $H_1: \mu_1 - \mu_2 \neq 0$

T-Value	DF	P-Value
-0.10	6	0.924

## Baseline Perpendicular vs. 150 Perpendicular (Hardness)

### Two-Sample T-Test and CI: 150 Per, Baseline Per

#### Method

$\mu_1$ : mean of 150 Per  
 $\mu_2$ : mean of Baseline Per  
Difference:  $\mu_1 - \mu_2$

*Equal variances are assumed for this analysis.*

#### Descriptive Statistics

Sample	N	Mean	StDev	SE Mean
150 Per	4	85.00	2.16	1.1
Baseline Per	4	85.250	0.645	0.32

#### Estimation for Difference

Difference	Pooled StDev	95% CI for Difference
-0.25	1.59	(-3.01, 2.51)

#### Test

Null hypothesis  $H_0: \mu_1 - \mu_2 = 0$   
Alternative hypothesis  $H_1: \mu_1 - \mu_2 \neq 0$

T-Value	DF	P-Value
-0.22	6	0.832

## Baseline Perpendicular vs. 205 Perpendicular (Hardness)

### Two-Sample T-Test and CI: 205 Per, Baseline Per

#### Method

$\mu_1$ : mean of 205 Per

$\mu_2$ : mean of Baseline Per

Difference:  $\mu_1 - \mu_2$

*Equal variances are assumed for this analysis.*

#### Descriptive Statistics

Sample	N	Mean	StDev	SE Mean
205 Per	4	90.750	0.645	0.32
Baseline Per	4	85.250	0.645	0.32

#### Estimation for Difference

Difference	Pooled StDev	95% CI for Difference
5.500	0.645	(4.383, 6.617)

#### Test

Null hypothesis  $H_0: \mu_1 - \mu_2 = 0$

Alternative hypothesis  $H_1: \mu_1 - \mu_2 \neq 0$

T-Value	DF	P-Value
12.05	6	0.0000198

## Baseline Perpendicular vs. 260 Perpendicular (Hardness)

### Two-Sample T-Test and CI: 260 Per, Baseline Per

#### Method

$\mu_1$ : mean of 260 Per

$\mu_2$ : mean of Baseline Per

Difference:  $\mu_1 - \mu_2$

*Equal variances are assumed for this analysis.*

#### Descriptive Statistics

Sample	N	Mean	StDev	SE Mean
260 Per	4	92.500	0.577	0.29
Baseline Per	4	85.250	0.645	0.32

#### Estimation for Difference

Difference	Pooled StDev	95% CI for Difference
7.250	0.612	(6.190, 8.310)

#### Test

Null hypothesis  $H_0: \mu_1 - \mu_2 = 0$

Alternative hypothesis  $H_1: \mu_1 - \mu_2 \neq 0$

T-Value	DF	P-Value
16.74	6	0.0000029

150 Perpendicular vs. 205 Perpendicular (Hardness)

## Two-Sample T-Test and CI: 150 Per, 205 Per

### Method

$\mu_1$ : mean of 150 Per

$\mu_2$ : mean of 205 Per

Difference:  $\mu_1 - \mu_2$

*Equal variances are assumed for this analysis.*

### Descriptive Statistics

Sample	N	Mean	StDev	SE Mean
150 Per	4	85.00	2.16	1.1
205 Per	4	90.750	0.645	0.32

### Estimation for Difference

Difference	Pooled StDev	95% CI for Difference
-5.75	1.59	(-8.51, -2.99)

### Test

Null hypothesis  $H_0: \mu_1 - \mu_2 = 0$

Alternative hypothesis  $H_1: \mu_1 - \mu_2 \neq 0$

T-Value	DF	P-Value
-5.10	6	0.00222

## 150 Perpendicular vs. 260 Perpendicular (Hardness)

### Two-Sample T-Test and CI: 150 Per, 260 Per

#### Method

$\mu_1$ : mean of 150 Per

$\mu_2$ : mean of 260 Per

Difference:  $\mu_1 - \mu_2$

*Equal variances are assumed for this analysis.*

#### Descriptive Statistics

Sample	N	Mean	StDev	SE Mean
150 Per	4	85.00	2.16	1.1
260 Per	4	92.500	0.577	0.29

#### Estimation for Difference

Difference	Pooled StDev	95% CI for Difference
-7.50	1.58	(-10.24, -4.76)

#### Test

Null hypothesis  $H_0: \mu_1 - \mu_2 = 0$

Alternative hypothesis  $H_1: \mu_1 - \mu_2 \neq 0$

T-Value	DF	P-Value
-6.71	6	0.00053



## 205 Perpendicular vs. 260 Perpendicular (Hardness)

### Two-Sample T-Test and CI: 205 Per, 260 Per

#### Method

$\mu_1$ : mean of 205 Per

$\mu_2$ : mean of 260 Per

Difference:  $\mu_1 - \mu_2$

*Equal variances are assumed for this analysis.*

#### Descriptive Statistics

Sample	N	Mean	StDev	SE Mean
205 Per	4	90.750	0.645	0.32
260 Per	4	92.500	0.577	0.29

#### Estimation for Difference

Difference	Pooled StDev	95% CI for Difference
-1.750	0.612	(-2.810, -0.690)

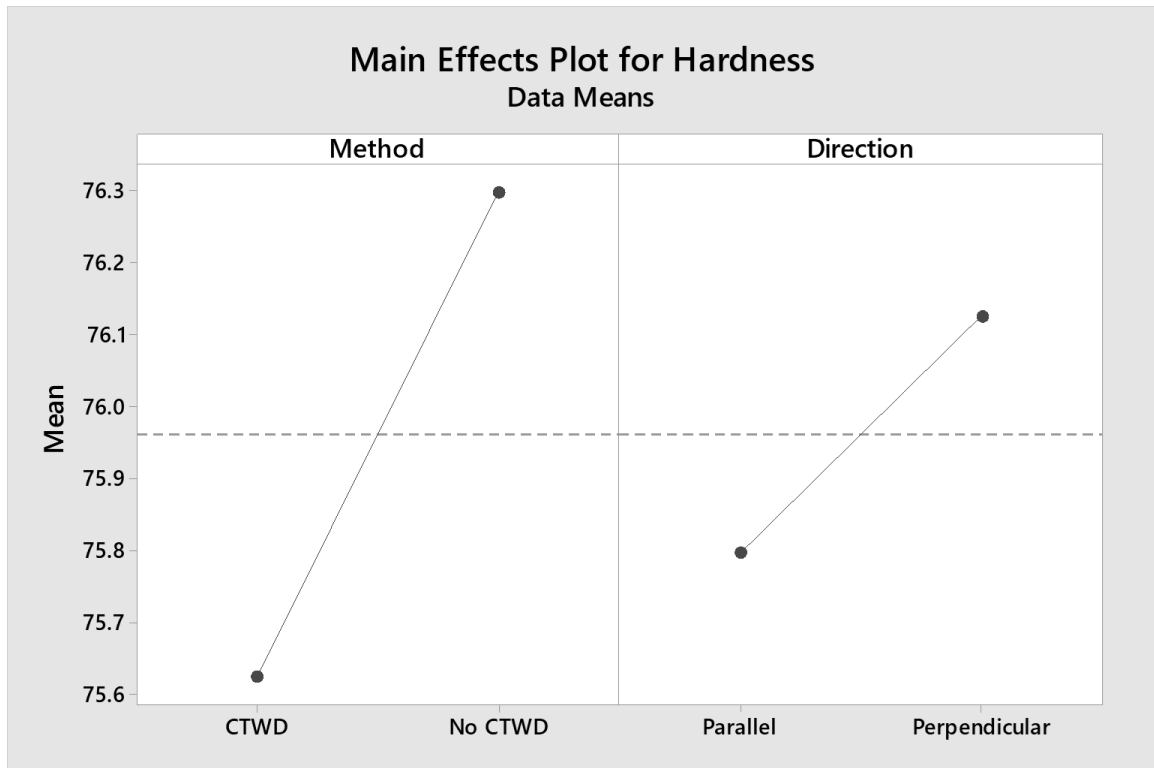
#### Test

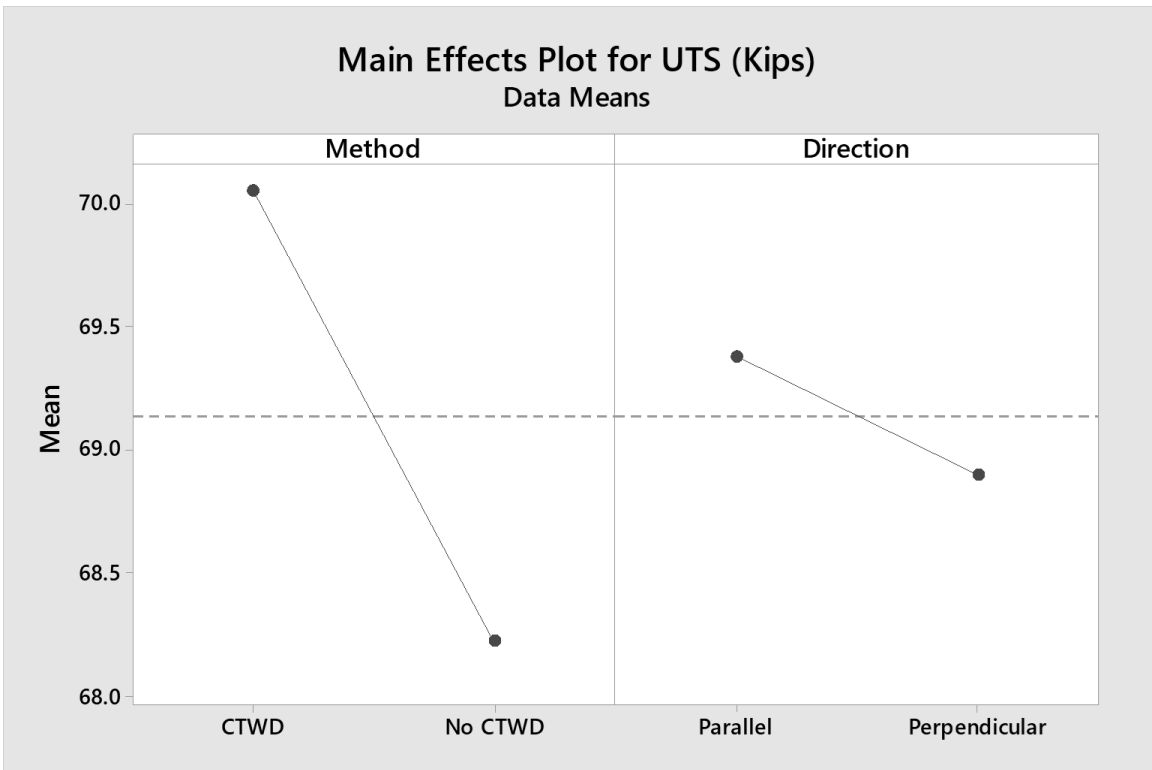
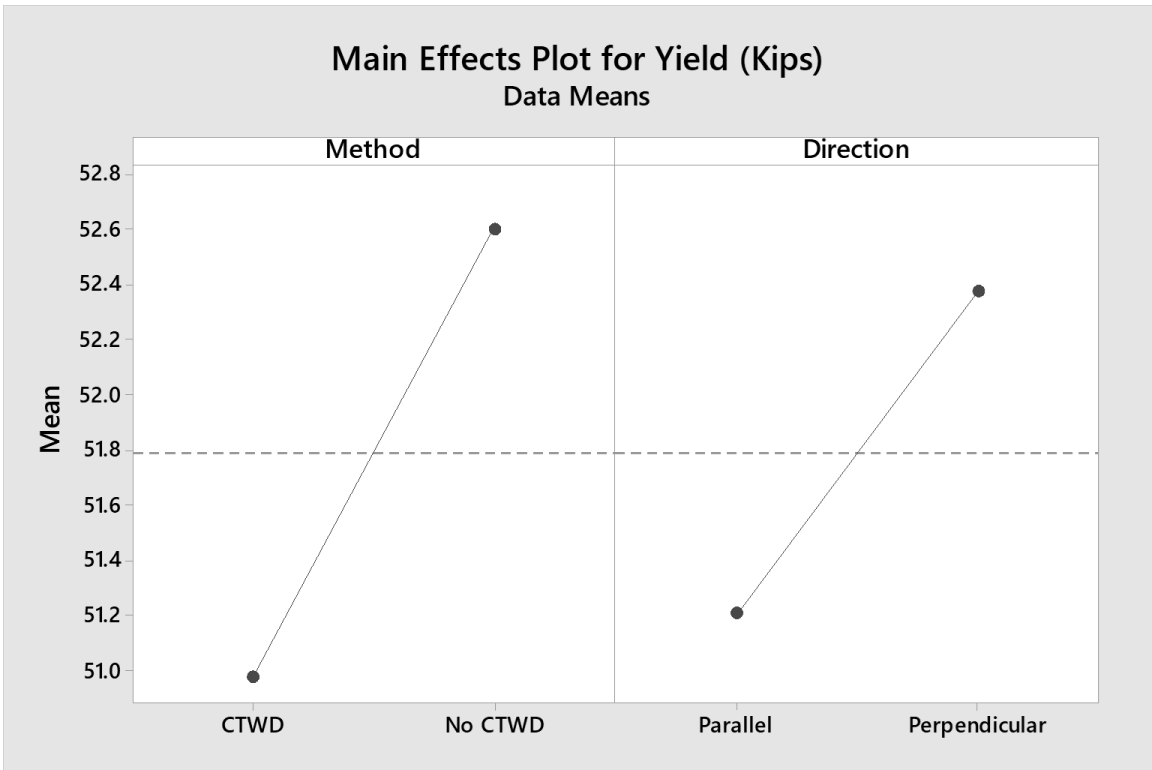
Null hypothesis  $H_0: \mu_1 - \mu_2 = 0$

Alternative hypothesis  $H_1: \mu_1 - \mu_2 \neq 0$

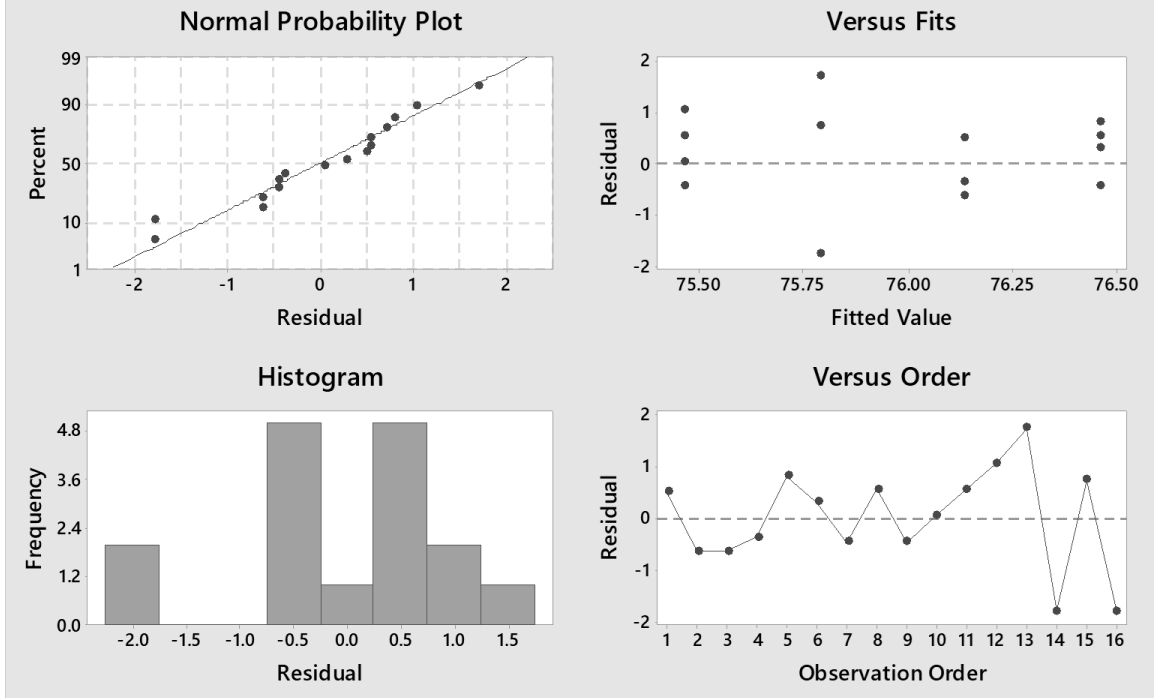
T-Value	DF	P-Value
-4.04	6	0.00679

# ER70S-6 ANOVA – CTWD

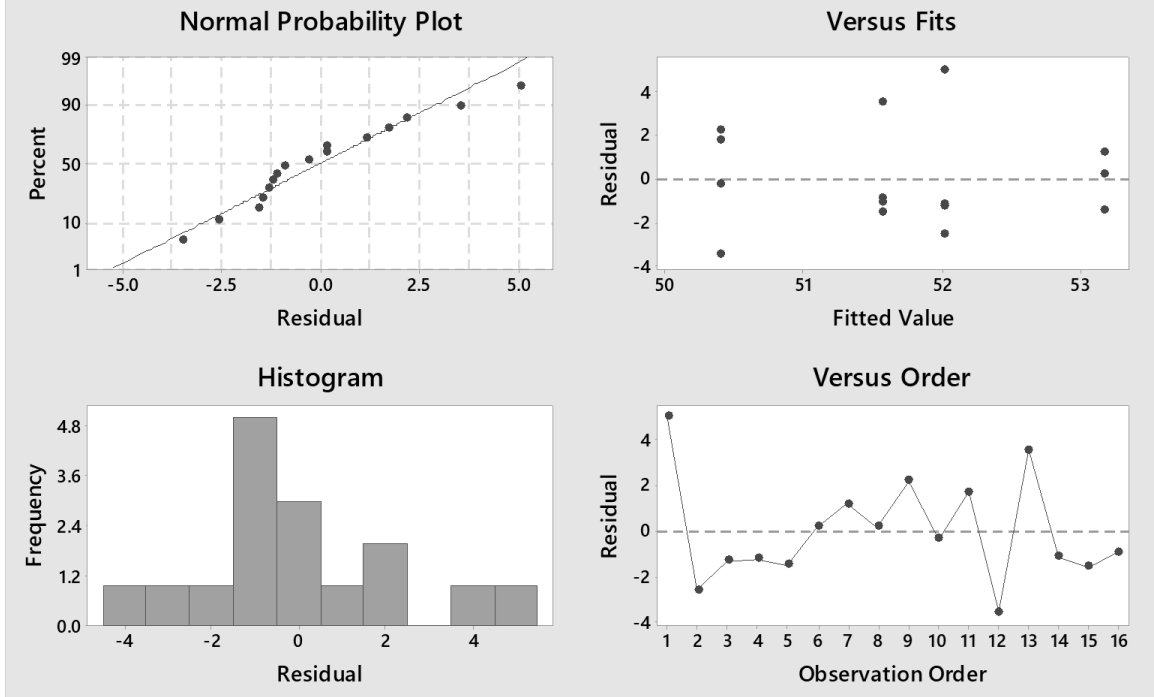




## Residual Plots for Hardness

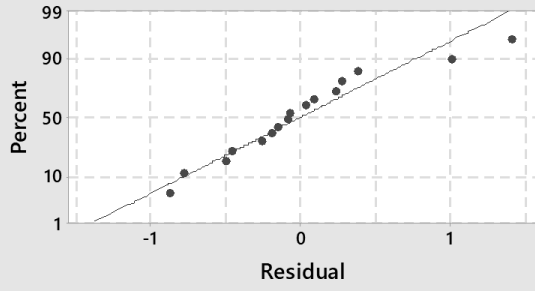


## Residual Plots for Yield (Kips)

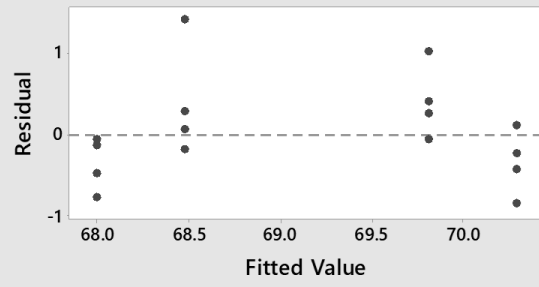


# Residual Plots for UTS (Kips)

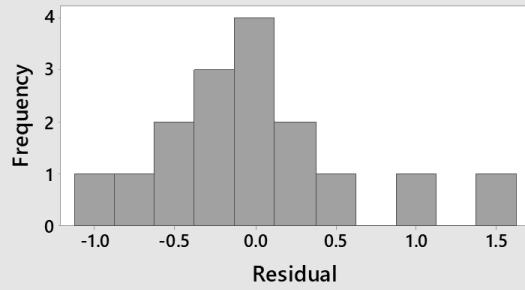
## Normal Probability Plot



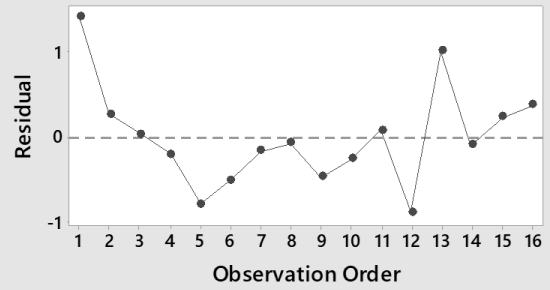
## Versus Fits



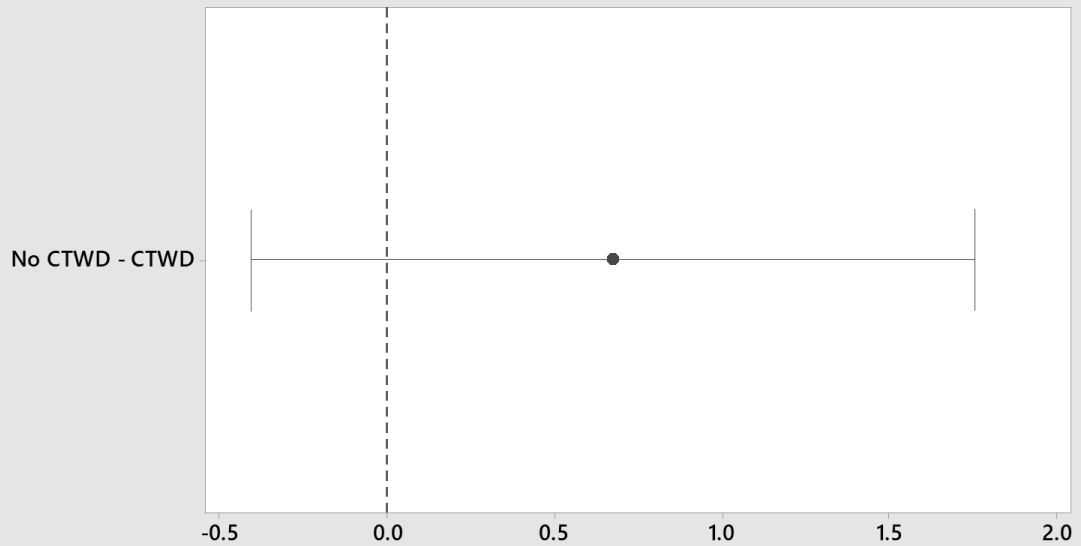
## Histogram



## Versus Order

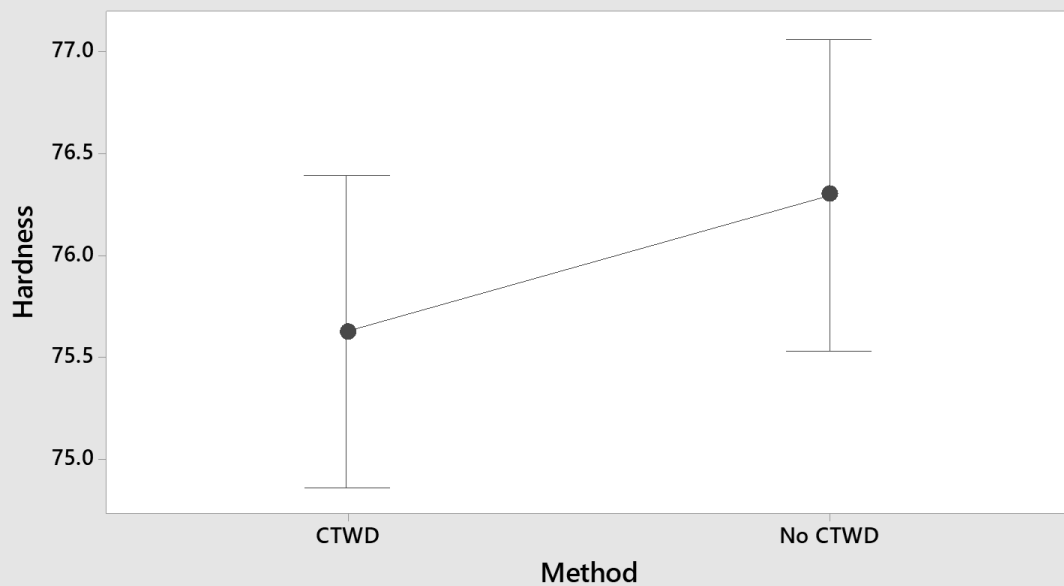


### Tukey Simultaneous 95% CIs Differences of Means for Hardness



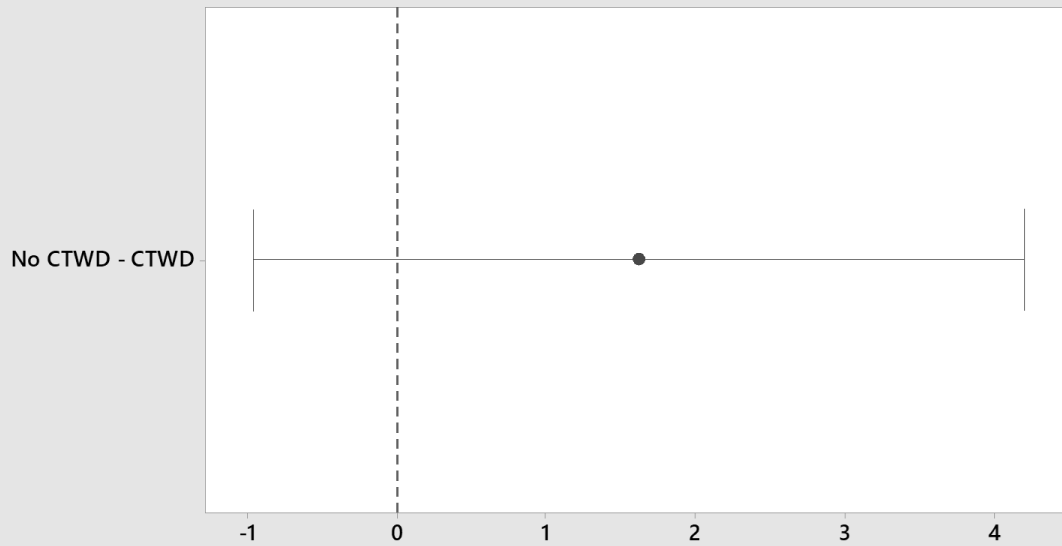
*If an interval does not contain zero, the corresponding means are significantly different.*

### Interval Plot of Hardness vs Method 95% CI for the Mean



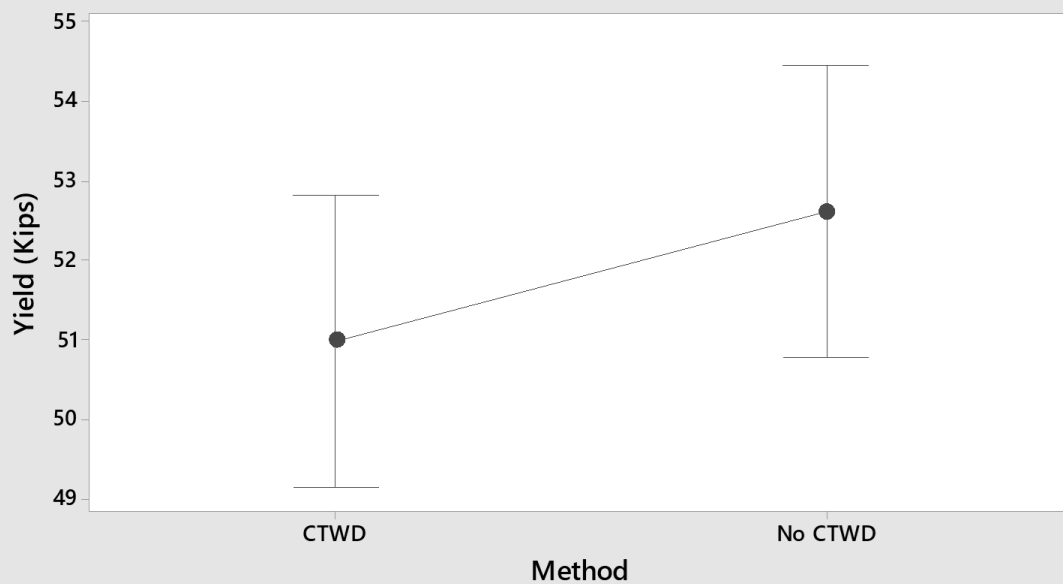
*The pooled standard deviation is used to calculate the intervals.*

### Tukey Simultaneous 95% CIs Differences of Means for Yield (Kips)



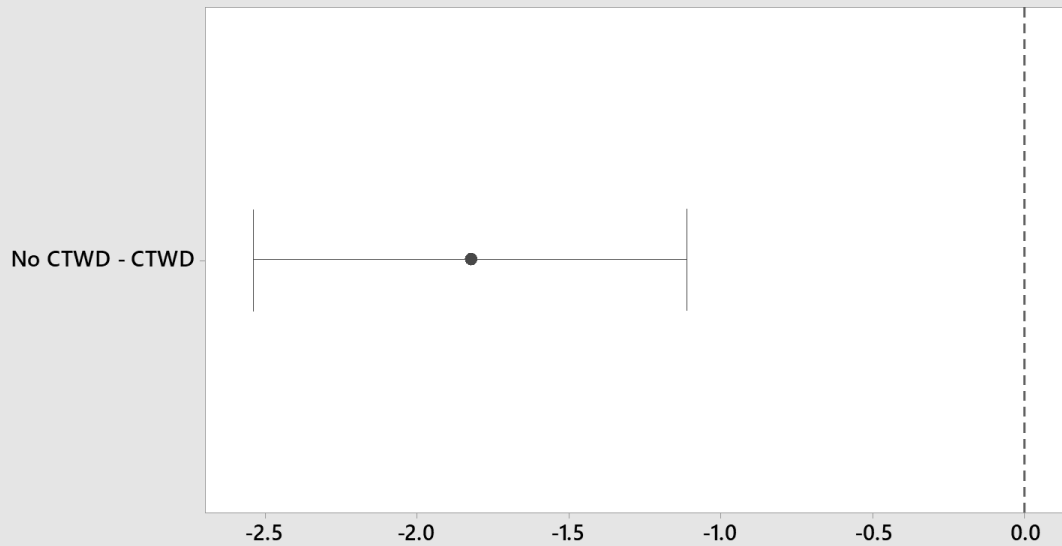
*If an interval does not contain zero, the corresponding means are significantly different.*

### Interval Plot of Yield (Kips) vs Method 95% CI for the Mean



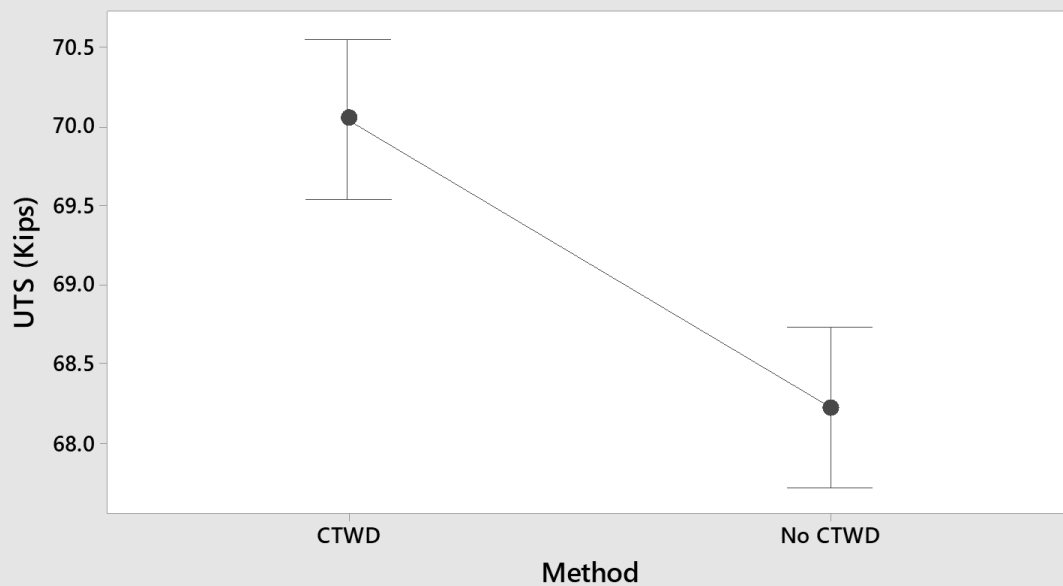
*The pooled standard deviation is used to calculate the intervals.*

### Tukey Simultaneous 95% CIs Differences of Means for UTS (Kips)



*If an interval does not contain zero, the corresponding means are significantly different.*

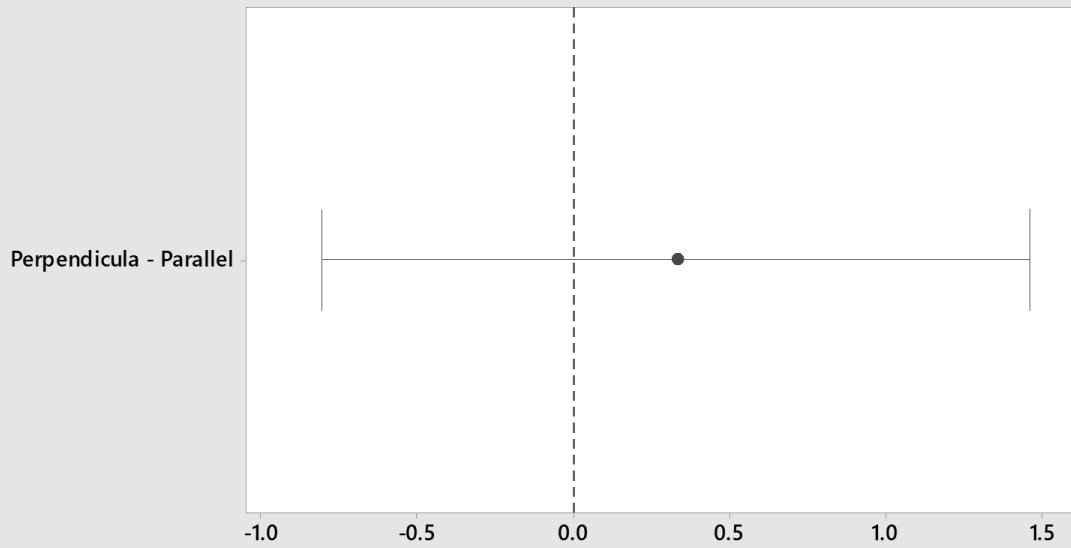
### Interval Plot of UTS (Kips) vs Method 95% CI for the Mean



*The pooled standard deviation is used to calculate the intervals.*

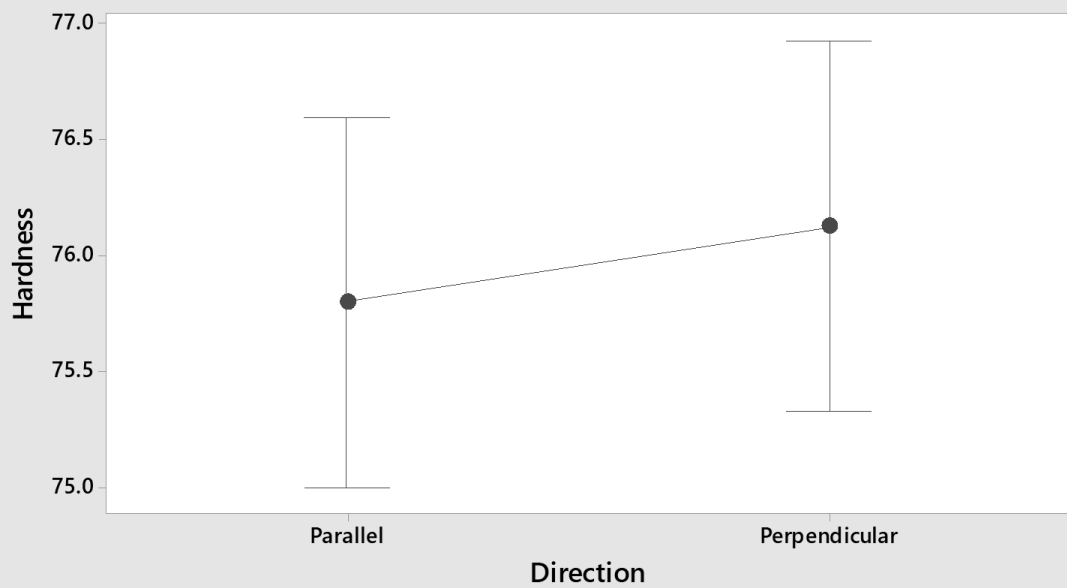


### Tukey Simultaneous 95% CIs Differences of Means for Hardness



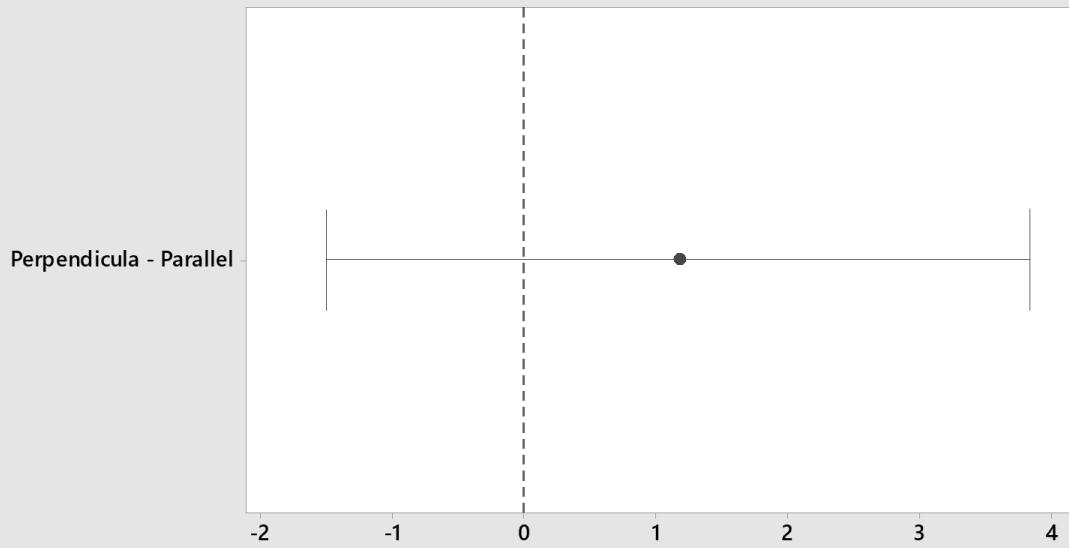
*If an interval does not contain zero, the corresponding means are significantly different.*

### Interval Plot of Hardness vs Direction 95% CI for the Mean



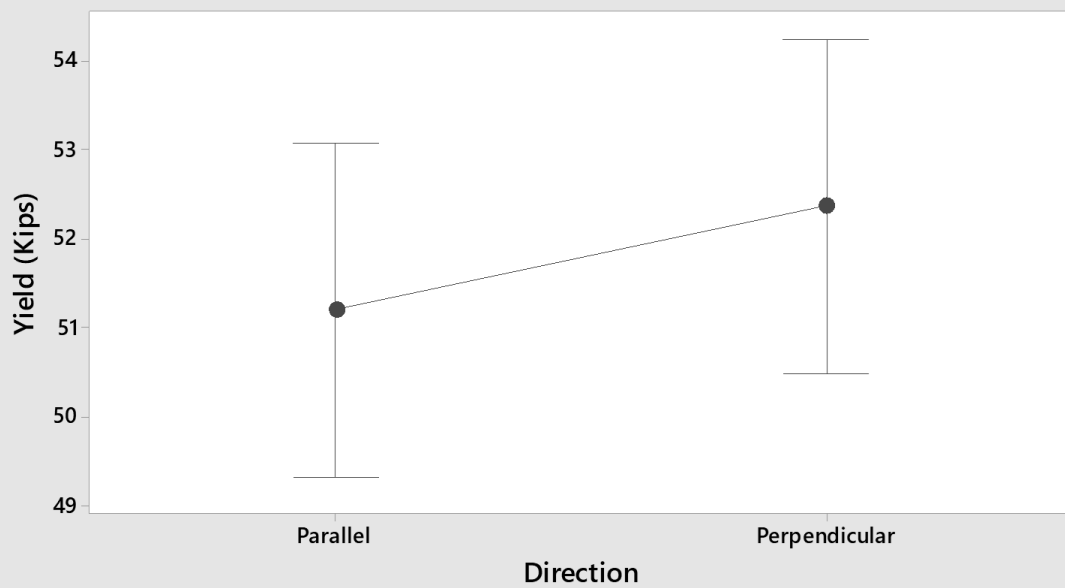
*The pooled standard deviation is used to calculate the intervals.*

### Tukey Simultaneous 95% CIs Differences of Means for Yield (Kips)



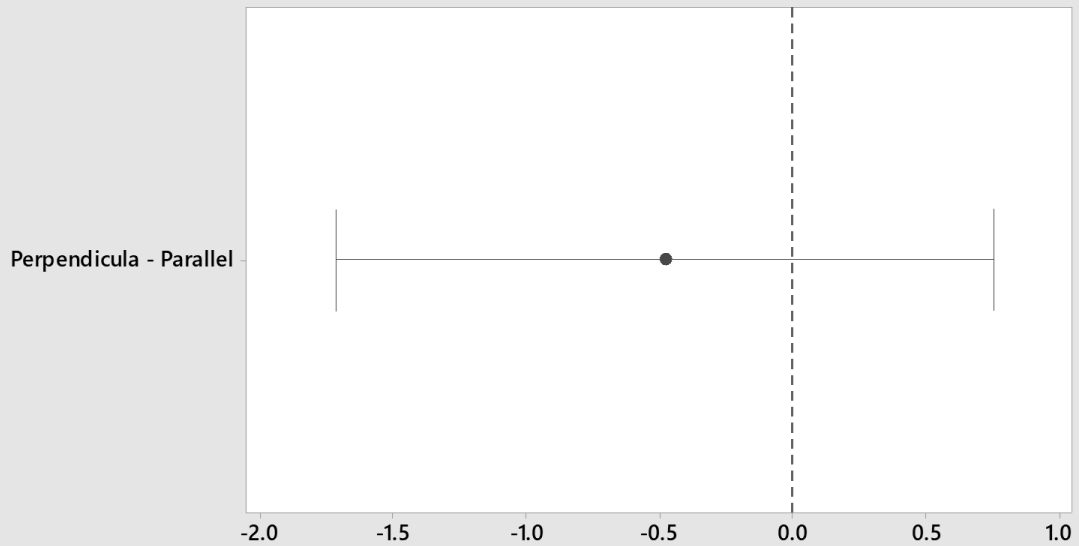
*If an interval does not contain zero, the corresponding means are significantly different.*

### Interval Plot of Yield (Kips) vs Direction 95% CI for the Mean



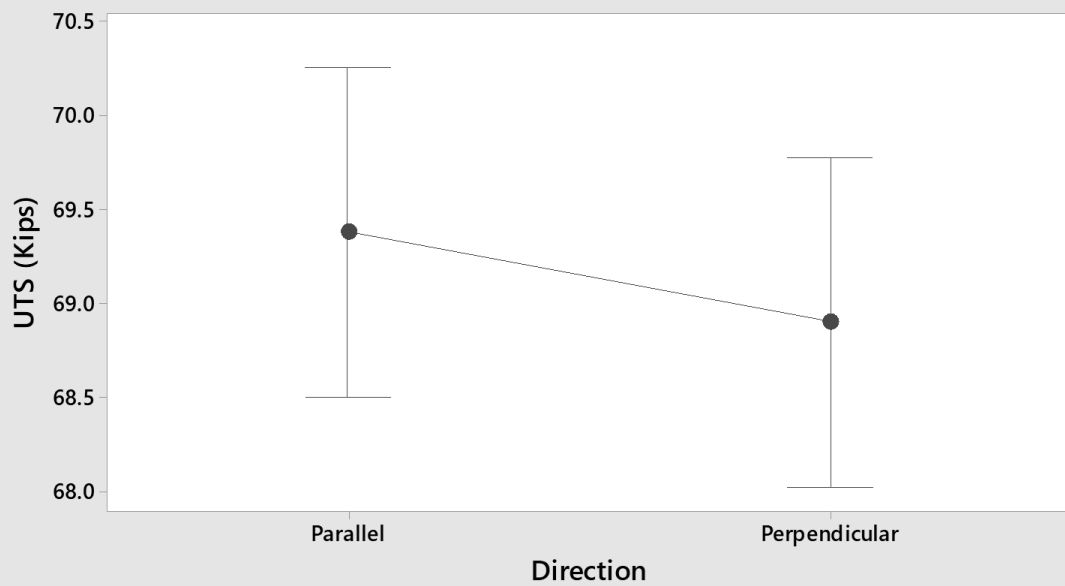
*The pooled standard deviation is used to calculate the intervals.*

### Tukey Simultaneous 95% CIs Differences of Means for UTS (Kips)



*If an interval does not contain zero, the corresponding means are significantly different.*

### Interval Plot of UTS (Kips) vs Direction 95% CI for the Mean



*The pooled standard deviation is used to calculate the intervals.*

### Analysis of Variance for Hardness

Source	DF	SS	MS	F	P
Method	1	1.8057	1.8057	1.70	0.215
Direction	1	0.4307	0.4307	0.41	0.535
Error	13	13.8174	1.0629		
Total	15	16.0537			

### Model Summary

S	R-sq	R-sq(adj)
1.03096	13.93%	0.69%

### Analysis of Variance for Yield (Kips)

Source	DF	SS	MS	F	P
Method	1	10.496	10.496	1.79	0.204
Direction	1	5.457	5.457	0.93	0.352
Error	13	76.167	5.859		
Total	15	92.120			

### Model Summary

S	R-sq	R-sq(adj)
2.42054	17.32%	4.60%

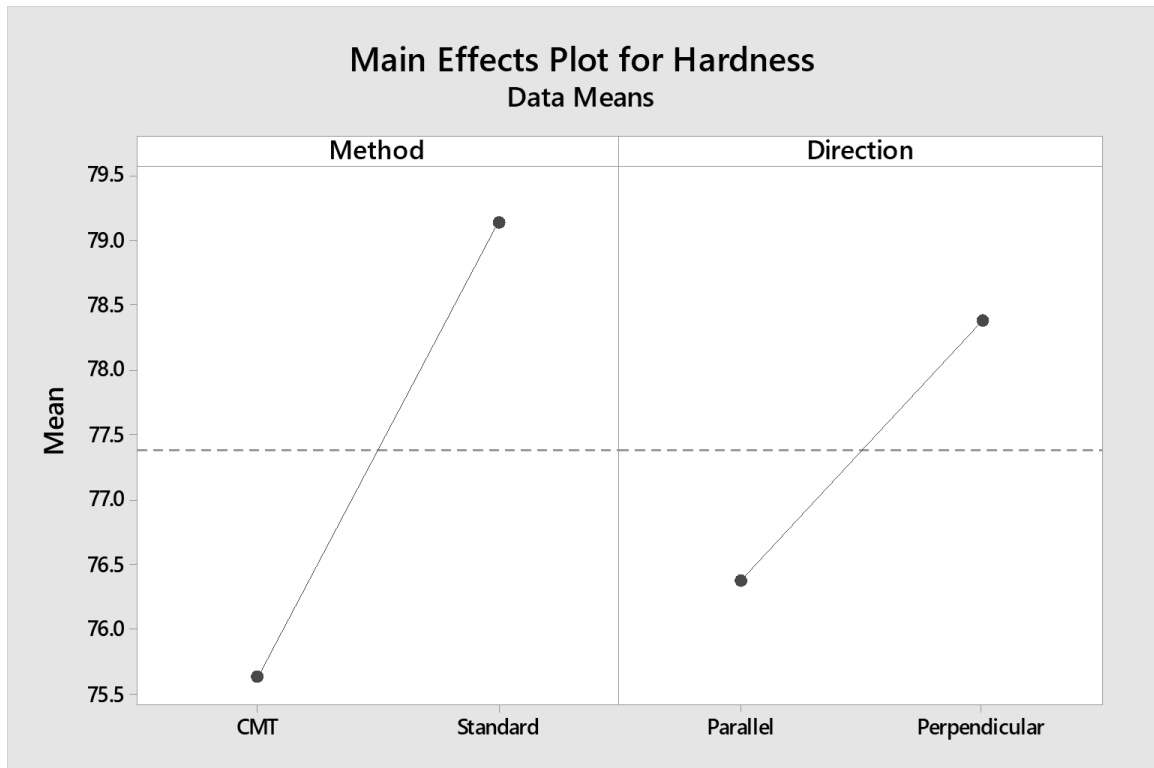
### Analysis of Variance for UTS (Kips)

Source	DF	SS	MS	F	P
Method	1	13.3551	13.3551	32.87	0.000
Direction	1	0.9264	0.9264	2.28	0.155
Error	13	5.2811	0.4062		
Total	15	19.5626			

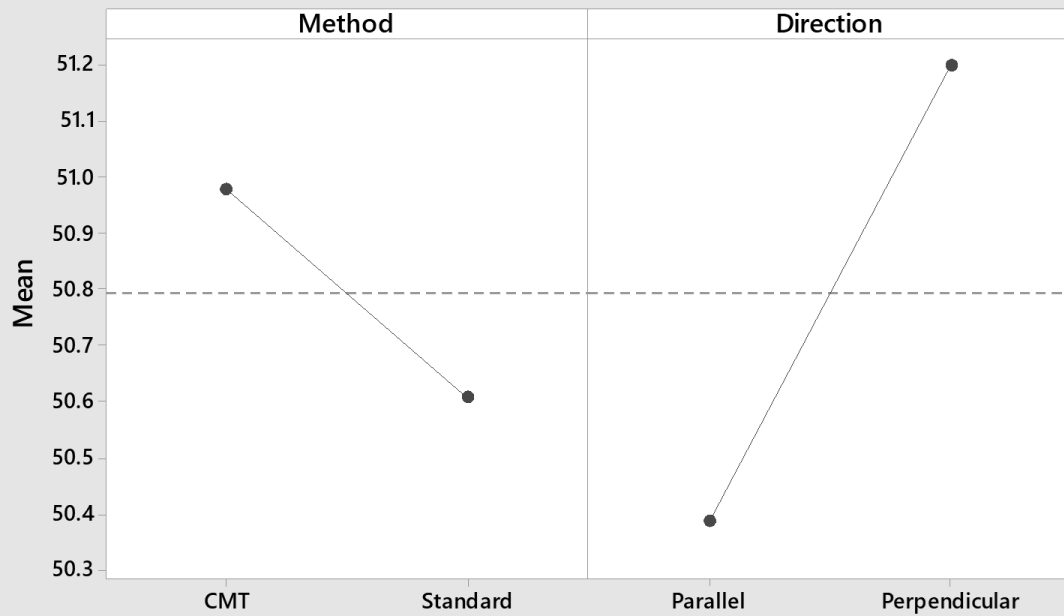
### Model Summary

S	R-sq	R-sq(adj)
0.637370	73.00%	68.85%

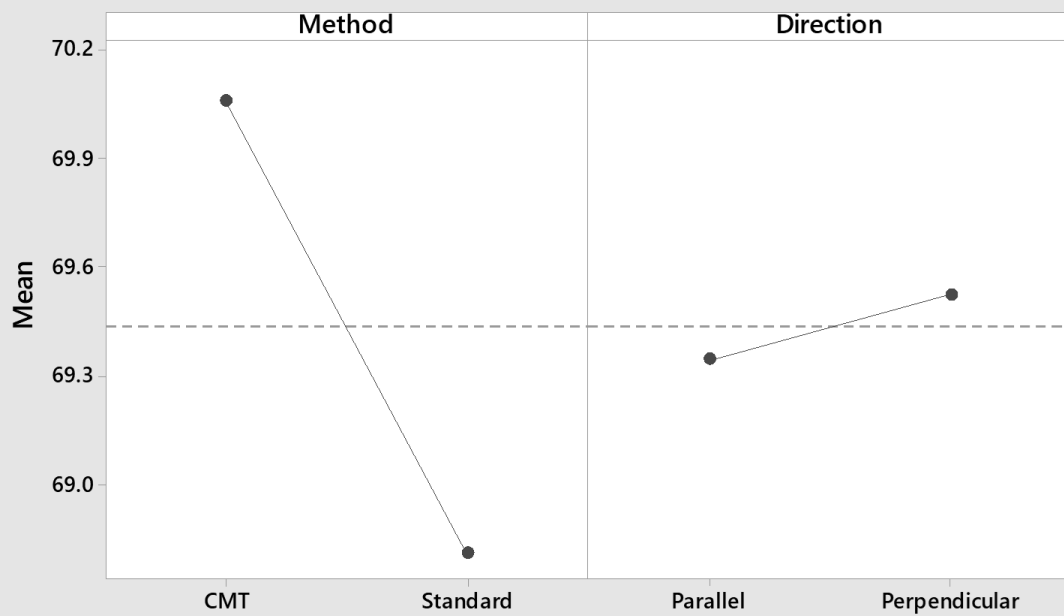
# ER70S-6 ANOVA – CMT



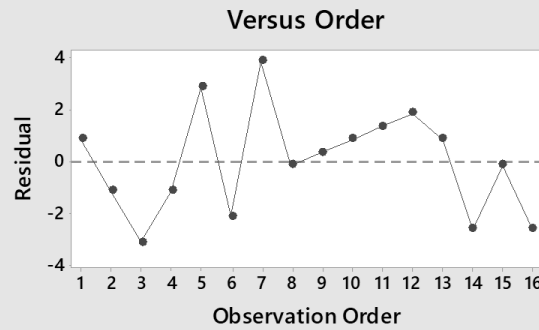
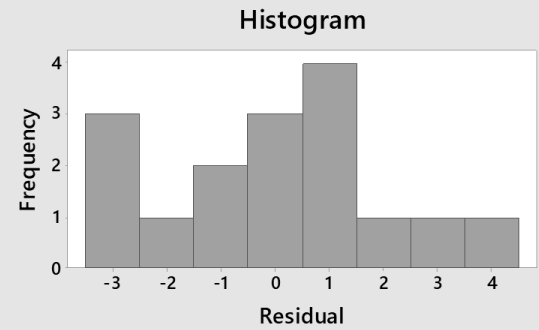
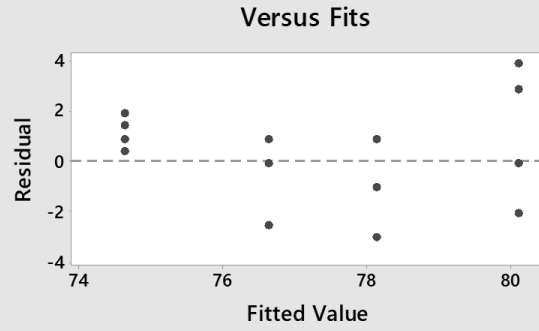
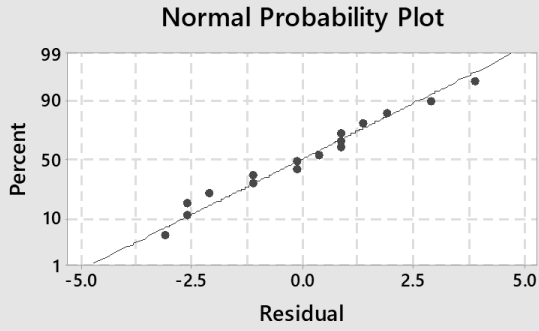
**Main Effects Plot for Yield (Kips)**  
Data Means



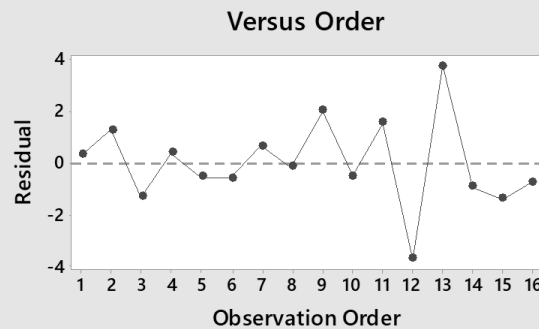
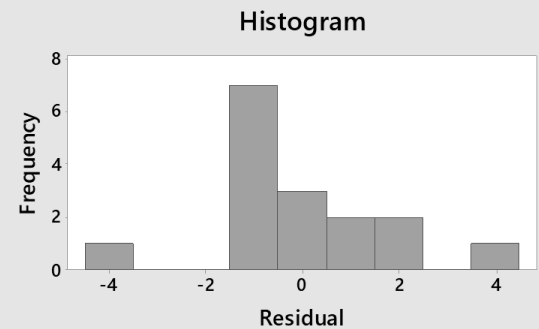
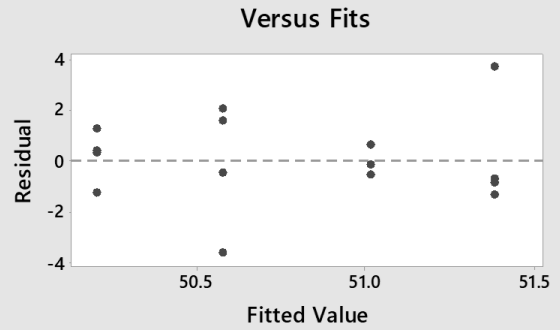
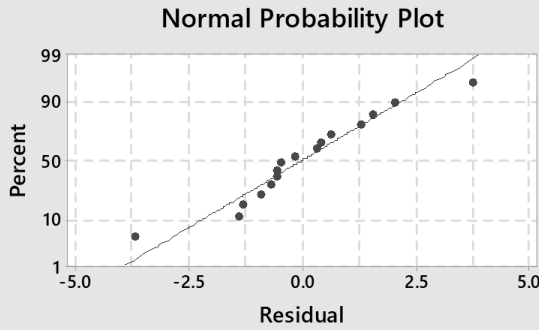
**Main Effects Plot for UTS (Kips)**  
Data Means



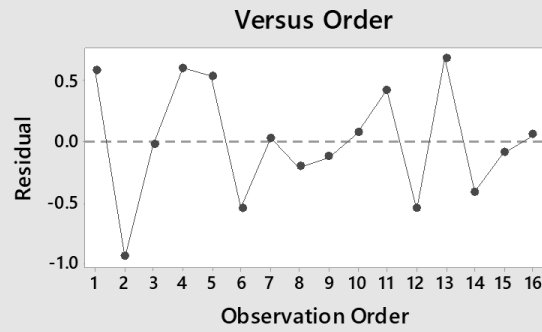
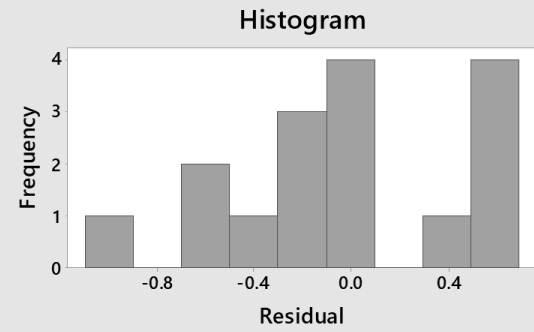
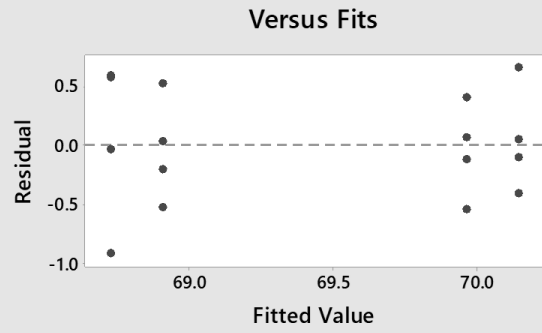
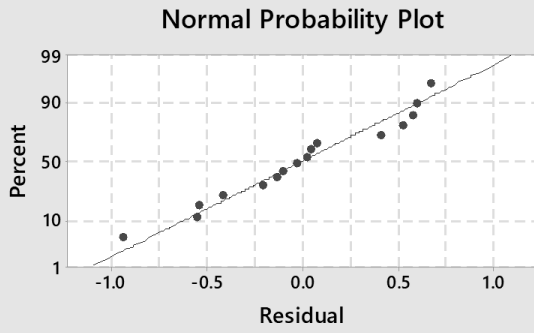
## Residual Plots for Hardness



## Residual Plots for Yield (Kips)

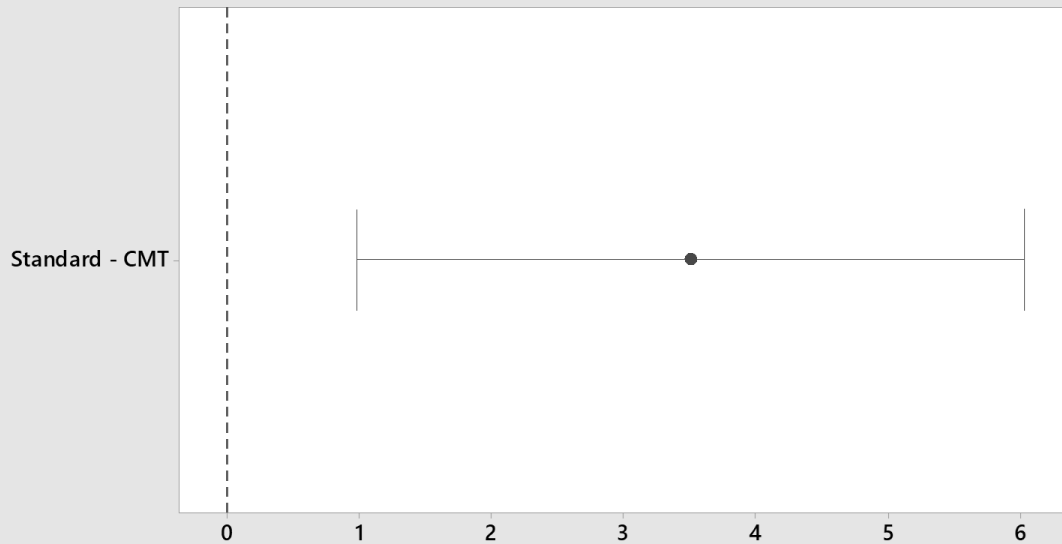


### Residual Plots for UTS (Kips)



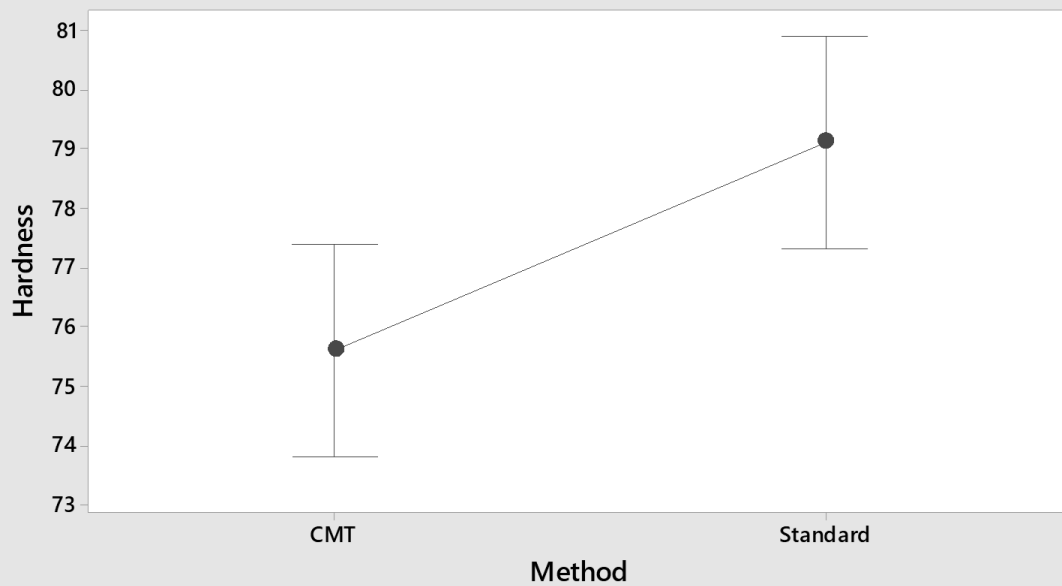


### Tukey Simultaneous 95% CIs Differences of Means for Hardness



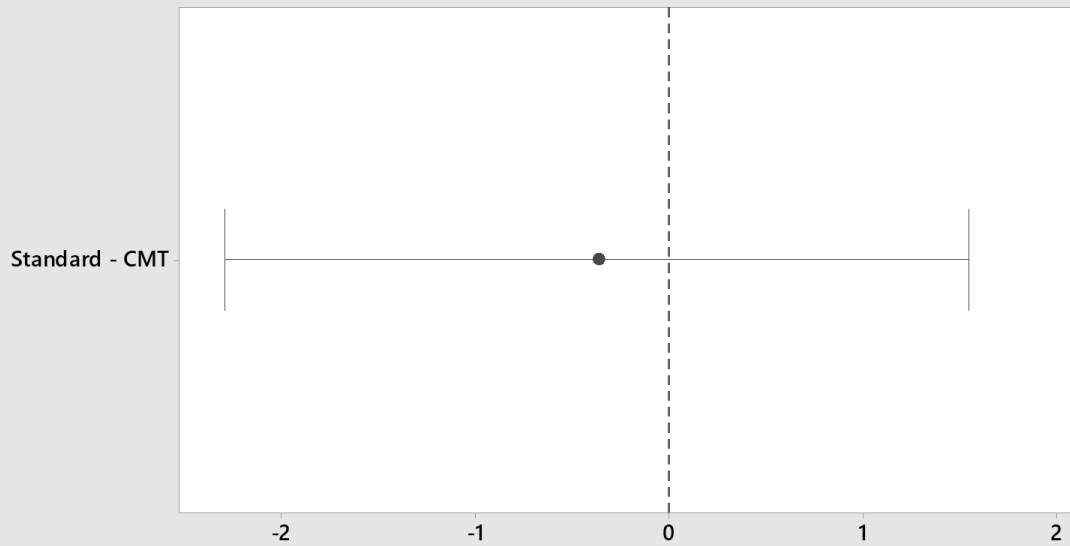
*If an interval does not contain zero, the corresponding means are significantly different.*

### Interval Plot of Hardness vs Method 95% CI for the Mean



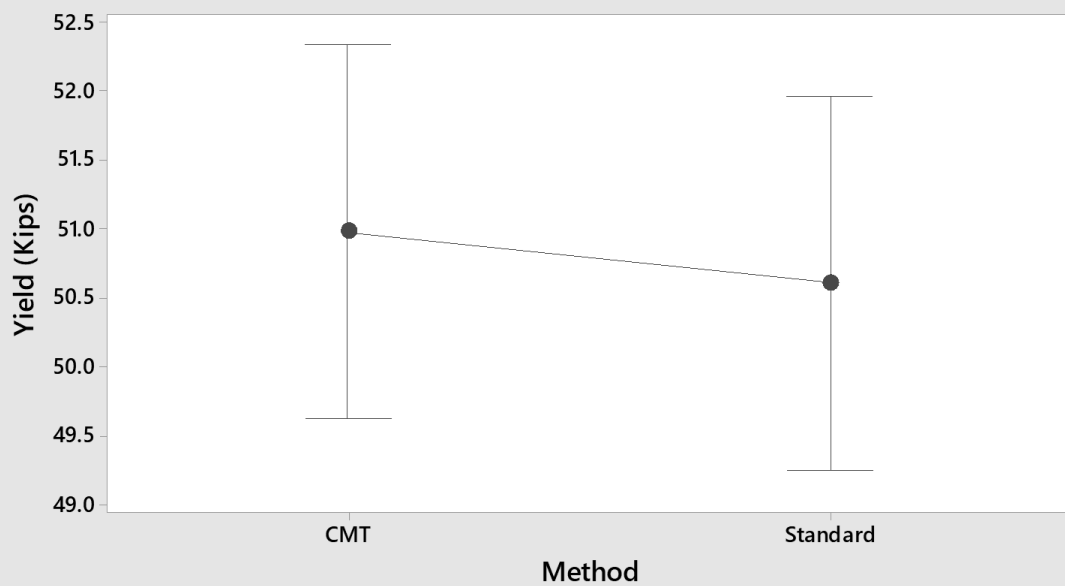
*The pooled standard deviation is used to calculate the intervals.*

### Tukey Simultaneous 95% CIs Differences of Means for Yield (Kips)



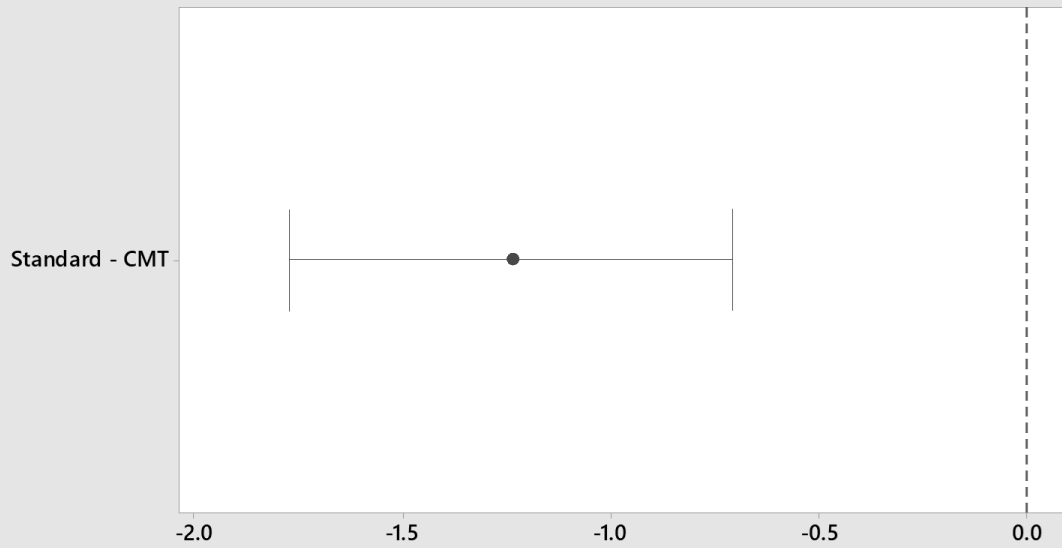
*If an interval does not contain zero, the corresponding means are significantly different.*

### Interval Plot of Yield (Kips) vs Method 95% CI for the Mean



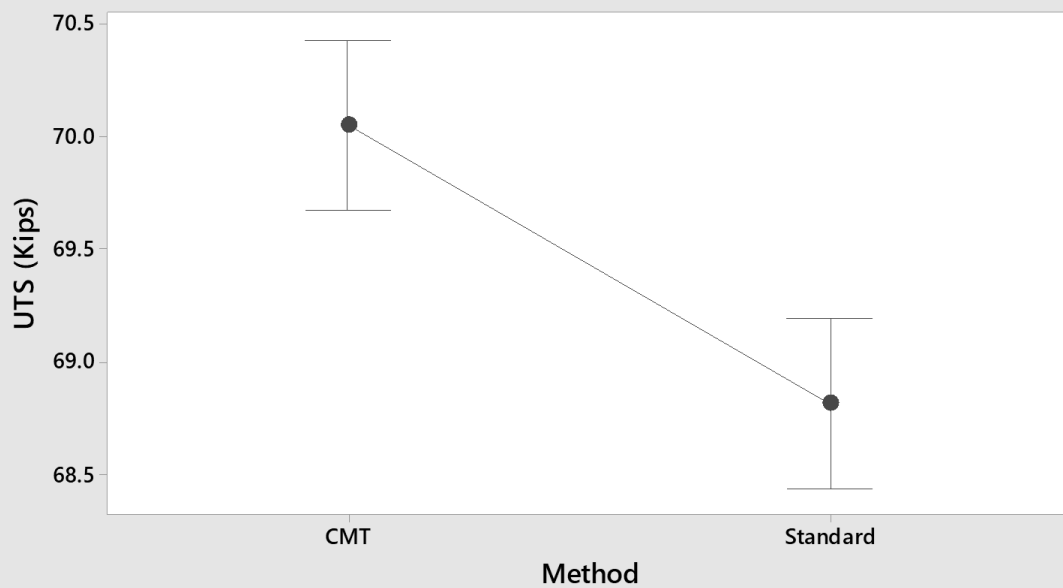
*The pooled standard deviation is used to calculate the intervals.*

### Tukey Simultaneous 95% CIs Differences of Means for UTS (Kips)



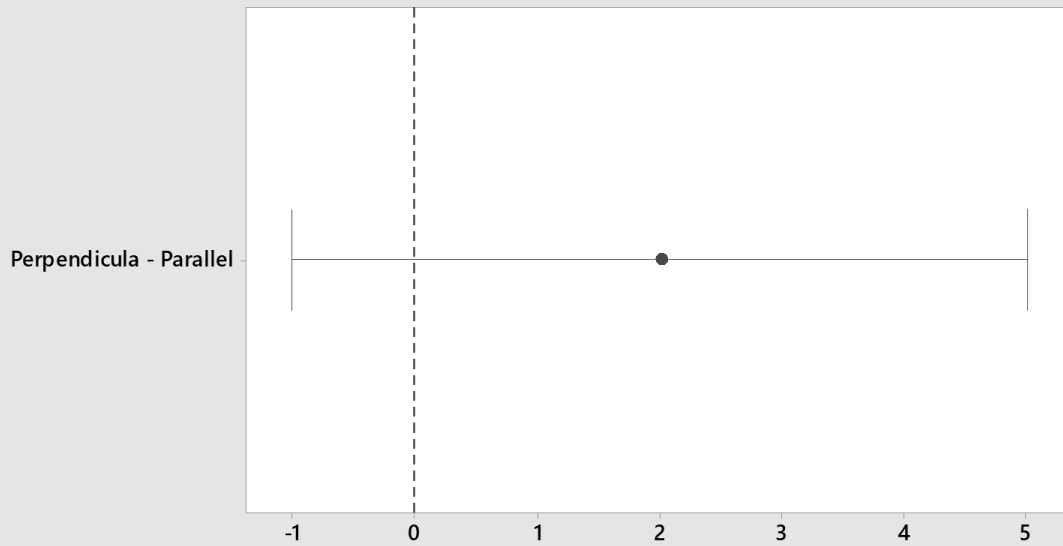
*If an interval does not contain zero, the corresponding means are significantly different.*

### Interval Plot of UTS (Kips) vs Method 95% CI for the Mean



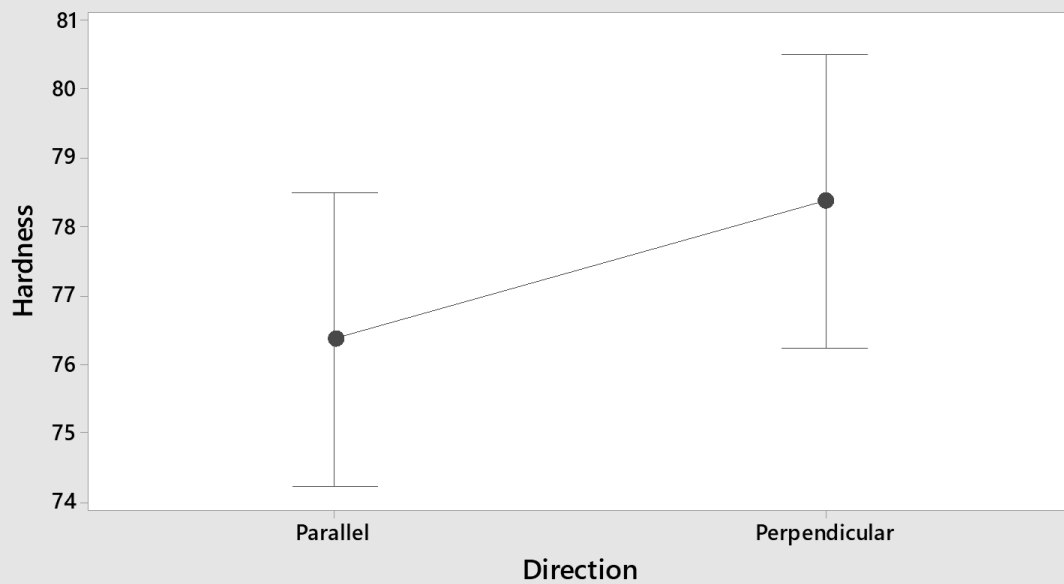
*The pooled standard deviation is used to calculate the intervals.*

### Tukey Simultaneous 95% CIs Differences of Means for Hardness



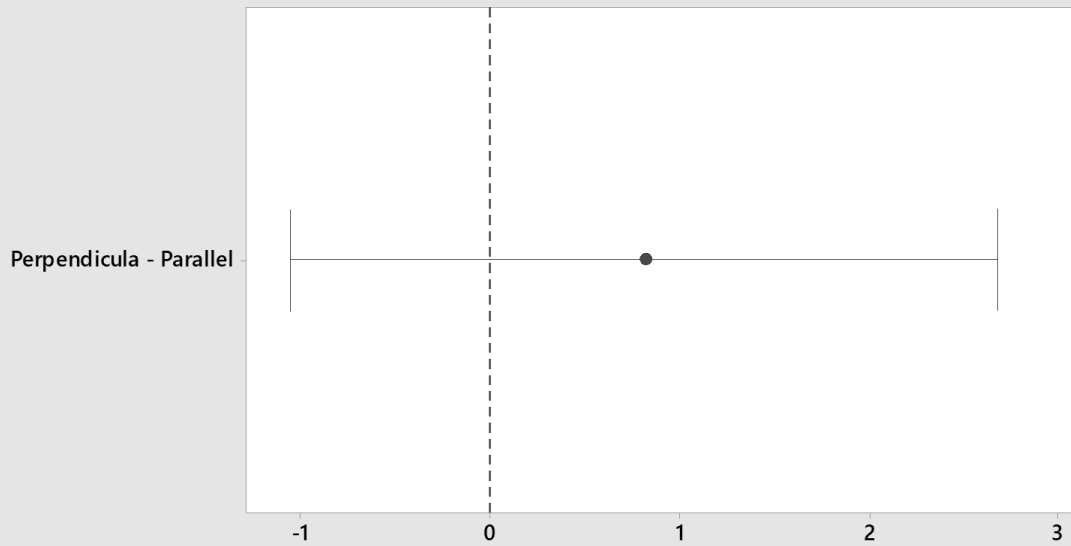
*If an interval does not contain zero, the corresponding means are significantly different.*

### Interval Plot of Hardness vs Direction 95% CI for the Mean



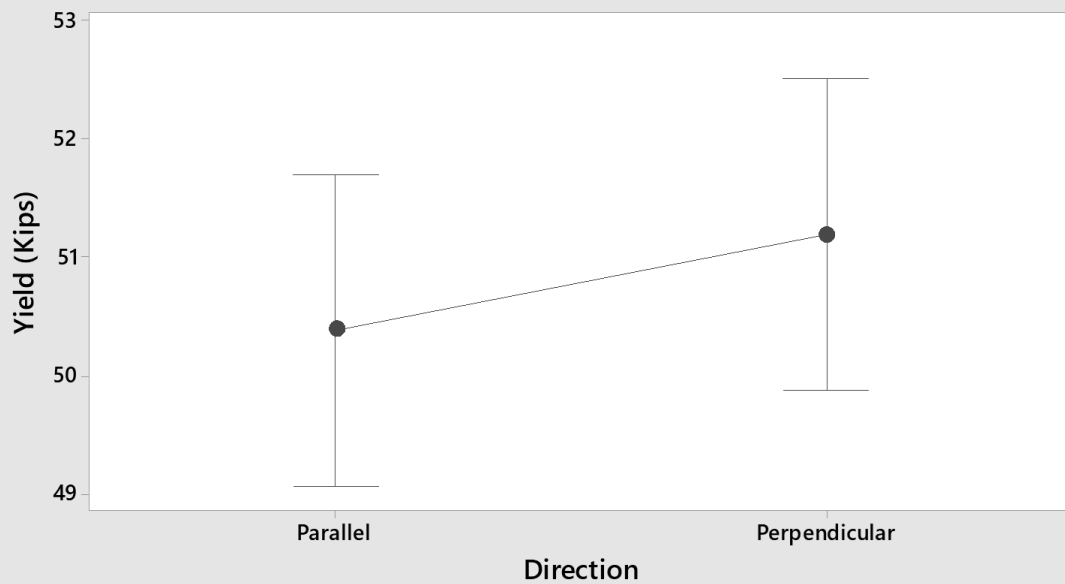
*The pooled standard deviation is used to calculate the intervals.*

### Tukey Simultaneous 95% CIs Differences of Means for Yield (Kips)



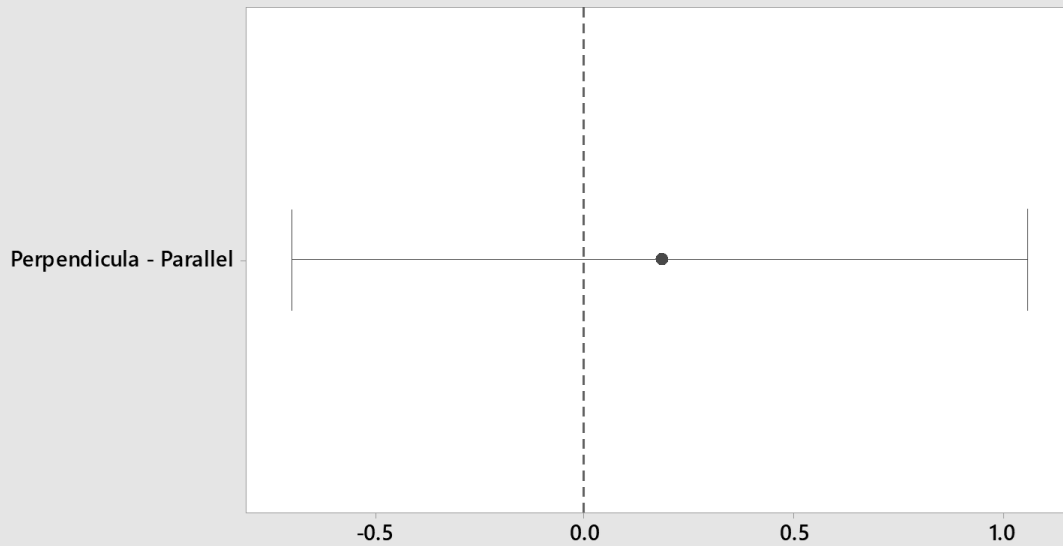
*If an interval does not contain zero, the corresponding means are significantly different.*

### Interval Plot of Yield (Kips) vs Direction 95% CI for the Mean



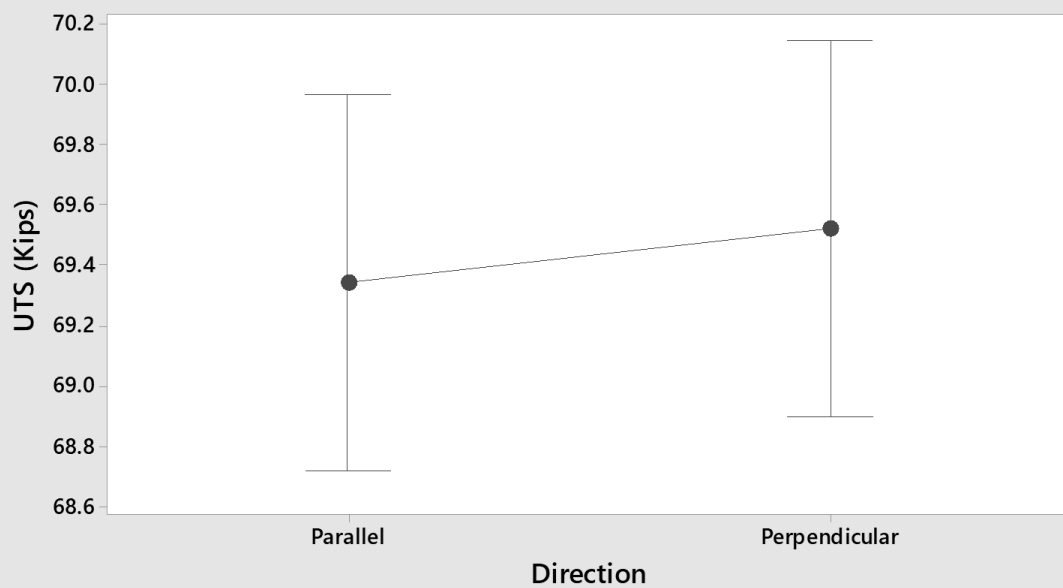
*The pooled standard deviation is used to calculate the intervals.*

### Tukey Simultaneous 95% CIs Differences of Means for UTS (Kips)



*If an interval does not contain zero, the corresponding means are significantly different.*

### Interval Plot of UTS (Kips) vs Direction 95% CI for the Mean



*The pooled standard deviation is used to calculate the intervals.*

### Analysis of Variance for Hardness

Source	DF	SS	MS	F	P
Method	1	49.00	49.000	10.32	0.007
Direction	1	16.00	16.000	3.37	0.089
Error	13	61.75	4.750		
Total	15	126.75			

### Model Summary

S	R-sq	R-sq(adj)
2.17945	51.28%	43.79%

### Analysis of Variance for Yield (Kips)

Source	DF	SS	MS	F	P
Method	1	0.5489	0.5489	0.17	0.688
Direction	1	2.6201	2.6201	0.81	0.385
Error	13	42.2183	3.2476		
Total	15	45.3874			

### Model Summary

S	R-sq	R-sq(adj)
1.80210	6.98%	0.00%

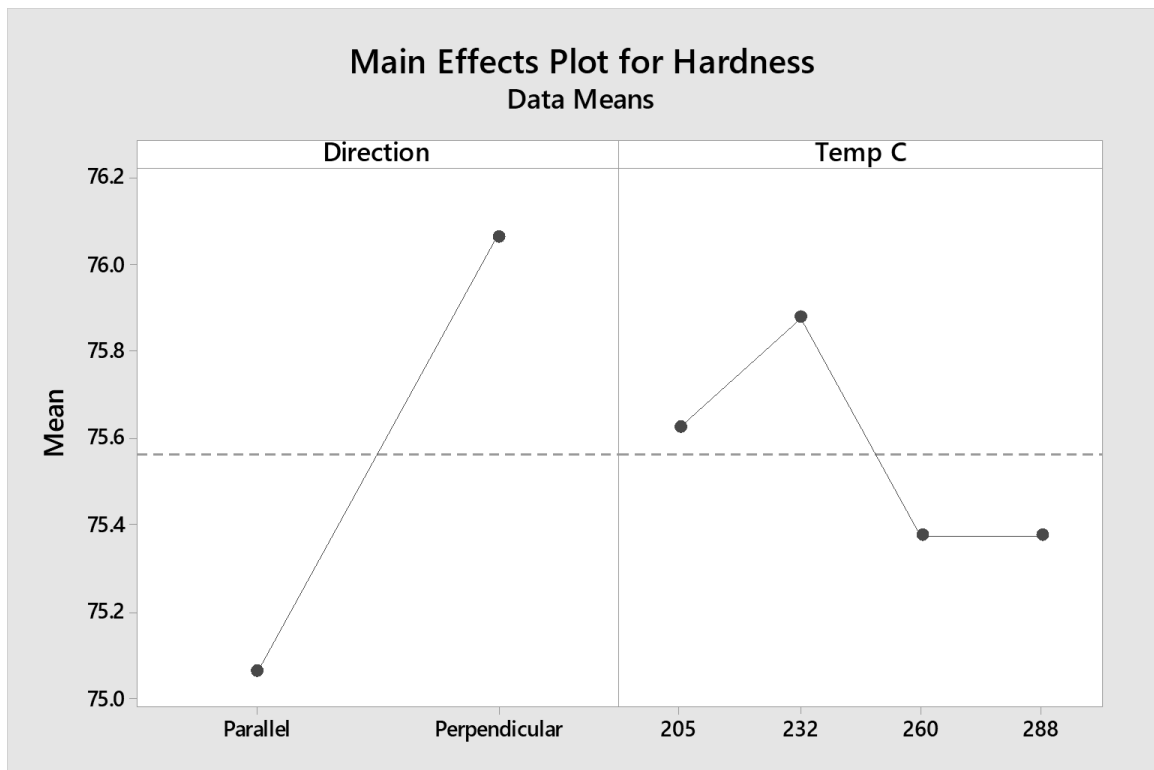
### Analysis of Variance for UTS (Kips)

Source	DF	SS	MS	F	P
Method	1	6.1515	6.1515	24.09	0.000
Direction	1	0.1265	0.1265	0.50	0.494
Error	13	3.3202	0.2554		
Total	15	9.5982			

### Model Summary

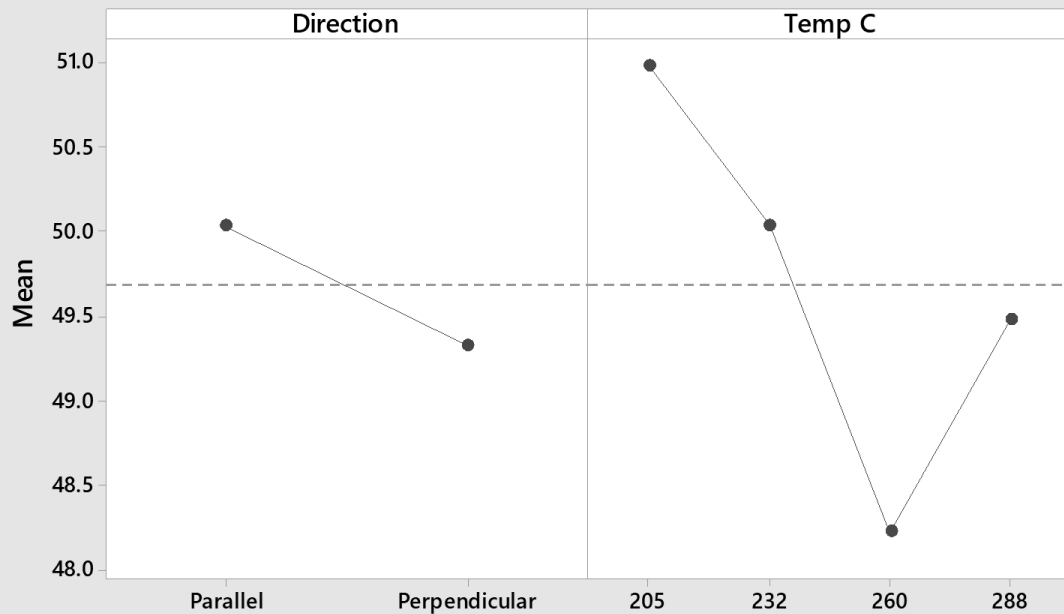
S	R-sq	R-sq(adj)
0.505368	65.41%	60.09%

## ER70S-6 ANOVA – Temperature

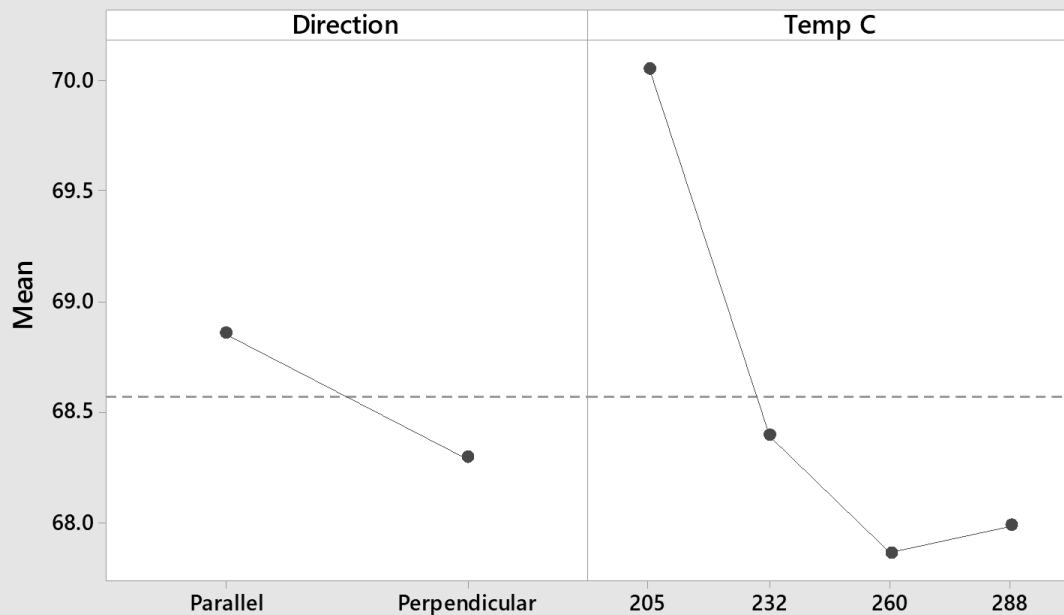




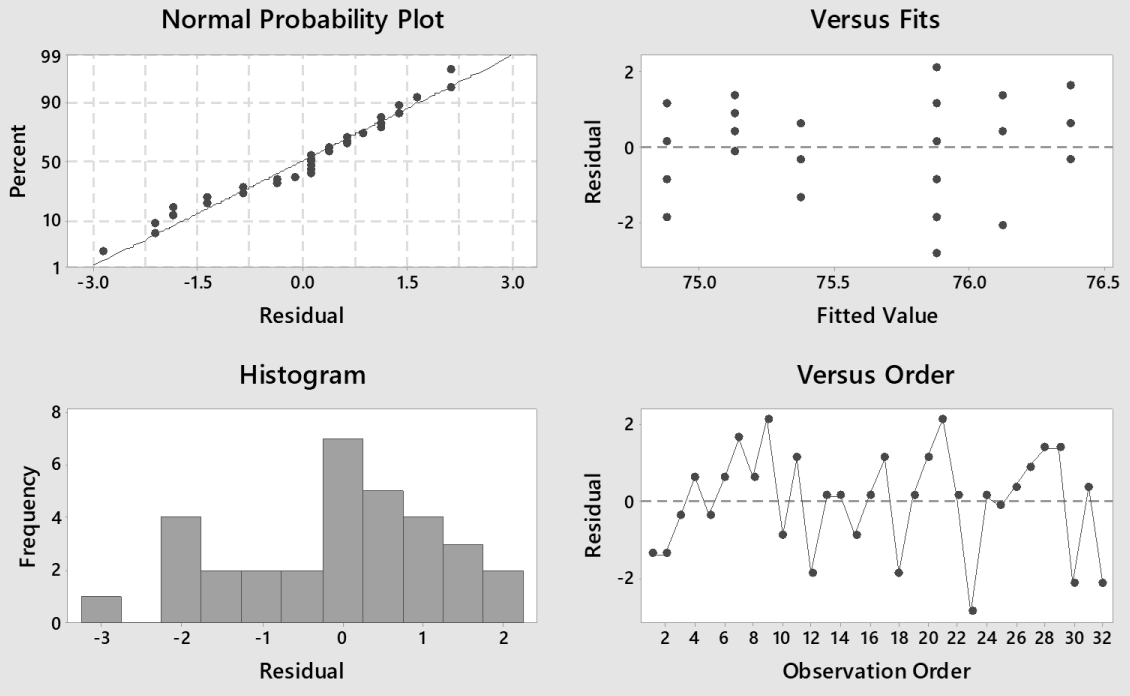
**Main Effects Plot for Yield (Kips)**  
Data Means



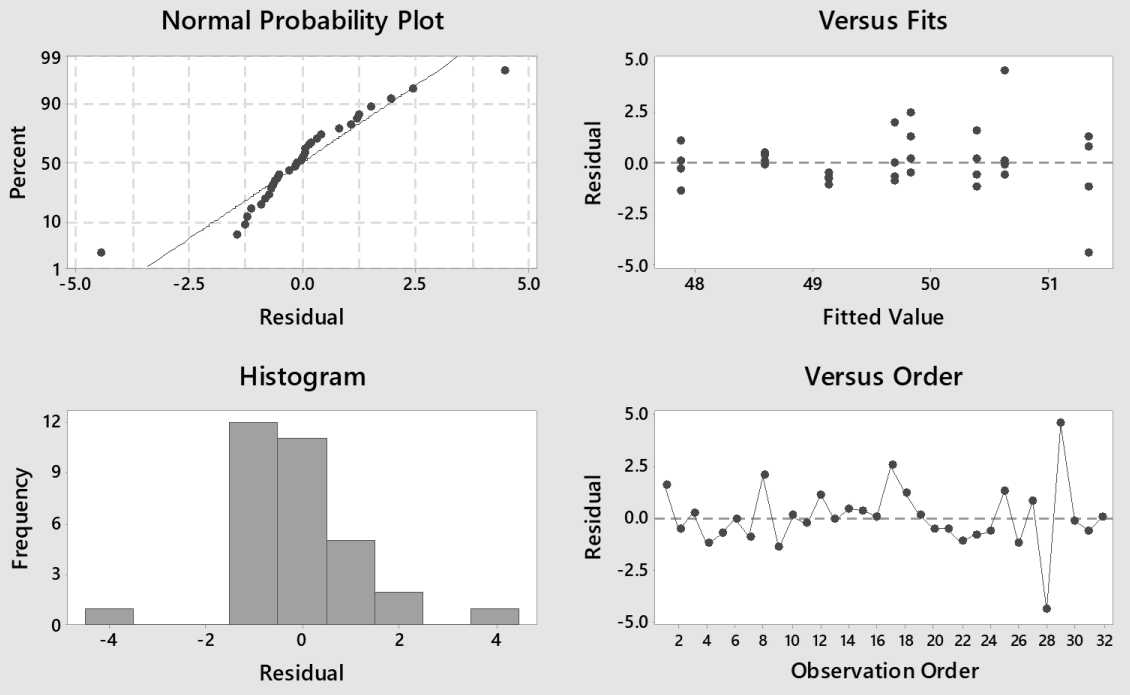
**Main Effects Plot for UTS (Kips)**  
Data Means



## Residual Plots for Hardness

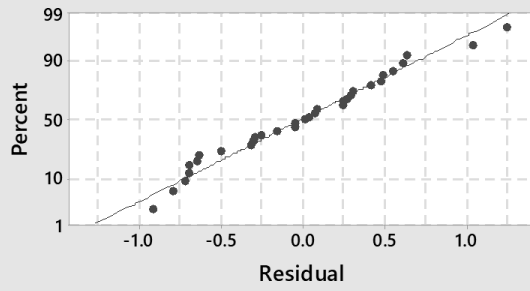


## Residual Plots for Yield (Kips)

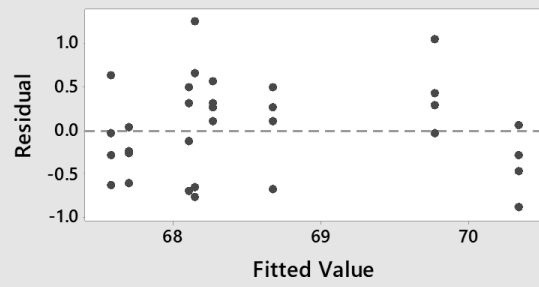


# Residual Plots for UTS (Kips)

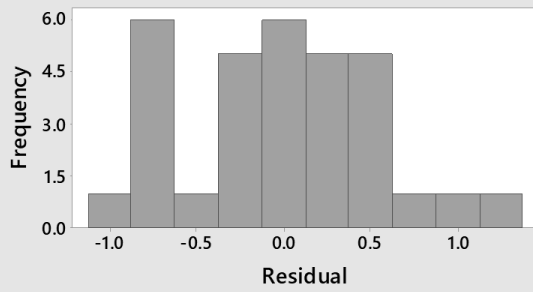
## Normal Probability Plot



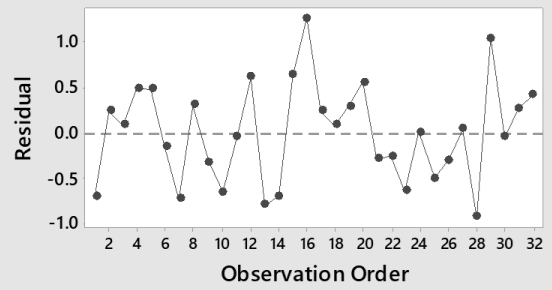
## Versus Fits



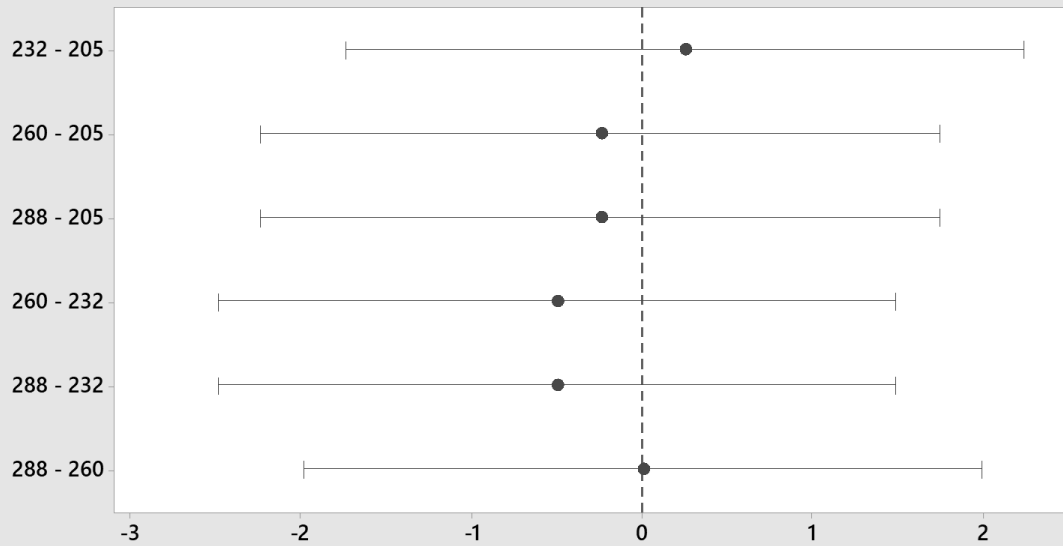
## Histogram



## Versus Order

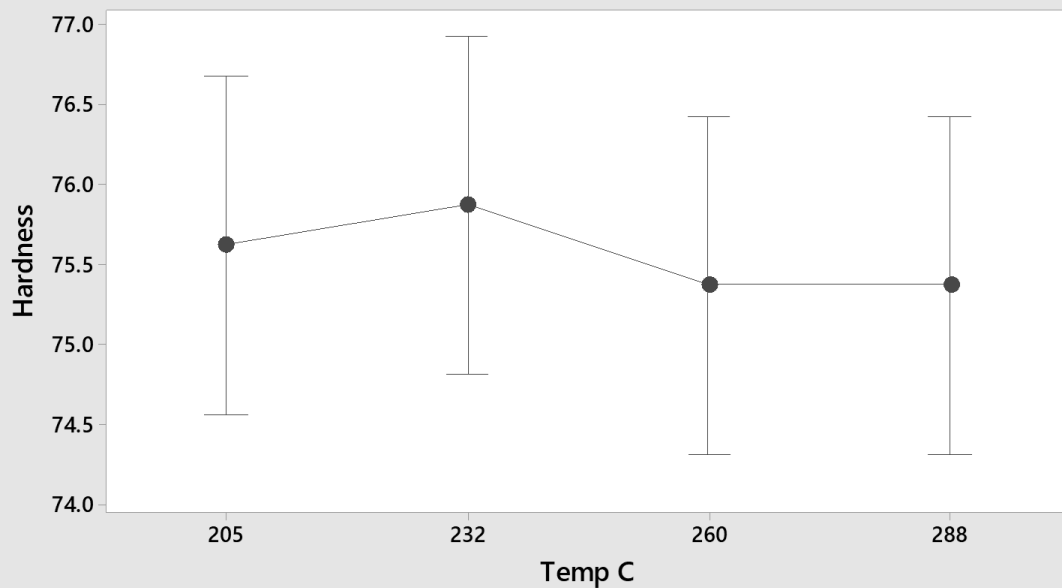


### Tukey Simultaneous 95% CIs Differences of Means for Hardness



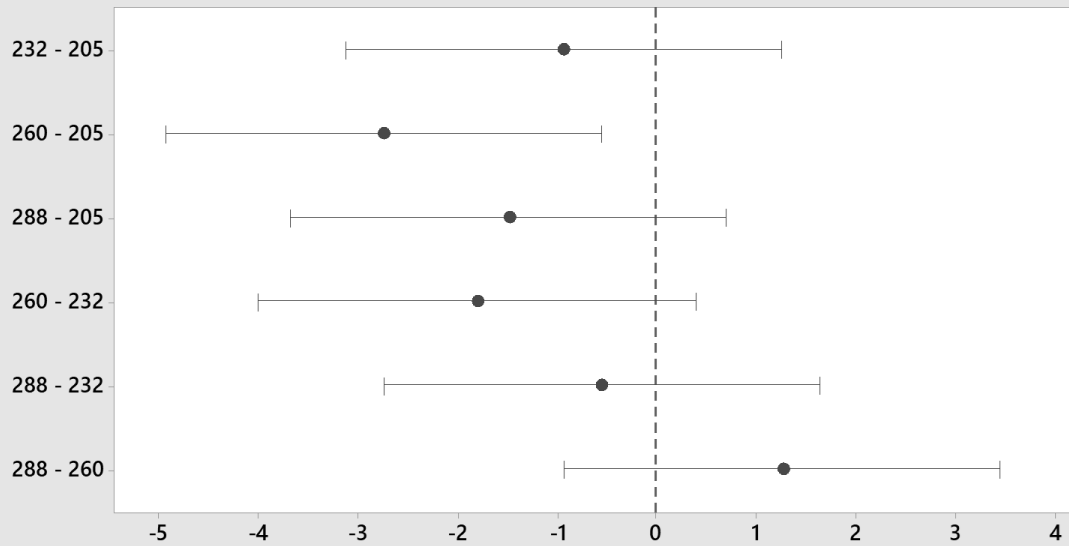
If an interval does not contain zero, the corresponding means are significantly different.

### Interval Plot of Hardness vs Temp C 95% CI for the Mean



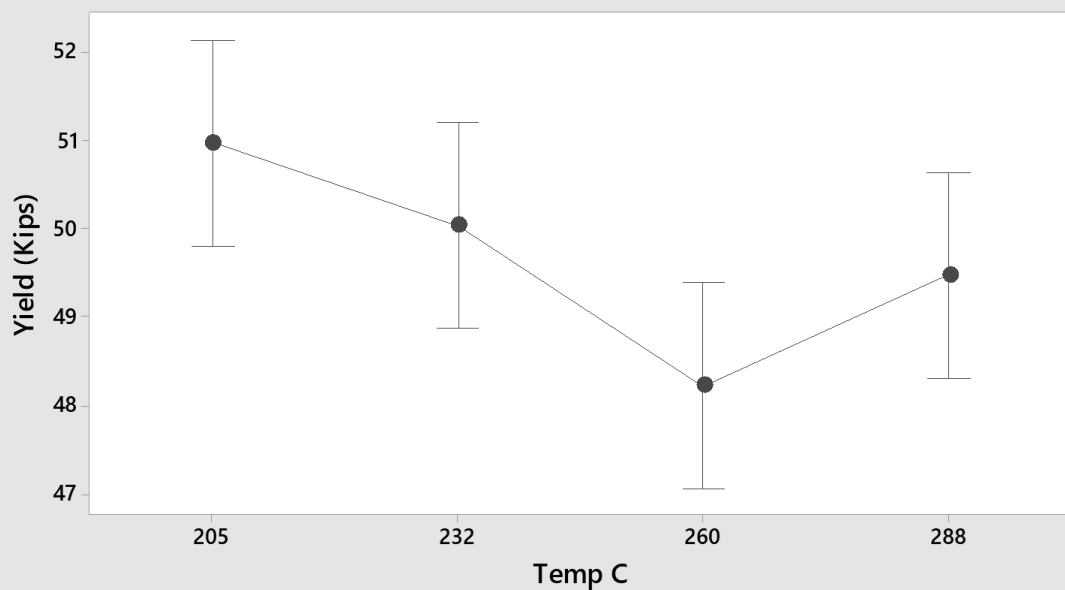
The pooled standard deviation is used to calculate the intervals.

### Tukey Simultaneous 95% CIs Differences of Means for Yield (Kips)



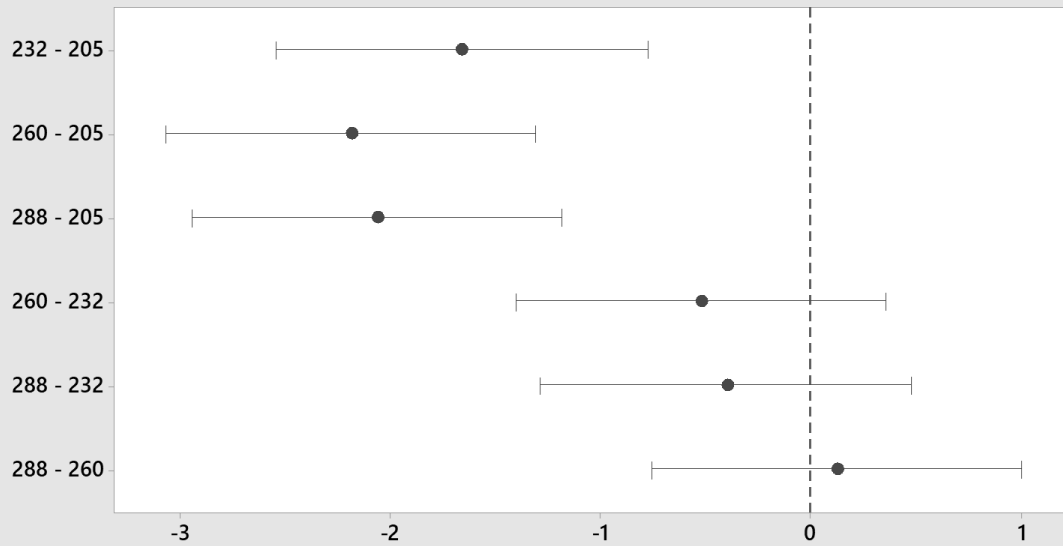
If an interval does not contain zero, the corresponding means are significantly different.

### Interval Plot of Yield (Kips) vs Temp C 95% CI for the Mean



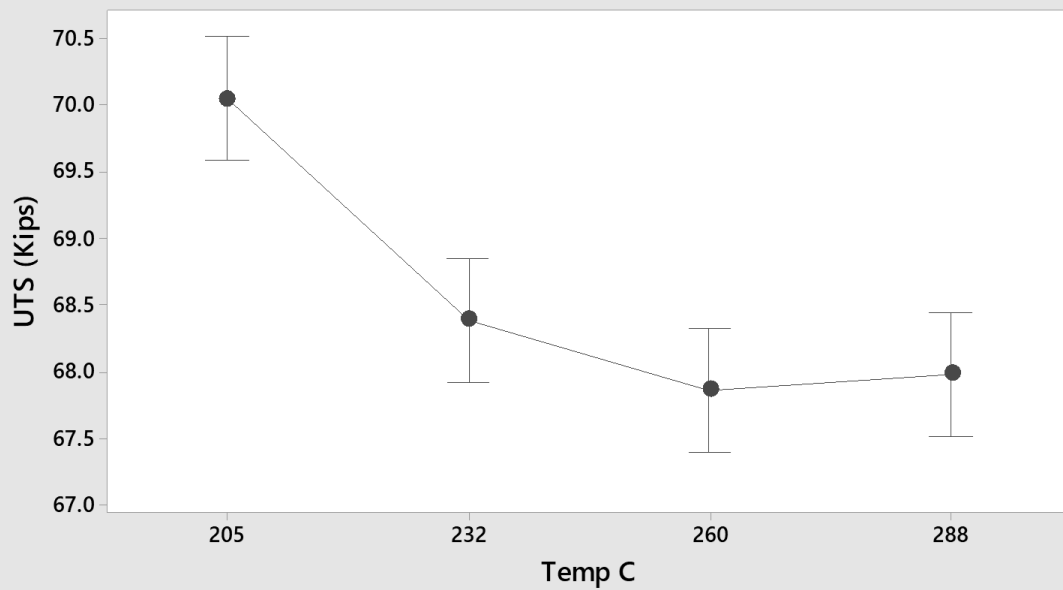
The pooled standard deviation is used to calculate the intervals.

### Tukey Simultaneous 95% CIs Differences of Means for UTS (Kips)



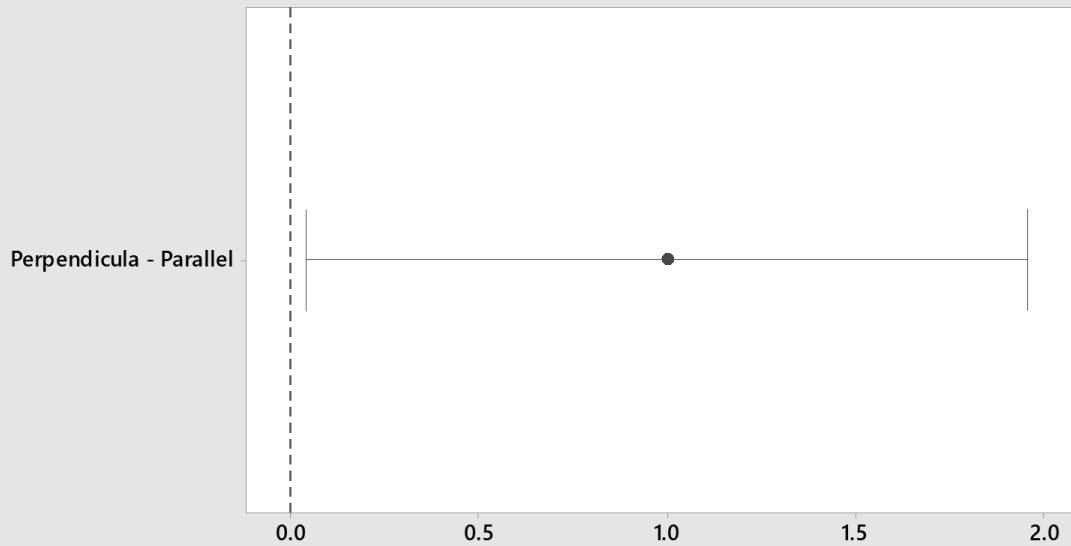
If an interval does not contain zero, the corresponding means are significantly different.

### Interval Plot of UTS (Kips) vs Temp C 95% CI for the Mean



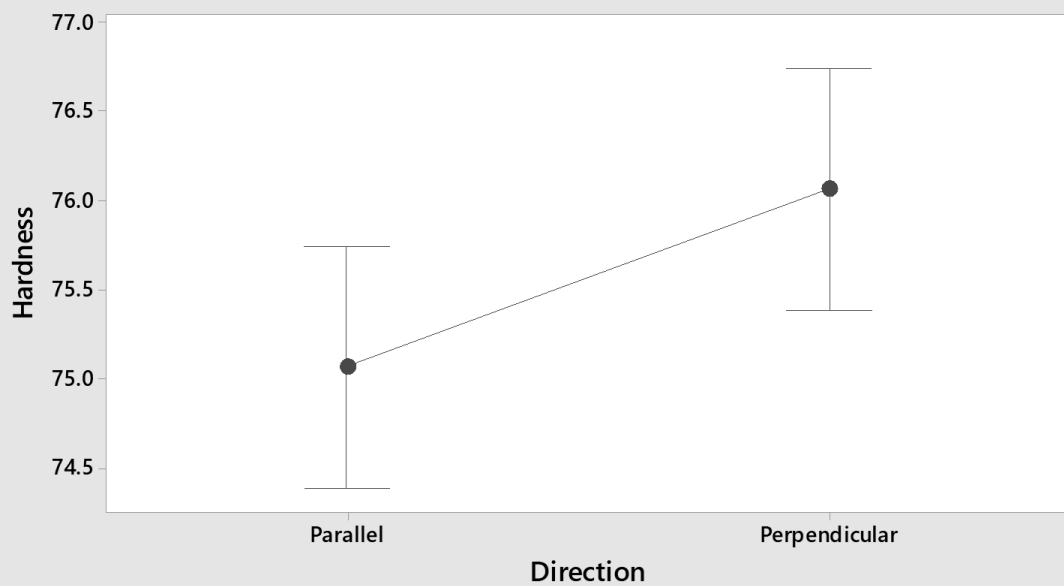
The pooled standard deviation is used to calculate the intervals.

### Tukey Simultaneous 95% CIs Differences of Means for Hardness



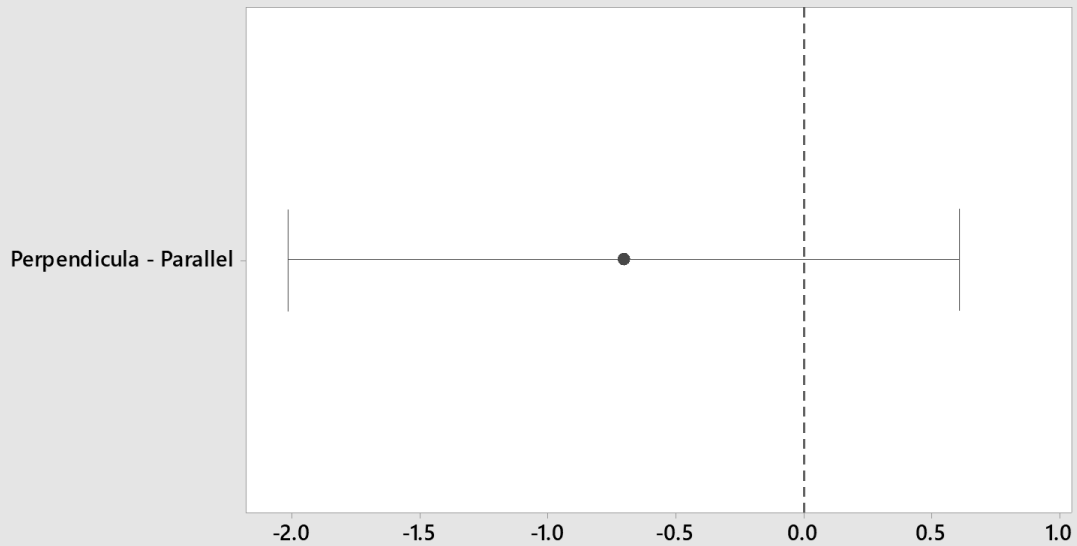
*If an interval does not contain zero, the corresponding means are significantly different.*

### Interval Plot of Hardness vs Direction 95% CI for the Mean



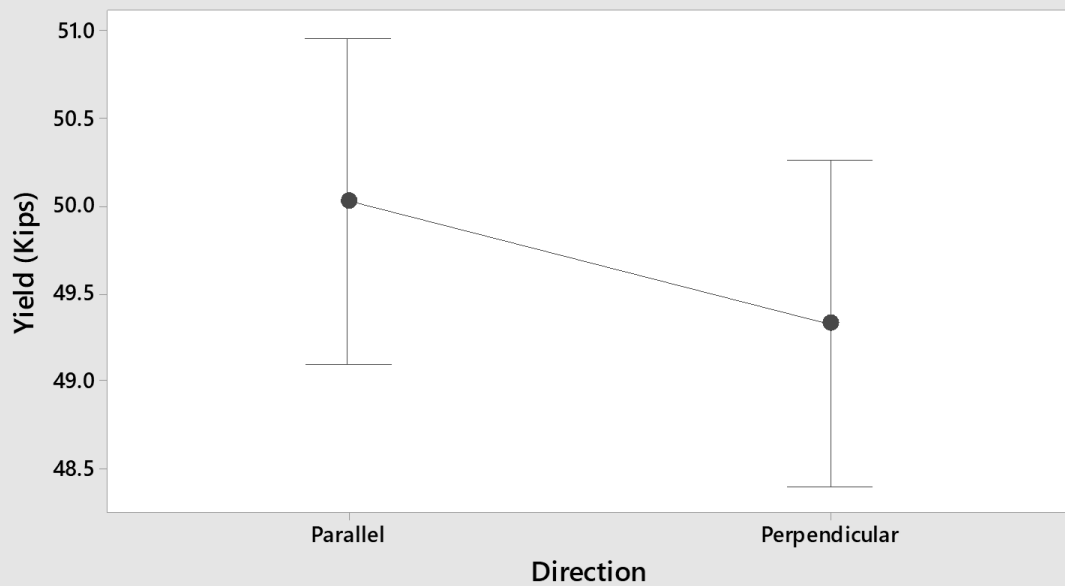
*The pooled standard deviation is used to calculate the intervals.*

### Tukey Simultaneous 95% CIs Differences of Means for Yield (Kips)



*If an interval does not contain zero, the corresponding means are significantly different.*

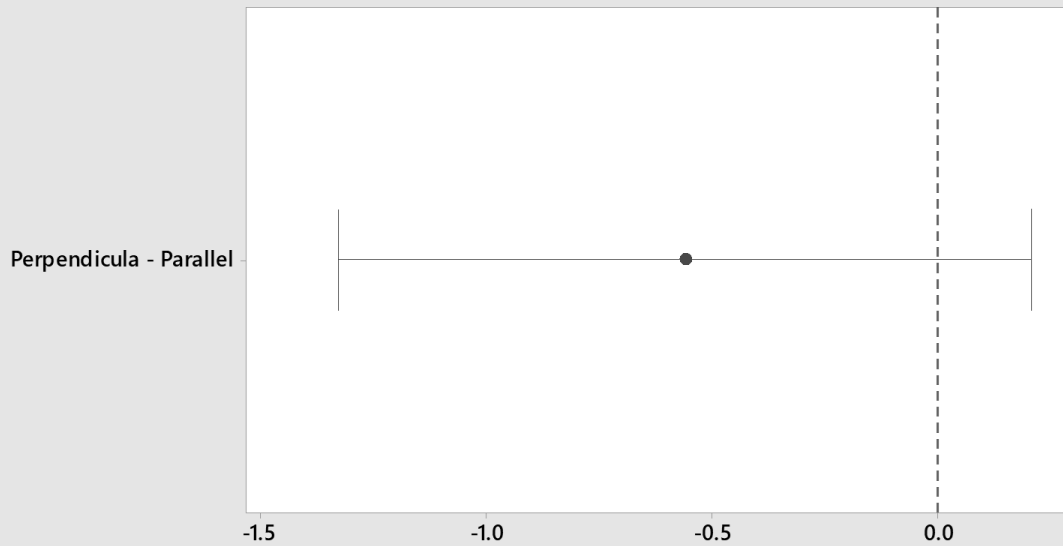
### Interval Plot of Yield (Kips) vs Direction 95% CI for the Mean



*The pooled standard deviation is used to calculate the intervals.*

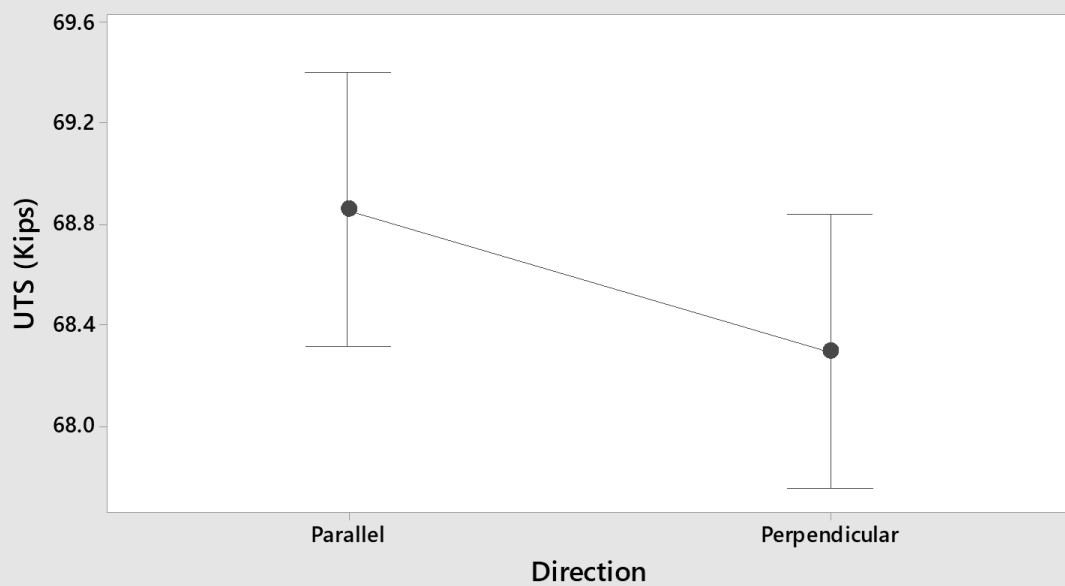


### Tukey Simultaneous 95% CIs Differences of Means for UTS (Kips)



*If an interval does not contain zero, the corresponding means are significantly different.*

### Interval Plot of UTS (Kips) vs Direction 95% CI for the Mean



*The pooled standard deviation is used to calculate the intervals.*

### Analysis of Variance for Yield (Kips)

Source	DF	SS	MS	F	P
Direction	1	3.969	3.969	1.58	0.220
Temp C	3	31.712	10.571	4.20	0.015
Error	27	67.962	2.517		
Total	31	103.643			

### Model Summary

S	R-sq	R-sq(adj)
1.58654	34.43%	24.71%

### Analysis of Variance for Hardness

Source	DF	SS	MS	F	P
Direction	1	8.000	8.0000	4.19	0.050
Temp C	3	1.375	0.4583	0.24	0.867
Error	27	51.500	1.9074		
Total	31	60.875			

### Model Summary

S	R-sq	R-sq(adj)
1.38109	15.40%	2.87%

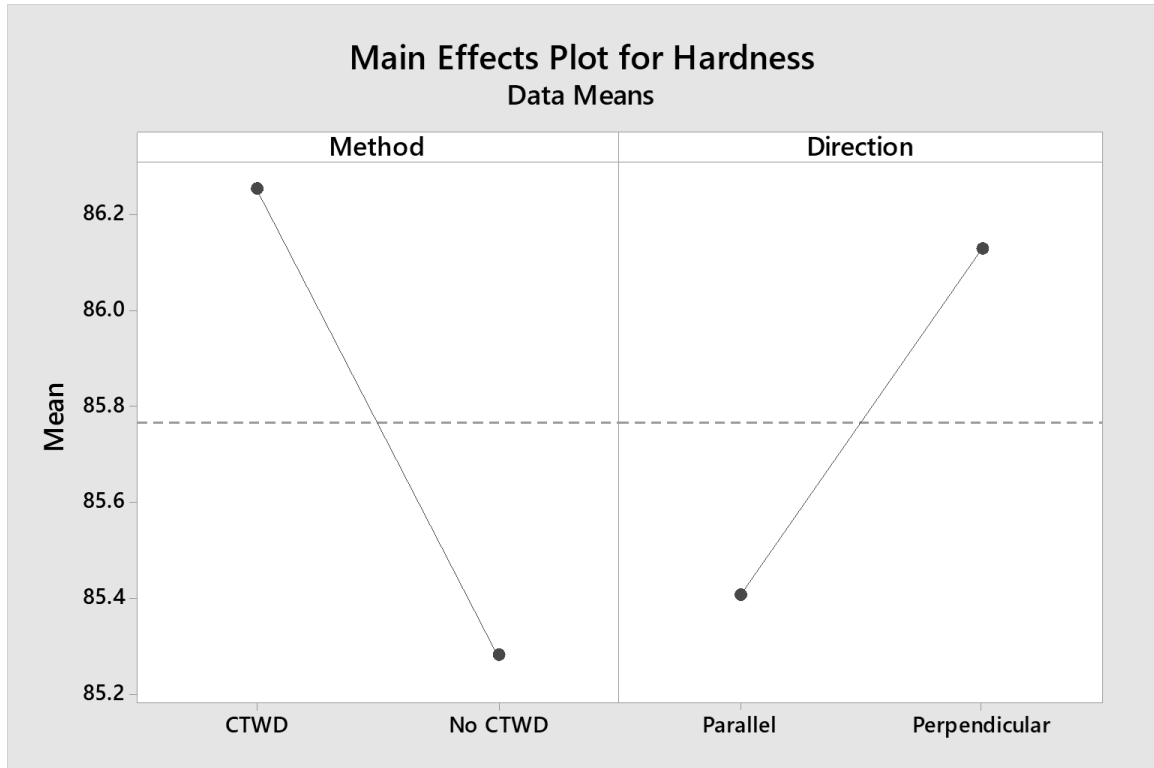
### Analysis of Variance for UTS (Kips)

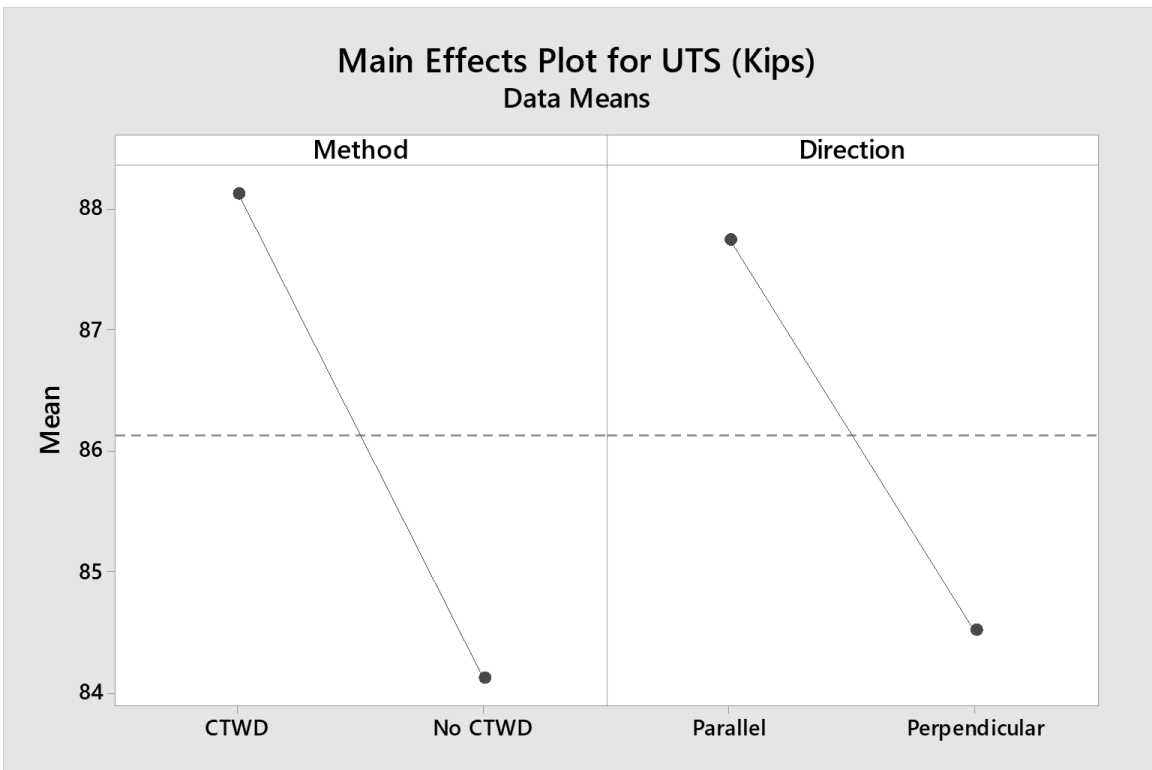
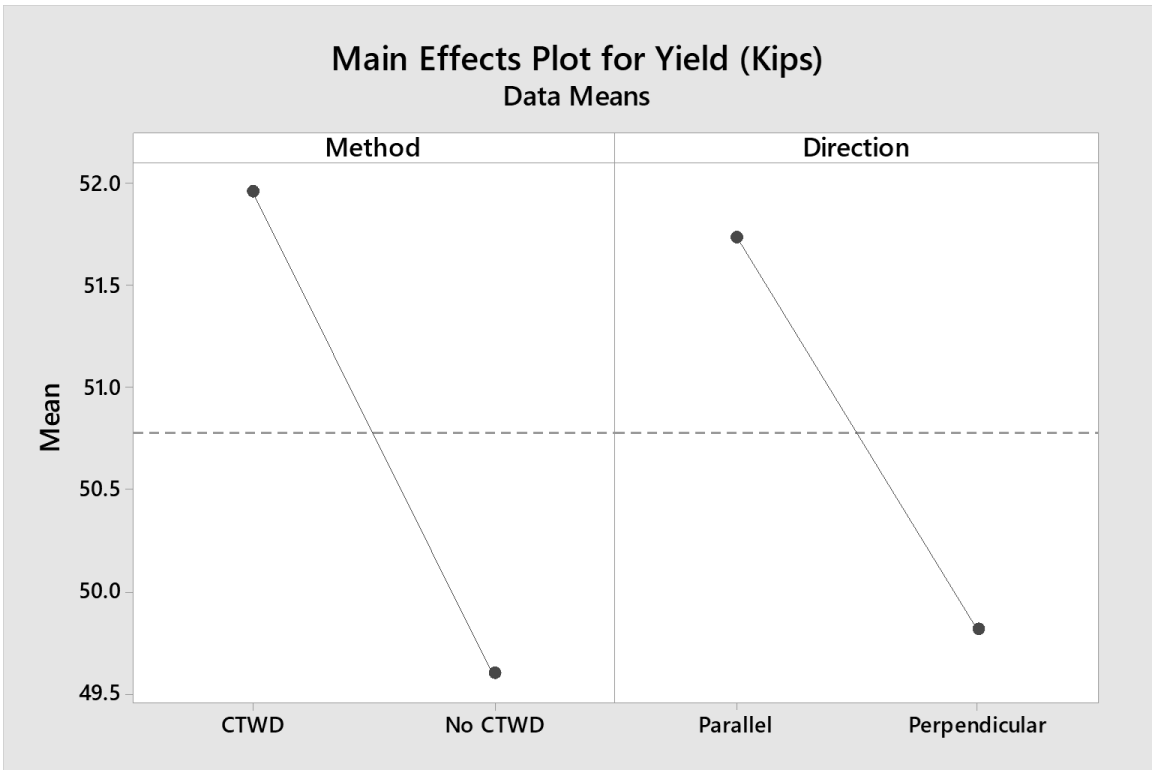
Source	DF	SS	MS	F	P
Direction	1	2.521	2.5211	7.43	0.011
Temp C	3	24.610	8.2033	24.17	0.000
Error	27	9.163	0.3394		
Total	31	36.294			

### Model Summary

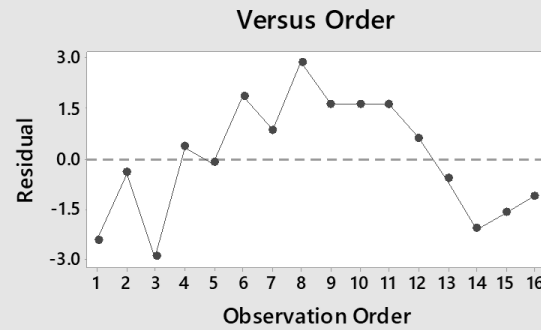
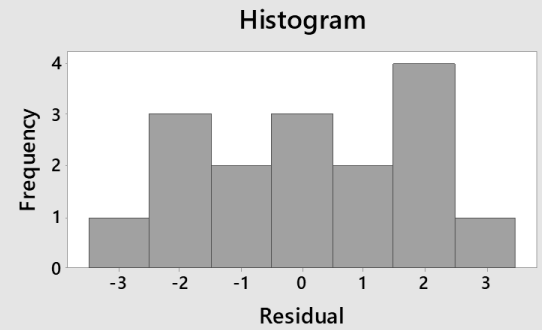
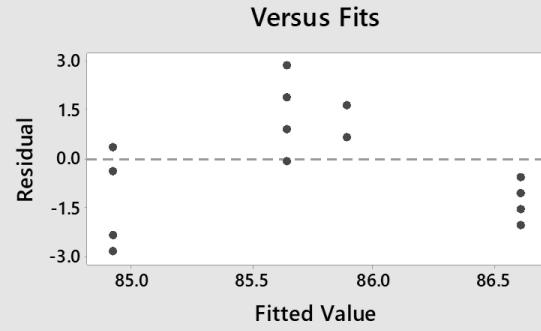
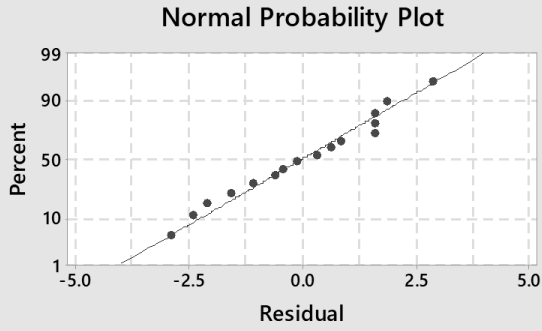
S	R-sq	R-sq(adj)
0.582544	74.75%	71.01%

# ER308L ANOVA – CTWD

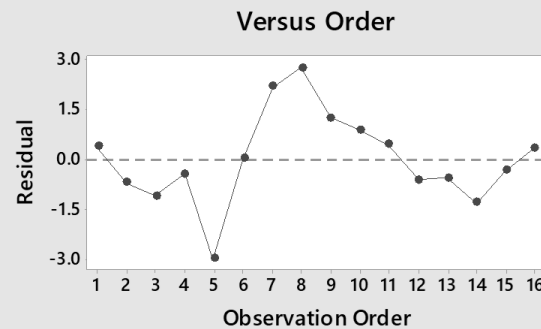
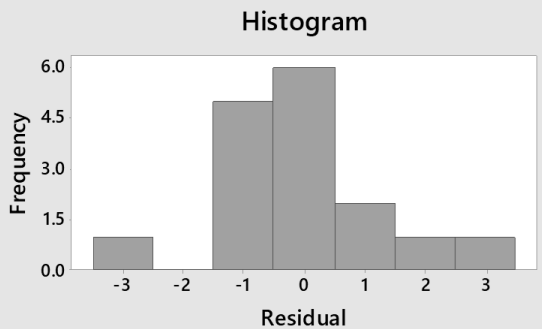
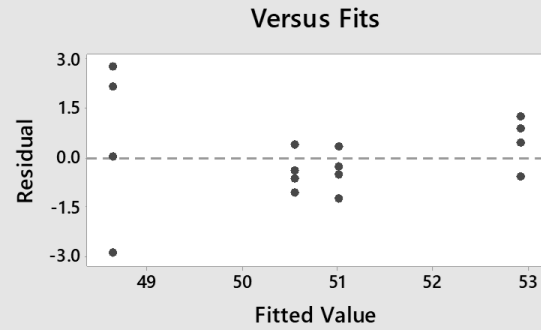
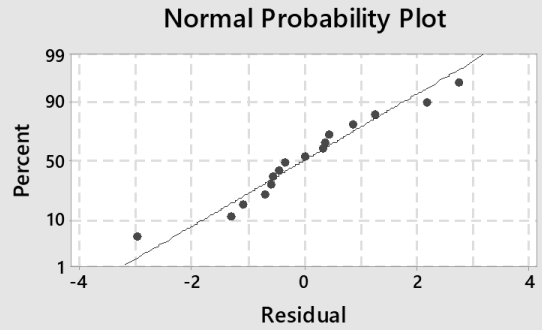




## Residual Plots for Hardness

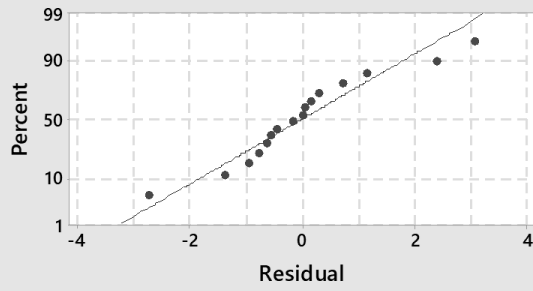


## Residual Plots for Yield (Kips)

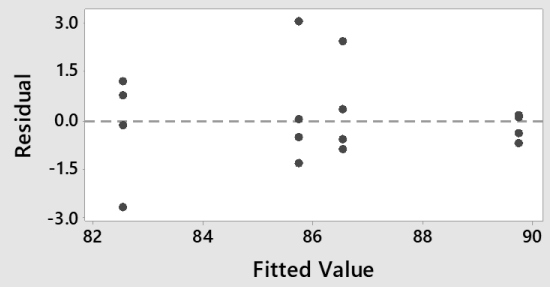


# Residual Plots for UTS (Kips)

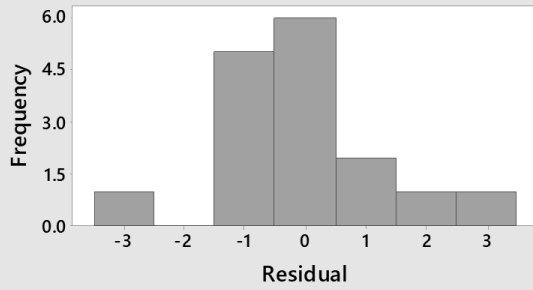
## Normal Probability Plot



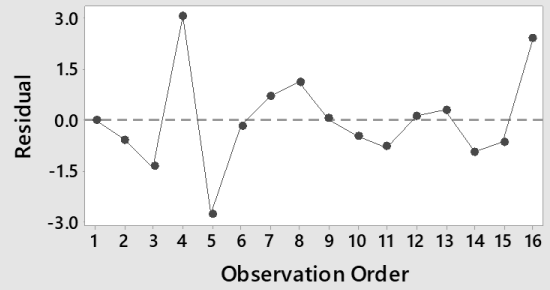
## Versus Fits



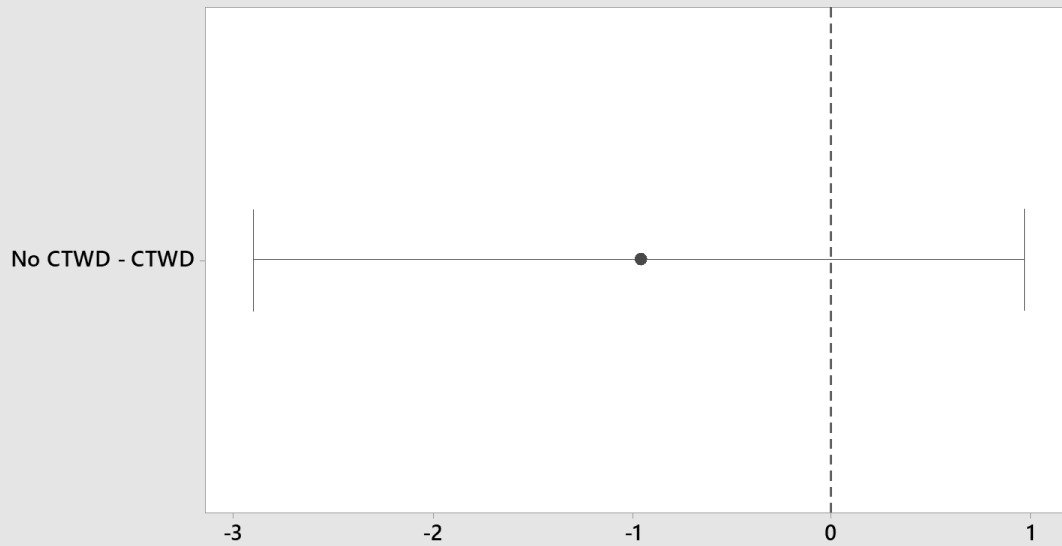
## Histogram



## Versus Order

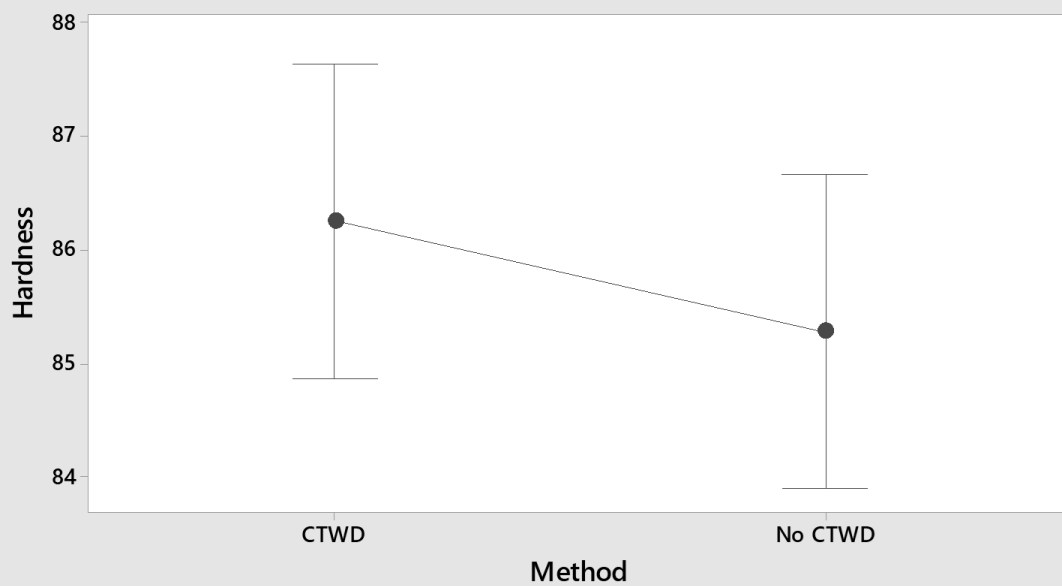


### Tukey Simultaneous 95% CIs Differences of Means for Hardness



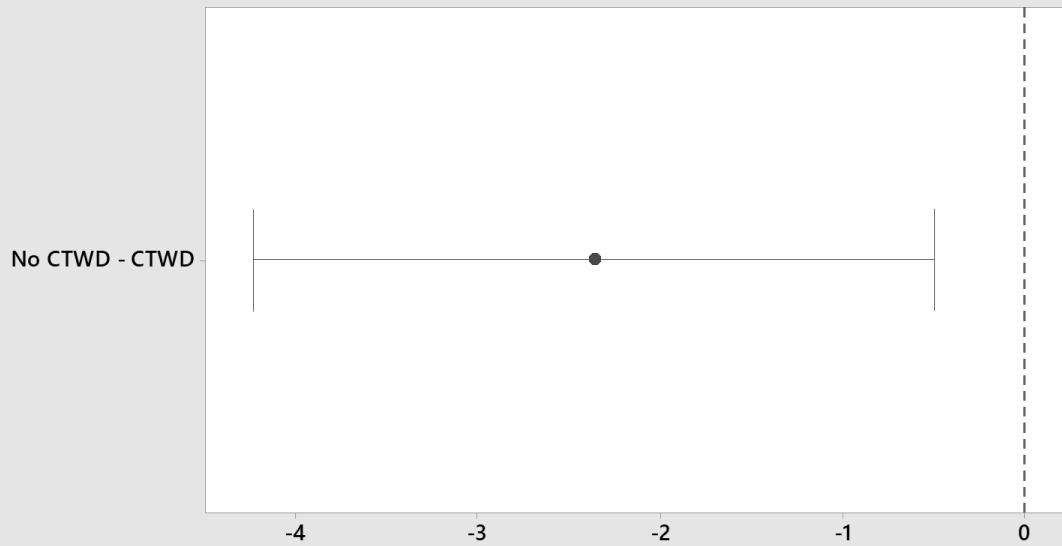
*If an interval does not contain zero, the corresponding means are significantly different.*

### Interval Plot of Hardness vs Method 95% CI for the Mean



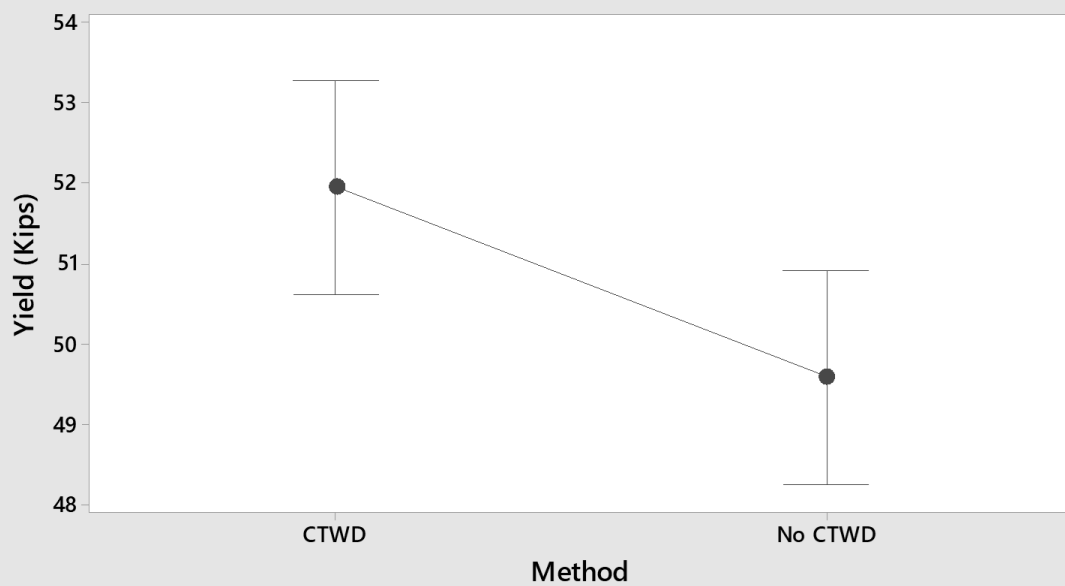
*The pooled standard deviation is used to calculate the intervals.*

### Tukey Simultaneous 95% CIs Differences of Means for Yield (Kips)



*If an interval does not contain zero, the corresponding means are significantly different.*

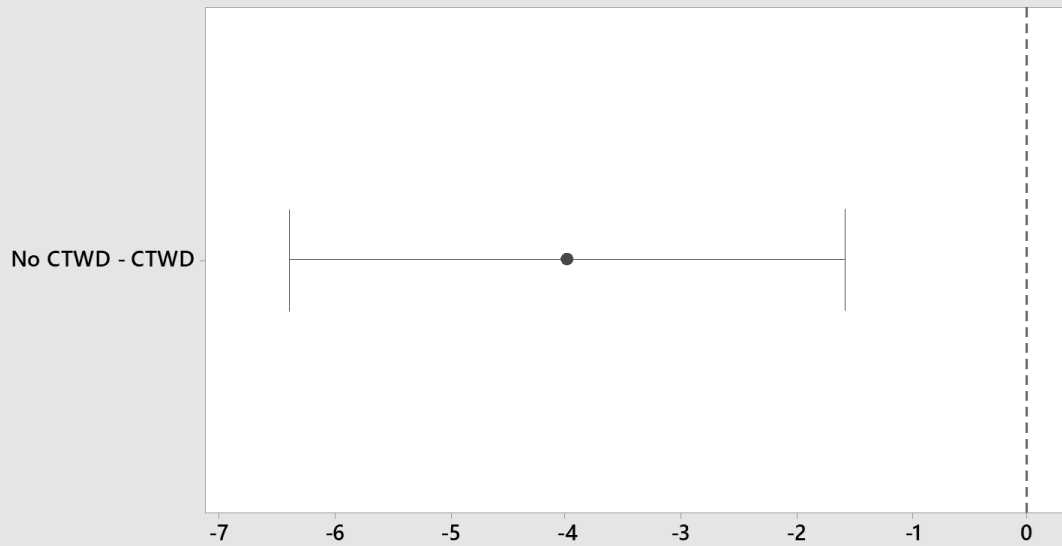
### Interval Plot of Yield (Kips) vs Method 95% CI for the Mean



*The pooled standard deviation is used to calculate the intervals.*

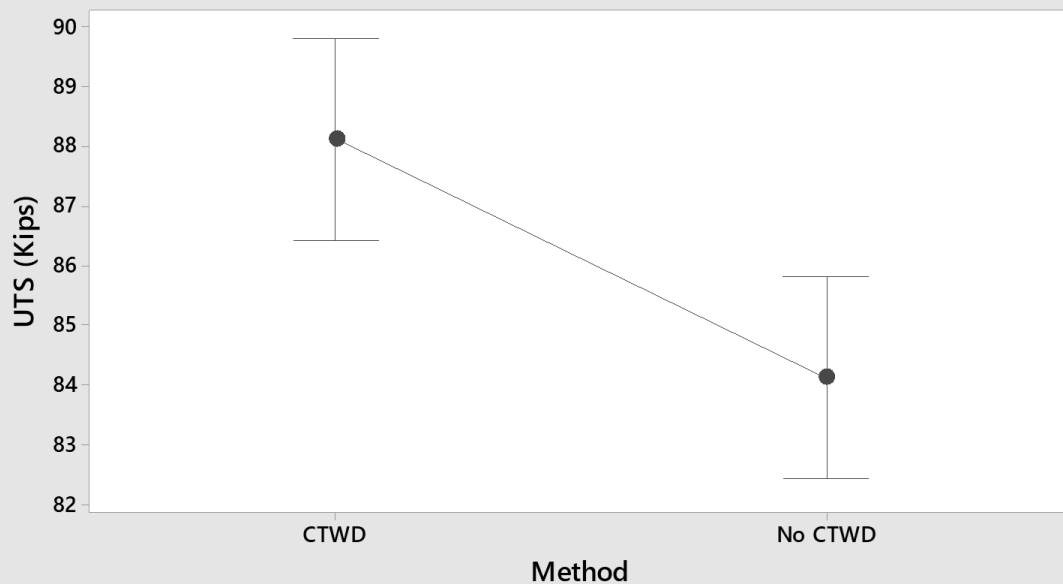


### Tukey Simultaneous 95% CIs Differences of Means for UTS (Kips)



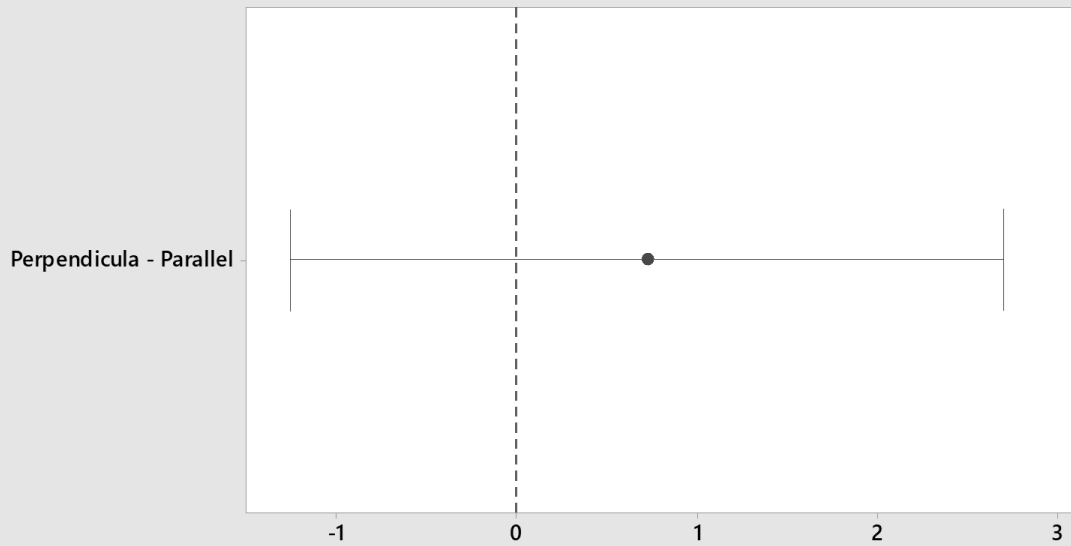
*If an interval does not contain zero, the corresponding means are significantly different.*

### Interval Plot of UTS (Kips) vs Method 95% CI for the Mean



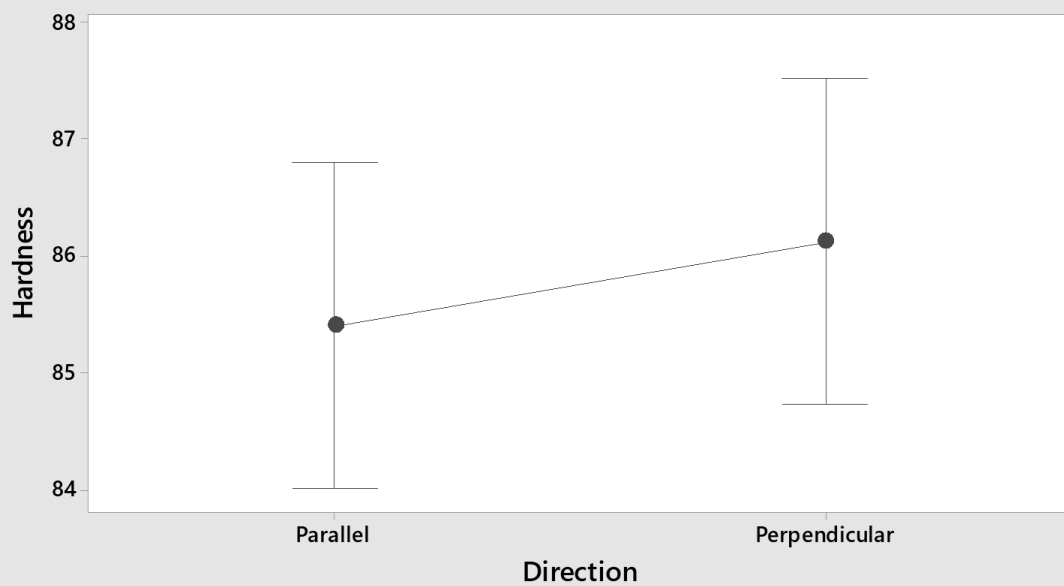
*The pooled standard deviation is used to calculate the intervals.*

### Tukey Simultaneous 95% CIs Differences of Means for Hardness



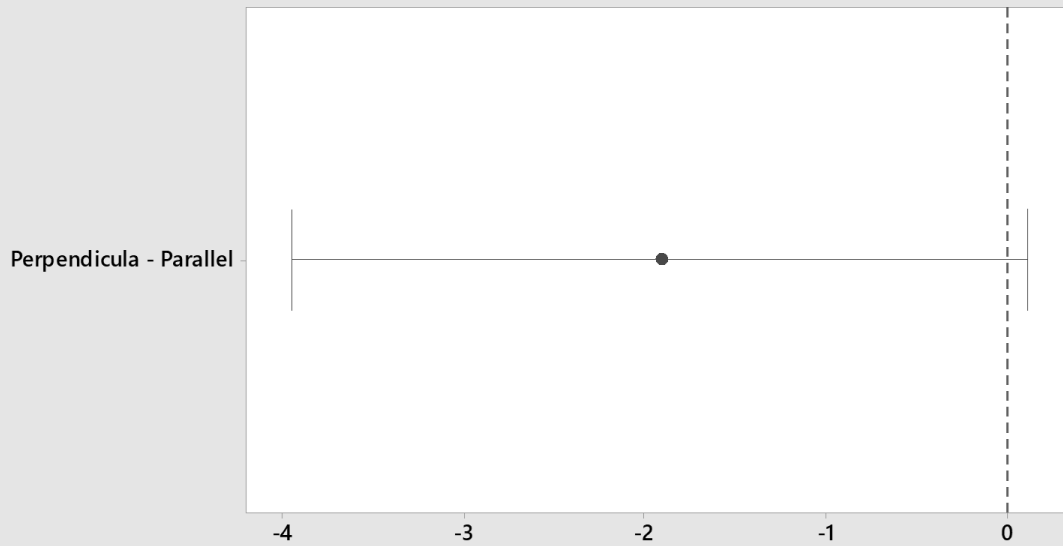
*If an interval does not contain zero, the corresponding means are significantly different.*

### Interval Plot of Hardness vs Direction 95% CI for the Mean



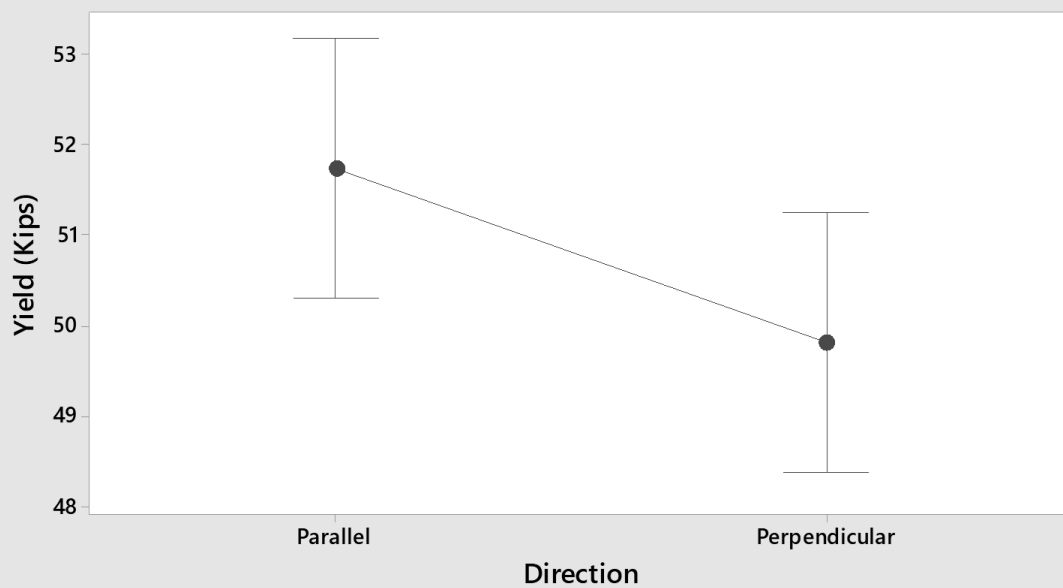
*The pooled standard deviation is used to calculate the intervals.*

### Tukey Simultaneous 95% CIs Differences of Means for Yield (Kips)



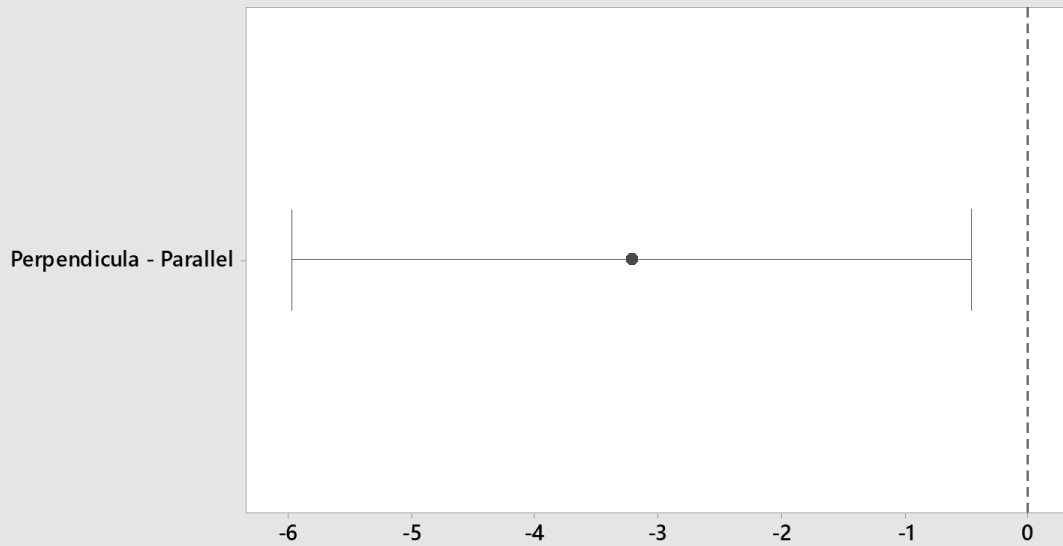
If an interval does not contain zero, the corresponding means are significantly different.

### Interval Plot of Yield (Kips) vs Direction 95% CI for the Mean



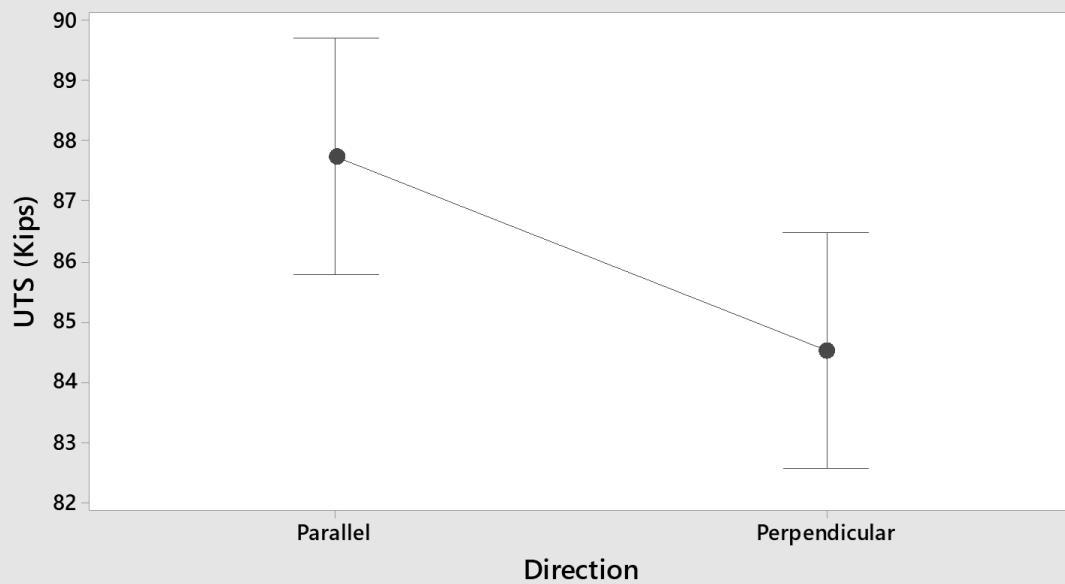
The pooled standard deviation is used to calculate the intervals.

### Tukey Simultaneous 95% CIs Differences of Means for UTS (Kips)



*If an interval does not contain zero, the corresponding means are significantly different.*

### Interval Plot of UTS (Kips) vs Direction 95% CI for the Mean



*The pooled standard deviation is used to calculate the intervals.*

### Analysis of Variance for Hardness

Source	DF	SS	MS	F	P
Method	1	3.754	3.754	1.11	0.311
Direction	1	2.066	2.066	0.61	0.448
Error	13	43.863	3.374		
Total	15	49.684			

### Model Summary

S	R-sq	R-sq(adj)
1.83687	11.71%	0.00%

### Analysis of Variance for Yield (Kips)

Source	DF	SS	MS	F	P
Method	1	22.40	22.397	10.39	0.007
Direction	1	14.73	14.726	6.83	0.021
Error	13	28.01	2.155		
Total	15	65.14			

### Model Summary

S	R-sq	R-sq(adj)
1.46798	56.99%	50.38%

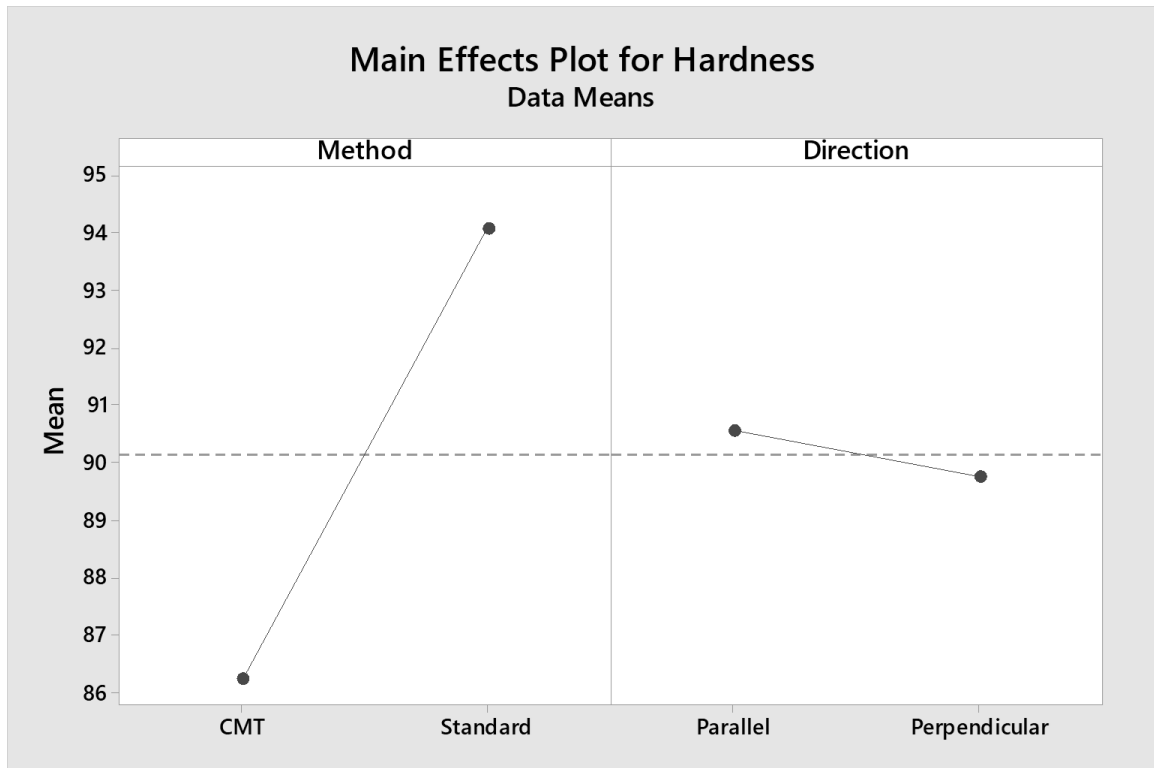
### Analysis of Variance for UTS (Kips)

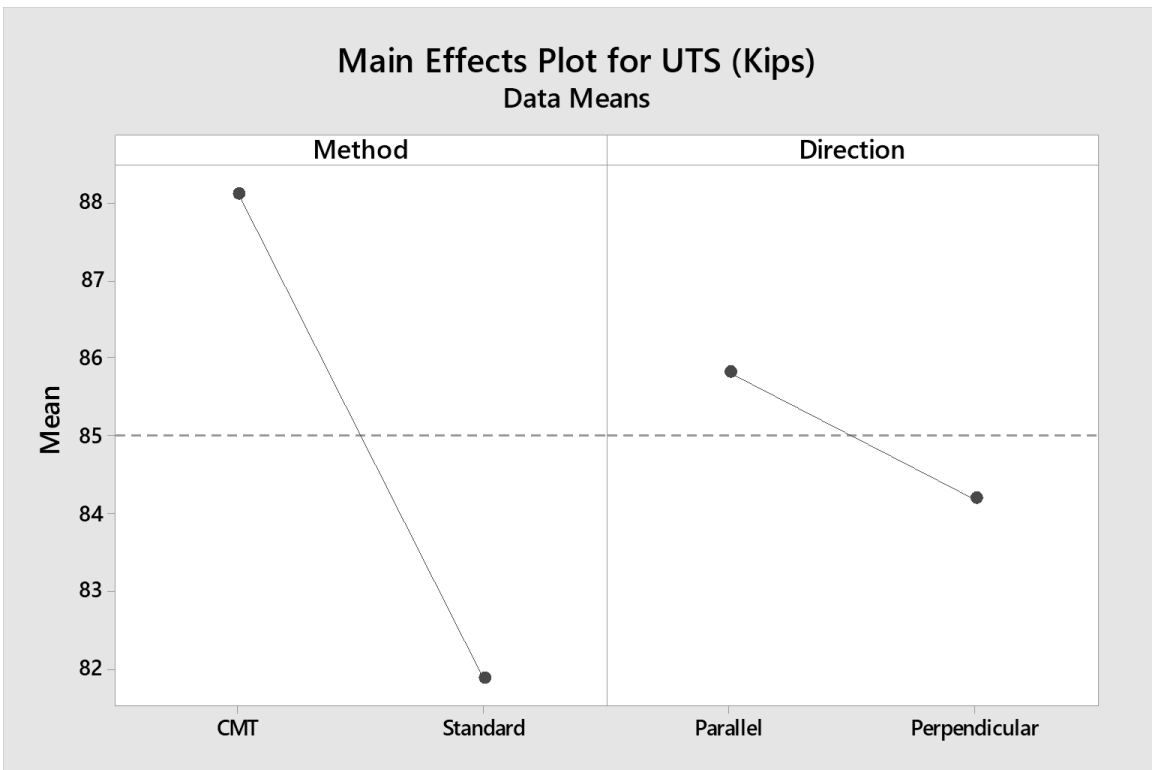
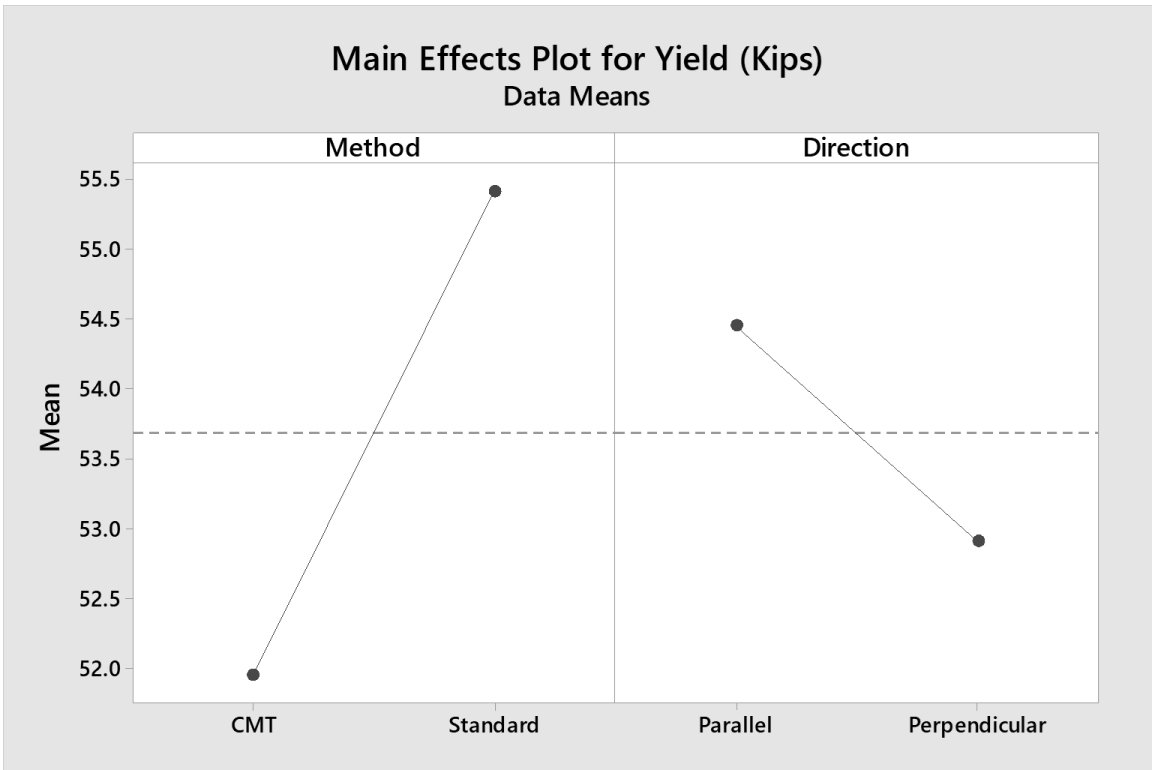
Source	DF	SS	MS	F	P
Method	1	63.92	63.920	28.77	0.000
Direction	1	41.47	41.474	18.67	0.001
Error	13	28.88	2.221		
Total	15	134.27			

### Model Summary

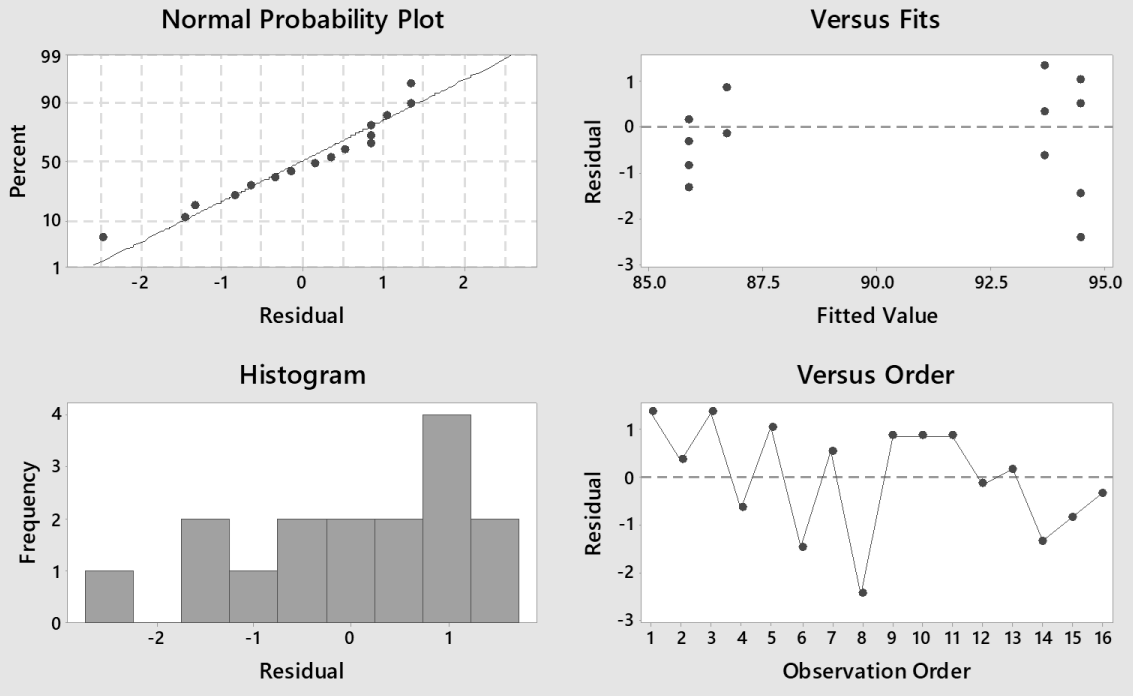
S	R-sq	R-sq(adj)
1.49046	78.49%	75.18%

# ER308L ANOVA – CMT

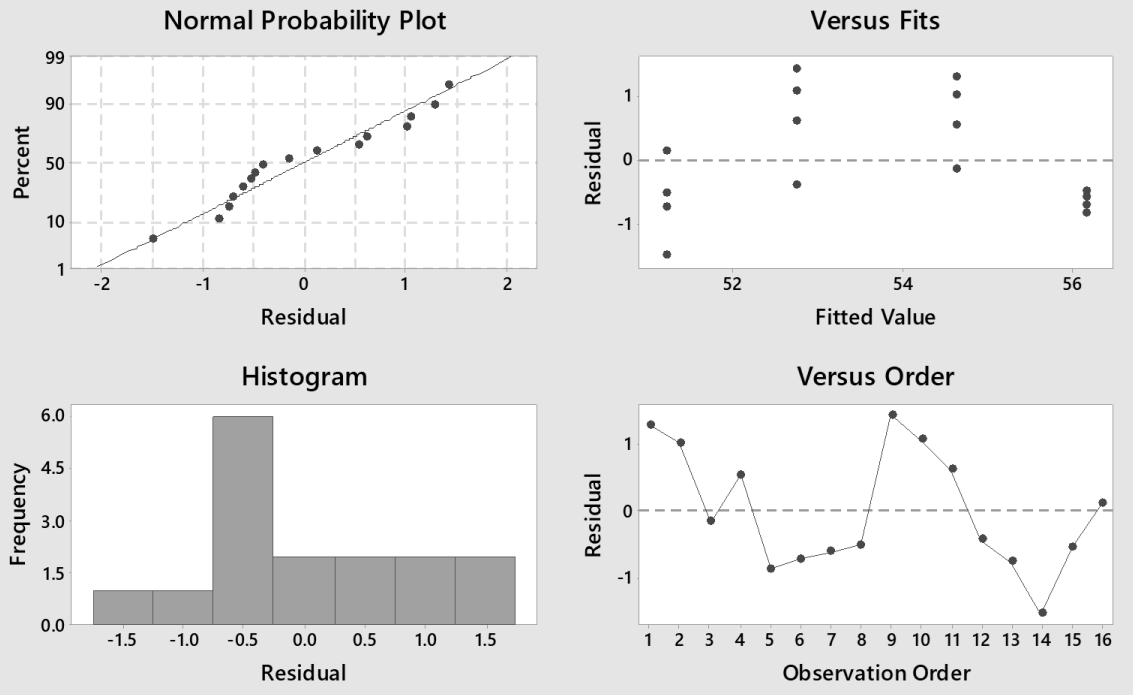




## Residual Plots for Hardness



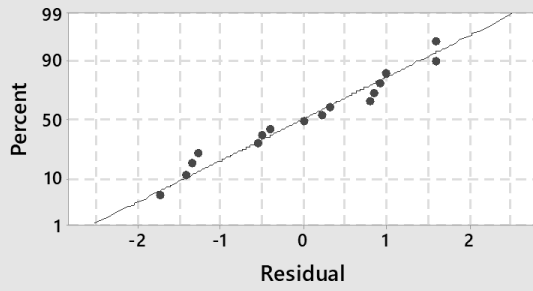
## Residual Plots for Yield (Kips)



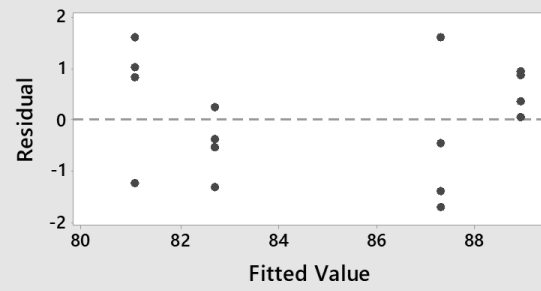


### Residual Plots for UTS (Kips)

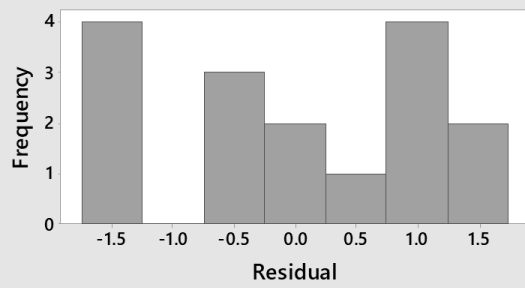
Normal Probability Plot



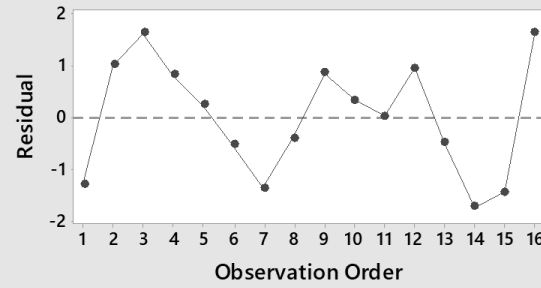
Versus Fits



Histogram



Versus Order

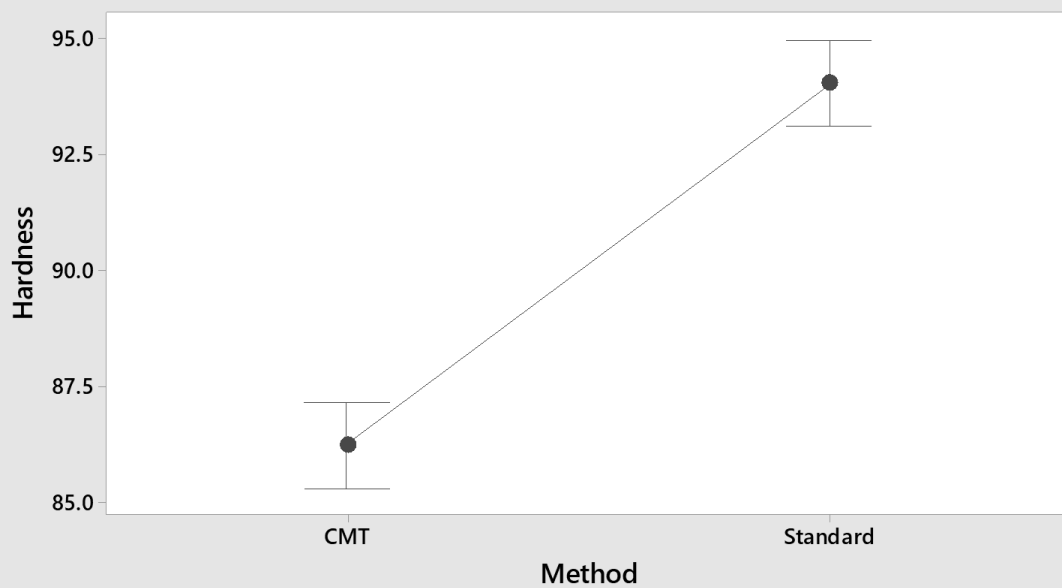


### Tukey Simultaneous 95% CIs Differences of Means for Hardness



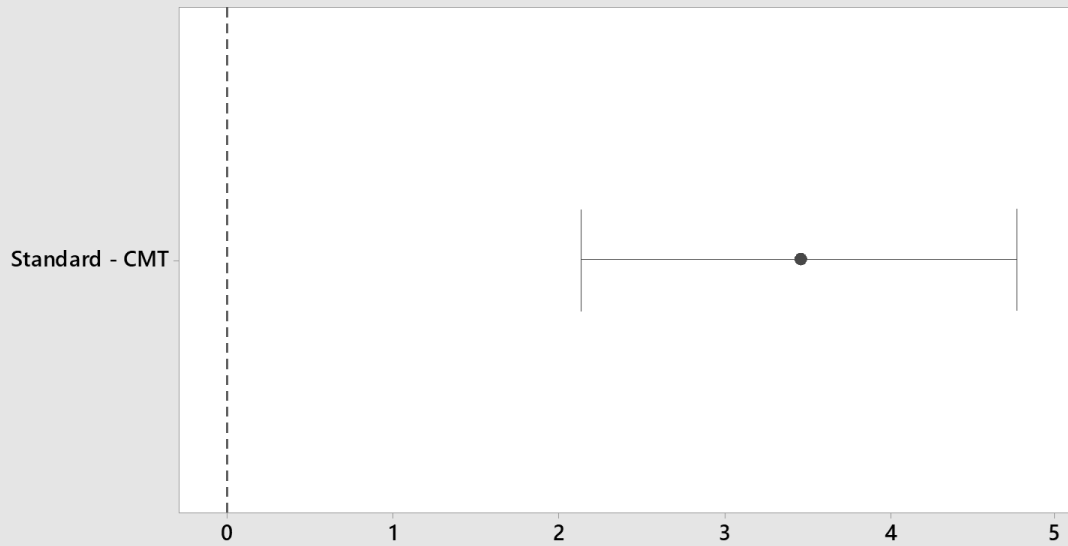
*If an interval does not contain zero, the corresponding means are significantly different.*

### Interval Plot of Hardness vs Method 95% CI for the Mean



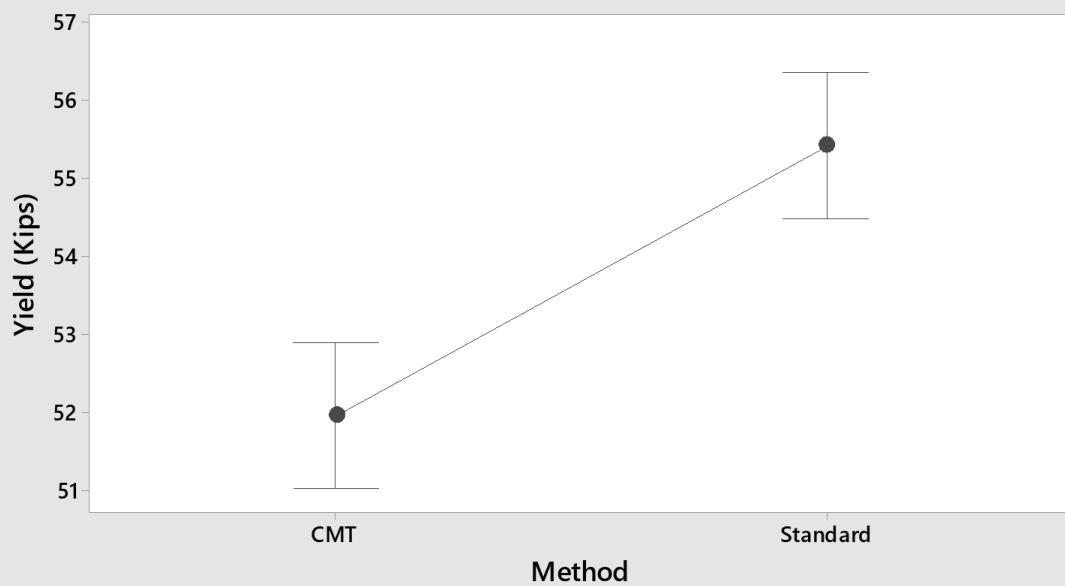
*The pooled standard deviation is used to calculate the intervals.*

### Tukey Simultaneous 95% CIs Differences of Means for Yield (Kips)



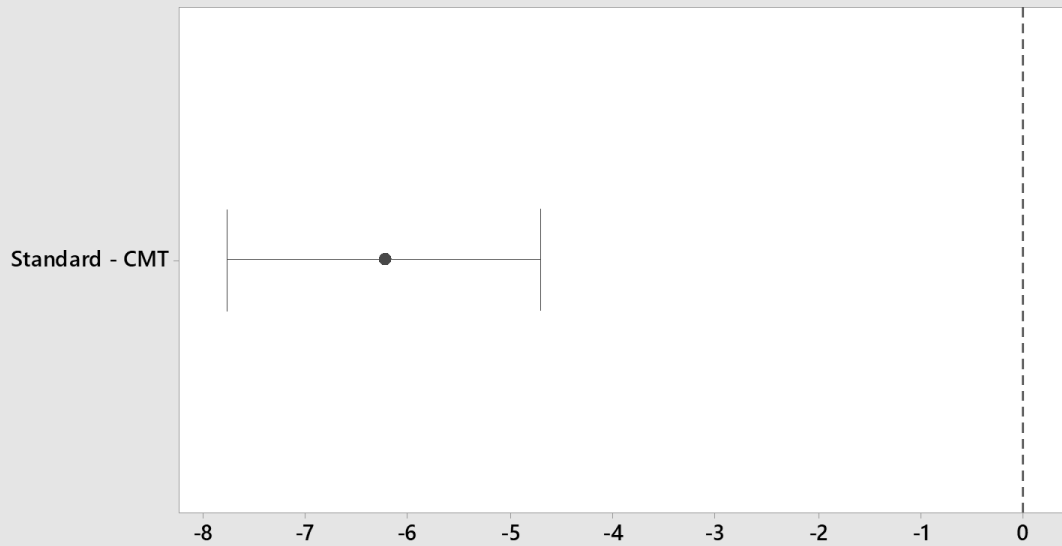
*If an interval does not contain zero, the corresponding means are significantly different.*

### Interval Plot of Yield (Kips) vs Method 95% CI for the Mean



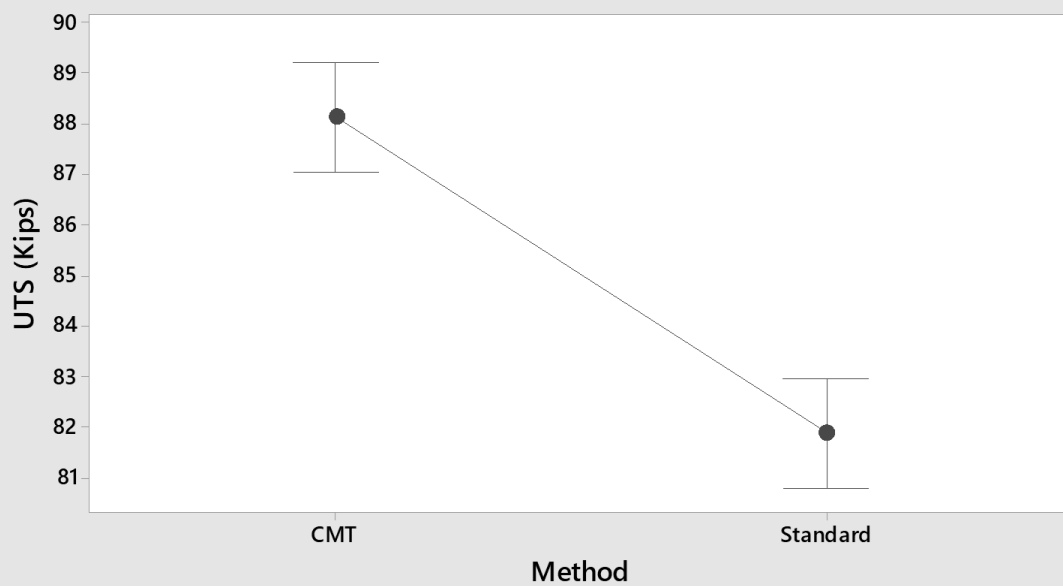
*The pooled standard deviation is used to calculate the intervals.*

### Tukey Simultaneous 95% CIs Differences of Means for UTS (Kips)



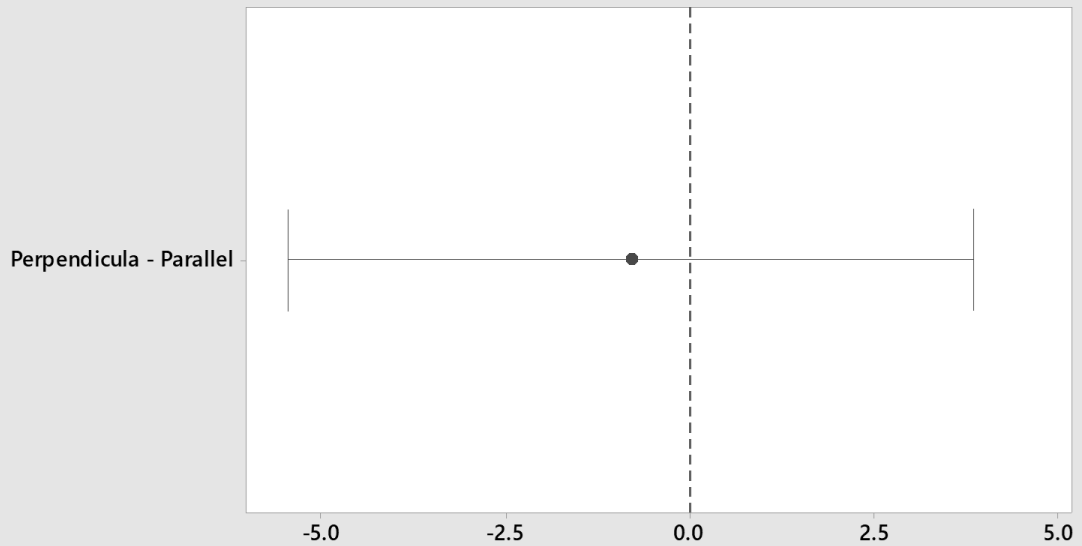
*If an interval does not contain zero, the corresponding means are significantly different.*

### Interval Plot of UTS (Kips) vs Method 95% CI for the Mean



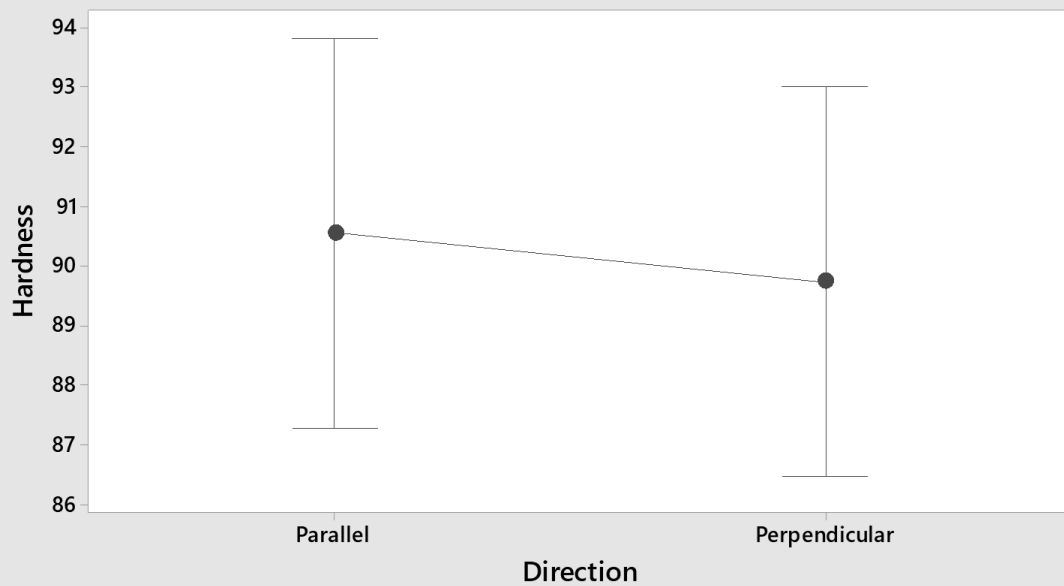
*The pooled standard deviation is used to calculate the intervals.*

### Tukey Simultaneous 95% CIs Differences of Means for Hardness



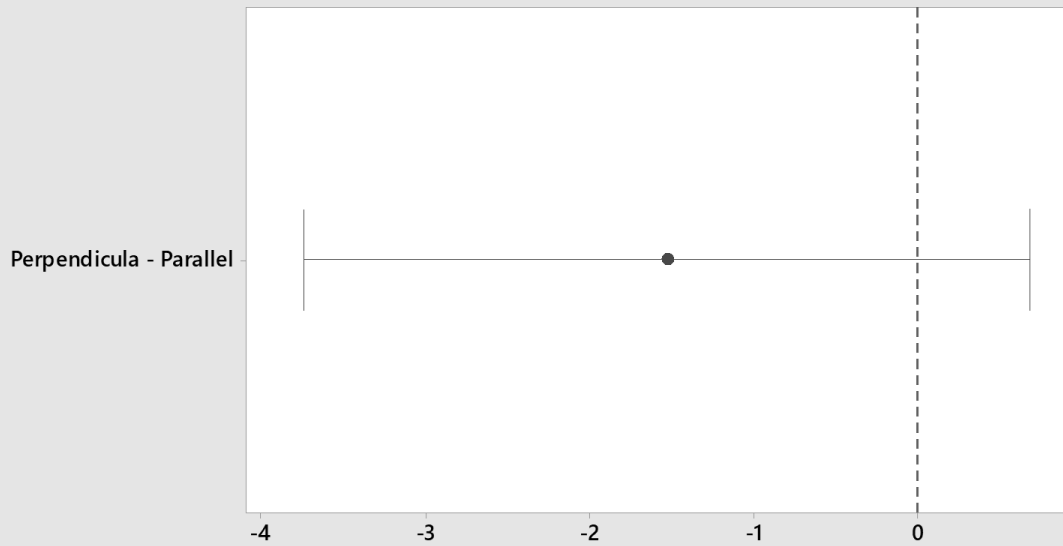
*If an interval does not contain zero, the corresponding means are significantly different.*

### Interval Plot of Hardness vs Direction 95% CI for the Mean



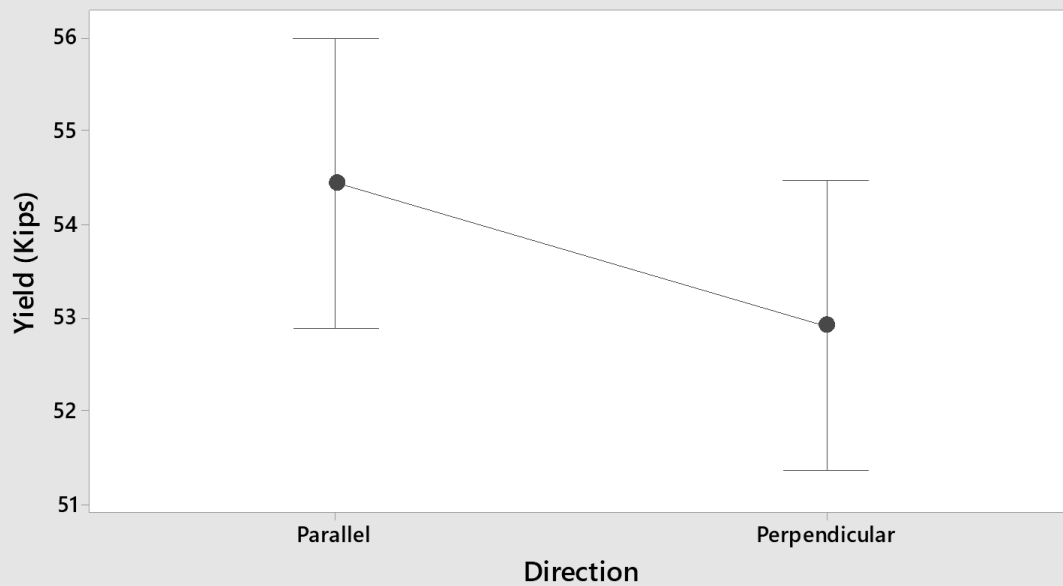
*The pooled standard deviation is used to calculate the intervals.*

### Tukey Simultaneous 95% CIs Differences of Means for Yield (Kips)



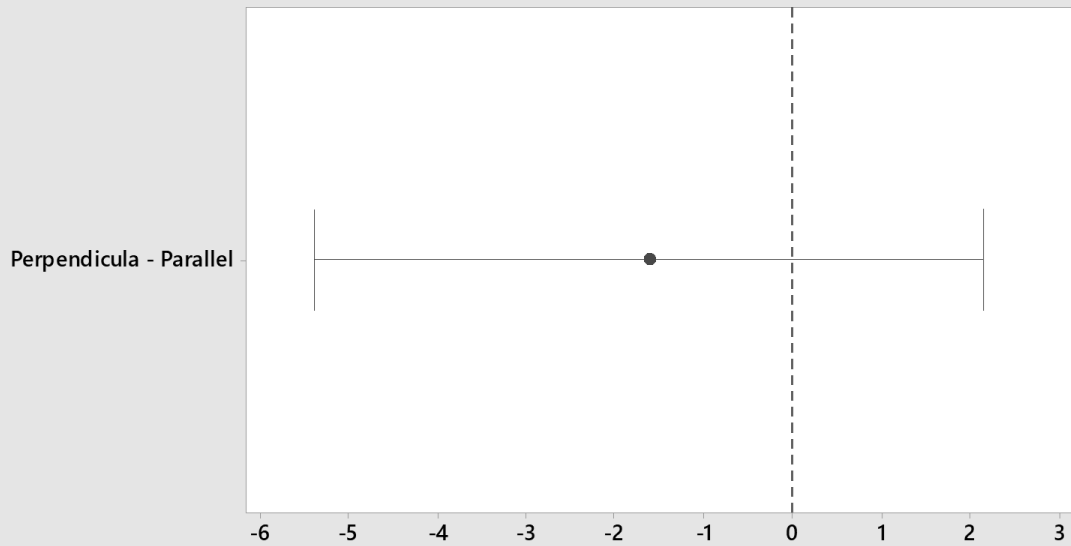
*If an interval does not contain zero, the corresponding means are significantly different.*

### Interval Plot of Yield (Kips) vs Direction 95% CI for the Mean



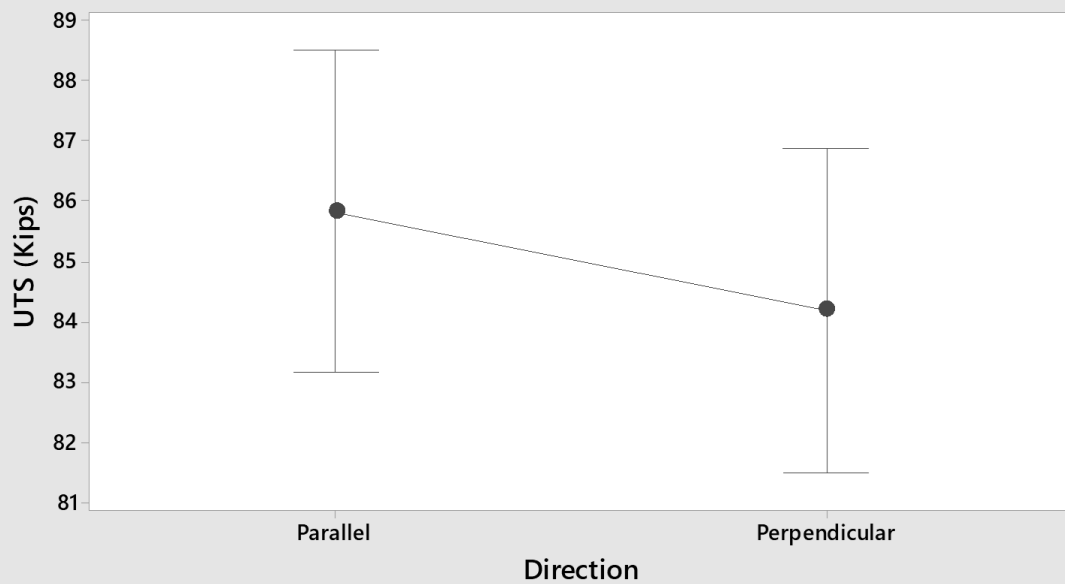
*The pooled standard deviation is used to calculate the intervals.*

### Tukey Simultaneous 95% CIs Differences of Means for UTS (Kips)



*If an interval does not contain zero, the corresponding means are significantly different.*

### Interval Plot of UTS (Kips) vs Direction 95% CI for the Mean



*The pooled standard deviation is used to calculate the intervals.*

### Analysis of Variance for Hardness

Source	DF	SS	MS	F	P
Method	1	244.141	244.141	170.84	0.000
Direction	1	2.641	2.641	1.85	0.197
Error	13	18.578	1.429		
Total	15	265.359			

### Model Summary

S	R-sq	R-sq(adj)
1.19544	93.00%	91.92%

### Analysis of Variance for Yield (Kips)

Source	DF	SS	MS	F	P
Method	1	47.636	47.6357	53.12	0.000
Direction	1	9.441	9.4411	10.53	0.006
Error	13	11.659	0.8968		
Total	15	68.735			

### Model Summary

S	R-sq	R-sq(adj)
0.947005	83.04%	80.43%

### Analysis of Variance for UTS (Kips)

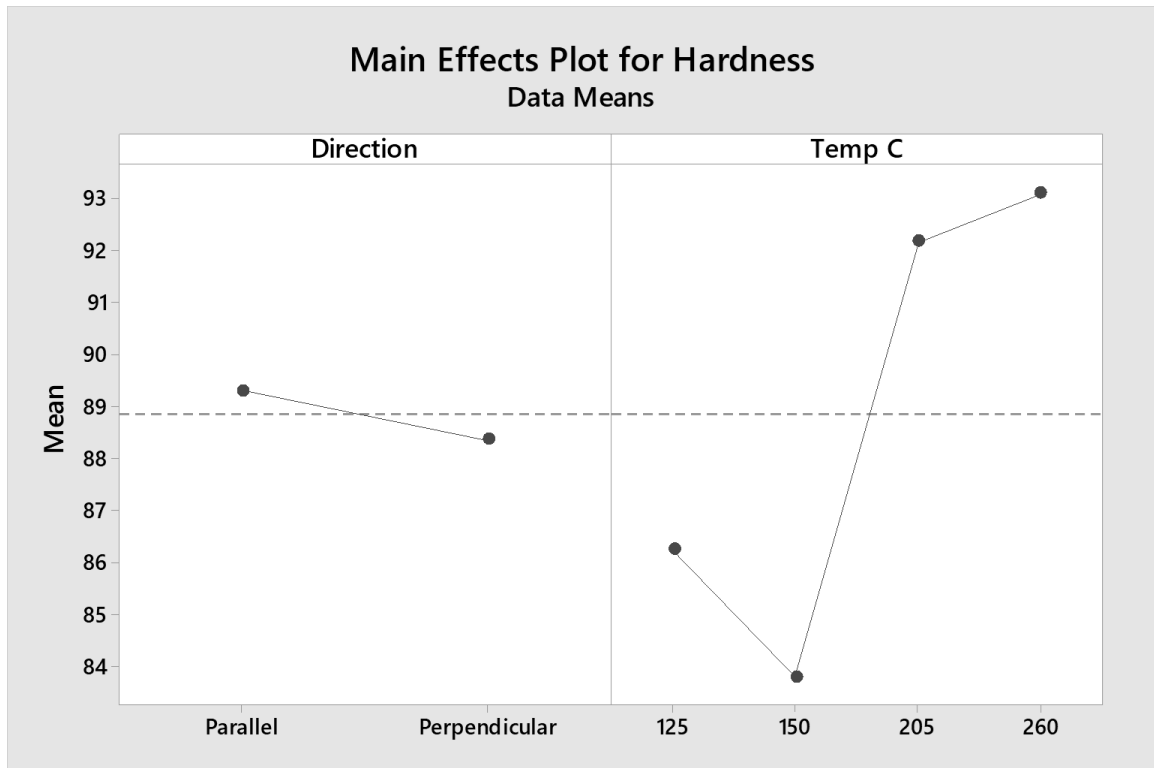
Source	DF	SS	MS	F	P
Method	1	155.58	155.585	113.97	0.000
Direction	1	10.62	10.615	7.78	0.015
Error	13	17.75	1.365		
Total	15	183.95			

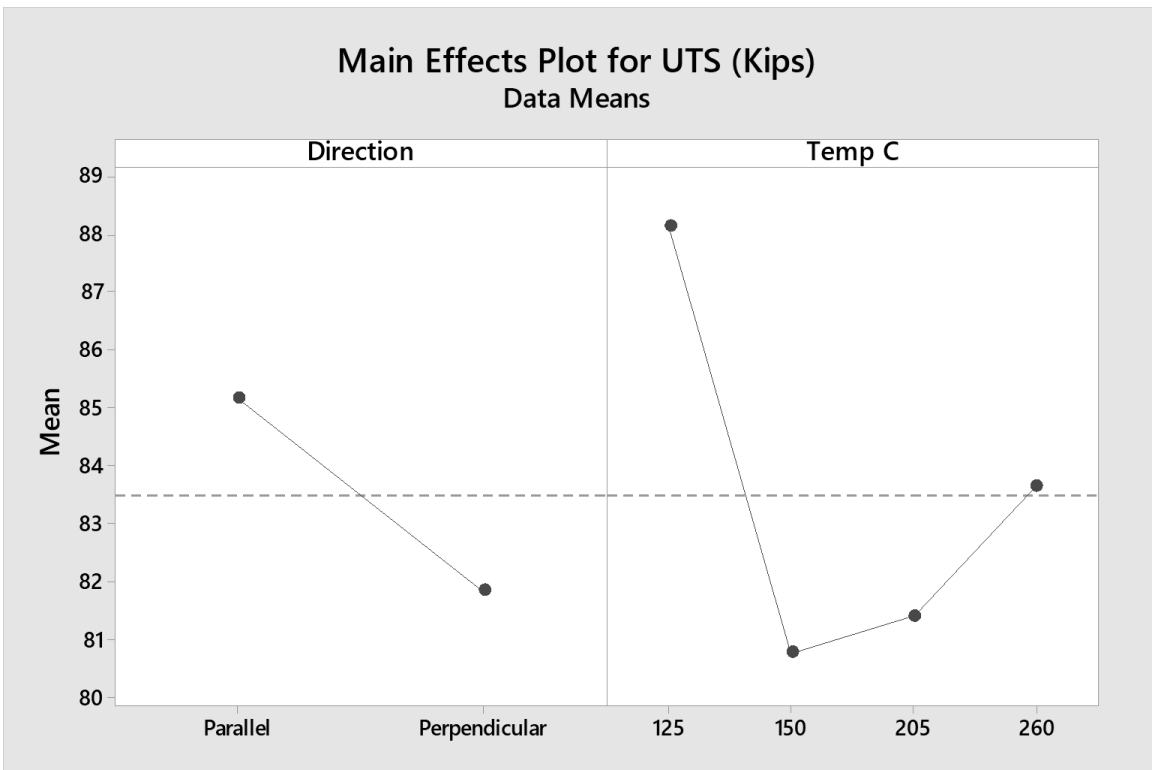
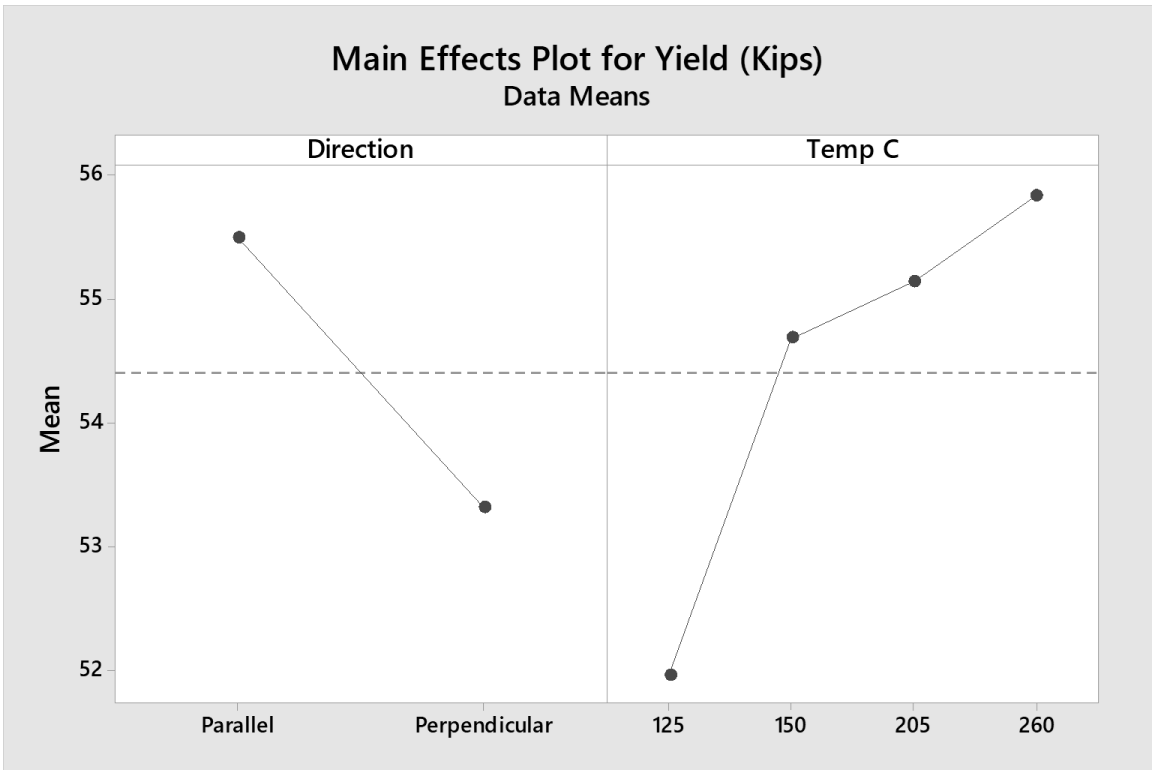
### Model Summary

S	R-sq	R-sq(adj)
1.16840	90.35%	88.87%

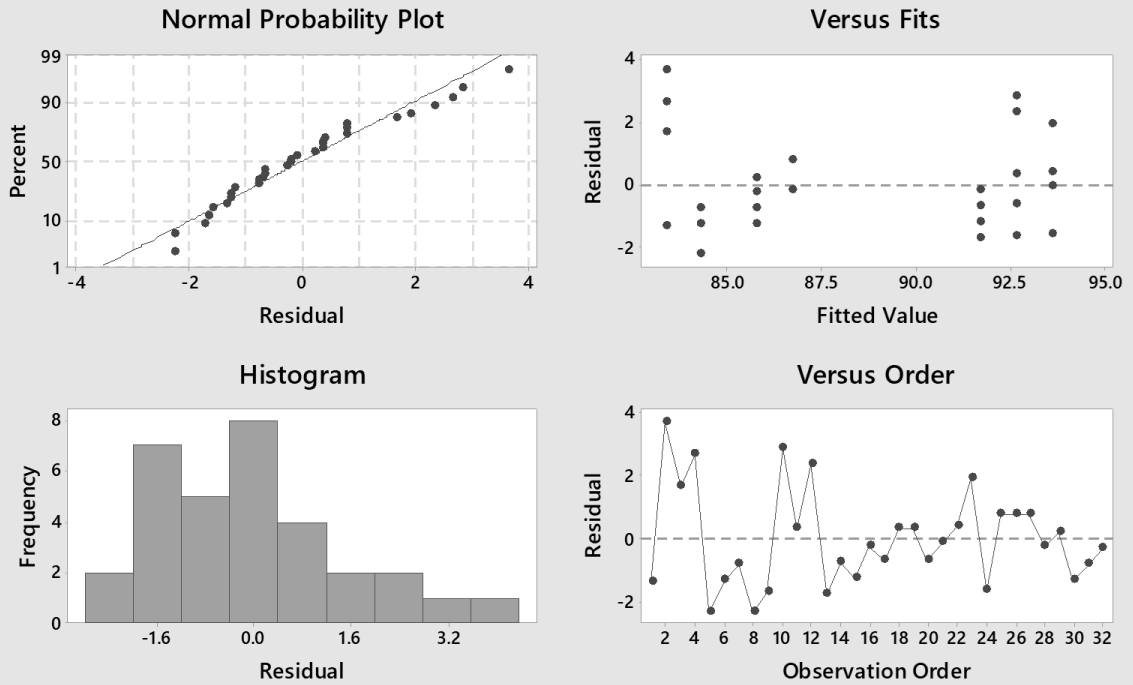


## ER308L ANOVA – Temperature

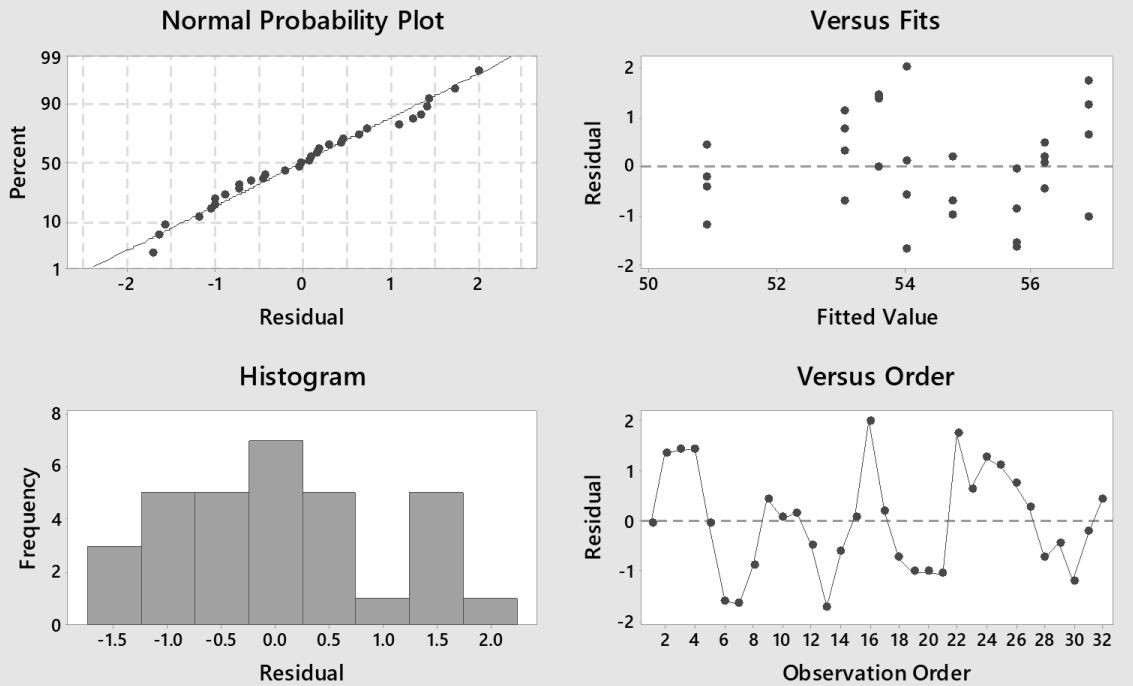




## Residual Plots for Hardness

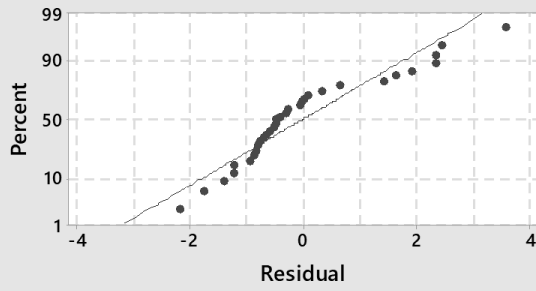


## Residual Plots for Yield (Kips)

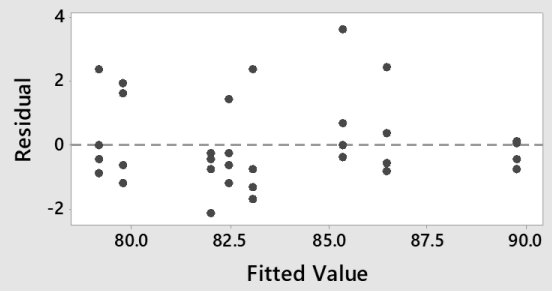


# Residual Plots for UTS (Kips)

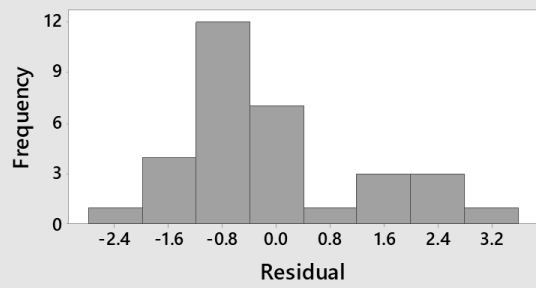
## Normal Probability Plot



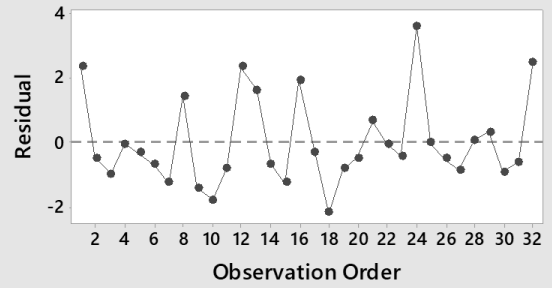
## Versus Fits



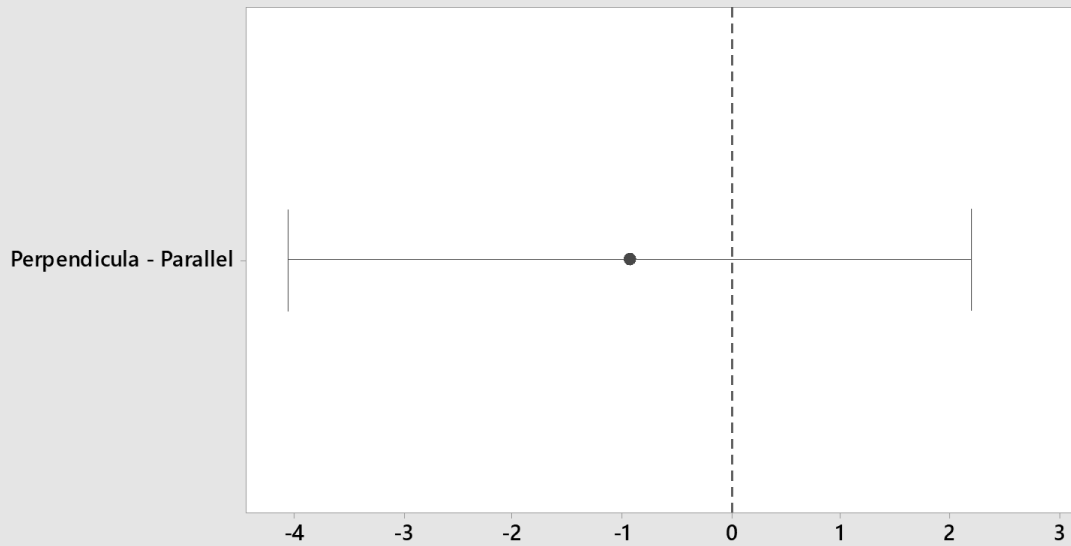
## Histogram



## Versus Order

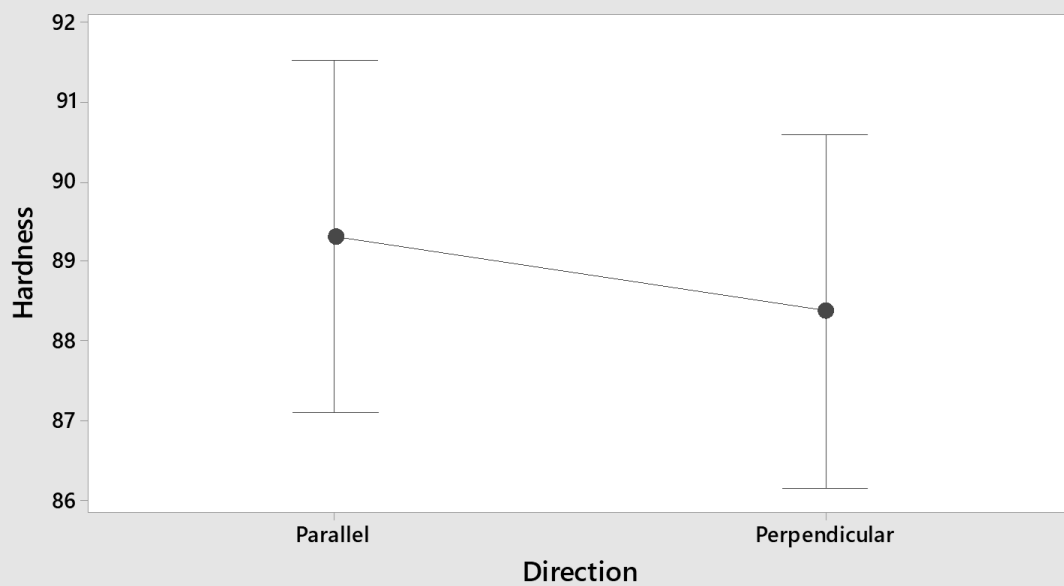


### Tukey Simultaneous 95% CIs Differences of Means for Hardness



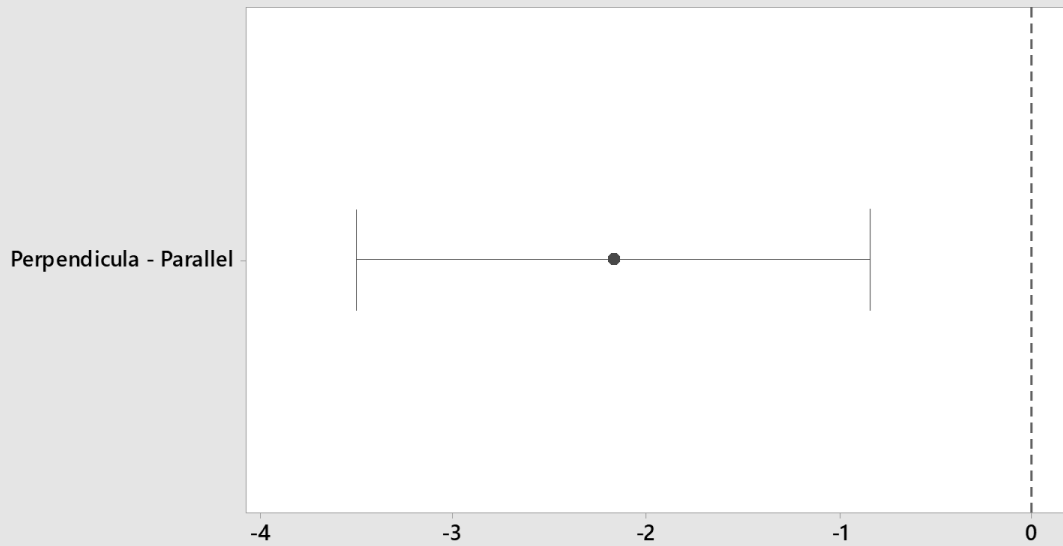
*If an interval does not contain zero, the corresponding means are significantly different.*

### Interval Plot of Hardness vs Direction 95% CI for the Mean



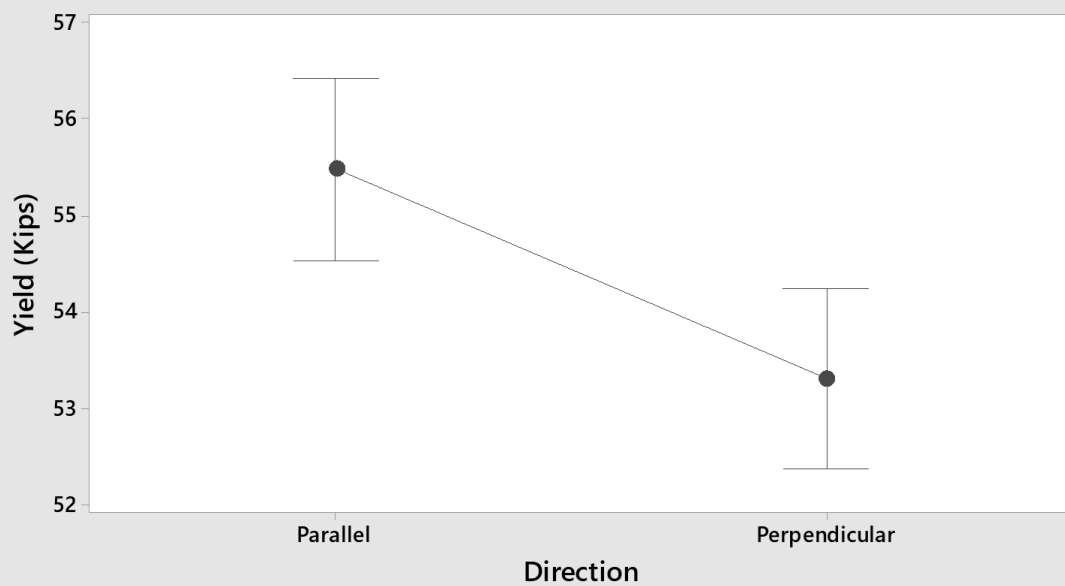
*The pooled standard deviation is used to calculate the intervals.*

### Tukey Simultaneous 95% CIs Differences of Means for Yield (Kips)



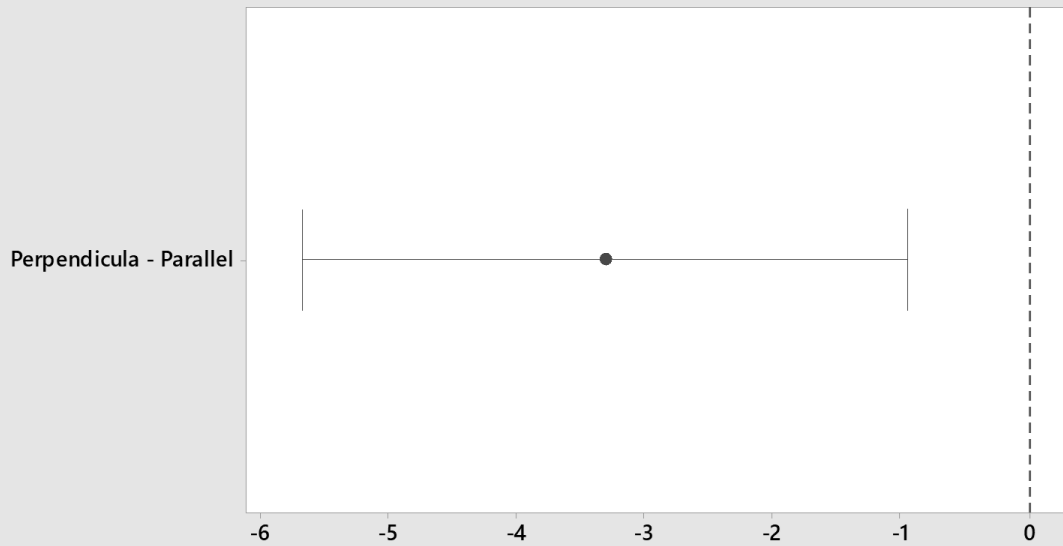
*If an interval does not contain zero, the corresponding means are significantly different.*

### Interval Plot of Yield (Kips) vs Direction 95% CI for the Mean



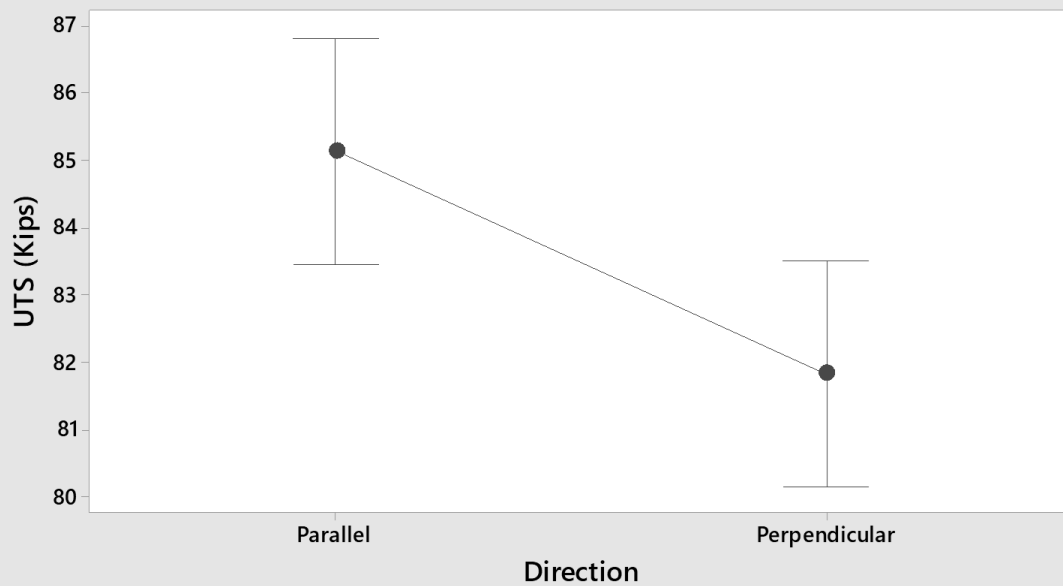
*The pooled standard deviation is used to calculate the intervals.*

### Tukey Simultaneous 95% CIs Differences of Means for UTS (Kips)



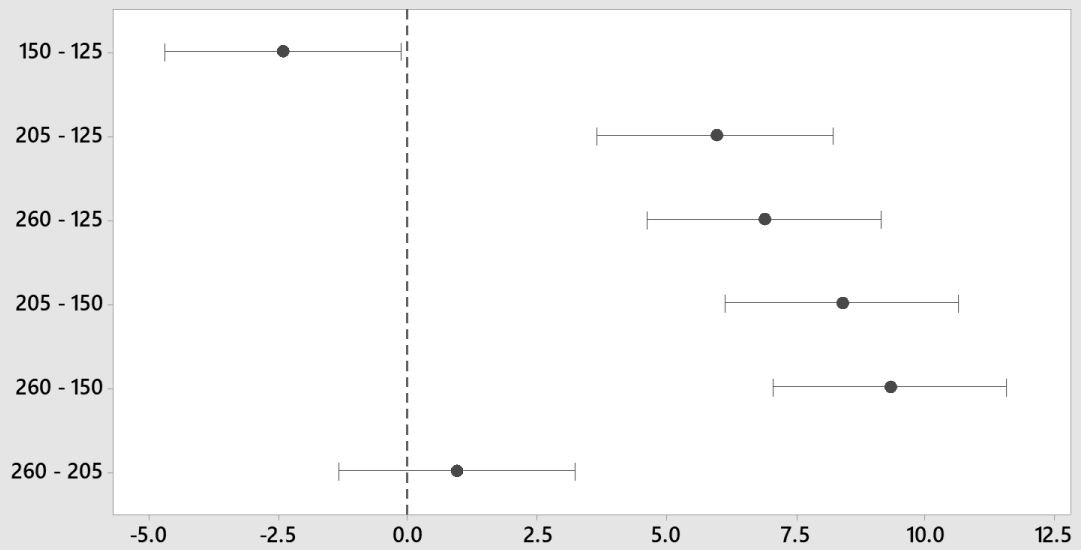
*If an interval does not contain zero, the corresponding means are significantly different.*

### Interval Plot of UTS (Kips) vs Direction 95% CI for the Mean



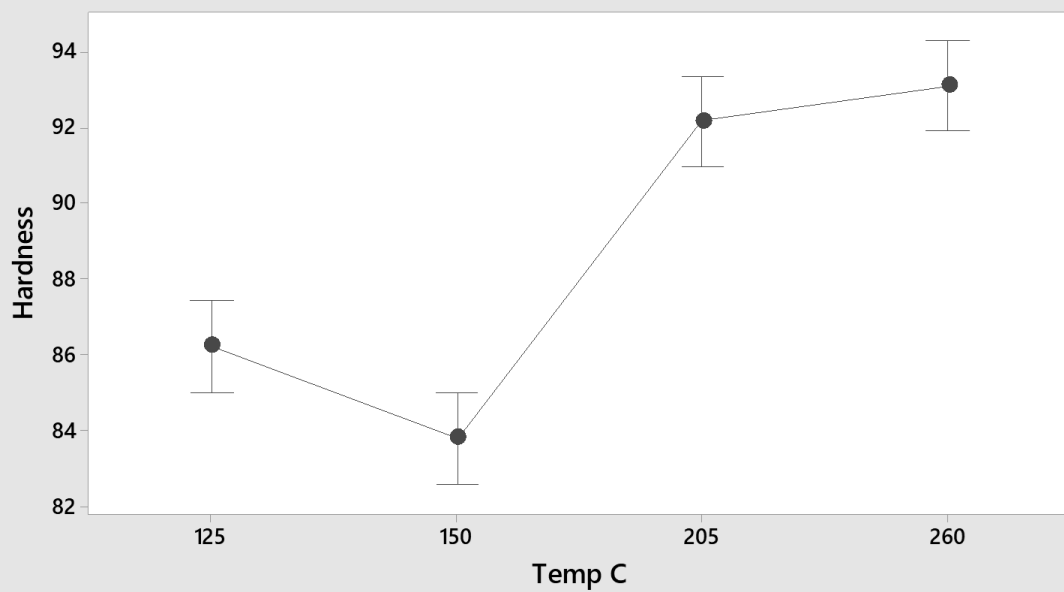
*The pooled standard deviation is used to calculate the intervals.*

### Tukey Simultaneous 95% CIs Differences of Means for Hardness



If an interval does not contain zero, the corresponding means are significantly different.

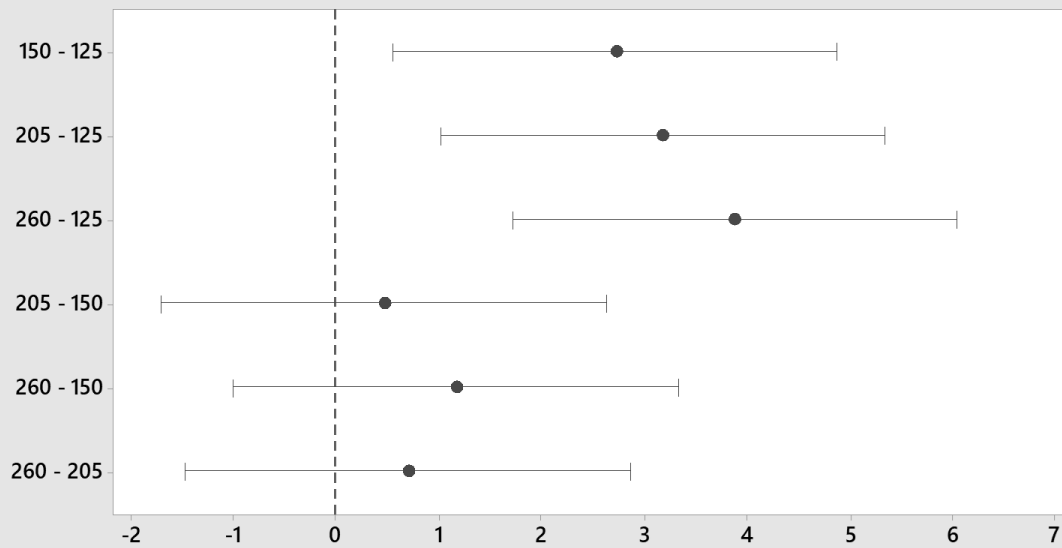
### Interval Plot of Hardness vs Temp C 95% CI for the Mean



The pooled standard deviation is used to calculate the intervals.

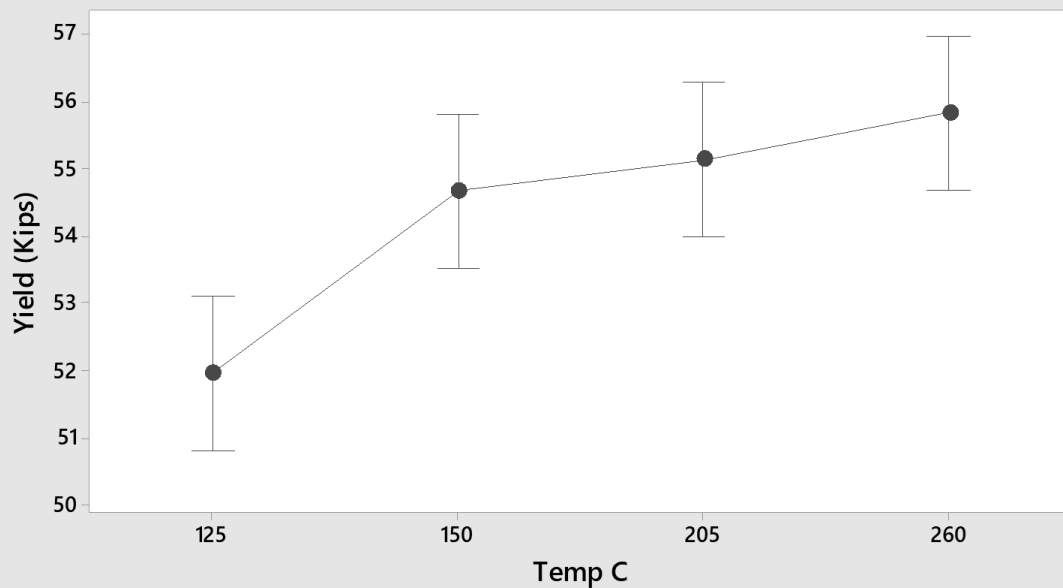


### Tukey Simultaneous 95% CIs Differences of Means for Yield (Kips)



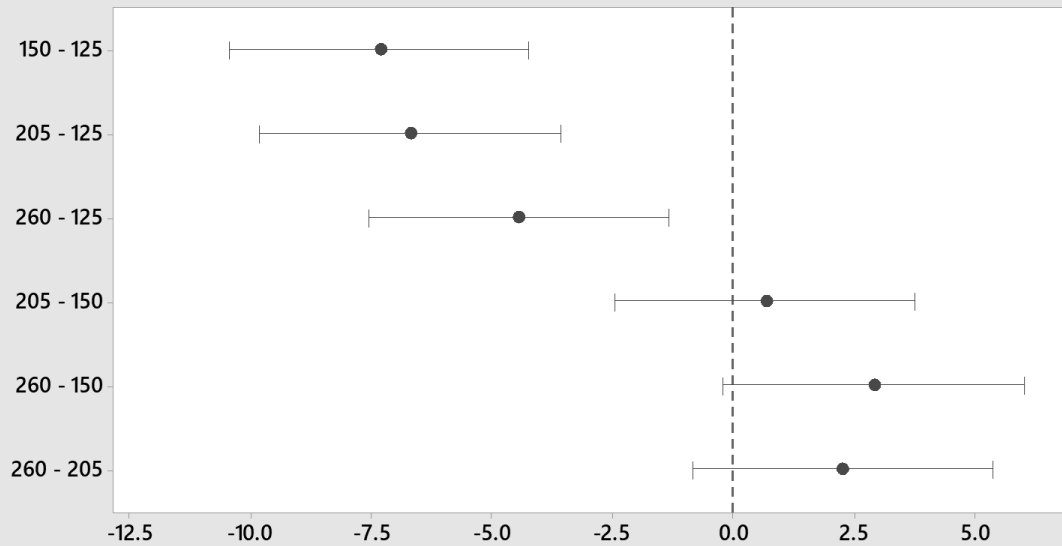
If an interval does not contain zero, the corresponding means are significantly different.

### Interval Plot of Yield (Kips) vs Temp C 95% CI for the Mean



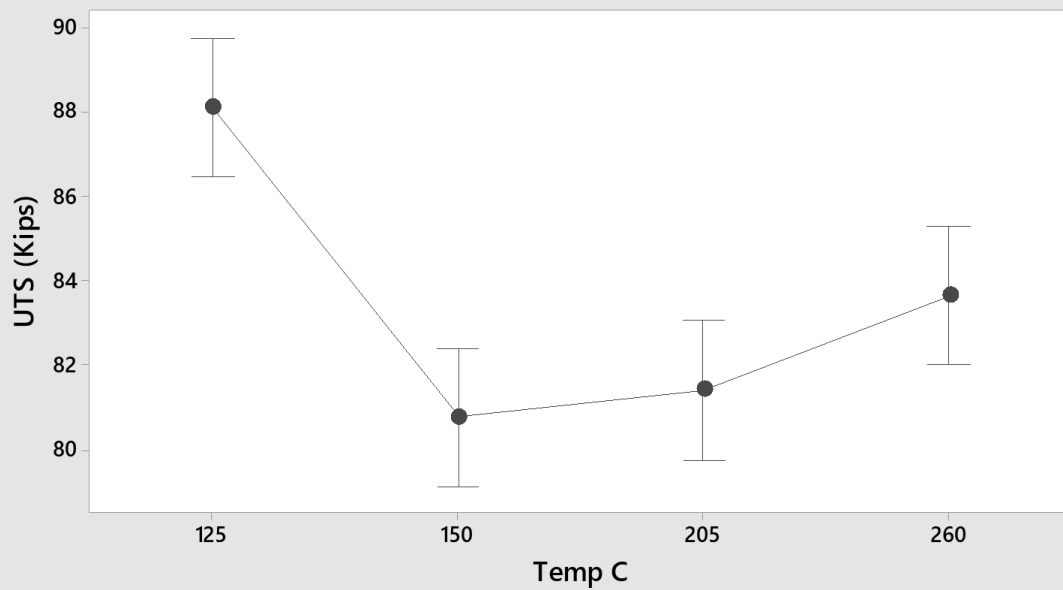
The pooled standard deviation is used to calculate the intervals.

### Tukey Simultaneous 95% CIs Differences of Means for UTS (Kips)



If an interval does not contain zero, the corresponding means are significantly different.

### Interval Plot of UTS (Kips) vs Temp C 95% CI for the Mean



The pooled standard deviation is used to calculate the intervals.

### Analysis of Variance for Hardness

Source	DF	SS	MS	F	P
Direction	1	7.031	7.031	2.68	0.113
Temp C	3	492.406	164.135	62.61	0.000
Error	27	70.781	2.622		
Total	31	570.219			

### Model Summary

S	R-sq	R-sq(adj)
1.61911	87.59%	85.75%

### Analysis of Variance for Yield (Kips)

Source	DF	SS	MS	F	P
Direction	1	37.73	37.728	31.24	0.000
Temp C	3	68.94	22.981	19.03	0.000
Error	27	32.61	1.208		
Total	31	139.28			

### Model Summary

S	R-sq	R-sq(adj)
1.09892	76.59%	73.12%

### Analysis of Variance for UTS (Kips)

Source	DF	SS	MS	F	P
Direction	1	87.84	87.842	41.28	0.000
Temp C	3	265.34	88.447	41.57	0.000
Error	27	57.45	2.128		
Total	31	410.63			

### Model Summary

S	R-sq	R-sq(adj)
1.45871	86.01%	83.94%

## **Appendix V – Material Data Sheets**

**COPPERFREE™ WELDING  
PARAMETERS AND PACKAGE OPTIONS**



**APPROXIMATE WELDING PARAMETERS:**

GRADE	DIA.	POLARITY	TRANSFER MODE	WIRE FEED SPEED in/min (m/min)		VOLTAGE		AMPERAGE	
				Min.	Max.	Min.	Max.	Min.	Max.
Copperfree™	0.030	DCEP	Short Circuit	75 (1.9)	300 (7.6)	17	22	45	130
Copperfree™	0.035	DCEP	Short Circuit	100 (2.5)	400 (10.1)	17	24	75	180
Copperfree™	0.035	DCEP	Spray	375 (9.5)	625 (15.9)	23	29	180	280
Copperfree™	0.045	DCEP	Globular	100 (2.5)	425 (10.8)	18	24	125	225
Copperfree™	0.045	DCEP	Short Circuit	125 (3.2)	450 (11.4)	18	24	125	225
Copperfree™	0.045	DCEP	Spray	350 (8.9)	500 (12.7)	26	30	250	350
Copperfree™	0.052	DCEP	Globular	175 (4.4)	300 (7.6)	18	26	150	250
Copperfree™	0.052	DCEP	Short Circuit	200 (5.1)	325 (8.3)	22	26	200	300
Copperfree™	0.052	DCEP	Spray	300 (7.6)	500 (12.7)	27	31	300	425
Copperfree™	0.062	DCEP	Globular	180 (4.6)	320 (8.1)	19	27	150	250
Copperfree™	0.062	DCEP	Short Circuit	190 (4.8)	325 (8.3)	23	27	200	325
Copperfree™	0.062	DCEP	Spray	200 (5.1)	375 (9.5)	27	31	325	425

PACKAGES
33-lb. Fiber Spool - Random Wound
45-lb. Fiber Spool - Random Wound
60-lb. Fiber Spool - Random Wound
250-lb. Smart Pak - 100% Recyclable
300-lb. Tru-Trac® NS
500-lb. Drum Pack
500-lb. Smart Pak - 100% Recyclable
900-lb. Drum Pack
900-lb. Smart Pak - 100% Recyclable
425-lb. Trigger Trac® NS
1,000-lb. Tru-Trac® NS
1,000-lb. Wood Reel

Note: See "Premium Packaging Options" for full description of packages. For additional packages, please contact NS Customer Service at 1-800-777-1618.

Exclusive to NS customers.

**DISCLAIMER:**  
The information contained or otherwise referenced herein is presented only in "typical" without guarantee or warranty, and National Standard expressly disclaims any liability incurred from any reliance thereon. Typical data are obtained when welded and tested in accordance with AWS specifications. Specification, other tests and procedures may produce different results. No data is to be construed as a recommendation for any welding condition or technique not controlled by National Standard LLC.

For Material Safety Data Sheets (MSDS) and Certificates of Compliance, visit our website at [www.nationalstandard.com](http://www.nationalstandard.com)

**National Standard** | 1-800-777-1618  
**Customer Service** | 405-372-7954 (fax)  
©2014 National Standard / Cat. # 062014



[www.nationalstandard.com](http://www.nationalstandard.com)

# AWS A5.18 ER70S-6

Quote This

Solid Electrodes and Rods, Welding Wire -- ER70S-6

## ER70S-6

**ER70S-6** [ER48S-6] are intended for both single- and multi-pass welding. They are especially suited for sheet metal applications, where smooth weld beads are desired, and structural and plate steels that have moderate amounts of rust or mill scale. These electrodes permit the use of higher current ranges with either CO<sub>2</sub> (AWS A5.32 Class SG-C) shielding gas or with mixtures of argon and oxygen (AWS A5.32 Class SG-AC-Y).

However, these electrodes do require a higher level of oxidation than the previously described electrodes when using either binary or ternary argon shielding gas mixtures per the AWS A5.32 specification. Typical base metal specifications are often the same as those for the "ER70S-2 [ER48S-2] classification.

Nominal Chemical Composition (%)												Tensile Strength		Yield Strength		Elongation	Average Impact Strength	
C	Mn	Si	P	S	Ni	Cr	Mo	V	Cu	Ti	Zr	Al	psi (min)	MPa (min)	psi (min)	MPa (min)	% (min)	20 ft·lbf @
0.06-0.15	1.40-1.85	0.80-1.15	0.025 max	0.035 max	0.15 max	0.15 max	0.15 max	0.03 max	0.50 max	-	-	-	70,000	480	58,000	400	22	-20°F

# AWS A5.9 ER308L

Quote This

**ER308L** or **Alloy 308L** has the same analysis as type 308 except the carbon content has been held to a maximum of .03% to reduce the possibility of intergranular carbide precipitation. Balanced chromium and nickel levels provide enough ferrite in the weld for high resistance to hot cracking.

## ER308L Applications

ER308L is used to weld metals with similar composition, such as 304L in wrought and cast forms. Ideal for welding Types 304L, 321, and 347 stainless steels. This is a suitable wire for applications at cryogenic temperatures.

## Specifications:

- AWS A5.9 ER308L
- UNS S30880

Nominal Chemistry Composition (%)									
C	Cr	Ni	Mn	Si	P	S	Mo	Cu	
0.03 max	19.5-22.0	9.0-11.0	1.0-2.5	0.30-0.65	0.03 max	0.03 max	0.75 max	0.75 max	

### Mechanical Properties

Tensile Strength (psi)	87,000
Yield Strength (psi)	57,000
Elongation (no units)	34%

## **Appendix VI – Wiring Diagram**

Here at Auburn University's Design and Manufacturing Laboratory (DML), research has been proceeding to develop an automation product that establishes new standards for quality, technological leadership, and operating excellence. With printing success as the primary focus, work has been proceeding on the crudely conceived idea of an instrument that would not only provide control of inverse reactive currents (CMT, CMT-Advanced Pulsed, Advanced, Pulsed), for use in unilateral layer deposition, but would also be capable of automatically synchronizing cardinal objectives. Basically, the only new principle involved is that instead of prints being generated by the relative motion of a conductor and flux, it is produced by the interaction of magnetic reluctance and capacitive reactance. Such an instrument comprised of MeanWell power supplies, Fronius' analog/digital control schemes, Sealevel's I/O board, Omega Engineering's process controller, and all monitored by Artsoft's Mach3 Software is the Wire + Arc Additive Manufacturing Control Encumulator (portmanteau: control enclosure/accumulator).

The Control Encumulator has a base plate of poly(methyl methacrylate), enclosed by a malleable acrylonitrile butadiene styrene casing in such a way that the units are in a direct line without the need for a passive fan. The lineup consists simply of four units, so fitted to the Deutsches Institut fur Normung guide (DIN-Rail) that signal side-fumbling is effectually prohibited. The Control Encumulator has now reached a fairly high level of development and is being successfully used in the operation of Cold Metal Transfer WAAM BAM (Wire + Arc Additive Manufacturing with Built-in Allowance for Machining) utilizing Hot Deposited Alloys of Metal (DAM). Figure 241 shows the wiring diagram for the Control Encumulator.



Sealevel RS-485 Modbus RTU

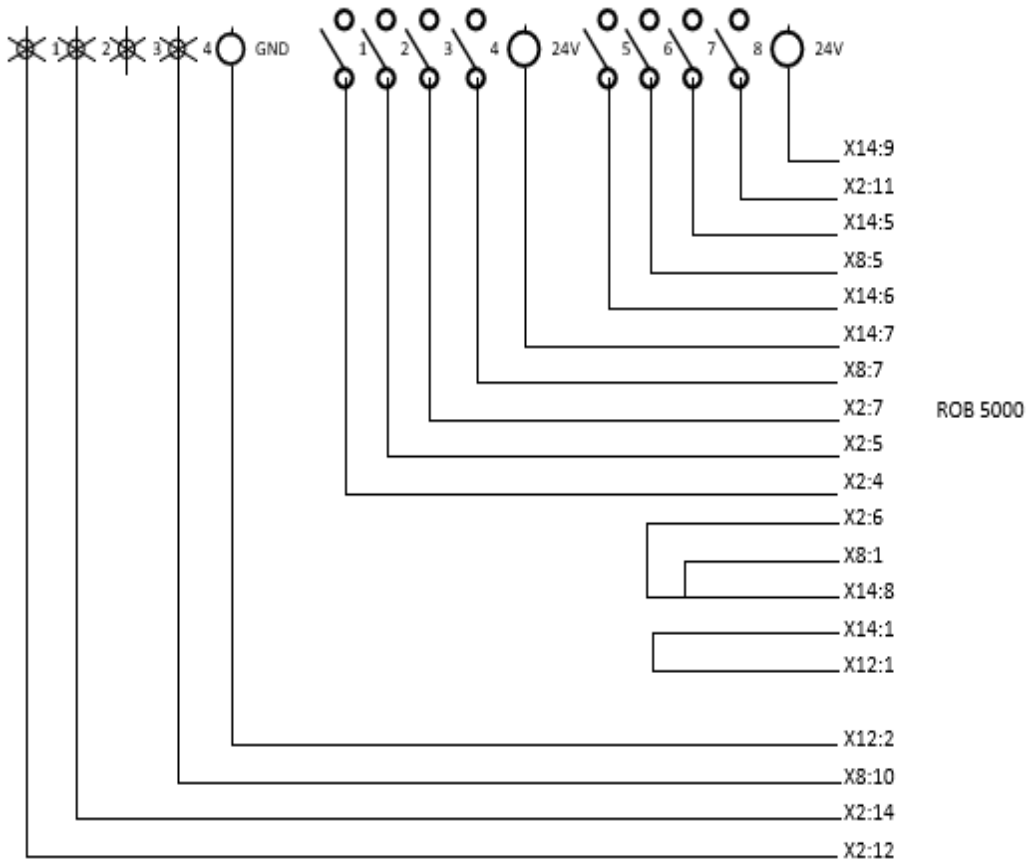


Figure 241: Control Encumulator Wiring Diagram

## **Appendix VII – Operating Manual**

## **Turning Everything On/Off**

The system requires multiple power inputs and shall be powered up according to the following schedule. The order for power up is as follows, turn on computer and launch Mach3 via the desktop icon, turn on the Probotix stepper motor drivers via red switch on the front of the stepper motor driver enclosure. Next, the control box containing the ROB 5000 is to be turned on via the switch on the side of the control box. The welder can now be turned on with a switch on the front of the unit.

Whenever the welder is turned on, go to the settings page on the RCU 5000 and change the parameters to 'Internal' instead of external before use. Once the parameters have been set, 'MIG/MAG' operation is to be selected. From here follow the on-screen prompts to select: material, wire diameter, gas, mode, etc. More detailed information can be found by reading the Fronius manual.

When operation of the machine is finished, the welder, control box, and stepper drivers should be turned off. If a print is not in progress the stepper drivers should be turned off due to heat issues. While the motors are off, care must be taken not to use Mach3 and move the welder, as the referenced coordinate system will be lost.

## **Controls Overview**

The welder is interfaced via the RCU as outlined in the equipment section. The wire offset distance probe control is programmed via M141 G-code command. To modify this command or other welder specific machine codes, one needs to go into the macros and adjust the VB scripts. The macros can be found via the file path: C:\Mach3\macros\3D\_Printer. They are saved as .m1s files. Before editing, one should become familiar with writing VB scripts and the nomenclature specific to Mach3.

## G-code

There is currently no software available to easily create G-code to produce a part for this machine. An adequate knowledge of G-code is necessary to operate the machine. One software that has been found to be very helpful in producing G-code is Autodesk's HSMWorks, which is a SolidWorks add-in and is available free download.

The creation of G-code is accomplished in HSMWorks by mimicking a milling toolpath using a trace or other function. For instance, if a wall is desired using the 1.25-mm zig zag, the path will be drawn out in a sketch and a trace path will be used. Setting the feed rate for the lead in and lead out to 700 mm/min and the feed rate for the desired in the print for the cutting feed rate will make post processing simpler. Figure 242 shows a sample of what this would look like.

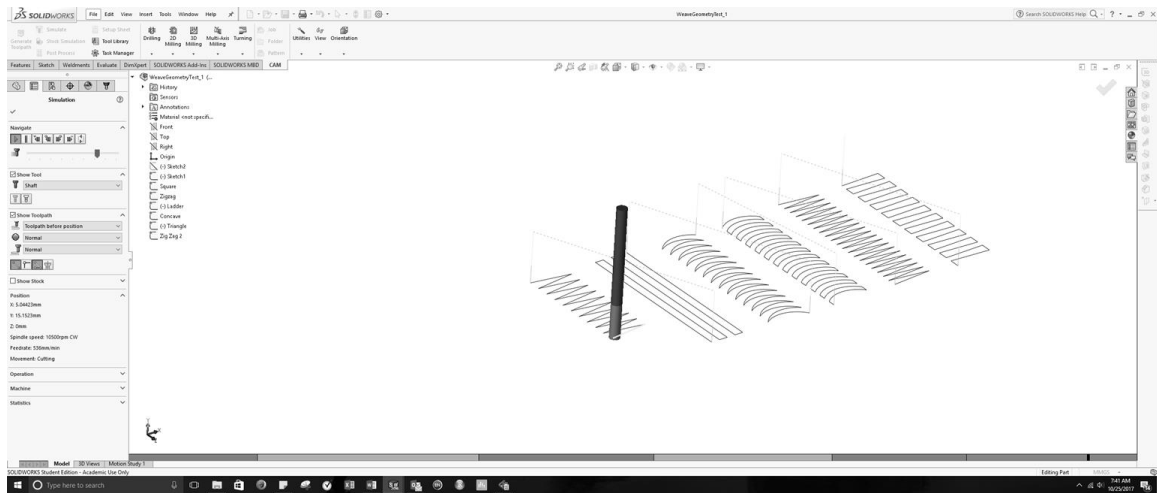


Figure 242. HSMWorks Toolpath Generation Shown for Stainless Geometries

Using the Mach3 specific post, the toolpaths are output and need to be post processed. The main codes needed to be added to the file are M111, M110, M141 codes to start and stop welding, and probe respectively. These codes are to be manually entered where appropriate. Between the layers, a G4 command with a P value shall be used to pause the code, for instance G4 P60 will perform a 60 second pause. Upon completion of

the welding program, have the torch move to the X0 Y0 Z150 position and preform a blow through with M171 and terminate the code with a M30. See Figure 243 below for reference.


<pre> 1 (TEST1) 2 G90 3 G21 4 G28 G91 Z0. 5 G90 6 7 (CONTOUR1) 8 M5 9 M9 10 T1 M6 11 S7850 M3 12 G54 13 M8 14 G1 15 G0 X-1.816 Y42.5 16 G43 Z95. H1 17 Z7.74 18 G1 Z0.5 F700. 19 Y84.761 F400. 20 X-1.813 Y84.921 21 X-1.798 Y85.08 22 X-1.771 Y85.24 23 X-1.729 Y85.4 24 X-1.678 Y85.546 25 X-1.673 Y85.56 26 X-1.6 Y85.719 27 X-1.518 Y85.866 28 X-1.51 Y85.879 29 X-1.399 Y86.039 30 X-1.359 Y86.089 31 X-1.261 Y86.199 32 X-1.199 Y86.261 33 X-1.089 Y86.359 34 X-1.039 Y86.399 35 X-0.879 Y86.51 36 X-0.866 Y86.518 </pre>		<pre> 1 (TEST1) 2 G21 3 G90 4 5 (CONTOUR1) 6 7 G0 X-1.816 Y42.5 Z7.74 8 9 G1 Z0.5 F700. 10 M11 11 G1 Y84.761 F400. 12 X-1.813 Y84.921 13 X-1.798 Y85.08 14 X-1.771 Y85.24 15 X-1.729 Y85.4 16 X-1.678 Y85.546 17 X-1.673 Y85.56 18 X-1.6 Y85.719 19 X-1.518 Y85.866 20 X-1.51 Y85.879 21 X-1.399 Y86.039 22 X-1.359 Y86.089 23 X-1.261 Y86.199 24 X-1.199 Y86.261 25 X-1.089 Y86.359 26 X-1.039 Y86.399 27 X-0.879 Y86.51 28 X-0.866 Y86.518 29 X-0.719 Y86.6 30 X-0.56 Y86.673 31 X-0.546 Y86.678 32 X-0.4 Y86.729 33 X-0.24 Y86.771 34 X-0.08 Y86.798 35 X0.079 Y86.813 36 X0.239 Y86.816 </pre>
---	---	--

Figure 243. Starting G-Code as Output (left) and as Post Processed (right).

Shown in Figure 243, G-code output for a program is edited in an NC Editor program (included with HSMWorks). The first two lines kept are G21, which lets Mach3 on the welder know were in millimeters, and G90 which is absolute coordinates. Reading down on the output file, Figure left, lines 7-14 are not useful to us. These are milling

specific G-codes contains information on what tool to use, what spindle speed, and turning on a coolant pump. Line 15 should be kept as it is a rapid (G0) move to the XY coordinate to the start of the toolpath where welding should begin. Line 16 can be removed as that is referencing the tool height, but line 17 should be kept and may be moved up to the prior line if desired to make it an XYZ rapid. Be aware this will move all three axes at the same time and may crash the machine if a clear path is not ensured.

G-code at the layer interface is shown in Figure 24. As you can see on output line 58 and 59, the trace ends and then moves up in the z-axis (Z5. F700.). As you can imagine, before moving to the next location for a milling machine, nothing really needs to happen. In our situation, the welder needs to be toggled off at this point. Therefore, performing a find replace option is done adding an M110, and a G1 before the z-axis move. The G1 is omitted in sequential lines to save space, however must now be added back after the M110.

The next chunk of code includes a z-axis rapid to the feed-height, an M9, and a rapid to the XY location where welding should resume. In our situation M9 is never used and is an easy way to find-replace to insert a pause, G4 P30 in this case. For the example shown in Figure 244, a probe cycle is run with the M141 code on line 66. A pause should always precede a probe, to allow any hot molten metal to cool, and a pause should follow a probe, to allow the machine to reorient itself and allow the operator to stop the program if for some reason the probe malfunctioned. Following probe contact, the M141 probe cycle retracts the torch to the correct wire offset distance and references that as the new Z0 plane. Therefore, welding should resume with at G1 Z0, to return to this level

before an M111 welding start. G1 needs to be added to the following line, shown in line 70 on Figure 24, right.


<pre> 50 Y9.5 51 X116. Y10. 52 Y7. 53 X104. Y7.5 54 Y4.5 55 X116. Y5. 56 Y2. 57 X104. Y2.5 58 Y-0.5 59 Z5. F700. 60 G0 Z15. 61 62 (ZIGZAG) 63 M9 64 G0 X84. Y50. 65 Z15. 66 Z5. 67 G1 Z0. F700. 68 X95.503 Y48.802 F720. 69 X96. Y48.75 F60. 70 X84.497 Y47.552 F720. </pre>		<pre> 50 Y9.5 51 X116. Y10. 52 Y7. 53 X104. Y7.5 54 Y4.5 55 X116. Y5. 56 Y2. 57 X104. Y2.5 58 Y-0.5 59 M110 60 G1 Z5. F700. 61 G0 Z15. 62 63 (ZIGZAG) 64 G4 P30 65 G0 X84. Y50. 66 M141 67 G4 P30 68 G1 Z0. F700. 69 M111 70 G1 X95.503 Y48.802 F720. 71 X96. Y48.75 F60. 72 X84.497 Y47.552 F720. </pre>
--	---	---

Figure 244. Layer Change G-Code as Output (left) and as Post Processed (right).

## Loading the Wire

Loading wire for the machine is detailed in the Fronius MIG Welding Equipment: Operations Guide very thoroughly. Reading the Fronius manual (RTFM) is encouraged as it contains more detail on the process, however, a brief overview will be discussed here. After installing the new spool, the wire needs trimmed and filed before being fed through the drive rollers, being careful not to let the spool unwind. Once the wire is in the drive rollers and the rollers are clamped, the wire feed switch in the VR 7000 is to be toggled to feed the wire through the first liner up to the wire buffer insert. Take the cover of the Robacta 5000 torch revealing the feed rollers. Open the feed rollers before feeding the wire further. Feed the wire again with the VR 7000 switch or the button on the

Robacata 5000 until the wire comes out of the liner in the Robacta 5000 Drive/Torch.

Make sure the wire is fed through the torch liner in the Robacta 5000 and close the cover.

Now the wire can be fed until the appropriate amount is fed out. Make sure the appropriate tip is in place for the specific material you are using.

### **Loading the Build Plate**

The build plate of choice is to be securely fastened to the steel platform by at least four finger clamps and ½-13 bolts to prevent uneven warpage. Black oxide, or uncoated, bolts should be used as zinc coatings will release toxic fumes when heated. The bolts should get coated in Loctite® 37616 copper anti-seize. The build plate should be adequately cleaned as any contaminants will alter the integrity of the print. Best practice is to mill the face of the build plates clean before use.

### **Setting the Gas Flow Rate**

Abiding to RTFM, the gas flow rate should be adjusted to the recommended setting per the wire diameter used. The shielding gas flow rate is controlled by the gas sensor and should not be altered with once initially set up. On the gas bottle, be sure to use a pressure regulator and not a flow regulator, as the gas sensor already regulates the flow and would only add an additional choke to the system. On the pressure regulator, just open the valve to the max flow and let the gas sensor take care of the rest. The level of the gas bottle shall be observed prior to a print and during a print to ensure sufficient flow. When empty, welding will be halted automatically, and ERROR NO GAS FLOW will read out on the RCU 5000.



## **Preparing Mach3 for Printing**

Open the Mach3 Software via the desktop icon labeled WAAM BAM (wire + arc additive manufacturing with built-in allowance for machining). If the prompt appears asking for which version of Mach3 you would like to run, you have opened the wrong version; however, this is ok, just select the '3D Printer' version.

The machined needs to be zeroed at the base plate. Using the aluminum standoff, probe the nozzle in the z-axis. Once the initial height is found, enter G92 Z87 in the prompt window to set the z-axis to 87 mm above the build plate (Z0). Now the x and y-axis need to be set according to the part's geometry. Also, do not forget to remove the aluminum standoff.

Load the G-code into Mach3 via the 'Load G-code' button. When the weld is ready to begin, click 'Cycle Start.'

## **Measuring the Voltage and Current and Wire Feed Speed**

The voltage/current/wire feed speed monitor begins recording when the weld is started. Fronius Explorer monitors these attributes automatically if the welder is online and the software open during the weld, therefore, ensure the software is open prior to running a print. The software records these values seam by seam and not as a 'print.' For example, if a print is 10 layers tall; the data for this part would be recorded as seam 1 through seam 10 in the Fronius software.

When collecting the data from the software, one should highlight the weld seams desired and select export to transfer the data for storage in the desired location. The data will then be able to open in Excel. One important note to mention is that Fronius

Explorer erases the files from its memory after midnight. Therefore, any late-night prints should be rescheduled if this data is to be collected.

### **Varying parameters in operation**

Parameters should not be modified during operation, as this thesis' main goal is to give more control and automation to the process. If desired, two significant parameters can be varied during the machine's operation. The machine's motion feed rate is modified by changing "feed rate" slider. The wire feed rate is modified by changing "Spindle Speed" slider. There are other various parameters that can be modified mid-weld; however, this should only be used for research purposes or to 'dial in' a new weld schedule (new material, etc.). If desired, addition pause duration can be added by changing the M110 script. Typically, after welding stops, the program waits 5 seconds to allow any crater fill and post flow gas to take place. By increasing this value, you can modify the layer pause times on the fly if the print is noticeably too hot.

**Appendix VIII – Continuation of Manual; Provided via Fronius**



Fronius International GmbH  
Froniusstraße 1  
4843 Paterbach

### CALIBRATION PROTOCOL

**Operating resources**

Manufacturer: Fronius International GmbH      Type: CMTAdv4030RMVUSA      Serial number: 20374374

**Ambient conditions**

Supply voltage: 380,20 V AC  
Ambient temperature: 24,13 °C

**Measuring equipment**

Agilent 34970A

The calibration was carried out by technicians trained especially for this following the example of a calibrating instruction. The precision of the calibration corresponds to the precision class under compliance the EN 60904. The load of the current source during the calibration was carried out by means of adjustable resistances.

Validation class      Precision      Open circuit voltage      54,51      V  
Validation type      Accuracy  
Number of measurements      2 measurements per measuring point

Visual inspection      Passed

**Measured data**

Operation mode:      Calibrate

	Desired value (setting)	Display			max. tolerance	Measured data			max. tolerance	Result
		Measure 1	Measure 2	Average		Measure 1	Measure 2	Average		
<b>Current measurement</b>										
Range 0 mA	40,00 A	40,00	40,00	40,00 A ± 4,00 A	40,11	40,10	40,10 A ± 4,00 A	OK		
Range 0 mA	120,00 A	120,00	120,00	120,00 A ± 4,00 A	120,40	120,36	120,38 A ± 4,00 A	OK		
Range 0 mA	200,00 A	200,00	200,00	200,00 A ± 4,00 A	200,55	200,55	200,55 A ± 4,00 A	OK		
Range 0 mA	300,00 A	300,00	300,00	300,00 A ± 4,00 A	300,72	300,63	300,67 A ± 7,00 A	OK		
Range 0 mA	400,00 A	400,00	400,00	400,00 A ± 4,00 A	400,79	400,60	400,79 A ± 10,00 A	OK		
<b>Voltage measurement</b>										
Range 300 mV	10,00 V	10,00	10,00	10,00 V ± 0,40 V	10,09	10,06	10,05 V ± 0,80 V	OK		
Range 300 mV	17,50 V	17,50	17,50	17,50 V ± 0,40 V	17,56	17,55	17,55 V ± 0,80 V	OK		
Range 300 mV	25,00 V	25,00	25,00	25,00 V ± 0,40 V	25,05	25,05	25,05 V ± 1,25 V	OK		
Range 300 mV	32,50 V	32,50	32,50	32,50 V ± 0,40 V	32,50	32,52	32,51 V ± 1,62 V	OK		
Range 300 mV	40,00 V	40,00	40,00	40,00 V ± 0,40 V	40,00	40,01	40,00 V ± 2,00 V	OK		

	Desired value (setting)	Measured data			max. tolerance	Result
		Measure 1	Measure 2	Average		
<b>Wire feeder speed VR 1</b>						
	-- m/min	--	--	-- rpm	--	--
	-- m/min	--	--	-- rpm	--	--
	-- m/min	--	--	-- rpm	--	--
	-- m/min	--	--	-- rpm	--	--

	Limit	Value	mOhm	mA	Result
Crash detection of protective Conductor	25,30 A	100,00	90,00	mOhm	OK
Input Circuit / Welding Circuit	5392,95 V	2,10	1,16	mA	OK
Input Circuit / exp. Conductive Parts	2950,47 V	1,00	0,41	mA	OK
Welding Circuit / exp. Conductive Parts	2491,70 V	1,10	0,78	mA	OK

This machine intended for industrial use has been successfully calibrated

Calibration engineer: Rozhan Patrick

## Digitally controlled GMA power sources

Heinz Hackl, Fronius International GmbH, Wels, Austria

### 1. Introduction

The ever more exacting demands nowadays being made of base and filler metals, and of materials-joining technology, have gone hand-in-hand with the continued development of power sources for GMA welding. This progress in the field of equipment technology has been largely underpinned by the enormous advances made by the electronics industry, and by the findings of arc physics. Thus it is that today, modern, fully digitally controlled power sources are available with extensive peripherals, improved ignition and welding behaviour and a good price-performance ratio.

### 2. Welding power-source designs

The high amperages required for arc welding, in conjunction with relatively low voltage values, can be generated with various different designs of power source. The characteristic feature of all the designs is the welding transformer, which serves to match the current and the voltage while at the same time functioning as an electrical isolation between the voltage supply and the welding current circuit. However, the decisive factor determining the size and the volume of the power source is the location of the transformer in the energy path.

The following diagram shows the various types of design of electronic power source.

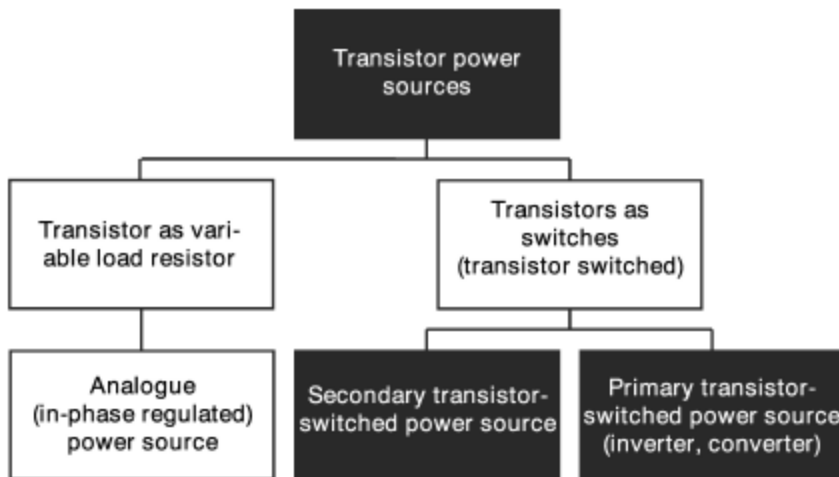


Fig. 1: Designs of power sources with power electronics

#### 2.1. Analogue power sources

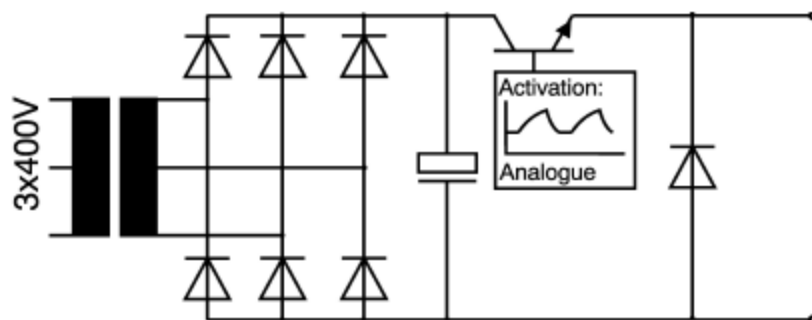


Fig. 2: Block diagram of an analogue power source

This power source consists of a 50Hz transformer, a rectifier and a transistor cascade (a large number of shunt-connected transistors) which serves as a continuously adjustable series resistor. The transistor cascade removes the voltage that is not needed for the welding process. The power loss that occurs here heats up the semiconductors - which is why these are generally cooled by an extra water cooling unit. The advantage of this configuration is its high response speed. The disadvantage is the huge power loss occurring on the power transistors. This results in very poor electrical efficiency, which is why this machine concept has more or less vanished from the market.

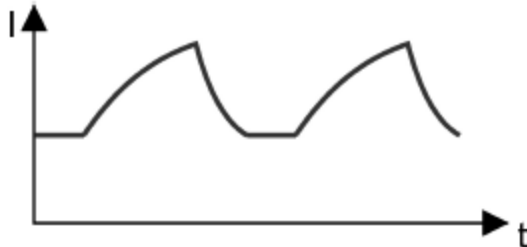


Fig. 3: Analogue current propagation

## 2.2. Secondary transistor-switched power sources

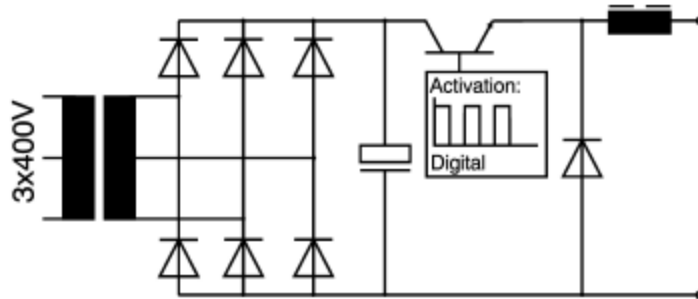


Fig. 4: Block diagram of a secondary transistor-switched power source

This power source consists of a voluminous 50Hz transformer, a rectifier and a transistor stage that acts as a switch.

The transistor stage is periodically turned on and off in the switching frequency (e.g. 20,000 times per second = 20 kHz). This periodical making and breaking is referred to as "transistor-switching".

We can picture the transistor in this configuration as a mechanical light-switch being turned on and off. With an ideal switch, no power loss occurs in either the 'open' or the 'closed' state. Thus a high electrical efficiency may be expected. Semiconductor switches are not ideal switching elements, of course, i.e. they too are affected by power-loss. However, this power loss is only very small. Another advantage of the transistors is their extraordinarily high switching speed.

In the power-range that is typical of welding, modern semiconductor switches can be switched on and off at up to 200 kHz (kilohertz). What is more, semiconductor switches can be activated using only very tiny electric currents - i.e. you can control a 20 kilowatt (500 A) power source with only a very few watts of control power.

Depending on the type of transistor used, the following switching frequencies are commonly used in the welding field:

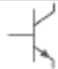


Semiconductor type	Graphic symbol	Switching frequency
Bipolar transistor		up to 30 kHz
MOS (Metal Oxide Semiconductor)		up to 200 kHz
IGBT (Isolated Gate Bipolar Transistor)		up to 40 kHz

Fig. 5: Power semiconductors

The higher the switching frequency of the transistor, the smaller is the output current ripple and the higher the response speed, all of which make for much better scope to influence the welding process. In order to make it possible to freely adjust the welding power across a wide range on transistor-switched power sources, the ratio of the make-time to the break-time must be changed. This method is called "pulse-width modulation" or "pulse-duration modulation" (PDM). If there is a large ratio of make-time to break-time, a high output power (mean value) results; if the ratio of make-time to break-time is small, a low output power results.

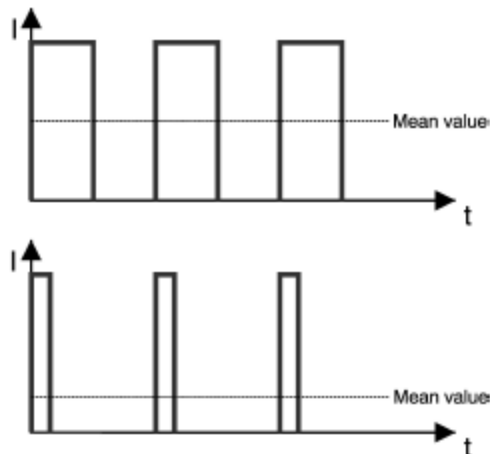


Fig. 6: Transistor-switched current propagation in PDM

### 2.3. Primary transistor-switched power sources (inverters)

In an inverter power source, the welding transformer is located after the switching transistor in the energy path. The reason for this is that a law of electrical engineering has it that the weight and volume of a transformer depend on the frequency at which it is operated. The higher the frequency, the smaller the volume.

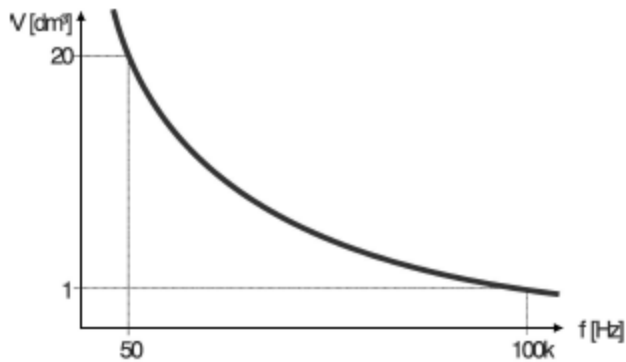


Fig. 7: Relationship between volume and frequency of a transformer at a given output power.

It is precisely this connection between volume and frequency that is exploited by inverter power sources. This is the reason why inverter power sources can have low weight and compact dimensions without sacrificing power and performance. As a result, they are much lighter to carry, which is particularly important for use out in the field. Also, thanks to their small volume, inverters take up less space in the often cramped conditions found in workshops.

Another advantage is their high electrical efficiency (up to 90%).

Before the high switching frequency can be exploited, the mains AC voltage must first be rectified - hence the term "inverter" power source. The DC voltage delivered by the primary rectifier is converted to a high frequency with the aid of a transistor switch.

The output voltage from the transformer is then rectified once again.

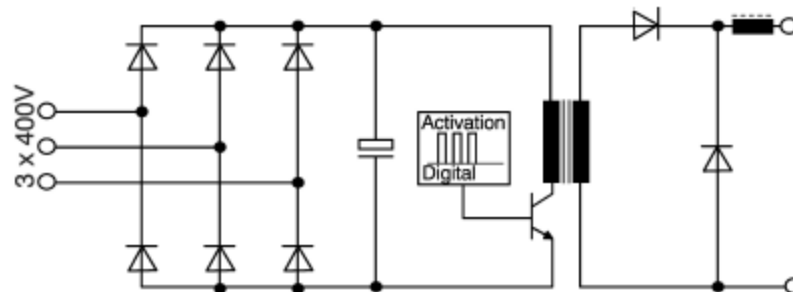


Fig. 8: Primary transistor-switched power source (inverter)

On transistor power sources, the welding properties do not depend on the design of the transformer and the output inductor. This makes it possible to flexibly adapt the power source characteristic to the job in hand.

### 3. Digitally controlled power sources

A revolutionary advance in the development of power sources has been brought about by 100% digitisation of the system. This quantum leap can be compared to the development of the music CD as a successor to the old vinyl LP record. Although previous computer-controlled power sources have also used microcontrollers, the process controller - the heart of the machine - has always been of analogue design. One of the main reasons for this is the high computing capacity required for such rapid processing of the data. It is only the use of digital signal processors (DSP's) that have made it possible to take this crucial step of complete digitisation. This means that the welding properties - by which we really mean the arc characteristic - are represented by software and not by inflexible, hard-to-alter hardware. Higher welding performance is the result.



This opens up unprecedented scope for influencing the welding process via software. What is more, the precision and replicability of the welding results are also enhanced, as the temperature-drift-prone analogue components are eliminated.

The use of a DSP is also the key feature differentiating a digitally controlled power source from a conventional, customary, computer-controlled one.

Mention should also be made of the fact that in fully digitised power sources, there is a significant reduction in the total number of electronic components.

Another advantage of modern equipment technology is the communication that takes place from the power source to the periphery (wirefeed drive, remote control units etc.). On the new digitised power sources from Fronius, this takes place via a serial data bus, which fulfils today's requirement for "Hot plug-and-play". By this we mean the facility for connecting or disconnecting peripherals during welding, with the system responding automatically to any such change. With certain types of bus (e.g. CAN bus), there is no provision for periodical bus initialisation. In such cases, then, the system must be "re-booted".

The serial data bus not only eliminates many of the interconnecting leads between the power source and the periphery, but also enables a convenient and comprehensive exchange of data. Fig. 9 gives a good example of the possibilities that this allows. Here, a display and an adjustment facility are integrated into the handle of the welding torch. This makes it possible to dispense with the extra workplace remote-control unit.



Fig. 9: Jobmaster welding torch with integrated remote control

In order to extend the advantages of digital data interchange to various different automation buses such as Interbus, Profibus etc., there are a large number of protocol interfaces that enable data adaptation. In this way, data on the operational status or parameter settings can be viewed and adjusted not only on the power source itself, but also e.g. directly on the robot control unit.

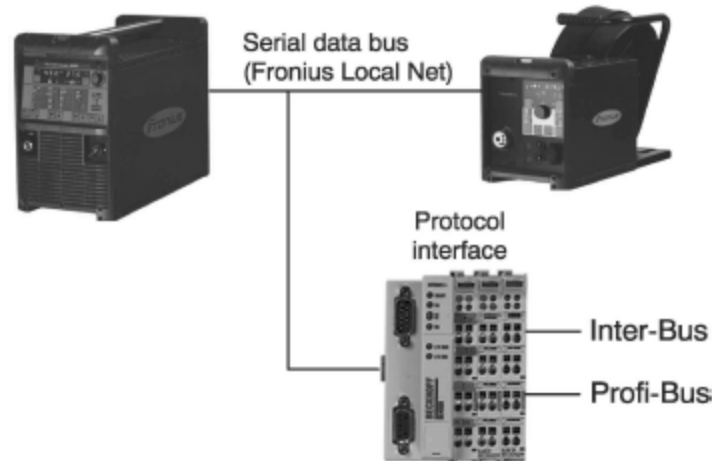


Fig. 10: Protocol interface

#### 4. Metal transfer

Depending on the current density, the arc power and the shielding gases used, it will be found that very different forms of metal transfer take place, each of which will be characterised by a particular type of arc.

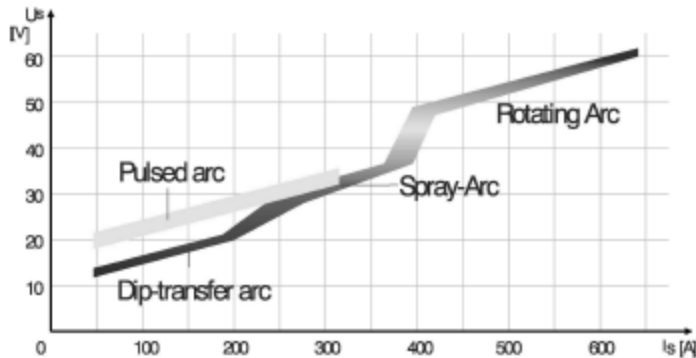


Fig. 11: Arc regions in GMA welding (Source: Linde AG)

Type of arc	Symbol	Droplet size	Metal transfer
Dip-transfer arc	k	Fine	Only in short circuit, uniform
Intermediate arc	ü	Fine to coarse	Partly in short circuit, partly short-circuit-free, irregular
Spray arc	s	Fine to super-fine	Short-circuit-free, uniform
Long arc	l	Coarse	Irregular, partly short-circuit-free in short circuit
Pulsed arc	P	Adjustable	Short-circuit-free, uniform

Fig. 12: Classification as per DIN 1910, Part 4

The decision as to which of these different types of arc to use will depend on the thickness of the sheet and the type of welding task to be performed.

The use of digitally controlled power sources enables very significant improvements indeed to be made in the metal transfer, particularly when welding with dip-transfer or pulsed arcs.

The main reasons for this are the high response speed of the inverter power source and - following from this - the many possibilities for influencing the metal transfer by software.

##### 4.1. Dip-transfer arc

The characteristic feature of the dip-transfer arc is the arcing period followed by a short-circuiting period in which the metal transfer takes place. On step-switched (thyristor-controlled) power sources, the short-circuit breaking phase can only be altered in steps (by changing the inductance tap). Sub-optimum results are the consequence.

On digital power sources, on the other hand, this phase can be "fine-tuned" to the wire quality, wire diameter and shielding gas being used. The result is a noticeably more stable arc and a low level of spattering - even under CO<sub>2</sub>.

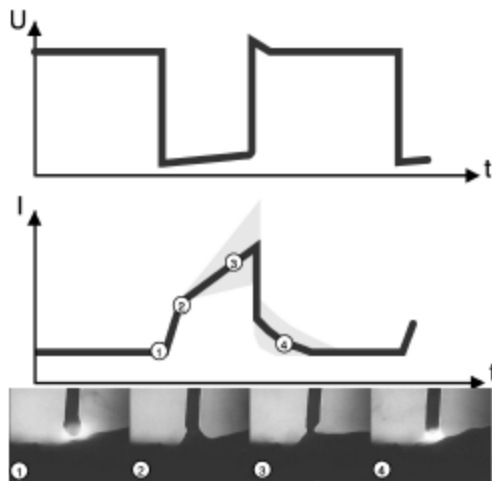


Fig. 13: Precision treatment of short circuits on transistorised power sources, by continuously adjustable inductance function.

#### 4.2. Pulsed arc

Under argon and argon-rich shielding gases it is possible to achieve a controlled, short-circuit-free metal transfer by selecting suitable parameters for the background current and pulsing current.

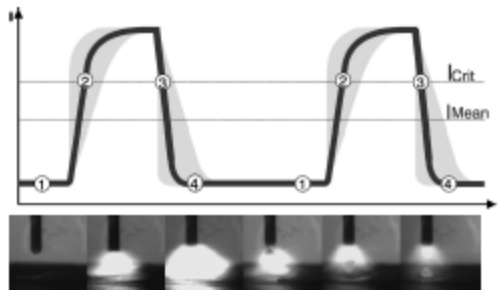


Fig. 14: Variable pulse form with a digitally controlled inverter power source

When optimum parameters are selected, exactly one droplet of filler metal per pulse is shed from the wire electrode. The result is virtually spatter-free welding.

Investigations carried out at Fronius have shown that differentiated pulse forms are necessary for different filler metals and shielding gases.

This has led to a "tailor-made" pulse form being used for every single filler metal.

The pulsed arc is used for welding aluminium and high-alloy steels, and for unalloyed steels in the region of the intermediate arc.

The pulsed arc makes it possible to use larger wire diameters, even when welding light-gauge sheet.

Larger wire diameters can be fed more easily - which is particularly important for soft wires such as aluminium - and are also generally less expensive.

Using a modern, high-quality pulsed-arc power source, a 0.8 mm aluminium sheet can be welded with a 1.2 mm wire electrode! Particularly in the case of aluminium, thicker wire electrodes are especially advantageous. Thicker wires have a more favourable ratio of volume to surface area, which means that fewer oxides are introduced into the weld pool.

Ideally, when changes are made to the wire extension length (the "stick-out", i.e. the length of wire exposed between the contact tube and the arc), little or no spattering should occur.

This is only the case if the process control can maintain a "one droplet per pulse" metal transfer even when stick-out changes are made.

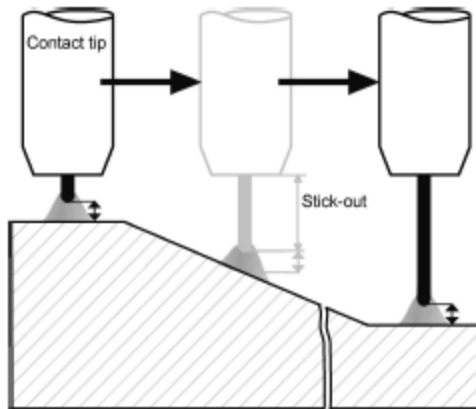


Fig. 15: Welding across a step

### 4.3. Arc ignition

On many transistorised power sources, the level of current necessary for exact, jerk-free ignition of the arc is determined with reference to the respective wire diameter and wire quality. There are also inverters that automatically remove the ball from the tip of the welding wire at the end of welding in the dip-transfer or spray arc.

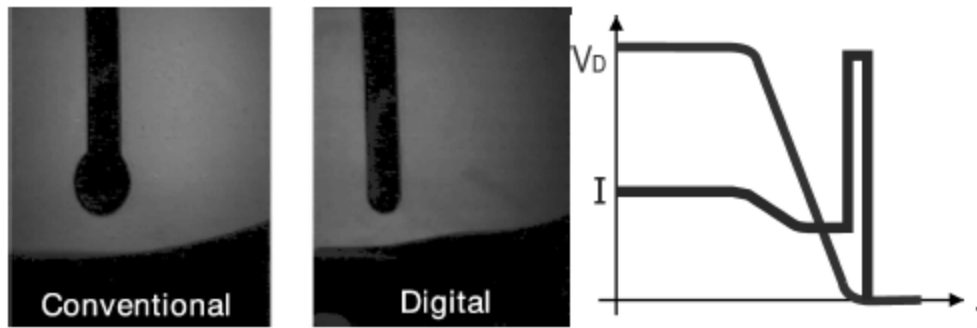


Fig. 16: Digitally controlled end-of-welding  $V_d$  ... Wirefeed speed in  $m/min$   $I$  ... Welding current in amperes

Jerk-free re-ignition is the result. This is particularly important for automated and mechanised applications, as ignition errors and arc-starting difficulties lead to costly down-times. Aluminium not only has a low density, but is also a good thermal conductor. This property causes a lack of fusion at the beginning of welding. With the "Aluminium Start-up Program", the welder can use the torch trigger to call up a higher welding power at the start of welding. In this way, the base metal starts to be fused even during the ignition phase. Once sufficient heat has been introduced into the weld pool, the welding power is lowered to the nominal level. Towards the end of the weld seam, when the heat starts to run ahead and there is a risk of weld-pool drop-through, the welding power is lowered again, this time to the crater-fill current.

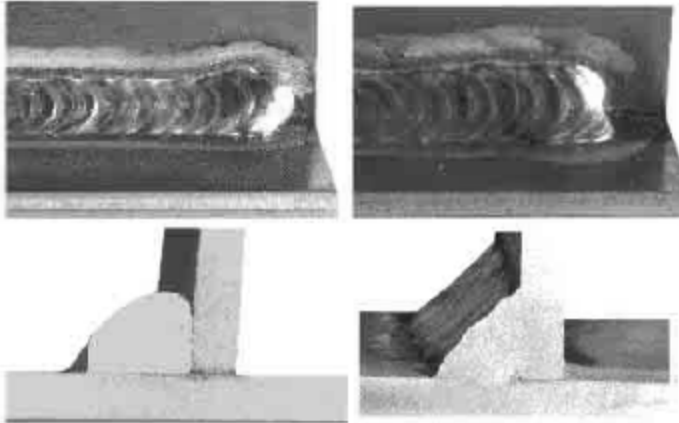


Fig. 17: Comparison of conventional ignition (left) with Aluminium Start-up Program (r) for preventing lack of fusion at start of weld

### 5. Synergic mode

The results described in Section 4 above are only possible with the aid of a large number of continuously adjustable parameters (around 60 in all). These make it possible to improve both droplet detachment in pulsed-arc welding and the treatment of the short circuit in dip-transfer welding, for a wide spectrum of filler metals. However, these additional parameters would make the power sources very much more difficult to operate and would mean that only a handful of experts would be able to use them.

This is where the "synergic mode" (single-dial operation) comes in. By providing pre-programmed parameters for any combination of wire and shielding gas, synergic operation makes the machine very easy for the welder to use.

In effect, the job of optimising the parameters for many different base and filler metals and shielding gases is done for the user by the equipment manufacturer. These empirical results are stored in an electronic memory module as a databank. The user simply selects the filler metal directly on the power source, and the integrated microprocessor enables the desired power to be selected on a continuous scale from minimum through to maximum.

There is a sheet-thickness indicator to help the user find the most suitable welding parameters. For fully mechanised tasks, the fillet-weld throat ("a"-dimension) can also be selected as a parameter. This of course only functions in conjunction with a pre-selected welding speed. The digitisation makes it possible to upload special welding programs directly to the power source by means of electronic data transmission.



Fig. 18: Innovative LCD-Remotecontrol-Unit, with welding-data-surveillance and logical (easy-to-use) userinterface

## 6. Summary

The latest development in the field of welding power sources is the completely digital machine. What this means is that not only the control sequences, but also the process controller are represented in digital terms - i.e. by software. The crucial difference as against customary computer-controlled power sources is the incorporation of a digital signal processor (DSP), which carries out the welding process control in a digital manner. Hitherto, this analogue part has always involved a great deal of hardware and time-consuming hardware adjustments.

The advantages of the fully digital power source are the much easier user guidance and outstanding welding properties that it makes possible. Particularly at the beginning and end of welding and in the dip-transfer and pulsed arcs, marked improvements over conventional power sources are apparent. Fig.19 and Fig. 20 show typical fields of application for digital inverter power sources.



*Fig. 19: Portable digital 270 A inverter power source being used in tank construction*



*Fig. 20: Digitally controlled 400 A inverter power source being used for steel construction work*

[69]